

Sheffield Hallam University

The effect of a magnesia based additive on fly ash deposition in a chain-grate boiler system.

HADJFOROOSH, Kambiz.

Available from the Sheffield Hallam University Research Archive (SHURA) at:

<http://shura.shu.ac.uk/19738/>

A Sheffield Hallam University thesis

This thesis is protected by copyright which belongs to the author.

The content must not be changed in any way or sold commercially in any format or medium without the formal permission of the author.

When referring to this work, full bibliographic details including the author, title, awarding institution and date of the thesis must be given.

Please visit <http://shura.shu.ac.uk/19738/> and <http://shura.shu.ac.uk/information.html> for further details about copyright and re-use permissions.



BRN 301 306

Sheffield Hallam University

REFERENCE ONLY

ProQuest Number: 10697040

All rights reserved

INFORMATION TO ALL USERS

The quality of this reproduction is dependent upon the quality of the copy submitted.

In the unlikely event that the author did not send a complete manuscript and there are missing pages, these will be noted. Also, if material had to be removed, a note will indicate the deletion.



ProQuest 10697040

Published by ProQuest LLC (2017). Copyright of the Dissertation is held by the Author.

All rights reserved.

This work is protected against unauthorized copying under Title 17, United States Code
Microform Edition © ProQuest LLC.

ProQuest LLC.
789 East Eisenhower Parkway
P.O. Box 1346
Ann Arbor, MI 48106 – 1346

**THE EFFECT OF A MAGNESIA BASED ADDITIVE ON
FLY ASH DEPOSITION IN A CHAIN-GRATE
BOILER SYSTEM**

KAMBIZ HADJFOROOSH

A thesis submitted in partial fulfilment of the
requirement of
Sheffield Hallam University
for the degree of Doctor of Philosophy

October 1993

Collaborating Organisation: Steetley Quarry Products Ltd.



TO
MY PARENTS AND MY BROTHER
KAMRAN
INSPIRATIONS EVERLASTING

Preface

The work described in this thesis is submitted for the degree of Doctor of Philosophy. It was carried out at Sheffield Hallam University in the period May 1986 to October 1993.

During this period, the author has attended post graduate level courses in the School of Engineering - Division of Materials and Environmental Engineering. These are:

- Advanced Refractories Technology
- Advanced Thermodynamics - Slag Chemistry
- Process Metallurgy

In addition, the author attended the first European conference on 'The Influence of Inorganic Constituents on Coal Combustion in Small to Medium Sized Boilers' held by the Institute of Energy in London in September 1987. A number of working papers and seminars have also been presented by the author to various industrial organisations and interested parties. These are:

- Steeley Quarry Products - Magnesia Materials Division, Hartlepool, 1986-1990
- West Belfast power station - Northern Ireland, November 1987
- British Coal Research Establishment, Stoke Orchard, June 1988 & December 1989
- Coal Research Forum - London, March 1989
- National Power - Thermal Division, Sheffield, November 1990

The work described herein is to the best of my knowledge original, except where reference is made to others, and no part of it has been submitted for an award at any college or university.

ACKNOWLEDGEMENTS

It is with immense relief and pleasure that I arrive at this final section to thank many people. First and foremost I would like to forward my sincere thanks and appreciation to Dr. G. Briggs whose didactic approach, guidance and support, particularly during the earlier stages of this work was paramount and significantly illuminating. Dr. R. Acheson takes the rest of my sincere thanks for his sustained supervision, his insight for the subject matter and his constructive criticism over many years, making this work possible.

I am thankful for all the help and technical advice which I received from time to time during the experimental work, from all the technical staff, particularly Mr. D. Latimer and Mr. N. Dziemidko. I would also like to thank the EOSA division and Mr. K. Blake for his availability and advice on X-Ray Diffraction work.

The receptivity, interest and financial assistance of Steetley Quarry Products Ltd. acting as the collaborating industrial organisation in this project is greatly appreciated. Particular thanks are due to Mr. G. Spoons and Mr. J. Turner.

Also I appreciate the assistance of personnel at West Belfast power station during residential monitoring of the boilers under study.

I am grateful for all the help and friendship which I enjoyed at various stages from the administrative staff, secretaries, librarians and my fellow research colleagues at the School of Engineering.

My final thanks and deepest gratitude are reserved for my family whose financial and moral support over many a long and sometimes arduous years was the most decisive factor which kept me going. To my aunt Mrs. T. Mostofi goes out my deep and sincere gratitude for her care, attention and encouragement.

ABSTRACT

THE EFFECT OF A MAGNESIA BASED ADDITIVE ON FLY ASH DEPOSITION IN A CHAIN-GRATE BOILER SYSTEM

By: Kambiz Hadjforoosh

Unlike in oil firing, the effective role of additives to alleviate deposition in coal fired power generation is still regarded with much scepticism and controversy amongst the power generators and boiler operators. The objectives of this research study were principally to explore the mechanisms involved in formation of coal ash deposits and thus determine the effectiveness of a magnesium based additive, namely Lycal 93HS, in reducing the bonding strength of ash deposits on boiler tube surfaces, by making them friable and easily removed by sootblowers during normal operation of the boiler.

The experimental techniques developed involved visual, optical and scanning electron microscopy examination of a wide range of matured deposit samples collected over a period of two years, with and without injection of Lycal 93HS into the boilers at West Belfast power station. Specimen deposit samples "fashioned" into the form of Seger cones and "reconstituted" from their crushed, powder form were tested for their softening behaviour at elevated temperatures with and without further additions of Lycal 93HS. This technique was further used to evaluate the effect of Lycal 93HS on the softening behaviour of a range of coal ash components separated by high temperature ashing of coarse particles of coal as well as the bulk ash from the coarse and fine sizes of coal particles. The softening behaviour on heating and crystallisation tendency behaviour on cooling for a selected range of the ash components was investigated without and with additions of Lycal 93HS, using Hot-Stage Microscopy. The possibility of surface adhesion between the fly ash and injected Lycal 93HS within the boiler environment was investigated through a series of laboratory based Surface leaching experiments of deposit and particulate samples with and without injection of Lycal 93HS. The variation in concentration profiles of silicon, iron and magnesium within the collected solutions over a period of time were analysed, using Atomic Absorption Flame Spectroscopy. The elemental chemical composition of bulk deposit samples, the average high temperature ash and its separated components was carried out using X-Ray Fluorescence. Qualitative study of the mineralogy of low temperature ash, selected ash components, as well as a range of deposit samples with Lycal injection was conducted using X-Ray Diffractometry.

The results of Lycal injection into a boiler were clearly evident from inspections of the boiler where Lycal injection over different periods of time had resulted in significantly cleaner boiler tube surfaces. Examination of deposit samples with Lycal injection showed lightly sintered, porous, friable textures compared to the highly sintered, fused and dense structures for samples without Lycal injection. The effect of Lycal on the softening behaviour of reconstituted deposit samples and various components of ash was shown to be dependent on their chemical composition, with iron oxide playing an important role. For a number of highly acidic ash components, additions of 5 and 10 mass% Lycal promoted crystallisation of their fluid melt, when cooled to specific temperatures. For the more ferriferous ash components, additions of 1 and 3 mass% Lycal enhanced the surface formation of spikes when their melts were cooled to specific temperatures. The results of leaching experiments showed that the initial magnesia concentrations were generally much higher for the deposit samples and fly ash particles from ash hoppers and grit arrestors with Lycal injection than those without.

CONTENTS

	<u>PAGE</u>
<u>ABSTRACT</u>	ii
<u>LIST OF FIGURES</u>	ix-xii
<u>LIST OF TABLES</u>	xiii-xxi
<u>LIST OF PLATES</u>	xxii-xxxii
CHAPTER 1 : <u>INTRODUCTION</u>	1
CHAPTER 2 : <u>LITERATURE SURVEY</u>	
2.1 THE BURNING OF COAL FOR POWER GENERATION	3
2.1.1 Introduction	3
2.1.2 Mechanical Stoker Firing Systems	3
2.1.3 The Combustion of Coal on a Grate	4
2.1.4 Fire-Side Boiler Deposits	9
2.2 MINERAL CONSTITUENTS OF COAL	12
2.2.1 Geological Origin of Mineral Matter in Coal	12
2.2.2 The Behaviour of Inorganic Mineral Matter When Heated	14
2.3 CHARACTERISATION AND FUSIBILITY OF COAL ASH WITH RESPECT TO IT'S CHEMICAL PROPERTIES	23
2.3.1 Introduction	23
2.3.2 The Effect of Chemical Composition on Ash Fusibility	24
(a) Oxidising Conditions	26
(b) Reducing Conditions	30
2.3.3 Flow Characteristics	35
2.4 THE FORMATION OF FLY ASH DEPOSITS IN BOILER SYSTEMS	39
2.4.1 Introduction	39
2.4.2 Factors influencing Deposition	41
(a) The Effect of Ash chemistry on Deposition	41
(b) The Influence of Flue Gas Composition on Deposition	48
(c) The Effect of Flue Gas Temperature on Deposition	49
(d) The Effect of Boiler Design on Ash Deposition	50
(e) The Effect of Boiler Operation on Ash Deposition	52

	<u>PAGE</u>
2.4.3 The Mechanism of Ash Deposition	53
(a) Formation and Accumulation of Coal Ash on Boiler Tube Surfaces	53
(b) Sintering and Coalescence of Coal Ash	58
(c) Formation of Monolithic and Layer - Structured Deposits	61
 2.5 ADDITIVES	 64
2.5.1 Additives in Coal-Based Power Generation	64
2.5.2 Implication of the Use of Additives	72
(a) Increased Flexibility and Efficiency in Fuel Selection	72
(b) Lower Cost Boiler Operation	73
(c) Reduction in Acid Smut, SO ₃ and Fly Ash Emission	74
2.5.3 Magnesium Compounds and their Effect on the Ash Deposition Process	75
 2.6 WEST BELFAST POWER STATION	 82
2.6.1 Introduction	82
2.6.2 Operation of the Plant	82
2.6.3 Boiler Operation	84
2.6.4 Additive Injection Equipment	87
 CHAPTER 3 : <u>EXPERIMENTAL METHODOLOGY</u>	
 3.1 INTRODUCTION	 90
3.2 RAW MATERIALS	92
3.2.1 Lycal 93HS	92
3.2.2 Ayrshire Coal	95
3.2.3 Boiler Ash Deposit Samples	95
 3.3 INVESTIGATION OF BOILER DEPOSITS	 100
3.3.1 Preliminary Examination of As Received Samples	100
(a) Chemical Analysis	100
(b) Visual Appearance and Texture of Deposits	100
(c) Stereo-Compound Microscopy (SCM)	101
3.3.2 Micro-Examination of As Received Samples	101
(a) Sample Preparation for Petrological Examination	101
(b) Optical Microscopy	103
(c) Scanning Electron Microscopy - EDX Elemental Analysis	103
3.3.3 X-Ray Diffraction Analysis of Deposits and Coal Ash Procedure	104 105

	<u>PAGE</u>
3.3.4 Determination of Softening and Melting Behaviour of Coal Ash Deposits Using the Cone Fusion Tests	106
(a) Introduction	106
(b) The Preparation of Cones for Fusibility Measurements	107
(c) Furnace Assembly Used for Fusibility Measurements	109
(d) Procedure	112
3.3.5 Heat Treatment of Selected Deposit Specimen	114
(a) Introduction	114
(b) High Temperature Muffle Furnace	115
(c) Procedure	115
3.3.6 Determination of the Magnesia Distribution Within Ash Deposit Particles	115
(a) Introduction	115
(b) Procedure	116
3.3.7 Ash Deposition on a Probe in West Belfast No.6 Boiler	118
3.4 INVESTIGATION OF AYRSHIRE COAL AND ITS ASSOCIATED MINERAL MATTER / ASH	127
3.4.1 Analysis of Ayrshire Coal	127
(a) Introduction	127
(b) Size Analysis of Coal	127
(c) Determination of Moisture Content	127
(d) Determination of the Ash Content	129
3.4.2 The Constitution and Properties of the Mineral Matter / Ash	129
(a) Evaluation of Ash Mineral Components	129
(b) Chemical and Mineral Constitution of Coal Ash	130
X-Ray Fluorescence (XRF) Chemical Analysis	
X-Ray Diffraction (XRD) Analysis	
(c) Determination of Softening and Melting Behaviour of Coal Ash	131
Cone Fusion Testing of Coal Ash	
Hot-Stage Microscopy of Coal Ash	
Procedure	
CHAPTER 4 : <u>EXPERIMENTAL RESULTS</u>	
4.1 INTRODUCTION	135
4.2 STRUCTURE, MORPHOLOGY AND CHEMICAL CONSTITUTION OF BOILER DEPOSITS	135
4.2.1 Boiler Observations	135
4.2.2 Bulk Chemical Analysis of Deposit Samples from Boilers No.5 & 6	137
4.2.3 Visual Examination of Boiler Deposits	142
(a) Pre Lycal 93HS Injection - Boiler No.6	142
(b) Post Lycal 93HS Injection - Boiler No.6	151
(c) No Lycal 93HS Injection - Boiler No.5	155

	<u>PAGE</u>
4.2.4 Microscopic Examination and Elemental Analysis	160
(a) Unpolished, As Received Samples from Boilers No.5 and No.6	160
(b) Polished, As Received Samples from Boilers No.5 and No.6	187
(c) Comparison of Deposit Samples from Boilers No.5 and No.6	219
4.2.5 Determination and Study of Crystallinity of Deposits	223
 4.3 SOFTENING CHARACTERISTICS OF DEPOSITS WITH AND WITHOUT ADDITIONS OF LYCAL 93HS	 224
4.3.1 Cones "Fashioned" from As Received Deposit Specimens	224
4.3.2 Cones Produced from "Reconstituted" Deposit Specimens	227
4.3.3 Effect of Additional Lycal 93HS on the Softening Behaviour of Deposits	229
4.3.4 Heat Treatment of Selected Deposits Under Controlled Conditions	234
 4.4 DEPOSITION PROBE SAMPLING OF THE COAL FLY ASH	 234
4.4.1 Chemical Analysis of the Collected Fly Ash	234
4.4.2 Determination of Deposition Rate	237
 4.5 THE SURFACE-LEACHING OF DEPOSIT SAMPLES	 237
 4.6 COAL CHARACTERISATION	 271
4.6.1 Proximate Analysis	272
4.6.2 Ultimate Analysis	272
4.6.3 Particle Size Analysis	272
4.6.4 Variation of Moisture With Coal Particle Size	275
4.6.5 Variation of Ash Content With Coal Particle Size	275
4.6.6 Variation of Ash Chemistry With Coal particle Size	275
4.6.7 Determination of the Softening Characteristics of Selected Ash Admixtures With and Without Additions of Lycal 93HS	281
 4.7 THE CHARACTERISATION OF ASH COMPONENTS IN AYRSHIRE COAL	 281
4.7.1 Separation of Coal Ash Components	284
4.7.2 Chemical Constituents of the Coal Ash Components	284
4.7.3 Mineralogy of the LTA and Separated HTA Components	293
4.7.4 Softening Characteristics of Selected Coal Ash Components With and Without Additions of Lycal 93HS	304
(a) Cone-Fusion Investigation	304
(b) Hot-Stage Microscopic Investigation	308

CHAPTER 5 : DISCUSSION

5.1 GENERAL INTRODUCTION	347
5.2 THE CHARACTERISATION AND BEHAVIOUR OF ASH DERIVED FROM AYRSHIRE COAL	348
5.2.1 Physical and Chemical Constitution of Ash Derived from Ayrshire Coal	349
5.2.2 Assessment of Softening Behaviour of High Temperature Ash and Its Relationship to Ash Deposition	354
(a) Critical Assessment of the Cone Fusion Technique	354
(b) Variation in the Softening Behaviour of Coal Ash With Respect to its Size and Composition and Its relevance to Deposition	356
(c) Variation in the Softening Behaviour of the Coal Ash Components and Its Relevance to Deposition	357
5.3 INTERPRETATION OF THE TRANSFORMATION AND CRYSTALLISATION BEHAVIOUR OF ASH COMPONENTS ON PROGRESSIVE HEATING	364
5.3.1 Without Additions of Lycal 93HS	364
5.3.2 With Additions of Lycal 93HS	366
5.4 CHARACTERISATION OF PARTICULATE FLY ASH SAMPLES FROM ASH HOPPERS AND GRIT ARRESTORS	369
5.4.1 Introduction	369
5.4.2 Variation in Fly Ash Morphology and Chemistry	370
5.4.3 Comparative Analysis of the Effect of Lycal 93HS on the Fly Ash and Ash Particles Collected on a Probe Surface	372
5.5 COMPARATIVE EXAMINATION AND ASSESSMENT OF THE EFFECT OF LYCAL 93HS ON BOILER DEPOSIT SAMPLES	374
5.5.1 Macroscopic-Scale Examination	374
5.5.2 Microscopic Examination and Analysis of Boiler Deposits	376
(a) Unpolished Deposit Samples	376
(b) Polished Deposit Samples	377
5.6 APPLICATION OF LABORATORY-BASED TECHNIQUES TO DEPOSIT SOFTENING BEHAVIOUR INSIDE THE BOILER SYSTEM	380
5.6.1 Correlation of the Softening Regimes for Fashioned Deposits to Boiler Environment	380
5.6.2 Relevance of Deposit Reconstitution to its Softening Behaviour Within the Boiler Environment	380

	<u>PAGE</u>
5.6.3 Role of Iron Oxide on the Softening Behaviour of Deposits on Boiler Tube Surfaces	381
5.7 PROPOSALS FOR THE ROLE OF LYCAL 93HS IN BOILER No.6	383
5.7.1 Introduction	383
5.7.2 The Role of Lycal 93HS as an Internal Modifier of Deposit Particles With Respect to their Softening Behaviour	384
5.7.3 The Role of Lycal 93HS as an External Modifier of Deposit Particles With Respect to their Surface Properties	387
5.8 PROPOSALS FOR A MECHANISM FOR THE EFFECT OF LYCAL 93HS ON DEPOSIT FORMATION	397
5.8.1 Introduction	397
5.8.2 Consideration of Factors Involved in Deposition	397
5.8.3 The Role of Lycal 93HS With Respect to Deposit Formation	400
CHAPTER 6 : <u>CONCLUSION</u>	405
CHAPTER 7 : <u>SUGGESTIONS FOR FURTHER WORK</u>	407
CHAPTER 8 : <u>REFERENCES</u>	408

Figure 2-1: The principle of operation for: (a) Overfeed (b) Underfeed and (c) Composite modes of combustion.	5
Figure 2-2: Section view of travelling grate stoker showing the form of the fuel bed.	6
Figure 2-3: Fuel-bed zones of a stoker fired boiler broken up into oxidation, reduction, distillation and volatile gas burning.	6
Figure 2-4: Fuel-bed temperature contours for travelling grate stoker.	8
Figure 2-5: Section through a deposit on a boiler tube.	11
Figure 2-6: Fe - S phase diagram.	21
Figure 2-7: Comparison of softening temperature under reducing and oxidising atmospheres for various percentages of basic constitutions.	33
Figure 2-8: Influence of iron on coal-ash fusion temperature under oxidising and reducing conditions.	33
Figure 2-9: Typical viscosity-temperature relationships of coal-ash slags in solidification range.	38
Figure 2-10: Deposit zones in a coal fired unit.	40
Figure 2-11: Approximate temperature regions for deposit formations in coal fired units.	40
Figure 2-12: Reaction sequence of iron oxides and alkalies with sulphur oxides.	46
Figure 2-13: The evolution of fly-ash during coal particle combustion.	55
Figure 2-14: The initial stage of sintering - Frenkel's two particle model.	60
Figure 2-15: Physical structure of a typical deposit from burning a highly fouling coal.	62
Figure 2-16: Arrangement of boiler no.6 - sectional view.	85
Figure 2-17: Diagram of draught system for boiler no.6.	88
Figure 2-18: Schematic representation of Lyclal 93HS injection apparatus.	88
Figure 2-19: Schematic representation of core and mass flow hoppers.	89

- Figure 3-1:** Lycal 93HS particle size distribution curve measured on a Sedigraph 5000D particle size analyser. 94
- Figure 3-2:** The surface area of magnesium oxide formed by the decomposition of magnesium hydroxide. 94
- Figure 3-3:** Schematic diagram of boiler no.6 - section view denoting deposit locations. 97
- Figure 3-4:** Characteristic shapes of the pyramidal deposit and coal-ash specimen during the heating regimes. 108
- Figure 3-5:** A diagram of the assembled apparatus used to study the softening and melting characteristics of ash cones. 111
- Figure 3-6:** Heating regime selected for the softening assessment of deposit and coal ash cone samples in a horizontal tube furnace. 113
- Figure 3-7:** A schematic diagram of the apparatus for the surface leaching of ash deposits. 117
- Figure 3-8:** Schematic diagram of air-cooled probe used for measuring ash deposition rate in full scale boiler at West - Belfast power station. 119
- Figure 3-9:** Apparatus for the determination of moisture content of coal (vacuum method): (a) furnace assembly, (b) absorption tube and weighing vessel. 128
- *****
- Figure 4-1:** Variation of unburned carbon content for size fractioned fly ash particles from economiser ash hoppers and grit-arrestors, with and without on-line injection of Lycal 93HS. 149
- Figure 4-2:** Particle size distribution curves for the economiser ash hopper samples collected with and without on-line injection of Lycal 93HS over the period of 12 hour tests. 178
- Figure 4-3:** Particle size distribution curves for the grit arrestor samples collected with and without on-line injection of Lycal 93HS over the period of 12 hour tests. 178
- Figure 4-4:** Effect of Lycal 93HS on the softening characteristics of the lower furnace rear wall deposit sample from the first batch of deposits before on-line injection of Lycal. 231

- Figure 4-5:** Effect of 3 mass% Lycal 93HS addition on the softening characteristics of the F1 and F2 type rear wall deposit samples received from the (i) A-side (normal injection) and (ii) B-side (reduced injection) of boiler no.6. 233
- Figure 4-6:** Comparison of probe deposition rates before the bottom screen tubes with and without on-line injection of Lycal in boiler no.6. 239
- Figure 4-7:** Determination of HF-solubility rates for (a) [SiO₂], (b) [Fe₂O₃] and (c) [MgO] concentrations for the front wall deposit samples from boilers no.5 and no.6, without and with on-line injection of Lycal 93HS respectively. 240
- Figure 4-8:** Determination of HF-solubility rates for (a) [SiO₂], (b) [Fe₂O₃] and (c) [MgO] concentrations for the rear wall deposit samples from boilers no.5 and no.6, without and with on-line injection of Lycal 93HS respectively. 245
- Figure 4-9:** Determination of HF-solubility rates for (a) [SiO₂], (b) [Fe₂O₃] and (c) [MgO] concentrations for the side wall deposit samples from boilers no.5 and no.6, without and with on-line injection of Lycal 93HS respectively. 249
- Figure 4-10:** Determination of HF-solubility rates for (a) [SiO₂], (b) [Fe₂O₃] and (c) [MgO] concentrations for the bottom screen tubes deposit samples from boilers no.5 and no.6, without and with on-line injection of Lycal 93HS respectively. 252
- Figure 4-11:** Determination of HF-solubility rates for (a) [SiO₂], (b) [Fe₂O₃] and (c) [MgO] concentrations for economiser ash hopper medium size (-500µm +63µm) particulate samples from boiler no.5 without and with on-line injection of Lycal 93HS respectively. 258
- Figure 4-12:** Determination of HF-solubility rates for (a) [SiO₂], (b) [Fe₂O₃] and (c) [MgO] concentrations for grit arrestor medium size (-500µm +63µm) particulate samples from boiler no.5 without and with on-line injection of Lycal respectively. 261
- Figure 4-13:** Determination of HF-solubility rates for (a) [SiO₂], (b) [Fe₂O₃] and (c) [MgO] concentrations for grit arrestor fine size particulate samples (-45µm) from boiler no.5 without and with on-line injection of Lycal respectively. 264

Figure 4-14: Particle size analysis for Ayrshire coal.	274
Figure 4-15: Variation in moisture content with particle size for the Ayrshire coal sample.	277
Figure 4-16: Variation in ash content with particle size for the Ayrshire coal sample batch on air-dried basis.	279
Figure 4-17: Effect of Lycal 93HS on the softening characteristics of the "IDT" ranges for the two ash admixtures as specified in Table 4-48.	283
Figure 4-18: Quantitative distribution analysis of various separated coal ash components.	290
Figure 4-19: X-ray diffraction spectrum for the LTA sample of Ayrshire coal.	294
Figure 4-20: X-ray diffraction spectra for the "acidic" HTA components.	295
Figure 4-21: X-ray diffraction spectra for the "basic" HTA components.	299
Figure 4-22: X-ray diffraction spectra for the "ferriferous" HTA components.	301

Figure 5-1: Variation in the dispersion of various ash components illustrated through a rationalised ternary SiO_2 - Al_2O_3 - Fe_2O_3 phase diagram at 1000°C.	351
Figure 5-2: Distribution profile of ash components with similar mineralogies illustrated in terms of five main regions on a rationalised ternary SiO_2 - Al_2O_3 - Fe_2O_3 phase diagram at 1000°C.	352

Table 2-1: Characteristics of overfeed, underfeed and composite combustion.	5
Table 2-2: Melting point of complex sulphates formed within depositing ash particles on boiler tube surfaces.	11
Table 2-3: Minerals commonly associated with coals.	13
Table 2-4: Effect of temperature on ash mineralogy.	15
Table 2-5: Transformation of selected mineral groupings due to heating.	18
Table 2-6: Major and minor abundance impurity elements in coal.	25
Table 2-7: Calculated solubility limit of FeO in coal ash slags.	46
Table 2-8: Design parameters - coal and coal ash.	51
Table 2-9: Degree of sintering based on the ratio of neck bond radius to particle radius (x/r).	60
Table 2-10: Considerations in choosing various techniques for controlling slag and corrosion.	65
Table 2-11: Physical form of oil and coal additive chemicals.	66
Table 2-12: Additives for control of slagging and corrosion on dry-bottom boilers.	69
Table 2-13: Additives for controlling slag fluidity on wet-bottom P.F. boilers.	70
Table 2-14: Additives for controlling convective pass fouling and corrosion on coal fired boilers.	71
Table 2-15: Methods of feeding additives to P.F coal fired boilers.	77
Table 2-16: Characteristic comparison of various types of magnesium fuel additives.	78
Table 2-17: Summary of the generating capacity of West - Belfast power station along with other power stations operating within Northern Ireland Electricity (N.I.E) supplies.	83
Table 2-18: Recommended hopper design values for Lycal 93HS.	89

Table 3-1: Chemical and physical properties of Lycal 93HS additive used in the operation of boiler no.6.	93
Table 3-2: Analysis of Ayrshire coal characteristics as received at West-Belfast power station.	96
Table 3-3: Summary of deposits received / collected for examination with and without Lycal 93HS injection.	98
Table 3-4: Summary of boiler operating parameters monitored during the scheduled deposition probe tests with and without on-line injection of Lycal 93HS.	122
Table 3-5: Operating data collected from boiler no.6 during the scheduled deposition probe tests with and without on-line injection of Lycal 93HS.	123

Table 4-1: Bulk chemical analysis of the first batch of deposit samples received before the commencement of Lycal 93HS additive treatment on boiler no.6.	143
Table 4-2: Bulk chemical analysis of the second batch of deposit samples received during the course of Lycal 93HS additive treatment on boiler no.6.	143
Table 4-3: Bulk chemical analysis of the third batch of deposit samples received during the course of Lycal 93HS additive treatment on boiler no.6.	144
Table 4-4: Bulk chemical analysis of the fourth batch of deposit samples received during the course of Lycal 93HS additive treatment on boiler no.6.	145
Table 4-5: Bulk chemical analysis of the fourth batch of deposit samples with "layering" orientation received during the course of Lycal 93HS additive treatment on boiler no.6.	145
Table 4-6: Bulk chemical analysis of the fifth batch of deposit samples received from boiler no.5 without any Lycal 93HS additive treatment	146
Table 4-7: Bulk chemical analysis of sieve size fractioned ash particulate samples from boilers no.5 and no.6 without and with Lycal additive treatment respectively, representing the sixth batch of samples.	147

Table 4-8: Bulk analysis of variation in the unburned carbon content associated with particulate fly ash matter in boiler no.6 with and without on-line injection of Lycal 93HS.	148
Table 4-9: Results of size fraction analysis of economiser ash hopper samples collected during the 12-hour trials on boiler no.6 with and without on-line injection of Lycal 93HS.	176
Table 4-10: Results of size fraction analysis of grit arrestor samples collected during the 12-hour trials on boiler no.6 with and without on-line injection of Lycal 93HS.	177
Table 4-11: X-ray diffraction analysis of crystalline phases within deposits from batches no.2 and no.3, received from boiler no.6.	225
Table 4-12: Results of cone-fusion tests for "fashioned" cone pieces of deposits from second batch received during the course of Lycal 93HS additive treatment on boiler No.6.	226
Table 4-13: Results of cone-fusion tests for "reconstituted" cone pieces of deposits from second batch received during the course of Lycal 93HS additive treatment on boiler No.6.	226
Table 4-14: Results of cone-fusion tests for the "reconstituted" cones of the two "friable" samples namely F1 and F2 received in the third batch of deposits from boiler no.6.	228
Table 4-15: Results of cone-fusion tests for the "reconstituted" cones of deposit samples from the first sample batch received, investigating the effect of laboratory additions of Lycal 93HS on the softening from boiler no.6 prior to injection of Lycal 93HS.	230
Table 4-16: Results of cone-fusion tests for the "reconstituted" cone samples of F1 and F2 type of deposits for selected deposits from the third sample batch, investigating the effect of 3 mass% additional Lycal 93HS.	232
Table 4-17: Result of heat treatment of typical "friable" deposits, F1 and F2, found most dominantly within the third batch of samples received from boiler no.6.	235
Table 4-18: Chemical analysis of deposited fly ash layer collected from the surface of test probe after 12 hours of exposure with and without injection of Lycal 93HS on boiler no.6.	236

Table 4-19: Result of deposition probe trials near the bottom screen tubes in boiler no.6 with and without on-line injection of Lycal 93HS.	238
Table 4-20: Results of surface leaching analysis of a front wall deposit sample received in the second batch of samples from boiler no.6 with on-line injection of Lycal 93HS.	241
Table 4-21: Results of surface leaching analysis of a bottom screen tube deposit sample received in the second batch of samples from boiler no.6 with on-line injection of Lycal 93HS.	242
Table 4-22: Results of surface leaching analysis of a passage between screen tubes and superheaters deposit sample received in the second batch of samples from boiler no.6 with on-line injection of Lycal 93HS.	243
Table 4-23: Results of surface leaching analysis of a F2 type of a deposit sample received in the third batch of samples from boiler no.6 with on-line injection of Lycal 93HS.	244
Table 4-24: Results of surface leaching analysis of a F2 type of a deposit sample received in the third batch of samples from boiler no.6 with on-line injection of Lycal 93HS.	246
Table 4-25: Results of surface leaching analysis of a F1 type of a deposit sample received in the third batch of samples from boiler no.6 with on-line injection of Lycal 93HS.	247
Table 4-26: Results of surface leaching analysis of a F1 type of a deposit sample received in the third batch of samples from boiler no.6 with on-line injection of Lycal 93HS.	250
Table 4-27: Results of surface leaching analysis of a front wall deposit sample received in the fourth batch of samples from boiler no.6 with on-line injection of Lycal 93HS.	251
Table 4-28: Results of surface leaching analysis of a rear wall deposit sample received in the fourth batch of samples from boiler no.6 with on-line injection Lycal 93HS.	253

Table 4-29: Results of surface leaching analysis of a bottom screen tubes deposit sample received in the fourth batch of samples from boiler no.6 with on-line injection of Lycal 93HS.	254
Table 4-30: Results of surface leaching analysis of "medium" sized particulate economiser ash hopper sample collected in the fifth batch of samples from boiler no.6 with on-line injection of Lycal 93HS.	255
Table 4-31: Results of surface leaching analysis of "medium" sized particulate economiser ash hopper sample collected in the fifth batch of samples from boiler no.6 without injection of Lycal 93HS.	256
Table 4-32: Results of surface leaching analysis of "medium" sized particulate grit arrestor sample collected in the fifth batch of samples from boiler no.6 with on-line injection of Lycal 93HS.	257
Table 4-33: Results of surface leaching analysis of "medium" sized particulate grit arrestor sample collected in the fifth batch of samples from boiler no.6 without injection of Lycal 93HS.	259
Table 4-34: Results of surface leaching analysis of "fine" sized particulate grit arrestor sample collected in the fifth batch of samples from boiler no.6 with on-line injection of Lycal 93HS.	260
Table 4-35: Results of surface leaching analysis of "fine" sized particulate grit arrestor sample collected in the fifth batch of samples from boiler no.6 without injection of Lycal 93HS.	262
Table 4-36: Results of surface leaching of a front arch deposit sample collected in the fifth batch of samples from boiler no.5 without any injection of Lycal 93HS.	263
Table 4-37: Results of surface leaching of a rear arch deposit sample collected in the fifth batch of samples from boiler no.5 without any injection of Lycal 93HS.	265
Table 4-38: Results of surface leaching of a front wall deposit sample collected in the fifth batch of samples from boiler no.5 without any injection of Lycal 93HS.	266

Table 4-39: Results of surface leaching of a rear wall deposit sample collected in the fifth batch of samples from boiler no.5 without any injection of Lycal 93HS.	267
Table 4-40: Results of surface leaching of a side wall deposit sample collected in the fifth batch of samples from boiler no.5 without any injection of Lycal 93HS.	268
Table 4-41: Results of surface leaching of a steam generating tubes deposit sample collected in the fifth batch of samples from boiler no.5 without any injection of Lycal 93HS.	269
Table 4-42: Results of surface leaching of a bottom screen tubes deposit sample collected in the fifth batch of samples from boiler no.5 without any injection of Lycal 93HS.	270
Table 4-43: Results of sieve analysis of the sample batch of coal collected from the chain-grate before it's introduction to boiler no.6.	273
Table 4-44: Results of inherent moisture determination for sieve size particle fractions of Ayrshire coal collected from the chain-grate before it's introduction to boiler no.6.	276
Table 4-45: Results of ash content determination (a.d.b) for sieve size particle fractions of Ayrshire coal collected from the chain-grate before it's introduction to boiler no.6.	278
Table 4-46: Description of various ash admixture groups derived from the Ayrshire coal size ranges present in the sample batch.	280
Table 4-47: Chemical analysis of ash admixture groups made from various coal size fractions.	280
Table 4-48: Results of cone-fusion tests for the ash admixture cone samples of the upper and lower size fractions (AM1 & AM4) with the effect of additions of Lycal 93HS on their softening behaviour.	282
Table 4-49: The characteristics of the coal ash components on the basis of texture and colour.	287
Table 4-50: Quantitative analysis of the separated ash composition from high temperature ashing of the coal particle size (+6350 μ m, -6350 +4760 μ m), stating the amount and frequency of occurrence of the ash components after a total of 100 ashing sessions.	289

Table 4-51: The chemical analysis of the major separated ash components.	291
Table 4-52: Minerals identified in the respective LTA, HTA components and deposit samples from batches no.2 and no.3 received from boiler no.6.	303
Table 4-53: Results of the cone-fusion tests for the selected ash components cone samples with and without Lycal addition.	305
Table 4-54: Hot - stage microscopic observation of softening and crystallisation behaviour of ash component No.(1) without and with additions of Lycal 93HS.	309
Table 4-55: Hot - stage microscopic observation of softening and crystallisation behaviour of ash component No.(2) without and with additions of Lycal 93HS.	310
Table 4-56: Hot - stage microscopic observation of softening and crystallisation behaviour of ash component No.(3) without and with additions of Lycal 93HS.	311
Table 4-57: Hot - stage microscopic observation of softening and crystallisation behaviour of ash component No.(4) without and with additions of Lycal 93HS.	312
Table 4-58: Hot - stage microscopic observation of softening and crystallisation behaviour of ash component No.(5) without and with additions of Lycal 93HS.	313
Table 4-59: Hot - stage microscopic observation of softening and crystallisation behaviour of ash component No.(6) without and with additions of Lycal 93HS.	314
Table 4-60: Hot - stage microscopic observation of softening and crystallisation behaviour of ash component No.(7) without and with additions of Lycal 93HS.	315
Table 4-61: Hot - stage microscopic observation of softening and crystallisation behaviour of ash component No.(11) without and with additions of Lycal 93HS.	316
Table 4-62: Hot - stage microscopic observation of softening and crystallisation behaviour of ash component No.(13) without and with additions of Lycal 93HS.	317

Table 4-63: Hot - stage microscopic observation of softening and crystallisation behaviour of ash component No.(14) without and with additions of Lycal 93HS.	318
Table 4-64: Hot - stage microscopic observation of softening and crystallisation behaviour of ash component No.(21) without and with additions of Lycal 93HS.	319
Table 4-65: Hot - stage microscopic observation of softening and crystallisation behaviour of ash component No.(27) without and with additions of Lycal 93HS.	320
Table 4-66: Hot - stage microscopic observation of softening and crystallisation behaviour of ash component No.(28) without and with additions of Lycal 93HS.	321
Table 4-67: Hot - stage microscopic observation of softening and crystallisation behaviour of ash component No.(29) without and with additions of Lycal 93HS.	322
Table 4-68: Hot - stage microscopic observation of softening and crystallisation behaviour of ash component No.(30) without and with additions of Lycal 93HS.	323
Table 4-69: Hot - stage microscopic observation of softening and crystallisation behaviour of ash component No.(32) without and with additions of Lycal 93HS.	324
Table 4-70: Hot - stage microscopic observation of softening and crystallisation behaviour of ash component No.(33) without and with additions of Lycal 93HS.	325
Table 4-71: Hot - stage microscopic observation of softening and crystallisation behaviour of ash component No.(46) without and with additions of Lycal 93HS.	326
Table 4-72: Hot - stage microscopic observation of softening and crystallisation behaviour of ash component No.(48) without and with additions of Lycal 93HS.	327
Table 4-73: Hot - stage microscopic observation of softening and crystallisation behaviour of a high temperature ash (HTA) sample without and with additions of Lycal 93HS.	328
Table 4-74: Hot - stage microscopic observation of softening and crystallisation behaviour of a low temperature ash (LTA) sample without and with additions of Lycal 93HS.	329

Table 5-1: Results of cone fusion tests for the selected range of acidic ash components showing the softening temperatures as determined in this study, compared to those evaluated in the literature for a range of high temperature ashes with identical basic oxide contents.	360
Table 5-2: Results of cone fusion tests for the selected range of basic ash components showing the softening temperatures as determined in this study, compared to those evaluated in the literature for a range of high temperature ashes with identical basic oxide contents.	361
Table 5-3: Results of cone fusion tests for the selected range of ferriferous ash components showing the softening temperatures as determined in this study, compared to those evaluated in the literature for a range of high temperature ashes with identical basic oxide contents.	362
Table 5-4: Percentage of elements leached from a typical coal fly ash.	396

Plate 2-1: Pictorial cross-section view of the travelling chain-grate boiler No.6, monitored for the deposition and additive injection studies. 86

Plate 3-1: The brass mould used to produce test cones. 110

Plate 3-2: The assembled form of the brass mould. 110

Plate 3-3: Illustration of ash fouling probe assembly in operation through a viewing port. 120

Plate 4-1: A view of the A-side of boiler No.6 after 3 months of Lycal 93HS injection, showing reasonably clean surfaces of front (LHS), rear (RHS) and side walls. 136

Plate 4-2: A view of the front wall tubes (LHS), from the A-side of boiler No.6 after 3 months of Lycal 93HS injection, showing a restricted area of deposit formation. 138

Plate 4-3: A view of the rear wall tubes from the A-side of boiler No.6 after 3 months of Lycal 93HS injection, showing a restricted region of deposit formation on the surface of the upper section tubes leading to the bottom screen tubes. 139

Plate 4-4: A view of the rear wall tubes from the B-side of boiler No.6, where due to the blockage of Lycal 93HS injection ports, an extended region of relatively thick deposits are formed on the surface of the upper section tubes leading to the bottom screen tubes. 140

Plate 4-5: A view of the bottom screen tubes from the B-side of boiler No.6, with partial blockage of Lycal 93HS injection ports, showing deposit formation between the tube surface at the top of the photograph. 141

Plate 4-6: Comparative illustration of a range of deposit samples from boilers No.5 and No.6. 150

Plate 4-7: A partially fused, particulate F1 type deposit sample with a "glazed" surface from lower furnace region of boiler No.6, with on-line injection of Lycal 93HS. 153

- Plate 4-8:** A particulate and friable F1 type deposit sample from the lower furnace region within boiler No.6, with on-line injection of Lycal 93HS. 153
- Plate 4-9:** A particulate and friable F2 type deposit sample from the lower furnace region within boiler No.6, with on-line injection of Lycal 93HS. 154
- Plate 4-10:** A protruded region within a largely F1 type deposit sample from the lower furnace region within boiler No.6, with on-line injection of Lycal 93HS, illustrating further the outer orange-brown colour layer covering the surface of the sample. 154
- Plate 4-11:** A piece of bottom grate clinker illustrating a porous, fused slag-like texture. 156
- Plate 4-12:** A piece of bottom grate clinker illustrating a stratified carbonaceous texture. 156
- Plate 4-13:** Cross-sectional view of a very hard lower furnace layered deposit from boiler No.5, without on-line Lycal 93HS injection, showing a black, vesicular, glassy outer layer, a grey middle layer and a brown lustered, smooth outer layer. 159
- Plate 4-14:** SEM-micrograph of an as received, unpolished deposit sample from the lower furnace region of boiler No.6 with on-line Lycal 93HS injection, showing limited degree of bonding and sintering between spherical ash particles of various sizes. 161
- Plate 4-15:** SEM-micrograph of bridged iron oxide particles over the surface of the bonded ash spheres in Plate 4-14. finer cenosphical ash beads are supported on the surface of the much larger ash particles. 162
- Plate 4-16:** SEM-micrograph of an as received, unpolished deposit sample from the lower furnace region in boiler No.6, with on-line Lycal 93HS injection. 164
- Plate 4-17:** SEM-micrograph of an as received, unpolished deposit sample from the bottom screen tubes in boiler No.6, with on-line Lycal 93HS injection, roughly surfaced aluminosilicate matrix exhibits the dispersion of iron oxide particles (area "A"). Further deposition of small solid ash spheres and cenospheres on the matrix are shown. 165

- Plate 4-18:** SEM-micrograph of an as received, unpolished deposit sample from the bottom screen tubes in boiler No.6, with on-line Lycal 93HS injection. Partial fusion of some of ash spheres and cenospheres depositing onto the roughly surfaced matrix are shown. 166
- Plate 4-19:** SEM-micrograph of an as received, unpolished deposit sample from the bottom screen tubes in boiler No.6, with on-line Lycal 93HS injection. It shows the textural and size difference between a number of very fine transparent ash cenospheres agglomerated at the base of a much larger solid ash sphere imbedded on the rough matrix. 168
- Plate 4-20:** SEM-micrograph of an as received, unpolished deposit sample from the bottom screen tubes in boiler No.6, with on-line Lycal 93HS injection. It shows the texture of some of the very fine ash cenospheres and the irregularly shaped particulate matter on the surface of the dark matrix. 168
- Plate 4-21:** SEM-micrograph of an as received deposit sample from the bottom screen tubes in boiler No.6, with on-line Lycal injection. It shows a string formation of softened ash spheres and ash matter bonded together with various degree of neck growth between the particles. Finer ash cenospheres with a transparent texture can further be seen adhering to the softened ash matter. 169
- Plate 4-22:** SEM-micrograph of an as received, unpolished deposit sample from the passage between screen tubes & steam generating tubes in boiler No.6, with on-line Lycal 93HS injection. It shows the various stages in the neck growth between solid ash spheres, forming a highly coalesced bulk of ash particulates. 169
- Plate 4-23:** SEM-micrograph of an as received, unpolished deposit sample from the front wall in boiler No.5, without Lycal injection. Extensive bonding and fusion between the spherical ash particles has formed a uniformly textured, continuous alumino-silicate matrix. The smaller smooth ash cenospheres absorbed onto the surface are further fused into the matrix. 170
- Plate 4-24:** SEM-micrograph of an as received, unpolished deposit sample from the rear arch in boiler No.5, without Lycal injection. Extended bonding and fusion between solid ash spheres of various sizes are shown to form a fairly continuous matrix. 171

- Plate 4-25:** SEM-micrograph of an as received, unpolished deposit sample from the rear wall in boiler No.5, without Lyclal injection. Extensive fusion of spherical ash particles has formed a coagulated, continuous and uniform matrix. Some transverse sections show the highly porous, vesicular character of this deposit. 173
- Plate 4-26:** SEM-micrograph of an as received, unpolished deposit sample from the bottom screen tubes in boiler No.5, without Lyclal 93HS. High degree of bonding and fusion is evident between spherical ash particles. Like the samples from the same location from boiler No.6, an extensive dispersion of iron oxide particles can be seen on the rough surface of the matrix. 174
- Plate 4-27:** SEM-micrograph of as received, unpolished deposit sample from the steam generating tubes in boiler No.5, without Lyclal 93HS injection. A continuous matrix contains a number of ash spheres with smaller, transparent, rounded and hexagonal siliceous matter imbedded on the surface. 175
- Plate 4-28:** High magnification of SEM-micrograph in Plate 4-27 showing the angular and rounded shape of the fine transparent siliceous particles, demonstrating their incomplete melting. 175
- Plate 4-29:** SEM-micrograph of economiser ash hopper particulate samples from boiler No.6, showing the spherical and non-spherical form of the particles with smooth and rough outer surfaces. the particle size range varies between -45 +700 μm . 180
- Plate 4-30:** High magnification of SEM-micrograph in Plate 4-29, showing the relatively smooth ash spheres as well as the roughly surfaced ash cenosphere and non-spherical particles. 181
- Plate 4-31:** SEM-micrograph of economiser ash hopper particulate samples from boiler No.6, showing the highly porous spheroids with surface crystallisation, and larger agglomeration of ash matter forming non-spherical and spherical particulates. 182
- Plate 4-32:** SEM-micrograph of a bottom grate clinker sample from boiler No.6, showing a fully fused, stratified morphology. 183
- Plate 4-33:** SEM-micrograph of a bottom grate clinker sample from boiler No.6, showing the lacey skeleton of a coke residue. 184

- Plate 4-34:** SEM-micrograph of a bottom grate clinker sample from boiler No.6, showing fine, smoothly surfaced ash cenospheres on a partially fluid and viscous matrix. 185
- Plate 4-35:** SEM-micrograph of a bottom grate clinker sample from boiler No.6, representing a carbonaceous ash matter with angular plates of iron oxide particles forming a crusty matrix. 186
- Plate 4-36:** Photo-micrograph of a polished lower furnace deposit sample from boiler No.6, with on-line Lycal injection. It shows the limited degree of bonding within the matrix of spherical and non-spherical porous ash matter, under oblique illumination. The iron oxide skeleton sphere (white) is in contrast to the other spherical (solid sphere with white rim) and non-spherical ash matter. 188
- Plate 4-37:** Photo-micrograph of the feature in Plate 4-36, under polarised, fully crossed illumination. The black and grey angular form of the iron oxide sphere is seemingly similar to the rim around the lower solid sphere, but different to the large, porous, ash skeleton (red) adjacent to the iron oxide sphere which had also shown large traces of the white matter. 189
- Plate 4-38:** Photo-micrograph of a upper furnace deposit sample from boiler No.6, with on-line Lycal 93HS injection. It shows two separate regions of discontinuous matrix under oblique incident illumination. The two regions appear to be identical in colour and texture. 191
- Plate 4-39:** Photo-micrograph of the feature in Plate 4-38, under polarised, fully crossed illumination. The black iron oxide region appears now to be distinctly different to the red and orange crystalline region, with a black outer edge similar to the RHS. A ferrosphere of iron oxide crystallisation appearing as a red sphere is also present. 192
- Plate 4-40:** Photo-micrograph of a deposit sample from bottom screen tubes in boiler No.6, with on-line Lycal 93HS injection. It shows a fused siliceous matrix with a scatter of angular cuboidal and euhedral iron-spinel crystals, and the very fine array of dendritic region at the centre or as a cluster at the top LHS of the photograph. 193

- Plate 4-41:** Photo - micrograph of the feature in Plate 4-40, under polarised, fully crossed illumination. The angular and euhedral iron-spinel phase, dendritic crystalline region at the centre and the very fine dendritic cluster at the top can be more clearly distinguished. 194
- Plate 4-42:** SEM-micrograph of a polished lower furnace deposit from boiler No.6, with on-line Lycal 93HS injection. The open skeletal structure is typical of post Lycal injected deposit samples. 196
- Plate 4-43:** Higher magnification SEM - micrograph of the deposit specimen in Plate 4-42, showing the extent of crystalline heterogeneity present within the sample. 197
- Plate 4-44:** SEM-micrograph of a lower furnace F2 type deposit sample from boiler No.6, with on-line Lycal 93HS injection. It shows the sintering as a range of spherical ash particles various sizes and textures. 198
- Plate 4-45:** SEM-micrograph of a deposit sample from the rear wall in boiler No.6, with on-line Lycal 93HS injection. An area of continuous matrix, "A-B-C" is connected to a highly porous, honeycomb textured area, "D". 199
- Plate 4-46:** SEM-micrograph of a F1 type deposit sample from the rear wall in boiler No.6, with on-line Lycal 93HS injection. It shows the neck growth between a large sphere and a smaller white sphere. 201
- Plate 4-47:** SEM-micrograph of a deposit sample from the rear wall in boiler No.6, with on-line Lycal 93HS injection. It shows the solidification of fine and large dendrites in a siliceous matrix with a white layer outlining the periphery of the ash sphere. 202
- Plate 4-48:** SEM-micrograph of a deposit sample from the front wall in boiler No.6, with on-line Lycal 93HS injection. It shows a broken spherical cluster of white crystals at the surface of a large pore. 203
- Plate 4-49:** SEM-micrograph of a deposit sample from the front wall in boiler No.6, with on-line Lycal 93HS injection. It shows cuboidal and euhedral crystals and large, long needles in a siliceous matrix. 204

- Plate 4-50:** SEM-micrograph of a deposit sample from the rear wall in boiler No.6, with on-line Lycal93HS injection. It shows an array of fine ($<5 \mu\text{m}$) crystalline needles. 205
- Plate 4-51:** SEM-micrograph of a deposit sample from the front wall in boiler No.6, with on-line Lycal 93HS injection. It shows a fibrous agglomeration of long laths inside a large pore within a siliceous matrix. 207
- Plate 4-52:** SEM-micrograph of a deposit sample from the front arch in boiler No.6, with on-line Lycal 93HS injection. It shows the bonding and neck growth between two ash spheres and the crystalline precipitates of fine and coarse needles in the lower sphere. 208
- Plate 4-53:** SEM-micrograph of a deposit sample from the bottom screen tubes in boiler No.6, with on-line Lycal 93HS injection. The iron rich phase acts as the binder in an open-skeletal matrix of large (100 - 400 μm) spherical ash particles. 209
- Plate 4-54:** SEM-micrograph of a deposit sample from the bottom screen tubes in boiler No.6, with on-line Lycal 93HS injection. A highly porous skeleton of sintered and fused, siliceous ash spheres and spheroids are connected together via a network of ferrous phase round the edge of the particles. 210
- Plate 4-55:** Optical photo-micrograph of a deposit sample from bottom screen tubes in No.6, with on-line Lycal 93HS injection. A number of large ash spheres and spheroids (200-700 μm) containing fine dendritic crystals of iron oxide are bonded together via a continuous network of a white phase around the ash particles. 210
- Plate 4-56:** Optical photo-micrograph of a deposit sample from the passage between screen tubes and steam generating tubes deposit sample from boiler No.6, with on-line Lycal 93HS injection. A number of ash spheres and spheroids are loosely sintered together through stretches of ferro-spheres and the other iron oxide rich phase, forming a porous skeletal matrix. 212
- Plate 4-57:** Optical photo-micrograph of a deposit sample from the passage between bottom screen tubes and steam generating tubes in boiler No.6, with on-line Lycal 93HS injection. A porous area of matrix is shown to contain a range of angular iron oxide, iron spinel type crystals within the matrix and around the porosity holes, with much finer dendritic hematite crystals scattered in the matrix. 212

- Plate 4-58:** SEM-micrograph representing the outer and middle layers of a deposit sample from the front wall in boiler No.5, without on-line Lycal 93HS injection. A highly porous, fully fused continuous matrix is shown. 213
- Plate 4-59:** SEM-micrograph representing the inner layer of the front wall deposit sample in Plate 4-58. It shows a continuous siliceous matrix with some fracture lines and very limited crystallinity in the centre of the plate. 214
- Plate 4-60:** SEM-micrograph of a deposit sample from the rear wall in boiler No.5, without on-line Lycal 93HS injection. It shows a fully fused, highly siliceous, porous matrix. 216
- Plate 4-61:** Optical photo-micrograph of the inner layer of a deposit sample from the rear wall in boiler No.5, without on-line Lycal 93HS injection. The discontinuous inner layer is in contrast to the continuous, porous outer layer. 216
- Plate 4-62:** Optical photo-micrograph of the outer layer of a deposit sample from the rear arch in boiler No.5, without on-line Lycal 93HS injection. It shows a porous, continuous matrix containing two precipitated crystalline phases. 217
- Plate 4-63:** Higher magnification optical photo-micrograph of Plate 4-62, showing the iron oxide dendritic precipitates, and long and large mullite-like needles. 217
- Plate 4-64:** SEM-micrograph of a deposit sample from steam generating tubes in boiler No.5, without on-line Lycal 93HS injection. It shows a highly porous, fully fused, continuous matrix. 218
- Plate 4-65:** Optical photo-micrograph of a deposit sample from steam generating tubes in boiler No.5, without on-line Lycal 93HS injection. It shows a porous, fused matrix with some residual spherical ash particles lodged at the outer boundaries of the matrix. Fine precipitates of iron oxide crystals are dispersed through the matrix. 220
- Plate 4-66:** SEM-micrograph of a deposit sample from bottom screen tubes in boiler No.5, without on-line Lycal 93HS injection. It shows a spherical ash particle, outlined by a fine dispersion of euhedral and angular iron oxide or iron spinel crystals, fused into the rest of the matrix. 220

- Plate 4-67:** High magnification SEM - micrograph of Plate 4-66, showing the euhedral and angular iron oxide or iron-spinel type crystals. 221
- Plate 4-68:** Optical photo-micrograph of a deposit sample from bottom screen tubes in boiler No.5, without on-line Lycal 93HS injection. It shows a porous, fully fused, continuous matrix with an extensive dispersion of particles within the matrix. 222
- Plate 4-69:** High magnification optical photo-micrograph of Plate 4-68, showing the euhedral and angular crystalline iron oxide or iron spinel and the pure iron oxide phase as well as fine ferriferous dendrites. 222
- Plate 4-70:** The separated high temperature coal ash components. 285
- Plate 4-71:** Illustration of the soft, powdery ash components of the high temperature coal ash. 285
- Plate 4-72:** Illustration of semi-hard, layered, ash components of the high temperature coal ash. 286
- Plate 4-73:** Illustration of hard, densely compacted or layered ash components of the high temperature coal ash. 286
- Plate 4-74:** Illustration of different stages of deformation for the separated ash components heated between thermocouple wires of the hot-stage microscope: (a) softening, (b) melting, (c) fluid. 330
- Plate 4-75:** Transformation of a drop of fluid ash component No.(1) with the addition of 10 mass% of Lycal 93HS, at 1400°C: (a) fluid (b) crystallisation of fluid melt after 10 minutes, (c) crystallisation of fluid melt after 15 minutes. 331
- Plate 4-76:** Formation and growth of fine needles from the surface of viscous fluid melt of ash component No.(3) with the addition of 1 mass% Lycal 93HS, after 20 minutes at 1350°C. 332
- Plate 4-77:** Transformation of fluid ash component No.(5) with the addition of 10 mass% Lycal 93HS at 1400°C: (a) formation of fine conically shaped stacks of crystalline needles after 30 seconds, (b) growth of the crystalline needles after 45 seconds, (c) growth of the crystalline needles after 1 minute, (d) fluid melt after 1 minute and 30 seconds. 334

- Plate 4-78:** SEM-micrograph of the fluid ash component No.(5) with the addition of 10 mass% Lycal 93HS, showing crystalline lozenges with well defined boundaries. 335
- Plate 4-79:** Transformation of fluid ash component No.(6) with the addition of 5 mass% Lycal 93HS, at 1350°C: (a) fluid pool, (b) formation of crystals from the meniscus and the tip regions, (c) growth of crystals into the centre of the pool, (d) further growth of crystals, (e) conversion of the pool into crystalline phase, (f) complete crystallisation of the fluid pool. 337
- Plate 4-80:** Formation of a precipitating phase within the fluid ash component No.(7) with the addition of 1 mass% Lycal, after 10 minutes held at 1300°C. 338
- Plate 4-81:** Formation of needles and arrow-head crystals from the surface and within the viscous fluid melt of ash component No.(7) with the addition of 5 Mass% Lycal 93HS, after up to 30 minutes held at 1100°C. 339
- Plate 4-82:** Formation and growth of fine needles from the surface of the viscous fluid melt of ash component No.(7) with the addition of 10 mass% Lycal 93HS, held at 1100°C: (a) initial formation of fine needles after 10 minutes. (b) growth of needles after 30 minutes, (c) further growth of needles after 45 minutes, (d) bending and bifurcation of further grown needles. 340
- Plate 4-83:** SEM-micrograph of the fully grown needles from the surface of fluid melt of ash component No.(7) with the addition of 10 mass% Lycal 93HS, quenched to room temperature: (a) matrix and the substrate to the fully grown laths from the surface, (b) high magnification of the fully grown laths with bifurcating ends. 342
- Plate 4-84:** Formation and growth of fine needles from the surface of the viscous fluid melt of ash component No.(13) with the addition of 1 mass% Lycal 93HS, after 1 hour at 1500°C. 343
- Plate 4-85:** Formation and growth of a single needle from the fluid meniscus of ash component No.(21), without and with addition of 3 mass% Lycal 93HS, at 1300°C: (a) after 10 minutes, (b) after 30 minutes, (c) after 45 minutes. 344

- Plate 4-86:** Formation and growth of fine needles from the surface of viscous fluid melt of ash component No.(21), with the addition of 10 mass% Lycal 93HS at 1300°C: (a) after 30 minutes, (b) after 1 hour. 345
- Plate 4-87:** Formation and growth of fine needles from the surface of viscous fluid melt of ash component No.(27), with the addition of 1 mass% Lycal 93HS, after 20 minutes at 1100°C. 346

1. INTRODUCTION

Coal is an extremely complex heterogeneous material. However, to simplify its constitution, it can be considered as a rock, comprised of different kinds of organic and inorganic matter. When coal is heated it ignites and undergoes loss of volatiles and pyrolysis. The organic matter is thus released and converted into volatile species, and the inorganic matter is released as ash.

In the environment of an industrial boiler where large quantities of coal are burned, the ash generated undergoes various reactions resulting in the production of some low melting point compounds. These compounds cause the ash to adhere to the boiler tube surfaces and promote further deposition of higher melting point alumino-silicate compounds. If these deposits are allowed to accumulate, heat transfer and consequently the efficiency of the boiler is effected. One method used to alleviate this problem, in addition to the conventional on-line cleaning techniques such as sootblowing, is chemical treatment in the form of additives to the coal.

Although the role of additives in alleviating deposition problems in oil-fired boilers through increasing the sintering temperature of deposits is well established, with coal firing however, where the ash burden is roughly 100 times that of fuel oil, the effectiveness of the regular use of modest and large amounts of additives is generally found to be dependent on the type of the boiler as well as the mode of operation.

The additive employed in this study is a magnesium based additive produced by Steetley Quarry Products Ltd under the name of Lycal 93HS. Lycal 93HS is a high quality grade of magnesium hydroxide precipitated from sea water and comes in the form of a finely divided, fully hydrated powder.

The opportunity to test Lycal 93HS on an industrial scale arose as a result of approaches made by Steetley to the West-Belfast power station in Northern Ireland. The power station employs thirteen boilers with a travelling grate combustion system to produce steam for generating electricity. The coal is fed into each boiler from a hopper on two chain grates and is spontaneously ignited due to the temperature inside the boiler. The Lycal 93HS additive was injected into the boiler through a series of secondary air ports along the length of the front and rear arches situated just above the grates, and was thus available for contact with the ash burden in the flue gases.

As a result of the apparent improvements observed during an initial three months "Lycal 93HS injection" trial, long term commitments extending over two years were undertaken by the power station operators. During this period deposit samples from various locations within the boiler were collected for examination at regular intervals. Furthermore, on-site probe sampling of deposits with and without Lycal injection over relatively short periods of time were carried out for comparative purposes. Samples of the coal as fed into the boiler were occasionally collected for size and ash analysis.

There is considerable conflict both with respect to the limited theoretical and practical methodologies explaining the controlling factors and steps in deposit formation mechanisms and effective role of any additive in alleviating this problem. The work presented here involved a series of both industrial and laboratory based investigations in order to elucidate a mechanism for the formation of fly ash deposits in West Belfast power station and the effect on these of the Lycal 93HS addition. Such understanding contributing to the possible use of the additive in other combustion systems.

2.1 THE BURNING OF COAL FOR POWER GENERATION

2.1.1 Introduction

All ranks of coal are capable of being combusted on an industrial scale to generate heat for conversion into electricity. Some ranks of coal are however more suited to combustion by certain techniques than others.¹ The three most important means for the large scale combustion of coal are:¹

- (1) Stoker firing
- (2) Cyclone furnace firing
- (3) Pulverised coal firing

The work reported in this thesis has been concerned entirely with a stoker fired system and therefore only this will be considered further in the next part of the literature review.

2.1.2 Mechanical Stoker Firing Systems

Mechanical stokers were developed early in the history of steam boilers as an improvement over hand firing. Today, despite the more dominant pulverized fuel firing systems, many small and medium size boilers employ mechanical stokers. Several types of stokers are available, but all are designed to feed coal onto a grate within a furnace and to remove the ash residue.

Mechanical stokers can be classified into three distinct groups according to the mode of introducing coal onto the grate for combustion:^{2,3}

- (1) Overfeed stokers: The main types are; chain and travelling grate, spreader, vibrating grate and coking stokers.
- (2) Underfeed stokers: The main types are; single and multiple retort stokers.
- (3) Composite stokers: This type of stoker is not commonly used and the best known of this type is the reciprocating stoker.

The principle of combustion for these three categories of stokers are schematically shown in Figure 2-1. The relative characteristics of the three modes of combustion are summarised in Table 2-1.²

The overfeed stokers are the most commonly used type still employed in industry and since the combustion system employed in the West Belfast power station was of the travelling grate type, this will now be considered further.

Figure 2-2⁴ shows a cross sectional view of a typical travelling grate stoker. The coal is fed by gravity from a hopper located at the front of the stoker onto a grate moving from the front to the rear of the furnace. The depth of fuel on the grate is regulated by a hand adjusted gate. Air enters the furnace from underneath through the openings in the grate, thereby promoting combustion of the coal.

Secondary air enters the furnace through ports situated at or above the front and rear arches in order to create turbulence for better mixing of the flue gases as well as controlling the position and length of the combustion flame.

The front arch promotes ignition by reflecting radiant heat onto the fuel bed. It also serves to break up and mix the combustion air with streams of volatile rich gases that might otherwise go through the unit unburned. The rear arch helps to further burn off the last remains of carbon before discharge of the ash clinker, by radiating heat from its surface onto the grate.

2.1.3 The Combustion of Coal on a Grate

Figure 2-3 illustrates the various combustion zones that exist as coal is continuously burned on a grate.^{5,6} As the bed is ignited from the top, the combustion front moves downward against an upward flow of primary air. The inherent moisture (H_2O) and volatile matter (CO, H_2, N_2 and hydrocarbons) are distilled

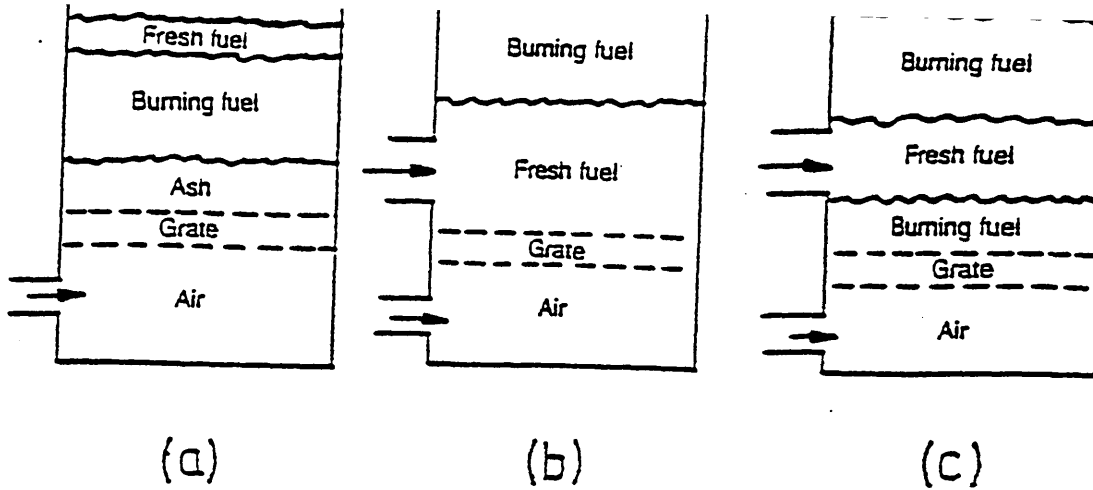


Figure 2-1: The principle of operation for: (a) Overfeed, (b) Underfeed and (c) Composite modes of combustion.²

Table 2-1: Characteristics of overfeed, underfeed and composite combustion.²

Mode of combustion	Advantage	Disadvantage
Overfeed	Rapid ignition, high response rate.	Smoke at low burning rates; not suitable for small coal. Can be sensitive to caking properties of coal.
Underfeed	Relatively smoke free, can burn strongly caking and small coals provided that these are properly conditioned with moisture and delivered uniformly over the grate.	Relatively slow ignition rate; can be difficult with coals with less than 20% volatile content.
Composite	Relatively smoke free, can burn small coal with up to 35% through 3 mm mesh.	Sensitive to caking properties of the coal.

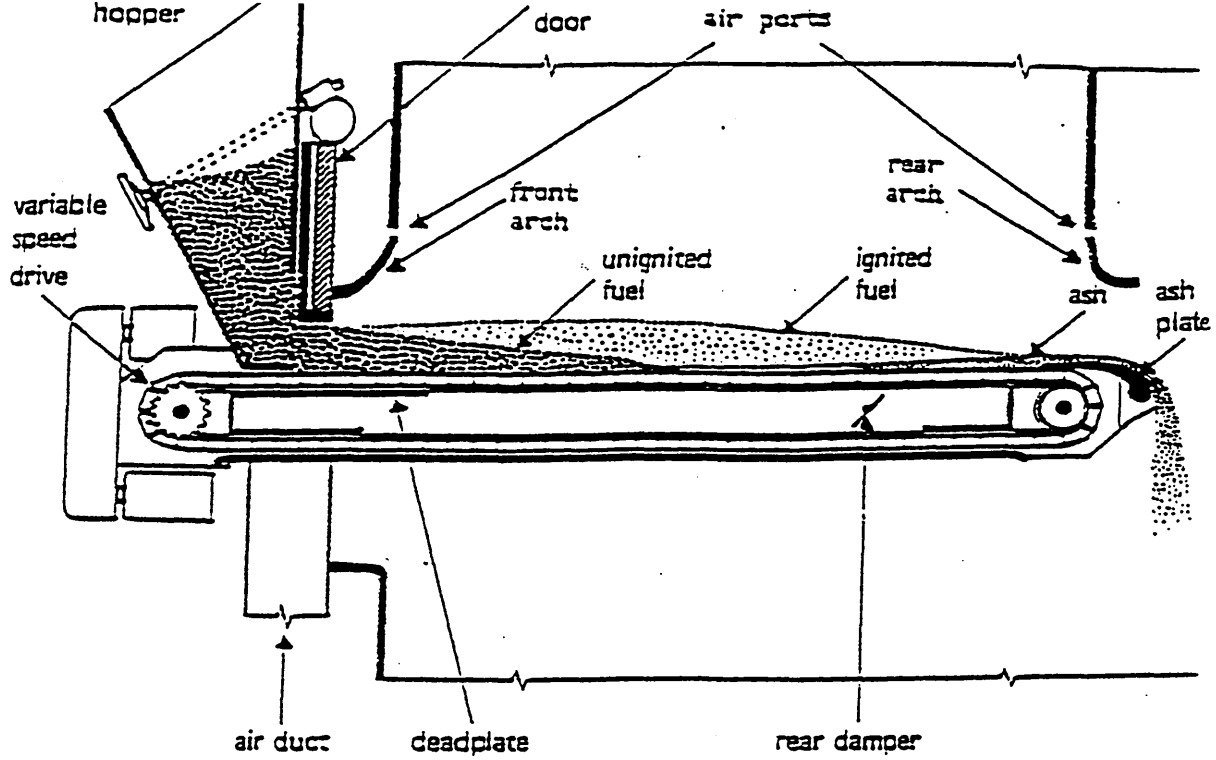


Figure 2-2: Section view of travelling grate stoker showing the form of the fuel bed.⁴

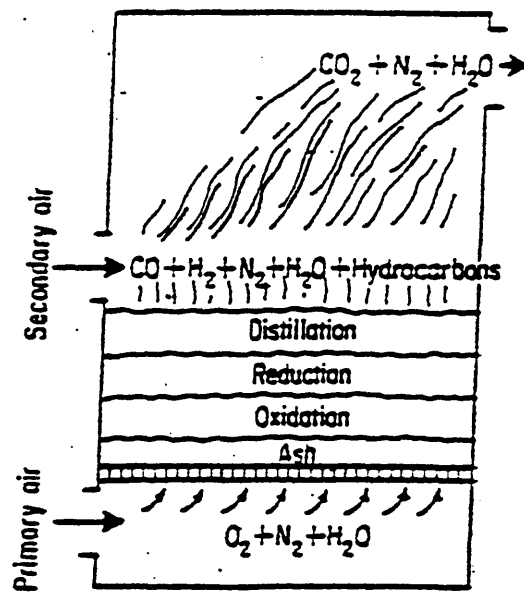


Figure 2-3: Fuel-bed zones of a stoker fired boiler broken up into oxidation, reduction distillation and volatile gas burning.^{5,6}

off in the "distillation" stage. The residual coke thus formed further promotes heat transfer down through the bed, leading to the evolution of more volatile matter. In the oxidation zone, coke is burned to carbon dioxide with the primary air rising through the bed. This carbon dioxide travels up through the zone above and is partly reduced to carbon monoxide by contact with the hot coke. The rate of CO formation becomes rapid at the beginning of the reduction zone. Usually the temperature within the bed is somewhat greater than at the surface. If this temperature is above that at which ash fuses, clinker may form which finally passes into the ash pit.

The travelling grate stokers are limited in their use by certain factors.^{7,8} These are:

- (1) The overall mass rate of combustion is limited due to the confined depth of the coal bed. The maximum practical rate per unit cross section is of the order of $250 \text{ Kg.m}^{-2}\text{hr}^{-1}$.
- (2) The area of the grate also has to be kept within some reasonable bounds, about 100m^2 will be an upper limit.
- (3) High levels of excess air, up to 40% can be required, to maximise combustion of the air-born fly ash, hence reducing loss of combustibles.
- (4) Smoke and the resulting atmospheric emission is a common problem.
- (5) Clinker formation, hot grate and hot ash problems in the bottom ash pit pose further maintenance problems. Furthermore carbon losses as high as 40 mass% has been reported⁹ in the bottom ash of some larger stokers. The extent of this problem is related to the bed temperatures which are achieved through the burning coal on the grate.

Figure 2-4² illustrates the temperature contours measured in the fuel bed of a travelling grate stoker.

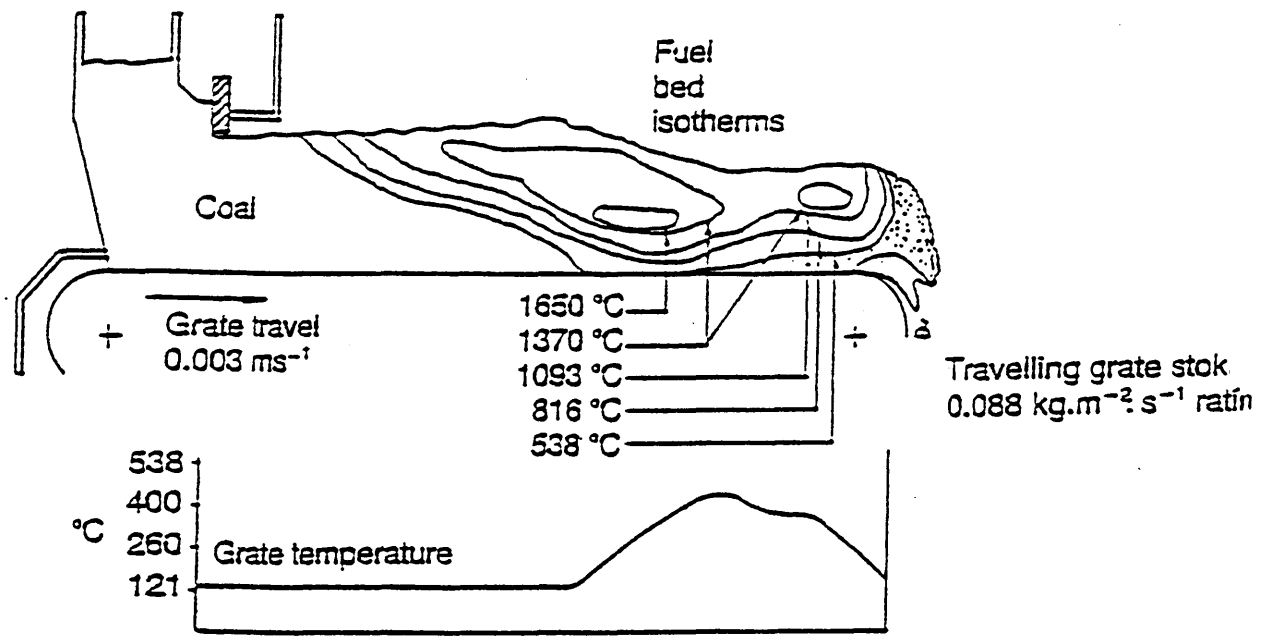


Figure 2-4: Fuel-bed temperature contours for a travelling grate stoker.²

A great variety of coals of varying quality can be burned on travelling grate stokers.¹⁰ However, the most satisfactory results have been found^{11,12,13} with coals having certain chemical and physical characteristics. These are chiefly as outlined below:

- Size range of 35mm or 25mm in diameter, with not more than 30% fines, less than 6 mm in diameter.
- Ash content of 6 to 15 mass% for forced draught stokers and 5 to 9 mass% for natural draught stokers.
- Moisture content should generally be low; of the order of 8 to 10 mass%, apart from "smalls" which should have a surface moisture of about 1.5 mass% per 10 mass% coal less than 3 mm.
- Volatile matter content of greater than 30 mass% on a dry ash free basis.
- Ash softening temperature should be as high as possible, with a minimum of 1150°C in order to avoid clinker formation as well as ash deposition on boiler tube surfaces.
- Alkali metal contents in the ash substances promote deposit formation on the heated boiler surfaces and thus should be at a minimum.

2.1.4 Fire-Side Boiler Deposits

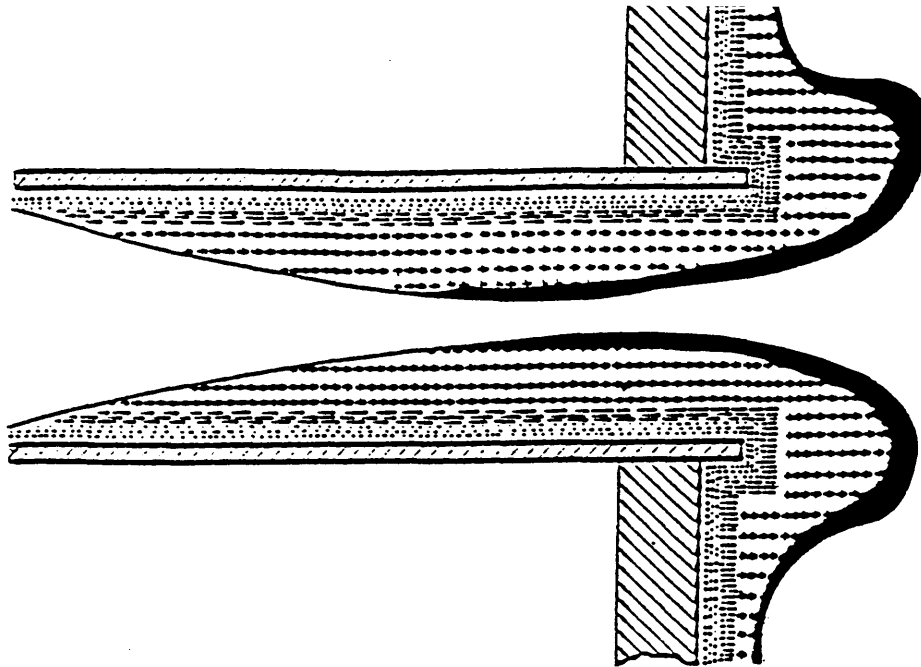
Deposits occur in those parts of the boiler where the metal temperature is high. Most significant are those deposits which are formed on the screen and superheater tubes and at the entrance to convection heating surfaces of the upper furnace regions. These types of deposits are usually referred to as fouling.

Those deposits which are generally limited to the lower furnace area where the flue gas temperatures are highest are known as slagging. These tend to be much harder and denser. Deposits form slowly at first but the rate of formation usually increases

with each successive layer.¹⁴ Figure 2-5¹⁵ illustrates a section through a deposit at the inlet to a convection tube of a boiler. The increase in the thickness of the outer layers is clearly evident. This in turn causes reduction in cross-sectional area and hence increases the resistance to gas flow.¹⁵ However, in practice the nature and extent of deposits can vary considerably. Apart from the temperatures experienced, it is most significantly the heterogeneity of the chemistry and structural complexity of the coal ash minerals that determines fly ash morphology and its role in the formation of deposits. At least 11 major morphological classes of coal fly ash particles have been identified¹⁶ on the basis of particle shape and opacity alone.

Fly ash may be partly infusible at furnace temperatures and partly quite readily fusible, so that a sticky film or layer may be deposited throughout the high temperature zone to which the remainder can adhere. In Figure 2-5¹⁵ distinct layers can be identified, the second of which is fused and thus helps to capture particles of fly ash which come into contact with it.

The main constituents of coal ash are silica and alumina, which are not easily fusible. Other substances present include oxides of iron, calcium, sodium and potassium, which are more easily fusible. The significance of these substances in terms of their individual as well as combined role in forming deposits has been studied by different workers^{17,18,19}. However, it is most significantly the oxides of sodium and potassium which play a dominant part in causing deposits to adhere to heated metal boiler surfaces. When in contact with the sulphur oxides present in the flue gases, formed by oxidation of sulphur which may be organically or inorganically combined within the coal or ash, sodium and potassium sulphates have been found¹⁹⁻²² to form various complex sulphates, by reacting with aluminium or iron oxides. The low melting temperatures of these complexes as depicted in Table 2-2



-  Thin layer of alkali sulphates
-  Fused layer of alkali sulphates (1 mm)
-  Friable layer of alkali sulphates (5 mm)
-  Fritted fly ash
-  Fused fly ash

Figure 2-5: Section through a deposit on a boiler tube.¹⁵

Table 2-2: Melting point of complex sulphates formed within depositing ash particles on boiler tube surfaces.^{19,20}

<u>COMPOUND</u>	<u>MELTING POINT (°C)</u>
$K_3Fe(SO_4)_3$	618
$K_3Al(SO_4)_3$	654
$KFe(SO_4)_2$	693
$Na_3Fe(SO_4)_3$	613
$Na_3Al(SO_4)_3$	646
$NaFe(SO_4)_2$	690

is believed^{19,20} to be responsible for the formation of the first layers of fly ash depositing over the boiler tube surfaces due to their fully softened or molten state.

2.2 MINERAL CONSTITUENTS OF COAL

2.2.1 Geological Origin of Mineral Matter in Coal

The geological environment in which the mineral deposits were laid down determines the mode of occurrence and the relative concentration of the mineral impurities.

Coal is a sedimentary rock composed principally of two basic classes of material:^{23,24} inorganic crystalline minerals and organic carbonaceous "macerals".

The latter form the combustible part of the coal and are in turn divided into three groups namely; vitrinite, exinite and inertinite.

Table 2-3^{24,25} lists the most common inorganic mineral components associated with coal.

The inorganic mineral matter in coal has frequently been classified^{24,26} as inherent or extraneous. The inherent mineral matter has its origin in the organic constituents of plants. The extraneous inorganic mineral matter is defined as that which was brought into the coal forming deposit from outside, for example as dust carried by winds, or as suspended or dissolved material carried by water, after the death of the plant.

The inherent minerals seldom exceed about 2 mass% of the coal and generally make up about 3 to 20 mass percentage of the total mineral matter.²⁷ These minerals are generally found to be rich in iron, phosphorus, calcium, potassium and magnesium which are mostly incorporated in the carbonaceous phases. Other elements such as silicon, aluminium, manganese and sodium known to be essential for plant life are also found to a lesser extent.²⁸

The extraneous minerals make up about 80 to 95 mass% of the total inorganic mineral matter in coal.²⁸ These minerals are principally found to be rich in the most abundant elements of the earth's crust such as silicon, aluminium, iron,

Mineral	Formula
Clay minerals	
Montmorillonite	$\text{Al}_2\text{Si}_4\text{O}_{10}(\text{OH})_2 \cdot \text{H}_2\text{O}$
Illite-sericite	$\text{K}_2(\text{Si}_6\text{Al}_2)\text{Al}_4\text{O}_{20}(\text{OH})_4$
Kaolinite	$\text{Al}_2\text{Si}_2\text{O}_5(\text{OH})_4$
Halloysite	$\text{Al}_2\text{Si}_2\text{O}_5(\text{OH})_4$
Chlorite	$\text{Mg}_5\text{Al}(\text{AlSi}_3\text{O}_{10})(\text{OH})_8$
Mixed-layer clay minerals	
Sulphide minerals	
Pyrite	FeS_2
Marcasite	FeS_2
Sphalerite	ZnS
Galena	PbS
Chalcopyrite	CuFeS_2
Pyrrhotite	Fe_{1-x}S
Arsenopyrite	FeAsS
Millerite	NiS
Carbonate minerals	
Calcite	CaCO_3
Dolomite	$(\text{Ca}, \text{Mg})\text{CO}_3$
Siderite	FeCO_3
Ankerite	$(\text{Ca}, \text{Fe}, \text{Mg})\text{CO}_3$
Witherite	BaCO_3
Sulphate minerals	
Barite	BaSO_4
Gypsum	$\text{CaSO}_4 \cdot 2\text{H}_2\text{O}$
Anhydrite	CaSO_4
Bassanite	$\text{CaSO}_4 \cdot 1/2\text{H}_2\text{O}$
Jarosite	$(\text{Na}, \text{K})\text{Fe}_3(\text{SO}_4)_2(\text{OH})_6$
Melanterite	$\text{FeSO}_4 \cdot 7\text{H}_2\text{O}$
Coquimbite	$\text{Fe}_2(\text{SO}_4)_3 \cdot 9\text{H}_2\text{O}$
Mirabilite	$\text{Na}_2\text{SO}_4 \cdot 10\text{H}_2\text{O}$
Kieserite	$\text{MgSO}_4 \cdot \text{H}_2\text{O}$
Chloride minerals	
Halite	NaCl
Sylvite	KCl
Bischofite	$\text{MgCl}_2 \cdot 6\text{H}_2\text{O}$
Silicate minerals	
Quartz	SiO_2
Biotite	$\text{K}(\text{Mg}, \text{Fe})_3(\text{AlSi}_3\text{O}_{10})(\text{OH})_2$
Zircon	ZrSiO_4
Tourmaline	$\text{Na}(\text{Mg}, \text{Fe})_3\text{Al}_6(\text{BO}_3)_3(\text{Si}_6\text{O}_{18})(\text{OH})_4$
Garnet	$(\text{Fe}, \text{Ca}, \text{Mg})_3(\text{Al}, \text{Fe})_2(\text{SiO}_4)_3$
Kyanite	Al_2SiO_5
Epidote	$\text{Ca}_2(\text{Al}, \text{Fe})_3\text{Si}_3\text{O}_{12}(\text{OH})$
Albite	$\text{NaAlSi}_3\text{O}_8$
Orthoclase	KAlSi_3O_8
Augite	$\text{Ca}(\text{Mg}, \text{Fe}, \text{Al})(\text{Al}, \text{Si})_2\text{O}_6$

calcium, magnesium, sodium, potassium and titanium.^{24,29}

In addition, other elements such as cadmium, antimony, arsenic, mercury, etc. which are usually detected at less than 0.02 mass% (200ppm) are present in coal as trace elements.²⁵

All these elements however are present as minerals in coal either singularly or as compounds in the form of oxides, hydroxides, sulphides and sulphates, carbonates and chlorides. The major groups and their constituents are listed in Table 2-3.²⁵

2.2.2 The Behaviour of Inorganic Mineral Matter When Heated

The inorganic mineral matter in coal undergoes many complex physical and chemical changes when it is heated. The chemical changes are essentially the thermal decomposition of minerals: the dehydration of hydrated minerals such as shales and clays, the loss of CO₂ from carbonates of Ca, Mg or Fe, the oxidation of pyrites (FeS₂) to Fe₂O₃ with evolution of SO_x and the volatilisation of alkalis and chlorides.^{30,31}

Further changes include interactions between mineral species, reactions between mineral matter and the char and reactions between the mineral matter and furnace gases.

Table 2-4³²⁻³⁵ represents the changes which have been observed on heating samples of ash formed by low temperature ashing³⁶ of pulverised coal particles. Low temperature ashing produces ash with its mineral matter in a relatively unaltered state. The changes illustrated in Table 2-4 are expressed more concisely in Table 2-5³⁷ for a range of selected components of various mineral groupings.

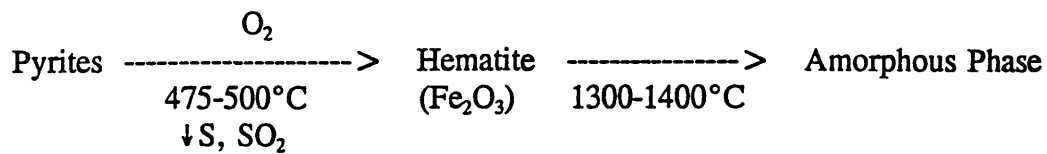
The physical changes include vaporisation, fusion, disintegration, agglomeration and the eventual release of mineral matter into the furnace gases.³⁸

The transformation of various inorganic mineral constituents of British coals in the flame within the combustion zone of a boiler have been comprehensively

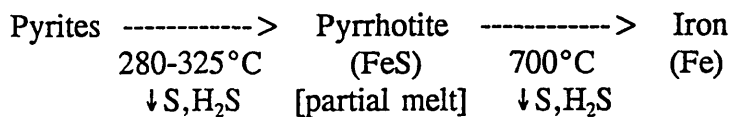
SULPHIDE GROUP

4. Pyrites [FeS₂]

Oxidising

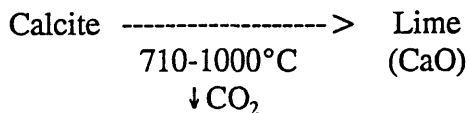


Reducing

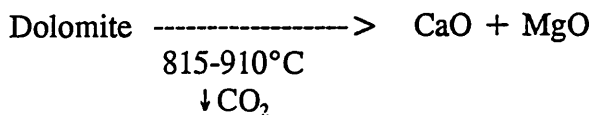


CARBONATE GROUP

5. Calcite [CaCO₃]

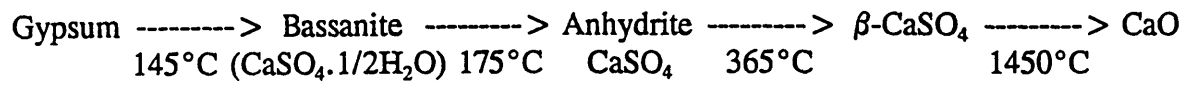


6. Dolomite [CaMg (CO₃)₂]



SULPHATE GROUP

7. Gypsum [$\text{CaSO}_4 \cdot 2\text{H}_2\text{O}$]



SILICATE GROUP

8. Quartz [SiO_2]

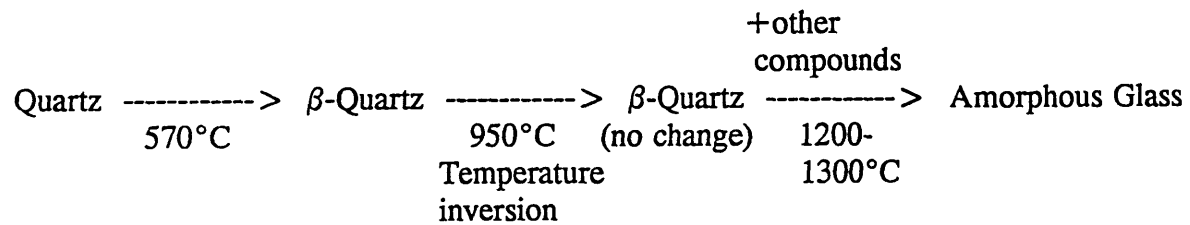
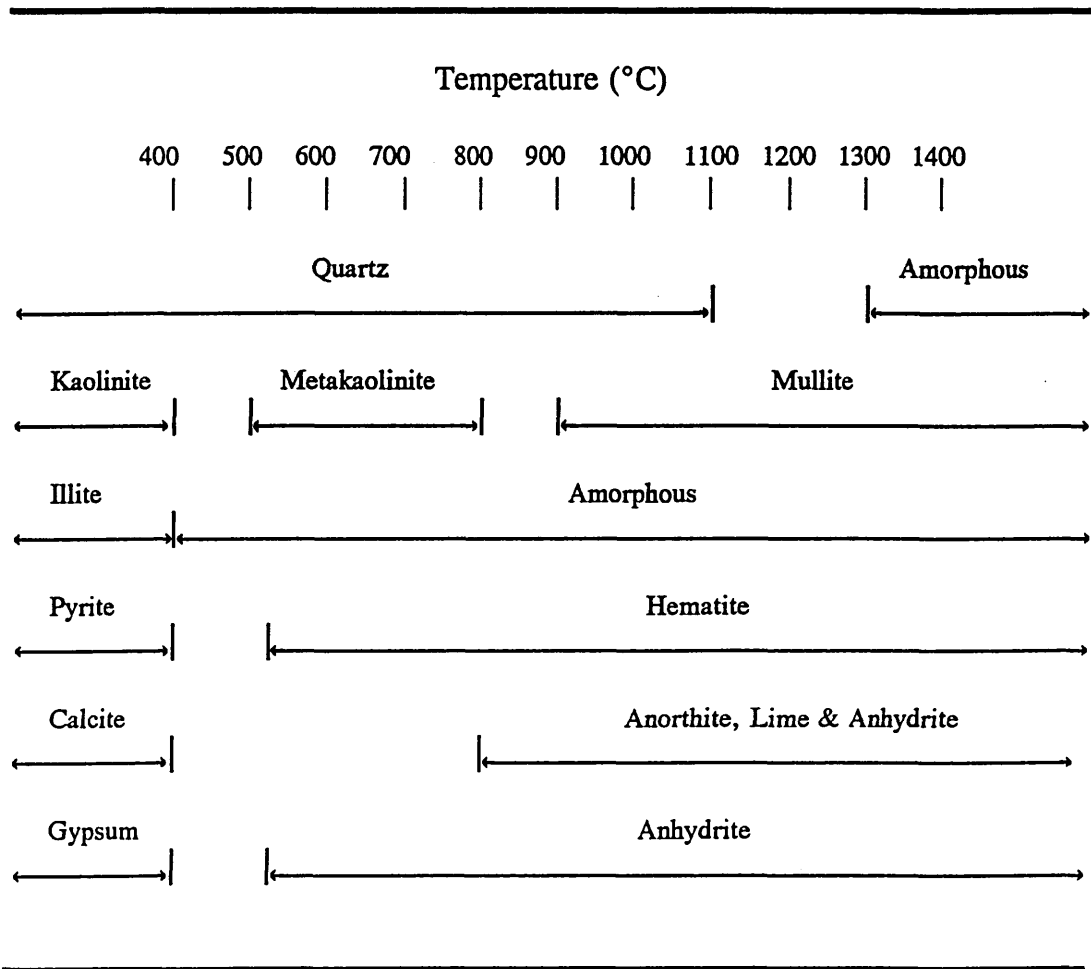


Table 2-5: Transformation of selected mineral groupings due to heating.³⁷



discussed.^{39,40,41} It has been inferred⁴² that the inorganic minerals associated with British coals are mainly shales and iron compounds. Shales, usually the result of consolidation of mud, silt and clay, are complex alumino-silicates in combination with a variety of metal compounds of calcium, iron, sodium and potassium. These minerals include illite $[K_2 (Si_6 \cdot Al_2) Al_4 O_{20} (OH)_4]$ and muscovite $[KA_2 (Si_3 AlO_{10}) (OH)_2]$. These are forms of mica. Kaolinite $[Al_2 Si_2 O_5 (OH)_4]$ is the most common of the clay (Kaolin) minerals which are found in coal in many forms.^{42,43} In the flame the shale minerals lose combined moisture and undergo lattice transformation. Those particles which are ejected from the flame do not complete either the process of fusion or the evolution of moisture before the change of shape of silicate particles commences.⁴² The particles which continue in the flame tend to complete both processes, particularly in relatively hot combustion chambers and thus, the small irregularly shaped particles are transformed into colourless, rounded, solid spheres.⁴² The change in shape of these irregularly shaped alumino-silicate particles on heating has been shown⁴⁴ to be the result of surface tension of the softened matter on their sharp edges.

The iron minerals are most commonly iron pyrite and Marcasite. The iron pyrite mineral (FeS_2) is known to occur in various physical forms within the coal, for example as nodules, lens-shaped masses, in veins and fissures or as discrete particles in veinlets.⁴³ When heated, the degree of liberation and the melting temperature of pyrite depends on its initial physical form, the fineness of the coal particles^{45,46} as well as the degree of sulphur reduction and iron oxidation.⁴⁷ It has been established⁴³ that ignition of pyrite occurs at low temperatures of about 200-500°C depending on particle size, the form of pyrites and the presence of oxygen. When pyrites is heated in the absence of air, it dissociates to form pyrrhotite (FeS) and sulphur gas, and at

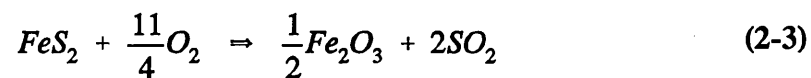
and sulphur gas, and at higher temperatures the pyrrhotite decomposes into sulphur and iron. The two step reaction can be summarised as follows:⁴⁸



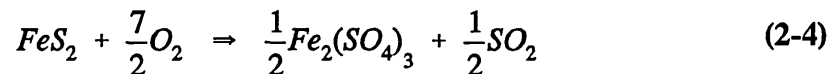
The first reaction proceeds at a rapid rate while the final reaction requires considerable time.

Under oxidising conditions, the reactions are found to be much more complex. Pyrites may be converted directly to sulphur dioxide and either ferrous or ferric oxide.

The overall reaction has been represented as follows:⁴⁹



In excess air the reaction can also proceed as follows:



The melting behaviour of the residue formed on heating iron pyrite mineral shows a complicated pattern. Some researchers⁴⁸ have published phase diagrams of the FeO-FeS system, with a minimum liquidus temperature appearing at 940°C. This has been supported by another study⁴⁷ which has claimed a minimum liquidus temperature of 948°C. In a study of the phase diagram for the Fe-S system, as shown in Figure 2-6⁵⁰, it appears that no liquid would form below 988°C. Hence,

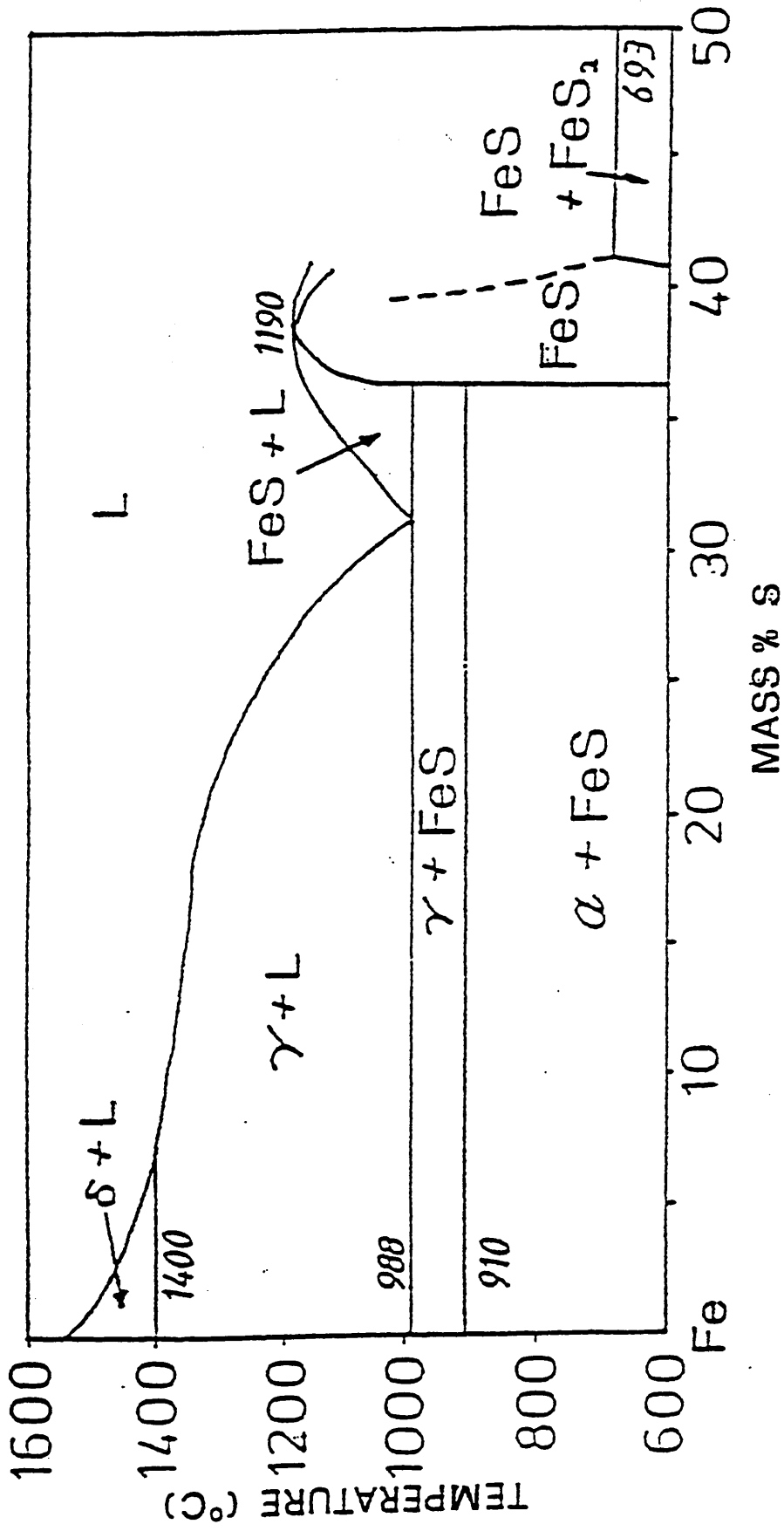
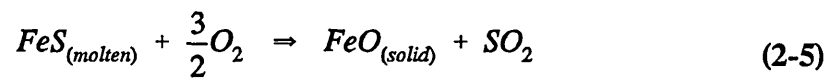


Figure 2-6: Fe - S phase diagram.⁵⁰

depending on the origins from which pyrrhotite is produced, the initial melting temperature of the product can be significantly different.

Under reducing conditions it has been shown⁴⁷ that pyrite can form melts at temperatures as low as 600°C.

Studies⁴⁸ of iron pyrite particles allowed to fall freely through an oxidising atmosphere in a laboratory furnace have exhibited the formation of a low melting phase, FeS, at 1027°C which had acquired a rounded shape. Furthermore iron oxide particles found in boilers as fly ash or deposits are spherical in shape, with a black colour⁴² this is taken as a proof that a liquid phase exists before oxidation of FeS to FeO:⁴⁸



In a stoker system, as the coal bed is ignited, various minerals previously bound up within the coal matrix are released. The coal ash thus formed exists in two forms; namely "clinker" and "fly ash".

Clinker is the ash which is mostly derived from the larger coal particles that as a result of high flame temperatures on the coal bed have formed extended liquid phases and consequently agglomerated.³⁰ The clinker remains on the grate and is dumped into ash pits at the other end of the grate's traverse. The clinker comprises between 40 to 60 mass% of the total ash content of the coal.²⁸ Depending on the mode of operation and the ease of combustion on the grate, carbon contents as high as 40 mass% have been found associated with the clinker.⁹

Fly ash is a heterogeneous mixture of inorganic mineral matter and unburned combustibles³⁰ which is lifted from the surface of the coal bed by air or gas entrainment, possibly burning and modifying in suspension as it travels upwards

inside the boiler environment, with the particle temperature continuously decreasing. Fly ash can exist in a solid or liquid state before it is deposited on heating surfaces. In stoker firing, fly ash is derived mainly from mixed minerals; only a few particles are pure shale or iron residues and the rest are mixtures in all proportions.⁴² Mixing of the minerals can take place in at least three ways:⁴²

- (1) During burning of relatively large particles of coal containing a variety of inorganic minerals when these are released and lifted above the bed.
- (2) If the coal forms swelling coke (i.e. becomes plastic at a temperature below the ignition point), minerals mix while it is plastic.
- (3) For a non-caking coal the minerals are mixed to some extent as a result of sintering and slagging during the pyrolysis and burning period of the coal on the grate.

The national average ash content for coals utilised by British power stations is estimated²⁸ at 16 mass%. The fly ash comprising about 50%²⁸ of the total ash content for a stoker system and 10% for a typical chain grate stoker⁵² suggests a comparatively limited amount of ash available within the boiler atmosphere to form deposits.

2.3 CHARACTERISATION AND FUSIBILITY OF COAL ASH WITH RESPECT TO ITS CHEMICAL PROPERTIES

2.3.1 Introduction

Characterisation of coal ash in terms of its fusibility was originally introduced as a means of providing guidance on the prediction of clinkering in coal fired stoker furnaces.⁵³

In spite of the fact that stoker firing has strongly declined and formation of clinker is no longer as important a problem as it once was, ash fusibility measurements are still widely used in their original form as a means of predicting the behaviour of coal

ash in combustion systems, in relation to their slagging propensity on heat receiving boiler surfaces.

The fusibility test is based on observing the temperature at which successive characteristic stages of fusion occur in a finely ground specimen of ash when heated in a laboratory furnace under specified conditions of atmosphere and rate of temperature rise.⁵²

Although many studies^{19,54-57} have regarded standard ash fusibility measurements as a relatively good indicator of the softening and melting behaviour of coal ash in combustion systems, others have shown⁵⁸⁻⁶⁰ major shortcomings. Never the less, as a relatively quick, easy, reliable and reproducible method, ash fusibility measurements are still widely used.

2.3.2 The Effect of Chemical Composition on Ash Fusibility

Coal ash, unlike a pure compound, does not exhibit a sharp melting point but rather softens over a temperature range as the temperature is increased. This temperature range corresponds to the plastic state and depends on the composition of the ash and gaseous environment.

The chemical composition of coal ash is usually described in terms of oxides of eight major elements. Table 2-6⁶¹ summarises these in addition to two other elements, (i.e. barium and strontium) as elements of major abundance and others as elements of minor abundance in coal. These oxides have been defined as "acidic" or "basic".^{62,63} The oxides of Al, Si and Ti are regarded as "acidic oxides", the oxides of Fe, Ca, Mg, K and Na are regarded as "basic oxides". The acidic oxides comprise the refractory part of the ash, helping to retard ash-melting, whereas the basic oxides acting as fluxes promote softening and melting of the ash.

Table 2-6: Major and minor abundance impurity elements in coal.⁶¹

Elements of Major Abundances (200 to 17,700 ppm)		Elements of Minor Abundances (Less than 200 ppm)	
Element	ppm in Coal	Element	ppm in Coal
Silicon, Si	17,700	Chromium, Cr	103
Aluminum, Al	11,300	Zirconium, Zr	64
Iron, Fe	3,690	Copper, Cu	56
Calcium, Ca	2,060	Boron, B	43
Potassium, K	1,370	Manganese, Mn	33
Magnesium, Mg	1,320	Rubidium, Rb	32
Titanium, Ti	738	Lithium, Li	31
Sodium, Na	546	Zinc, Zn	26
Barium, Ba	266	Nickel, Ni	20
Strontium, Sr	171	Niobium, Nb	19
		Caesium, Cs	15
		Tin, Sn	15
		Neodymium, Nd	14
		Vanadium, V	13
		Cobalt, Co	12
		Lanthanum, La	11
		Lead, Pb	11
		Scandium, Sc	7.2
		Arsenic, As	4.5
		Gallium, Ga	3.3
		Molybdenum, Mo	3.2
		Praseodymium, Pr	2.3
		Cesium, Cs	2.3
		Thorium, Th	2.2
		Beryllium, Be	1.3
		Antimony, Sb	< 0.65
		Uranium, U	< 0.56
		Cadmium, Cd	0.48
		Germanium, Ge	0.35
		Mercury, Hg	< 0.33
		Tungsten, W	< 0.33

Major-abundance elements are 98.7 weight percent of these 41 elements. Minor-abundance elements are the remaining 1.3 percent.

Nonmetal elements have appreciable ppm levels, e.g., average values of 4360 (S), 229 (Cl), 116 (P), 15 (F), and 0.34 (Se).

In terms of the ash melting retardation, the most desirable constituent of ash is considered⁵⁸ to be Al_2O_3 and the most undesirable constituents to be Fe_2O_3 , CaO and K_2O . Another factor which affects the softening temperatures of the ash is the atmosphere. Reducing atmosphere provides a more dependable basis for standardisation of ash fusion temperature measurements. However it is generally oxidising conditions which are prevalent in local areas or other parts of the furnace and may alter the behaviour of the ash independently of actual change in temperature.⁵² This effect is significant in the fouling of heating surfaces as will be discussed in later sections.

2.3.2 (a) oxidising conditions

Behaviour of Alumina (Al_2O_3)

Alumina is the most refractory component of the ash and is therefore expected to increase the softening temperature of the coal ash. In a comprehensive study⁶⁴ of the fusion characteristics of a range of coal ashes, it is shown that for four different coal ash mixtures the softening temperature of the ashes increased on average between 9 to 17°C for every 1.0 mass% of alumina added to the coal ashes. It has further been suggested^{58,64} that mineralogically it is mostly due to the alumina in kaolin minerals such as kaolinite, rather than alumina in the shales such as Illite, Muscovite or other minerals in this group, that coal ashes rich in alumina retain their refractoriness up to relatively high temperatures.

Behaviour of Silica (SiO_2)

Silica is the major constituent of coal ash and is also regarded as a refractory oxide. However it can act as a flux for the more refractory alumina. Additions of silica in the various proportions to three different ash mixtures with original silica contents varying between 49 to 59 mass% showed⁶⁴ only a slight decrease in

softening temperatures with increasing silica content. Addition of silica was believed to produce two opposing effects:

(i) An increase in the silica/alumina ratio in the ash which would be expected to reduce the softening temperature.

(ii) Lowering of the content of other fluxes present in the coal ash, thereby increasing the softening temperature.

Hence, the net lowering in softening temperature is a compromise between these two opposite effects.

In the results published by another study⁶⁵, additions of up to 20 mass% of silica as quartz showed a marked decrease in the softening temperature of the ash from the washed and then ground large particles of coal. However, no significant effect was observed on the softening behaviour of the ash collected from the fines in the coal sample. The large coal particles were found to be richer in the basic oxides than the fines. It was concluded that should an acidic oxide like silica be introduced into a coal, having predominantly basic minerals, on burning of the coal they would react together leading to formation of eutectic mixtures of low melting point, thereby lowering the softening temperature range.

Behaviour of Iron Oxide (Fe_2O_3)

As an amphoteric transition metal oxide, iron can exist in various oxidation states; FeO, Fe_2O_3 , Fe_3O_4 or even pure Fe, depending on the availability of oxygen as well as mixing of air with the burning coal.

In an oxidising atmosphere, iron is present mostly as Fe_2O_3 within the coal ash. This causes the softening temperatures of the coal ash to be higher than in the presence of a mildly reducing atmosphere where iron may be present as FeO.⁶⁴

Coal ashes and deposits from coal fired units most often are shown^{62,63,66} to contain compounds of about 80% basic FeO plus 20% acidic Fe₂O₃ compounds. Hence, iron oxide is invariably classified with the bases, even though they are usually listed as Fe₂O₃ in the chemical analysis of coal ashes.

The fluxing effect of Fe₂O₃ in lowering the softening temperature of ash has been shown^{64,67} to be dependent on the original softening temperature and the Fe₂O₃ content of the ash. This has been estimated at 15-16°C per 1.0 mass% Fe₂O₃ at Fe₂O₃ contents less than 15 mass%. Beyond this point, the fluxing effect becomes negligible and sometimes even results in the rise of softening temperature with further increase of Fe₂O₃ content. Similar results have been documented⁶⁸ whereby the fluxing effect of the Fe₂O₃ content for a series of ash samples increased up to 20 mass% of Fe₂O₃. However, in the range of 20 to 40 mass% Fe₂O₃ progressively increased the melting temperature. In another study⁶⁹, removal of the magnetic iron fraction from fly ash reduced both the softening and melting temperatures by 10 to 15°C. It has also been shown⁶⁸ that large particles of iron oxide formed on dissociation of carbonates and oxidised pyrite species in the superheater flue gas are comparatively inert in an oxidising atmosphere.

Behaviour of Alkali Earth Oxides (CaO, MgO)

The effect of CaO and MgO on softening temperature of a series of coal ash samples of varying composition has been investigated.⁶⁴ It was shown⁶⁴ that the fluxing effect of CaO decreases with increase in CaO content, up to 45 mass% for any particular ash considered. The extent of the fluxing effect of CaO has been divided into three ranges according to the amount of lime added:

- (1) For increase in CaO content between 0 to 13 mass%, the softening temperature was lowered by 18 to 25°C per mass% of CaO in the ashes.

(2) For increase in CaO content between 13 to 30 mass%, the fluxing effect of CaO is very small, about 4 to 5°C per mass% of CaO. Sometimes the fluxing effect is even negative at the lower end of the range but increases as the CaO content approaches 30 mass%.

(3) For increases in CaO content between 30 to 45 mass%, the softening temperature rises progressively.

However in consideration of the above observations, it should be added that the changes in the softening temperature of the coal ash mixtures as CaO is added, is also due to the reduction in the proportion of other oxides in the ash, such as MgO, Na₂O, K₂O and Fe₂O₃ or FeO, which possess considerable fluxing affect.

In a study of fusion behaviour of selected ash components⁷⁰, a contrasting effect of CaO content on ash softening and melting temperatures of two low temperature ashes was investigated. It was observed that for a coal ash with an original CaO content of 34.10 mass%, the first liquid phase was observed at 1240°C and the sample was fully liquid by 1400°C. In contrast, a coal ash with a much lower original CaO content of 13.60 mass% did not exhibit an observable liquid phase formation and formed a fully liquid melt at a lower temperature of 1310°C. These observations exemplify the complex softening behaviour of coal ash which can not be predicted from its chemical composition.

Magnesium oxide is normally present in coal ash in smaller quantities than CaO. As an individual entity, it is highly refractory with a melting point of 2800°C. The changes observed⁶⁴ on softening temperature of two coal ash samples showed the fluxing effect of MgO additions to be similar to a limited extent to that of CaO at the lower ranges. The fluxing effect was shown to be restricted to an MgO content

of 4 mass%, with no further lowering in the softening temperatures of the two ash samples beyond that.

Additions of MgO to a selected range of coal ash samples rich in iron oxide is reported⁵³ to have rendered the ash more refractory by forming the high melting compound of magnesium ferrite.

Behaviour of Alkali Oxides (K_2O , Na_2O)

The fluxing action of alkali oxide additions has been investigated⁶⁴ for two coal ashes. The lowering of the softening temperature per mass% of alkali oxide additions was between 24 to 26°C which is more pronounced than with CaO or MgO.

The effectiveness of alkali oxides as fluxes is particularly dependent on their occurrence as "active alkalies" such as simple inorganic salts (e.g. NaCl, KCl) or as "inactive alkalies", bonded to organo-metallic molecules, such as those in clays and shale minerals.⁶⁶ Whereas the effective fluxing action of the latter group of alkalies is restrained and defined by the alumino-silicate matrix boundaries of coal ash minerals, the former group can undergo various reactions to form simple or complex silicates and sulphates which are influential in depressing ash softening temperatures to varying degrees.

It has been shown⁵⁸ by analysis of coal ash quenched from temperatures less than 1200°C, that the most important fluxing oxide is K_2O . Above 1200°C, CaO and to a lesser extent Fe_2O_3 also become important fluxing agents.

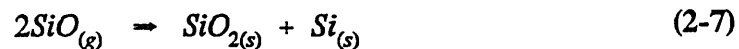
2.3.2 (b) reducing conditions

This condition can exist within restricted regions of the lower furnace atmosphere, due to wide variations in oxygen concentration, from undiluted air to fuel rich regions, depending on the degree of mixing and the local rate of combustion. Even with ideal

mixing in the flame, strongly reducing conditions with O₂ mole fraction < 10⁻¹⁰ are thought⁷¹ to exist within the burning char due to the limiting rate of diffusion of oxygen in the pore system.

Behaviour of Silica (SiO₂) and Alumina (Al₂O₃)

In the majority of coals, silica is present as quartz or is derived from the decomposition of clay minerals. However during combustion, silica may interact with other components of the ash, e.g. CaO, FeO and alkalis in the furnace gases to form low viscosity oxides. In addition, under reducing conditions, silica in close association with the char may undergo carbothermal reduction^{44,70,71} to its more volatile suboxide, SiO. This is a gaseous product and is only thermodynamically stable above 1870 °C. On cooling, SiO dissociates to SiO₂ and Si, the Si subsequently reoxidising to SiO₂.⁷²

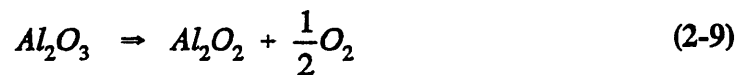


The SiO₂ thus formed consists of particles of submicron size sometimes known as "silica fume". The emission of silica fume has frequently been observed in stoker boilers.⁷¹

The evidence given in support of the formation of the initial SiO sub-micron size fume particles has been challenged by some researchers⁴² suggesting that if silicon is vaporized as the element, the monoxide or sulphides, the vapour will be completely oxidised to silica in the combustion chamber. Silica would then condense

immediately after formation to form a collidal suspension or aerosol.

Alumina existing almost entirely in clay and shale minerals is relatively unreactive. However studies⁷¹ of coal ash slag heated in a graphite crucible in an argon atmosphere containing a trace amount of oxygen, showed that a substantial amount of Al_2O_3 was volatilised at $1900^\circ C$ and subsequently condensed at about $1330^\circ C$. It is purported that volatile suboxides of aluminium were formed at high temperatures and condensed and reoxidised on cooling:



Behaviour of Iron Oxide (FeO)

The softening temperature of coal ash under reducing atmosphere is lower than in its temperature under oxidising atmosphere, as typically illustrated in Figure 2-7.⁵⁴

This has been attributed^{53,73} to the difference in the fluxing action of the different states of oxidation of iron oxide in different atmospheres. In an oxidising atmosphere, iron is mostly present as Fe_2O_3 whereas in a mildly reducing atmosphere, it is present as FeO and in a strongly reducing atmosphere it is completely reduced to metallic iron.

Figure 2-8⁵² illustrates the effect of total iron content on ash fusion temperatures of coal ash under oxidising and reducing conditions.

A laboratory based study of ash melting behaviour showed⁵⁸ that melting was greatly accelerated under reducing conditions. The percentage of melted ash increased rapidly between $900^\circ C$ and $1100^\circ C$, with no further increases above

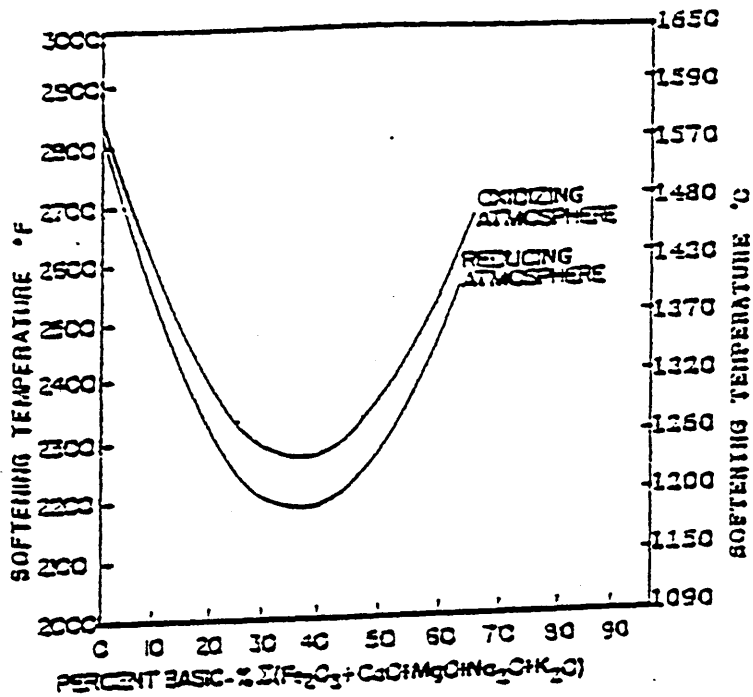


Figure 2-7: Comparison of softening temperatures under reducing and oxidizing atmospheres for various percentages of basic constituents.⁵⁴

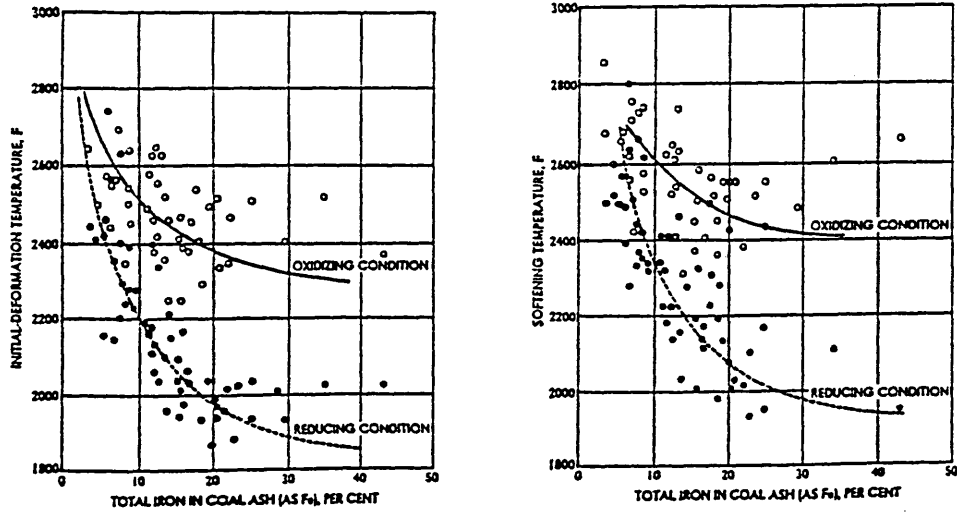


Figure 2-8: Influence of iron on coal-ash fusion temperatures under oxidizing and reducing conditions.⁵²

1200°C. It is primarily due to the predominant occurrence of iron as FeO, rather than Fe₂O₃, as the principal fluxing oxide controlling ash melting, that reducing conditions become pertinent to the combustion regime within the boiler environment. The fluxing effect of iron oxide as Fe₂O₃ has been shown⁷³ to diminish considerably as its amount in the coal ash, as well as that added to synthetic ash samples was increased to 35 mass%. Further increases in the iron oxide content up to 50 mass% had no effect on the softening temperatures which varied between 1075 and 1155°C for the ashes considered. It was further shown in the same study that for some ash mixtures with SiO₂/Al₂O₃ ratios greater than 1.50 and (CaO + MgO) content greater than 10 mass%, further increases in the iron oxide content as FeO beyond 40 mass% increased the softening temperatures. Similar studies of ash fusion behaviour have established⁷⁴ analogous results with the maximum fluxing effect of FeO at 30 mass% with slight increase in ash fusion temperature beyond this point.

Behaviour of Calcium Oxide (CaO) and Alkalies (Na₂O, K₂O)

An investigation of the softening behaviour of a range of ash mixtures with CaO contents varying from 3 to 43 mass% showed⁷⁴ that the ash fusion temperature was at its highest between 3 to 8 mass%. On further additions of CaO, the fusion temperatures decreased, reaching a minimum at 22 mass%, beyond which the fusion temperatures continued to increase up to 43 mass%. However, the lowering of softening temperature by the addition of CaO to a coal ash with high Fe₂O₃ content has been observed⁷³ to be very low or even insignificant in reducing conditions, when the original CaO content of the ash is low. Similar observations were made in the same study regarding the role of the alkalies.

2.3.3 Flow Characteristics

An understanding of the behaviour of coal ash in the molten state and its subsequent mode of solidification is crucial for any boiler designer and operator whatever the mode of operation and firing involved. In stoker systems, the flow characteristics are important with respect to the formation of clinker on the grate as well as deposition of fly ash on boiler tube surfaces.

The flow characteristics of coal ash slags and deposits formed on boiler tube surfaces have been correlated^{75,76,77} to temperature-viscosity-composition measurements for a wide range of coal ashes. The results of one study⁷⁵ have been published in the form of a nomogram relating these properties, with composition expressed in terms of the "silica ratio" defined by the expression:

$$\text{Silica ratio} = \frac{\text{mass\% SiO}_2}{\text{mass\%} [(\text{SiO}_2 + \text{Equivalent Fe}_2\text{O}_3 + \text{CaO} + \text{MgO})]} \quad (2-11)$$

where;

$$\text{Equivalent Fe}_2\text{O}_3 = \text{Fe}_2\text{O}_3 + 1.11 \text{ FeO} + 1.43 \text{ Fe} \quad (2-12)$$

The silica ratio of an ash was considered to be a good guide to assessing its behaviour in the plant.

In the most comprehensive studies^{77,78} covering most of the British coals likely to be used in practice, correlations have been made between the temperature, viscosity and composition of a range of slags derived from blending ashes from actual British coals. The viscosities of coal ash slags were generally correlated under two conditions:

(a) For fully liquid slags a logarithmic equation was derived,⁷⁷ giving satisfactory accuracy for the viscosity values:

$$\text{Log}_{10} \eta = \frac{10^7 * m}{(t-150)^2} + c \quad (2-13)$$

where;

η - Viscosity (poises)

$$m = 0.00835 \text{mass\% SiO}_2 + 0.00601 \text{mass\% Al}_2\text{O}_3 - 0.109 \quad (2-14)$$

$$c = 0.0415 \text{mass\% SiO}_2 + 0.0192 \text{mass\% Al}_2\text{O}_3 + 0.0276 \text{Equivalent}$$

$$\text{mass\% Fe}_2\text{O}_3 + 0.1060 \text{mass\% CaO} + 3.92 \quad (2-15)$$

t - Temperature ($^{\circ}\text{C}$)

(b) For devitrified slags, the temperature of critical viscosity (T_{cv}), which is the temperature at which, on cooling, crystallisation of the slag is first likely to interfere with its flow properties, is expressed⁷⁸ as follows:

$$T_{cv} = 2990 - 1470(A) + 360(A^2) - 14.7(B) + 0.15(B^2) \quad (2-16)$$

where;

$$T_{cv} \text{ is in } ^{\circ}\text{C}, \quad A = \frac{\text{mass\% SiO}_2}{\text{mass\% Al}_2\text{O}_3}, \quad B = \text{mass\% [Fe}_2\text{O}_3 + \text{CaO} + \text{MgO]}$$

This expression was shown to be best suited to ashes with:

$$A < 2.0, \quad \text{based on } \sum (\text{SiO}_2 + \text{Al}_2\text{O}_3 + \text{Fe}_2\text{O}_3 + \text{CaO} + \text{MgO}) = 100.$$

The importance of T_{cv} is that it greatly influences the thickness of coal fly ash depositing on boiler tube surfaces where there is a temperature gradient through the overlaying deposit layers. The outermost layer of deposit, being fluid, flows under gravitational forces, but the innermost layer behaving as a solid, is unaffected by gravity. Hence, the temperature at which this transition occurs between liquid and solid, as well as the viscosity of the liquid phase is important in establishing just how thick the deposit layer will be.⁷⁶

Figure 2-9⁷⁵ illustrates the four distinct ways in which coal fly ash deposits can act during cooling generated as the result of temperature gradients within the maturing deposits. Curve 1 is that for a deposit consisting of pure glass, cooling uniformly without formation of any solid phases as precipitates within the coal ash melt. Curve 2 represents deposits approaching a glass in behaviour, cooling to a low temperature before separation of solids causes the development of plastic flow of coal ash melt, with T_{cv} being very low. Curve 3 represents coal ash slags which have a long cooling range but which begin to slowly separate solids at a relatively high temperature and freeze to a complete solid at a much lower temperature. T_{cv} is usually high in this case. Curve 4 represents slag deposits having a short freezing range, separation of solids being very rapid with the possibility that T_{cv} may be high or low.

In terms of the individual effect of various components of the coal fly ash on the silicate slag deposits, it has been shown^{79,80} that alumina reduces the viscosity of highly siliceous slags, but in highly alkaline melts, it acts to increase the viscosity. Additions of alkali or alkali earth oxides usually decreases the viscosity of aluminosilicate melts. However, the effect of potassium oxide can be an exception to this rule due to its "inactive" status in aluminosilicate shale minerals. Iron being present

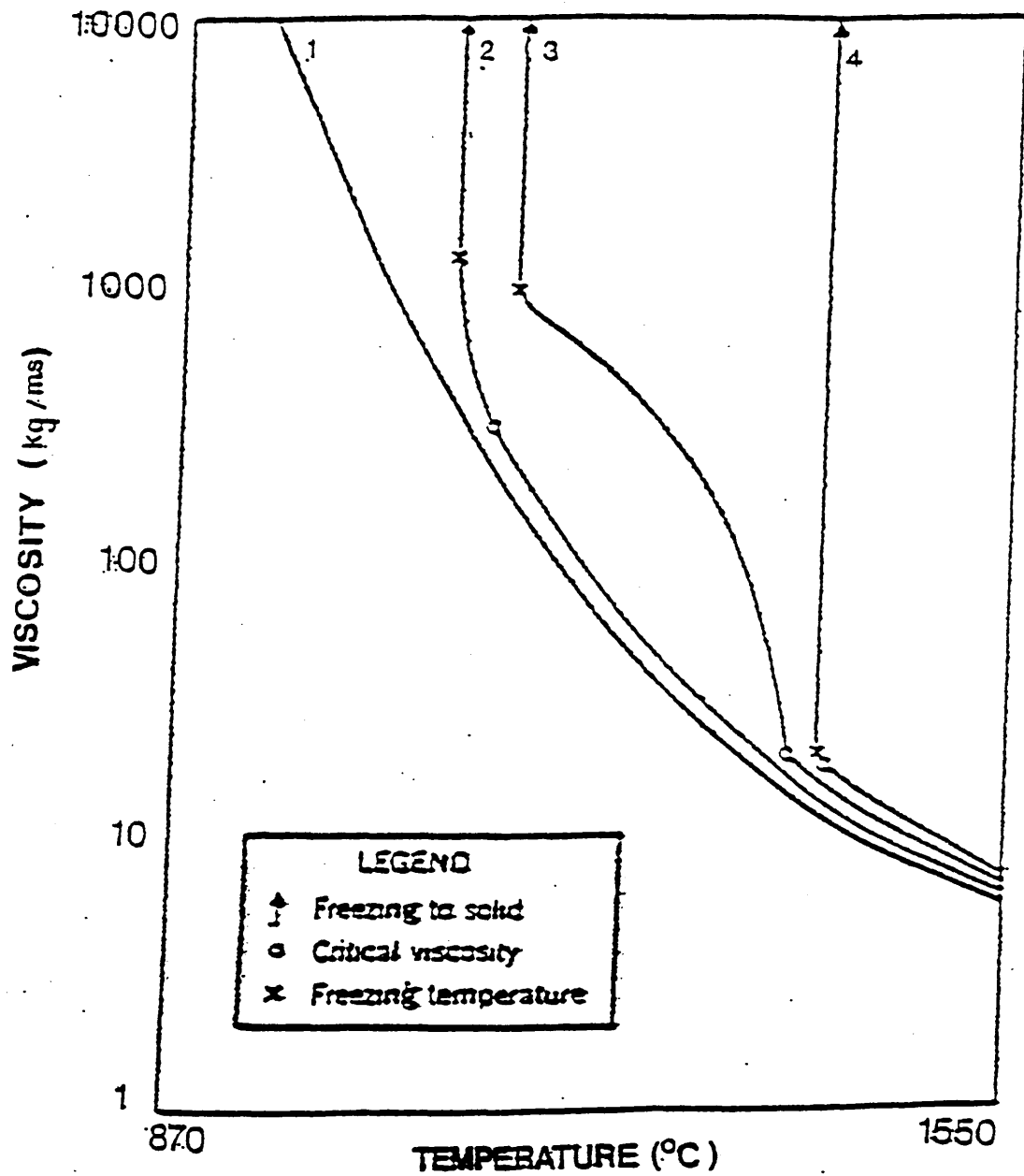


Figure 2-9: Typical viscosity-temperature relationships of coal-ash slags in solidification range.⁷⁵

as ferric iron under oxidising conditions, increases the viscosity by behaving as a silicate network extender in a manner similar to that of alumina. The slag viscosity will also increase as a result of crystallisation of iron-alumina spinels and iron containing silicates. In a strongly reducing atmosphere at high temperatures iron oxide is reduced and separates out as liquid metal. As a ferrous oxide, it reduces the viscosity.

The measurement of viscosity is time consuming, arduous and requires specialised equipment not commonly available. Efforts have thus been made to correlate the viscosity of coal ash with parameters such as "silica ratio", "ferric percentage", "base to acid ratio" and "dolomite percentage".^{81,82}

2.4 THE FORMATION OF FLY ASH DEPOSITS IN BOILER SYSTEMS

2.4.1 Introduction

Generally, formation, growth and consolidation of a deposit is a long term process possibly proceeding over periods of thousands of hours in a boiler. The study of deposition phenomenon is complicated by the physical and chemical reactions and changes of the depositing fly ash particles as well as those within the maturing deposit.

The two distinct types of deposits, namely slagging and fouling, have already been defined in section 2.1.4. However these types have further been divided into high and low temperature deposits according to the region within the boiler unit that they are formed as schematically illustrated in Figure 2-10.⁸³ The approximate temperature ranges for the various deposition zones are presented in Figure 2-11.⁸³

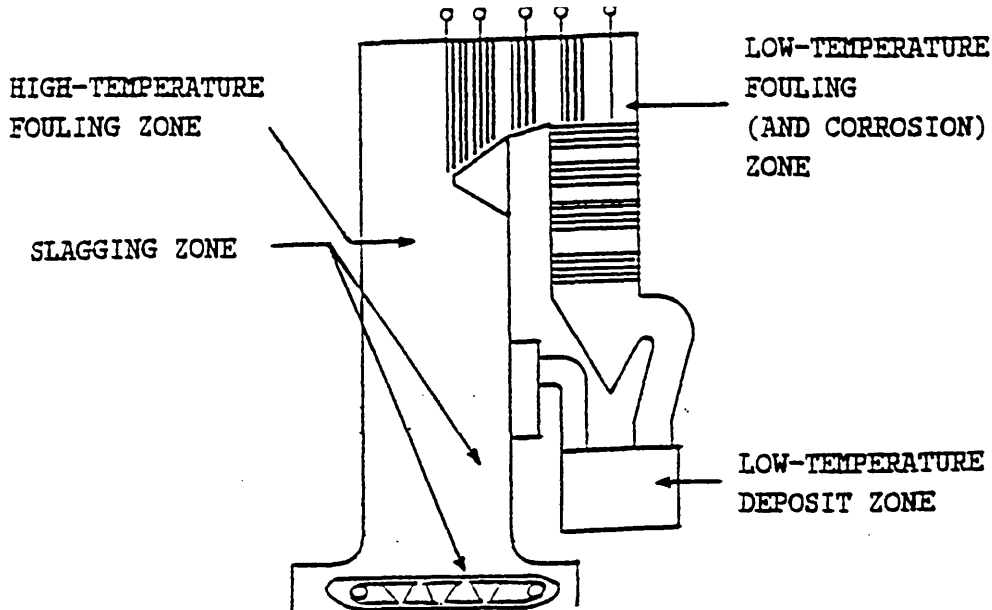


Figure 2-10: Deposit zones in a coal-fired unit.⁸³

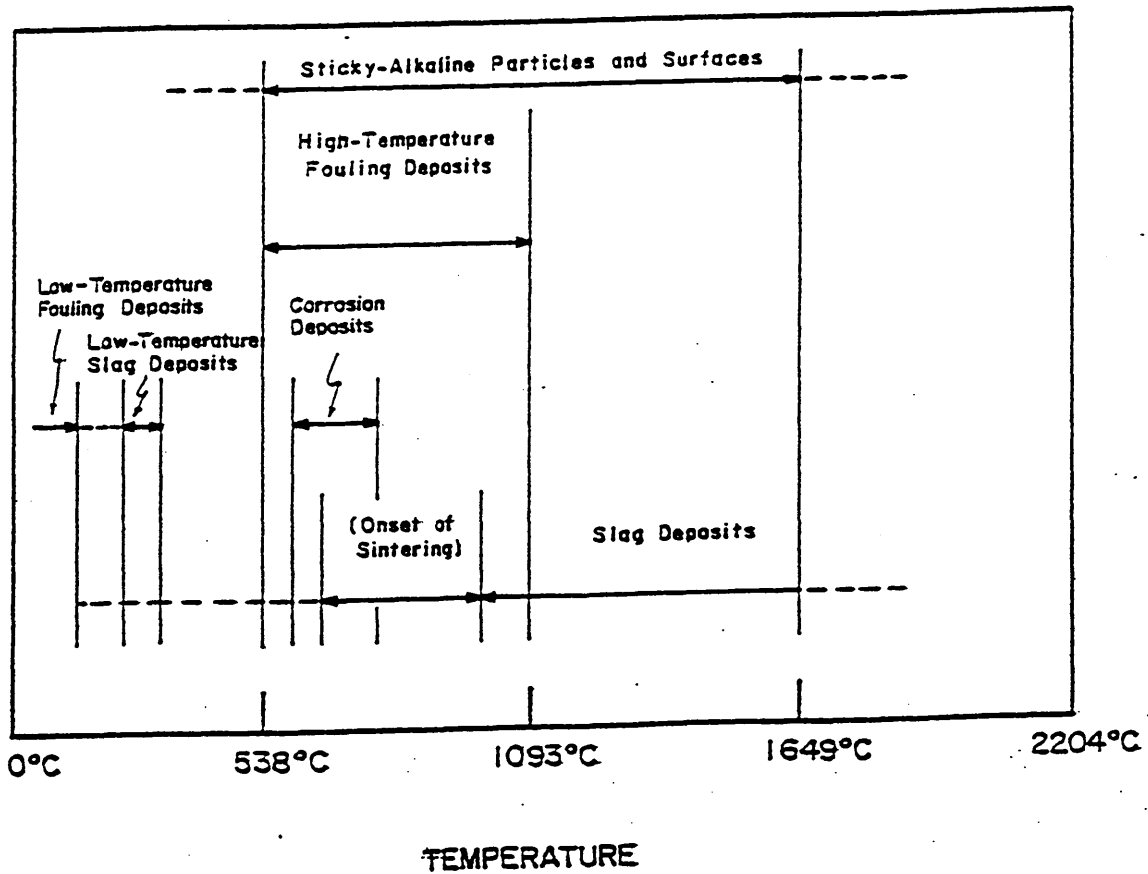


Figure 2-11: Approximate temperature regions for deposit formations in coal-fired units.⁸³

2.4.2 Factors Influencing Deposition

2.4.2 (a) The Effect of Ash Chemistry on Deposition

The influence of ash chemistry on deposition has been investigated by many workers. However, as yet no comprehensive study of all the chemicals present in the ash and their interactive effect on the build up of deposits has been made.

In an investigation of the sintering behaviour of ash from Australian brown coals, the effect of five oxides which appeared to influence the rate of deposition of the coal ash was considered¹⁷ with respect to the amount of deposit formed. It was shown that of the five oxides, silica, iron oxide and sodium oxide were consistently significant, magnesium oxide was partially significant and calcium oxide was of varying significance. On the basis of statistical examination of data from many tests determining the fouling rates, the mass of the deposit formed was related to the mass composition of the ash in the coal, as follows:

$$\begin{aligned} \text{Mass of deposit} &= 0.030 (\%SiO_2) + 0.092 (\%Fe_2O_3) + 0.061 (\%CaO) \\ &+ 0.264 (\%MgO) + 0.423 (\%Na_2O) - 10.6 \quad (2-17) \end{aligned}$$

Good agreement was found between the mass of the deposit collected and the mass predicted from the above equation.¹⁷

Silica - The role of silica in deposit formation is complex. As quartz, it remains essentially unaltered if heated in isolation. However, within the boiler atmosphere it may interact with other components of the ash, such as CaO and FeO or Fe₂O₃ and alkalis in the furnace gases, to form low viscosity silicates. Clay minerals may be involved in similar reactions.²²

The rates of deposition for three bituminous coals with varying ash composition showed⁸⁴ that the coal ashes with higher SiO₂ contents (at 51.2 and 46.7 mass%) and relatively lower Fe₂O₃ + CaO (12.8 and 13.4 mass%) were deposited at less than one third of the rate of the coal ash with SiO₂ content of 40.1 mass% and Fe₂O₃+CaO content of 21.3 mass%. This illustrates the significance of the role of the potentially strong fluxing components of the coal ash over the SiO₂ content of the ash in determining the deposition rate.

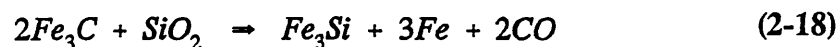
The silicate ash particles comprising the bulk of the deposits are by and large of a spherodised shape which is acquired through transformation of irregularly shaped particles passing through the boiler.^{44,84} These particles whether present in larger quantities as cenospheres, plerospheres (i.e large hollow spheres containing lots of smaller spheres) or just dense, solid spheres, or in much smaller quantities as dermaspheres and ferrospheres (i.e small, solid spheres containing large amounts of iron oxide as fine particles) will be the major "collectors" of various other mineral constituents of fly ash such as sulphates of sodium, potassium or calcium or pyrite particles which either diffuse through or reside and blend into the siliceous matrix to form the deposit agglomerate.⁸⁴

In Germany, studies⁸⁵ of the initiation of deposits from bituminous coals in stoker fired boilers provided evidence of reaction between SiO₂ and iron sulphides to form iron oxide and silicon sulphide (SiS₂) which was subsequently oxidised in the deposit to SiO₂, hence acting as the carrier of iron oxide to boiler tube surfaces.

Examination of slags formed in large industrial boilers burning Victorian brown coals from Australia revealed⁸⁶ that slags were formed only when silica in the form of sand or clay as part of the coal was introduced into the boiler units.

Alkali - alumino - silicates with inclusions of other oxides such as ferrous oxides were considered⁸⁷ to be the major reason for slag at the walls of the radiative section and glassy bridges between particles in the superheater and reheater regions of the highest temperature zones of the combustion chamber of a pulverised coal fired boiler.

Iron Oxides and Iron Pyrites - The effect of iron oxide on the expansion of molten ash droplets has been studied and it has been shown⁸⁸ that at least 5 mass% iron oxide should be contained in the ash if any significant quantities of cenospheres are to be produced in the flame zone of the boiler unit. The occurrence of hollow ash spheres, commonly known as "cenospheres", has been shown⁴⁴ to increase sharply with the iron oxide content of the molten fly ash, reaching its maximum when the iron oxide content of the ash comprised 9%⁸⁸ of the total mass of the ash. This increase is thought to be due to volatilisation of iron in the form of metal vapour or via formation of volatile iron carbide within the fly ash particles.⁴⁴ After deposition of carbide fly ash particles on the surface of boiler tubes and the gradual formation of deposit accretion, the iron carbide within the ash reacts with the SiO₂ to release carbon monoxide:^{44,72}



This catalytic effect of iron has further been observed⁸⁸ through evolution of residual gases such as carbon dioxide and nitrogen with traces of oxygen and carbon monoxide, when iron was added to silicate melts in the form of oxide or metal powder. However, ashes with higher than 20 mass% Fe₂O₃ have been found⁸⁹ to produce insignificant quantities of cenospheres. This is probably because the

iron-rich ashes have a low viscosity and the gas evolution is too rapid for the formation of stable cenospheres.

Such considerations are particularly justified in the case of stoker systems where relatively large quantities of unburned carbon are associated with the fly ash.

The results from operational units have indicated^{90,91} that iron oxides, FeO and/or Fe₂O₃ acting as fluxes to form low-melting glasses can also be an important factor in slagging of the heat exchanger surfaces. An approximate solubility limit of FeO in silicate ashes of different compositions has been expressed in the form of the following equation:⁹²

$$FeO_{SOL} = 1.2(SiO_2 - Al_2O_3) - 0.6(CaO + MgO + Na_2O + K_2O + TiO_2) \quad (2-19)$$

where;

FeO_{SOL} is the mass% solubility limit of iron oxide in slag.

(M_xO_y) is the mass% of the major oxides in the ash (e.g. SiO₂, K₂O).

Table 2-7⁹² gives the calculated solubility limits of FeO in bituminous coal ashes of differing composition. The difference between the FeO solubility limit, and the amount of iron oxide present in an ash as FeO, has been considered⁹² as a measure of the strength of the ash for developing an adhesive bond with the heat exchanging metal surfaces.

Furthermore, the catalytic effect of Fe₂O₃ on the conversion of SO₂ to SO₃ can influence the reactions of alkaline constituents in the ash. Iron oxide has been found in deposits in the form of iron alkali trisulphates. These are believed^{93,94} to have formed from the reaction between iron oxide and alkali sulphates present in the ash, thereby producing sticky ash particles which would further promote the corrosion

of the boiler tube surfaces. Figure 2-12³⁰ summarises the probable sequence of reactions involved in the formation of injurious iron-alkali-sulphate complexes in fouling deposits which leads to external corrosion of the tube surfaces by the trisulphate route below 650°C and by pyro-sulphates below 480°C, within the convective zones of a boiler unit.

In a non-oxidising atmosphere, molten residues of pyrites appeared to be the only coal mineral impurities that have an observable tendency for particle-to-particle bridging.⁷¹ This is helped by the low viscosity, probably below 10 N.s.m⁻² of the pyrite residue. According to the Frenkel equation⁷¹, this would give the time required for the formation of a degree of partial bonding at less than 1 ms. The low melting point liquids derived from pyrite minerals in the coal ash have been suggested^{53,90} as being instrumental in forming the first layer of deposit on boiler tube surfaces through either the formation of a eutectic of FeS and ferrous orthosilicate (Fe₂SiO₄) or by accelerated slagging through formation of a low melting temperature ferrous meta-silicate (FeSiO₃) compound.⁴⁶

The selective role of iron pyrites as an independent species of the ash in the promotion of slagging, by forming the initial layer of deposit, has been suggested by many workers^{43,47,95,96} based on observations of deposits formed on probes and heat exchanger tubes from furnace and convection zones near the furnace exit regions. In addition, microstructural examination of laboratory prepared deposits has shown⁵⁰ that porous iron sulphide droplets deformed on impact to give a consolidated deposit on an oxidised metal surface.

Table 2-7: Calculated solubility limit of FeO in coal-ash slags.⁹²

Ash number	Percent by mass							FeO		
	SiO ₂	Al ₂ O ₃	CaO	MgO	Na ₂ O	K ₂ O	TiO ₂	Solubility limit	Amount present	Difference
	1	50.7	34.1	1.7	1.7	0.3	1.8	1.2	15.9	6.8
2	48.6	28.0	3.4	1.9	1.9	3.1	1.0	17.9	8.1	9.8
3	43.6	24.6	7.7	2.9	0.7	2.2	1.0	14.1	11.3	2.8
4	42.2	28.1	4.3	1.1	0.9	1.7	0.8	11.6	15.0	-3.6
5	37.2	21.4	8.1	1.6	0.6	1.4	0.8	11.5	21.4	-9.9

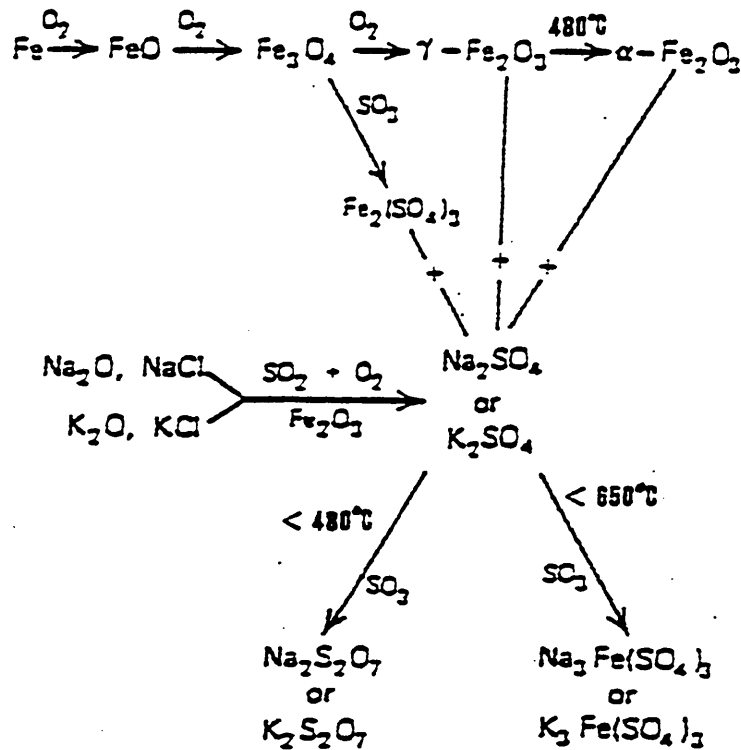


Figure 2-12: Reaction sequence of iron oxides and alkalis with sulphur oxides.³⁰

Sodium and Potassium Oxides - Sodium oxide can be considered as the principal promoter of corrosive ash formation and deposition in combustion systems. Sodium is mostly found in deposits as chloride (NaCl) or sulphate (Na_2SO_4), depending on temperature conditions at the collecting surface⁹³ as well as the chlorine content of the coal. These are invariably concentrated in the first layer of deposits forming a sticky layer adjacent to the boiler tube surface in the convective zones.^{93,97-99} Laboratory based investigations have shown^{22,100} that the deposition of sodium on the surface of thin silicate fly ash particles promotes the formation of sodium silicate. This would make the fly ash particle more sticky and therefore easier to adhere to boiler tube surfaces. Detailed examination of deposit and fly ash specimen from power station boilers has^{21,101,102} further shown a similar mechanism involved in the depositing ash over the surface of heat exchanger tubes.

In other studies²⁰ of boiler deposits which had caused severe corrosion of superheater tubes, a large proportion of complex sulphates of potassium-aluminium, potassium-iron and sodium-iron were found in the inner layer of deposits. Potassium sulphate having a higher temperature stability limit compared with that of sodium and calcium sulphates, can be preferentially transported across the ash deposit to the surface of cooled boiler tubes when there is a steep temperature gradient. The K_2SO_4 containing phase, when molten, can cause severe corrosion of tube metals.⁸⁴

In the absence of silicate ash, a typical value for the mass of sulphate fume ($\text{Na}_2\text{SO}_4 + \text{K}_2\text{SO}_4$) produced per unit mass of coal, for a series of coals of different volatile alkali-metal content, formed in pulverised coal fired boilers has been given as 0.4 with a typical value of the mean diameter of the sulphate fume particles being $0.12\mu\text{m}$.⁶⁹

Low fouling deposits usually contain less than 1.0 mass% sodium,¹⁰³ while ashes with more than 3 mass% sodium content are regarded as high fouling.

Calcium and Magnesium Oxide - The role of these oxides in the deposition of fly ash on boiler surfaces has not received much attention. Calcium, mostly found as sulphate, is frequently found in deposits, but it is considered¹⁰⁴ that the sulphate does not take part in the initial sintering process. However, this is dependent on the availability of calcium sulphate on the surface of fly ash particles, where it can inhibit the cohesion of fly ash particles. Conversely, the growth of crystalline CaSO_4 material inside the porous matrix of sintered ash may increase the strength of deposits. The presence of small amounts of calcium sulphate in sodium-rich ashes may enhance the rate of sintering, but in large concentrations it may retard the process of deposit formation.⁶⁹ Calcium sulphate has also been recognised as the bonding agent in the outer, bulky layer of deposits from Victorian brown coals.⁹⁵

It has been suggested⁸⁸ that the amount of calcium oxide in the ash may be influential in the tendency for the formation of cenospheres rather than dense ash particles, with higher calcium oxide contents favouring the latter. However, other investigations of the possibility that cenosphere production is limited by the quantity of calcium oxide in the ash has not established any correlation for different types of ash⁸⁹.

It has been shown¹⁰² that magnesium sulphate and calcium sulphate in the presence of alkali sulphates form low melting eutectics that might lead to serious fouling problems. Furthermore, calcium and magnesium are known to have an inhibiting effect on the formation of potassium and sodium iron trisulphates by formation of the more stable compounds of $\text{K}_2\text{Ca}_2(\text{SO}_4)_3$ and $\text{K}_2\text{Mg}_2(\text{SO}_4)_3$.¹⁰⁵

2.4.2 (b) The Influence of Flue Gas Composition on Deposition

The chemical composition of the flue gases in a boiler environment has been considered an important factor in determining the extent of sintering of fly ash and the subsequent

texture of deposits formed.¹⁰⁶ Invariably all flue gases contain major proportions of various chemical combinations of four elements; carbon, oxygen, hydrogen and nitrogen. In coals with significant quantities of chlorine and sulphur compounds, further gaseous compounds result when the coal is combusted creating a corrosive environment with high fouling potential.

Studies have shown^{106,107} that areas of superheater tubes and other heat receiving surfaces exhibiting high corrosion rates due to fouling within the combustion chamber, existed where high CO levels were present. The sulphur content of particulate matter was relatively higher in these areas than the areas which were depleted in CO and richer in oxygen.

In a study¹⁰⁸ of factors affecting the corrosion of boiler tubes, it has been suggested that when oxides of sulphur, carbon monoxide and steam are dissolved as gases in the fused slag at temperatures of approximately 1300-1700°C, their presence could facilitate the break down of the metal anions such as SiO_4^{4-} and SiO_3^{2-} , into SiO_2 and O^{2-} , hence enhancing the stability of silicate cohesion within the slag.

An investigation of the composition and origin of gas in ash cenospheres has shown⁸⁸ that CO_2 and N_2 were the main constituents of gas locked in the ash spheres with CO_2 being produced via dissociation of carbonates and combustion of carbonaceous matter.

2.4.2 (c) The Effect of Flue Gas Temperature on Deposition

The effect of temperature on the mineral matter as well as the flow properties of the coal ash, has already been discussed in sections 2.2.2 and 2.3.3 respectively. Of all the factors influencing deposition, temperature and composition of the coal ash are probably the most significant. The effect of increasing gas temperature has been found¹⁰³ to be very pronounced, indicated by a three-fold increase in the deposition

rate over the temperature range of 980°C to 1150°C.

A theoretical study of the effect of flame temperature on the surface temperature and thickness of deposits has been carried out.^{91,109} It was calculated that with a flame temperature of 1500°C, even an initial deposit of 0.5 mm would be enough to raise the surface temperature by 450°C whereas with a flame temperature of 1200°C, the same increase in surface temperature would not be achieved until a deposit layer of 1.2 mm was formed on the boiler tube. Similar observations on the degree of sintering and fusion of various coal ashes as a function of flue gas temperature have also been made.¹¹⁰

The importance of flue gas temperatures below 1000°C on the balance between the rate of deposition of fly ash and sodium sulphate in the ash and also the effect on the physical nature of deposits has also been investigated.¹¹¹ It was shown that at flue gas temperatures greater than 900°C, formation of hard deposits was increased. These observations have been confirmed by other workers.¹¹²

2.4.2 (d) The Effect of Boiler Design on Ash Deposition

Ash deposition in various boiler zones is an important factor to be considered in boiler design and operation. As explained earlier, the occurrence and severity of ash deposition depends largely on the coal ash composition and amount of coal ash, but can be strongly influenced by the method of firing, design of equipment, and the operating conditions.⁸² Some of the design considerations are shown in Table 2-8.

In practice, the design parameters and operating conditions are determined by the characteristics of the ash. For example if ash does not tend to form troublesome deposits, the furnace wall surface will require few, if any, sootblowers for cleaning. The boiler can be designed with deep banks of closely spaced superheater or reheater

Fuel characteristics

1. Properties of coal substances

- a. Physical, including density, hardness, specific heat, thermal expansion and thermal conductivity
- b. Chemical-behaviour during heating i.e. carbonization, gasification and combustion

Technological properties

1. Proximate analysis
2. Ultimate analysis
3. Free-swelling index
4. Differential thermal analysis
5. Thermogravimetric analysis
6. Effluent gas analysis
7. Grindability
8. Calorific value
9. Sieve analysis
10. Ignitability
11. Abrasiveness

2. Properties of coal ash

Determined by the concentration and type of minerals in the coal containing the following elements:

- | | |
|---------------|----------------------|
| a. Alkalies | e. Calcium-Magnesium |
| b. Sulphur | f. Iron |
| c. Chlorine | g. Silica |
| d. Phosphorus | h. Alumina |

Technical properties

1. Fusion temperature
2. Viscosity of slag
3. Surface tension of slag
4. Volatility of constituents in slag
5. Sintering temperature and strength of ash

Boiler design and operation

- | | |
|--|--------------------------------|
| 1. Firing method | 4. Combustion conditions |
| a. Slag tap, PC and cyclone | a. Excess air |
| b. Dry ash, PC | b. Air temperature |
| c. Fuel bed, chain-grate and spreader stoker | c. Load cycle |
| | d. Residence time |
| 2. Furnace design | 5. Properties of flue gases |
| a. rating | a. Temperature |
| b. Wall construction | b. Flow patterns |
| c. Type, number and arrangement of burners | c. Composition |
| d. Exit-gas temperature | |
| 3. Tube bank design | 6. Properties of entrained ash |
| a. Horizontal or vertical tubes | a. Dust loading |
| b. Spacing, side and back | b. Size consist |
| c. Depth of bank | c. Composition |
| d. Alignment | d. Microstructure |
| e. Freedom of tube movement | |

Sootblower design and operation

1. Blowing medium
 - a. Air or steam
 - b. Pressure
 - c. Temperature
2. Type of sootblower
 - a. Short retractable
 - b. Long retractable
 - c. Fixed position rotating
 - d. Travelling frame
3. Location and spacing of sootblowers
4. Sootblower nozzles
 - a. Type, size, number
 - b. Angle of attack
5. Lance-tube attack
 - a. Rotational
 - b. Axial
6. Frequency of operation

tubes located in high - gas - temperature zones. Relatively few sootblowers will be required and these can be operated at high speed, with small nozzles and low pressures. On the other hand, if the ash produces hard, massive deposits, the superheater and reheater tube banks must be designed to permit ease of deposit removal. For instance, lateral tube spacing is increased, tube bank depth is decreased and the banks are located in cooler gas temperature zones. Additional sootblowers, operating at maximum capability, may be required.⁸²

Further design considerations such as furnace dimension, burner location, heat input and width and arrangement of convective tube banks, with respect to the slagging of lower and upper furnace regions, have been adequately discussed elsewhere.^{113,114}

2.4.2 (e) The Effect of Boiler Operation on Ash Deposition

Boiler operating conditions can significantly effect deposition. Some of the operating factors that have been studied^{82,52} are:

- Excess air requirements
- Firing method
- Gas/tube temperature
- Selection and blending of coal
- Humidification of combustion air
- Mixing of flue gases with combustion air
- Compound firing of pulverized coal over stoker fuel beds
- Operating within loading capacity
- Cleaning of the heat receiving boiler tube surfaces at regular intervals either by using additives or by soot blowing of these surfaces.

2.4.3 The Mechanism of Ash Deposition

2.4.3 (a) Formation and Accumulation of Coal Ash on Boiler Tube surfaces

Three types of ash species have been identified¹⁰³ in the flue gas stream in boiler units:

- (1) The relatively physically unaltered extraneous inorganic matter such as quartz, kaolinite and iron pyrites which undergo further oxidation.
- (2) The coalesced or agglomerated ash particles formed largely from the less volatile inherent inorganic ash made up of calcium, magnesium, aluminium and iron compounds. Small extraneous silica particles may serve as condensation nuclei for these agglomerates.
- (3) Sodium, potassium and sulphur compounds derived from organically bound volatile constituents of ash.

Similar categorisation of the particulate matter in fly ash has been made in other studies.¹¹⁵ It has been proposed that the formation of particulate matter takes place in three different ways:

- (i) By transportation of solid particles of inorganic ash with the flue gas up through the boiler unit.
- (ii) By volatilisation of portions of the ash and their subsequent transportation with the flue gas. The volatilised particulate matter thus formed is the product of condensation of vaporised inorganic constituents, such as SiO. On reaching the lower temperature zones of the boiler unit, some degree of reaction can occur between these particles. The products of these condensation processes generally form very small fly ash particles.
- (iii) By reaction of metal oxides such as Na₂O and K₂O in the ash with condensed sulphuric acid in the lower temperature zones of the boiler unit.

Figure 2-13¹¹⁶ gives a simplified view of the evolution of the inorganic ash components of fly ash during coal particle combustion.

In a comprehensive study by CEGB workers,¹¹⁷ of the inhomogeneity of a wide range of bituminous coals heated in air, it was observed that the coal particles consistently formed ash particulates of four main types. These were described as:

- (a). "solid" particles, retaining the original irregular shape of the particles of coal;
- (b). thin-walled, hollow cenospheres (balloon type);
- (c). "lacey" cenospheres with intricate internal partitions;
- (d). thick-walled cenospheres.

The ash derived from the inherent and extraneous mineral matter within the burning char substance are released as particles of varying size and composition, as the coal is burnt in the furnace region of a mechanical stoker or pulverised fuel burner within a boiler unit. In mechanical stokers the majority of particles are from 1 to 150 μm in size with some solid particles up to 300 μm and a few hollow particles even larger. In pulverised fuel units, there are very few particles outside the range of 1 to 120 μm .⁴²

Studies relating the morphology of the evolved ash particles to their size ranges have demonstrated¹¹⁸ that whereas the relative abundance of amorphous, vesicular and cenospherical ash particles decreased with decreasing ash particle size, the abundance of solid, non-opaque spherical ash particles increased with decreasing particle size.

Variations in the structure and morphology of ash matter have been observed and catalogued¹⁶ with the proportion of various ash particle types depending on the origin of the coal. These studies have described the heterogeneity and structural complexity of coal fly ash in great detail. In other studies^{111,119} spherical particles of

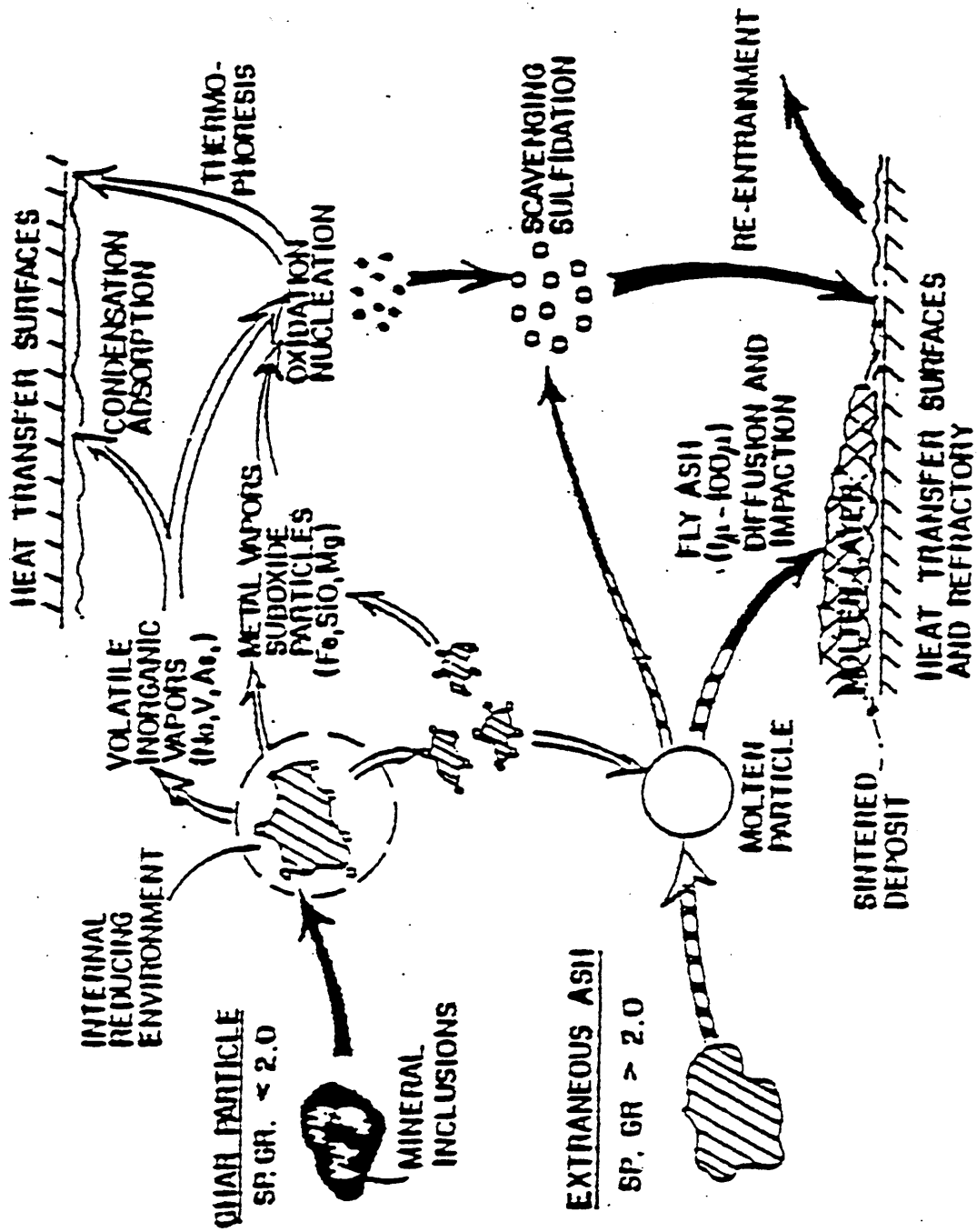


Figure 2-13: The evolution of fly-ash during coal particle combustion. 16

various shapes, sizes, mass and colour were found to be the most dominant structures in sampled deposits from boilers. Other studies^{88,89,120} have exclusively dealt with the formation of solid ash spheres and cenospheres.

Accumulation of fly ash particles on boiler surfaces involves at least four physical processes:^{102,121}

(1). ***Inertial impaction*** - This is the dominant mechanism in transporting flue gas particles with a threshold size of about $5\ \mu\text{m}$ in diameter to boiler tubes. At typical flue gas velocities between 10 to $25\ \text{m}\cdot\text{s}^{-1}$ in pulverised and other conventional coal fired boilers, the particles above about $10\ \mu\text{m}$ in diameter have kinetic energy in excess of what can be dissipated at impaction on clean tube surfaces, resulting in their re-entrainment in the flue gas.⁸⁴

(2). ***Brownian motion (particle diffusion)***-This mechanism may account for deposition of some fume particles below $0.1\ \mu\text{m}$ in diameter. It has been suggested¹²² that sulphate particles in the boundary layer of flue gas surrounding a cooled target as well as a small mass fraction of silicate ash in the form of fume can be deposited via this mechanism.

(3). ***Molecular (vapour) diffusion*** - Flame volatilised species chiefly Na_2SO_4 , K_2SO_4 , are deposited on cooler boiler tubes as condensable salts. This could account for over 50 mass% of the total of these sulphates,⁸⁴ the remainder being carried onto the surface of the tubes by the silicate fume particles. This is believed to be a more significant transport mechanism than particle diffusion.

(4). ***Thermophoresic (eddy) and electrophoresic diffusion*** - These mechanisms are likely to have a marked influence in cooled boiler tubes. Thermophoresis is the particle movement resulting from a heat flux¹²¹. This is particularly relevant in the

initial stages of deposit formation, when the surface temperature of a clean boiler tube is around 430°C and that of the flame exceeds 1430°C⁸⁴.

As all heat transfer and combustion systems contain areas of high thermal gradients, this form of particle deposition is very significant. Conversely, if the combustion gases are being heated, deposition due to thermophoretic effects will be negligible. Electrophoretic diffusion is responsible for the preferential deposition of ash particles of comparatively high conductivity. The electrostatic charge is acquired by the moving particles in the flue gas as a result of flame ionization or the frictional forces on particle collision. The silicate ash surface, enriched by alkalies and iron oxide particles are partly deposited via this mechanism.⁸⁴

An overall schematic representation of the formation and deposition of coal fly ash particles through various physical processes, as discussed previously, is depicted in Figure 2-13.¹¹⁶

It is believed that as the size of ash particles increase, the process of accumulation changes from (4) to (1) above. However, the combined effects of deposition mechanisms (1)-(4) are most conducive to the deposition of 0.1 to 10 μm fly ash particles on boiler tubes.

In the initial stages of deposition the formation of an adhesive bond involves two stages; wetting and then bonding. Wetting involves the viscous flow processes required to bring the possible liquid phases of the ash in contact with the solid surface.¹²³ The rate of wetting is determined by the interfacial energy of both the liquid and solid, the viscosity of the liquid, and the roughness of the solid surface. Bonding may involve either the formation of a chemical, physical or electrostatic bonds at the interface.⁹⁴ The area of contact required between a depositing fly ash particle and a tube to prevent

detachment of the particle under the influence of gravity, its tendency to rebound on impaction, and its ability to resist detachment due to abrasion by other fly ash particles depends on various factors. These include the mass of the particle, its velocity at the time of impaction, its surface tension, its affinity for the metal oxide and other factors relating to viscoelastic properties of the particle. When the particle impacts onto a deposit layer already formed on the tube, its retention will also be determined by the condition of the deposit surface, especially with respect to any liquid phases present.²²

A strength of 10 kN.m^{-2} is regarded as just sufficient to withstand sootblower action. At the adhesive bond strength of 100 kN.m^{-2} , a 500 mm length of boiler tube could support a 10 kg mass of slag deposit.¹²⁴

2.4.3 (b) Sintering and Coalescence of Coal Ash

The term "sintering" is variously defined and it can connect either individual or compound processes of bonding, densification and / or recrystallisation. However in general terms it is the extension of the contact area between powder particles in the solid state, by the transport of material across or around pores, under appropriate conditions of time, temperature, pressure and atmosphere.¹²⁵ The driving force in the sintering process is the reduction in the surface energy by decreasing the surface area. There are four possible mechanisms: 1) viscous flow, 2) vapour condensation, 3) surface diffusion and 4) volume diffusion.¹²⁵⁻¹²⁹

The process of sintering by viscous flow is believed¹²⁶ to play a dominant role in the formation of deposits in coal fired boilers. It has been suggested¹³⁰ that sintering by viscous flow can occur via two mechanisms:

- densification governed by shrinkage of large pores with a sufficient excess of liquid phase to fill initial porosity.

- densification with an abundance of a liquid phase allowing for complete filling of the pore spaces.

The dominance of one mechanism over the other is dictated by temperature and chemical composition of the liquid phase. In order to quantify the sintering process, a model that describes the rate of coalescence of particles, in terms of measurable parameters, has been developed.¹³¹ The growth of the interface between two spherical particles or a particle and a semi-infinite body as shown in Figure 2-14 is thus defined:

$$x^2 = \frac{3r\gamma t}{2\eta} \quad (2-20)$$

where;

x = radius of interface assumed to be circular
r = radius of the spherical particle
 γ = surface tension
t = time
 η = viscosity

Rearranging equation (2-20) in terms of "x/r" and "t", it becomes:¹²⁶

$$\frac{x}{r} = 1.225 \left(\frac{\gamma}{\eta r}\right)^{\frac{1}{2}} t^{\frac{1}{2}} \quad (2-21)$$

This equation is applicable when $x/r < 0.3$.

The ratio x/r can be used to characterise stages in the sintering of ash deposits on boiler tubes, as shown in Table 2-9¹²⁶ from the initial contact between the particles to the formation of fused slag where the shape of initial constituent particles is no longer distinguishable.

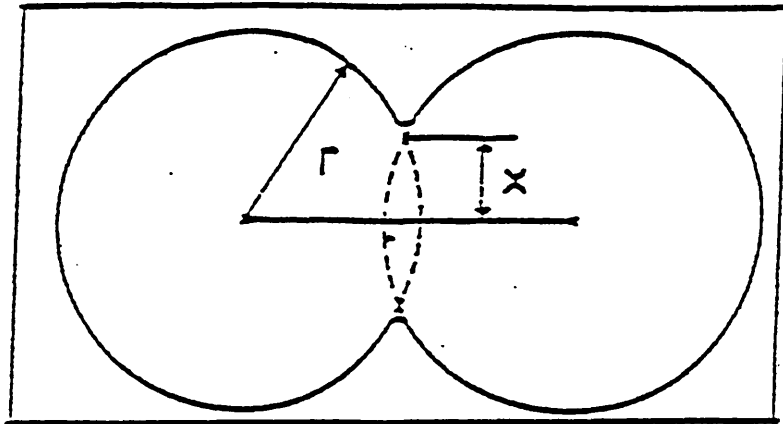


Figure 2-14: The initial stage of sintering - Frenkel's two particle model.^{47,123}

Table 2-9: Degree of sintering based on the ratio of neck bond radius to particle radius (x/r).¹²⁶

Value of x/r	Degree of sintering	Comment
0.001	Onset of sintering	The deposit of this degree of sintering on boiler tubes has no significant cohesive strength and would probably fall off under the action of gravity and boiler vibration.
0.01	Slightly sintered matrix	The deposit on boiler tubes would probably be removed by soot blowing.
0.1	Strongly sintered deposit	The deposit on boiler tubes would be difficult to remove by soot blowing.
>0.3	Slagging	The ash particles lose their original identity and the deposit on boiler tubes cannot be removed by soot blowing.

The sintering characteristics of coal ash are effected by many factors such as the chemical composition of the ash, the nature of minerals in the original coal, the time-temperature history during combustion of the coal, the atmosphere, temperature and the time during which the ash particles are in contact with each other on a heat receiving surface.

Although the complexity of coal ash systems makes it difficult to relate composition to sintering tendency, the alkali content of the coal has been shown¹³² to correlate well with sinter strength. In a similar study¹³³ the effect of iron oxide and water soluble alkalis on the temperatures corresponding to the maximum expansion on heating of precipitator ashes was examined. It was shown that this temperature was lowered by increasing the iron oxide content of an ash and increased by reducing the soluble alkalis present in the ash.

Changes in the iron oxide content and silica ratio of coal ash have been used¹²⁴ as indices for a range of temperatures indicative of slow (10 hours), rapid (2-3 minutes) and very rapid (1 second) sintering processes.

2.4.3 (c) Formation of Monolithic and Layer - structured Deposits

By far the most widely investigated feature in ash deposition is the formation of "layer-structured" deposits. These are often encountered with high alkali and sulphur coals.

Figures 2-5¹⁵ and 2-15⁹⁹ are the schematic representations of the variations in the form, thickness and the role of alkali-sulphates in the formation of layers of ash depositing on boiler tube surfaces. In the first investigation¹³⁴ of these type of deposits, it was concluded that the mechanism whereby these deposits are formed is as follows:

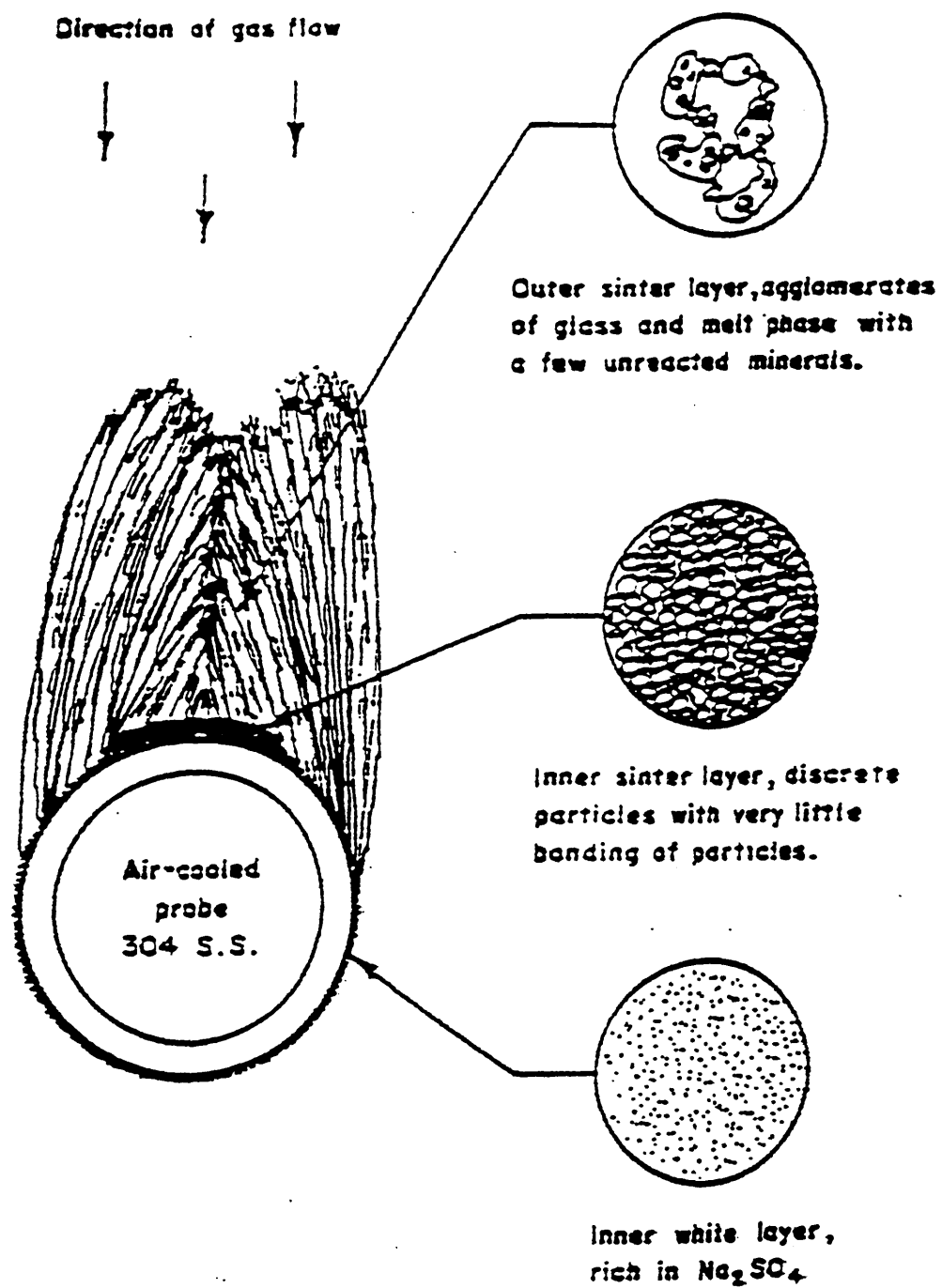


Figure 2-15: Physical structure of a typical deposit from burning a highly fouling coal.⁹⁹

1. Loose unbonded fly ash accumulates on the tube surface.
2. Alkali compounds in this deposit form alkali sulphates by a reaction with SO_3 in the deposit. The SO_3 may have originated in the flue gas stream and/or has been formed from the catalytic oxidation of sulphite by another oxide such as Fe_2O_3 , in the ash deposit (see Figure 2-12).
3. The deposit nearest the tube metal continuously becomes enriched with SO_3 until a major portion of the alkali compounds are converted to sulphates. Up to this point there has been no formation of a "white inner layer".
4. In the presence of alkali sulphates, the red iron oxide (Fe_2O_3) and SO_3 react to form alkali iron sulphates $\text{Na}_3\text{Fe}(\text{SO}_4)_3$ and $\text{K}_3\text{Fe}(\text{SO}_4)_3$, in a layer immediately next to the tube. This is white or yellow-white in colour.
5. In the presence of alkali sulphates, the alkali iron and alkali aluminium sulphates form low melting point phases which soften at the tube metal temperatures and form a tightly adherent bond to the tube metal.
6. Both the inner and the outer layers of the deposit increase in thickness, so that the temperature of the outer layer is raised and sintering occurs.
7. The surface temperature of the deposit ultimately becomes high enough to melt the alkali sulphates capturing more fly ash and thus accelerating the rate of deposit build up. In the higher temperature regions, alkali silicates, aluminium silicates as well as other complex oxides of silicon, aluminium, iron, sodium and potassium can form, producing strong fused, glassy outer layers.

One of the principal reasons for the formation of layer-structured deposit in coal fired boilers is that the chief constituents of ash, namely silicates and sulphates such as alkali-metal and calcium sulphates, are immiscible.⁸⁴

Investigations carried out by other researchers^{99,135} burning high-fouling coals, have established similar mechanisms, whereby three distinct layers, namely; "inner white layer", "inner sinter layer" and "outer sinter layer", which differed in physical character but had similar chemical analysis, were formed. In another study⁹² the role of iron oxide in forming layered deposits on the surface of superheater and reheater tubes with different physical as well as chemical characters has been recognised. Other studies^{86,97,103} have only identified two layers as inner and outer layers. Figure 2-15⁹⁹ shows the various layers as they are progressively formed on a boiler tube.

2.5 ADDITIVES

2.5.1 Additives In Coal-Based Power Generation

The treatment of fuels by addition of certain chemicals directly or indirectly to the fuel or fuel ash, has been tried since corrosion and deposits first became a problem in industrial and utility boilers. However, chemical additives are just one amongst nine potentially applicable techniques for controlling slagging, fouling and corrosion in coal-fired boilers. These techniques are briefly summarised in Table 2-10¹³⁶ along with some of the economic considerations in choosing between them.

The range of chemicals and minerals which have been employed in order to assist in addressing the various fireside problems is quite diverse. Some perception of this diversity can be gained from Table 2-11¹³⁷ which classifies additives by physical form as well as chemical ingredient.

Generally there are four main reasons for using additives:¹³⁸

- To minimise catalytic formation of SO₃ on hot surfaces.
- To prevent formation of corrosive substances on heat receiving surfaces (high temperature corrosion).

Table 2-10: Considerations in choosing various techniques for controlling slag and corrosion.¹³⁶

<u>Techniques</u>	<u>Considerations</u>
Drop boiler load.	Costly if load demand requires use of less efficient generation.
Reduce flame temperature by increasing excess air or by flue gas recirculation.	Hurts thermal efficiency, increase erosion.
Increase frequency of soot blowing.	Increase tube erosion and operation expences.
Add more soot blowers or water blowers.	Increases capital investment and operating cost.
Switch to clean or blended fuels.	Increases cost of alternate fuel or blending expense. Cleaning coal may aid or worsen problems.
Grind coal more finely.	Increases mill capacity requirement, causes higher operating expense.
Boiler modification.	Increases capital cost.
Closely monitor combustion system maintenance/operation.	Increases maintenance cost.
Chemical additives.	Evolving technology, continuing cost may require small investment for feed equipment. Feed method, location and frequency are important.

Table 2-11: Physical form of oil and coal additive chemicals.¹³⁷

Chemical	Powder	Form		Emulsions	Gas
		Dispersions oil	Water		
Magnesium oxide	x	x			
Magnesium hydroxide	x	x	x		
Aluminium trihydrate		x			
Manganous oxide	x	x			
Limestone, dolomite	x	x	x		
Water-soluble metal salts Mg, Mn, Cr, Ba, Si, Fe	x	x	x		
oil-soluble metal salts Mg, Mn, Cr, Ba, Si, Fe		x	x	x	
Ammonia					x
Rare earth oxides	x	x			
Silica	x	x			
Vermiculite	x				
Sulphur trioxide					x
Borates	x				
Amines			x		
Copper oxychloride	x	x			

- To decrease the sintering tendency of high-temperature deposits.
- To neutralise acids normally condensing on cool surfaces.

In oil-fired boilers, additives have been used for many decades, mainly to prevent corrosion on the cooler parts of the system. The extent of their use to date, is a measure of their success which has been proven and accepted for many years.

A number of studies concerned with the use of magnesia, the most widely used additive in oil-fired boilers have been carried out. In a comprehensive review¹³⁸, the role of magnesia along with some of the more frequently used additives in oil firing has been considered.

In coal fired boilers, the use of additives has by no means been as extensive as with oil-firing and chemicals have mostly been used to deal with the waterside of the boilers, ignoring the potential benefits of fireside chemical treatment. The main reason for this seems to originate from the higher ash content of the coal (at 10% or greater) compared with the ash content of oil (at around 0.1%). Thus, with nearly one hundred times greater solid burden in the flue gas relatively larger quantities of additive (from 0.4 to 3 mass% of the coal burned compared with 0.025 mass% for oil)^{132,139} have been required to have any significant effect on ash deposition. This makes the application of additives to coal-firing uneconomical.

Some studies^{140,141} have however suggested that it is sometimes possible to use chemical treatment effectively to inhibit deposit build ups in coal-fired boilers. Trials carried out during the early 1970's,¹⁴² employing fine particle size MgO dispersion in pulverized coal fired boilers burning widely different kinds of coal yielded a reduction in deposits at very low treatment rates, 0.015 mass% or less.

In addition to magnesia which is probably the most widely used additive, dolomite and limestone are also frequently used with pulverized fuel slag-tap furnaces to lower the viscosity of the slag.^{96,143}

In the early 1960's the use of copper oxychloride to control slag formation was introduced as a relatively cheap, easy to use and readily available additive.¹⁴⁴ By the early 1970's application of small amounts of copper oxychloride directly to the coal being burnt at over twenty five power stations in England and Wales,¹⁴⁵ mostly utilising chain-grate systems, to combat slagging, produced results varying from marked improvement to marginal or no improvement. The only ineffective use of copper oxychloride was associated with the power station burning a coal with a high alkali content. The cost of this treatment was usually between 0.1 and 0.3 pence per tonne of coal.

Investigations of the effective use of additive mixtures to combat high temperature corrosion and fouling of heat exchange surfaces showed that mixtures of magnesia-alumina and magnesia-silica¹⁴⁶ as well as silica-antimony¹⁴⁷ at various compositions performed satisfactorily by forming friable, high-melting products under laboratory and furnace conditions.

The choice of any additive used is governed by the particular desired changes in slag properties (e.g. more fluid or more powdery) and fuel ash chemistry, coupled with cost effectiveness, ease of handling/addition and any side effects.

Tables 2-12, 2-13¹³⁶ and 2-14¹⁴⁸ provide an overview of the range of additives most widely used for controlling and alleviating slagging and corrosion on dry-bottom boilers and on wet-bottom boilers and fouling of the convective passages of coal-fired boilers, respectively.

Table 2-12: Additives for control of slagging and corrosion on P.F dry-bottom boilers.¹³⁶

<u>Additive Type^a and form</u>	<u>Treatment Rate</u>		<u>Treatment cost</u>	<u>Remarks</u>
	<u>ppm</u>	<u>lb/ton coal</u>	<u>\$/ton coal</u>	
HIGH RANK COAL				
Copper oxychloride powder	2-6	0.004-0.012	0.006-0.018	(1)
Magnesium oxide water slurry	50-70	0.11-0.15 ^b	0.05-0.075	(2)
oil slurry	500-900	1.1 - 1.8 ^b	0.40-0.90	
Manganese organic oil solution	22	0.04	0.20	(3)
Limestone fine powder	c	400	c	(4)
LOW RANK COAL				
Limestone gravel	500-1500	1-3	0.03-0.09	(5)
Magnesium oxide oil slurry	100-160	0.2-0.33	0.075-0.12	
Copper oxychloride diluted powder	5-50 ^d	^d	0.20-1.00	(6)

^a In order of suggested consideration by fuel class.

^b Pounds of MgO fed in proprietary slurries which typically weigh 1.5 to 2.0 times the numbers shown.

^c Not meaningful.

^d Equivalent copper oxychloride.

- (1) Rate based on current utility practice.
- (2) Applied only to the 15-20% of furnace surface that slags.
- (3) Only good data is on a cyclone furnace.
- (4) Aimed at SO_x control; slagging is secondary benefit.
- (5) Not effective on cyclone-fired units.
- (6) In a proprietary additive, costs are high compared to the pure copper oxychloride because of the accompanying inert or other active ingredients, service, and benefit for the additive vendor.

Table 2-13: Additives for controlling slag fluidity on wet-bottom P.F boilers.¹³⁶

Additive Type and form	Treatment Rate Continuous Feed lb/ton	Treatment Cost \$/ton	Feed Point
Limestone ^a gravel	1 to 200	0.01 to 1.00	Coal mill
Boron minerals ^b Granular	1 to 10	0.18 to 0.80	Coal mill
Mill scale powder	per test	Negligible ^c	Coal mill
Sodium compounds ^d	per test	^e	Coal mill

^a Dolomite or waste calcium products are alternates.

^b variety of boron minerals are effective.

^c Waste from steel making is potentially very low cost.

^d Can cause fouling problems; sodium bearing wastes offer low costs.

^e Cost dependent on additive source and treatment rate, which are best determined by test.

Table 2-14: Additives for controlling convective pass fouling and corrosion on coal-fired boilers.¹⁴⁸

<u>Additive Type and Form</u>	<u>Feed Point</u>	<u>Feed Method</u>	<u>Treatment Rate lb/ton coal</u>	<u>Treatment Cost \$/ton coal</u>
HIGH-RANK COAL				
MgO powder	Burner	Intermittent	0.33	0.04
Mg(OH) ₂ water dispersion	Furnace outlet	Continuous	0.26 ^a	0.20
Vermiculite powder	Furnace outlet	Continuous	0.6 to 2.0	0.03 to 0.10
CaO-Limestone powder	Coal mill	Continuous	20	0.60
CaCl ₂ solution	On coal	Continuous	0.2 to 7.0 ^a	0.02 to 0.56
Clay-Kaolin powder	Lower furnace	Continuous	7.5	0.25
Mn-Organic solution	Burners	Continuous	0.04 ^a	0.20
LOW-RANK COAL				
CaO-Limestone powder	Coal mill	Continuous	1.0 to 1.5	0.07 to 0.15
Vermiculite powder	Furnace outlet	Continuous	1.0 to 4.0	0.07 to 0.25
MgO-oil dispersion	Burner	Continuous	0.3 to 0.6 ^a	0.15 to 0.30

^a Pounds of active ingredient contained in the additive compound per ton of coal.

2.5.2 Implication of the Use of Additives

2.5.2 (a) Increased Flexibility and Efficiency in Fuel Selection

In most cases of boiler slagging, the cause can be traced back to particular coals with low ash fusion temperatures, to specific variations in the boiler operation or to some other features of boiler design. Since the formation of deposits is very much a function of reactions between the coal ash minerals, any variations in the nature and type of coal used can exaggerate any existing fouling and slagging problems with inevitable cost penalties incurred.

In addition to the significant expenses and time involved in fuel evaluation and in negotiating new supply contracts, the fuel related options are also likely to result in increased shipping cost since proximity to the mine normally is a criterion for initial selection of fuel. Furthermore, if cleaning or blending of the selected fuel is needed, the as-fired expenses will increase significantly.¹³⁶

In addition to a wide range of troublesome coals liable to cause slagging, the inhibition of external fouling and slagging in a peat-fired chain-grate stoker, through the use of copper salts, has further been reported.^{145,149}

Effective use of magnesia on a few selected lignitic, sub-bituminous and bituminous coals burnt in various industrial boilers has been demonstrated.¹⁵⁰

Coals from the Western USA, which included a range of sub-bituminous and lignitic fuels, containing large quantities (10 - 30 mass%) of CaO with substantial sodium levels were successfully fired using additional limestone as an additive.¹⁵¹

Cleaner convection passes will allow a reduction in excess air levels; each 1% reduction being equivalent to an increase in efficiency of about 0.05%.¹⁵⁰

In a number of studies concerned with the catalytic effect of some proprietary metallic compound (DG-807) used in different types of stoker boiler systems, boiler efficiency gains of 1.25%¹⁵² to 1.7%⁹ via lower excess air and carbon losses in fly ash were achieved. The treatment rates of additive added onto coal varied between 80-365 ppm of coal. In another similar study¹⁵³ steam generation increased by 6.1% per tonne of coal burnt as well as an 18% reduction in excess air requirements and additional reduction of unburnt carbon and deposits were realised.

Efficiency gains of up to 4.5% for precipitator performance have been reported¹⁵⁴ through injection of a magnesia solutions (liquimag) into a pulverised coal fired boiler. Other workers¹⁵⁵ have reported gains of between 15-30% in collection efficiency of precipitators through conditioning of fly ash with a range of additives at a concentration of 50 ppm.

2.5.2 (b) Lower cost boiler operation

Additives can offer a rapid solution to slagging and corrosion problems with minimum capital investment and acceptable operating costs.^{136,145,148,172}

Injection of minor quantities of magnesia into the superheater area on boilers firing both high and low fouling coals has resulted in cleaner convection surfaces which would result in an increase in superheater temperatures hence increasing thermal cycle efficiency of power generation. Consequently boilers can be designed for higher heat releases and/or higher steam temperatures. Other cost related activities and factors which can lower capital and operating costs are:^{150,156}

- Boiler shutdown time,
- Reduction in heat transfer and loss in efficiency,
- Metal damage and cost of replacement of tubes,

- Cleaning and lower rating of units resulting in loss of power output capacity,
- Dependability

2.5.2 (c) Reduction in Acid Smut, SO₃ and Fly Ash Emission

Acid smuts are effectively the entrained agglomerates of condensed sulphuric acid in combination with sticky carbonaceous and particulate matter of the ash. These can contain up to 50% H₂SO₄ and therefore environmentally it is imperative to capture these injurious particles before release into the atmosphere.

Injection of magnesium hydroxide and a mixture of magnesium oxide and sodium bicarbonate in a 500 MW boiler have been shown¹⁵⁷ to reduce the free acidity of deposits to a level which would be unlikely to cause an acid smut problem. In the same study the overall amount of smut in the flue gases at the top and bottom of the stack was greatly reduced after long term trials with magnesium hydroxide and sodium bicarbonate injection.

Generally materials effective in reducing SO₃ levels in flue gases can be classified into three main groups:⁵²

- (1) Materials that physically absorb SO₃, such as silica or carbon.
- (2) Materials that combine preferentially with the atomic oxygen in the flame zone or which promote recombination of the oxygen atoms with consequent inhibition of the reaction:



Carbon tetrachloride and tetraethyl lead are examples of this category of additive.

- (3) Materials that combine with SO₃ to form non-corrosive compounds, which are carried away in the stack gases. Compounds of magnesium fall into this category.

Three mechanisms have been suggested as being influential in reducing soot emissions:¹⁵¹

- Ionization effects, which reduce coagulation of soot particles into large agglomerations. Na, K, Cs, Ba as elements are believed to act in this way.
- Promotion of oxidizing radicals such as OH[•]. Ba, Ca, Sr compounds are believed to be OH[•] promoters.
- Oxidation catalysis: Mn, Fe, Co, Ni are recognised catalysts, along with many other metals.

Additives are also gradually being accepted as tools for enhancing precipitator performance. The characteristics of the fly ash greatly influence the efficiency with which an electrostatic precipitator (ESP) can collect fly ash. The most notable of these characteristics, is the electrical resistivity of the fly ash, which controls the rate at which the electrical charges placed on the fly ash particles by the ionising wires can be caught by the collecting plates of the precipitator. This is considered to be directly related to the neutralising effect of additives. Additives such as MgO or CaO help to neutralise the SO₃ and Na₂O levels in the flue gas which lowers the electrical resistivity and therefore reduces the efficiency of the collection process.¹⁵⁸

2.5.3 Magnesium Compounds and their Effect on the Ash Deposition Process

Magnesium oxide (MgO) is a hygroscopic powder, usually supplied as a fuel additive with a size range such that 98% passes through a 325 mesh sieve (44 μm). MgO is produced by calcining either mineral magnesite (MgCO₃) or magnesium hydroxide (Mg(OH)₂) which has been precipitated from magnesium chloride contained in brine or sea water.¹³⁷ The reactivity of magnesium oxide and hydroxide is a function of the time-temperature history during calcination, thermal exposure in the boiler, the surface

area, particle size and agglomeration state of the powder.^{14,142}

Magnesium oxide and hydroxide have been successful in treating fireside problems, deposits and fouling problems, as well as high-temperature and low-temperature corrosion in all types of coal-fired boilers.^{142,150,159,160}

The form in which the magnesium based additives have been applied whether as a powder or a water/oil based solution, is very much dependent on the particular type of boiler, the feeding position, the mode of firing, the nature of the dominating problems and the relevant economics.^{136,137} Table 2-15¹³⁶ and Table 2-16¹⁶¹ highlight some of the factors mentioned here, involved in utilising magnesium oxide, hydroxide or its compounds as additives for different coal fired boilers. A number of other additives have also been included in Table 2-15 for comparison.

When fine particulate magnesium oxide is injected separately from the coal, it yields a "base" which seems to be more available chemically than the far larger quantities (ten to thirty times as much) of alkaline materials in the coal ash. The naturally occurring alkaline earth material in the coal ash is present as a silicate which would render it "unreactive".¹⁵⁰

When introduced into the boiler atmosphere, magnesia can act as a "scavenger" by contacting and absorbing SO_3 in the combustion gases. The resultant reaction produces the high melting point compound, magnesium sulphate.^{142,146,150,151}



Removal of sulphur trioxide in this way, reduces not only the amount of sulphur available for condensation on the surface of silicate ash particles in the flue gases but also restricts the amount of low melting point sodium and potassium sulphates,

Table 2-15: Methods of feeding additives to P.F coal-fired boilers.¹³⁶

<u>Additive Type and Form</u>	<u>Feed Point</u>	<u>Method</u>	<u>Capital Investment</u>	<u>Labour Intensive</u>
<u>Dry-Bottom Boilers - High Rank Coal</u>				
Copper oxychloride powder	Coal mill	Intermittent	Negligible	No
Magnesium oxide water slurry	Sprayed on furnace wall	Continuous	Minor	Yes
oil slurry	furnace injection	Continuous	Modest	No
Manganese organic oil solution	Special burner	Continuous	Modest	No
Limestone fine powder	Furnace injection	Continuous	Significant	No
<u>Dry-Bottom Boilers - Low Rank Coal</u>				
Limestone gravel	Coal mill	Intermittent	Significant	No
Magnesium oxide oil slurry	Ignitors	Continuous	Modest	No
Copper oxychloride diluted powder	Coal bunkers	Continuous	Modest	Yes
<u>Wet-Bottom Boilers</u>				
Limestone gravel	Coal crusher	Continuous	Significant	No
Boron minerals granular	Coal crusher Slag tap	Continuous As needed	Significant Modest	No Yes
Mill scale powder	Coal crusher	Continuous	Significant	No
Sodium compounds Various	Coal crusher	Continuous	Significant	No

Table 2-16: Characteristic comparison of various types of magnesium fuel additives.¹⁶¹

Comparing Key Characteristics of Various Types of Magnesium Fuel Additives

Characteristic	Soluble	oil or water dispersions	Powders
Class example	Magnesium sulphonate	MgO or Mg(OH) ₂ suspended in light oil or water	MgO, MgCO ₃ , Mg(OH) ₂
Typical concentration active metal (%)	8 to 10	19 to 42	28 to 58
Purchase cost, (\$/lbMg)	Very high 8 to 10	Moderate to high 0.47 to 4.17	Low, 0.18 to 1.25
Freight/unit Mg cost	High	Moderate	Low
Handling and feeding	Meter into furnace	Meter into furnace	Powder feeder to boiler
Feed system investment	Low	Low	High
Effective particle size	<0.1 μ m	0.7 to 2.0 μ m	20 μ m
Typical dosage for high-temperature corrosion and deposits (lbs Mg / ton coal)	NR ¹	0.06 to 1.2	0.6 to 5.0
Control of acid and plume	Very good	Fair	Some help
Shelf life	Excellent	Poor to excellent depending on manufacture	Good, protect from moisture

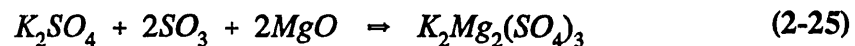
(1) Not recommended.

which can form the initial sticky layer on heat receiving surfaces.^{108,150,151,162} However, it has been reported¹⁶³ that the reactivity of MgO decreases above 970°C, due to a sharp reduction in the "reactive" surface due to the formation of non-porous crystalloids. However, in another study¹³⁸ it has been claimed that the scavenging effect of MgO is not as important as its coating of the otherwise receptive tube surfaces with a thin layer of inactive MgO thus preventing the adhesion of sticky ash particles.

Formation of low melting point alkaline iron trisulphates has been shown^{138,142} to be inhibited, due to the fact that magnesium oxide reacts faster than iron oxide in the coal ash to produce more stable complexes with alkaline sulphates such as $\text{Na}_2\text{Mg}_4(\text{SO}_4)_4$:



In the absence of iron oxide, other researchers^{94,105} have suggested that MgO can form complex systems with potassium and sodium sulphates, e.g.:



In a similar study,¹⁶⁴ it was concluded that the magnesium oxide additive reduced corrosion rates by preventing the formation of a molten phase in the inner layer of deposits.

The main advantage of using magnesium oxide or hydroxide injection is probably the change in the character of deposits which form on superheater tubes. Without the additive, the deposits are very dark and extremely difficult to remove. With additive

the deposits are soft, friable and lightly bonded to the tubes. They are reddish brown and can be easily brushed from the tubes.¹⁶⁵ Similar observations have been made on deposits collected on sampling probes¹⁴² showing the gas stream reaction between MgO and SO₃ to have been significant resulting in the formation of more friable deposits on the probe surface.

In a comprehensive laboratory based study,¹⁶⁶ the addition of 1 mass% of magnesia with particle sizes of 2, 10 and 50 μm reduced the strength of various types of coal ashes by half or more. Surface reactions between the ash particles was shown to have been modified as a result of diffusion of various species of the ash such as Si, P, Fe and Al, as vapours into the magnesia particle. An extension to this work¹⁶⁷ showed that iron, one of the main components of the ash, was more evenly distributed through the "magnesia" particles than the other elements, demonstrating its high intra-particle mobility.

The role of magnesium based additives as ash and ash deposit fusion modifiers which would consequently bring about a change in the physical form of the deposit, rendering it more easily removed by normal sootblowing has been demonstrated in a number of studies.^{168,169} It was found¹⁶⁸ that a 10-20 mass% addition of magnesium hydroxide to a reconstituted powder sample of a slag fired at a furnace temperature of 1200°C raised the liquid phase formation temperature by about 200 °C, thus extending the vitrification range sufficiently to alter the deposit texture from a fused mass to a light, friable mass. Regular addition of 10-20 mass% Mg(OH)₂ to the coal ash would be prohibitively expensive. However, other work¹⁵¹ has suggested that such large additions of Mg(OH)₂ may not be necessary to modify the nature of ash deposits.

The proposed influence of additives on surface devitrification of silicate ash particles has been extensively reviewed.¹⁶³ The influence of the ratio of glassy to crystalline components of the ash on the rate of sintering has been defined by the relationship:

$$R_d = a * \left(\frac{x_g}{1-x_g} \right)^b \quad (2-26)$$

where;

- R_d = rate of deposit formation
- x_g , $1-x_g$ = the glassy and crystalline fractions of the ash
- a = constant
- b = rate index

It has been shown¹⁶³ that the glassy fraction of typical bituminous coal ashes from pulverized coal fired boilers was between 71 and 88 mass%. The glass content has been estimated by difference:

$$G = 100 - (X + C + S) \quad (2-27)$$

where;

- G = the glassy material
- X = crystalline species
- C = carbon content of ash
- S = sulphur content of ash

The rate of ash sintering could thus be significantly reduced when an additive captured on flame-borne ash acts as a nucleating agent, resulting in the transformation of glass to crystalline species on the surface layer of silicate ash particles, hence forming a surface material of relatively high viscosity.¹⁶³

Measurements of the rate of ash deposition are quite varied. Whereas in some studies it has been determined⁹⁹ that magnesium and calcium additives had little effect on the deposition rate, in other studies¹⁶⁰ the mass of deposit collected for most of the additive injection trials, including MgO, were higher than the mass of deposit with no additive. However in the same study¹⁶⁰ the intermittent injection of high dosages of MgO (at 45 kg per tonne of coal, injected for a period of 30 seconds at six minute intervals) with a resultant average injection of 2.2 - 4.5 kg per tonne of a high fouling coal, was shown to reduce the deposit rate by up to 40 mass%.

2.6 WEST BELFAST POWER STATION

2.6.1 Introduction

West Belfast power station is one of the four power stations operating in Northern Ireland, producing electricity for provincial consumption. This power station is the one which this study is primarily concerned with. The generating capacity of this station along with others are summarised in Table 2-17.¹⁷⁰

West Belfast power station was commissioned in the period between May 1955 and October 1958 and is capable of generating up to 240 MW of electricity.

2.6.2 Operation of the Plant

Whilst many power stations operate under a unitized generating system with one boiler to one generator, West Belfast power station employs a range system in generating electricity from the steam produced by its thirteen boilers. This means that each generator is connected to a number of boilers and vice versa, using pressurised collection vessels known as receivers. This system provides scope for maintenance and power generation as it allows for operation of all other units should any particular boiler or generator fail.

Table 2-17: Summary of the generating capacity of West-Belfast power station along with other power stations operating within Northern Ireland Electricity (N.I.E) supplies.¹⁷⁰

STATION	SIZE OF SET (MW)	NO. OF	TOTAL POWER GENERATED (MW)	GENERATION METHOD
COOLKEERAGH (360 MW)	30	2	60	OIL-FIRED
	60	5	300	OIL-FIRED
	60	1	60	GAS-TURBINE
BALLYLUMFORD (960 MW)	120	3	360	OIL-FIRED
	200	3	600	OIL-FIRED
	60	2	120	GAS-TURBINE
KILROOT (960 MW)	300	2	600	OIL-FIRED
	180	2	360	COAL-FIRED
	30	2	60	GAS-TURBINE
WEST BELFAST (240 MW)	60	3	180	COAL-FIRED
	30	2	60	COAL-FIRED

The power station burns 600,000 tonnes of coal per annum at full load, producing 70,000 tonnes of ash. The flue gases are released into three 73 meter high chimneys, with the power station generating electricity of 11.8 kv from the fire generators.^{170,171}

2.6.3 Boiler Operation

The boiler monitored in the course of this study was supplied by Babcock and Wilcox Ltd. Figure 2-16¹⁷¹ and Plate (2-1) show cross-sectional views of the boiler.

The boiler is capable of producing 99,660 kg of steam per hour at a pressure of 6.55 MPa and a temperature of 496°C. The coal is fed into the boiler from a hopper onto two chain grates and is spontaneously ignited due to the temperature inside the boiler. The ash falls off the grate at the other side of the boiler and is collected in an ash hopper, where it is sluiced away by water to the ash handling plant.

Combustion of coal is supported by passing air up through the coal bed on the grate (primary air) using a forced draught fan and is enhanced using secondary air which enters the firing area through ports situated in the front and back walls of the boiler just above the level of the grate.

The heat produced by combustion is transferred by radiation and convection in the firing chamber of the boiler to the wall tubes and screen tubes and by conduction to the water contained within the tubes. The pressurized water rises by natural convection to the steam/water drum where the steam is separated from the water. This saturated steam is then superheated in the superheater section of the boiler, using some of the remaining heat of the flue gases, before passing to the receiver. The heat contained in the flue gases is further utilized by passing the gases over the economiser tubes, containing the boiler feed water returning from the generator turbines as condensate.

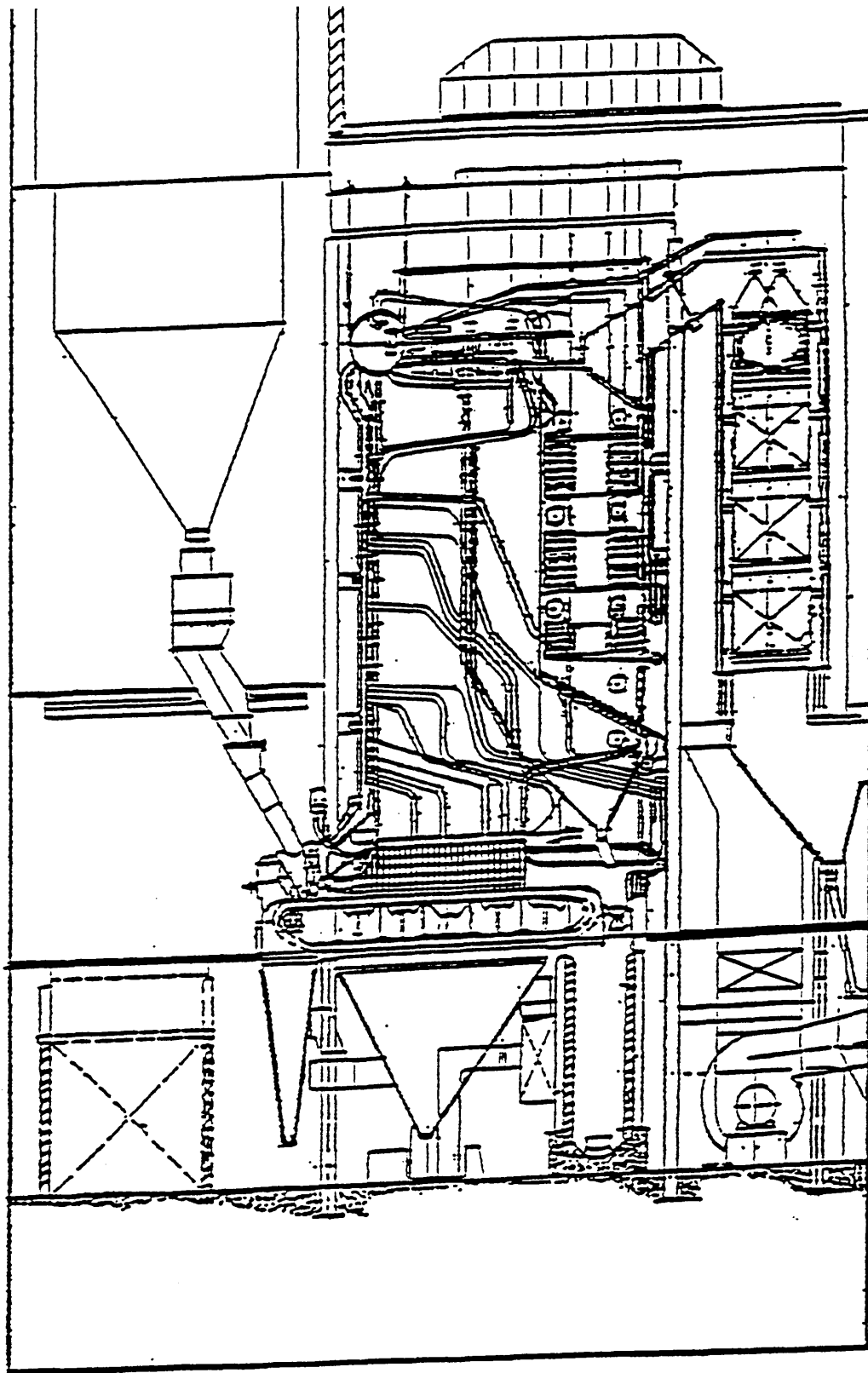


Figure 2-16: Arrangement of boiler no.6 - sectional view.¹⁷¹

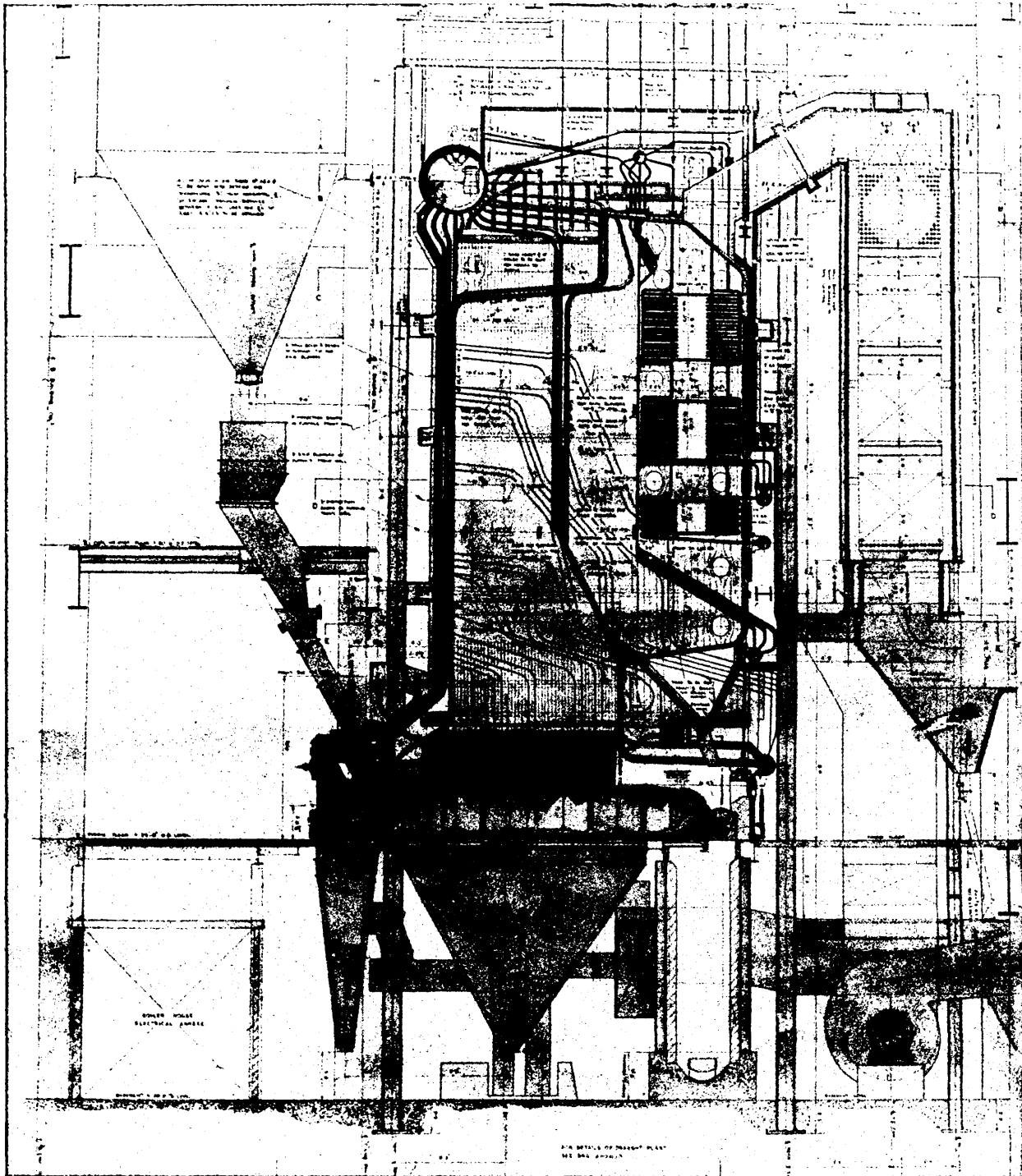


Plate 2-1:

Pictorial cross-section view of the travelling chain-grate boiler No.6, monitored for the deposition and additive injection studies.

The exit flue gases also heat up the inlet air (taken from the warm area at the top of the boiler) in the corrugated air heaters. This is illustrated in Figure 2-17.¹⁷¹ The flue gases are drawn through the ducting by induced draught fans which pass the gases out to the chimneys. The entrained grits present in the flue gases are removed by a series of grit arrestors taking the form of cyclones with incorporated trickle valves, and are positioned prior to the airheaters.

2.6.4 Additive Injection Equipment

The apparatus used to inject the powder was only temporary since the Lyclal 93HS was being added as part of a test. The design of the apparatus was based on the Nyflow feeder system¹⁷², operating essentially with a wedge shaped hopper of approximately 25 kg capacity, a discharge screw and a variable speed drive. The powder was screw fed into a venturi system where it was drawn into the air stream and passed immediately through a venturi orifice. This assembly is shown schematically in Figure 2-18. The air conveying the powder was supplied from the plant compressed air supply. The powder was injected with the secondary air through the many secondary air ports, ensuring good mixing, into the combustion chamber at both the front and rear walls, just above the level of the grate.

The design of the hopper was such that discharge should be by mass flow, where the material moved down the hopper as a solid mass with little relative movement between the particles; in preference to core flow, where the material slides over itself at a place remote from the hopper walls. The configuration of the two type of hoppers is schematically shown in Figure 2-19.¹⁷² The recommended hopper design values for Lyclal 93HS are further outlined in Table 2-18.¹⁷²

It should be noted however that for the assembled test injection apparatus the discharge from the hopper was in fact by core flow.

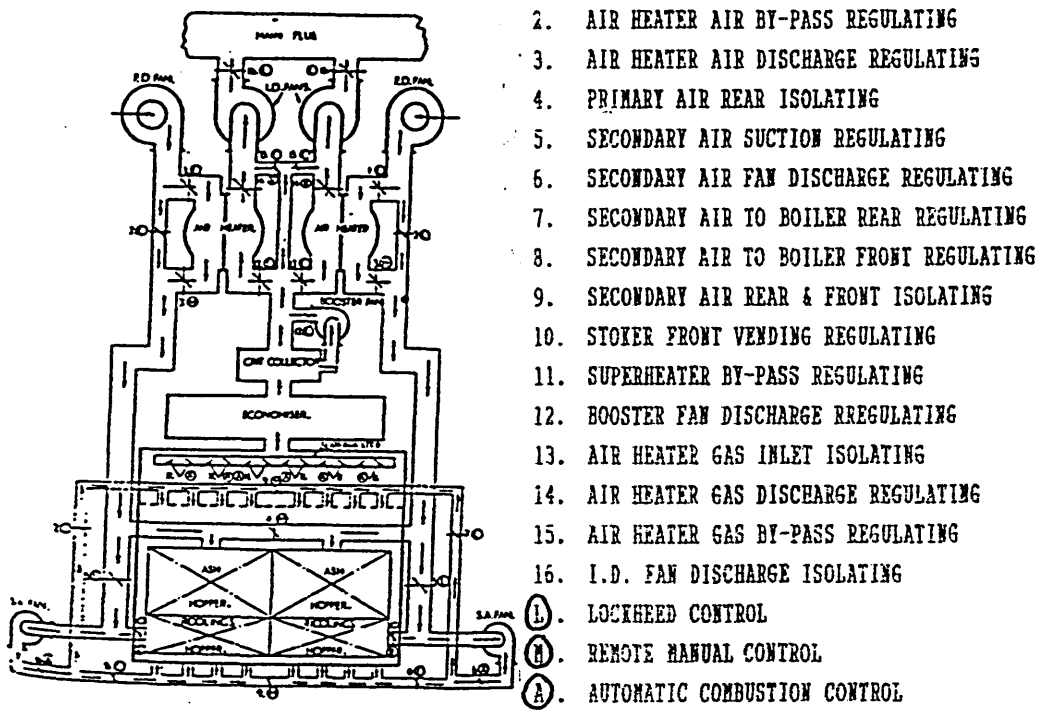


Figure 2-17: Diagram of draught system for boiler no.6.¹⁷¹

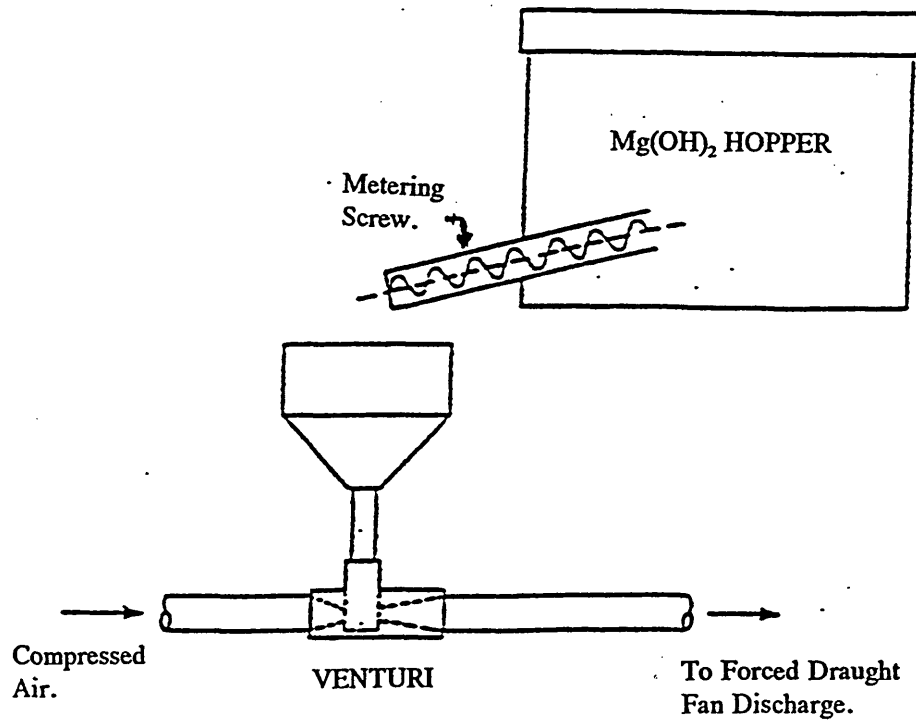


Figure 2-18: Schematic representation of Lycal 93HS injection apparatus.¹⁷¹

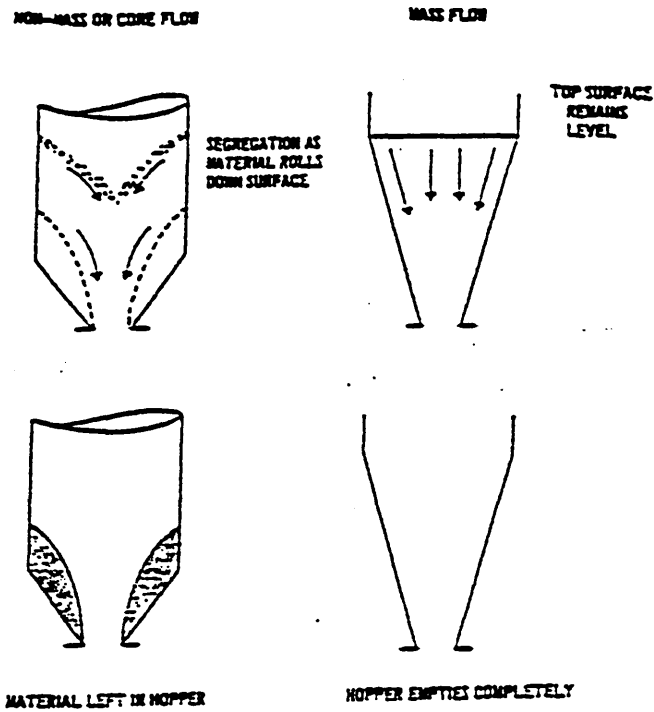


Figure 2-19: Schematic representation of core and mass flow hoppers.¹⁷²

Table 2-18: Recommended hopper design values for Lycal 93HS.¹⁷²

Measured angle of wall friction, deg	Recommended angle of hopper wall to the horizontal, deg	Bulk density in hopper, kg/m ³	Recommended diameter of hopper outlet (instantaneous conditions), cm
28	79	500	25
30	81	500	25

CHAPTER

(3)

EXPERIMENTAL METHODOLOGY

3.1 INTRODUCTION

Short term injection trials investigating the role of Lycal 93HS in alleviating high and low temperature ash deposition problems on boiler surfaces had been carried out by investigators from the Magnesium Materials Division of Steetley Quarry Products Ltd. Trials had been carried out on a variety of combustion systems. These included a refuse incinerator at Wolverhampton, an oil-fired boiler at CEGB in Surrey and a coal fired chain-grate shell stoker operated by Rowntree Mackintosh in Halifax. All had exhibited marked reductions in fly ash deposition and slagging upon application of Lycal 93HS.

Following the success of this work, a long-term investigation extending over a period of two years was carried out on a larger boiler unit at West Belfast power station where the operators were experiencing slagging and fouling problems, particularly on screen and steam generating tubes. It is this part of the work with which the author was involved.

Batches of ash deposit samples were obtained at intervals by Steetley personnel from West Belfast Power Station. These were mainly from boiler No.6 which had been set up to operate with Lycal 93HS injection through its secondary air ports. In addition one batch of deposits was collected from boiler No.5 operating similarly to No.6 but without any additive injection. These samples were sent to Sheffield Hallam University for detailed examination by the author.

The deposits observed within boilers No.5 and No.6 clearly showed that whereas the deposits formed under the influence of Lycal 93HS injection in boiler No.6 were generally soft, friable and easier to remove as much smaller accretions, the undoped deposits in boiler No.5 were mostly dense, hard, glassy accumulations of ash, producing larger pieces on removal.

During the early stages of the research, as a result of the coal strike in 1984/5, West Belfast Power Station had become committed to using a variety of imported coals from as far afield as China and Australia, long after the strike was over.

The first batch of samples received in February 1986 had therefore resulted from a variety of coals of uncertain origin, from which little could be reliably deduced and hence were used only to establish different investigative techniques.

By the middle of 1986 a consistent supply of coal from open-cast coal fields in Ayrshire, Scotland had become a permanent feature of the operation at the power station.

Samples of deposits from various regions within the two boilers were investigated using:

- visual and macroscopic examination.
- optical and SEM-EDX microscopic examination.
- X-ray fluorescence chemical analysis.
- X-ray diffractometry.
- cone fusion tests.
- size fraction analysis.
- surface dissolution of deposit samples and chemical analysis of the leachant.

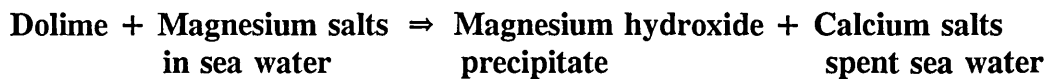
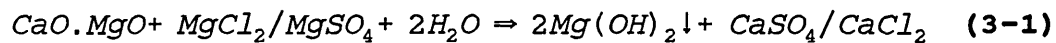
During the course of the investigation it became apparent that an understanding of the mineral matter associated with the Ayrshire coal was required. Hence a series of experiments investigating this aspect was embarked on involving:

- high and low temperature ashing of Ayrshire coal
- particle size distribution of the coal
- ash and moisture content determination of coal particle size fractions
- separation of various components of the coal ash
- determination of the effect of Lycal 93HS on softening/melting and crystallisation behaviour of separated components of the ash, using Hot-Stage Microscopy
- X-ray fluorescence chemical analysis of ash admixtures
- X-ray diffractometry of separated ash components

3.2 RAW MATERIALS

3.2.1 Lycal 93HS

Lycal 93HS is the additive which was employed in this study and is produced by the Magnesium Materials Division of Steetley Quarry Products Ltd. Lycal 93HS is a high quality, technical grade of magnesium hydroxide precipitated from sea water and takes the form of a finely divided, fully hydrated powder. The production process essentially consists of calcining dolomite to produce dolime and reacting this with sea water to precipitate magnesium hydroxide:



The chemical and physical properties of Lycal 93HS are presented in Table 3-1.¹⁷¹

The particle size distribution of Lycal 93HS, is depicted in Figure 3-1.¹⁷² The fineness of the particles, all less than 50 μm , ensures that the powder is free flowing with a high specific surface area and large number of particles per unit mass.

On exposure to high temperatures, Lycal 93HS calcines to produce magnesium oxide particles with a large effective surface area, as illustrated in Figure 3-2.¹⁷¹

The Lycal injected into the combustion zone of a boiler experiences high temperature, short retention time conditions which are analogous to a flash calcination process. It is to be expected that the resulting oxide is significantly more reactive than if it was pre-calcined prior to injection.

Table 3-1: Chemical and physical properties of Lycal 93HS additive used in the operation of boiler No.6.¹⁷¹

CHEMICAL ANALYSIS (%)		TYPICAL	RANGE
AS RECEIVED BASIS			
MgO		66.7	66.0 - 68.0
CaO		0.6	0.5 - 0.9
SiO ₂		0.6	0.5 - 0.8
Fe ₂ O ₃		0.9	0.8 - 1.0
Al ₂ O ₃		0.3	0.2 - 0.4
Sulphates as SO ₃		0.9	0.7 - 1.1
Loss at 950 C		30.0	29.0 - 31.0
		100.0	
sodium as Na ₂ O		0.1	0.05 - 0.2
Chlorides as NaCl		0.4	0.2 - 0.7
Carbonates as CO ₂		1.4	1.0 - 2.0
PHYSICAL PROPERTIES			
SIEVE ANALYSIS (GALLIE PORITT METHOD)			
%GREATER THAN			
Microns	B.S.S		
150	100	0.005	0.0 - 0.02
75	200	0.40	0.2 - 0.7
53	300	0.65	0.4 - 0.9
PARTICLE SIZE DISTRIBUTION (%FINER)			
Microns			
53		99.3	99.1 - 99.6
20		97.0	95.0 - 99.0
6		85.0	80.0 - 90.0
4		68.0	60.0 - 80.0
2		35.0	25.0 - 45.0
1		20.0	10.0 - 30.0
PACKAGING DENSITY B.S.1460 (kg/m³)		570	550 - 590

N.B. Lycal 93HS is packed in 25 kg moisture proof, multi-ply paper sacks which can be safely stored.

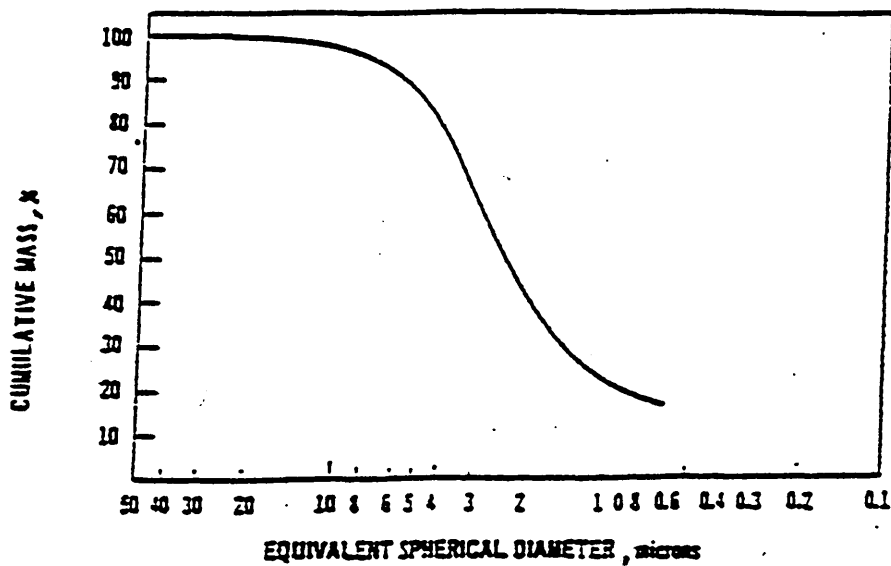


Figure 3-1: Lycal 93HS particle size distribution curve measured on a Sedigraph 5000D particle size analyser.¹⁷²

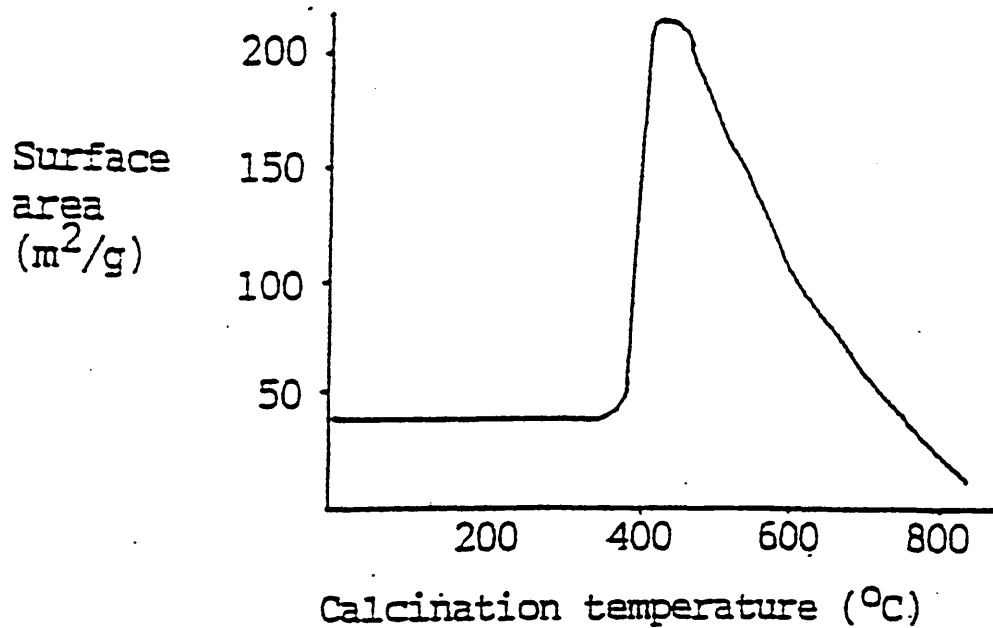


Figure 3-2: The surface area of magnesium oxide formed by the decomposition of magnesium hydroxide.¹⁷¹

3.2.2 Ayrshire Coal

The coal delivered to West Belfast power station during all but the earliest period of this investigation, was a bituminous coal, originating from the open-cast coal fields of Ayrshire in Scotland. The coal specification as received and analysed at the power station and Sheffield Hallam University is shown in Table 3-2.

3.2.3 Boiler Ash Deposit Samples

A wide range of deposit samples were taken from various locations within boilers No.6 and No.5, which operated with and without on-line injection of Lycal 93HS respectively, over a period of two years. The sampling positions are denoted in the schematic diagram shown in Figure 3-3, for the boiler system under study. Table 3-3 summarises the various positions sampled in each batch of deposits collected over the period of the investigation.

All the deposit sample batches, except the fifth which was collected by the author in person during a ten day trial period, were collected by Steetley representatives, while the boiler was "down" for inspection and/or maintenance.

Batch Number 1 - Samples of deposits taken from boiler No.6 before the commencement of Lycal 93HS treatment, were received in February 1986. The origin of the coal from which these deposits had been derived was rather uncertain since at the time, the power station was burning a variety of Chinese, Australian as well as other coals. Four samples were received, taken from the rear wall, the furnace corner, the bottom screen tubes and the passage between the screen tubes and superheater tubes.

Batch Number 2 - Samples of deposits were received from boiler No.6, after three months of continuous operation with Lycal 93HS injection, in September 1986. Regular

Table 3-2: Analysis of Ayrshire coal characteristics as received at West Belfast power station.

<u>PROXIMATE ANALYSIS (%)</u>		<u>ULTIMATE ANALYSIS (%)</u>		<u>ADDITIONAL DATA</u>	
Fixed Carbon	47.46	Carbon	71.7	Swelling index No.	1-2
Total Moisture	12.14	Hydrogen	4.7	Volatile Matter	29.10
Nitrogen	1.7	Sulphur (ave.)	0.6	B.S.Sieve-size	All < 1"
Ash	11.30	Oxygen (diff.)	9.7		30% < 1/8"
Net C.V (kj/kg)	24,900	Chlorine (max.)	0.37	N.C.B.Rank	702
		Phosphorous (max.)	0.02		
 <u>ASH COMPOSITION (%)</u>			 <u>ASH SOFTENING DATA (Oxidising) / (°C)</u>		
SiO ₂	48.90	<i>High Temperature Ash</i>			
Al ₂ O ₃	29.65				
TiO ₂	1.22	Initial deformation temperature	1432		
Fe ₂ O ₃	9.65	Hemisphere temperature	1450+		
CaO	6.20	Flow temperature	1450+		
MgO	1.62				
K ₂ O	1.89	<i>Low Temperature Ash</i>			
Na ₂ O	0.50				
P ₂ O ₅	0.20	Initial deformation temperature	1450+		
SO ₃	n.d	Hemisphere temperature	1450+		
		Flow temperature	1450+		
 <u>SPECIFICATIONS FOR UNTREATED SMALLS</u>					
	<u>Datum</u>	<u>Range</u>			
Moisture	11%	9-13%			
Ash	10.5%	9-12%			
Volatile Matter	28.5%	25-32%			
Fixed Carbon	48.5%	40-57%			
Net C.V (kj/kg)	25,900	25,000-27,800			
Sulphur	not more than 1.2% with an average of < 1%.				
Chloridne	not more than 0.1%.				

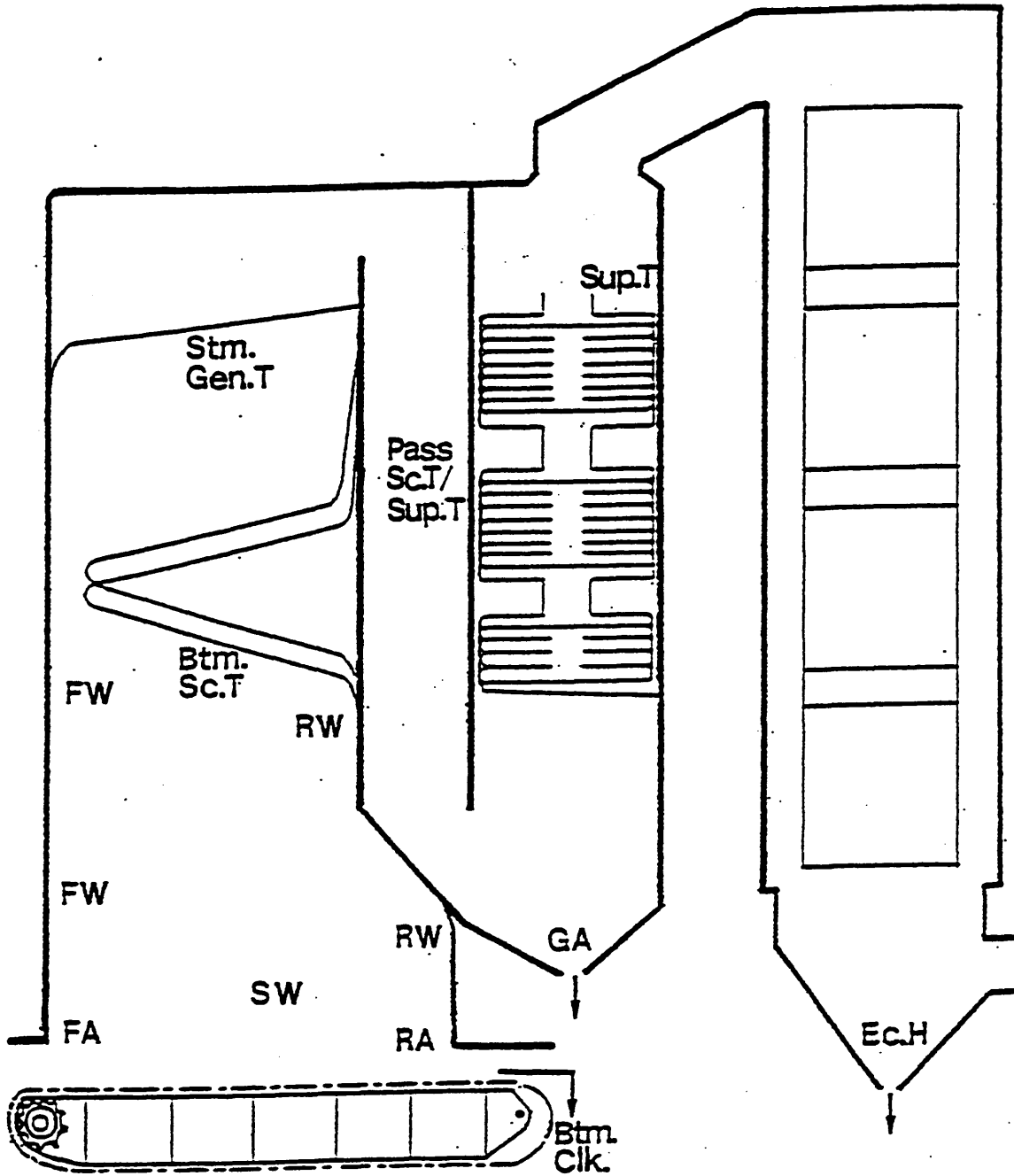


Figure 3-3: Schematic diagram of boiler no.6 - section view denoting deposit locations. (See Table 3-3 for key to abbreviations).

Table 3-3: Summary of deposits received / collected for examination with and without on-line injection of Lycal 93HS.

Batch No.	Date Received	Deposit Sampling Position	Boiler No.	Period of Continuous Lycal 93HS Injection (hour)
1	20-6-86	RW, Cor., Btm. Sc. T., Pass. Sc.T & Sup. T.	6	0
2	5-9-86	FA, FW, RW, Btm.Sc.T., Pass.Sc.T & Sup. T.	6	2100
3	10-3-87	FW _A , FW _B , RW _A , RW _B , SW _A , SW _B , Btm. Sc. T _A , Btm. Sc. T _B	6	2800
4	31-8-87	FW _A , FW _B , RW _A , RW _B , SW _A , SW _B , Btm. Sc.T _A , Btm. Sc.T _B , Ec.H _A , Ec.H _B , Btm. Clk.	6	4100
5	24-11-87	FA _B , FW _A , FW _B , RA _B , RW _B , SW _A , Btm. Sc. T _A , Stm. Gen. T _A , Sup. T _B , Ec.H _A , Ec.H _B Ec.H _A , Ec.H _B , GA _A , GA _B	5	-
			6	12
6	10-12-87	GA _A , GA _B GA _A , GA _B / GA _A , GA _B	5	-
			6	4 / -

Key to abbreviation:

FA: Front Arch, FW: Front Wall, RA: Rear Arch, RW: Rear Wall,
SW: Side Wall, Btm. Sc. T.: Bottom Screen Tubes, Stm. Gen. T.: Steam Generating
Tubes, Pass. Sc. T. & Sup.T.: Passage between Screen Tubes and Superheater Tubes
Sup. T.: Superheater Tubes, Ec. H.: Economiser Ash Hoppers, GA: Grit Arrestors,
Btm. Clk.: Bottom Grate Clinker, A / B: Side A or B

supplies of coal from the Ayrshire coal-field had been restored since March 1986. Five deposit samples were received, taken from the front arch near the secondary air ports, the front wall tubes above the secondary air ports, the rear wall arch near the secondary air ports, the bottom screen tubes, and finally the passage between the screen tubes and the superheater section.

Batch Number 3 - Samples of deposits were received from boiler No.6 after nearly four months of continuous operation with Lycal 93HS injection, in March 1987. As a result of earlier observations made by Steetley, it had become apparent that due to the uneven injection of Lycal 93HS into the furnace region in boiler No.6, deposits formed on the left hand side of the boiler, referred to as side A, were lighter and more friable than deposits formed on the right hand side of the boiler, referred to as side B, which also exhibited some bridging. Hence the samples were taken from both sides, of the front wall tubes above the secondary air-ports, the rear wall tubes above the secondary air-ports, the side walls and the screen tubes.

Batch Number 4 - Samples of deposits were received from boiler No.6 after almost six months of continuous operation with Lycal 93HS injection, in September 1987. The deposit samples were taken from the front wall above the secondary air-ports, the rear wall above the secondary air-ports, the side walls, the screen tubes, the economiser ash hoppers, the soot hopper and a sample of the bottom grate clinker was also received.

Batch Number 5 - Samples of deposits were collected by the author from boiler No.5 after one month of continuous operation in November 1987. These deposit samples were collected principally for comparative purposes, since boiler No.5 had never been

operated under the influence of any additive injection. The deposit samples from boiler No.5 were obtained from the rear arch, the front arch, the front wall above the secondary air-ports, the rear wall above the secondary air-ports, the steam generating tubes, the screen tubes, the superheater tubes, the economiser ash hopper and grit arrestors.

At this time also, short term sampling of fly ash deposition with and without Lycal 93HS injection was carried out by the author on boiler No.6, using the deposition probe described in Section 3.3.7.

Batch Number 6 - This batch consisted only of particulate samples taken from the grit arrestors at the back-end of the boiler No.6 at periods when Lycal had been both on-line and off-line. Similar samples were also taken from boiler No.5 for the purpose of comparison.

3.3 INVESTIGATION OF BOILER DEPOSITS

3.3.1 Preliminary Examination of As Received Samples

3.3.1 (a) Chemical Analysis

X-ray fluorescence analysis was used to determine the elemental composition of deposit samples. The deposit specimens had to be in the form of a fine powder (-72 mesh) before analysis could take place and hence a mechanically driven pestle and mortar assembly was used to grind the samples to size.

The analysis was carried out by Mr. J. Hippy of Steetley Refractories in Worksop.

3.3.1 (b) Visual Appearance and Texture of Deposits

All as received samples were first examined visually and general features such as colour, texture, friability, strength, layering effects as well as the size of the bulk samples were noted.

More detailed morphological and micro-textural examination of deposit samples was carried out by the use of stereo, optical and scanning electron microscopy techniques. These techniques are described separately in the following sections.

3.3.1 (c) Stereo-Compound Microscopy (SCM)

SCM was chiefly used to examine and characterize various topographical and morphological constituents of deposit samples, by providing a realistic three-dimensional image of the specimen.

It was particularly useful for studying the variation in the colour and texture of the ash cenospheres which were found to make up the bulk of the friable samples within sample batches 2, 3 and 4.

Almost no preparation was required nor desired for the preliminary examination of the deposit specimen. For the examination of the fly ash particles from the grit arrestors and the economiser ash hoppers in sample batches 4, 5 and 6, it was necessary to spread the particles out uniformly over a smooth surface using a salt shaker. The particles spread out in this way could easily be manipulated with a probe so that the surface of each particle could be looked at in its entirety. A limitation in the SCM however, was found to be its power of magnification, attaining a maximum of x40, which was mostly used in this investigation, as well as the limited depth of focus at this magnification.

3.3.2 Micro-Examination of As Received Samples

3.3.2 (a) Sample Preparation For Petrological Examination

Hard deposit samples approximately 10 mm to 15 mm across were cut from the bulk samples, using a diamond wheel.

Alcohol was used as the lubricant in order to avoid any possible dissolution of

soluble phases which might be present in the deposit. Those samples which were softer, were broken down to approximately the same size.

The samples were oven dried at 100°C for a minimum of one hour. Each sample was immersed in a mixture of a cold setting resin and Metset hardener and was then impregnated in a vacuum dessicator connected to a single stage rotary pump. The vacuum was applied for a minimum of 30 minutes. After setting, the mounted specimen was removed and allowed to cure for 24 hours.

Having removed the mounted samples from their moulds, the diamond wheel was further used to slice away a layer of a few millimeters thick, to produce a smooth exposed deposit surface. The mounted samples were then prepared for micro-examination by grinding on 240, 400 and 600 grit silicon carbide papers, using paraffin as the lubricant and cooling agent. The samples were then polished using 25 μ m, 14 μ m, 6 μ m and 1 μ m diamond paste on the polishing papers. The polishing time with each diamond paste was kept to the minimum necessary to remove all scratches from the previous stage, to minimise damage to the deposit specimen. Each sample was ultrasonically cleaned in alcohol after polishing on each diamond paste in order to remove any loose particles of the deposit as well as any residual abrasive paste trapped in the pores. Care was taken to thoroughly wash the samples with alcohol and dry them with the aid of a warm air-blower, between each polishing operation.

All samples were stored in a desiccator containing silica gel, so that their surfaces would not be contaminated by any extraneous and injurious matter in the air, such as moisture, dust, etc.

The prepared samples were examined using Ultraphot and Vanox optical microscopes.

3.3.2 (b) Optical Microscopy

An Ultraphot compound photomicroscope and an Olympus Vanox photomicroscope, using reflected light, 35mm PANF film and operating in an automatic exposure mode were used to examine and photograph deposit specimens in an unpolished and polished state. The Ultraphot photomicroscope was further used to obtain colour photographs of the morphology of selected deposit samples under cross-polarised light conditions, using a blue filter and 50 ASA high-sensitivity film. Magnifications of x10 to x200 were typically employed.

3.3.2 (c) Scanning Electron Microscopy - EDX Elemental Analysis

Samples of deposits and grit were examined using a Phillips (PSEM) 500 scanning electron microscope, operating at an accelerating voltage of 25 kv, and a JEOL 840 scanning electron microscope operating at an accelerating voltage of 20 kv and beam current of approximately 5×10^{-8} A. The JEOL 840 microscope, being equipped with back-scattered electron probes in addition to the secondary electron probes, was primarily used to obtain micrographs of those features within the samples with limited contrast, using the variation in the atomic number of the various elements present in the microstructural phases.

Representative as received and polished deposit samples were attached to aluminium stubs by means of colloidal silver and were left in air for a few minutes to dry. For examination of the particulate matter, from, for example the grit arrestors, economiser ash hoppers and superheater section, double-sided adhesive tape was used to mount them instead of the colloidal silver. The particles were randomly scattered onto the tape. All specimens were coated with a layer of carbon a few microns thick, to render the surface electrically conducting, by placing them within the vacuum chamber of a carbon-coating machine.

The mounted and coated specimens were then examined using the scanning electron microscopes identified above. Photo-micrographs were taken as required.

The EDX ("Energy dispersive analysis of X-rays") detector was used to analyse for chemical elements in the specimen down to atomic number 11 i.e sodium. This was carried out by intensity measurements of the characteristic X-rays generated by each individual element present, as a result of bombardment of the specimen by a finely focused electron beam. This was set to produce a 50 nm spot on the sample. The spectral X-ray peaks thus formed were usually quite easily identifiable. However, when features of interest found within cavities or pores were to be analysed, more time and better manipulation of spot size and location was essential in order to obtain sufficient X-ray counts to give a recognisable peak. The elemental composition of the wide ranging phases observed were further characterised.

A hard copy of the elemental peak distributions was obtained by transferring the data onto a printer. These could thus be reproduced accompanying the photomicrograph of the various features of the specimen.

Both of the EDX micro-analyser units utilised by the PSEM 500 and JEOL 840A systems were manufactured by the Link analytical suppliers, with the former microscope being fitted with the 860 series unit and the latter with an AN 10,000 series unit.

3.3.3 Analysis of X-Ray Diffraction Spectra from Deposits and Coal Ash

A Phillips Norelco X-ray diffractometer was used to analyse and identify the crystalline minerals in the deposit samples. In addition, high and low temperature ash derived from a mixed size representative sample of Ayrshire coal, as well as the entire range of separated high temperature ash components as explained in Section 3.4.2 (b), were also analysed.

3.3.3 (a) Procedure

A representative specimen taken from a deposit sample was firstly ground, using a pestle and mortar, to a fine powder passing through a 300-mesh screen.

The powdered sample specimen was then gently compacted into the sample holder and the smooth surface of the powder was levelled. The sample in the holder was then fitted into the diffractometer. The specimen holder was rotated during the exposure in order to produce uniform diffraction lines by increasing the number of crystallographic planes in diffracting positions.

The X-ray detector connected to a counting-rate meter was set at an angle of $15^\circ 2\theta$ at the commencement of each separate analysis. The output from the counting rate meter was fed into a fast-acting automatic recorder. The detector was driven at a constant angular velocity through increasing values of 2θ until the whole angular range which was considered to be of significance at $15-70^\circ 2\theta$ had been scanned. At the same time, the paper chart on the recorder moved at a constant speed, so that distances along the length of the chart were proportional to 2θ . The result was a chart which gave a record of radiation counts per second (proportional to diffracted intensity) on the vertical axis against diffraction angle 2θ on the horizontal axis.

The diffractometer was used with monochromatic X-ray radiation, with cobalt or copper as the metal target. Diffraction occurred whenever the Bragg law¹⁷³ was satisfied:

$$n\lambda = 2.d.\sin\theta \quad (3-2)$$

where;

n = the order of reflection (equal to unity for diffraction)

λ = the wavelength of the radiation (i.e. Co: 1.790 Å or Cu: 1.542 Å)

d = inter-planar distance (Å)

θ = angle of incidence of X-ray beam

With n and λ , depending on the metal target (i.e. cobalt or copper), being constant for all the runs and values of θ easily read from the chart recordings, equation (3-1) was used to evaluate the corresponding d-spacing values for the recorded diffraction peaks. The relative intensities of various peaks was evaluated by measuring their proportional heights. These were compared with the relative diffraction peak intensities of a range of crystalline mineral substances which were suspected of being present, as a result of previous XRF and SEM-EDAX analysis of deposit samples which had given specific indications of elements and therefore the groups of compounds possibly present. Comparison was facilitated by reference to the standard ASTM card index system, classifying an extensive range of crystalline substances on the basis of their relative diffraction peak intensities and corresponding d-spacing values.

In order to make a positive identification of any crystalline phase present, at least three strongest peaks, as suggested in literature¹⁷⁴, had to be in close agreement with their standard values on the ASTM cards. However, in the case of some minerals with very weak second and third peaks, the strongest peak was considered for possible identification.

3.3.4 Determination of Softening and Melting Behaviour of Coal Ash Deposits **Using the Cone Fusion Test**

3.3.4 (a) Introduction

The cone fusion test, as described in B.S.1016¹⁷⁵, is probably the most common method of determining coal ash and coke ash fusibility under oxidising or reducing conditions. The test as performed in this study, is an empirical test to simulate the behaviour of coal ash and its admixtures as well as doped and undoped deposit powder specimens, when heated in a oxidising atmosphere. Whereas oxidising conditions are

generally considered as characteristic of the furnace area, particularly with respect to the formation of deposits on heating surfaces, reducing conditions are regarded as characteristic of the fuel bed and the area just above it.

The test consisted of observing the transformation in shape of triangular pyramidal cones of crushed deposit powder specimens in a furnace in which the temperature was continuously increasing. In addition to the three characteristic ash fusion temperatures as defined by B.S 1016¹⁷⁵, a further mid-point in the softening stages, namely the (ST), was also considered as being relevant in the thermal behaviour of the ash. These stages are as follows:

- Initial deformation temperature (IDT) - The temperature at which the first sign of rounding of the tip of the specimen occurs.
- Softening temperature (ST) - The temperature at which the height of the specimen is equal to the length of the base.
- Hemisphere temperature (HT) - The temperature at which the height of the specimen is equal to half the base, its shape being approximately hemispherical.
- Flow temperature (FT) - The temperature at which the height of the specimen is equal to one-third of that at the softening or hemisphere temperatures.

These stages have been illustrated in Figure 3-4.

3.3.4 (b) The Preparation of Cones for Fusibility Measurements

Small amounts of the bulk deposit samples were crushed in a mechanically driven pestle and mortar until a fine powder, passing through a 240 mesh (63 μ m) B.S sieve was obtained. After weighing out approximately 2.0 grams of powdered specimen, 8% by mass of ammonium chloride was added to the powder as a binder. The mixture was mixed by hand in a small silica dish, using a spatula. Alcohol was added to

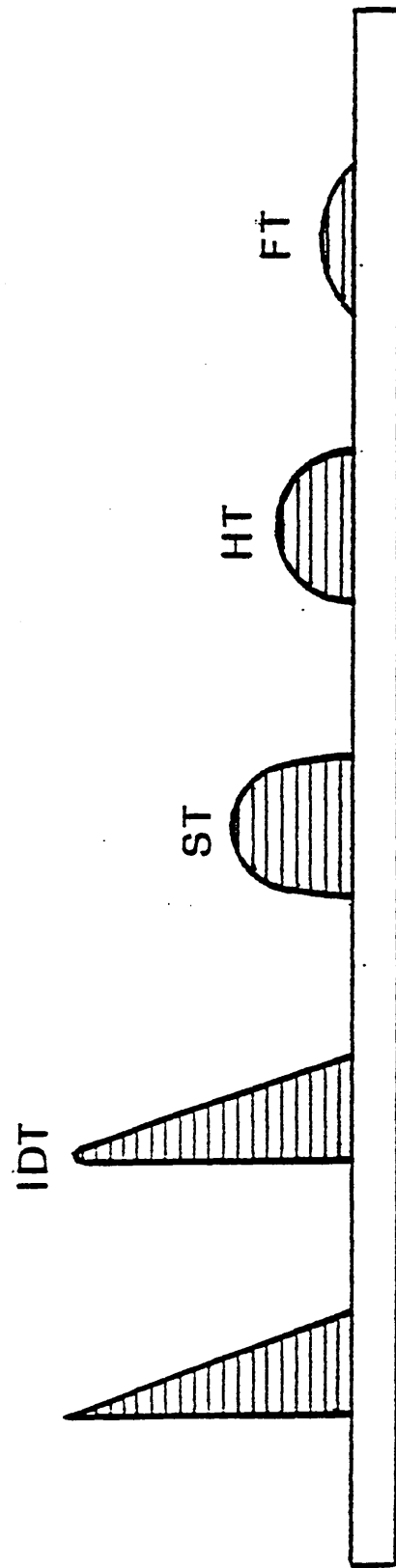


Figure 3-4: Characteristic shapes of the pyramidal deposit and coal ash specimen during the heating regime.

produce a stiff paste. A three piece brass mould, as shown in Plate 3-1 and Plate 3-2 was employed to produce a trilateral pyramidal cone. This particular mould produced cones which at 26 mm height and 9 mm length of the side of the base, were considerably larger than standard cones, as described in B.S.1016¹⁷⁵. The larger cone size meant a larger surface area of the cone was heated, thus making the observation of the cone fusion easier. Furthermore, a larger droplet of molten deposit was thus obtained at the end of the test making its subsequent micro-examination easier.

The mould was lined with "Cling film" before the pasty mixture was pressed into the cavity, to facilitate the removal of the cone. After careful removal from the mould, each cone was mounted on a base made from C60 alumina hydraulic cement, using a little C60 powder and water paste as the "glue". The mounted specimen was then dried in an oven for at least 1.0 hour at 100°C.

In order to investigate the effect of further additions of Lycal 93HS on the fusion characteristics of the already doped deposit samples, cones were made from powdered deposit to which up to 8 mass% of Lycal 93HS had been added.

In addition to these "reconstituted" deposit cones, pyramidal shaped test pieces of similar size were "fashioned" from the bulk deposit samples for fusibility tests.

3.3.4 (c) Furnace Assembly Used For Fusibility Measurements

The furnace assembly is shown in Figure 3-5. The furnace principally consisted of a non-porous, pure, recrystallised alumina tube (50 mm diameter) which was heated by silicon-carbide electrical resistance elements surrounding the middle section of the tube and covered by the furnace outer casing. The front end of the tube was closed by a quartz window and the back end was closed by a metallic disc containing a hole, through which the thermocouple sheath was pushed into position at the furnace hot



Plate 3-1:

The brass mould used to produce test cones.



Plate 3-2:

The assembled form of the brass mould.

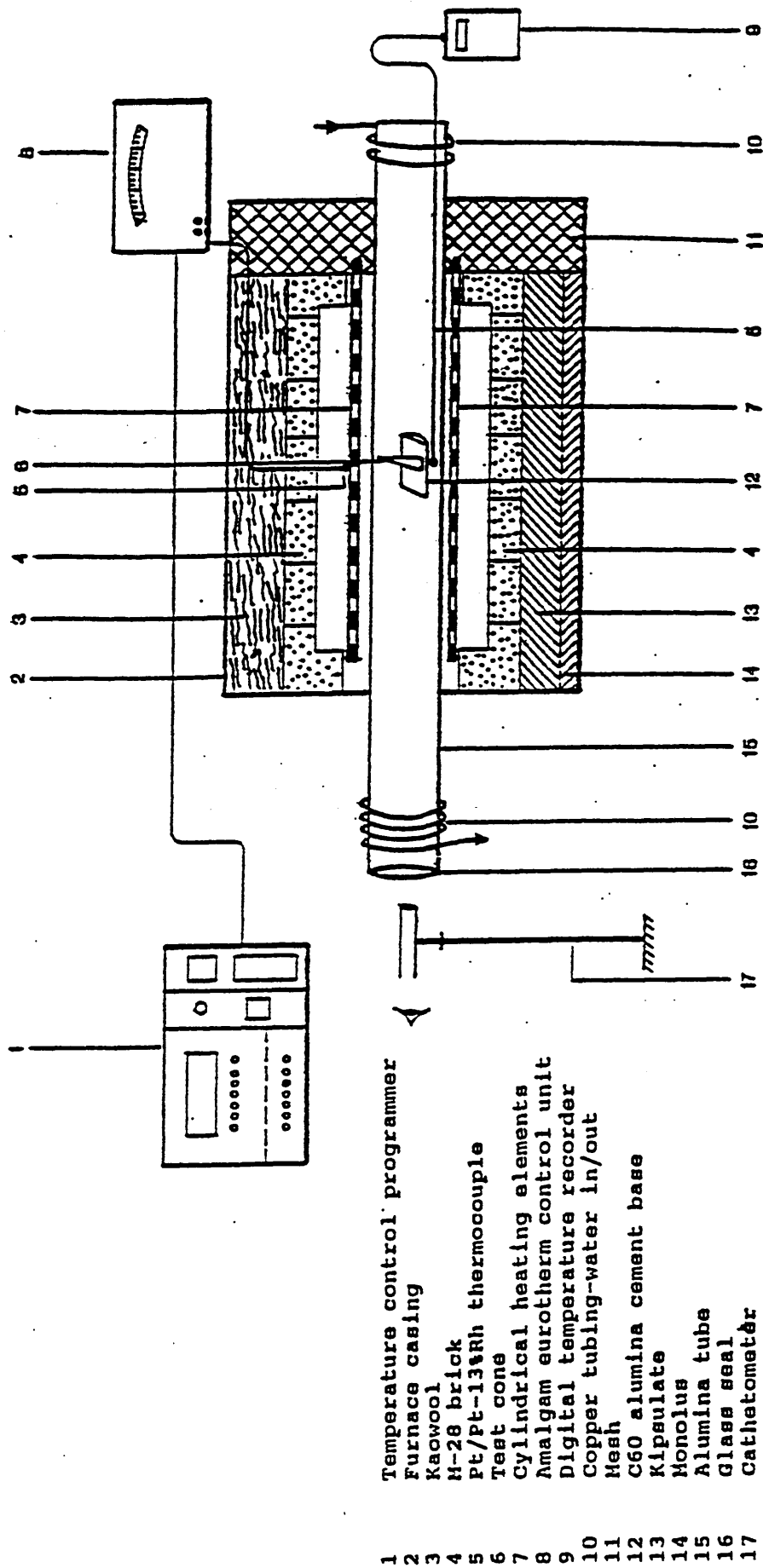


Figure 3-5: A diagram of the assembled apparatus used to study the softening and melting characteristics of ash cones.

zone. The end fittings were water-cooled and also carried the gas inlet and outlet tubes for introduction of various gases, if so required. The gaseous environment for the whole series of tests carried out was static air. The temperature was measured using a platinum / platinum-13% rhodium thermocouple.

A series of standard pyrometric "Seeger" cones, covering a range of temperatures from 1000 - 1400°C, representative of the critical softening and melting temperature range of the deposit cones, were used to calibrate the furnace. The accuracy of the furnace tube thermocouple was found to be between +8°C and -8°C.

3.3.4 (d) Procedure

The test-piece mounted on its aluminous base was pushed to the centre of the cold furnace tube so that it was close to the hot junction of the Pt/Pt-13% Rh thermocouple. The other end of the thermocouple was connected to a digital temperature recorder, with the cold junction temperature set at room temperature.

Care was taken to try and ensure that the vertical face of the cone was perpendicular to the longitudinal axis of the tube, but this was difficult as visibility was poor.

The furnace was then switched on. The heating rate of the furnace was controlled via a multi - channel programmable controller, type 211 manufactured by Eurotherm Instrumentation Ltd. Co. Figure 3-6 illustrates the heating regime which was adopted. This allowed the cone to be heated without cracking or disintegrating during the earlier stages of heating, as had previously been experienced. A steady temperature rise of approximately 5°C per minute from 1000°C to the maximum temperature at 1450°C, as recommended by B.S 1016¹⁷⁵ was also achieved.

A cathetometer, supplied by Foster Instruments Co. Ltd. was used to observe the specimens within the glowing furnace hot-zone during heating at temperatures above

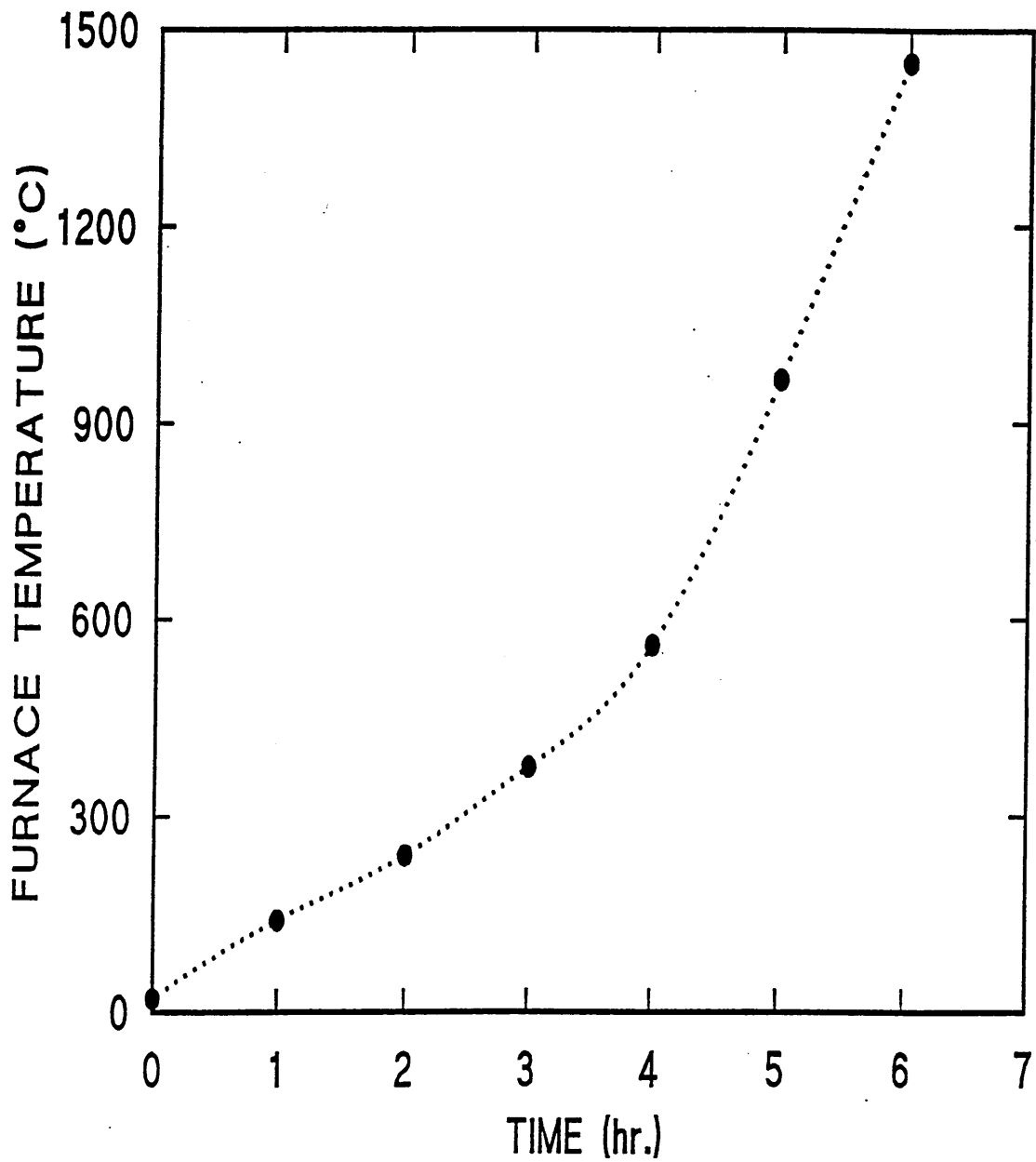


Figure 3-6: Heating regime selected for the softening assessment of deposit and coal ash cones samples in a horizontal tube furnace.

800°C. The horizontal line of a "cross-wire" on the lens of the cathetometer was adjusted to coincide with the top of the specimen, thereby facilitating the observation of its reduction in height as a measure of its progressive softening. The "cross-wire" was also helpful in recognising the onset of the various stages in the fusion process, as described in Section 3.3.4 (a) and Figure 3.4.

The temperature of the furnace was raised until cone fluidity had occurred, or the maximum furnace temperature, of 1450°C, was attained. The furnace was then switched off and cooled to room temperature which took about 6 hours. The sample could then be removed for examination. Optical microscopic and scanning electron microscopic examination was carried out on selected cones, after the test.

3.3.5 Heat Treatment of Selected Deposit Specimen

3.3.5 (a) Introduction

Two types of deposits from the third batch of samples which upon visual and stereomicroscopic examination been found to have apparently distinct textural differences were heat treated for various times and temperatures in an air atmosphere. Chemical analysis of these two types of deposits revealed an enrichment of iron oxide in one type as compared with the other.

This particular investigation arose from the observation by Steetley personnel that there had been a variation in deposition build up in boiler No.6 due to the uneven distribution of Lycal 93HS injection into the furnace region.

The heat treatment was envisaged to demonstrate the sticking ability of the two friable deposit types onto the surface of the silicon-carbide tray containing the two deposit types.

3.3.5 (b) High Temperature Muffle Furnace

A muffle furnace supplied by Carbolite Co. equipped with built in programmable temperature controller, capable of achieving a maximum temperature of 1400°C was used. The furnace was heated by silicon-carbide electrical resistance heating elements situated vertically along the side walls of the inner jacket of the silicon-carbide muffle. The temperature inside the furnace chamber was measured using a Pt/Pt-13%Rh thermocouple installed at the rear wall inside the furnace.

3.3.5 (c) Procedure

A small specimen approximately 10 mm x 7 mm, from the two types of deposits in Batch number 3, was introduced into the muffle furnace, using a silicon-carbide tray as a sample holder. The temperature of the relatively small deposit specimen was accurately monitored using a Pt/Pt-13% Rh thermocouple, with its hot junction placed adjacent to the specimen tray. The specimens were "soaked" for time periods of 10, 30 and 60 minutes at temperatures of 1200°C, 1275°C and 1350°C.

At the end of each experiment the specimen was air-cooled outside the furnace, and the degree of softening or melting and the extent of the "wetting" of the silicon-carbide tray by the specimen was assessed.

3.3.6 Determination of the Magnesia Distribution Within Ash Deposit Particles

3.3.6 (a) Introduction

In order to assess the role of Lycal 93HS as a "surface-modifier" of boiler fly ash particles, a technique was developed to selectively dissolve the outer layer of ash particles from a range of boiler ash deposits, using hydrofluoric acid (HF) as the leaching agent. The samples for this work were selected from all of the batches received from West Belfast power station during the course of this research programme.

Initially, in order to optimise the experimental conditions, HF - solutions of varying concentrations, ranging from 1.0 to 0.01 molar were used to leach the ash deposit specimens.

The temperature of the solution was also varied between room temperature at 20°C to 85°C. The time scale for the tests was also varied up to a maximum of 8 hours.

These initial experiments established that an HF-solution concentration of 0.05 molar at a temperature of 22°C produced a moderate rate of dissolution of the surface layer of the deposit specimens, after five to six hours.

3.3.6 (b) Procedure

The apparatus for the leaching experiments is illustrated schematically in Figure 3-7.

A water bath was heated to a constant temperature of 22°C by a controllable thermostatic heater. The bath was continuously stirred to keep the temperature uniform.

A 0.05 molar HF - solution was prepared by diluting 22.0 ml of AnalaR grade 40 mass% HF with distilled water in a 10 dm³ plastic beaker.

150 ml of the prepared 0.05 molar HF-solution was transferred to a 500 ml cylindrical plastic beaker, which was fitted with a perspex lid through which a plastic stirrer passed. The beaker with the stirrer in position was lowered into the bath and positioned as shown in Figure 3-7. Once the temperature of the solution had reached the predetermined temperature of 22°C, 1.0 gram of ash deposit bulk sample in the form of a lump was placed in the solution and the stirrer was switched on.

A 10 ml sample of the leaching solution was removed after 1.0 minute and at further intervals of 5, 15, 30, 60, 120, 180, 240, and 300 minutes, using a plastic graduated pipette. After each 10 ml sample had been removed, an equal amount of fresh HF solution which had been brought to the bath temperature was added to the beaker.

- | | | | |
|---|-------------------------------|----|----------------------|
| 1 | Water tank | 7 | Two-speed motor |
| 2 | Stand & clamp assembly | 8 | Plastic pipette |
| 3 | HF-solution | 9 | Plastic beaker & lid |
| 4 | Thermometer | 10 | Plastic stirrer |
| 5 | Thermostatic heater & stirrer | 11 | Deposit sample |
| 6 | Cork | | |

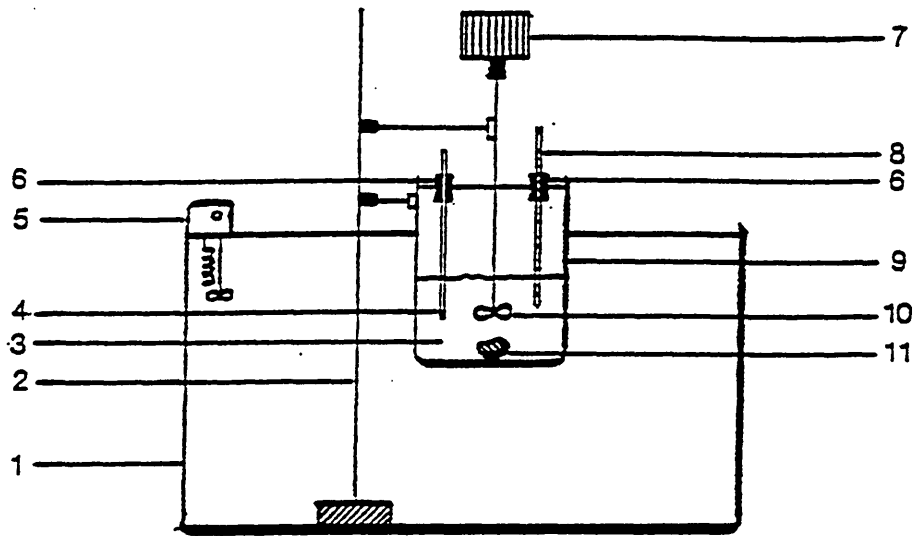


Figure 3-7: A schematic diagram of the apparatus for the surface leaching of ash deposits.

In order to neutralise the HF-solutions, at the end of each experiment the residual leach solution was mixed and washed thoroughly by a concentrated solution of BaCl₂ and tap water before being discarded.

The collected samples of leaching solutions were analyzed for silicon (Si), iron (Fe) and magnesium (Mg) by the Chemical Analysis Department within the Division of Materials and Process Engineering, using Flame Atomic Absorption Spectrometry.

3.3.7 Ash Deposition on a Probe in West Belfast No.6 Boiler

A limited number of trials were carried out by the author using an air-cooled ash fouling probe to collect ash deposits from within the No.6 boiler at West Belfast. The main objective of this test program was to determine the effect of Lycal 93HS injection on the rate and texture of ash deposits formed on the probe. Tests were carried out for varying exposure times, ranging from 1.0 hour to 12.0 hours with and without continuous injection of Lycal 93HS.

The probe used in this study was a single tube probe manufactured from 25 mass% Cr/20 mass% Ni stainless steel. The length of the probe was approximately 3.0 m, with an inner diameter of 20 mm and outer diameter of 25 mm. A sketch of the fouling probe is shown in Figure 3-8. The actual probe used is shown in Plate 3-3, inserted into the boiler through a viewing port on the side wall of the boiler, with its axes perpendicular to the direction of gas flow.

The probe contained a total of five thermocouples, embedded into its walls, three of which, all located on the upper side of the probe, were essentially used to measure the variation in the temperature of the boiler flue gases in contact with the probe.

However, only one thermocouple position, namely position 3, was monitored during this work, for reasons that will be described later.

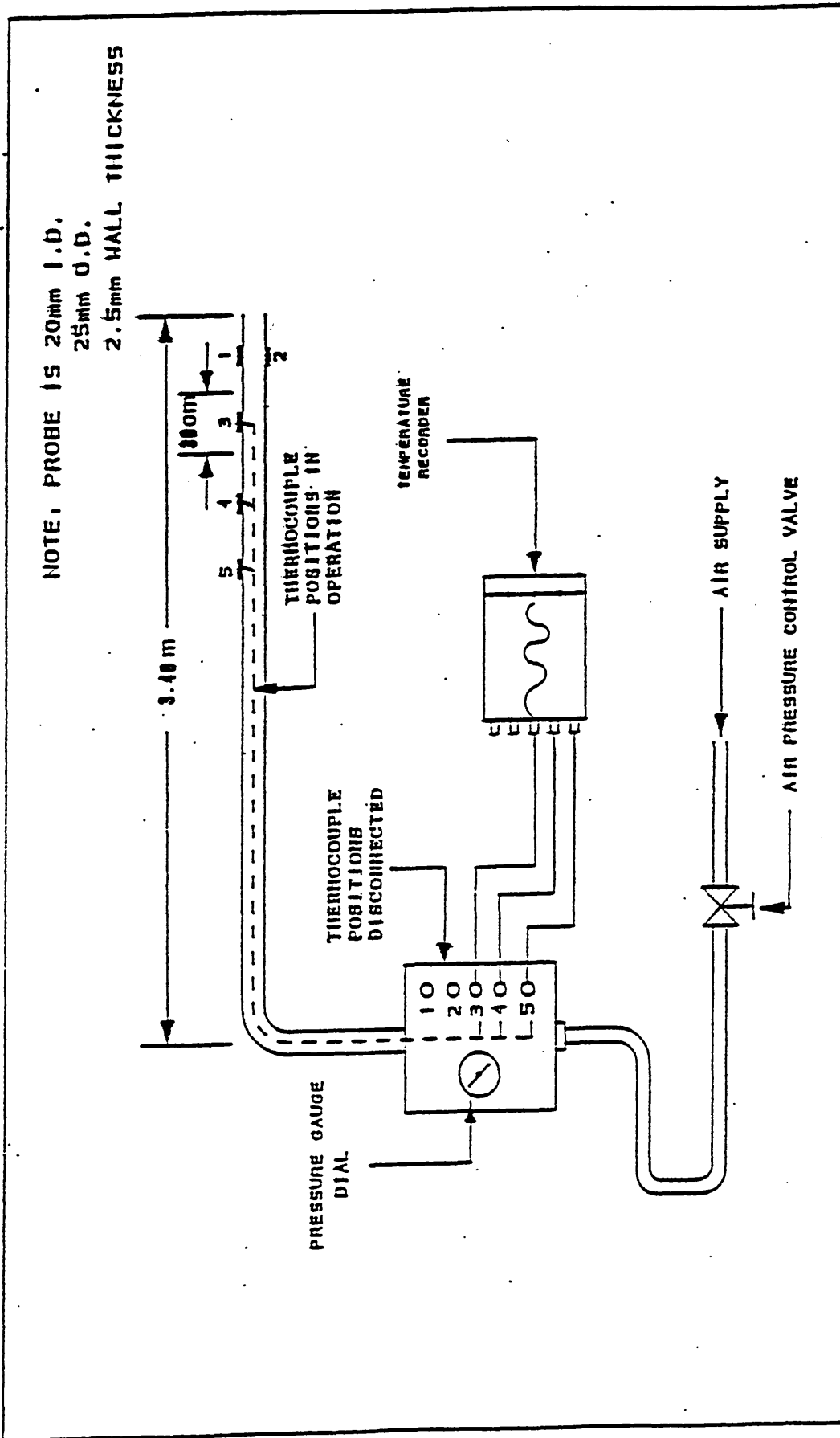


Figure 3-8: Schematic diagram of air-cooled probe used for measuring ash deposition rate in full scale boiler at west belfast power station.

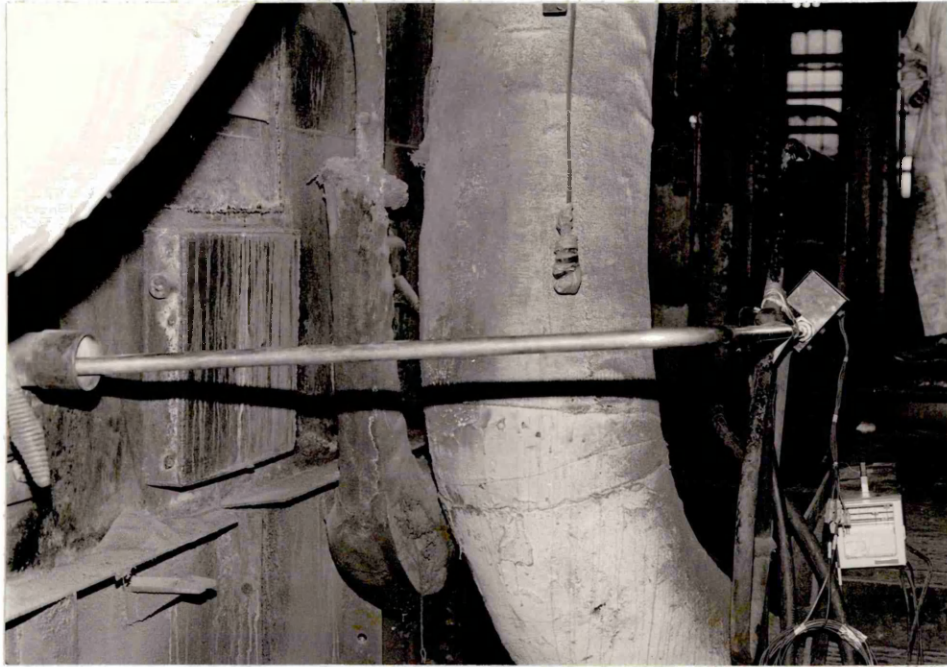


Plate 3-3:

Illustration of ash fouling deposition probe assembly in operation through a viewing port.

Ash deposits were collected from the surface at thermocouple position 3 as well as an area approximately 15 cm on each side of the thermocouple position.

The probe was positioned at the level of the screen tubes, since this was one region where the effective use of Lycal 93HS was of particular importance. It had been intended that the temperature of the probe would be maintained in the range of 330-350°C in order to simulate the thermal conditions that existed at the surface of the screen tubes. However, due to difficulties in maintaining the air flow pressure at high enough levels along the probe, temperatures in the range of 350-390°C could only be achieved for thermocouple position 3, for the durations of the tests. The air pressure was maintained at around 11×10^4 Pa.

An ash deposit had been expected to form on the probe after a short time. However, after the initial two and four hour trials, the amount of ash deposited was very small and it became apparent that longer exposure periods would be required to obtain a significant sample. Unfortunately test runs for longer than twelve hours were not deemed feasible due to certain restrictions at the plant such as shortage of personnel to assist in monitoring the boiler conditions.

Various boiler conditions and operating parameters were observed and recorded during each test by experienced power plant operators. These test parameters are summarised in Table 3-4 and recorded using the form shown in Table 3-5.

During periods while the probe was in use, soot-blowing was terminated within the lower and upper furnace regions, to avoid any interference with ash flow and Lycal injection.

The ash deposits collected at the end of each trial were weighed and XRF-chemical analysis of deposits collected after 12 hour tests, with and without Lycal 93HS injection was carried out.

Table 3-4: Summary of boiler operating parameters monitored during the scheduled deposition probe test with and without on-line injection of Lycal 93HS.

BOILER OPERATING PARAMETERS	BOILER SIDE	FREQUENCY
1. STEAM		
Flow Rate (kg/hr)	—	hourly
Final Temperature (°C)	—	"
Secondary Superheater Outlet Temperature (°C)	A,B	"
Primary Superheater Outlet Temperature (°C)	A,B	"
Superheater Steam Pressure (Pa)	—	"
2. GASES		
Boiler Outlet Temperature (°C) (Before Economiser)	A,B	"
Economiser Outlet Temperature (°C)	A,B	"
Air Heater Outlet Temperature (°C)	A,B	"
3. AIR		
Air Heater Outlet Temperature (°C)	A,B	"
Secondary Air Temperature (°C)	A,B	"
Maximum Air Flow (%)	—	"
4. FEED WATER		
Economiser Inlet Temperature (°C)	—	"
Economiser Outlet Temperature (°C)	A,B	"
5. OXYGEN (%)	—	"
6. SMOKE DENSITY	—	"

Table 3-5: Operating data from boiler No.6 during the scheduled deposition probe tests with and without on-line injection of Lycal 93HS.

BOILER No. 6

LYCAL 93HS	TIME	STEAM				GASES				AIR				WATER									
		FLOW Kg/hr	TEMP °C	SUP. HEAT. OUTLET °C		PRIMARY OUTLET °C	BOILER OUTLET °C		ECONOMIS. AIR HEAT. OUTLET °C		W. WORK %	AIR HEAT. OUTLET °C		SECONDARY AIR °C		CONDENS. WATER °C		ECONOMIS. OUTLET °C					
				L.H.	R.H.		L.H.	R.H.	L.H.	R.H.		L.H.	R.H.	L.H.	R.H.	L.H.	R.H.	L.H.	R.H.	L.H.	R.H.		
ON	11.30	168	486	-	518	453	478	521	444	262	256	215	138	0.95	143	163	140	118	131	282	271	6.38	0.70
ON	12.30	171	485	-	518	453	481	522	444	264	257	217	138	1.00	143	166	138	117	131	282	271	6.41	0.71
ON	13.30	162	482	-	510	453	478	504	-	257	251	215	139	0.95	146	166	134	115	130	282	268	6.41	0.62
ON	14.30	179	491	-	521	455	486	-	-	263	259	217	140	0.92	143	163	142	119	131	283	271	6.38	0.72
ON	15.30	177	489	-	518	455	485	-	-	263	258	217	140	0.92	144	163	143	121	129	282	271	6.40	0.70
ON	11.00	165	485	-	502	460	391	519	-	260	248	212	123	0.83	149	149	126	109	132	283	264	6.45	0.67
ON	12.00	172	485	-	504	464	419	519	-	262	249	213	124	0.88	149	149	136	122	132	283	265	6.45	0.61
ON	13.00	172	485	-	499	466	428	534	-	261	250	213	142	0.86	152	169	147	111	130	283	260	6.45	0.70
ON	14.00	180	485	-	493	469	464	529	-	258	245	213	142	0.85	152	171	146	106	129	282	259	6.45	0.61
ON	15.00	182	485	-	493	472	471	536	-	259	247	214	142	0.80	152	168	152	105	132	284	262	6.48	0.61
ON	9.30	170	485	499	-	458	468	514	493	-	264	224	139	0.80	149	168	134	121	163	283	274	6.48	0.61
ON	10.30	171	485	504	-	456	474	516	493	-	270	226	142	0.85	149	171	141	123	162	284	276	6.45	0.61
ON	11.30	174	485	504	-	449	472	524	500	-	269	225	141	0.85	149	171	140	123	162	283	278	6.48	0.61
ON	12.30	177	485	504	-	453	469	522	497	-	268	225	141	0.87	149	171	140	124	162	283	274	6.48	0.61
ON	13.30	174	485	503	-	448	468	521	498	-	268	225	142	0.90	149	171	139	123	162	282	276	6.49	0.61

Table 3-5: (Continued).

BOILER No. 6

ON/OFF	TIME	STEAM						GASES						AIR						WATER						
		% CONDENSATE		SUP. HEAT. OUTLET °C		PRIMARY OUTLET °C		BOILER OUTLET °C		ECONOMIS. OUTLET °C		AIR HEAT. OUTLET °C		% O ₂		% SMOKE		AIR HEAT. OUTLET °C		SECONDARY AIR °C		% ECONOMIS. INF. L ₂		ECONOMIS. OUTLET °C		
		L.H.	R.H.	L.H.	R.H.	L.H.	R.H.	L.H.	R.H.	L.H.	R.H.	L.H.	R.H.	L.H.	R.H.	L.H.	R.H.	L.H.	R.H.	L.H.	R.H.	L.H.	R.H.	L.H.	R.H.	L.H.
ON	15.30	180	485	-	510	443	485	-	-	274	268	223	141	7.9	0.90	149	168	132	127	161	283	279	6.48			
ON	16.30	182	485	-	513	446	483	-	-	271	267	222	141	7.9	0.92	149	167	131	127	163	282	279	6.48			
ON	9.30	170	488	-	510	457	471	500	414	242	254	208	129	9.2	0.85	135	152	126	143	128	268	282	6.41			
ON	10.30	170	482	-	510	457	476	496	416	241	253	207	130	9.1	0.90	135	154	127	144	127	265	282	6.38			
ON	11.30	170	482	-	510	453	474	493	416	240	253	207	131	9.3	0.85	135	154	129	144	128	265	282	6.38			
ON	13.30	169	482	-	504	461	469	495	404	242	251	208	130	9.4	0.95	135	152	127	139	127	269	279	6.38			
ON	14.30	163	485	-	516	454	477	638	422	245	258	210	134	10.0	0.90	135	154	128	142	128	273	282	6.38			
ON	15.30	160	485	-	510	454	477	525	503	276	261	210	134	9.5	0.90	135	154	128	142	127	271	282	6.38			
ON	10.30	190	485	-	499	454	473	-	-	272	263	224	138	8.2	0.95	146	163	136	128	161	284	271	6.48			
ON	11.30	190	485	-	499	460	472	-	-	276	264	226	146	8.2	0.95	146	171	142	125	161	284	274	6.48			
ON	12.30	188	485	-	498	462	471	-	-	275	266	226	143	8.1	0.95	146	171	135	131	159	282	271	6.48			
OFF	9.30	177	485	-	516	460	473	528	438	263	256	217	139	9.1	0.90	143	166	137	117	132	283	267	6.34			
OFF	10.30	165	487	-	518	455	478	528	444	335	254	215	138	9.8	0.95	145	165	137	117	129	281	269	6.36			
OFF	11.30	170	486	-	517	454	475	528	447	338	254	219	139	9.0	0.95	143	159	137	117	128	282	271	6.36			

Table 3-5: (Continued).

TIME		STEAM		GASES			AIR		WATER								
		Wt. %	Temp. °C	Temp. °C	Temp. °C	Temp. °C	Temp. °C	Temp. °C	Temp. °C	Temp. °C							
ON	12.30	160	485	L.H. 510 R.H. -	L.H. 453 R.H. 472	L.H. 516 R.H. 498	L.H. 269 R.H. 269	L.H. 222 R.H. 233	L.H. 269 R.H. 268	L.H. 222 R.H. 133	9.3%	0.90	L.H. 141 R.H. 157	L.H. 129 R.H. 148	162	L.H. 283 R.H. 284	6.48
ON	13.30	169	485	L.H. 504 R.H. -	L.H. 450 R.H. 473	L.H. 511 R.H. 493	L.H. 271 R.H. 268	L.H. 222 R.H. 133	L.H. 271 R.H. 268	L.H. 222 R.H. 133	9.1%	0.90	L.H. 141 R.H. 157	L.H. 130 R.H. 144	162	L.H. 283 R.H. 281	6.41
ON	14.30	171	485	L.H. 504 R.H. -	L.H. 451 R.H. 471	L.H. 509 R.H. 496	L.H. 280 R.H. 266	L.H. 222 R.H. 131	L.H. 280 R.H. 266	L.H. 222 R.H. 131	8.2%	0.88	L.H. 141 R.H. 157	L.H. 130 R.H. 142	162	L.H. 283 R.H. 281	6.41
ON	15.30	172	485	L.H. 507 R.H. -	L.H. 453 R.H. 476	L.H. 521 R.H. 501	L.H. 279 R.H. 268	L.H. 224 R.H. 132	L.H. 279 R.H. 268	L.H. 224 R.H. 132	8.4%	0.89	L.H. 141 R.H. 152	L.H. 130 R.H. 142	163	L.H. 283 R.H. 279	6.45
ON	16.30	166	485	L.H. 507 R.H. -	L.H. 452 R.H. 474	L.H. 516 R.H. 503	L.H. 275 R.H. 269	L.H. 223 R.H. 131	L.H. 275 R.H. 269	L.H. 223 R.H. 131	8.8%	0.86	L.H. 141 R.H. 152	L.H. 128 R.H. 139	163	L.H. 283 R.H. 281	6.41
ON	17.30	165	485	L.H. 500 R.H. -	L.H. 451 R.H. 476	L.H. 512 R.H. 504	L.H. 277 R.H. 268	L.H. 224 R.H. 133	L.H. 277 R.H. 268	L.H. 224 R.H. 133	8.7%	0.88	L.H. 141 R.H. 159	L.H. 130 R.H. 138	166	L.H. 283 R.H. 280	6.42
ON	18.30	174	485	L.H. 510 R.H. -	L.H. 446 R.H. 477	L.H. 512 R.H. 506	L.H. 278 R.H. 270	L.H. 224 R.H. 133	L.H. 278 R.H. 270	L.H. 224 R.H. 133	8.0%	0.90	L.H. 141 R.H. 157	L.H. 126 R.H. 142	161	L.H. 283 R.H. 282	6.45
ON	19.30	173	485	L.H. 513 R.H. -	L.H. 446 R.H. 476	L.H. 513 R.H. 509	L.H. 271 R.H. 271	L.H. 225 R.H. 134	L.H. 271 R.H. 271	L.H. 225 R.H. 134	8.0%	0.86	L.H. 141 R.H. 157	L.H. 124 R.H. 143	163	L.H. 283 R.H. 283	6.45
ON	20.30	171	485	L.H. 510 R.H. -	L.H. 447 R.H. 476	L.H. 517 R.H. 507	L.H. 271 R.H. 270	L.H. 223 R.H. 133	L.H. 271 R.H. 270	L.H. 223 R.H. 133	8.4%	0.90	L.H. 141 R.H. 157	L.H. 122 R.H. 143	162	L.H. 283 R.H. 283	6.48

3.4 INVESTIGATION OF AYRSHIRE COAL AND ITS ASSOCIATED MINERAL MATTER/ASH

3.4.1 Analysis of Ayrshire Coal

3.4.1 (a) Introduction

As a result of the investigation of the earlier samples of boiler deposits, particularly those found in the third batch, it had become evident that an understanding of the coal and the mineral matter in its ash would be essential if the mechanism of deposit formation was to be understood.

3.4.1 (b) Size Analysis of Coal

A sample of air-dried coal weighing 4.783 kg, collected by one of the boiler operators at West Belfast power station, from the hopper feeding the chain grate in boiler No.6, was provided for analysis.

The particle size distribution of the coal sample was analysed according to B.S 410¹⁷⁶, using sieve mesh sizes of 1/4", 3/16", 8, 14, 18, 25, 44, 52, 100, 200, 300 and 350. The sieving time was kept to a minimum in order to avoid undue fracturing and breakage of the larger coal particles.

3.4.1 (c) Determination of Moisture Content

The "inherent" moisture of representative samples of each size fraction of the original air-dried batch of Ayrshire coal was determined. Samples were obtained by "cone and quartering" each size fraction, and then crushed using a mechanically driven pestle and mortar, to pass through a 72 mesh (210 μ m) sieve. The inherent moisture content was determined by the "vacuum" method, using the apparatus illustrated in Figure 3-9 and according to the procedure specified in B.S 1016.¹⁷⁷

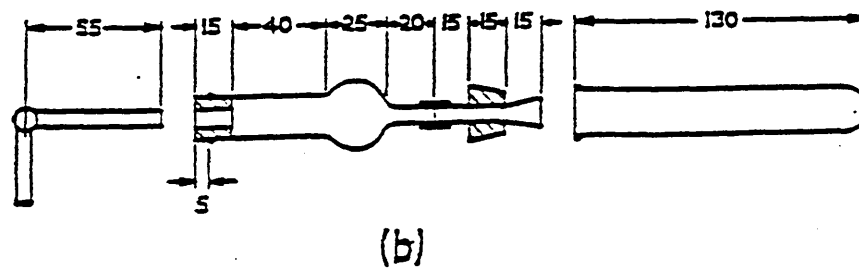
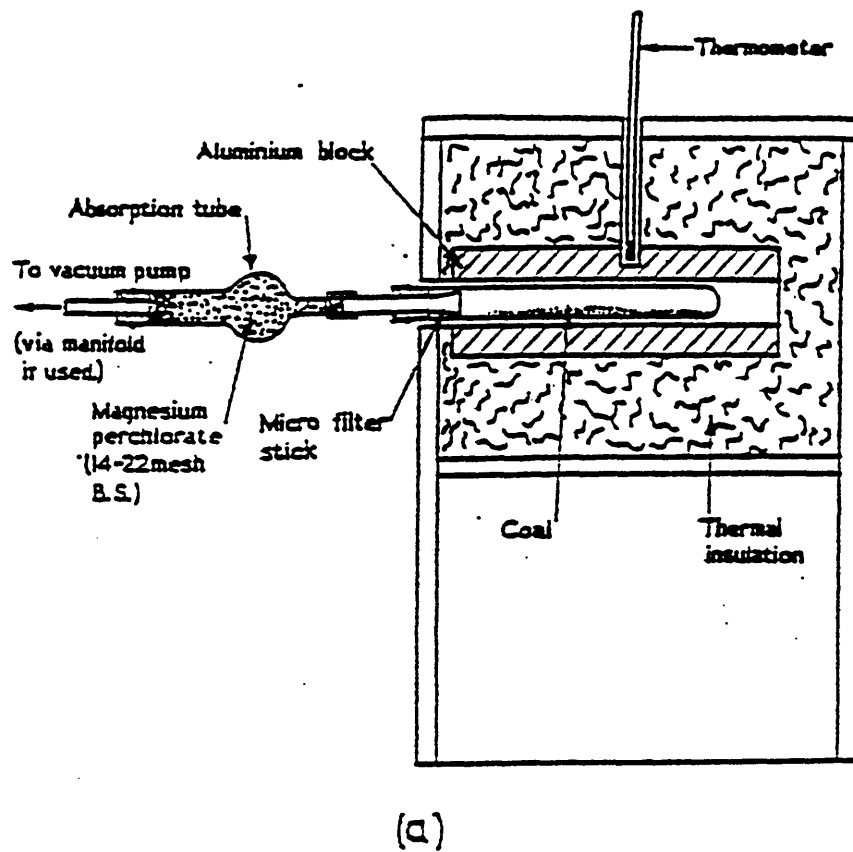


Figure 3-9: Apparatus for the determination of moisture content of coal (vacuum method):
 (a) furnace assembly, (b) absorption tube and weighing vessel (dimensions in millimeters).¹⁷⁵

3.4.1 (d) Determination of the Ash Content

The ash content of representative samples of each size fraction of the original coal batch was determined using the high temperature ashing (HTA) technique described in B.S 1016.¹⁷⁷

With each individual size fraction further crushed down to -72 mesh, an average of twenty separate ashings in batches of five 1.0 gram samples were carried out in order, not only to examine the reproducibility of the results, but also to accumulate large enough quantities of ash from each size fraction to carry out further chemical analysis and fusibility tests.

The principle of the ashing operation consisted of heating a 1.0 gram sample of coal in air to 500°C in 30 minutes and maintaining it at this temperature for another 30 minutes, in a confined atmosphere muffle furnace. The sample was further heated at 815°C in air, using another larger atmosphere muffle furnace, until the sample mass remained constant. The percentage of ash was calculated from the mass of residue remaining after incineration.

In addition, "low-temperature ash" (LTA) from a 100 gram sample of the Ayrshire coal was provided by British Coal Research Establishment (BCRE), using low-temperature plasma ashing. This technique involves oxidation of the carbonaceous matrix by electronically excited oxygen at comparatively low temperatures (< 150°C), leaving the minerals essentially unchanged.¹⁷⁸

3.4.2 The Constitution and Properties of the Mineral Matter/ Ash

3.4.2 (a) Evaluation of Ash Mineral Components

On attempting to ash coarse particles of the coal, it was noted that the mineral matter constituents of the coal ash could be distinguished and separated on the basis of

texture and colour. The individual coal particulates had to be large enough so that when combusted under high temperature ashing conditions, the individual particles of ash could be easily distinguished. It was found that only coal particles of +6350 μ m and +4760 μ m (i.e +1/4" and 3/16" mesh) size would yield sufficiently large ash residues to facilitate a rigorous separation on the basis of the stated criteria.

In total, over 910 nodules of coal, weighing over 522 grams were ashed under high temperature conditions, as described in Section 3.4.1 (d), except that the coal particles were not crushed.

Individual components of the ash thus obtained were subsequently identified and separated on the basis of the previously stated criteria, using visual and stereo-microscopic examination. As the work progressed, the frequency of occurrence as well as the mass of the individual coal ash components was documented. Thus an assessment of the relative abundance of the various coal ash species, which could be related to the mineral matter in the original coal, was obtained.

Furthermore XRF-chemical analysis of the more dominant ash species (based on either their frequency of occurrence or their mass percentage) was carried out.

3.4.2 (b) Chemical and Mineral Constitution of Coal Ash

X-Ray Fluorescence (XRF) Chemical Analysis

XRF analysis was carried out by Steetley Refractories Ltd. of Worksop, to determine the elemental composition of bulk boiler deposit samples including the fly ash samples taken from the deposition probe, the high and low temperature ashes, the ash from various coal size fractions and a selected range of separated coal ash species.

The analyses are reported as the mass percentages of the most stable oxides of the elements determined. In this study only the eight major oxides mainly present in the

coal ash have been reported, balanced to 100%. However, occasionally data has also been reported for sulphur content of samples as SO₃.

X - Ray Diffraction (XRD) Analysis

The principle operation and procedure for this technique has already been described in Section 3.3.3.

The technique which is sensitive to the presence of minerals in concentrations of greater than a few mass percentage, was used to determine the crystalline minerals and phases in low and high temperature ash sample specimens, as well as the separated high temperature ash components.

However, some of the ash components were not found in large enough quantities to fill the standard sample plate, and hence the technique had to be modified. A small specimen taken from the ash component was sprinkled onto the surface of a micro-thin circular glass plate, smeared with a small amount of petroleum jelly. The specimen was spread out to form a uniform layer covering the surface area of the glass plate and then the plate was mounted onto the sample holder, of the diffractometer, using the standard sample plate as the supporting base to rotate it into position inside the sample holder assembly.

3.4.2 (c) Determination of Softening and Melting Behaviour of Coal Ash

Cone fusion testing of coal ash

A series of cone fusion tests were carried out to determine the softening and melting characteristics of high temperature ash samples, with and without additions of Lycal 93HS. These were carried out in three different "fashions":

- Representative specimens of the bulk coal ash sample, with various additions of Lycal 93HS between 2.0 to 8.0 mass%

- Ash admixtures formed from the coarse (i.e. +6350 +2057 μm) and the smaller (i.e. +150 +53 μm) coal size fractions, with additions of Lycal 93HS between 0.5 to 3.0 mass%.
- Representative specimens of selected components of separated ash, with an addition of 0.5 mass% of Lycal 93HS.

The furnace operation and cone sample preparation were identical to the procedure described in section 3.3.4(a)-(d).

Hot-Stage Microscopy of Coal Ash

A hot-stage microscope was used to study the softening/melting behaviour of HTA, LTA and a selected number of components of the high temperature ash. In addition, the effect on the melting and crystallisation behaviour of the HTA, LTA and the ash components, of varying additions of Lycal 93HS between 1.0 to 10.0 mass% was investigated.

The hot-stage microscope used was manufactured by Alison Instruments, a division of Alison Engineering Ltd. A 30% Rh/Pt wire and a 6% Rh/Pt wire, approximately 3 cm. in length each, comprise the arms of the thermocouple junction which when welded together at the tip; supports, heats and measures the temperature of the sample. The temperature was recorded on a digital temperature display. Reactions occurring at temperatures up to 1800°C could be observed. In operation, the thermocouple was connected to a power supply generating pulses at 300 Hz. For half a cycle, power is supplied to the thermocouple to raise the temperature of the sample, while the emf generated at the thermocouple tip is measured during the remaining half of each cycle. The thermocouple was mounted in a cell fitted with glass windows. The thermal behaviour of the ash samples was observed through adjustable binocular x10

eyepieces and two parfocal objectives of power x5 and x10 mounted in front of the cell, all assembled on a turret. At the rear, the lamp assembly containing a 20 watt quartz-iodine source fitted with an adjustable iris, was used to illuminate the sample within the cell.

The temperature of the sample could be raised or lowered in the range 20-1800°C within a few seconds. It was thus possible to melt the ash samples and, by rapidly lowering the temperature, quench to a glass. Subsequent reheating of the ash specimens allowed the crystallisation process to be observed.

Procedure

The apparatus was calibrated using a range of reagents which included Na₂SO₄ (melting point = 884°C), K₂SO₄ (melting point = 1069°C) and 2CaO.Al₂O₃.SiO₂ [Gehlenite- (melting point = 1582-1596°C)], covering the temperature range of interest in this study.

Ash samples were crushed to -240 mesh (-63µm) and when applicable 0.2 gram specimens were mixed with various quantities of Lycal 93HS in a silica dish, using a spatula. Microgram samples of ash to be studied were mounted at the tip of the V-shaped junction of the thermocouple. The thermocouple was then introduced into the cell and fastened to the microscope stage by means of clamping screws. A small amount of argon was passed continuously through the cell to reduce the amount of volatile material condensing on the cell windows. The flow rate was monitored using a small liquid bubbler.

With the thermocouple centered in the field of view of the objective lens and in focus, the sample was heated to about 900°C in a fraction of a second. Further heating was carried out more slowly at approximately a rate of between 25°C to 50°C per minute.

Various stages of melting, from sintering to complete fluidity were directly observed through the binocular eyepieces. For each stage of melting the corresponding temperature was recorded by direct reading off the digital temperature display.

Equilibrium was achieved at each stage by holding the sample at the specific temperature for at least 5 minutes. The temperature was taken up to a maximum of 1600°C to ensure complete fluidity and homogeneity of the melt.

The nature and the extent of crystallisation was investigated for the whole range of HTA, LTA and selected components of ash samples with and without additions of Lycal 93HS.

The crystallisation range was determined by cooling the fluid ash to a pre-decided temperature at which samples were held for a minimum of 30 minutes in order to allow for maximum crystal growth to occur. This process was repeated for lower temperatures and the observations were recorded. The various melting stages as well as the crystallisation regimes were recorded photographically through the attachment of an automatically driven camera which was mounted on the turret extension of a single stage eyepiece.

4.1 INTRODUCTION

The results of the detailed analyses carried out during the course of this investigation on coal, coal ash and coal ash deposits, with and without Lycal 93HS are described hereafter. The results are presented in two major parts:

In the first part, deposits from boilers No.6 and No.5 are considered for various characterisation studies. These include the structural, morphological and chemical composition of the deposit samples, the softening characteristics of deposits with and without additions of Lycal 93HS, determination of fly ash deposition and its composition as well as surface-leaching characterisation of deposit samples from boilers No.6 and No.5.

In the second part, characteristics of Ayrshire coal are investigated. These include the physical and chemical properties of the coal and its ash as well as the characterisation of various ash components in terms of its composition, mineralogy and its softening behaviour with and without additions of Lycal 93HS.

4.2 STRUCTURE, MORPHOLOGY AND CHEMICAL CONSTITUTION OF BOILER DEPOSITS

4.2.1 Boiler Observations

An overall view of the water wall tubes in the furnace area of boiler No.6 can be seen in Plate 4-1. The photograph shows the extent of deposition on the front, rear and side wall tubes after a period of three months of continuous operation with Lycal 93HS. As can be seen, the boiler tubes are in a relatively clean condition.

The effectiveness of Lycal 93HS was demonstrated when the injection ports became partially blocked in one half of the boiler, namely B-side. The deposits received at the end of this period of injection in March 1987, constituted the third batch of deposits.

CHAPTER

(4)

EXPERIMENTAL RESULTS

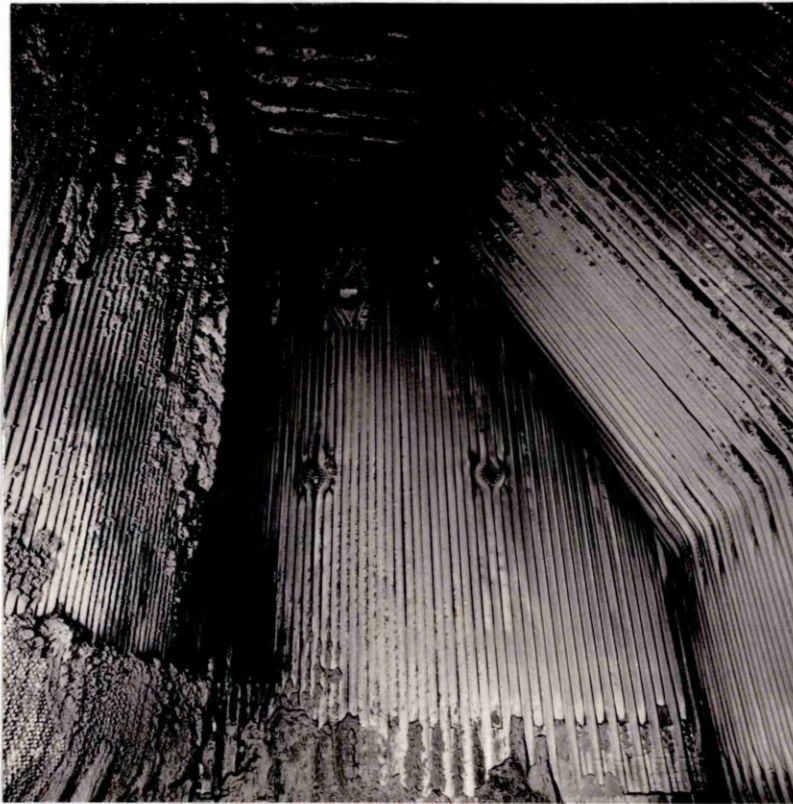


Plate 4-1:

A view of the A-side of boiler No.6 after 3 months of Lycal 93HS injection, showing reasonably clean surfaces of front (LHS), rear (RHS) and side wall tubes.

Plates 4-2 and 4-3 show the extent of deposit formation on the front and rear walls respectively of the left hand side (A-side) of the boiler where Lycal 93HS delivery had been normal. With the exception of some patches of slag on the front wall and partially covered surface of the reclining rear wall tubes, the deposit build-up is very small. In comparison, on the right hand side of the boiler (B-side), where Lycal 93HS injection had been temporarily hindered, the extent of deposit build-up as shown in Plates 4-4 and 4-5 is more pronounced.

It is reasonable to suggest that as a consequence of Lycal 93HS depletion, the deposits formed are more tenacious than those formed on the A-side of the boiler, and proved more difficult to remove by sootblowing.

4.2.2 Bulk Chemical Analysis of Deposit Samples From Boilers No.5 and No.6

The bulk analyses of samples of deposits received at various intervals before and after the injection of Lycal 93HS into boiler No.6 as well as those collected from boiler No.5 under normal operational conditions, i.e. without Lycal 93HS injection, are presented in Tables 4-1 to 4-7. All the deposits were essentially made up of aluminosilicates with varying amounts of iron, calcium and magnesium compounds, and only small traces of sodium and potassium compounds present.

Some interesting aspects of the analyses are worthy of comment:

(a). For all the samples from boilers No.5 and No.6, it is evident that whereas the deposits taken from the lower furnace regions have an iron oxide content compatible with that of the average coal ash i.e. 11 mass% (see Section 3.2.2, Table 3-2), the samples from the upper furnace regions have iron oxide contents up to and greater than three times that amount (14%-39%).

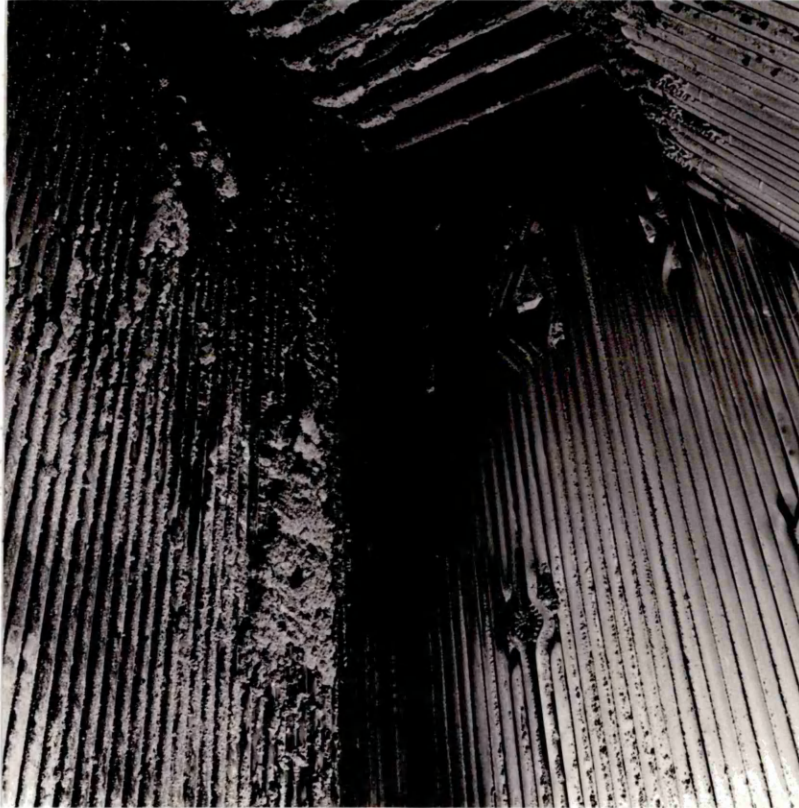


Plate 4-2:

A view of the front wall tubes (LHS), from the A-side of boiler No.6 after 3 months of Lycal 93HS injection, showing a restricted area of deposit formation.

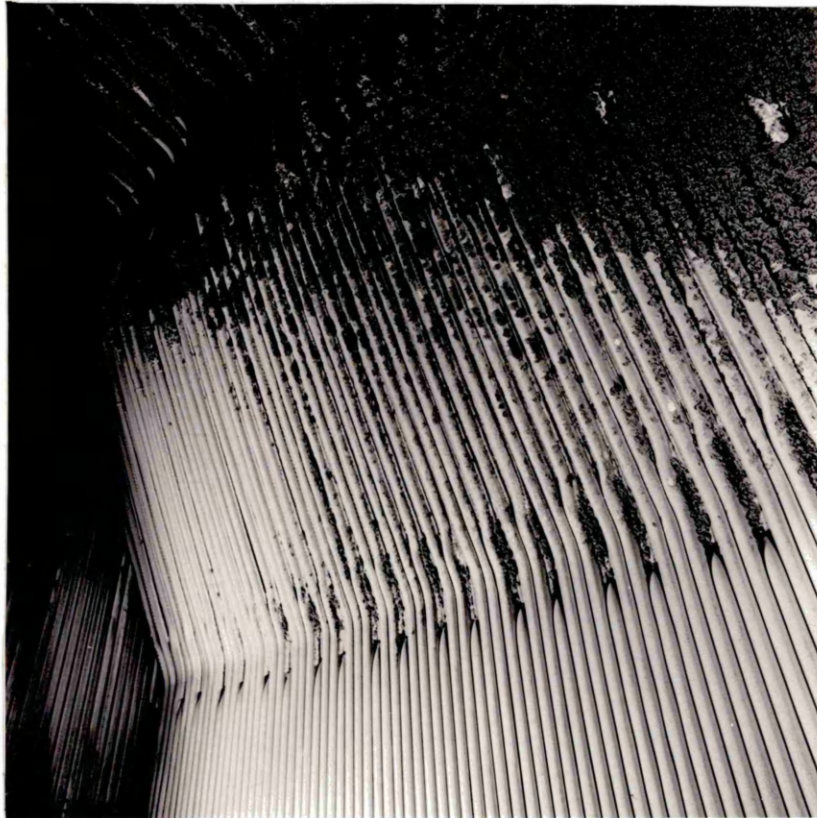


Plate 4-3:

A view of the rear wall tubes from the A-side of boiler No.6 after 3 months of Lycal 93HS injection, showing a restricted region of deposit formation on the surface of the upper section tubes leading to the bottom screen tubes.

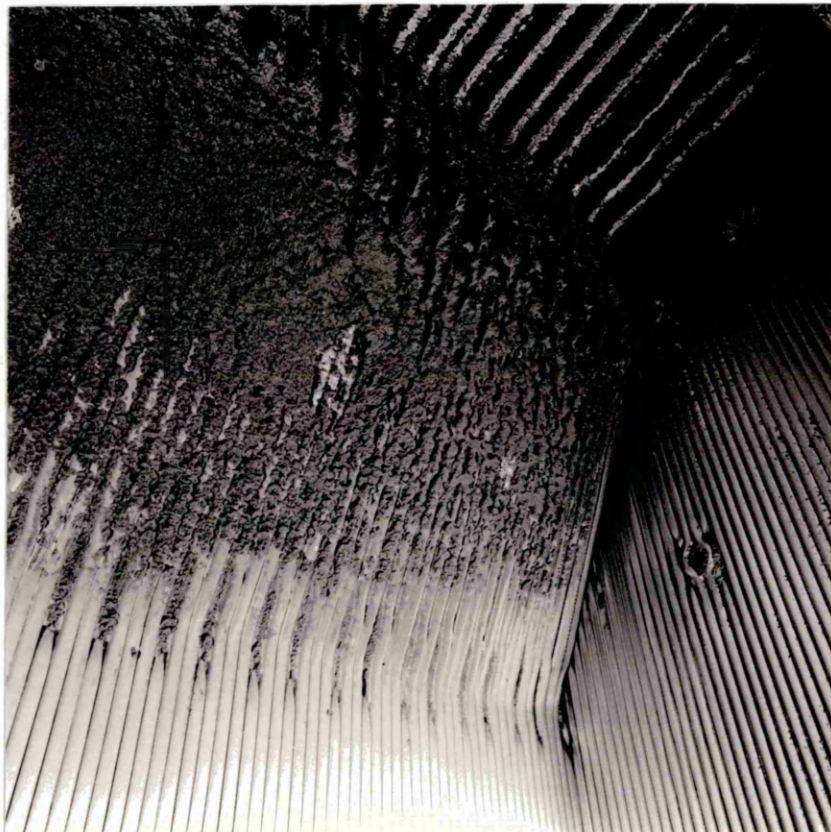


Plate 4-4:

A view of the rear wall tubes from the B-side of boiler No.6, where due to the blockage of Lical 93HS injection ports, an extended region of relatively thick deposits are formed on the surface of the upper section tubes leading to the bottom screen tubes.

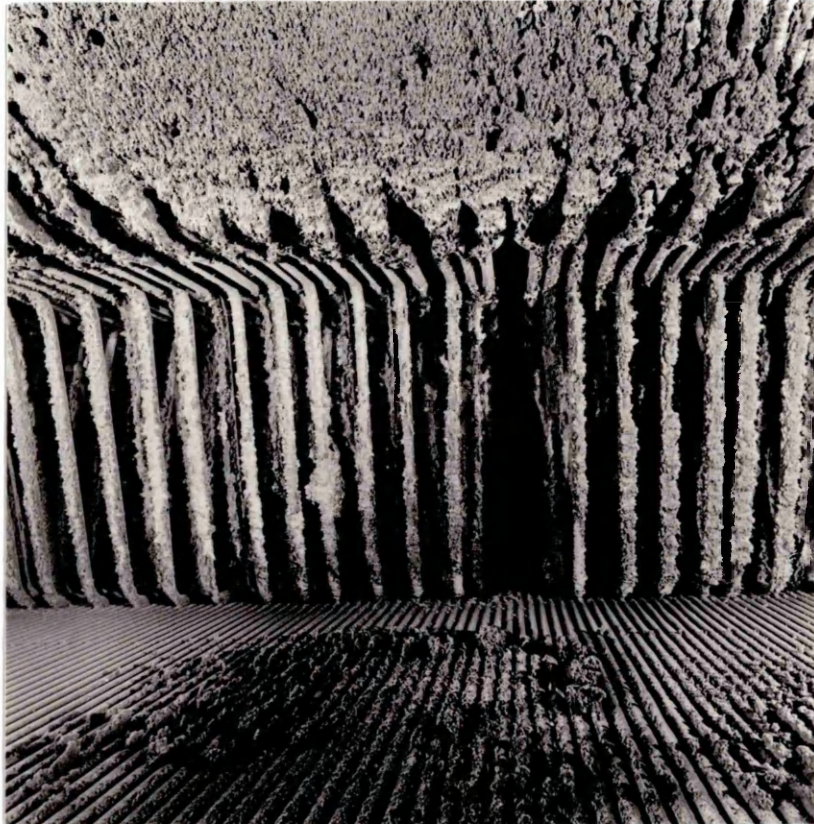


Plate 4-5:

A view of the bottom screen tubes from the B-side of boiler No.6, with partial blockage of Lycal 93HS injection ports, showing deposit formation between the tube surfaces at the top of the photograph.

(b). Where there is a layering effect within the deposits, as mainly was observed in boiler No.5 samples (see Section 4.2.3), in the lower furnace deposits the outer layer is enriched in iron compounds whereas in the upper furnace it is the inner layer which is enriched.

(c). For the post Lycal 93HS injection samples from boiler No.6 (Tables 4-2 to 4-5), the higher iron oxide contents whether within the bulk or layering of a sample is invariably associated with higher magnesium oxide values.

(d). For the "grit arrestor" and "economiser ash hopper" particulate samples (Table 4-7) it can be seen that whereas a high concentration of iron oxide is consistently associated with increased amounts of magnesium oxide for samples from boiler No.6, for the samples collected from boiler No.5 such a pattern does not emerge. The increase in the amount of iron oxide and magnesium oxide is particularly revealing for the fine ($-45\mu\text{m}$) particulates. The variation in the carbon content of the size fractioned grit arrestor and economiser ash hopper particulate samples with and without injection of Lycal 93HS is further shown in Table 4-8 and Figure 4-1. This is a measure of the ash's ability to form spheres, as explained in Section 2.4.2.

4.2.3 Visual Examination of Boiler Deposits

The deposit samples from boilers No.5 and No.6, without and with on-line injection of Lycal 93HS respectively, over the period of the injection trials, exhibited a wide range of textures, colours and thicknesses. The extent of this variation is illustrated in Plate 4-6, showing samples taken from various locations within boilers No.5 and No.6.

4.2.3 (a) Pre Lycal 93HS Injection - Boiler No.6

A limited number of deposit samples were received for analysis before the commencement of the course of Lycal 93HS injection. These constituted the first

Table 4-1: Bulk chemical analysis of the "first" batch of deposit samples received before the commencement of Lycal 93HS additive treatment on boiler No.6.

SIDE OF BOILER	SAMPLE ORIGIN	COMPOUND MASS PERCENTAGE (%)								
		SiO ₂	Al ₂ O ₃	TiO ₂	Fe ₂ O ₃	CaO	MgO	K ₂ O	P ₂ O ₅	SO ₃
A	CORNER	46.67	26.22	0.56	13.32	5.78	4.34	2.71	0.38	0.0
A	REAR WALL	42.09	26.47	1.02	16.62	5.63	3.76	2.30	2.07	0.0
A	Btm. Sc.T	22.52	14.05	0.65	47.18	5.73	3.54	2.49	1.69	2.1
A	Ps.Sc.T&Sup.T	24.11	14.79	0.62	38.30	6.32	3.57	5.79	3.15	3.2

Note: Btm. Sc.T - Bottom Screen Tubes.

Ps.Sc.T & Sup.T - Passage Between Screen Tubes and Superheater Tubes.

Table 4-2: Bulk chemical analysis of the "second" batch of deposit samples received during the course of Lycal 93HS additive treatment on boiler No.6.

SIDE OF BOILER	SAMPLE ORIGIN	COMPOUND MASS PERCENTAGE (%)								
		SiO ₂	Al ₂ O ₃	TiO ₂	Fe ₂ O ₃	CaO	MgO	K ₂ O	P ₂ O ₅	SO ₃
-	FRONT ARCH	47.51	25.35	0.95	16.23	3.91	3.14	2.43	0.46	0.01
-	REAR ARCH	23.72	67.74	1.69	1.90	2.55	1.04	0.98	0.15	0.16
-	FRONT WALL	52.04	29.68	1.11	9.98	2.21	1.77	3.07	0.11	0.01
-	Btm. Sc.T	47.83	25.33	0.90	16.24	4.79	2.15	2.37	0.37	0.01
-	Ps.Sc.T&Sup.T	47.40	25.29	0.95	16.19	3.90	3.13	2.42	0.45	0.01

Table 4-3: Bulk chemical analysis of the "third" batch of deposit samples received during the course of Lycal 93HS additive treatment on boiler No.6.

SIDE OF BOILER/ TX.TYPE	SAMPLE ORIGIN	COMPOUND MASS PERCENTAGE (%)								
		SiO ₂	Al ₂ O ₃	TiO ₂	Fe ₂ O ₃	CaO	MgO	K ₂ O	P ₂ O ₅	SO ₃
A / F1	FRONT WALL	46.24	31.55	0.93	12.43	5.30	1.66	1.64	0.22	0.01
A / F2	FRONT WALL	33.14	20.17	0.66	32.28	8.87	2.73	1.20	0.56	0.35
B / F1	FRONT WALL	46.27	31.85	1.03	12.24	5.03	1.60	1.64	0.31	0.01
B / F2	FRONT WALL	27.67	17.80	0.62	40.49	9.05	2.56	0.84	0.56	0.35
A / F1	REAR WALL	47.66	33.98	1.11	9.83	5.75	1.66	1.72	0.18	n.d
A / F2	REAR WALL	34.98	22.65	0.86	29.27	7.47	2.31	1.58	0.85	n.d
B / F1	REAR WALL	44.98	31.55	1.03	12.92	5.93	1.66	1.53	0.36	n.d
B / F2	REAR WALL	39.26	25.04	0.83	24.93	5.76	1.87	1.73	0.58	n.d
A / F1	SIDE WALL	49.16	29.33	1.23	11.30	5.42	1.45	1.83	0.26	n.d
B / F1	SIDE WALL	48.92	28.77	1.21	11.70	5.66	1.51	1.97	0.24	n.d
B / F1	Btm. Sc. T.	47.59	29.25	1.31	12.12	6.16	1.62	1.71	0.32	n.d
B / F2	Btm. Sc. T.	40.39	22.25	1.09	24.65	6.72	2.04	1.86	0.96	n.d

Note: F1 and F2 are the two "Friable" types of deposits which were dominant in this batch, with the latter type particularly enriched in Fe₂O₃.

Table 4-4: Bulk chemical analysis of the "fourth" batch of deposit samples received during the course of Lycal 93HS additive treatment on boiler No.6.

SIDE OF BOILER	SAMPLE ORIGIN	COMPOUND MASS PERCENTAGE (%)								
		SiO ₂	Al ₂ O ₃	TiO ₂	Fe ₂ O ₃	CaO	MgO	K ₂ O	P ₂ O ₅	SO ₃
B	FRONT WALL	46.81	31.11	0.76	12.78	4.63	1.78	1.46	0.34	0.08
A	SIDE WALL	47.83	33.57	0.87	10.65	3.69	1.26	1.44	0.58	0.04
B	SIDE WALL	47.60	34.31	0.90	10.94	3.37	1.17	1.25	0.44	0.03
B	Btm. Sc. T.	41.80	29.33	0.91	14.83	4.77	1.84	2.41	3.06	0.29
A	Btm. Sc. T.	38.26	25.58	0.78	24.57	6.37	1.73	1.29	0.70	0.34
B	Ec. ASH Hop	46.72	31.38	0.81	11.94	5.54	1.79	1.26	0.40	0.36
A	Ec. ASH Hop	47.52	31.85	0.83	10.90	5.01	1.69	1.39	0.40	0.50
-	Btm. Clk.	52.38	35.12	0.91	4.35	4.42	1.07	1.63	0.06	0.11

Table 4-5: Bulk chemical analysis of the "fourth" batch of deposit samples with "layering" orientation received during the course of Lycal 93HS additive treatment on boiler No.6.

SIDE OF BOILER/ LAYER	SAMPLE ORIGIN	COMPOUND MASS PERCENTAGE (%)								
		SiO ₂	Al ₂ O ₃	TiO ₂	Fe ₂ O ₃	CaO	MgO	K ₂ O	P ₂ O ₅	SO ₃
A / I	FRONT WALL	46.28	28.48	0.75	18.71	5.37	1.92	0.99	0.82	0.13
A / O	FRONT WALL	27.78	16.05	0.53	39.87	6.89	2.71	1.27	0.69	3.97
A / I	REAR WALL	48.12	35.65	0.96	9.05	3.11	1.26	1.33	0.60	0.01
A / O	REAR WALL	46.94	38.27	0.96	8.67	2.28	0.86	1.27	0.58	0.21
B / I	REAR WALL	47.87	36.05	0.95	9.38	2.91	0.90	1.37	0.58	0.04
B / O	REAR WALL	47.69	34.93	0.92	10.17	3.39	1.09	1.31	0.56	0.01
A / I	Btm. Sc. T.	24.77	14.52	0.50	39.89	7.49	2.00	3.45	0.77	6.11
A / O	Btm. Sc. T.	28.33	16.83	0.56	39.92	7.48	2.15	1.24	0.54	2.78

Table 4-6: Bulk chemical analysis of the "fifth" batch of deposit samples received from boiler No.5 without any Lycal 93HS additive treatment.

SIDE OF BOILER/ LAYER	SAMPLE ORIGIN	COMPOUND MASS PERCENTAGE (%)								
		SiO ₂	Al ₂ O ₃	TiO ₂	Fe ₂ O ₃	CaO	MgO	K ₂ O	P ₂ O ₅	SO ₃
B / I*	FRONT ARCH	9.34	34.30	0.22	12.38	0.67	17.80	0.20	0.02	0.06
B / O	FRONT ARCH	35.67	25.05	0.63	24.10	7.46	6.24	0.57	0.40	0.09
B / I	REAR ARCH	49.63	41.54	1.10	3.78	2.44	0.69	0.64	0.69	0.01
B / O	REAR ARCH	49.30	35.27	0.96	8.70	3.39	1.21	0.93	0.74	0.01
A / -	FRONT WALL	38.38	24.48	0.78	23.87	7.30	2.75	0.76	0.98	0.58
B / I*	FRONT WALL	9.64	31.46	0.22	12.50	0.52	17.98	0.11	0.02	0.75
B / M*	FRONT WALL	18.30	30.21	0.32	13.95	1.84	13.90	0.45	0.07	0.66
B / O	FRONT WALL	46.50	31.80	0.76	10.43	5.82	3.01	1.26	0.34	0.39
B / -	REAR WALL	45.66	33.55	0.97	10.47	4.34	1.96	1.07	0.77	1.06
A / -	SIDE WALL	47.02	34.79	1.09	9.83	4.73	1.42	0.72	0.76	0.04
A / I	Btm. Sc. T.	30.86	19.88	0.65	35.57	6.73	2.23	0.51	0.87	0.64
A / O	Btm. Sc. T.	47.18	33.89	0.99	10.56	3.70	1.19	1.15	0.77	0.33
A / I	Stm. Gen. T.	45.19	29.17	0.84	15.82	5.77	1.66	1.23	0.70	0.14
A / O	Stm. Gen. T.	44.77	31.95	0.93	12.82	3.87	1.11	1.75	1.59	1.57
A / -	Sup. T.	48.44	31.95	0.93	10.41	4.39	1.59	1.08	0.59	0.59
A / -	Ec. ASH Hop.	46.30	33.48	1.03	10.02	3.49	1.07	1.21	1.65	1.77

Note: I=Inner layer, M=Middle layer, O=Outer layer

*Samples were found to contain Cr₂O₃ > 20% - these results have not been normalised.

Table 4-7: Bulk chemical analysis of sieve size fractioned ash particulate samples from boilers No.5 & No.6 without and with Lycal 93HS additive treatment respectively, representing the "sixth" batch of samples.

SIDE OF BOILER/ +/-LYC.	SAMPLE ORIGIN	COMPOUND MASS PERCENTAGE (%)								
		SiO ₂	Al ₂ O ₃	TiO ₂	Fe ₂ O ₃	CaO	MgO	K ₂ O	P ₂ O ₅	SO ₃
B / +	G.A (C)	51.44	33.10	1.66	6.35	2.68	1.53	1.71	0.85	0.65
B / +	G.A (M)	51.11	29.62	1.46	9.65	4.07	1.53	1.79	0.50	0.27
B / +	G.A (F)	48.03	29.94	1.69	11.17	3.56	2.14	1.68	1.00	0.77
A / +	G.A (C)	51.59	32.68	1.61	6.07	2.99	1.43	2.15	0.79	0.66
A / +	G.A (M)	48.01	27.50	1.29	9.01	4.47	1.51	1.92	0.51	0.01
A / +	G.A (F)	47.36	28.96	1.75	10.87	4.15	2.12	2.22	1.35	1.19
A / -*	G.A (C)	53.22	33.26	1.47	5.85	2.59	0.91	2.06	0.60	0.01
A / -	G.A. (M)	50.18	28.40	1.36	10.47	4.84	1.69	1.92	0.56	0.30
A / -	G.A (F)	48.47	28.68	1.61	11.86	4.04	1.44	2.05	1.06	0.74
A / +	Ec. Hop. (C)	52.92	31.94	1.55	5.89	3.11	1.42	1.90	0.72	0.47
A / +	Ec. Hop. (M)	48.26	27.04	1.33	11.00	6.94	2.68	1.61	0.82	0.23
A / -*	Ec. Hop. (C)	50.15	34.90	1.55	6.74	2.90	1.30	1.55	0.40	0.56
A / -	Ec. Hop. (M)	49.57	29.78	1.31	10.56	4.35	1.79	1.67	0.50	0.01

Note: C=Coarse (+500 μ m), M=Medium (-500 μ m +63 μ m), F=Fine (-45 μ m)

*samples collected from boiler No.5 and the rest from boiler No.6.

Carbon contents increased in the range of 8%, 18% and up to 75% for the fine, medium and coarse particulates respectively.

Table 4-8: Bulk analysis of variation in the unburnt carbon content associated with particulate fly ash matter in boiler No.6 with and without on-line injection of Lycal 93HS.

ECONOMISER ASH HOPPERS					
+LYCAL 93HS			-LYCAL 93HS		
Side of Boiler	Fly Ash Size (μm)	Unburned Carbon (mass%)	Side of Boiler	Fly Ash Size (μm)	Unburned Carbon (mass%)
B	+500	71.8-74.8	B/A	+500	73.8-75.1
B/A	-500 +63	14.9-18.0	B/A	-500 +63	13.0-15.7
B	-45	6.0-6.8	B/A	-45	4.7-5.8
GRIT ARRESTORS					
-	+500	63.6-67.8	B/A	+500	58.2-74.5
-	-500 +63	5.8-9.5	B/A	-500 +63	8.0-16.0
-	-45	5.7-7.1	-	-45	5.1-8.7

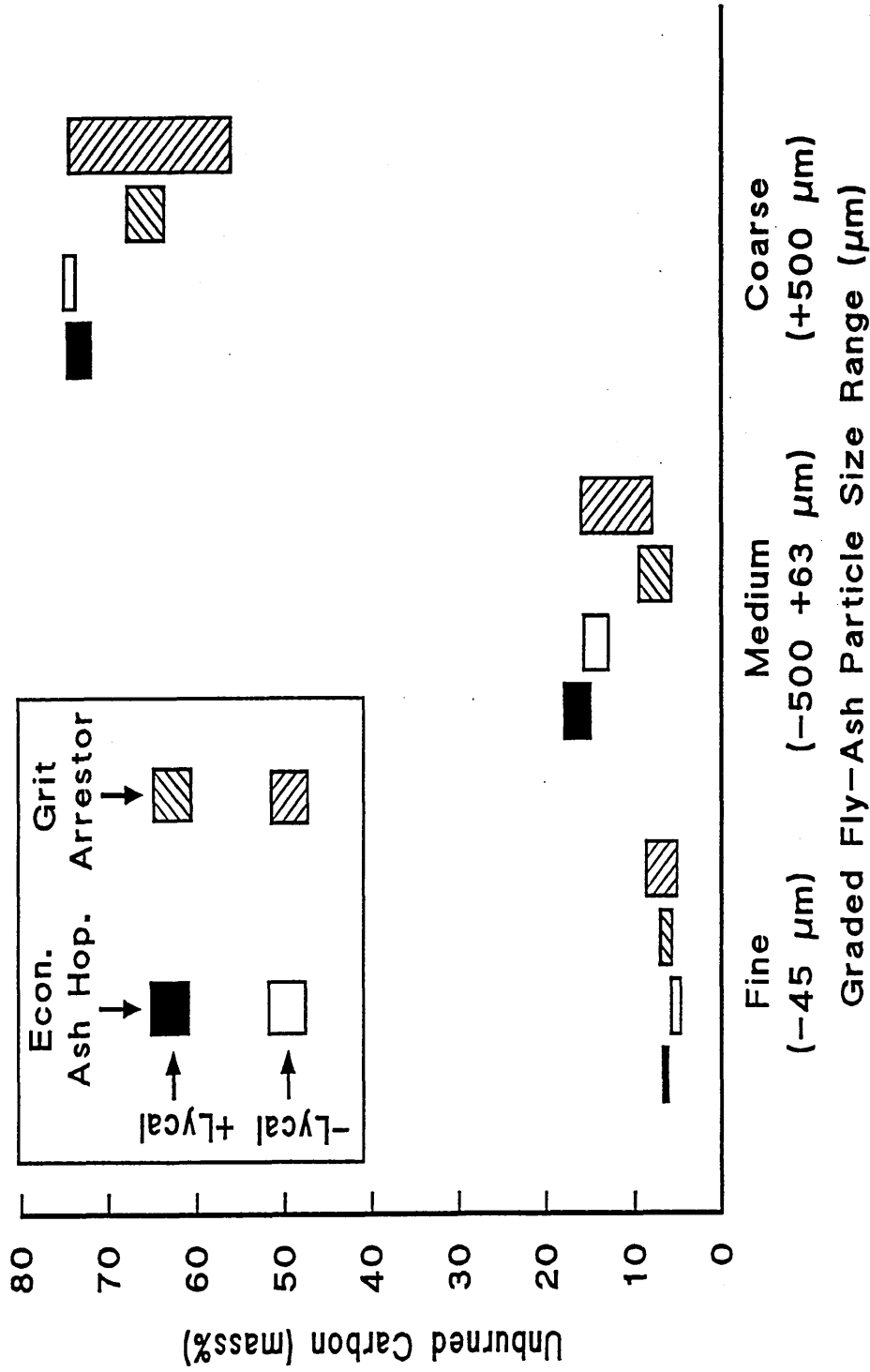


Figure 4-1: Variation of unburned carbon content for size fractionated fly ash particles from economiser ash hoppers and grit arrestors, with and without on-line injection of Lyclal 93HS.



Plate 4-6:

Comparative illustration of a range of deposit samples from boilers No.5: (A = FA, B = RA, C = RW, D = FW, E = Stm.Gen.T) and No.6: (F = FA, G = RW, H = SW, J = Btm.Sc.T, K = Pass Sc.T & Sup.T).

batch of deposits summarised in Table 3-3.

The deposits were predominantly made up of hard, dense, fully or partially fused structures, ranging from 40 mm to 50 mm in diameter. Investigation of these deposits revealed them to have been formed from highly siliceous, fully bonded phases exhibiting a limited degree of heterogeneity.

4.2.3 (b) Post Lycal 93HS Injection - Boiler No.6

The range of deposits which were received over a period of two years of Lycal 93HS injection have been summarised in Table 3-3. The nominated locations within boiler No.6 from which these deposits were taken have been identified in Figure 3-3. The general characteristics of the deposits from each of these locations is summarised as follows:

Front Arch - A light and porous deposit which would break down into granules when only lightly pressed by hand. It had a dark brown, tinted grey colour with a thickness typically of the order of 25-30 mm.

Rear Arch - This material was very similar to the front arch samples, however deposited ash particles nearest to the tube surface were very loosely bonded, whereas in the rest of the deposit, some degree of bridging and sintering was evident. The deposit was a mixture of light and dark brown colours and had a thickness of about 10 mm.

Front Wall - These samples were mostly taken from above or near the secondary air ports. The deposits had a porous, lightly sintered, coarse, brittle structure. The degree of sintering varied. Whereas some samples were only slightly sintered with limited bridging, others had external surfaces which were more continuous and sometimes appeared to have a "glazed" look. This is shown in Plate 4-7, as the less ferrous "F1" type deposit sample of the two friable types of deposit samples, namely

"F1" and "F2", which were characteristic of all of the samples received within the third batch. (see Section 3.2.3 and Table 3-3).

Rear Wall - These samples also had a porous, lightly sintered, coarse, brittle structure. Like the rear arch samples; a soft, dusty layer of 2-3 mm thickness comprised the inner layer. A relatively hard and brittle layer with an outermost surface formed from sharp and pointed particles of ash, impinging onto the previously molten ash layer, comprised the bulk of the deposit.

In some deposit batches, particularly in the third batch, the presence of some softer pieces covered by a yellow/orange dust was noted. These constituted as much as 40 mass% of the total bulk deposit sample. Similar material was also present, but in more limited amount, in the front wall samples. Despite their distinctive appearance, structurally and chemically, they were found to be identical to the other, more prevalent pieces of deposit, which were also "friable". These two types of deposits are thus referred to as "friable-undusted" or "F1" and "friable-dusted" or "F2". They are illustrated in Plates 4-7 to 4-10.

Side Wall - These samples were identical to the front and rear wall samples but with the total absence of the F2 type of deposit.

Screen Tubes - These samples were mostly received from the bottom screen tubes. Once again these samples were of a particulate constitution but with more extensive bridging between the particles. The samples were closely compacted and relatively dense. In some batches, the (F2) type of deposit comprised as much as 50% by mass of the total bulk deposit sample.

The deposits were mostly dark brown to dark red in colour, suggesting iron enrichment. In size they varied between 10-20 mm across and about 10-15 mm in thickness.

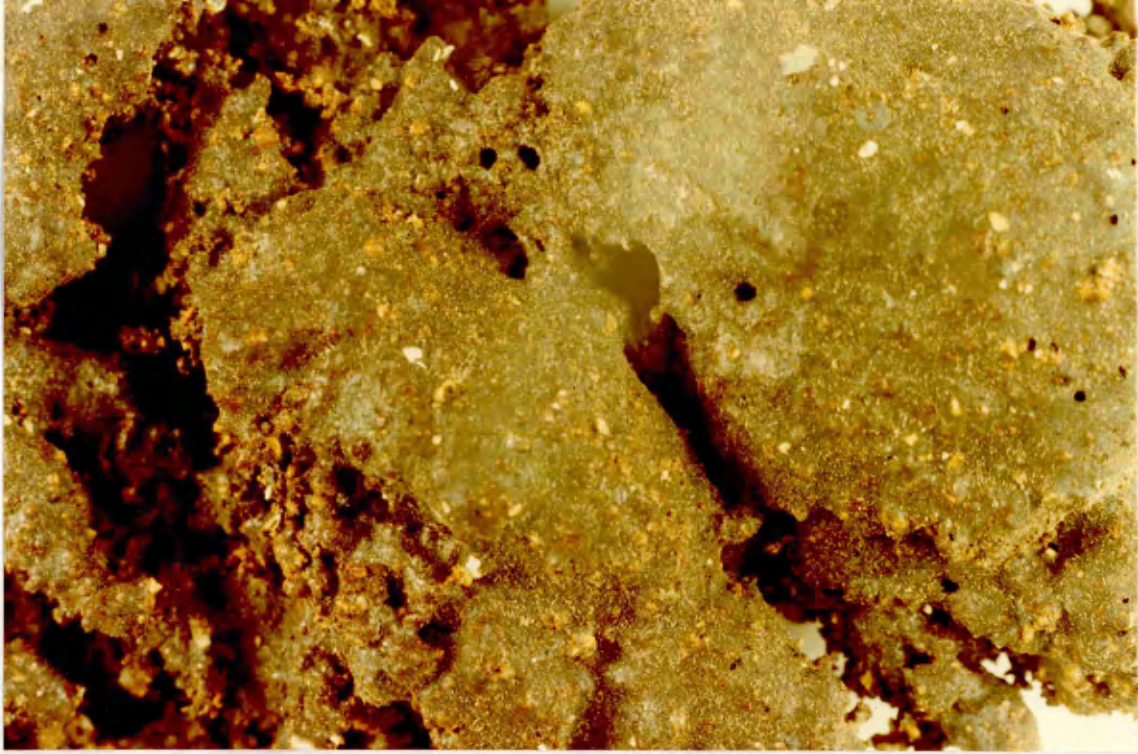


Plate 4-7:

A partially fused, particulate "F1" type deposit sample with a "glazed" surface from lower furnace region of boiler No.6, with on-line injection of Lycal 93HS. [Mag: x4]



Plate 4-8:

A particulate and friable "F1" type deposit sample from the lower furnace region within boiler No.6, with on-line injection of Lycal. [Mag: x4]



Plate 4-9:

A particulate and friable "F2" type deposit sample from the lower furnace region within boiler No.6, with on-line injection of Lycal 93HS. [Mag: x4]



Plate 4-10:

A protruded region within a largely "F1" type deposit sample from the lower furnace region within boiler No.6, with on-line injection of Lycal 93HS, illustrating further the outer orange-brown colour layer covering the surface of the sample. [Mag: x4]

Passage Between Screen Tubes and Superheaters - These samples resembled the bottom screen tube deposits. They were either in pieces 10-25 mm thick or smaller pieces 5-10 mm thick. When squeezed they would break into smaller pieces. They were generally found to have a yellowish brown colour.

Grit Arrestors / Economiser Ash Hoppers - These consisted of individual particles of fly ash with varying sizes and shapes. The major bulk of the particles were spherical, with lesser amounts of non-spherical particles. The larger particles tended to have rough surfaces, while the smaller ones were smooth. The colour of the particles was from light to dark grey and they could be opaque or translucent.

Bottom-grate clinker - Considerable variation existed amongst the received samples. Some larger particles which were probably the product of the fusion of the residual mineral matter and ash on the grate, had a fully fused, shiny texture whilst others were clearly carbonaceous. Plates 4-11 and 4-12 represent typical examples of each of these types of sample.

4.2.3 (c) No Loyal 93HS Injection - Boiler No.5

Like boiler No.6, deposit samples were collected from both sides of the boiler; i.e. the left hand side (side A) and the right hand side (side B). Table 3-3 summarises the deposits which were collected from boiler No.5 after one month (720 hours) of continuous operation before the shut down.

The most striking difference between these samples and those received from boiler No.6 was their much greater size, thickness and density. Furthermore, whereas the samples received from boiler No.6 were generally monolithic, the boiler No.5 samples were mostly of a multi-layered structure with a wider colour variation between samples.



Plate 4-11:

A piece of bottom grate clinker illustrating a porous, fused, slag-like texture. [Mag: x4]



Plate 4-12:

A piece of bottom grate clinker illustrating a stratified carbonaceous texture. [Mag: x4]

Front Arch - This was a very hard, dense deposit which could be divided into two layers:

(a) *Inner layer*: This was the layer closest to the boiler tube surface. This was a very hard, dense and fairly smooth layer. The thickness varied between 10 and 15 mm. It had a mixed dark and light brown colour.

(b) *Outer layer*: This was the layer closest to the flame and gas flow. It was a hard layer with a spikey texture. This layer was fairly porous and had a thickness of 2-3 mm. The colour was a mixture of dark brown and grey particles.

Rear Arch - This was hard and brittle with a relatively high degree of sintering and fusion between the spherical ash particles. This deposit consisted of two layers:

(a) *Inner layer*: This was the layer closest to the boiler tube surface. This was a soft, powdery particulate layer with a thickness of 2-4 mm. It exhibited a yellow/orange range of colours.

(b) *Outer layer*: This layer comprised the bulk of the deposit, formed closest to the gas flow. The sample had a thickness of about 20-30 mm and had a light leadish grey colour.

Additionally, some deposit samples with a monolithic, well sintered structures of approximately 25-30 mm thick were also found within the deposit batch.

Front Wall - A hard deposit with three layers:

(a) *Inner layer*: This was hard and dense and well fused into the next layer. The layer had a thickness of 1-2 mm and ranged in colour from brown to orange.

(b) *Middle layer*: This had a very hard, dense, glassy structure with an abrasive surface. The thickness of this layer was approximately 4 mm and ranged in colour from grey to dark brown.

(c) *Outer layer*: This was a black, fully vitrified layer about 20-23 mm thick and comprised the bulk of the deposit. It had a porous structure, but despite this, it had a hard and abrasive character. Plate 4-13 shows this deposit with its three distinctly coloured and textured layers.

Rear Wall - This was a bulky, highly porous, fully fused, homogenous, vitreous deposit. Despite the porosity voids, the deposit was very hard. The thickness of the sample was approximately 30-33 mm. It was black in colour.

Side Wall - This sample was identical to the rear wall sample. In some of the smaller sample pieces, varying degree of sintering was evident between the ash particles.

Steam Generating Tubes - This deposit was comprised of two layers:

(a) *Inner layer*: This was a porous, hard, abrasive deposit with a moderate degree of sintering. It had a thickness of 50-55 mm and had a dark brown and dark grey mixture of colours.

(b) *Outer layer*: This was a soft, dusty, thin layer which enveloped the inner layer. It was of a mixed dark brown and orange colours.

Screen Tubes - This deposit sample was collected from the bottom screen tubes and was identical to those samples received from the same position within boiler No.6.

Superheater Tubes - This was a very fine powder sample and could only be collected from the area underneath the superheater tubes since the tubes were clean of any particulate matter. This was identical to the following sample from the economiser ash hopper samples.

Grit Arrestors and Economiser Ash Hoppers - The samples collected were identical to the corresponding samples received from boiler No.6 for the same locations.



Plate 4-13:

Cross-sectional view of a very hard lower furnace layered deposit from boiler No.5, without on-line Lycal 93HS injection, showing a black, vesicular, glassy outer layer, a grey middle layer and a brown lustered, smooth outer layer.

4.2.4 Microscopic Examination and Elemental Analysis

All deposit specimens were examined in both the unpolished and polished conditions using a stereo-microscope, a standard optical photo-microscope and scanning electron microscopes equipped with EDX qualitative elemental analysis.

4.2.4 (a) Unpolished, As Received samples from Boilers No.5 and No.6

Regardless of their source location within the boiler unit, all deposits mainly comprised of agglomerations of a wide range of spherical ash particles of varying size, colour and composition, sintered or fused together.

Under the stereomicroscope, the spherical ash particles varied from colourless or white, through shades of orange, red and maroon to brown and black, suggesting a complex range of compositions, mineralogy and physical states within the deposit samples. Scanning electron microscopy, together with EDX analysis, was used to examine the ash particles in more detail and to identify their elemental constitution. A range of some of the typical structures observed with the aid of the SEM are illustrated in plates 4-14 to 4-28.

Boiler No.6 - Plates 4-14 to 4-22 are representative of deposits taken from boiler No.6 with on-line injection of Lycal 93HS.

Plates 4-14 and 4-15 show a typical surface morphology of a "front arch", a "front wall" or a "side-wall" sample from boiler No.6 after Lycal injection. It exhibits a limited degree of bonding and sintering between spherical ash particles.

Points "A" and "B" respectively illustrate examples of smooth and rough surface textured ash particles with different compositions. Plate 4-15 is a higher magnification of the B-region in Plate 4-14. It shows the wide spread, clustered dispersion of particles of pure iron oxide covering the surface of the alumino-silicate rich ash

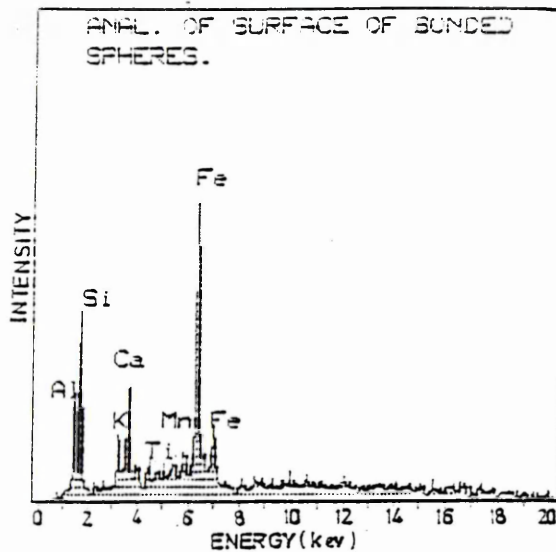
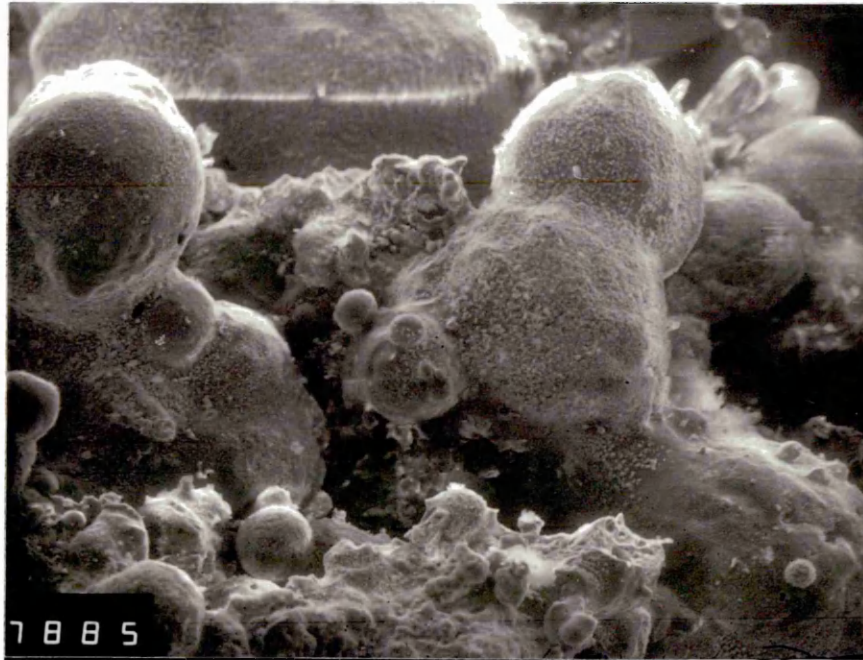


Plate 4-14:

SEM-micrograph of an as received, unpolished deposit sample from the lower furnace region (i.e. FA, FW or SW) of boiler No.6 with on-line Lyclal 93HS injection, showing limited degree of bonding and sintering between spherical ash particles of various sizes. The EDX-analysis shows the surface composition of the smooth "A" and rough "B" textured regions respectively (see Plate 4-15 for analysis of area "B"). [Mag: x130]

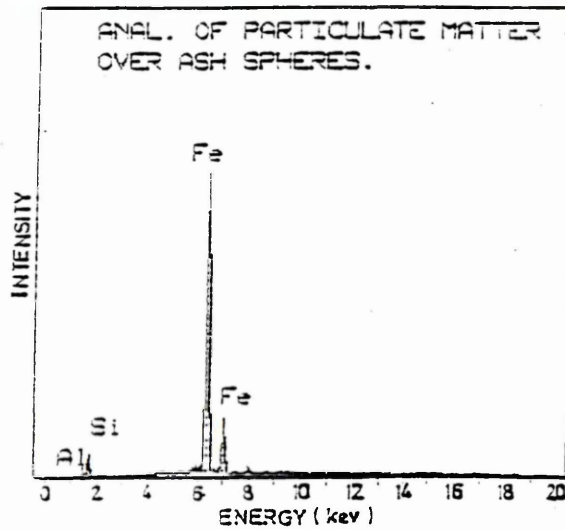
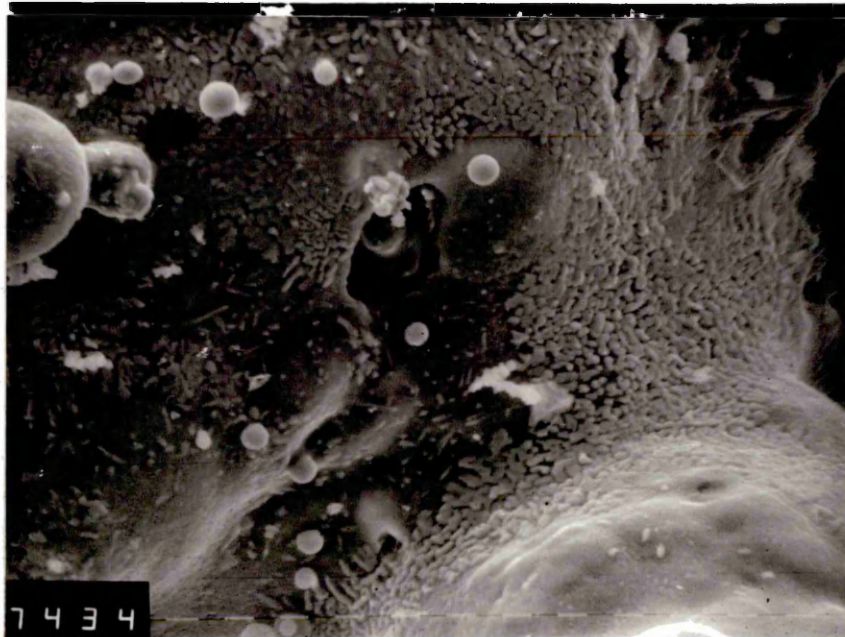


Plate 4-15:

SEM-micrograph of bridged iron oxide particles over the surface of the bonded ash spheres in Plate 4-14. Finer cenospherical ash beads are supported on the surface of the much larger ash particles. The EDX-analysis of the particulate iron oxide dispersion is shown. [Mag: x520]

matrix. The appearance of such iron oxide dispersions, although encountered in all the samples taken from various locations within the boiler No.6, was most commonly present in samples from the upper furnace regions. The EDX analysis illustrates the ferriferous nature of these particulates.

Plate 4-16 shows a typical morphology of a "rear arch" or a "rear wall" sample from boiler No.6, exhibiting a dispersion of alumino-silicate ash particles of various sizes illustrated by points "A" and "B" imbedded in a crusty iron-silicate matrix, identified as point "C". There is very little direct bonding between the ash particulates.

Plate 4-17 shows the surface morphology of a "screen tube" deposit sample from boiler No.6. The main feature of these samples is the extensive dispersion of the fine iron rich particles, spread over the surface of the deposits (see the EDX analysis for area A). The spherical ash particles are further deposited onto the surface, gradually dissolving into the body of the deposit.

Plate 4-18 shows further capture of spherical ash particles of various sizes into the molten surface of the body of the "screen tube" deposit from boiler No.6. The rounded shape outline of some of the larger ash particles which have become incorporated into the body of the deposit is evident.

The wide scale dispersion of fine iron oxide particles, as previously shown in Plate 4-15 is further evident.

Plates 4-19 to 4-21 are particularly representative of "screen tube" deposit samples.

Plate 4-19 shows the agglomeration of a group of smooth ash cenospheres exhibiting considerable diversity of size. The large spherical ash particle clearly shows a different texture and transparency compared to the ash cenospheres.

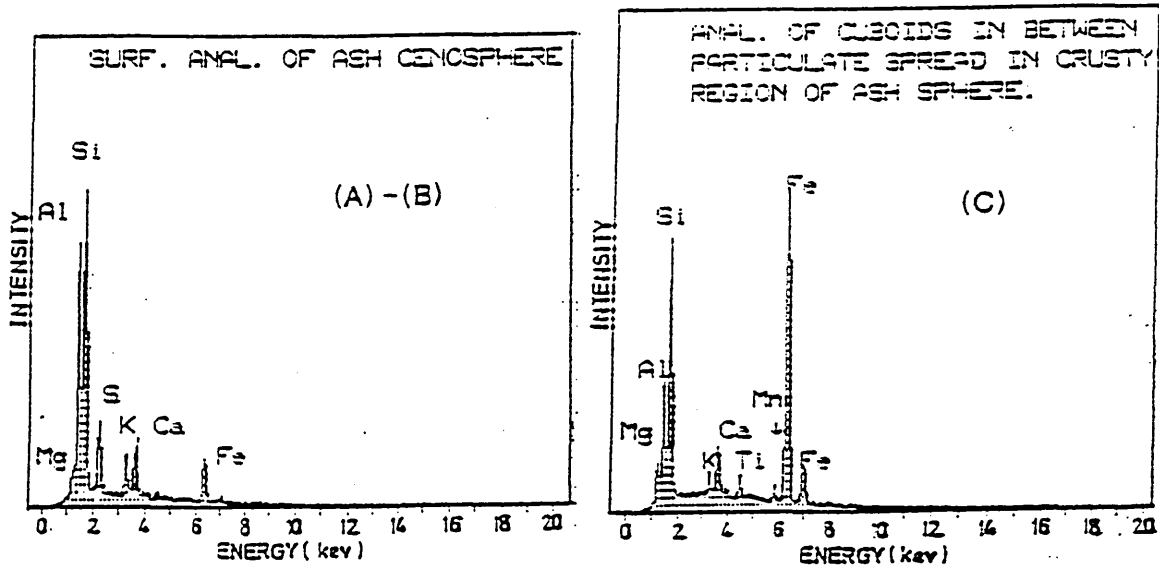
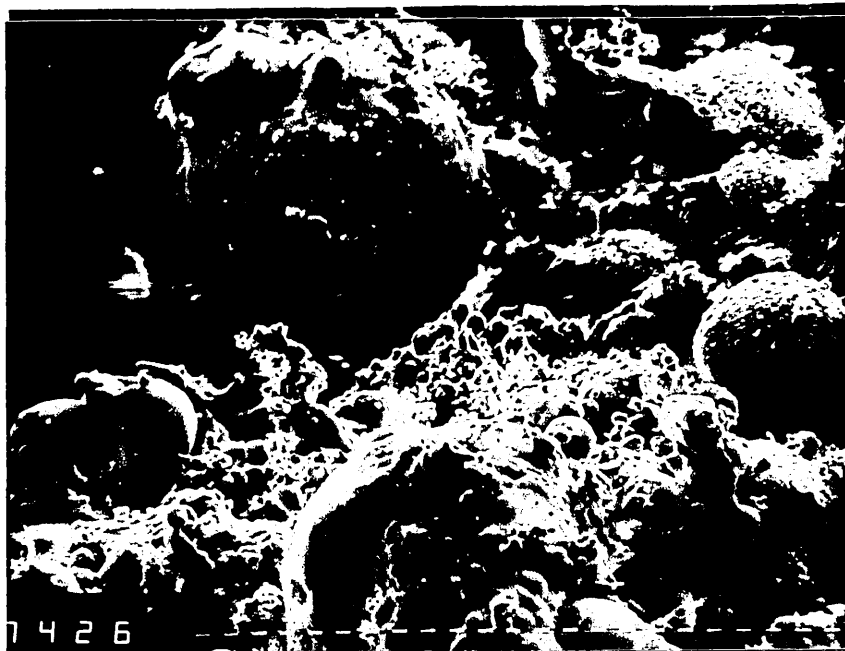


Plate 4-16:

SEM-micrograph of an as received, unpolished deposit sample from the lower furnace region (i.e RA, RW) in boiler No.6, with on-line Lycl-93HS injection. The EDX-analysis shows the surface composition of the Smooth "A" and rough "B" surfaced ash spheres of different sizes, imbedded in a crusty iron-silicate matrix, area "C". [Mag: x220]

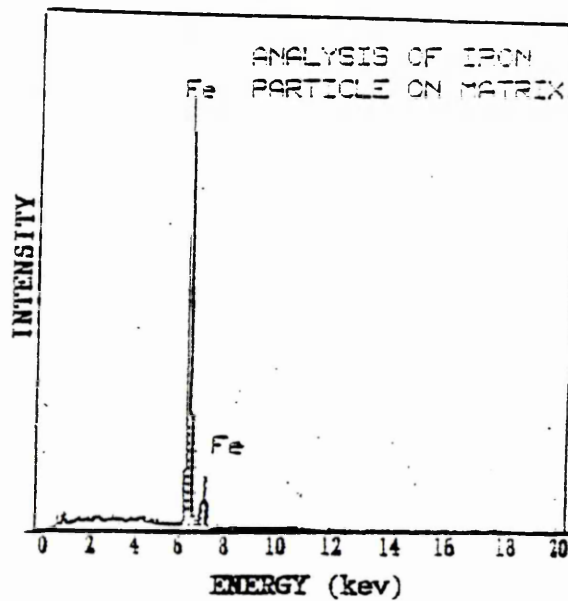
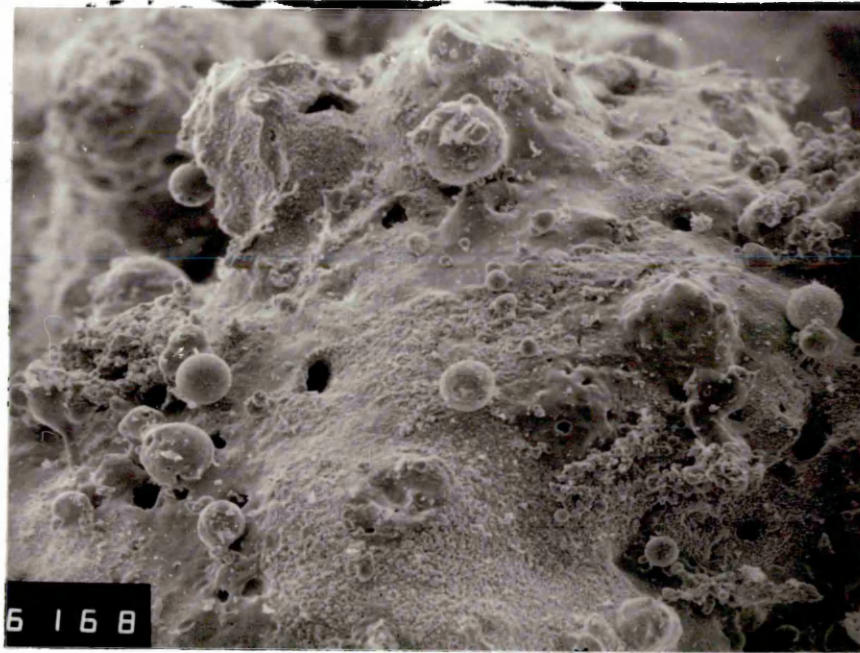


Plate 4-17:

SEM-micrograph of an as received, unpolished deposit sample from the Bottom Screen Tubes in boiler No.6, with on-line Lycal 93HS injection. Roughly surfaced alumino-silicate matrix exhibits the dispersion of iron oxide particles (area "A"). Further deposition of small solid ash spheres and cenospheres on the matrix are shown. The EDX-analysis shows the composition of the fine particulates (area "A"). [Mag: x70]

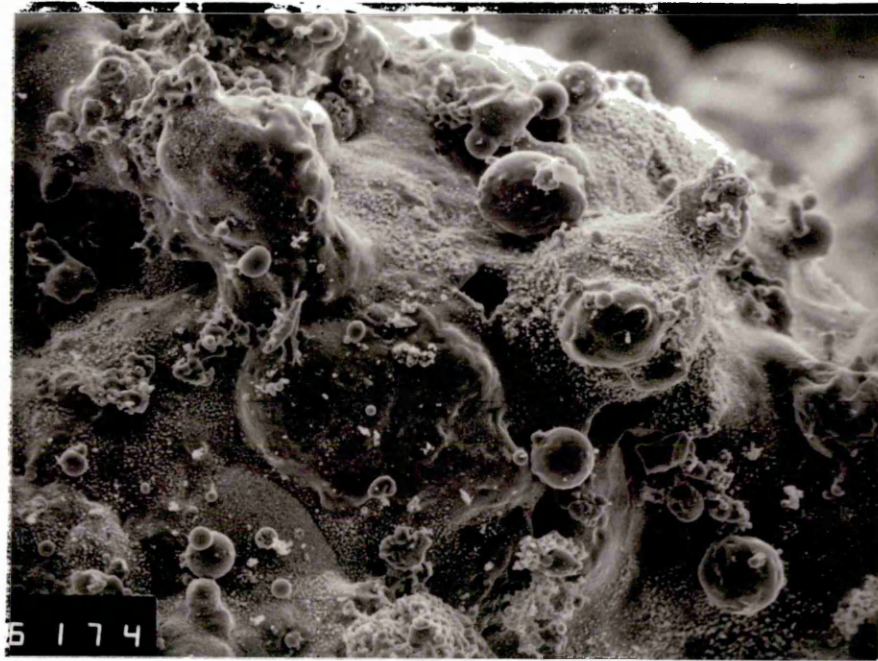


Plate 4-18:

SEM-micrograph of an as received, unpolished deposit sample from the Bottom Screen Tubes in boiler No.6, with on-line Lycal 93HS injection. Partial fusion of some of ash spheres and cenospheres depositing onto the roughly surfaced matrix are shown. [Mag: x140]

Plate 4-20 shows the surface of an ash particle which is encrusted with a range of fine, irregularly shaped particles as well as a collection of much smaller, fully or partially developed spherical ash particles, growing independently of the underlying matrix.

Plate 4-21 illustrates a string of spherical and non-spherical ash particles of different sizes coalescing together. The bonding process between the ash particles is evidently as a result of full or partial melting of the ash matter. This illustration is indicative of the early stages of deposition as fly ash particles come into contact together on the tube surfaces.

Plate 4-22 is representative of the deposit taken from the passage between screen tubes and steam generating tubes in boiler No.6. It shows the various stages of "neck" formation and growth between spherical ash particles of different sizes which would bring about a more fully sintered or fused deposit. The dispersion of iron particles is again apparent with the necking areas particularly affected.

Boiler No.5 - Plates 4-23 to 4-28, are representative of deposits taken from boiler No.5, operating without Lycal 93HS. Plate 4-23 is typical of a front wall sample, showing a high degree of bonding and fusion between the ash particulate matter, forming a more uniform and continuous structure than was evident in samples from the same position in boiler No.6. The smaller ash particles would be readily collected and absorbed into the surface of such deposits, forming dense accretions.

Plate 4-24 is illustrative of the general bulk of the rear arch sample. A large section of spherical ash particles are fused together with further deposition of smaller ash particulates being evident. The surface of the agglomerated spherical ash particles was observed to be covered by a very fine dispersion of iron oxide particles, as illustrated by the EDX analyses.

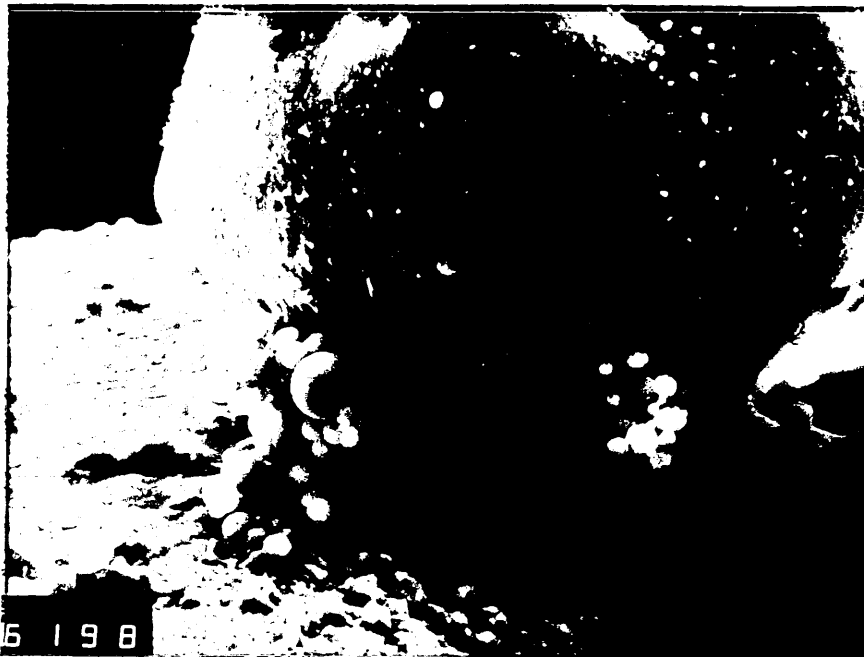


Plate 4-19:

SEM-micrograph of an as received, unpolished deposit sample from the Bottom Screen Tubes in boiler No.6, with on-line Lycal 93HS injection. It shows the textural and size difference between a number of very fine transparent ash cenospheres agglomerated at the base of a much larger solid ash sphere imbedded on the rough matrix. [Mag: x1040]

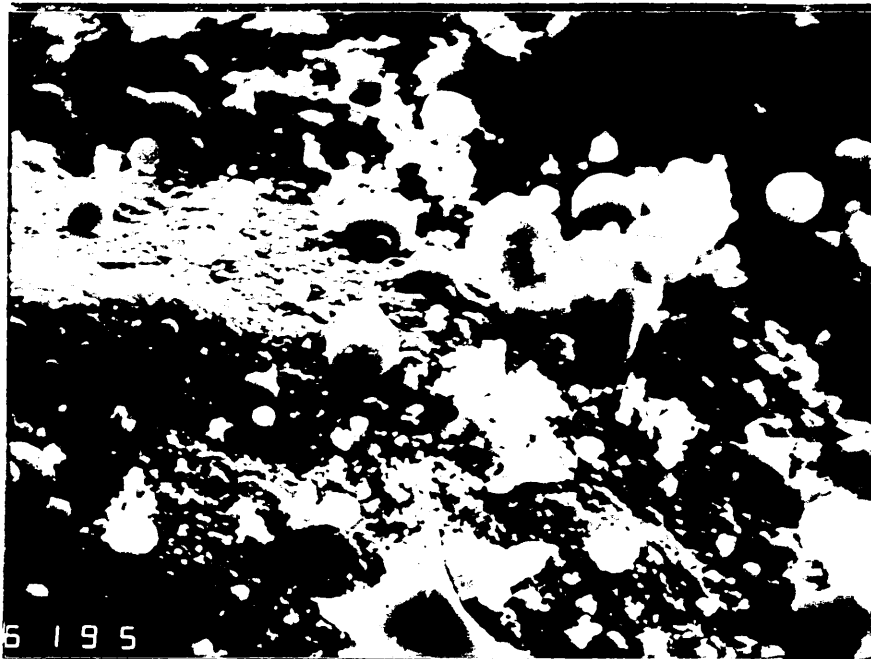


Plate 4-20:

SEM-micrograph of an as received, unpolished deposit sample from the Bottom Screen Tubes in boiler No.6, with on-line Lycal 93HS injection. It shows the texture of some of the very fine ash cenospheres and the irregularly shaped particulate matter on the surface of the dark matrix. [Mag: x2040]

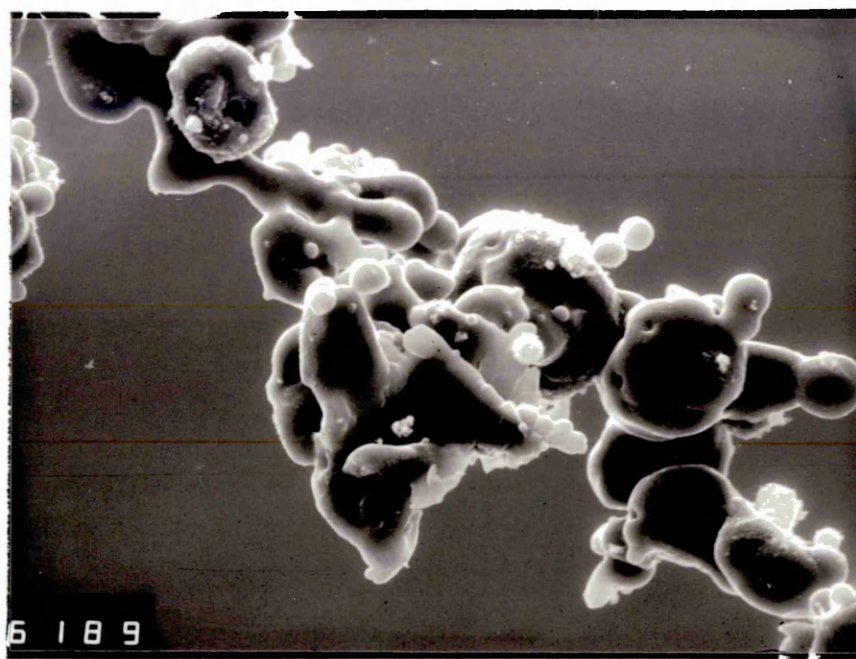


Plate 4-21:

SEM-micrograph of an as received, unpolished deposit sample from the Bottom Screen Tubes in boiler No.6, with on-line Lyclal 93HS injection. It shows a string formation of softened ash spheres and ash matter bonded together with various degrees of neck growth between the particles. Finer ash cenospheres with a transparent texture can further be seen adhering to the softened ash matter. [Mag: x1040]

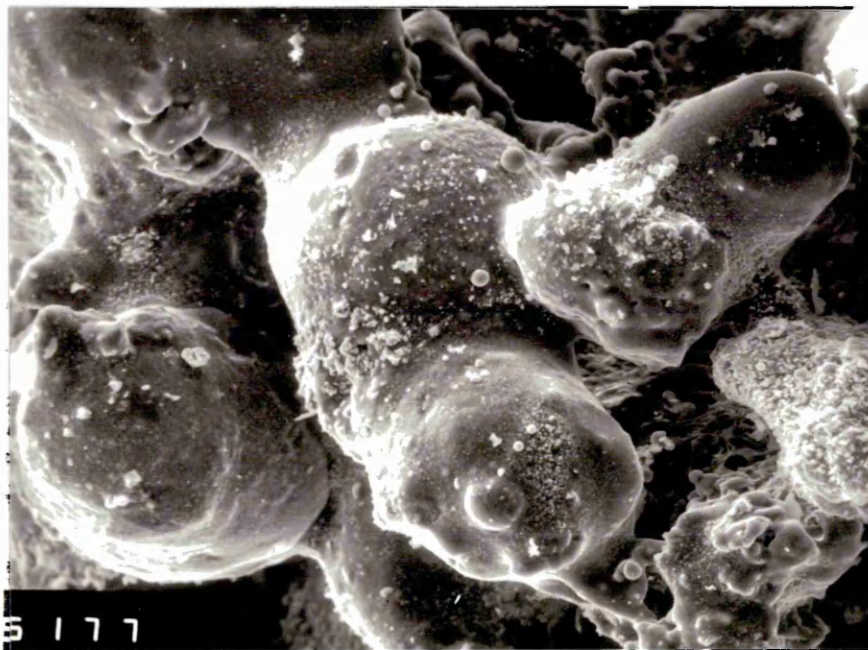


Plate 4-22:

SEM-micrograph of an as received, unpolished deposit sample from the Passage between Screen Tubes & Steam Generating Tubes in boiler No.6, with on-line Lyclal 93HS injection. It shows the various stages of neck growth between solid ash spheres, forming a highly coalesced bulk of ash particulates. [Mag: x240]

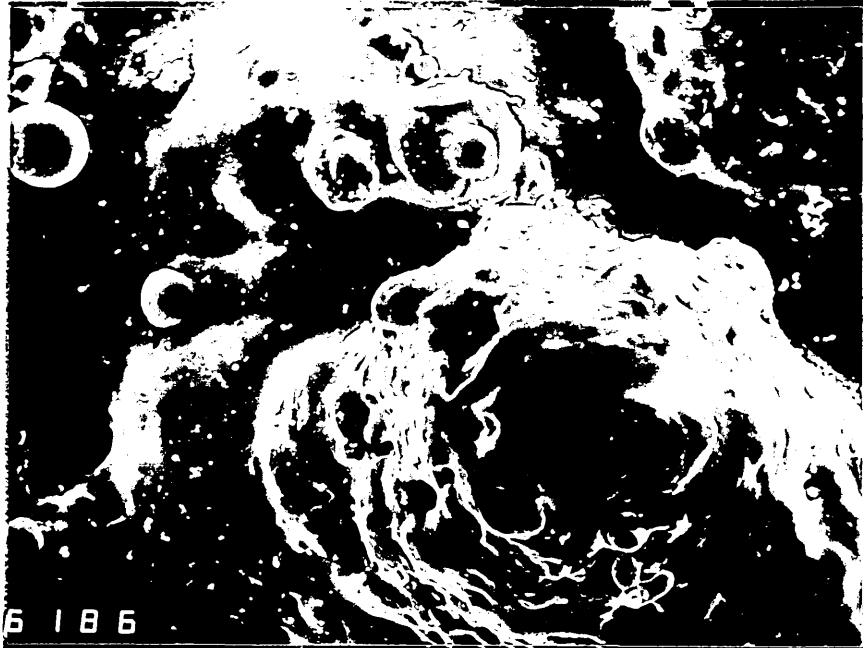


Plate 4-23:

SEM-micrograph of an as received, unpolished deposit sample from the Front Walls in boiler No.5, without Lyclal 93HS injection. Extensive bonding and fusion between the spherical ash particles has formed a uniformly textured, continuous alumino - silicate matrix. The smaller smooth ash cenospheres adsorbed onto the surface are further fused into the matrix. [Mag: x260]

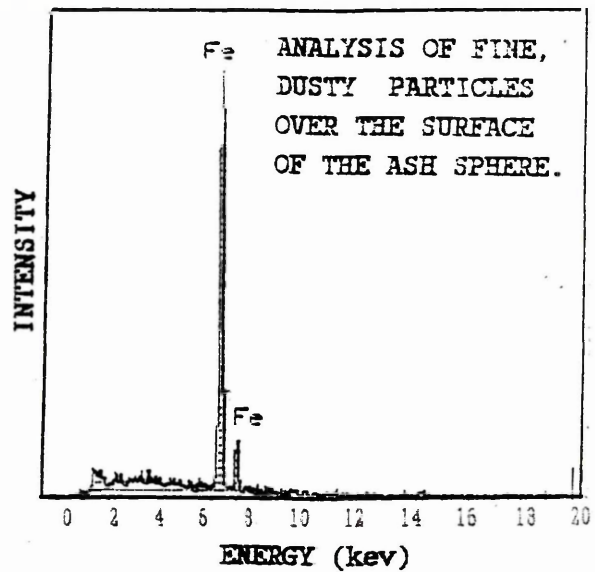
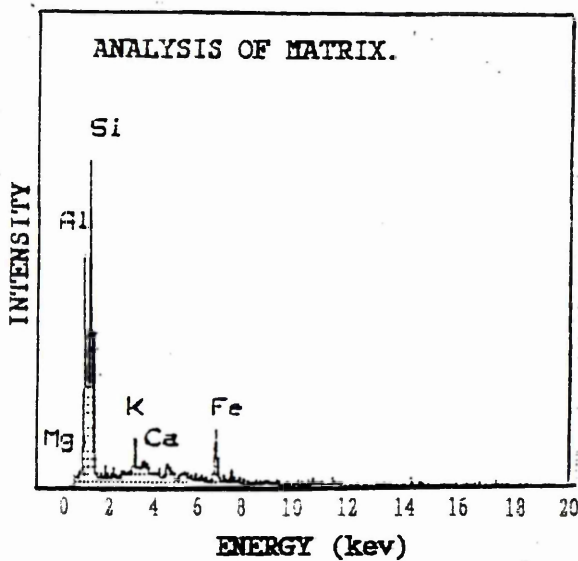
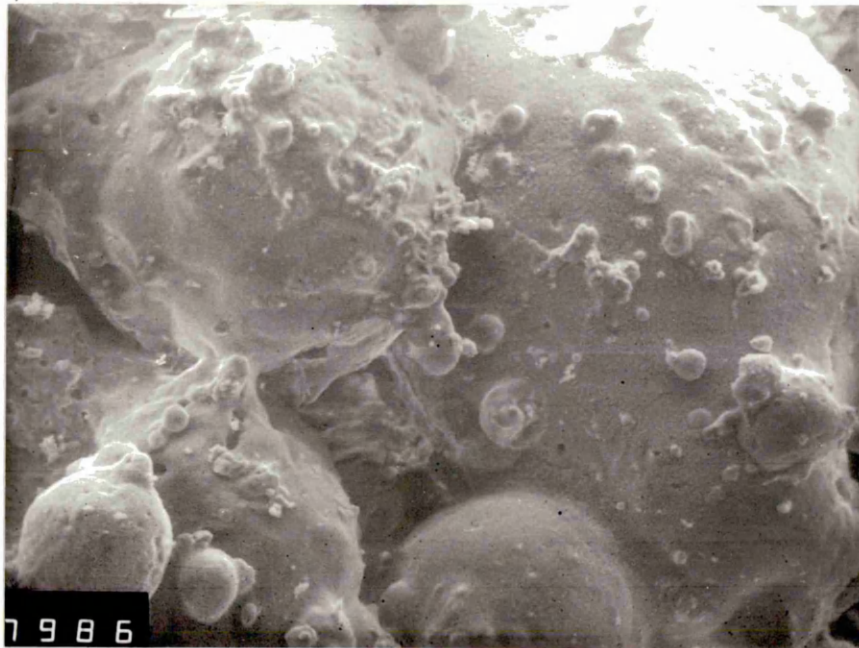


Plate 4-24:

SEM-micrograph of an as received, unpolished deposit sample from the Rear Arch in boiler No.5, without Lycal 93HS injection. Extended bonding and fusion between solid ash spheres of various sizes are shown to form a fairly continuous matrix. The EDX-analyses show an aluminosilicate matrix with the enrichment of fine iron oxide particles on the outer surface of the matrix. [Mag: x240]

Plate 4-25 is a general view of the surface morphology of a Rear Wall sample. The extensive degree of fusion between the apparently molten, spherical ash particles has helped to form a continuous and uniform structure. The presence of iron enriched particles associated with the surface chemistry of this samples was significantly less than that associated with similar samples from boiler No.6.

Plate 4-26 is representative of the bottom screen tube sample. Like the samples for the same location from boiler No.6, this sample has an extensive dispersion of iron enriched particles covering the outer surface of the deposit. Some degree of fusion and neck growth is apparent between the spherical ash particles.

Plate 4-27 is illustrative of the general matrix of the steam generating tube sample. As shown in the plate, the spherical ash particles have undergone extensive fusion, producing a continuous, uniform matrix. A large number of fine angular and rounded particles, forming small clusters could also be observed as the less prevelant feature of this deposit.

Plate 4-28 shows such a cluster of small angular and rounded particles.

Plates 4-29 to 4-31 characterise features which were commonly encountered in the SEM-EDX analysis of the particulate matter from the economiser ash hoppers in both boilers No.5 and No.6.

Size fraction analyses were carried out on the grit arrestor and economiser ash hopper samples collected from boiler No.6 with and without Lycal 93HS being on-line, in order to establish a quantitative measure of the texture of the as received particulate samples. The results tabulated in Tables 4-9 and 4-10 and presented graphically in Figures 4-2 and 4-3 show little difference in the particle size distributions with and without injection of Lycal. The extent of size variation across the whole number of samples from different batches received has been illustrated by range-bars.

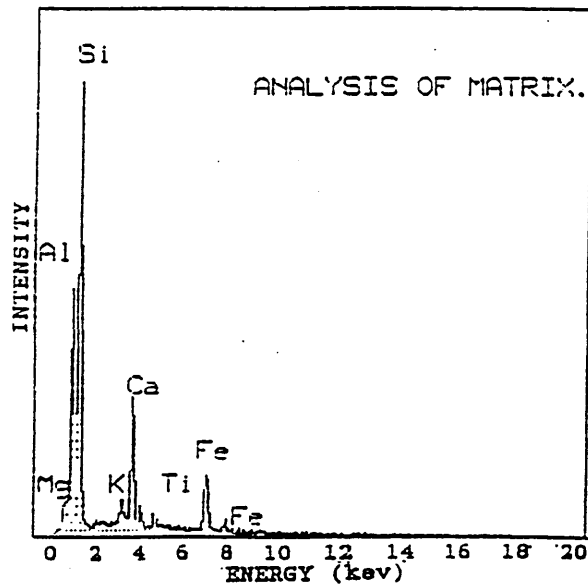
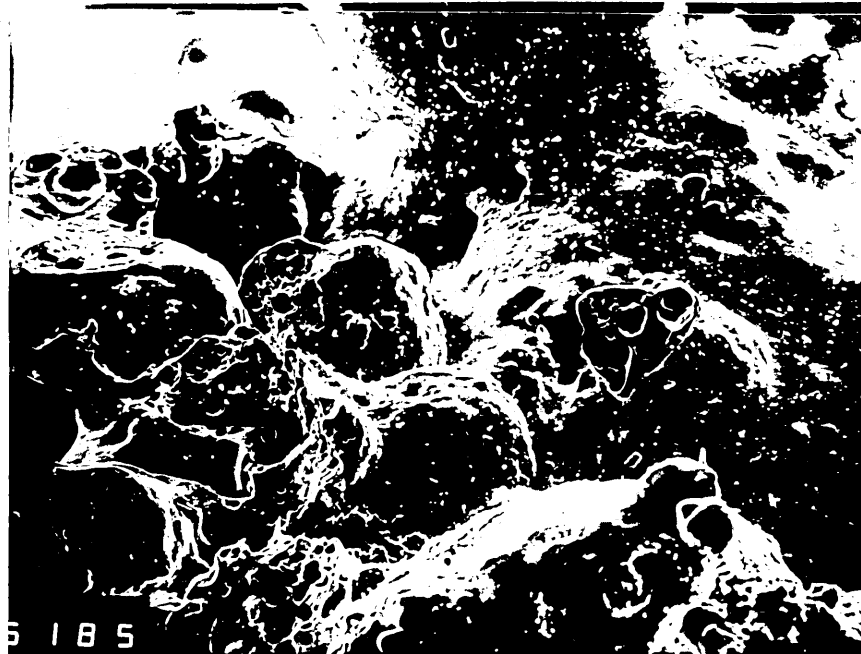


Plate 4-25:

SEM-micrograph of an as received, unpolished deposit sample from the Rear Wall in boiler No.5, without Lycal 93HS injection. Extensive fusion of spherical ash particles has formed a coagulated, continuous and uniform matrix. Some transverse sections show the highly porous, vesicular character of this deposit. The EDX-analysis shows the matrix composition. [Mag: x70]

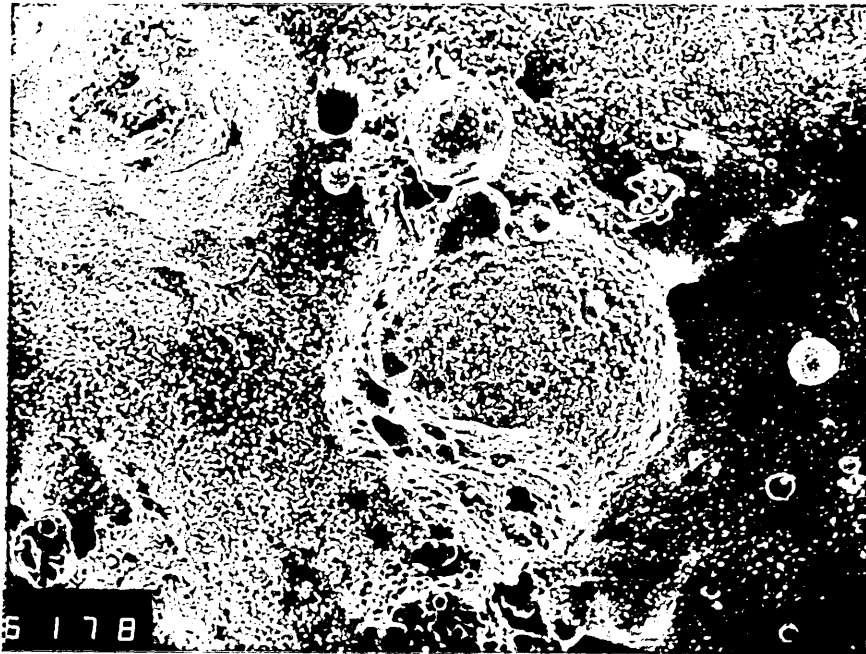


Plate 4-26:

SEM-micrograph of an as received, unpolished deposit sample from the Bottom Screen Tubes in boiler No.5, without Lycal 93HS injection. High degree of bonding and fusion is evident between spherical ash particles. Like the samples from the same location from boiler No.6, an extensive dispersion of iron oxide particles can be seen on the rough surface of the matrix. [Mag: x140]

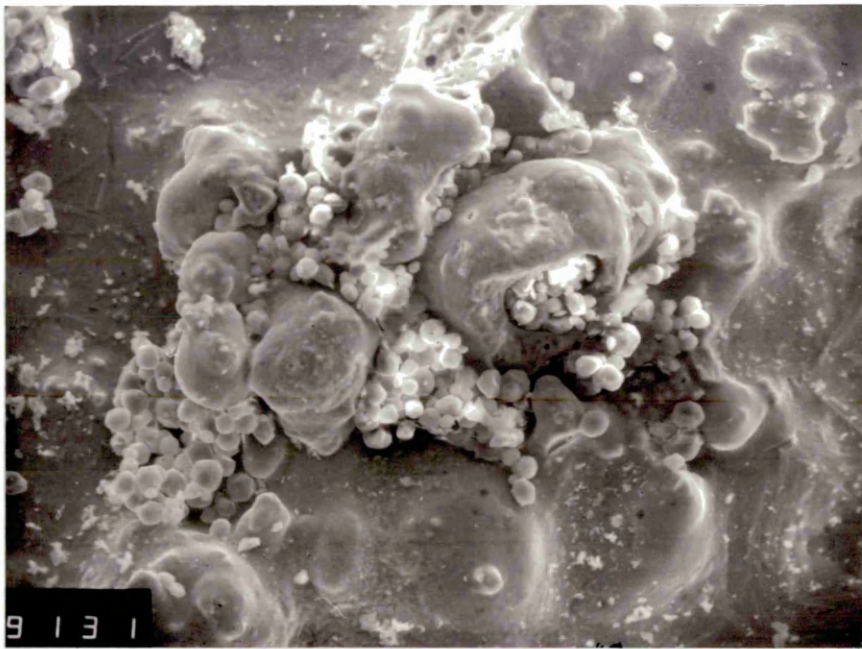


Plate 4-27:

SEM-micrograph of an as received, unpolished deposit sample from the Steam Generating Tubes in boiler No.5, without Lycal 93HS injection. A continuous matrix contains a number of ash spheres with smaller, transparent, rounded and angular siliceous matter imbedded on the surface. [Mag: x240]

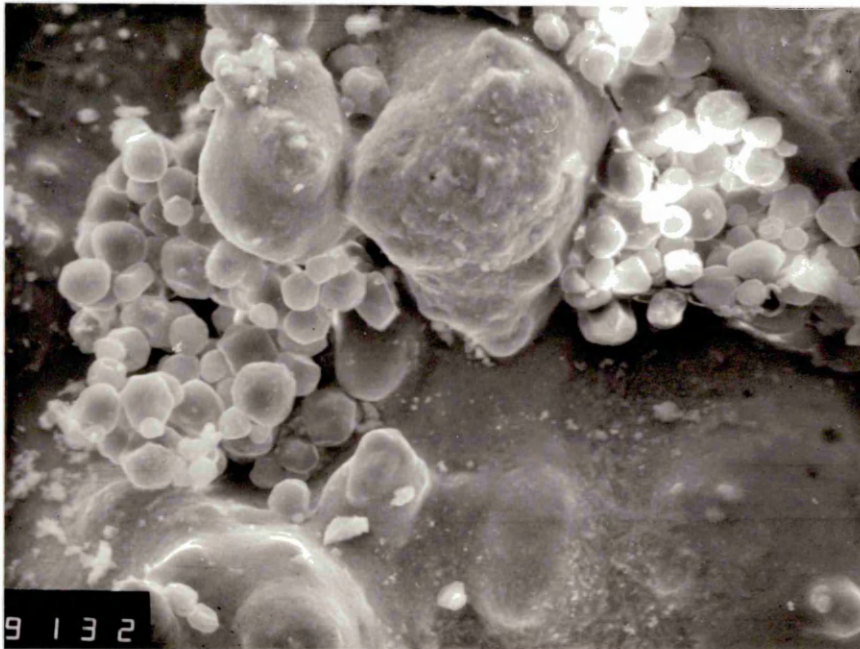


Plate 4-28:

High magnification of SEM - micrograph in Plate 4-27 showing the angular and rounded shape of the fine transparent siliceous particles, demonstrating their incomplete melting. [Mag: x480]

Table 4-9: Results of size fraction analysis of "Economiser ash hopper" samples collected during the 12-hour trials on boiler No.6 with and without on-line injection of Lycal 93HS.

ECONOMISER ASH HOPPER					
+LYCAL 93HS			-LYCAL 93HS		
Particle size (μm)	Mass collected (g)	Mass percent (%)	Particle size (μm)	Mass collected (g)	Mass percent (%)
+1200	1.181	2.363	+1200	0.794	1.597
-1200 +1000	2.223	4.448	-1200 +1000	1.552	3.121
-1000 +710	7.679	15.369	-1000 +710	7.173	14.422
-710 +500	8.107	16.225	-710 +500	8.373	16.834
-500 +355	13.380	26.778	-500 +355	12.408	24.947
-355 +250	9.460	18.934	-355 +250	9.689	19.480
-250 +150	5.594	11.196	-250 +150	6.773	13.616
-150 +75	1.572	3.147	-150 +75	2.187	4.397
-75 +45	0.155	0.310	-75 +45	0.333	0.669
-45	0.614	1.229	-45	0.456	0.917
	-----	-----		-----	-----
	49.965	99.999		49.738	100.00

Table 4-10: Results of size fraction analysis of "Grit arrester" samples collected during the 12-hour trials on boiler No.6 with and without on-line injection of Lycal 93HS.

GRIT ARRESTORS					
+LYCAL 93HS			-LYCAL 93HS		
Particle size (μm)	Mass collected (g)	Mass percent (%)	Particle size (μm)	Mass collected (g)	Mass percent (%)
+1200	0.042	0.042	+1200	0.020	0.021
-1200 +1000	0.097	0.098	-1200 +1000	0.070	0.071
-1000 +710	0.989	0.984	-1000 +710	0.774	0.785
-710 +500	2.251	2.272	-710 +500	1.858	1.884
-500 +355	5.013	5.060	-500 +355	4.127	4.185
-355 +250	7.309	7.377	-355 +250	6.745	6.840
-250 +150	15.177	15.320	-250 +150	14.594	14.799
-150 +75	25.735	25.978	-150 +75	25.682	26.042
-75 +45	11.706	11.816	-75 +45	11.503	11.664
-45	30.748	31.038	-45	33.244	33.710
	-----	-----		-----	-----
	99.067	99.985		98.617	100.201

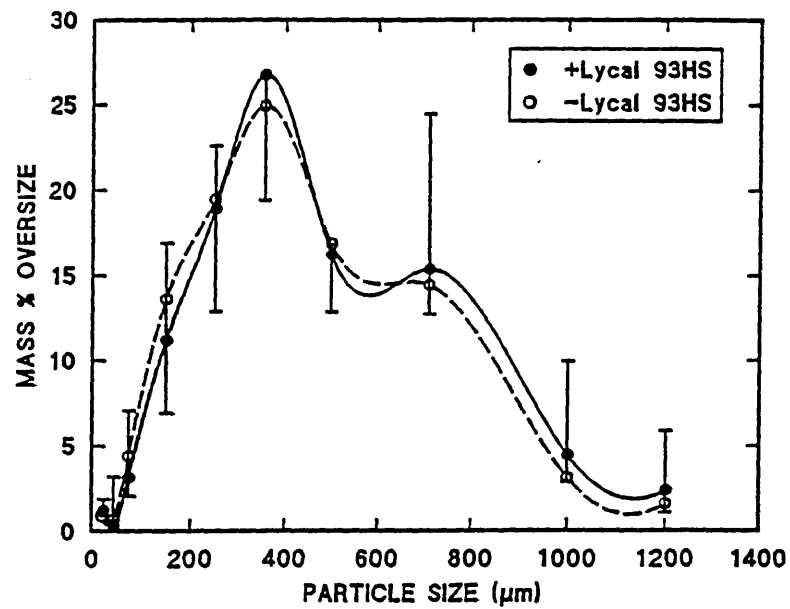


Figure 4-2: Particle size distribution curves for the "economiser ash-hopper" samples collected with and without on-line injection of Lycal 93HS over the period of 12 hour tests.

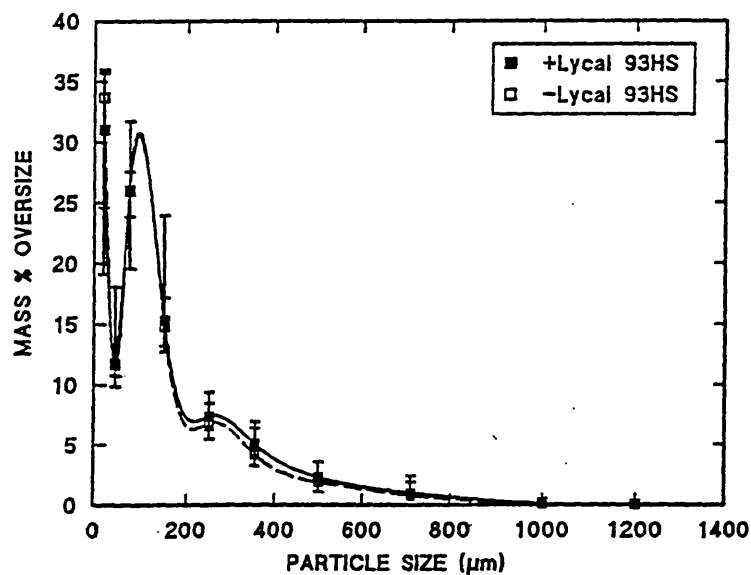


Figure 4-3: Particle size distribution curves for the "grit arrestor" samples collected with and without on-line injection of Lycal 93HS over the period of 12 hour tests.

Plate 4-29 shows both smooth and rough surfaced spherical ash particles in the size range between 150 μm to 700 μm in diameter.

Plate 4-30 shows in more detail a rough surfaced, cenosphere as well as a number of relatively smooth surfaced spherical ash particles. The EDX-analyses illustrate the differences in composition for the two types of spherical ash particles as well as the coagulated matter between two ash spheres. The first appearance of Mg can be seen from the EDX spectra for the white particles over the rough ash sphere.

Plate 4-31 shows a number of highly porous, thick-walled, spherical ash particles and larger ash agglomerations forming non-spherical particulate matter. The EDX analysis shows the surface composition of the porous and smooth, non-porous ash agglomerates.

Plates 4-32 to 4-35 characterise features which were commonly encountered in the SEM-EDX of the "ash clinker" formed on the travelling chain grate.

Plate 4-32 shows a stratified structure which was typically found in the harder, vitreous type of residual clinker matter. The matrix composition as shown by the EDX-analysis, was found to be silica-alumina rich.

Plate 4-33 shows a highly porous, honeycomb surface texture creating a lace-like network appearance. The EDX-analysis shows the enrichment of aluminum, sulphur and calcium in this sample, as oxides or compounds, which in appearance was also considerably different from the previous clinker sample in Plate 4-32.

Plate 4-34 shows the presence of small, smooth surfaced ash cenospheres in what appears to be a molten and fluid matrix. This again shows an entirely different morphology to the two previous photomicrographs of the clinker samples, illustrating the diversity of clinker samples found on the chain grates in boiler No.6.

Plate 4-35 is representative of carbonaceous clinker samples which were rich in iron oxides, as shown by the EDX-analysis. The angular ferrous plates embedded

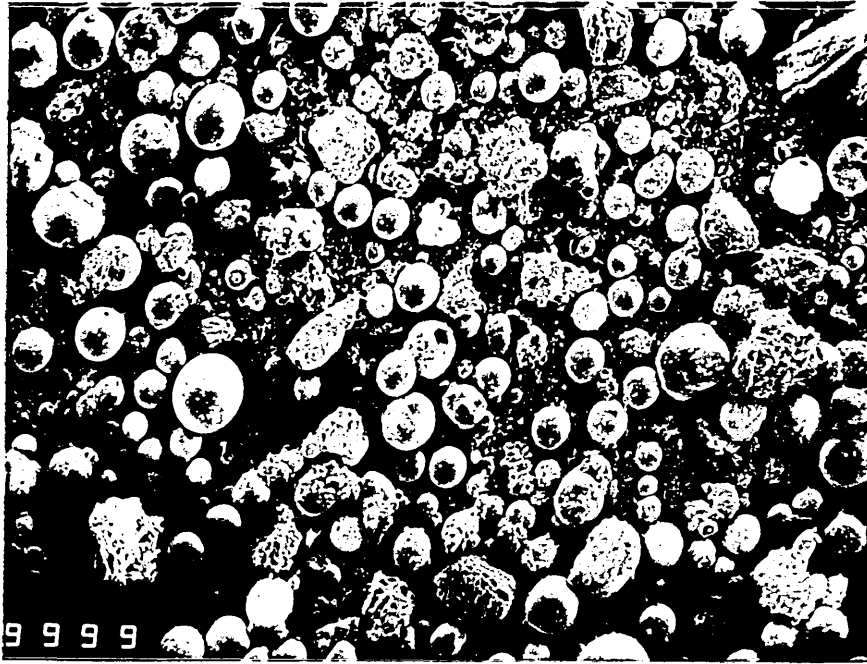


Plate 4-29:

SEM-micrograph of Economiser Ash Hopper particulate samples from boiler No.6, showing the spherical and non-spherical form of the particles with smooth and rough outer surface. The particle size range varies between -45 +700 μm . [Mag: x24]

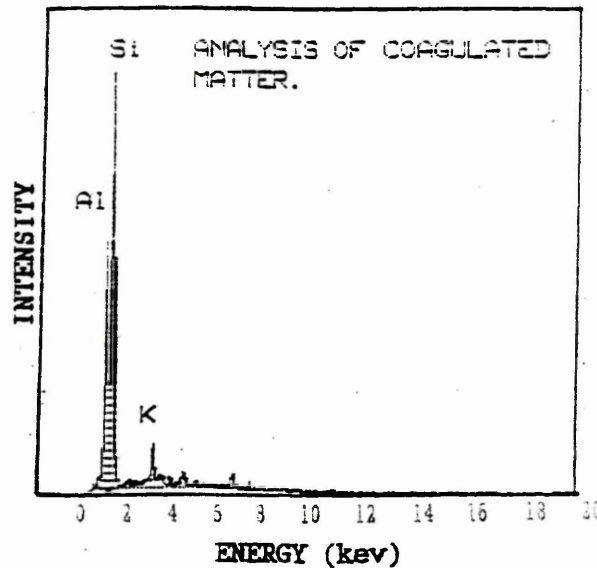
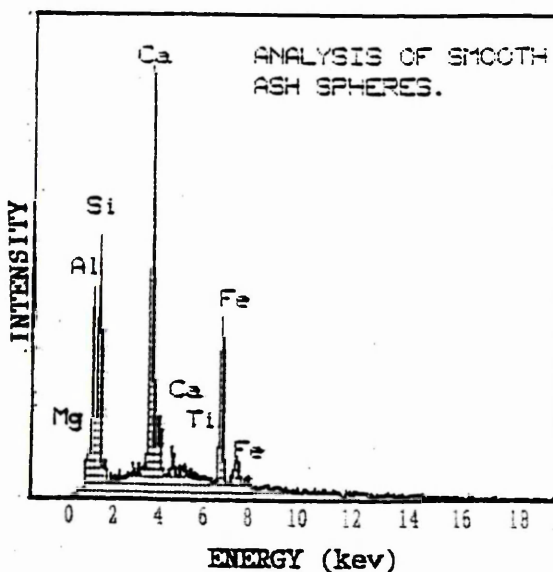
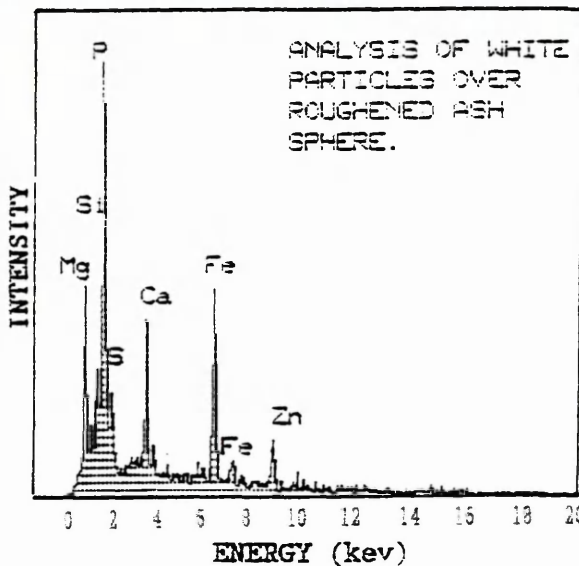
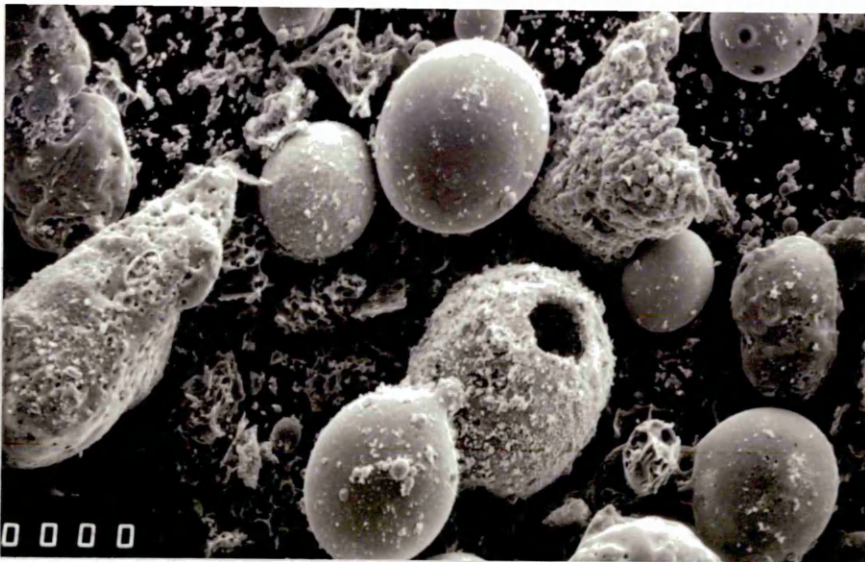


Plate 4-30:

High magnification of SEM-micrograph in Plate 4-29, showing the relatively smooth ash spheres as well as the roughly surfaced ash cenosphere and non-spherical particles. The EDX-analyses shows the variation in the surface composition of the smooth, rough and coagulated fly ash particulates. [Mag: x95]

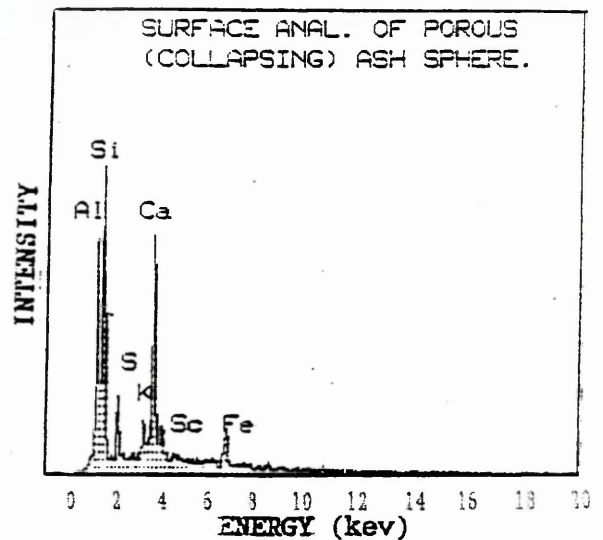
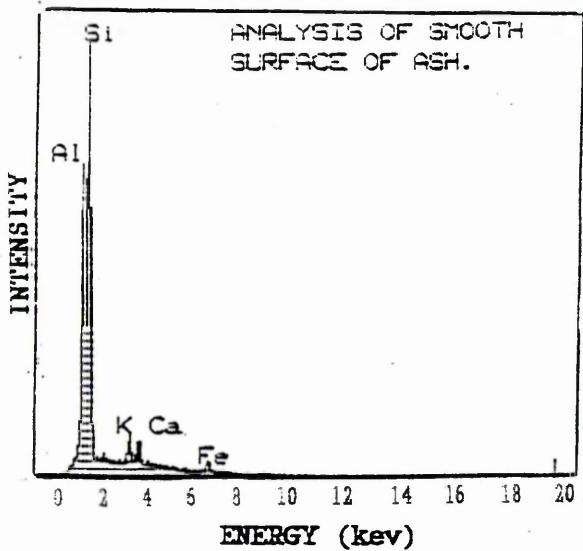
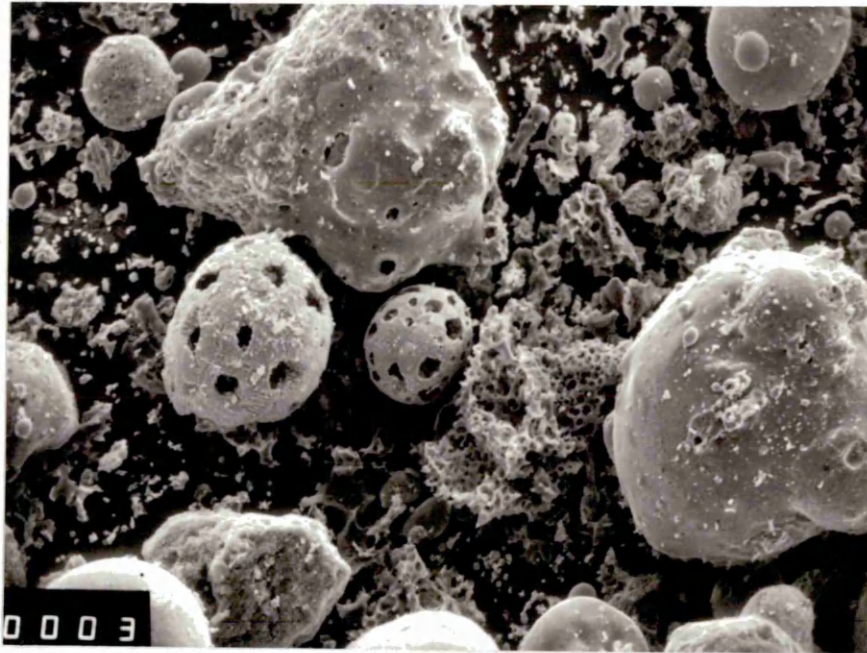


Plate 4-31:

SEM-micrograph of Economiser Ash Hopper particulate samples from boiler No.6, showing the highly porous spheroids with surface crystallisation, and larger agglomeration of ash matter forming non-spherical and spherical particulates. The EDX - analyses show the surface composition of porous spheroids and non-porous ash spheres and agglomerates. [Mag: x100]

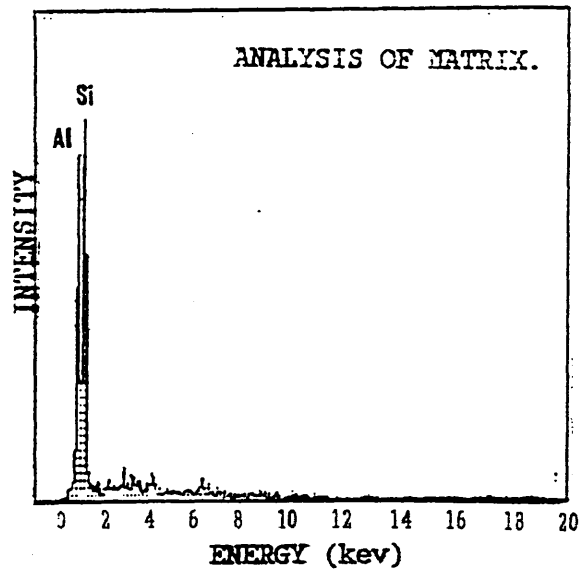
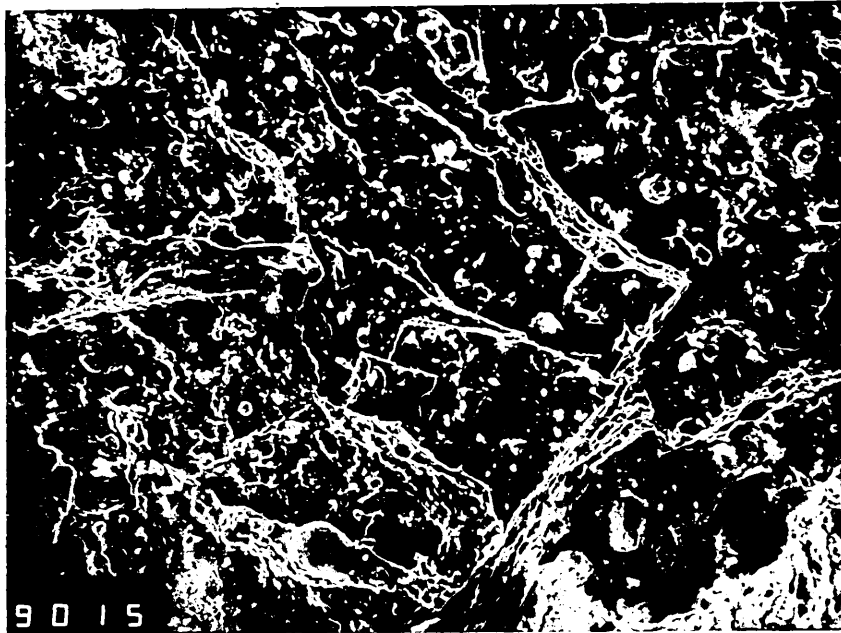


Plate 4-32:

SEM-micrograph of a Bottom Grate Clinker sample from boiler No.6, showing a fully fused, stratified morphology. The matrix composition is characterised by the EDX-analysis. [Mag: x120]

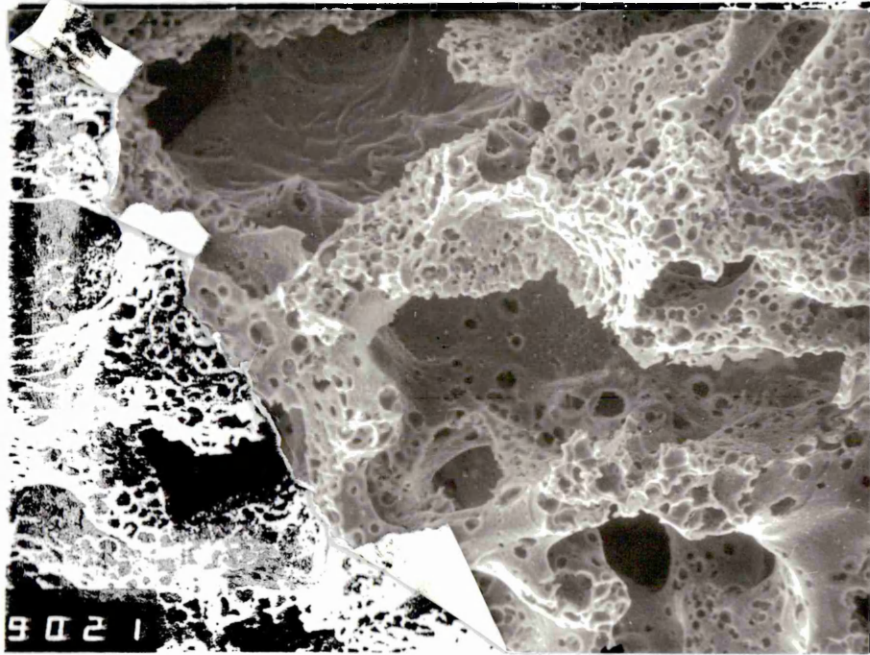


Plate 4-33:

SEM-micrograph of a Bottom Grate Clinker sample from boiler No.6, showing the lacey skeleton of a highly porous, honeycomb coke residue containing ash matter. [Mag: x110]

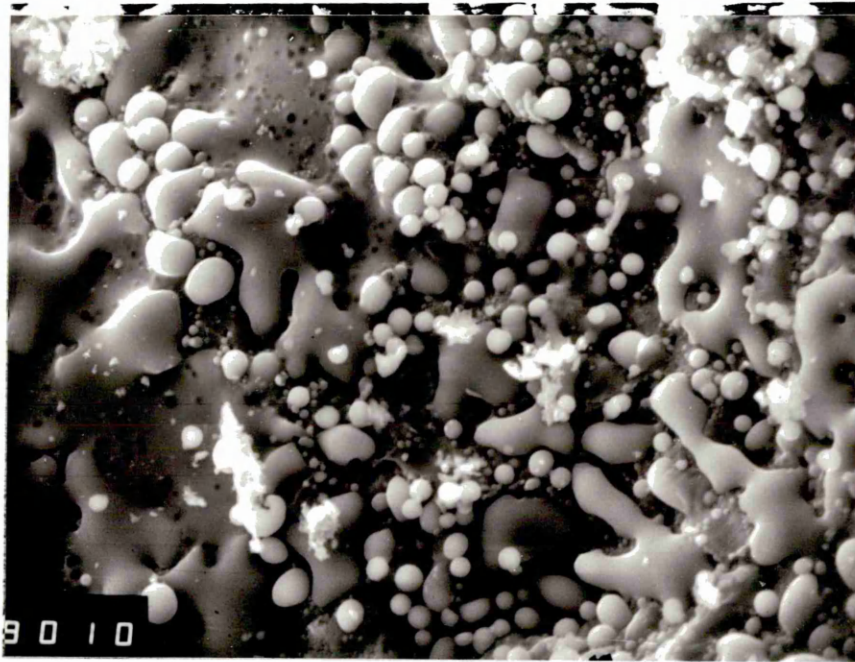


Plate 4-34:

SEM-micrograph of a Bottom Grate Clinker sample from boiler No.6, showing fine, smoothly surfaced ash cenospheres on a partially fluid and viscous matrix. [Mag: x960]

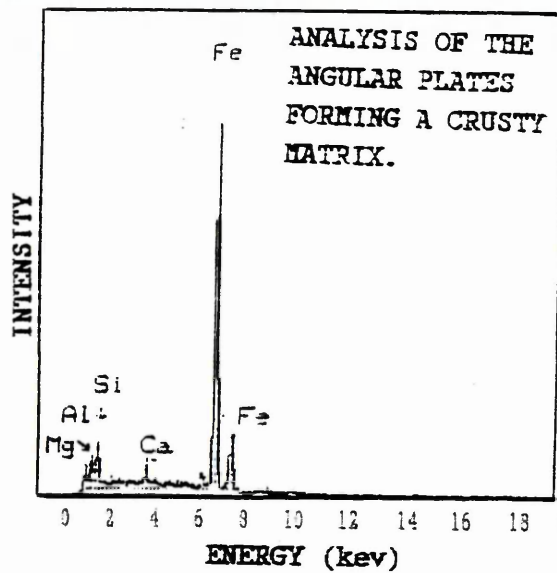
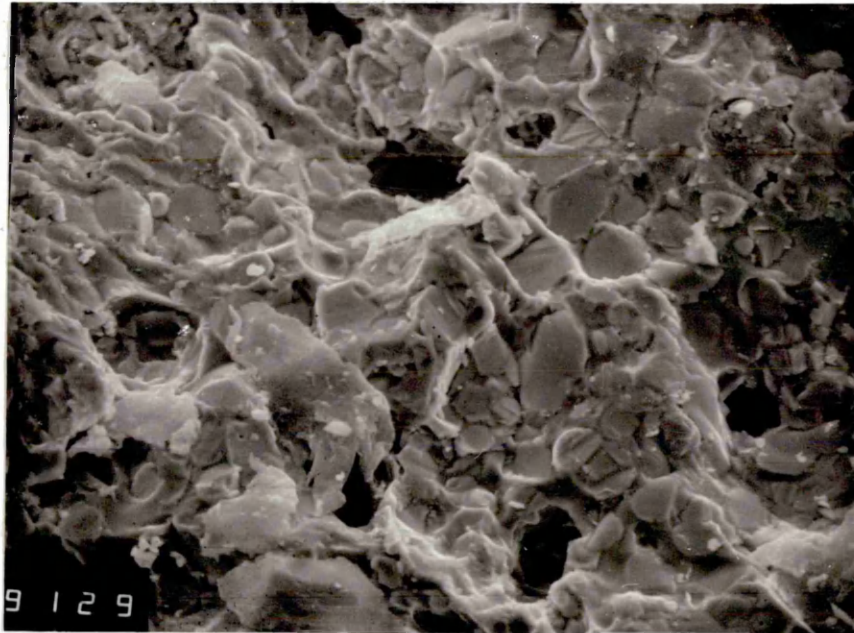


Plate 4-35:

SEM-micrograph of a Bottom Grate Clinker sample from boiler No.6, representing a carbonaceous ash matter with angular plates of iron oxide particles forming a crusty matrix. The EDX-analysis shows the ferriferous composition of this matrix. [Mag: x560]

within the surface of the sample, essentially forms the bulk of these samples, creating a differently textured, less siliceous material compared to the previous clinker samples shown in Plates 4-32 to 4-34.

4.2.4 (b) Polished, As Received Samples from Boilers No.5 and No.6

Polished specimens from various locations and sample batches from boilers No.6 after Lyclal 93HS injection and from boiler No.5 were examined using both optical and scanning electron microscopy.

Boiler No.6 - The range of structures observed in the samples from boiler No.6, are illustrated in Plates 4-36 to 4-57.

Plate 4-36 is a photo-micrograph representative of a front, rear or side wall deposit. It shows the limited degree of bonding between the various spherical and non-spherical, porous ash particles under oblique illumination. The spherical, ferriferous ash particle (white sphere) features prominently, with sintered and fused regions exhibiting an open matrix.

Plate 4-37 is a photo-micrograph of the identical region represented in Plate 4-36 but using polarised, fully crossed incident light for illumination. The morphological diversity of various ash components which previously appeared to be the same is now further evident through their textural and colour variation. The white particle in Plate 4-36 now appears as a finely grained, black and grey coloured sphere. Furthermore whereas the ring around the bottom ash sphere (black area) appears to be the same as that of the upper one, the dispersion of other white, fine particles in Plate 4-36 distinctly appears here as red in colour, suggesting the presence of hematite(α -Fe₂O₃) crystals.

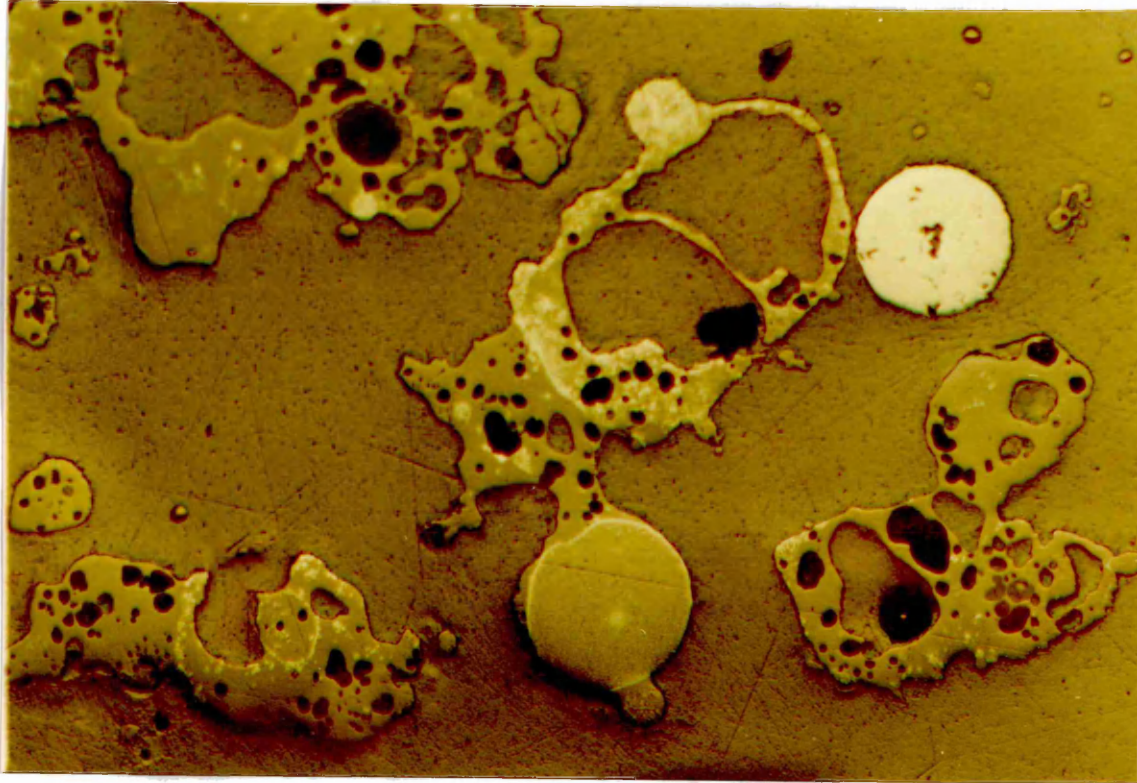


Plate 4-36:

Photo-micrograph of a polished lower furnace (i.e FW, RW or SW) deposit sample from boiler No.6, with on-line Lyclal 93HS injection. It shows the limited degree of bonding within the matrix of spherical and non-spherical porous ash matter, under oblique illumination. The Iron oxide skeleton sphere (white) is in contrast to the other spherical (solid sphere with white rim) and non-spherical ash matter. [Mag: x32]



Plate 4-37:

Photo-micrograph of the feature in Plate 4-36, under polarised, fully crossed illumination. The black and grey angular form of the iron oxide sphere is seemingly similar to the rim around the lower solid sphere, but different to the the large, porous, ash skeleton (red) adjacent to the iron oxide sphere, which had also shown large traces of the white matter.

[Mag: x32]

Plate 4-38 is a photo-micrograph representative of the deposit from the bottom screen tubes or the passage between screen and steam generating tubes. It shows two separate regions of discontinuous matrix under oblique incident illumination. The two regions appear to be identical in colour and texture.

Plate 4-39 is a photo-micrograph of the identical region displayed in Plate 4-38, using polarised, fully crossed incident light for illumination. Clearly the two segments which appeared to have an identical internal texture have distinctly different compositions and textures represented by the variation in colour, mainly black and red. The spherical ash particle at the top is markedly red in colour, suggesting the presence of hematite crystals. The other distinguishable spherical ash particles within the left hand side segment, each appear as orange and black in colour, further illustrating the textural and compositional variation between spherical ash particles.

Plate 4-40 is a photo-micrograph representative of a screen tube deposit. It shows the continuous area of the matrix under oblique incident light. The angular cuboid particles (creamy white) are scattered in a matrix (dark grey) marked with the presence of another phase (light grey) as well as a very fine array of dendritic crystals (cream-white) at the top of the micrograph.

Plate 4-41 is a photomicrograph of the identical region in Plate 4-40, but using polarised, fully-crossed incident light. The various features mentioned previously are thus further shown through colour variations. The various crystalline constituents such as the angular ferrous cuboids (greyish green), the fine array of dendrites (orange) and the other phase (bright yellow) are clearly evident and can be distinguished within the matrix.

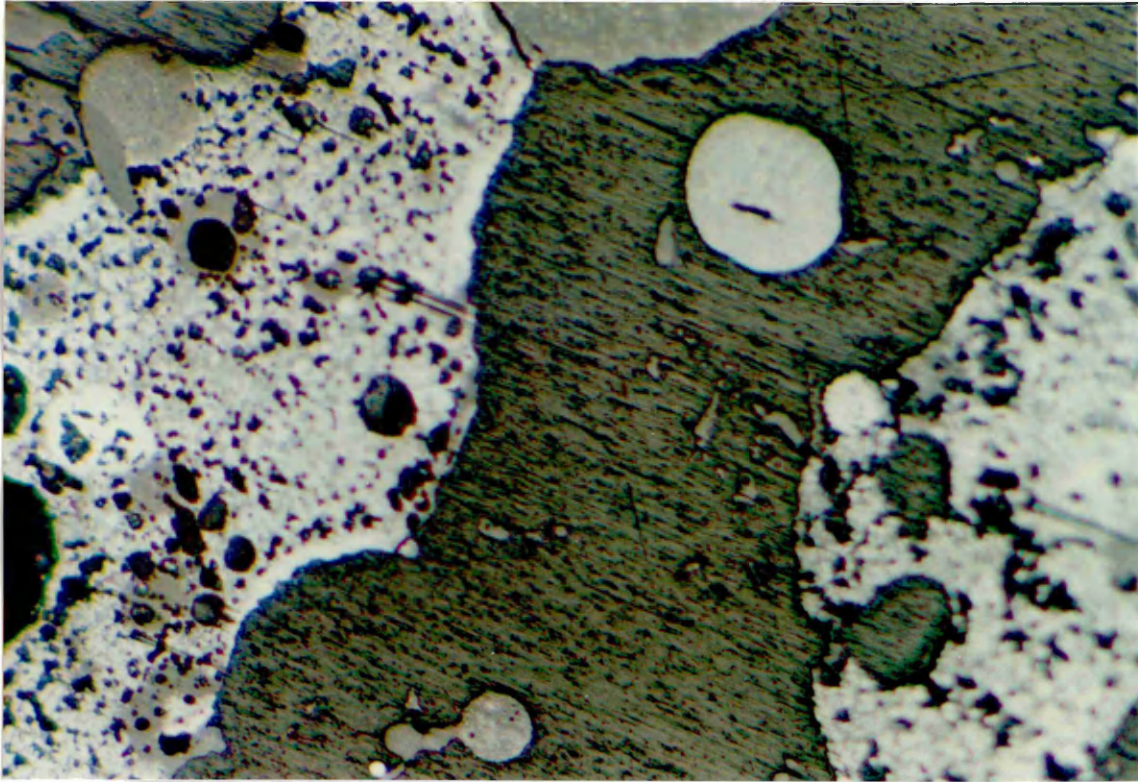


Plate 4-38:

Photo-micrograph of a upper furnace (Btm Screen Tubes or Steam Gen. Tubes) deposit sample from boiler No.6, with on-line Lycal 93HS injection. It shows two separate regions of discontinuous matrix under oblique incident illumination. The two regions appear to be identical in colour and texture.

[Mag: x64]

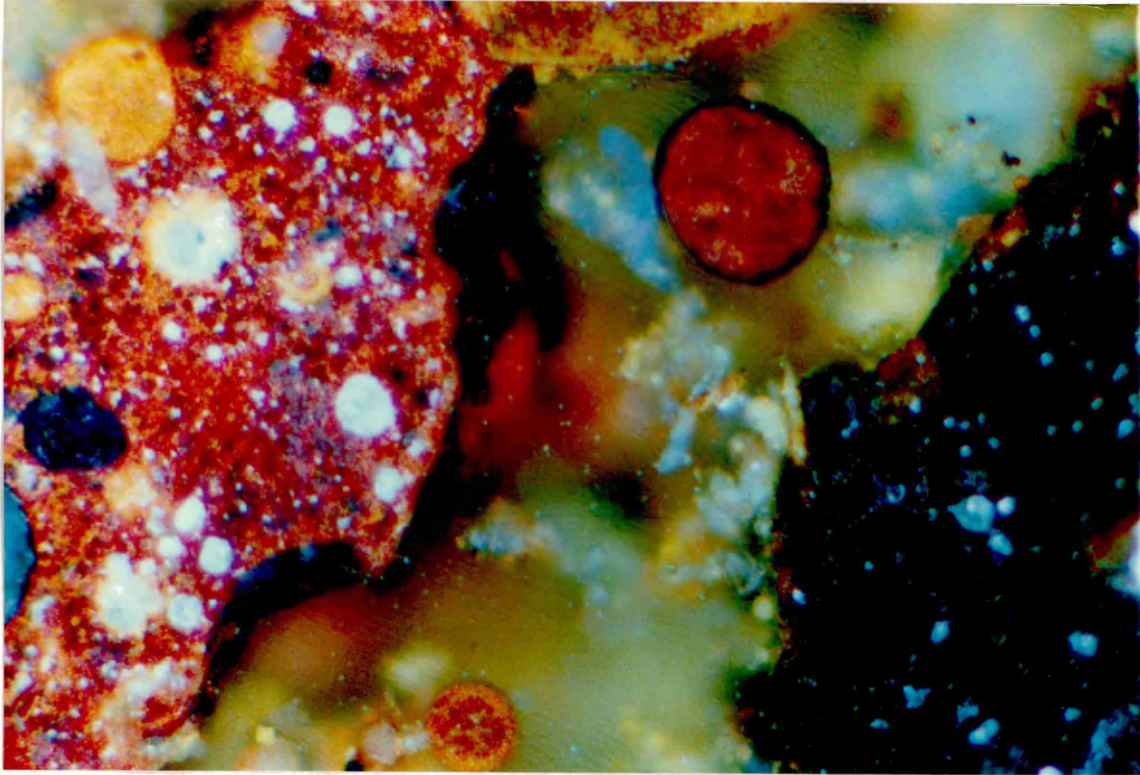


Plate 4-39:

Photo-micrograph of the feature in Plate 4-38, under polarised, fully crossed illumination. The black iron oxide region (RHS) appears now to be distinctly different to the red and orange crystalline region (LHS), with a black outer edge similar to the RHS. A ferrosphere of iron oxide crystallisation appearing as a red sphere is also present. [Mag: x64]

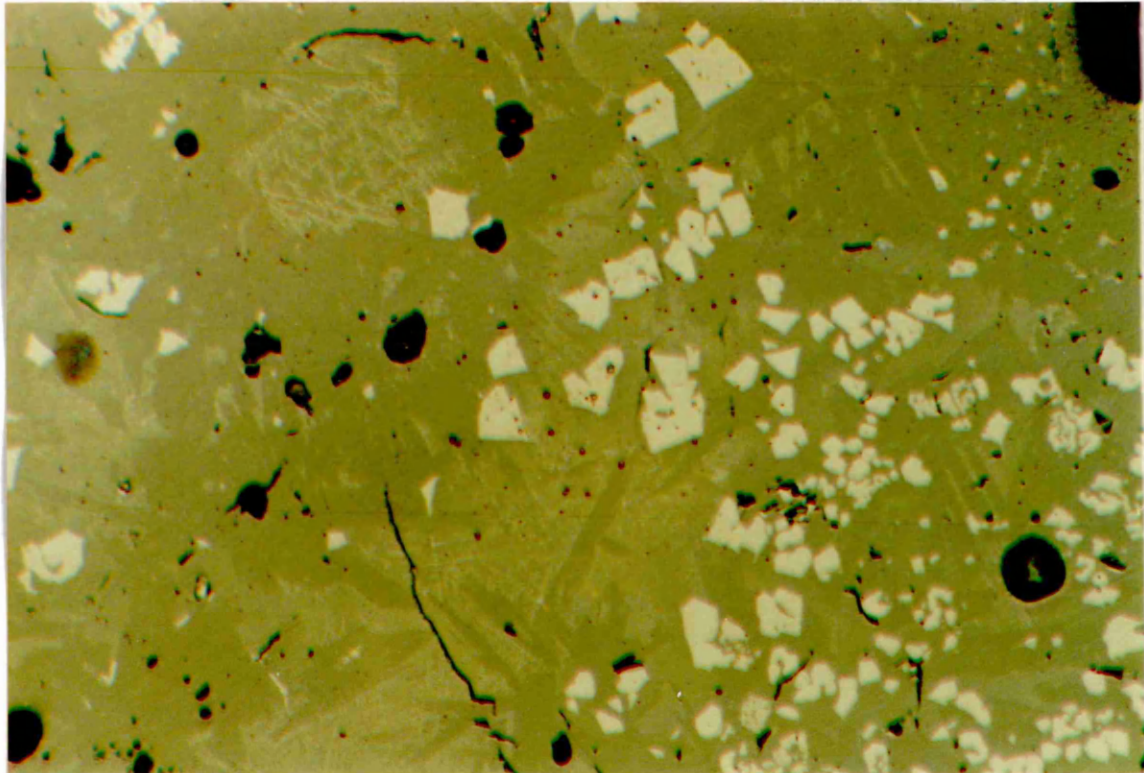


Plate 4-40:

Photo-micrograph of a deposit sample from Bottom Screen Tubes in boiler No.6, with on-line Lycal 93HS injection. It shows a fused siliceous matrix (dark grey) with a scatter of angular cuboidal and euhedral iron-spinel crystals (creamy white), and the very fine array of dendritic region (cream-white crossing lines) at the centre or as a cluster at the top LHS of the photograph.

[Mag: x64]

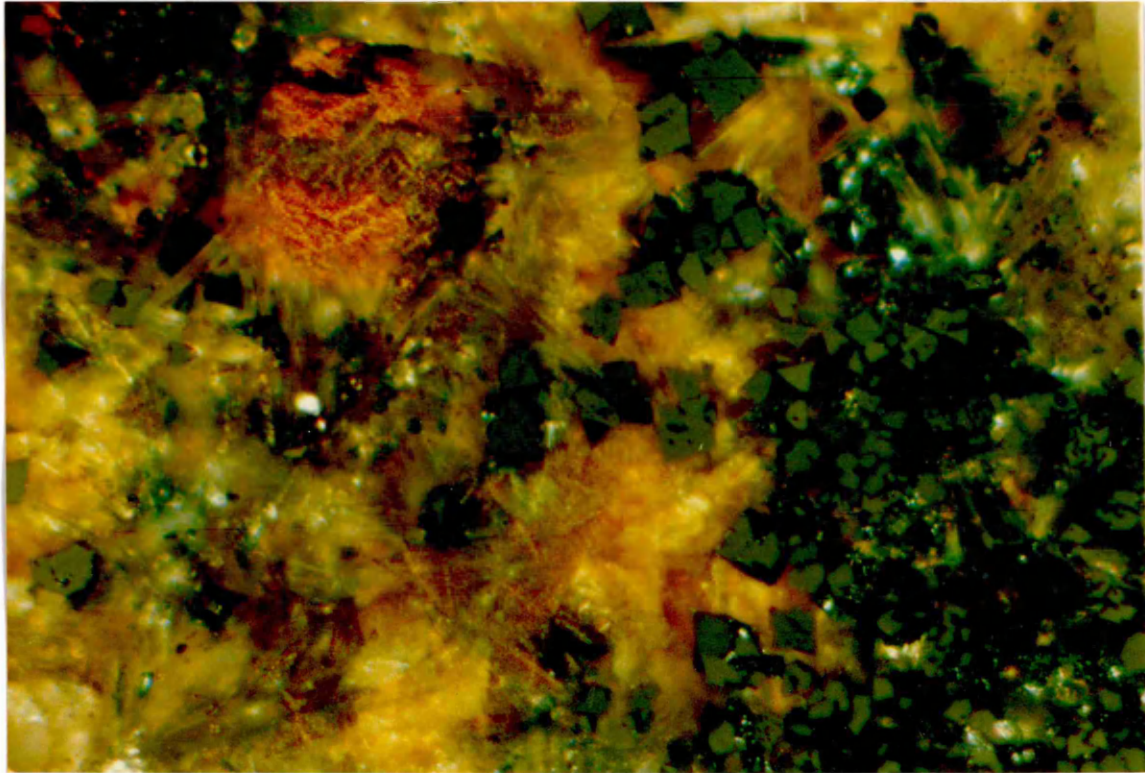


Plate 4-41:

Photo-micrograph of the feature in Plate 4-40, under polarised, fully crossed illumination. The angular and euhedral iron spinel phase (greyish-green), dendritic crystalline region at the centre (yellow and orange) and the very fine dendritic cluster at the top LHS (red) can be more clearly distinguished.

[Mag:x64]

Plate 4-42 shows the typical open skeletal structure which is representative of the deposits received from the front or rear arches / walls or side walls from boiler No.6, at the lower furnace region, during the course of Lyclal 93HS injection.

Plate 4-43 is a higher magnification back-scattered electron image (BSE) of the same sample, demonstrating the chemical and phase heterogeneity within the deposit sample. The photomicrograph shows the formation of a range of truncated laths (dark grey) as precipitates within the underlying matrix (darker grey), with a spread of angular iron oxide rich cuboids (light grey), a large spherical formation of dendritic hematite (top right) and a pure metallic iron oxide ash sphere (bottom left). The black areas are porosity.

Plate 4-44 is representative of an "F2" type front or rear wall deposit sample from the third batch. It shows the sintering of a range of spherical ash particles of various sizes and chemical composition as illustrated by the EDX-analyses. The large ash sphere denoted by "A" was found to be silica, iron oxide and calcium oxide rich. The boundary region between the large perforated spherical ash particle and the smaller smooth ash particle which is denoted by "B" is most probably a calcium sulphate rich phase. The perforated ash sphere denoted by "C" is enriched in a mixture of calcium, magnesium, iron and sulphur as oxides and/or sulphates. The EDX-analysis further demonstrates the chemical heterogeneity of such samples despite their homogenous external appearance.

Plate 4-45 illustrates the variation in matrix composition of a lower furnace deposit from the rear wall; showing a continuous phase (areas "A", "B" and "C"), with area "C" showing evidence of dendritic solidification and the honeycomb, porous phase (area "D"). The EDX-analyses show areas "A" and "B" to be siliceous, area "C" to be iron oxide rich crystallisation on solidification of the deposit, and area "D"

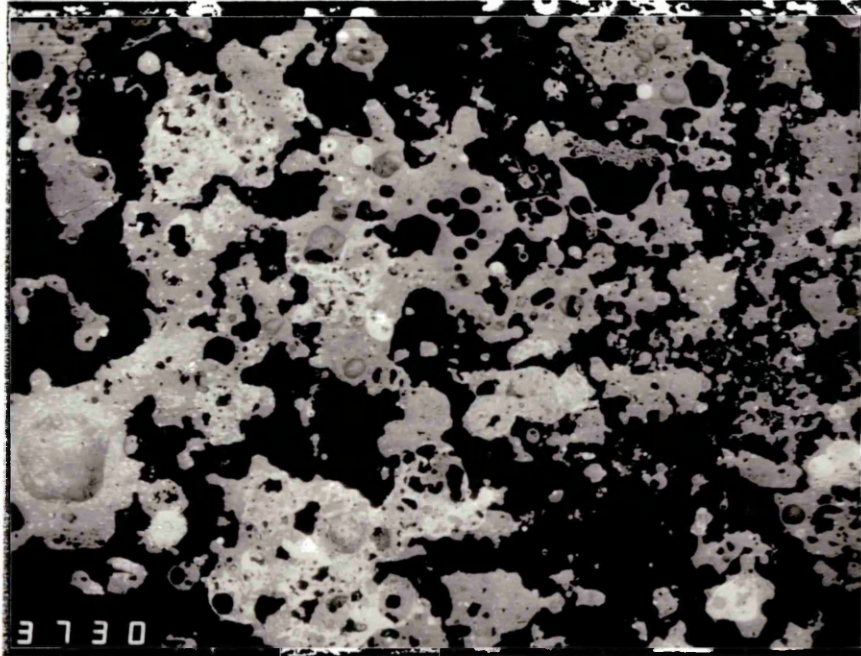


Plate 4-42:

SEM-micrograph of a polished lower furnace deposit (i.e. FA, RA, FW, RW and/or SW) from boiler No.6, with on-line Lycal 93HS injection. The open skeletal structure is typical of post Lycal injected deposit samples. [Mag: x30]

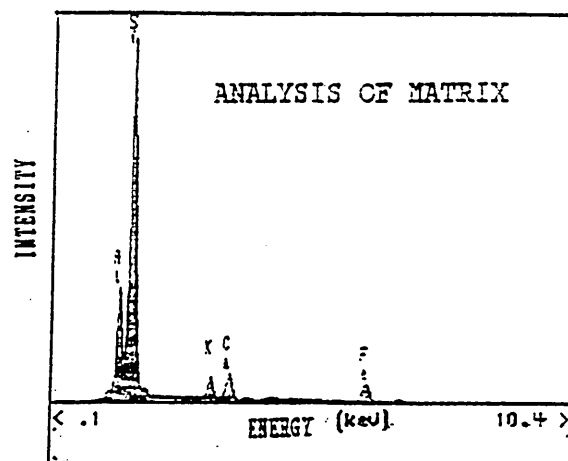
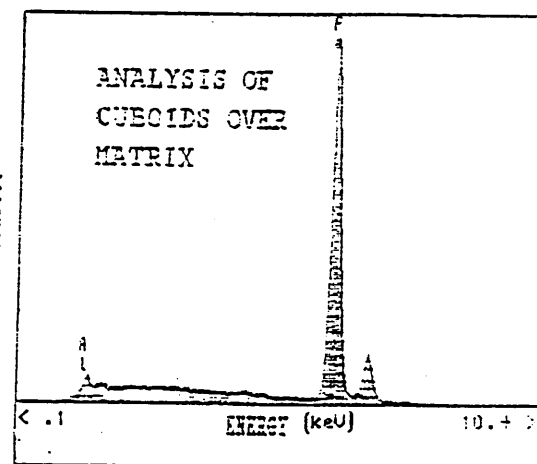
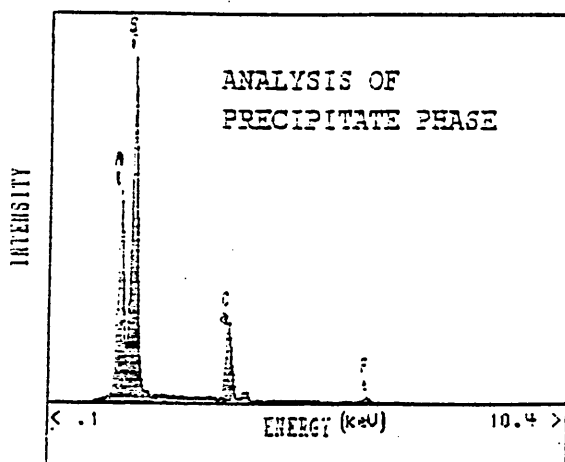
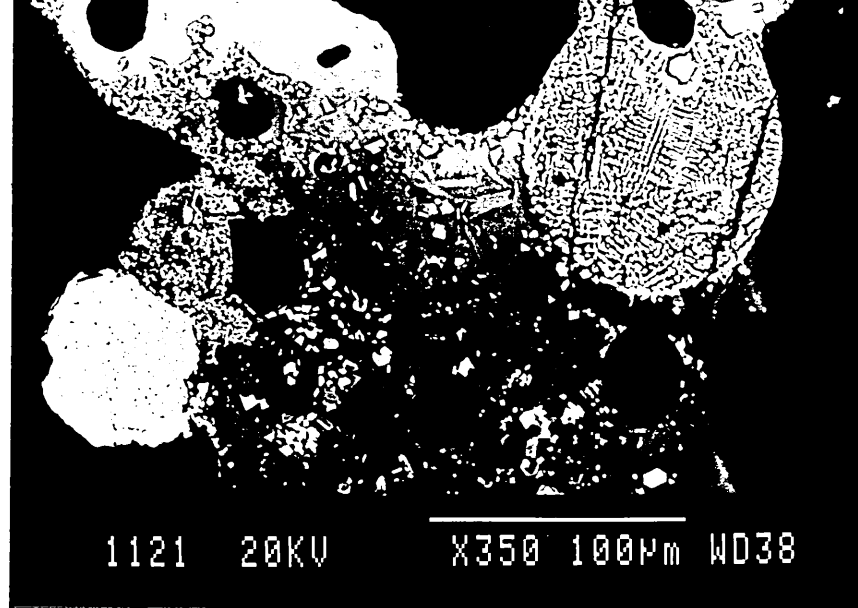


Plate 4-43:

Higher magnification SEM-micrograph of the deposit specimen in Plate 4-42, showing the extent of crystalline heterogeneity present within the sample. The EDX-analyses show the composition of the precipitate phase within the matrix (dark grey), the angular cuboids (light grey) and the siliceous matrix. A large sphere of hematite dendrites (creamy white) at the top RHS and a deformed sphere of pure iron oxide crystal (white) at the bottom LHS of the photograph are further evident.

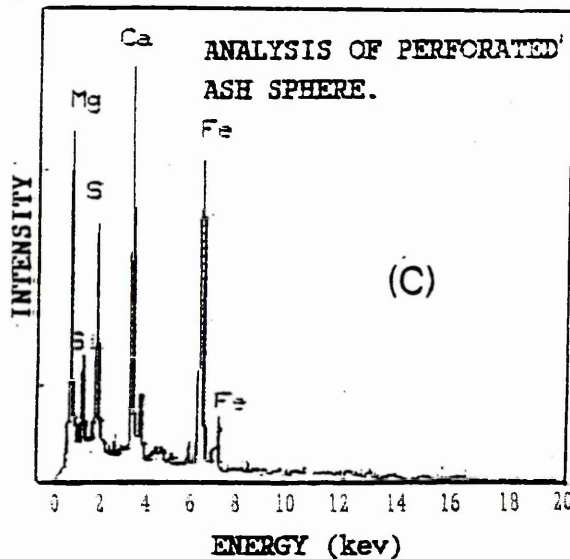
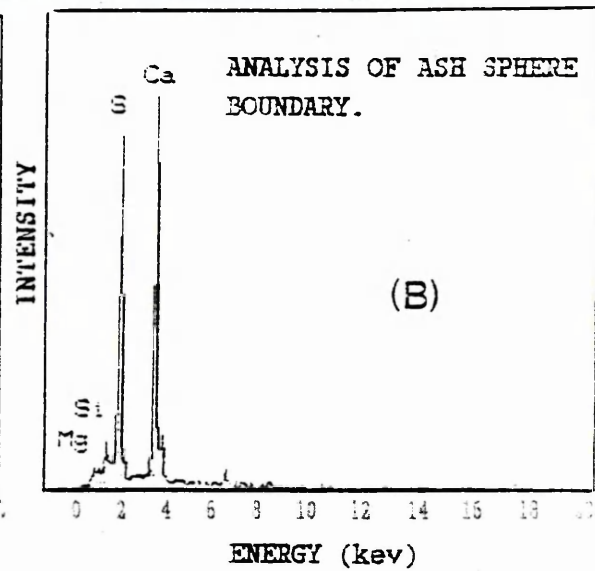
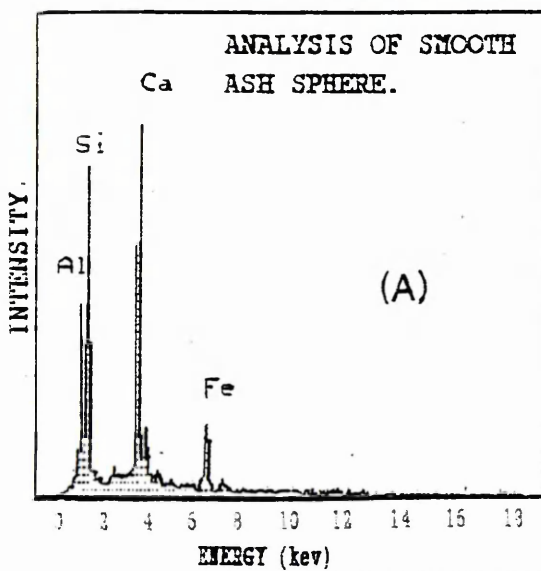
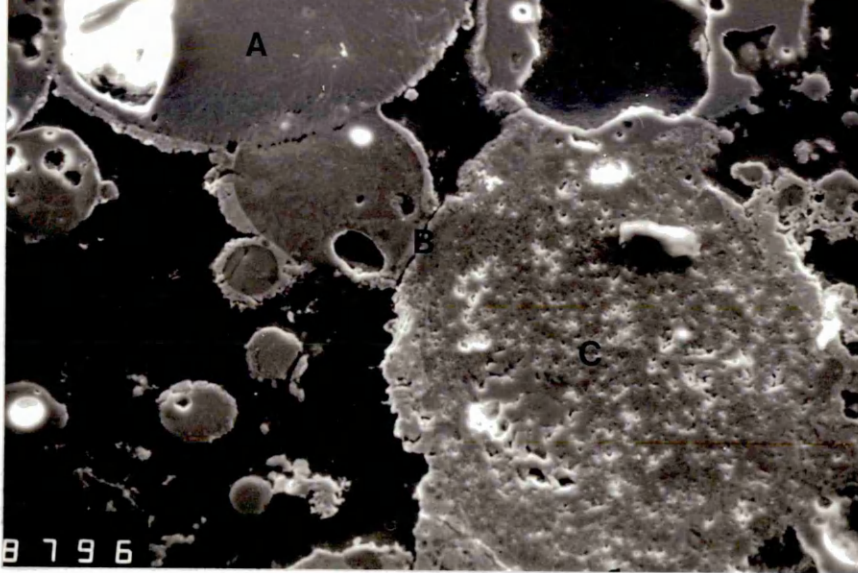


Plate 4-44:

SEM-micrograph of a lower furnace (i.e. FW, RW) "F2" type deposit sample from boiler No.6, with on-line Lycal 93HS injection. It shows the sintering of a range of spherical ash particles of various sizes and textures. The EDX-analyses show the composition of the areas "A", "B" and "C".

[Mag: x460]

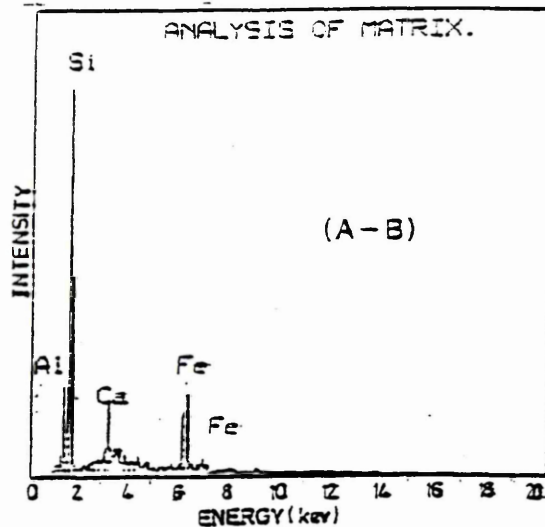
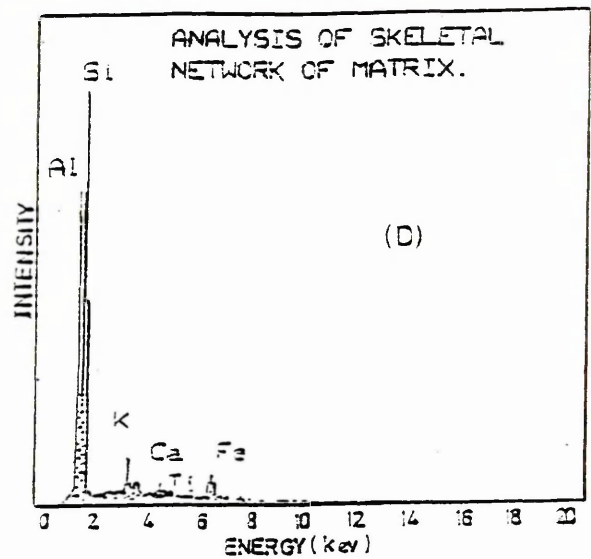
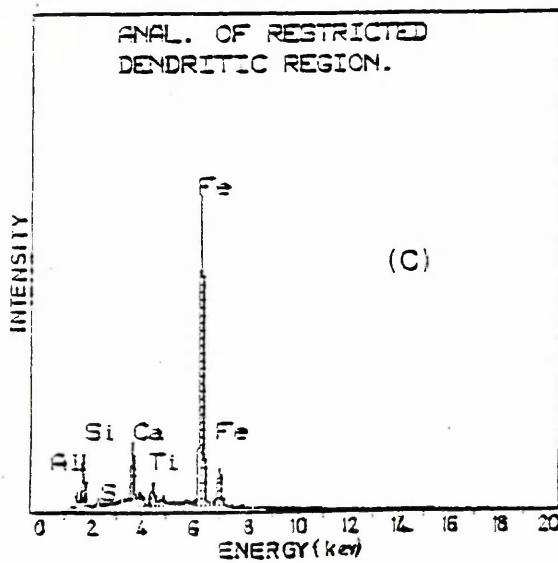
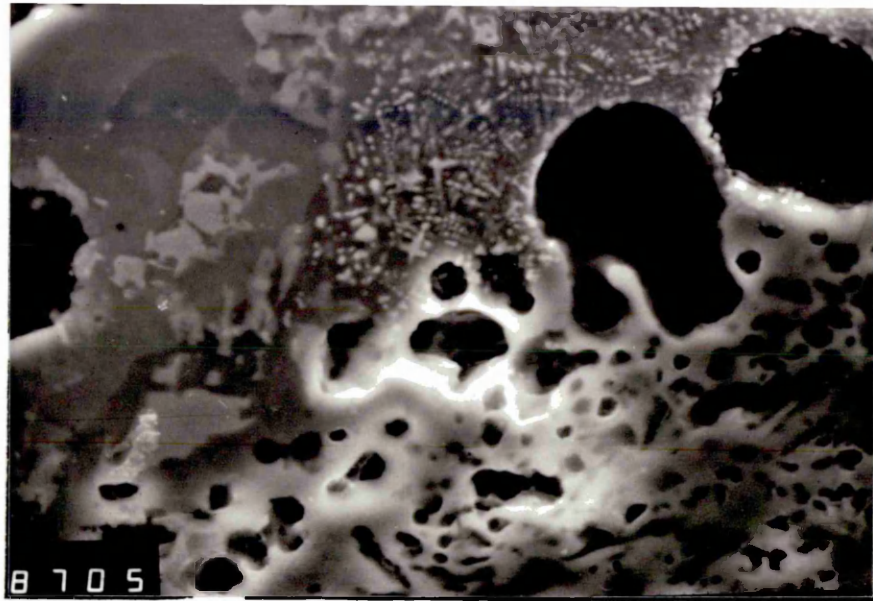


Plate 445:

SEM-micrograph of a deposit sample from the Rear Wall in boiler No.6, with on-line Lycal 93HS injection. An area of continuous matrix, "A-B-C" is connected to a highly porous, honeycomb textured area, "D". The EDX-analyses show the composition of the siliceous matrix, "A-B" with crystalline phase, "C" and skeletal matrix, "D". [Mag: x1040]

is shown to be of an alumino-silicate composition.

Plate 4-46 is the BSE image of neck growth between two spherical ash particles within an "F1" type rear wall deposit sample from the third batch. The EDX analysis shows that the larger sphere has a siliceous matrix (grey). There are small dendritic iron-alumina enriched precipitates at the inner periphery of the larger ash sphere and larger lath shaped growths, enriched in titanium oxide, as well as alumina, silica and iron oxide, towards the centre. The smaller ash particle at the top is shown to be made up of fine crystals of hematite (white) with minor impurity oxides.

Plate 4-47 reveals the occurrence of iron oxide-alumina dendritic crystals (light grey) which may possibly be $\text{FeO} \cdot \text{Al}_2\text{O}_3$ spinels, hercynite, in a siliceous matrix (dark grey). The EDX-analysis shows a finer iron oxide enriched surface layer (white) outlining the edge of the spherical ash particle. The black areas are porosity.

Plate 4-48 is a BSE-image of a broken cluster of what could be angular, iron oxide-alumina spinel crystals, hercynite, concentrated at the surface of a large pore within a front wall sample. The angular shape of these crystals is evidently different to the dendritic type crystals observed in Plate 4-47, illustrating a variation in crystalline structure despite an identical chemical composition.

Plate 4-49 is the BSE-image of a front wall deposit sample, containing fine cuboidal crystals (white) dispersed within a siliceous matrix (dark grey) with a range of laths (light grey). The presence of minor quantities of magnesium oxide with silica, alumina and iron oxide as the major components is shown by the EDX analysis.

Plate 4-50 is the BSE-image from a front wall deposit sample showing an area within the periphery of a cavity, where extremely fine crystalline needles (white) have grown. The EDX analysis illustrates the silica-alumina enrichment in the relative proportions which could suggest the fine needles to be mullite crystals. A range of

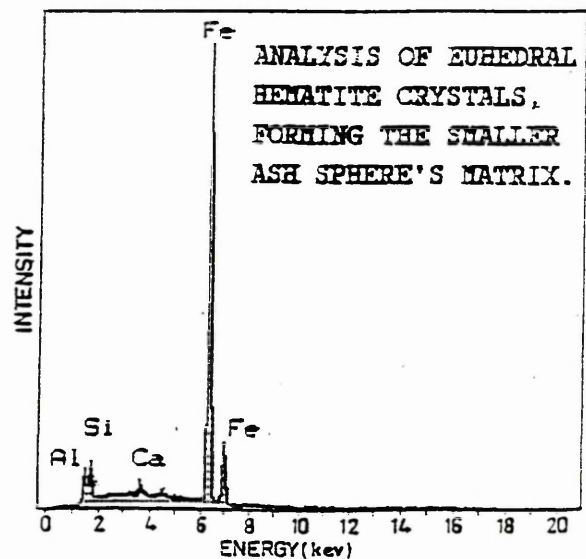
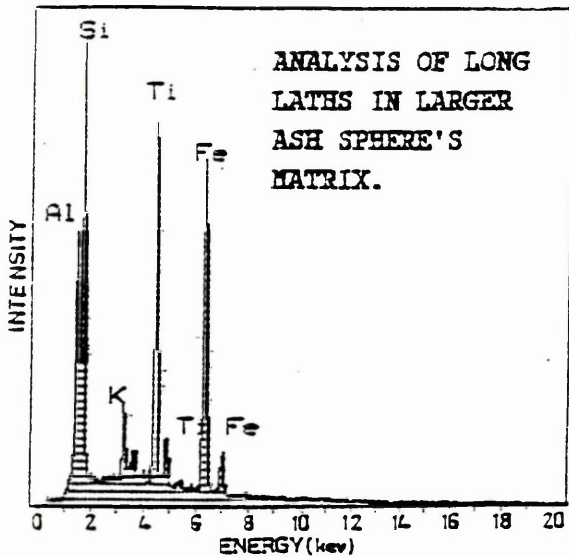
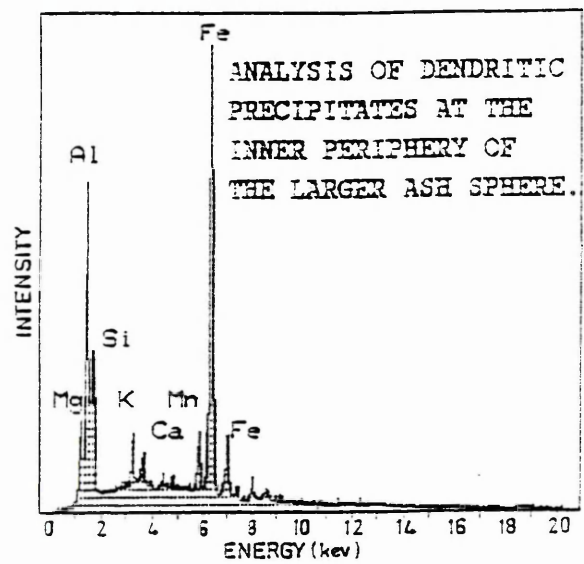
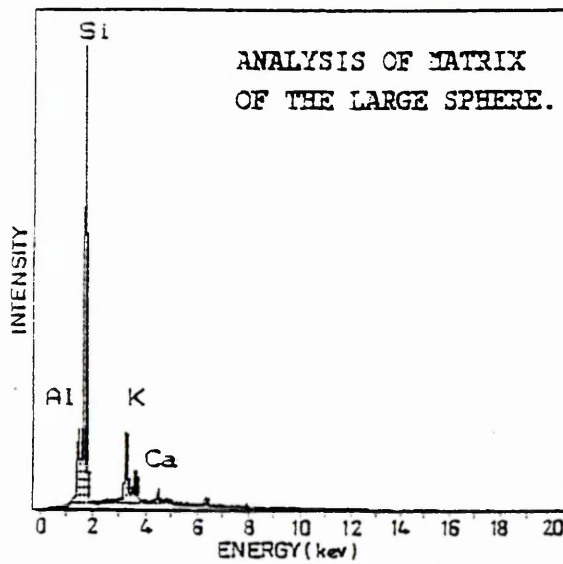
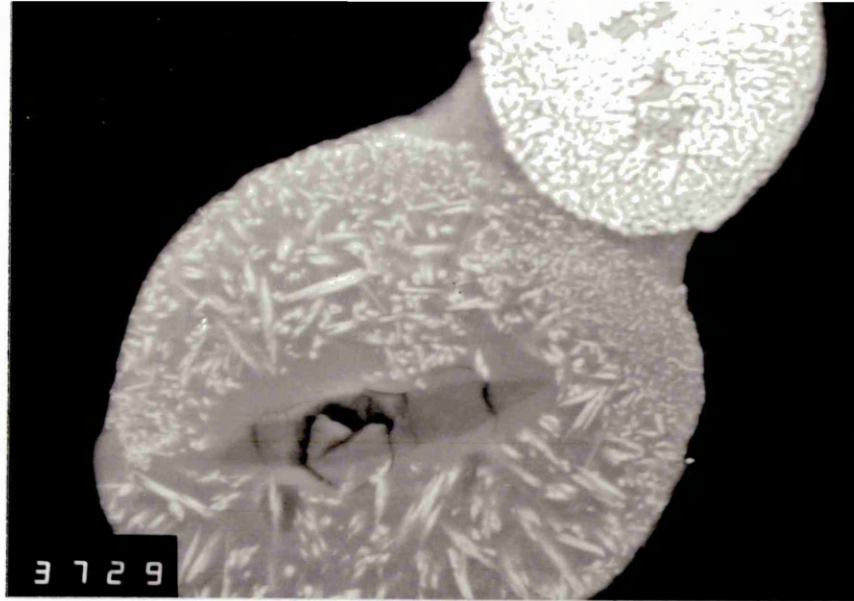


Plate 446:

SEM-micrograph of a "F1" type deposit sample from the Rear Wall in boiler No.6, with on-line Lycal 93HS injection. It shows the neck growth between a large sphere and a smaller white-sphere. The EDX-analyses illustrate the composition of different phases. [Mag: x960]

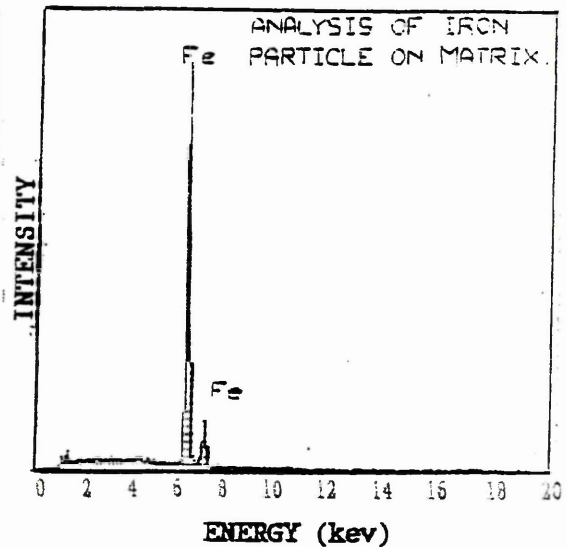
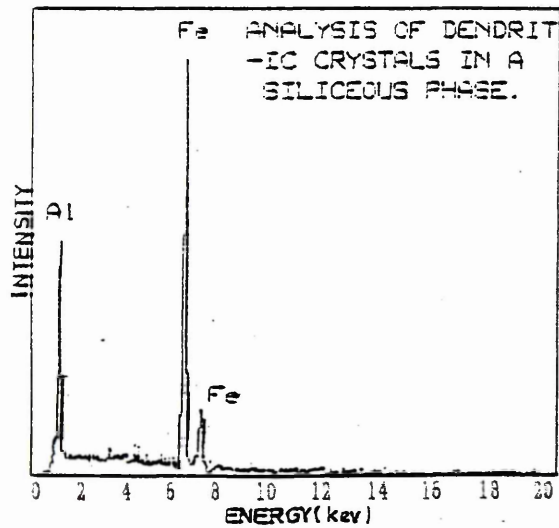
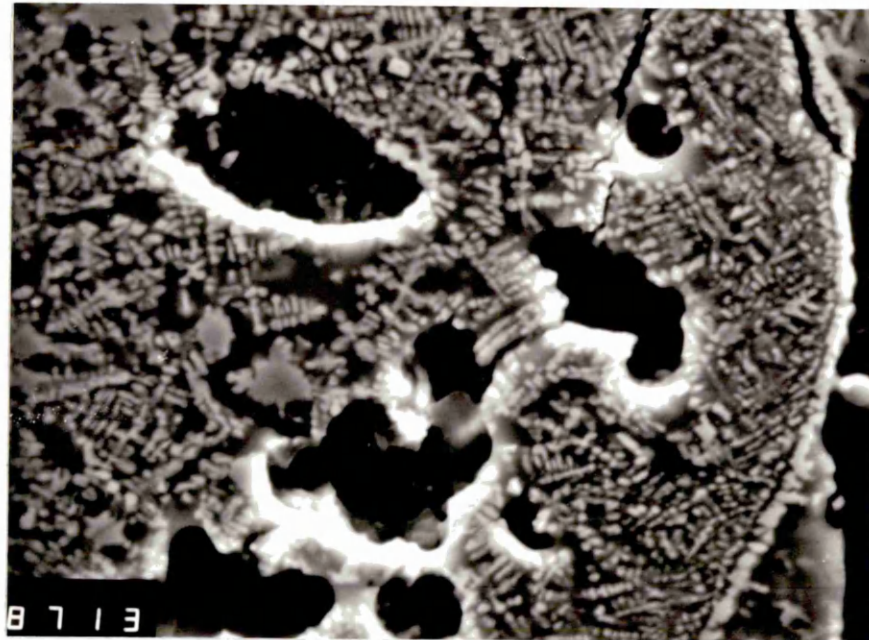


Plate 4-47:

SEM-micrograph of a deposit sample from the Rear Wall in boiler No.6, with on-line Lyclal 93HS injection. It shows the solidification of fine and large dendrites in a siliceous matrix (dark grey) with a white layer outlining the periphery of the ash sphere. The EDX-analyses show the dendrites to be of the iron-spinel type and the white layer is pure iron oxide. [Mag: x1120]

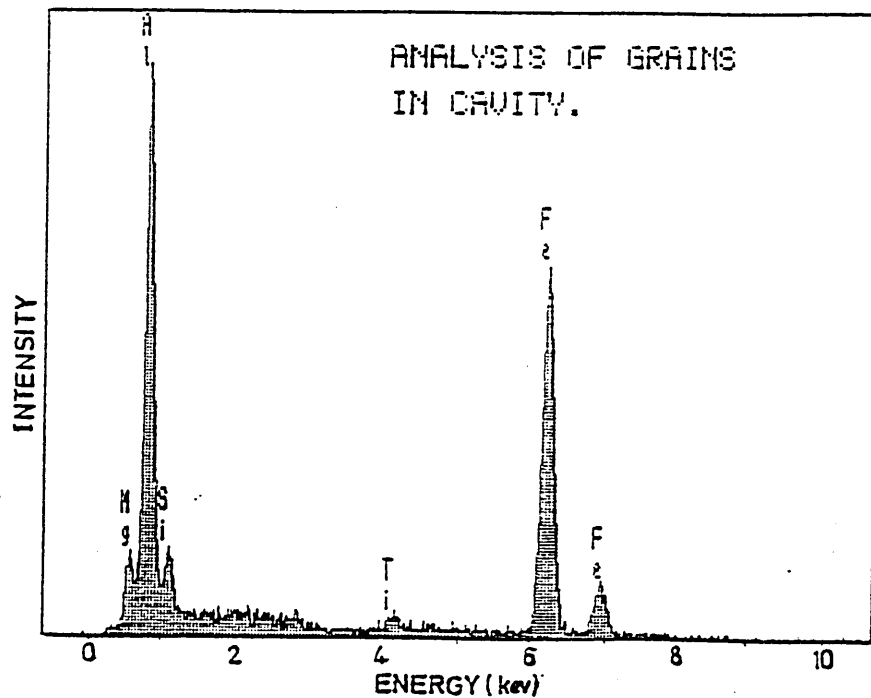
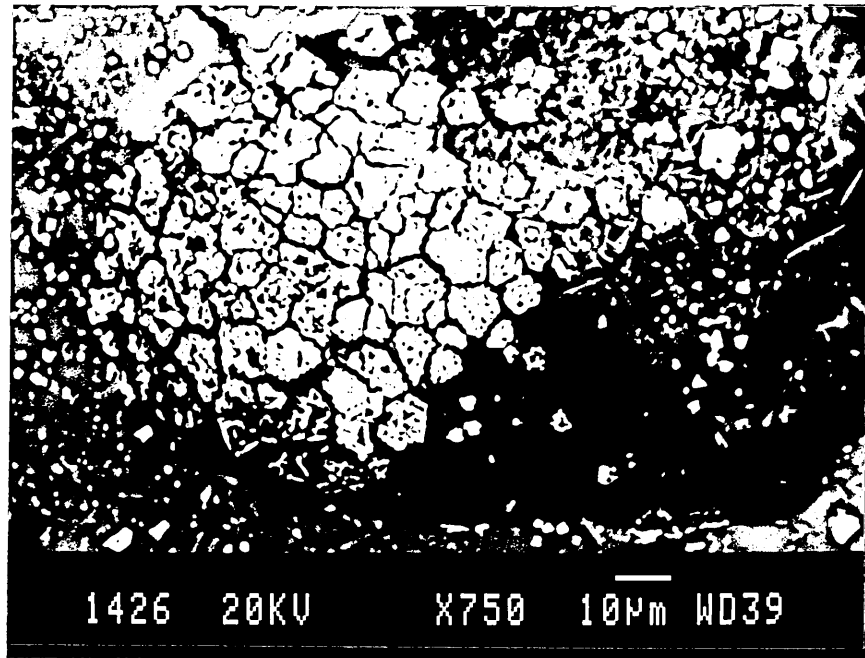


Plate 4-48:

SEM-micrograph of a deposit sample from the Front Wall in boiler No.6, with on-line Lycal 93HS injection. It shows a broken spherical cluster of white crystals at the surface of a large pore. The EDX-analysis shows the crystals to be iron oxide-alumina rich, suggesting iron-spinel crystals.

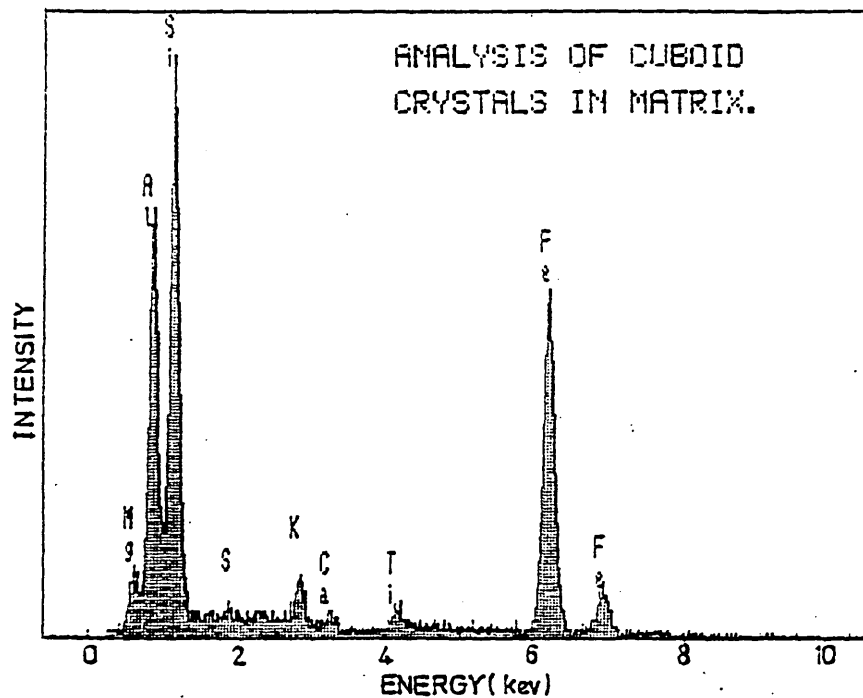
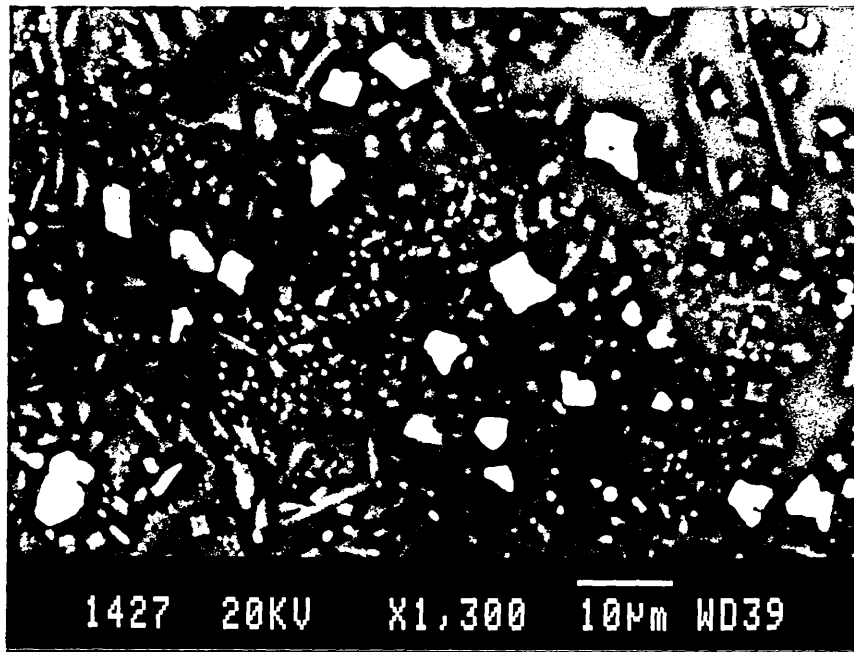


Plate 4-49:

SEM-micrograph of a deposit sample from the Front Wall in boiler No.6, with on-line Lyclal 93HS injection. It shows cuboidal and euhedral crystals (white) and large, long needles(light grey) in a siliceous matrix (dark grey). The EDX-analysis shows the composition of cuboid crystals.

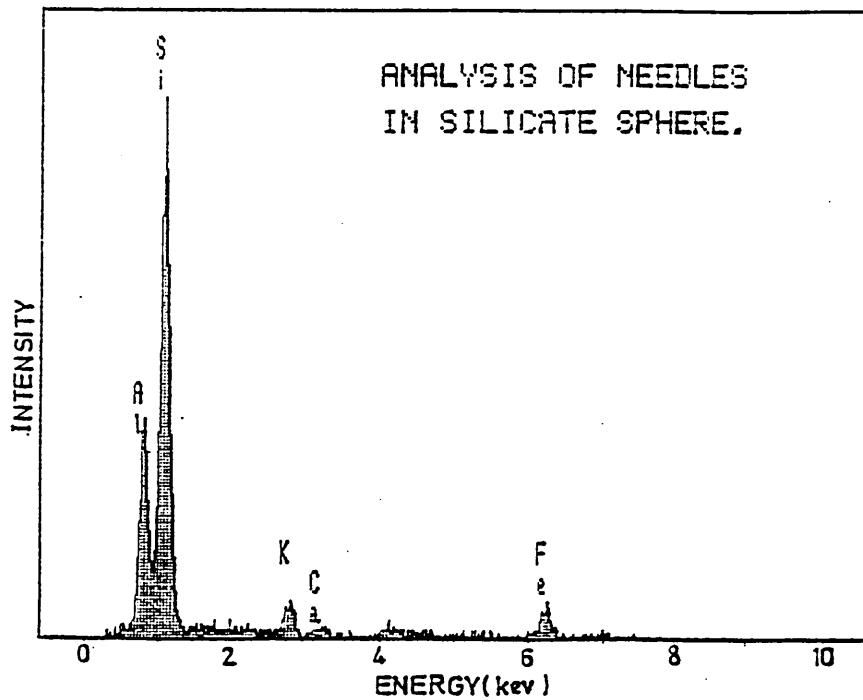
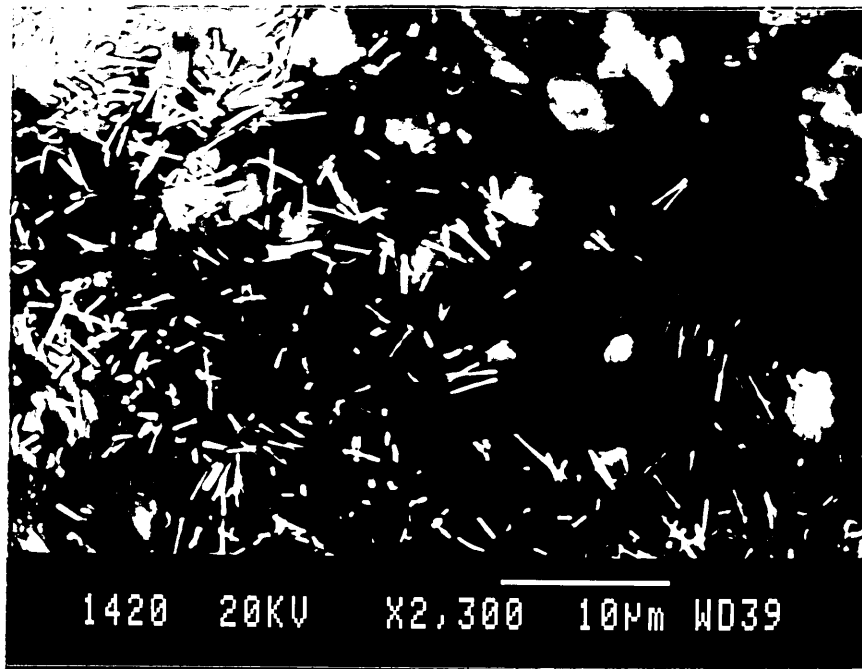


Plate 4-50:

SEM-micrograph of a deposit sample from the Rear Wall in boiler No.6, with on-line Lyclal 93HS injection. It shows an array of fine ($< 5\mu\text{m}$) crystalline needles (white). The EDX-analysis is characteristic of the mullite phase.

angular iron rich cuboids as well as lathes can be seen in the background.

Plate 4-51 shows a large porosity hole in a front wall deposit filled with a "fibrous" agglomeration. The EDX-analysis shows these to be mostly made up of a silica-alumina phase enriched with oxides of iron and titanium. This observation was not very common and furthermore was only evident in lower furnace deposits.

Plate 4-52 shows the neck between two sintering spherical ash particles in a front arch deposit sample. Fine needle shaped crystals have precipitated at the periphery of the lower ash sphere and coarse ones at its centre. The EDX-analysis shows the needles to be relatively enriched in the four major oxides in the ash matter, namely; silica, alumina, iron oxide and calcium oxide.

Plate 4-53 shows the arrangement of sintering ash particles within an upper furnace screen tube deposit sample. The iron oxide rich phase (white) acts as a bridge between spherical alumino silicate ash particles (dark and lightgrey) to form a discontinuous matrix with an extensive dispersion of finer spherical ash particles of a few micrometers in size. The EDX- analysis shows the composition of the two major components in this micrograph.

Plate 4-54 shows a highly porous (black), screen tube deposit containing a number of highly sintered and deformed siliceous (dark grey) ash particles which are bonded together via a network of iron oxide enriched phase (white).

Plate 4-55 is a photo-micrograph of a bottom screen tube sample, showing a number of larger spherical ash particles with fine dendritic crystals of hematite or iron-spinel (white-lines) within the matrix of the joined ash spheres and iron oxide rich phase as the bonding layer (white area) around the periphery of the ash spheres.

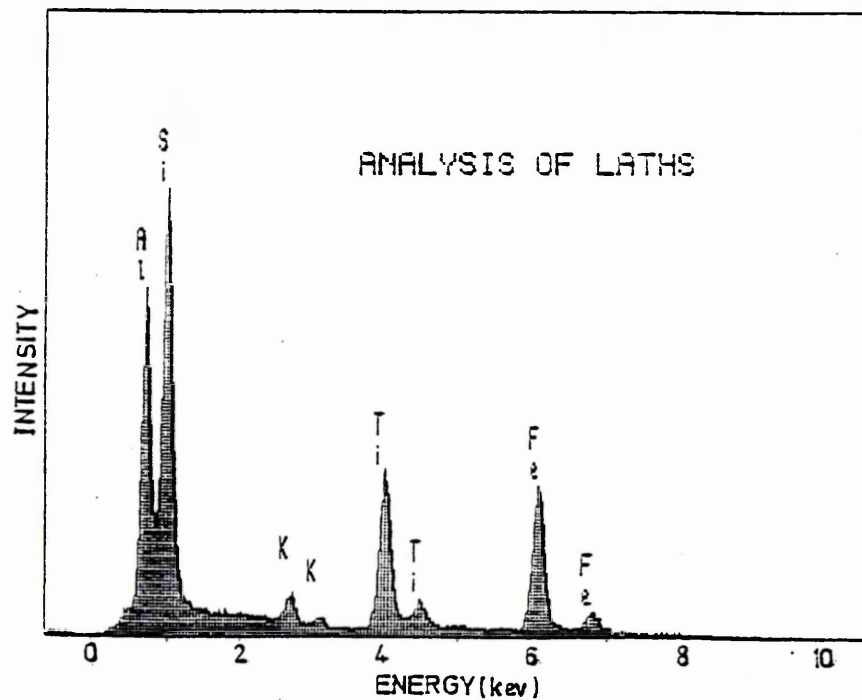
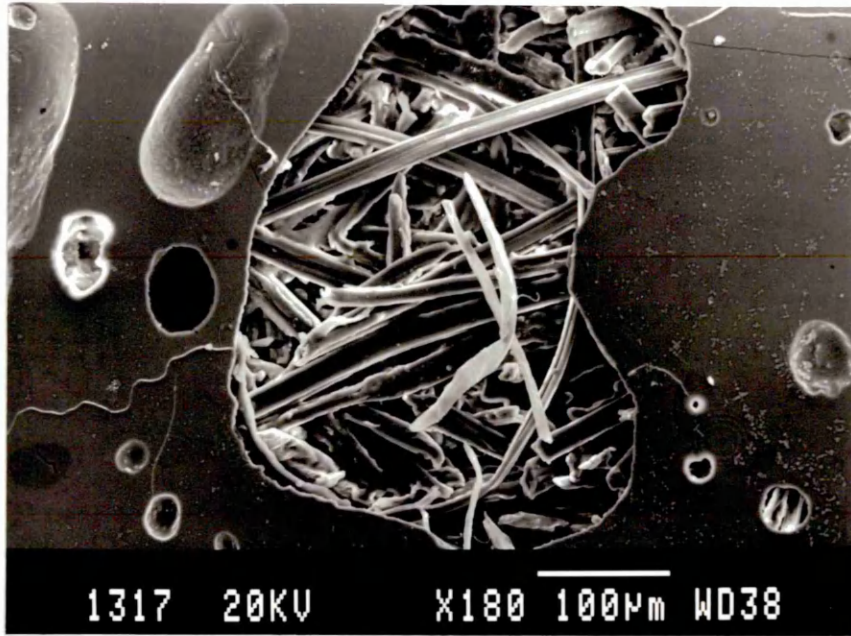


Plate 4-51:

SEM-micrograph of a deposit sample from the Front Wall in boiler No.6, with on-line Lyclal 93HS injection. It shows a fibrous agglomeration of long laths inside a large pore within a siliceous matrix. The EDX-analysis of the laths is alumino-silicate, enriched with iron oxide and titania.

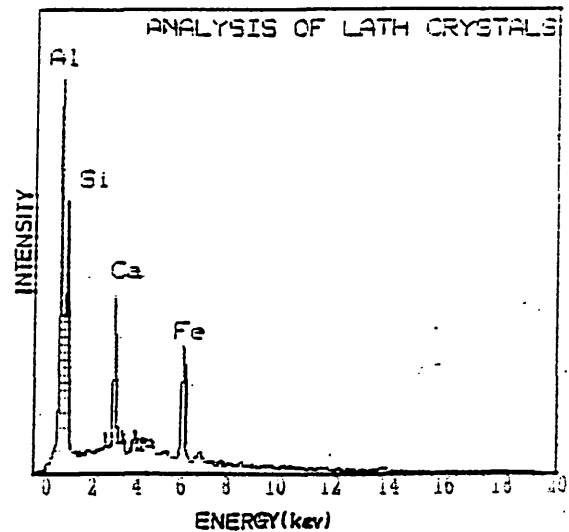
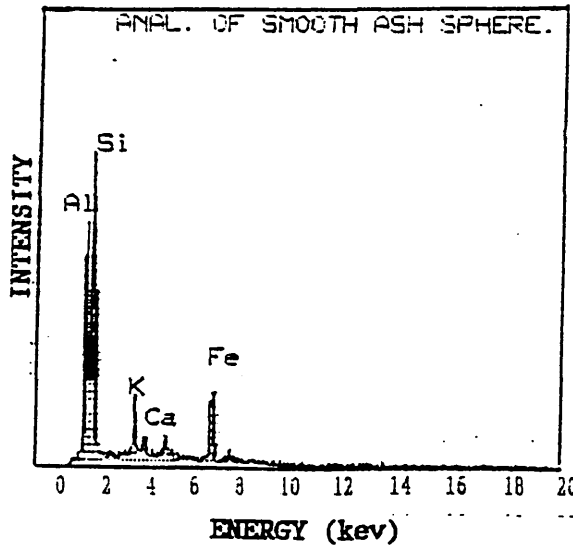
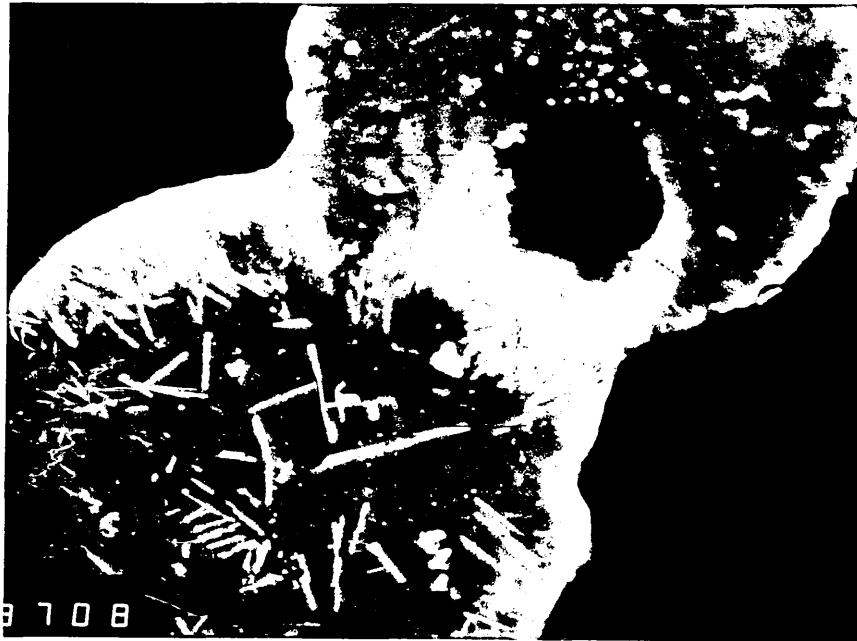


Plate 4-52:

SEM-micrograph of a deposit sample from the Front Arch in boiler No.6, with on-line Lycal 93HS injection. It shows the bonding and neck growth between two ash spheres and the crystalline precipitates of fine and coarse needles in the lower sphere. The EDX-analyses characterise the composition of matrix and the fine needles. [Mag: x1120]

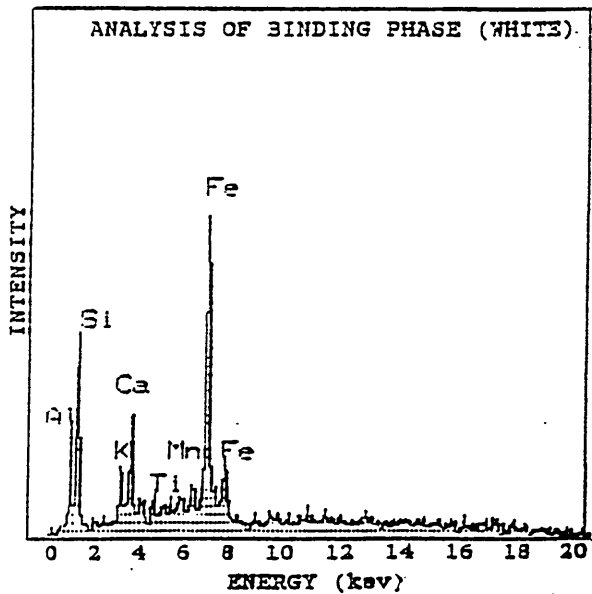
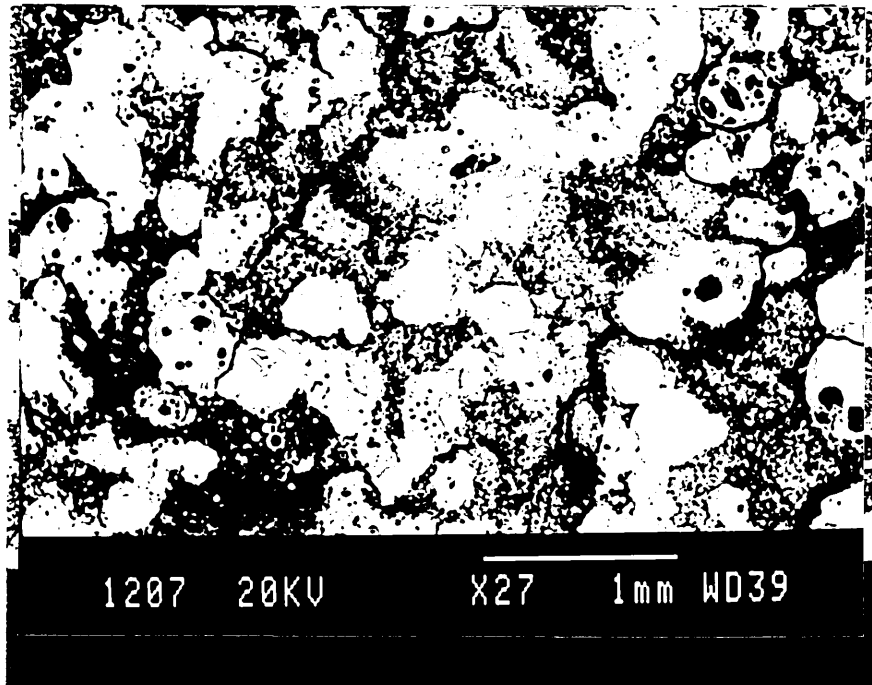


Plate 4-53:

SEM-micrograph of a deposit sample from the Bottom Screen Tubes in boiler No.6, with on-line Lycl 93HS injection. The iron rich phase (white) acts as the binder in an open - skeletal matrix of large (100-400 μ m) spherical ash particles. The EDX-analysis illustrates the composition of the binding phase.

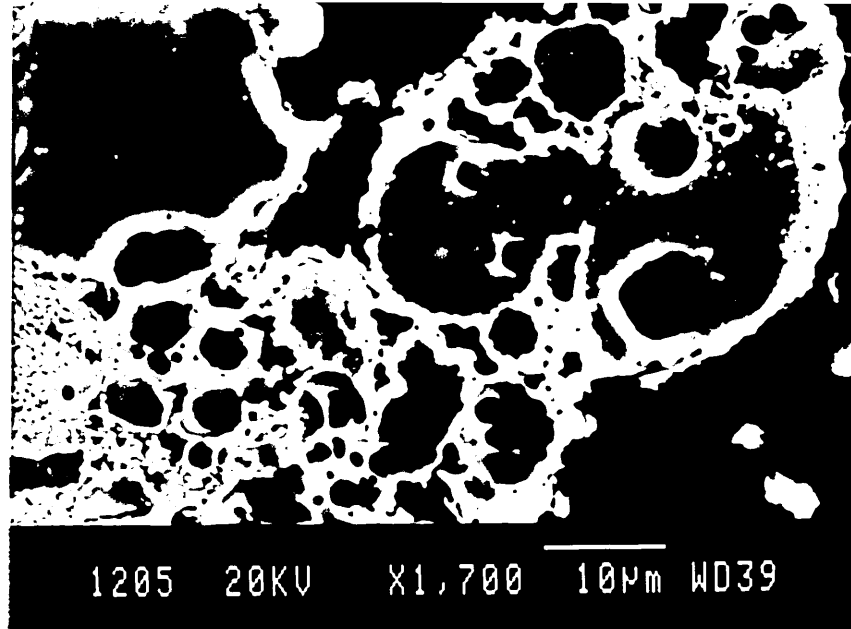


Plate 4-54:

SEM-micrograph of a deposit sample from the Bottom Screen Tubes in boiler No.6, with on-line Lycal 93HS injection. A highly porous (black) skeleton of sintered and fused, siliceous ash spheres and spheroids (dark grey) are connected together via a network of ferrous phase (white-light grey) round the edge of the particles.

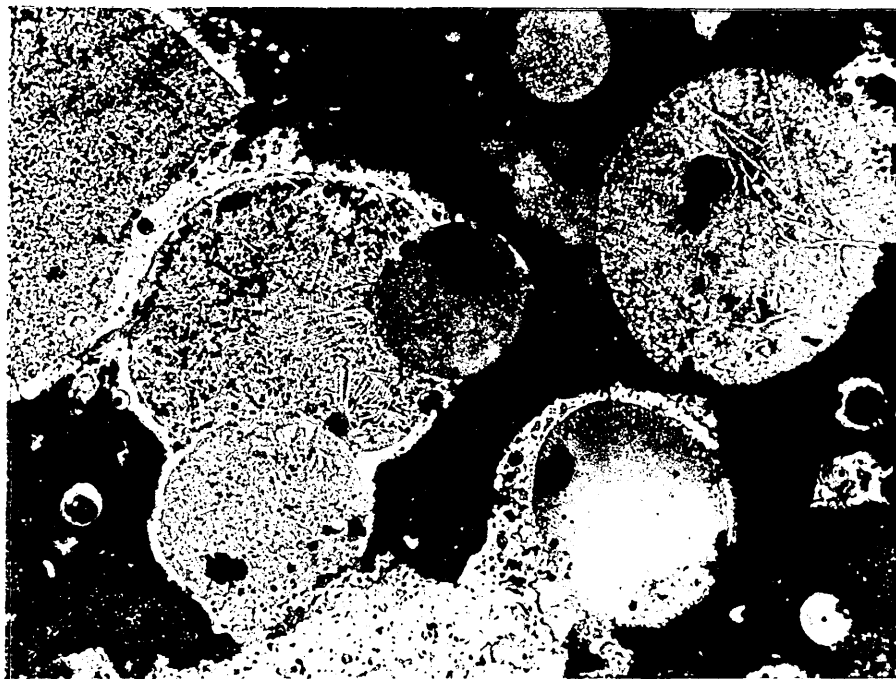


Plate 4-55:

Optical photo-micrograph of a deposit sample from Bottom Screen Tubes in No.6, with on-line Lycal 93HS injection. A number of large ash spheres and spheroids (200-700 μm) containing fine dendritic crystals of iron oxide (hematite) are bonded together via a continuous network of a white phase around the ash particles. [Mag: x50]

Plate 4-56 is a photo-micrograph of a deposit from the passage between screen tubes and steam generating tubes. It shows a number of loosely sintered spherical ash particles with iron rich spherical and non spherical ash particles (white) forming a layer around and between the joining ash particles.

Plate 4-57 is a photo-micrograph of a deposit from the "passage between screen tubes and steam generating tubes". It shows a porous (black areas) surface, with angular iron oxide- alumina spinel type particles (white) as well as finer dendrites (white) scattered throughout the matrix (dark grey).

Boiler No.5 - The range of structures observed for samples from boiler No.5, are illustrated in Plates 4-58 to 4-69.

Plate 4-58 is a micrograph typical of the outer and middle layers within the front wall deposit from boiler No.5. It shows a porous, fully fused, chemically uniform structure. The EDX-analysis shows these layers to be mainly alumino-silicate compounds.

The most notable feature of this deposit compared with the deposits taken from the same region of boiler No.6 with Lycal 93HS injection (see plate 4-42), is its continuity and physical uniformity which results in the formation of a hard, non-friable and dense structure.

Plate 4-59 is a micrograph typical of the inner layer within the same front wall deposit. It shows a continuous matrix with some fracture lines which were probably caused during sampling and sample preparation. The EDX-analysis illustrates the siliceous nature of the matrix (dark grey) and randomly dispersed iron oxide - silica rich particulate phase (light grey) within some sections of the matrix.

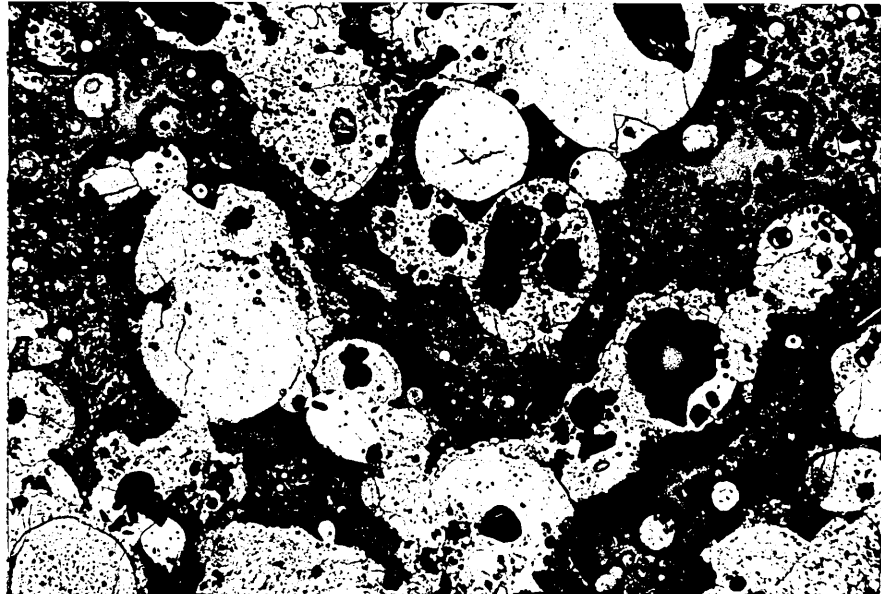


Plate 4-56:

Optical photo-micrograph of a deposit sample from the Passage between Screen Tubes and Steam Generating Tubes deposit sample from boiler No.6, with on-line Lyclal 93HS injection. A number of ash spheres and spheroids are loosely sintered together through stretches of ferro-spheres and the other iron oxide rich phase (white), forming a porous, open-skeletal matrix. [Mag: x75]

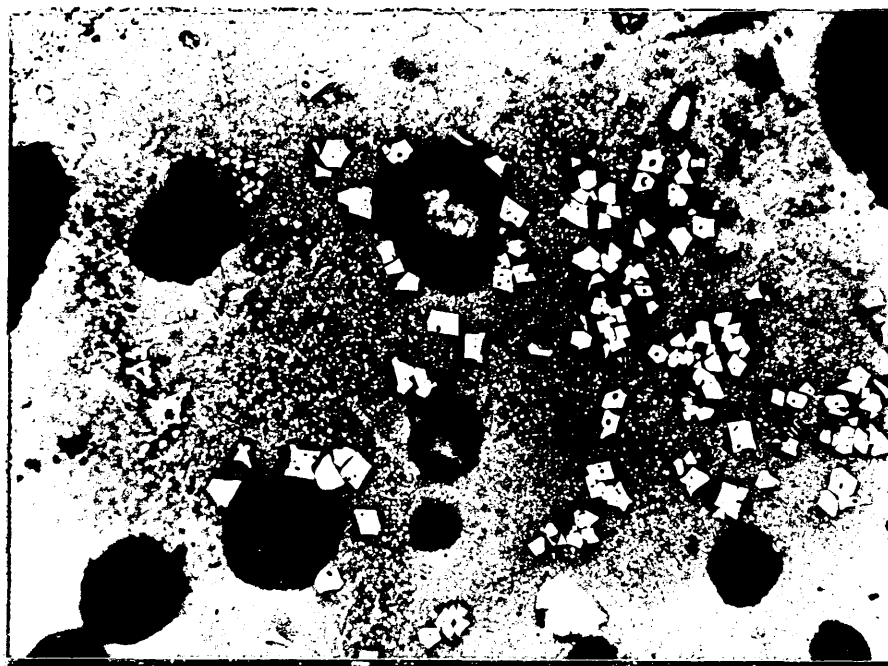


Plate 4-57:

Optical photo-micrograph of a deposit sample from the Passage between Screen Tubes and Steam Generating tubes in boiler No.6, with on-line Lyclal 93HS injection. A porous area of matrix is shown to contain a range of angular iron oxide, iron spinel type crystals (white-light grey) within the matrix and around the porosity holes, with much finer dendritic hematite crystals (white-light grey) scattered in the matrix. [Mag: x125]

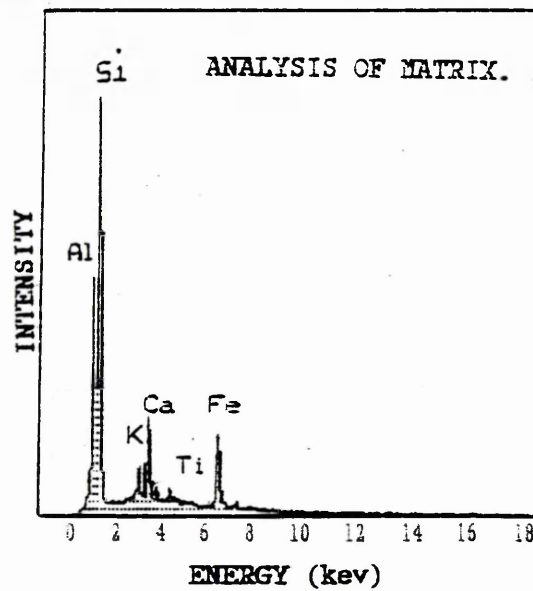
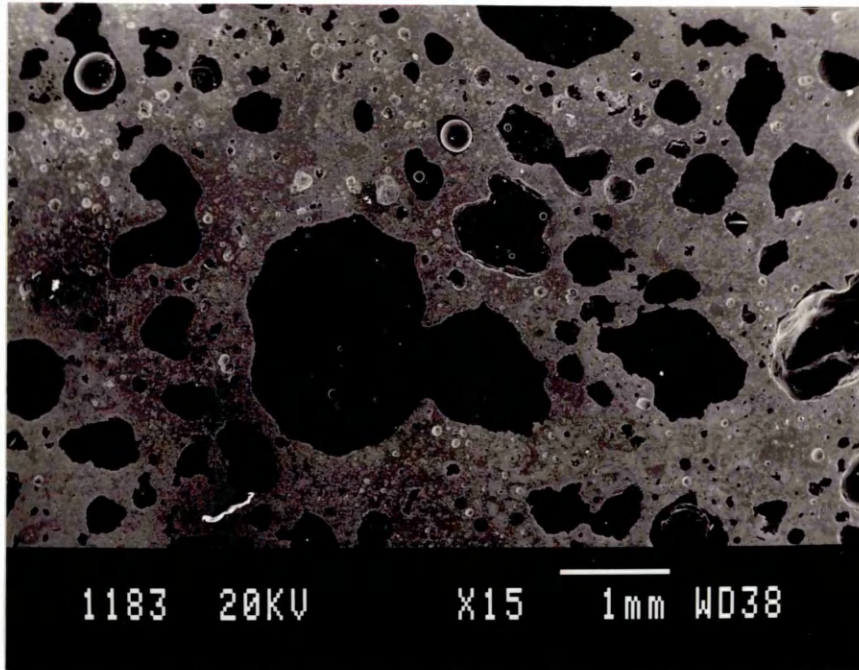


Plate 4-58:

SEM-micrograph representing the outer and middle layers of a deposit sample from the Front Wall in boiler No.5, without on-line Lycal 93HS injection. A highly porous, fully fused, continuous matrix is shown. The EDX-analysis shows an alumino-silicate rich matrix.

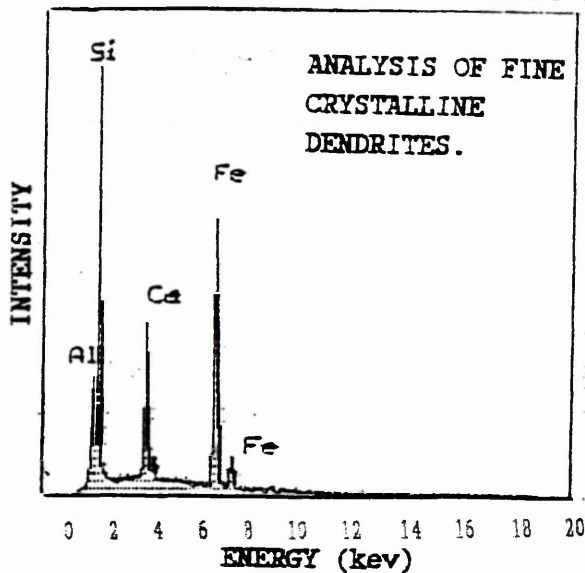
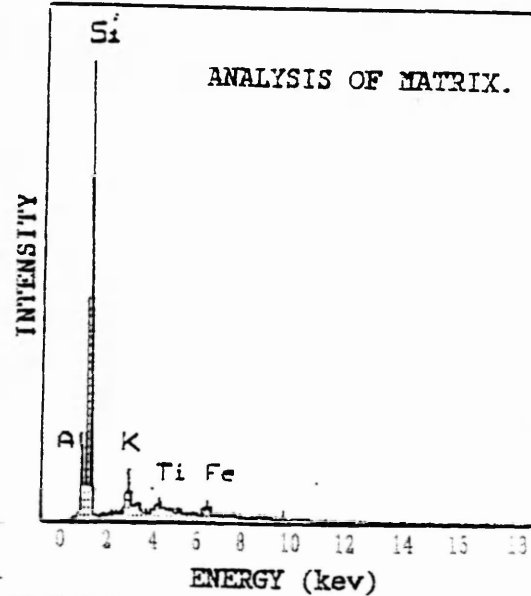
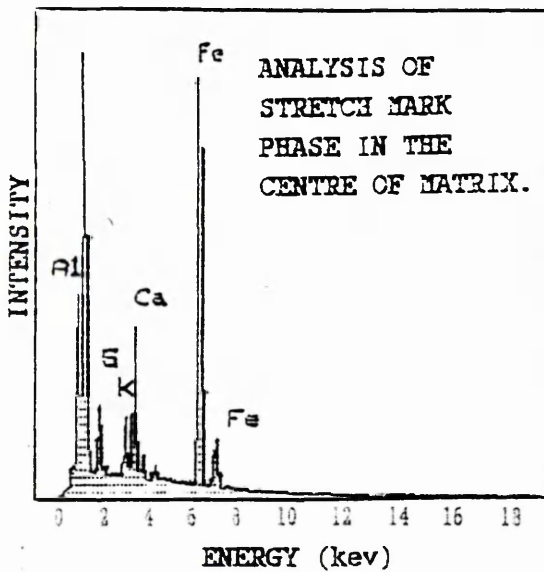
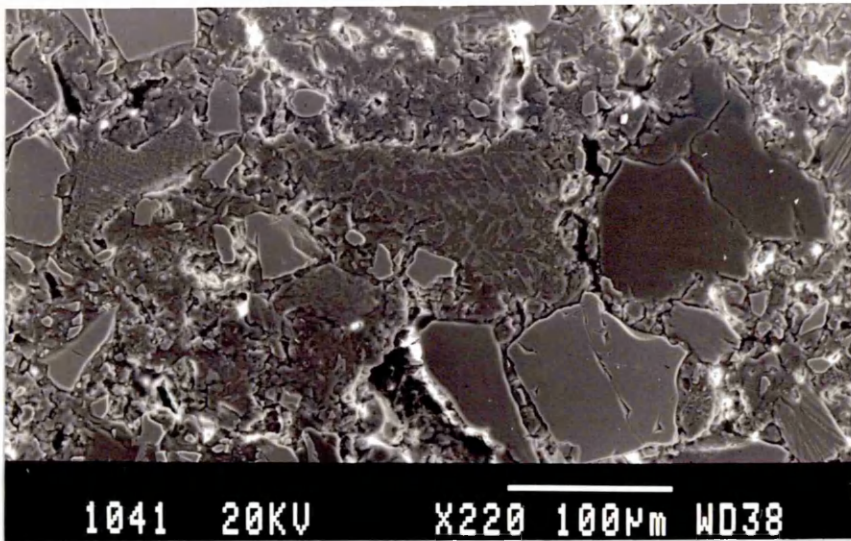


Plate 4-59:

SEM-micrograph representing the inner layer of the Front Wall deposit sample in Plate 4-58. It shows a continuous siliceous matrix (dark/light grey) with some fracture lines and very limited crystallinity (dark grey) in the centre of the plate. The EDX-analyses show the phase compositions of matrix and crystalline matter.

Plate 4-60 is a micrograph typical of the structure associated with the rear wall deposit sample. It shows a fully molten ash network with an irregular distribution of porosity. The notable feature of this sample compared with a sample taken from the same region in boiler No.6 with Lycal 93HS injection (see plate 4-42), is its continuity and physical uniformity. As a result of coalescence, the ash particles seem to have lost their original spherical shape.

Plate 4-61 is a micrograph of the rear arch deposit sample showing the discontinuous nature of the inner layer matrix (left hand side) and the relatively continuous matrix of the outer layer (right hand side). The limited bonding which evidently exists between the two layers suggests the discrete formation of these layers from each other compared to that of the front wall deposit sample in Plates 4-58 and 4-59.

Plate 4-62 is a micrograph of the outer layer from the rear arch sample showing a porous but continuous matrix, containing distributions of two precipitated crystalline phases. These latter phases are shown in more detail in Plate 4-63 where they are seen to take the form of laths (light grey) and dendritic crystals of ferriferous type precipitate (white) within the matrix phase (dark grey).

Plate 4-64 is a micrograph typical of the structure associated with the steam generating tube deposit sample. It shows a molten lattice network with extensive porosity. The EDX- analysis illustrates the ferriferous nature of the matrix of this deposit.

Plate 4-65 is a micrograph of the steam generating tube sample. It shows a porous, fully fused matrix (light grey) with some residual spherical ash particles lodged in the pores at the outer boundary of the sample. A distribution of fine precipitates (white) can also be seen throughout the matrix.

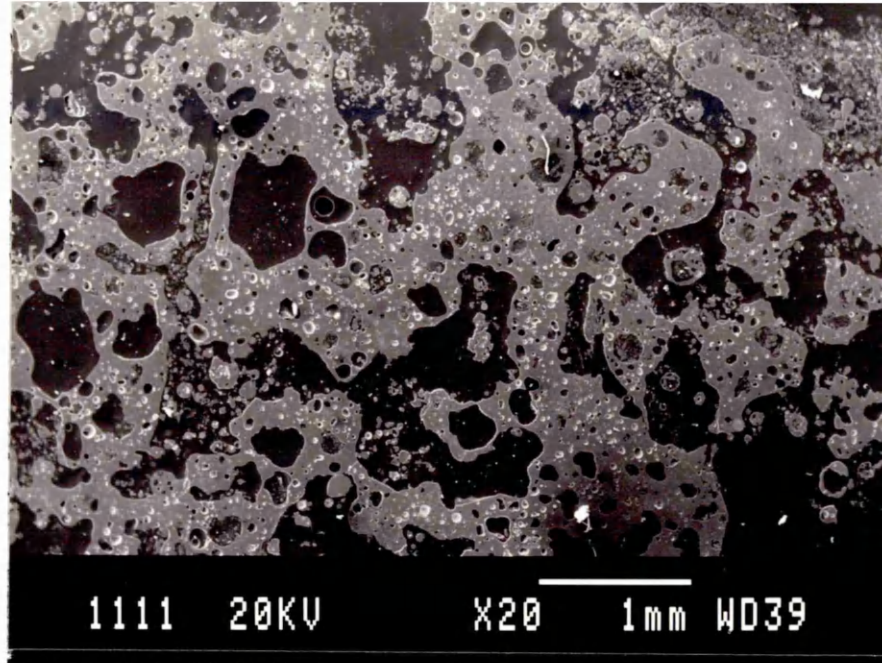


Plate 4-60:

SEM-micrograph of a deposit sample from the Rear Wall in boiler No.5, without on-line Lycal 93HS injection. It shows a fully fused, highly siliceous, porous matrix. The EDX-analysis was similar to that of Plate 4-59.

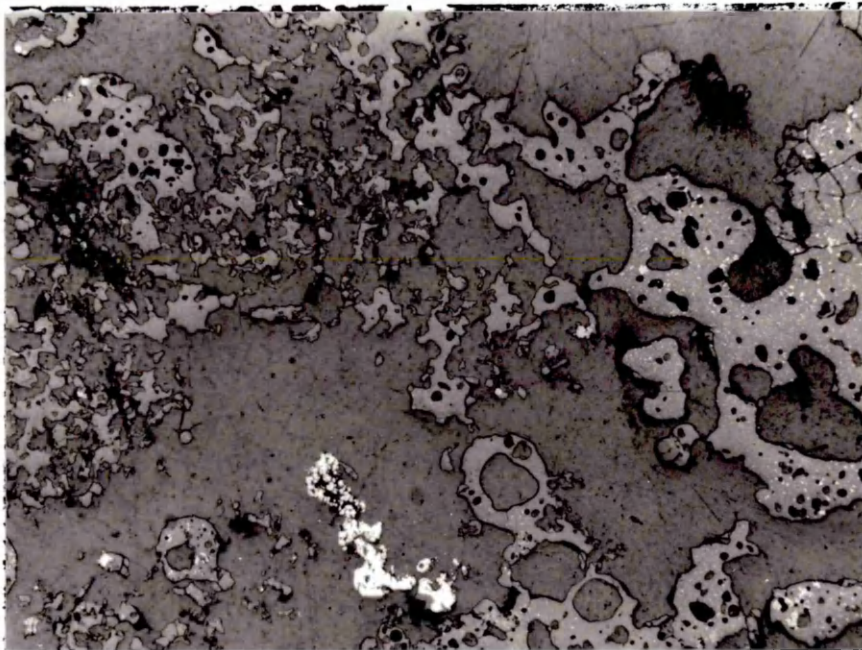


Plate 4-61:

Optical photo-micrograph of the inner layer of a deposit sample from the Rear Wall in boiler No.5, without on-line Lycal 93HS injection. The discontinuous inner layer (LHS) is in contrast to the continuous, porous outer layer (RHS). **[Mag: x13]**

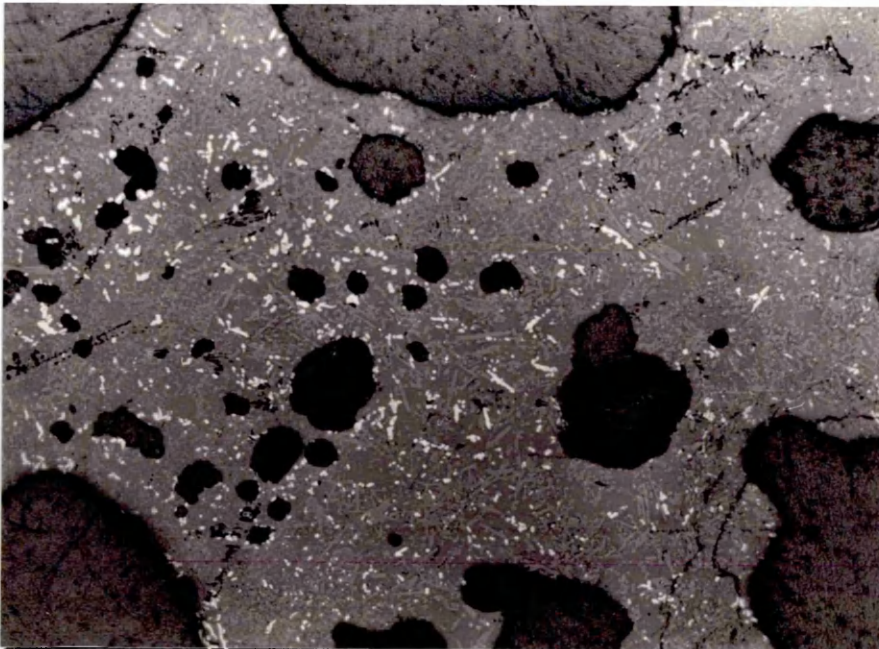


Plate 4-62:

Optical photo-micrograph of the outer layer of a deposit sample from the Rear Arch in boiler No.5, without on-line Lyclal 93HS injection. It shows a porous (black/dark grey), continuous matrix (light grey) containing two precipitated crystalline phases (white and light grey). [Mag: x25]



Plate 4-63:

Higher magnification optical photo-micrograph of Plate 4-62, showing the iron oxide dendritic precipitates (white), and long and large mullite-like needles. [Mag: x125]

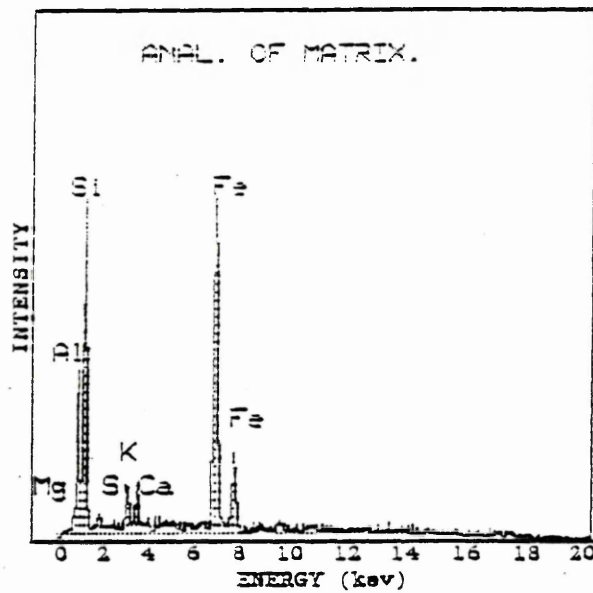
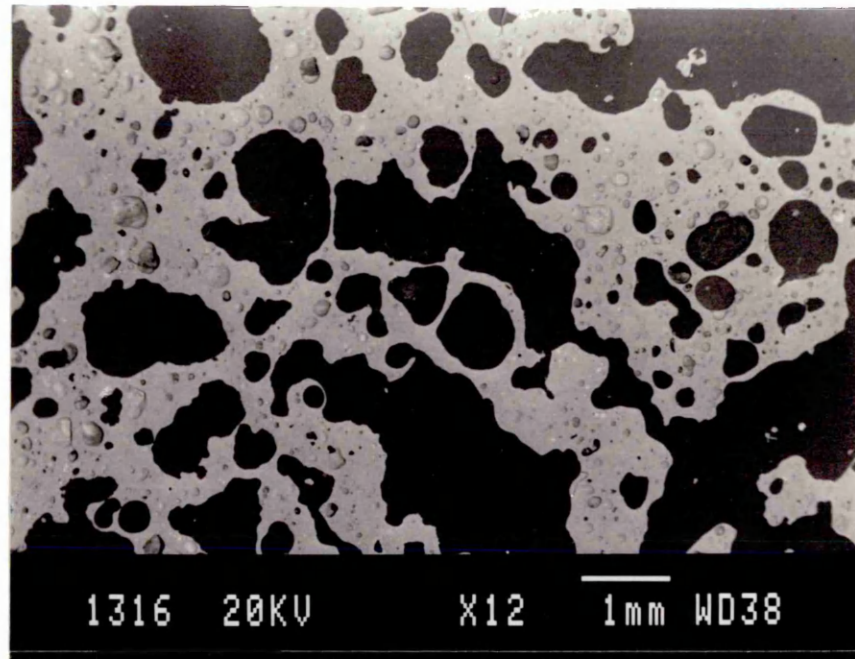


Plate 4-64:

SEM-micrograph of a deposit sample from Steam Generating Tubes in boiler No.5, without on-line Lycal 93HS injection. It shows a highly porous, fully fused, continuous matrix. The EDX-analysis of the matrix shows a iron rich composition.

Plate 4-66 is a BSE-image from the bottom screen tube deposit sample. The spherical shape of an ash particle, which has been fully incorporated into the rest of the matrix, is defined by a fine dispersion of iron oxide crystals around its boundary. The extent of the dispersion of iron oxide crystals in these deposits, is similar to the deposits taken from the same region within boiler No.6 with Lycal 93HS injection.

Plate 4-67 is a higher magnification view of the iron oxide crystals and a cluster of dendrites. The angular shape of these crystals suggests that they have precipitated at temperatures before they had become softened and therefore the edges have not become rounded as would otherwise be expected.

Plate 4-68 is a micrograph of the screen tube deposit showing a uniformly fused matrix (light grey) with a number of pores (dark grey/black) and an extensive dispersion of iron oxide crystals (white). The continuity and the physical uniformity of this sample is in total contrast to those from boiler No.6 with Lycal 93HS injection. This is evident when compared with Plates 4-53 to 4-56. However, the extent of iron oxide dispersion in these deposits is identical to those from the same region within boiler No.6.

Plate 4-69 is a higher magnification view of angular cuboidal and irregularly shaped iron oxide crystals (white) as well as a dispersion of fine dendritic crystals of iron oxide as hematite (white). The EDX-analysis is identical to that in Plate 4-67.

4.2.4 (c) Comparison of Deposit Samples from Boilers No.5 and No.6

The range of similarities and differences observed for the deposits from boilers No.5 and No.6 can be summarised as follows:

(a) For the range of post Lycal 93HS injection samples received from the upper and lower furnace regions within boiler No.6, the general matrix was of a discontinuous and

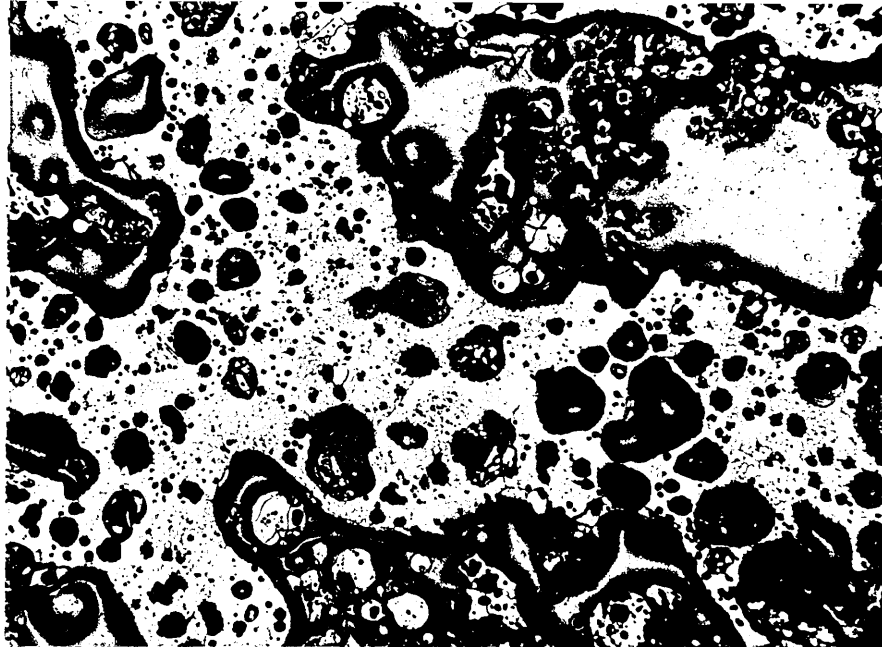


Plate 4-65:

Optical photo-micrograph of a deposit sample from Steam Generating Tubes in boiler No.5, without on-line Lycal 93HS injection. It shows a porous, fused matrix (light grey) with some residual spherical ash particles lodged at the outer boundaries of the matrix. Fine precipitates of iron oxide (white) crystals are dispersed throughout the matrix.

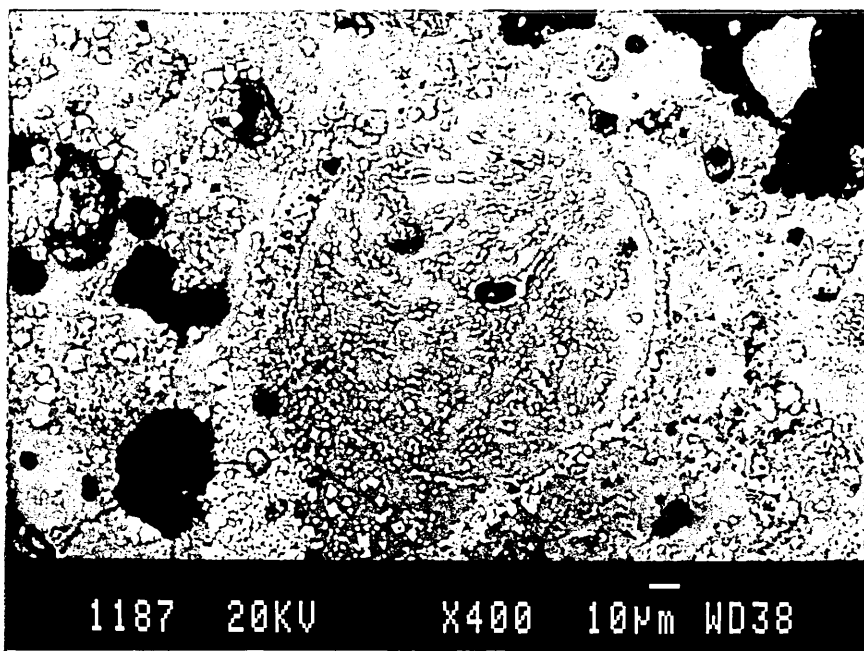


Plate 4-66:

SEM-micrograph of a deposit sample from Bottom Screen Tubes in boiler No.5, without on-line Lycal 93HS injection. It shows a spherical ash particle, outlined by a fine dispersion of euhedral and angular iron oxide or iron spinel crystals (light grey), fused into the rest of the matrix.

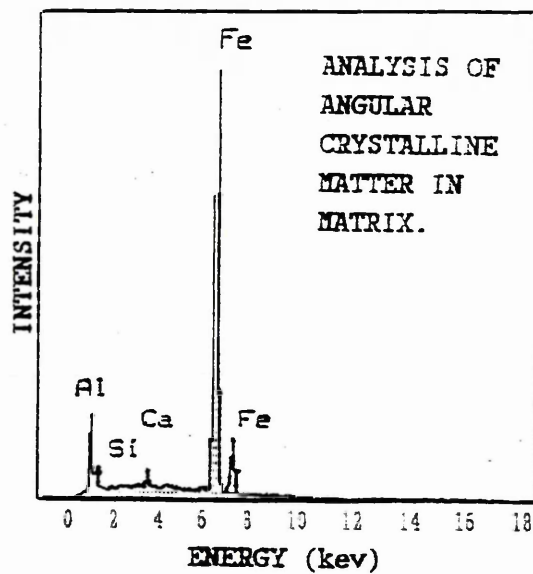
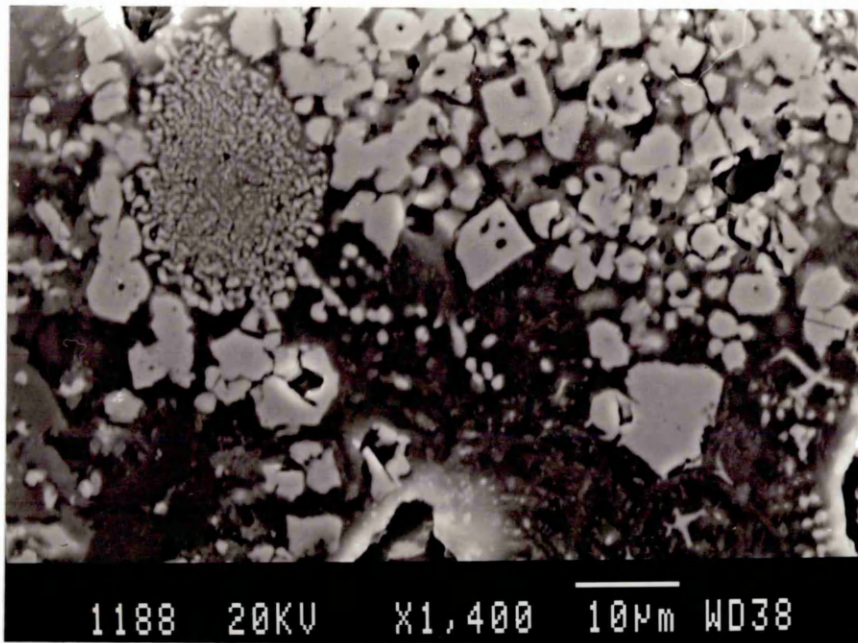


Plate 4-67:

High magnification SEM-micrograph of Plate 4-66, showing the euhedral and angular iron oxide or iron spinel type crystals. The EDX-anlysis shows the composition of the crystalline phase.

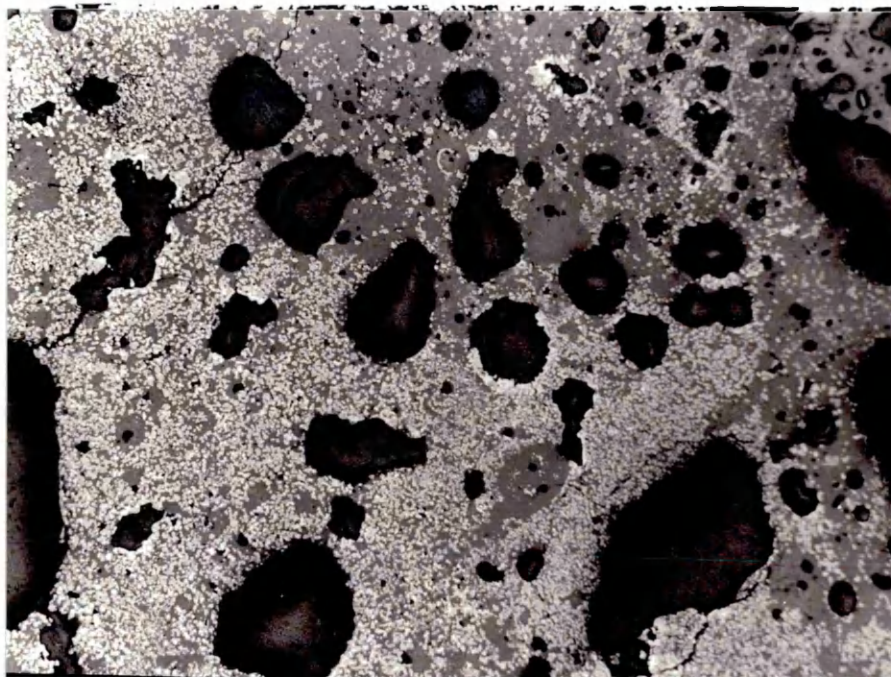


Plate 4-68:

Optical photo-micrograph of a deposit sample from Bottom Screen Tubes in boiler No.5, without on-line Lycal 93HS injection. It shows a porous, fully fused, continuous matrix (grey) with an extensive dispersion of particles (white/light grey) within the matrix. [Mag: x12]

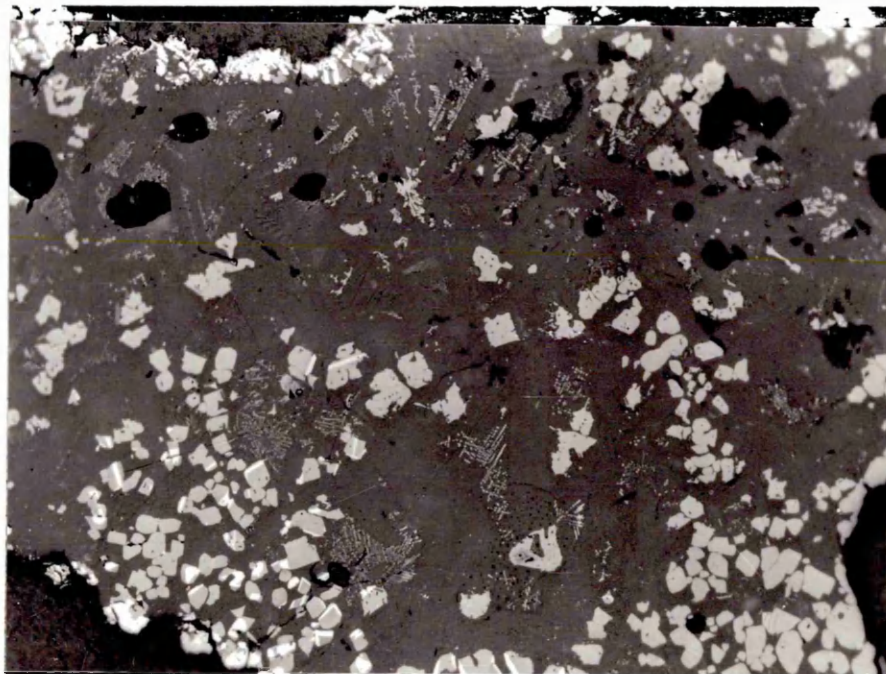


Plate 4-69:

High magnification optical photo-micrograph of Plate 4-68, showing the euhedral and angular crystalline iron oxide or iron spinel (light grey) and the pure iron oxide phase (white) as well as fine ferriferous dendrites.

[Mag: x66]

highly porous alumino-silicate form. The limited samples collected from corresponding regions within boiler No.5 predominantly displayed a structure which had been fully molten, physically uniform and continuous siliceous matrix with limited cavities and pores.

(b) Whereas the deposit samples received from boiler No.6 over the two years period of Lycal 93HS injection trials were predominantly "monolithic", the deposit samples collected from boiler No.5, particularly those from the lower furnace region were found to be of a "layered" structure with significant chemical and limited morphological variation across the layers.

(c) Despite apparent homogeneity of the samples, extensive variations in morphological and textural combinations were common place for the whole range of samples from both boilers No.6 and No.5. This was particularly significant for the upper furnace samples.

(d) Dispersion and segregation of ferriferous crystalline matter in the form of precipitates of angular particles as iron oxides or iron oxide - alumina spinel type cuboidal and dendritic crystalline matter were found to be prevalent. This was particularly significant in the case of upper-furnace deposit samples compared to the lower furnace samples from both boilers No.6 and No.5, where the iron oxide segregation at the surface boundary of spherical ash particles acted as bridges between these particles.

4.2.5 Determination and Study of Crystallinity of Deposits

This study was primarily carried out in order to investigate the possible effects of Lycal 93HS on the crystallisation behaviour of the deposits formed on boiler tube surfaces. The crystalline mineral compounds present were determined by carrying out

x-ray diffractometry on powdered samples of various deposits from boilers No.5 and No.6. The previously obtained SEM-EDX analyses as well as the bulk chemical analyses of the samples previously obtained were utilised to assist in recognition of the crystalline phases present. The results are listed in Table 4-11.

4.3 SOFTENING CHARACTERISTICS OF DEPOSITS WITH AND WITHOUT ADDITIONS OF LYCAL 93HS

The softening behaviour of the deposit samples obtained from boiler No.6, with on-line injection of Lycal, was investigated with and without further additions of Lycal 93HS, as described in Section 3.3.4. Cones for testing were produced in two ways:

- (a) "Fashioned" from as received deposit specimens,
- (b) "Reconstituted" deposit specimens,

4.3.1 Cones "Fashioned" From As Received Deposit Specimens

A series of samples were "fashioned" out of the bulk deposits in the form of cones as described in section 3.3.4(b). The results of the cone fusion tests carried out are presented in Table 4-12. With no further additions of Lycal 93HS into these deposits, the results simulate the softening behaviour of the fully formed as opposed to forming bulk deposits. It is evident from the results that the lower furnace deposit samples, i.e. front, rear arch and front, rear wall samples, have a more refractory nature, compared to the upper furnace bottom screen tube deposits and the deposits from the passage between screen tubes and superheaters. This would also be expected from the composition of the upper and lower furnace deposits in Table 4-2, with the former deposits having a much higher basic oxides content compared to the lower furnace deposits which are shown to have a higher acidic oxide content.

Table 4-11: X-ray diffraction analysis of crystalline phases within deposits from batches No.2 and No.3, received from boiler No.6.

Batch No.	Side of Boiler	Deposit Location	Text. Type	Crystalline Phases
2	-	FRONT ARCH	-	M, Mag, Her, (Cor)
2	-	REAR ARCH	-	M, Her, Cor, U, (Cs.)
2	-	FRONT WALL	-	M, (α Cs.), U
2	-	Btm. Sc. T.	-	M, H, W, (Cs., Sil)
2	-	Pas.Sc.T&SupT	-	M, H, U
3	A	FRONT WALL	F1	M, H, A, Cs., U
3	A	FRONT WALL	F2	M, H, A, Her, Cor, Cs., U
3	B	FRONT WALL	F1	M, Her, U, (Cor, Cs.)
3	B	FRONT WALL	F2	H, Mag, Her, Ca.mAl, (α Cs)
3	A	REAR WALL	F1	M, H, A, α Cs., U, (Ca.mAl)
3	A	REAR WALL	F2	M, H, Her, Cs., U
3	B	REAR WALL	F1	M, H, A, α Cs., Ca.mAl., U
3	B	REAR WALL	F2	M, H, Cs., U, (Ca.mAl.)
3	A	SIDE WALL	F1	M, H, (α Cs.,A)
3	B	SIDE WALL	F1	M, H, A, W, Mag, Cor, Cs., U
3	A	Btm. Sc. T.	F1	M, H, A, W, Cs, Her, U, (Cor)
3	B	Btm. Sc. T.	F1	M, H, α Cs., U
3	B	Btm. Sc. T.	F2	H, α Cs., U

Note: The symbols for the crystalline phases identified are as follows:

M: Mullite, Mag: Magnetite, Her: Hercynite, Cor: corundum, Cs: Cristobalite
H: Hematite, α Cs: α -Cristobalite, W: Wustite, Sil: Sillimanite, A: Anhydrite,
Ca.mAl: Calcium mono-Aluminate, U: Unknown.

The mineral phases in brackets could also be present as minor phases.

Table 4-12: Results of cone-fusion tests for "fashioned" cone pieces of deposits from "second" batch received during the course of Lycal 93HS additive treatment on boiler No.6.

DEPOSIT SPECIFICATION	SOFTENING TEMPERATURE (°C)			
	IDT	ST	HT	FT
FRONT ARCH	1435	>1450	-	-
REAR ARCH	1384	>1450	-	-
FRONT WALL	1385	>1450	-	-
Btm. Sc.T	1355	1374	1394	1411
Pas. Sc.T & Sup.T	1345	1382	1428	1440

Note: All of the softening temperature values presented for each location in this and other tables are average values for two samples tested from each location, with a maximum variation of $\pm 10^{\circ}\text{C}$.

Table 4-13: Results of cone-fusion tests for cones produced from "Reconstituted" deposit samples from the "second" batch received during the course of Lycal 93HS additive treatment from boiler No.6.

DEPOSIT SPECIFICATION	SOFTENING TEMPERATURE (°C)			
	IDT	ST	HT	FT
FRONT ARCH	1311	1395	>1450	-
REAR ARCH	1420	>1450	-	-
FRONT WALL	1430	>1450	-	-
Btm. Sc.T	1309	1385	1413	1446
Pas. Sc.T & Sup.T	1292	1312	1354	1436

4.3.2 Cones Produced From "Reconstituted" Deposit Specimens

Additional pieces taken from identical regions within the deposits used to produce the "fashioned" cones were crushed into powder form as described in Section 3.3.4(b) and were made into cones using the brass mould illustrated in Plate 3-1 and Plate 3-2. These are referred to as "reconstituted" samples and are intended to simulate the process of formation of the thick agglomerates as the coal fly ash sticks onto the surface of boiler tubes and then undergoes sintering and fusion to form finally the coalesced bulk of the coal ash deposits. Table 4-13 presents the results of fusion tests carried out on the "reconstituted" samples from the second batch of deposits, on an as received basis without any further additions of Lycal 93HS. Like the previous results in Table 4-13, the lower furnace deposit samples were found to have higher softening temperatures than the upper furnace deposits. On comparison of the results in Tables 4-12 and 4-13, it is evident that the reconstituted lower furnace samples had higher softening temperatures and the upper furnace samples had lower softening temperatures compared to the corresponding fashioned samples. This identifies the significance of the morphological variation of the various coal ash particles in the make up of deposits in terms of their softening characteristics.

Table 4-14 presents the results of similar fusion tests performed on "reconstituted" samples of the two type of friable deposits, "F1" and "F2" found within the third batch and the clinker sample from boiler No.6.

The softening temperatures for all the samples were higher for the "F1" type of samples than the "F2". It is further evident that whereas the "F1" type deposits did not assume the fluidity state range, the "F2" type samples formed fluid melts within the experimental temperature range. In addition the "F1" type samples taken from

Table 4-14: Results of cone-fusion tests for the "reconstituted" cones of the two "friable" samples namely F1 and F2 received in the "third" batch of deposits from boiler No.6.

DEPOSIT SPECIFICATION	BOILER SIDE	TEXT. TYPE	SOFTENING TEMPERATURE (°C)			
			IDT	ST	HT	FT
FRONT WALL	A	F1	1406	1440	> 1450	-
FRONT WALL	B	F1	1380	1393	> 1450	-
FRONT WALL	A	F2	1338	-	1366	1420
FRONT WALL	B	F2	1350	-	1380	> 1450
REAR WALL	A	F1	1358	1406	1446	> 1450
REAR WALL	B	F1	1351	1368	1416	> 1450
REAR WALL	A	F2	1320	1363	1395	1428
REAR WALL	B	F2	1325	1344	1378	1422
SIDE WALL	A	F1	1375	1418	> 1450	-
SIDE WALL	B	F1	1358	1415	> 1450	-
Btm. Sc.T	A	F1	1354	1386	1419	> 1450
Btm. Sc.T	B	F1	1372	1383	1450	> 1450
Btm. Sc.T	B	F2	1320	1350	1386	1402
Btm. Clink.	-	-	1436	> 1450	-	-

side "A" of the lower furnace region, where Lycal 93HS injection was unhindered, displayed higher softening temperatures than those samples taken from side "B" where temporary blockage of Lycal 93HS injection ports had occurred. This trend was reversed in the case of "F2" type deposit samples.

4.3.3 Effect of Additional Lycal 93HS on the Softening Behaviour of Deposits

The effect of adding 2 and 8 mass% Lycal 93HS on the softening and fusion behaviour of deposits was investigated for samples from the first batch received from boiler No.6. These samples were received prior to the commencement of the course of Lycal 93HS injection. The results of these experiments are tabulated in Table 4-15 and presented graphically in Figure 4-4. Additions of Lycal 93HS are shown to decrease the softening temperatures for the lower furnace deposit samples whereas for the upper furnace samples, the softening temperatures show an increase on further additions of Lycal at 8 mass%.

Further cone fusion tests were carried out on reconstituted cone samples to which a single addition of 3 mass% Lycal 93HS had been made. The two "friable" types of textures, namely "F1" and "F2", found within the third batch of deposits received from boiler No.6 were considered for this experiment. The results of this study are shown in Table 4-16, with the variation in the extent of the fluxing effect of Lycal 93HS further depicted in Figure 4-5. On comparison of the results from Tables 4-14 and 4-16, it is evident that the softening temperatures of the "F1" type deposit samples were significantly reduced but the reduction in the softening temperature of the "F2" type samples was relatively restrained.

Table 4-13: Results of cone - fusion tests for the reconstituted cones of deposit samples from the "first" sample batch received, investigating the effect of laboratory additions of Lycal 93HS on the softening behaviour of deposits from boiler No.6 prior to injection of Lycal 93HS.

DEPOSIT SPECIFICATION	LYCAL ADDITION (mass%)	SOFTENING TEMPERATURE (°C)			
		IDT	ST	HT	FT
CORNER	0	1335	1365	1372	1418
CORNER	2	1293	1310	1320	1342
CORNER	8	1262	1284	1303	1340
REAR WALL	0	1330	1352	1363	1392
REAR WALL	2	1246	1269	1318	1380
REAR WALL	8	1223	1260	1325	1399
Btm. Sc.T	0	1315	> 1450	-	-
Btm. Sc.T	2	1297	1395	> 1450	-
Btm. Sc.T	8	1345	> 1450	-	-
Pas.Sc.T & Sup.T	0	1315	1345	1364	1397
Pas.Sc.T & Sup.T	2	1256	1319	1369	1415
Pas.Sc.T & Sup.T	8	1301	1329	1368	1430

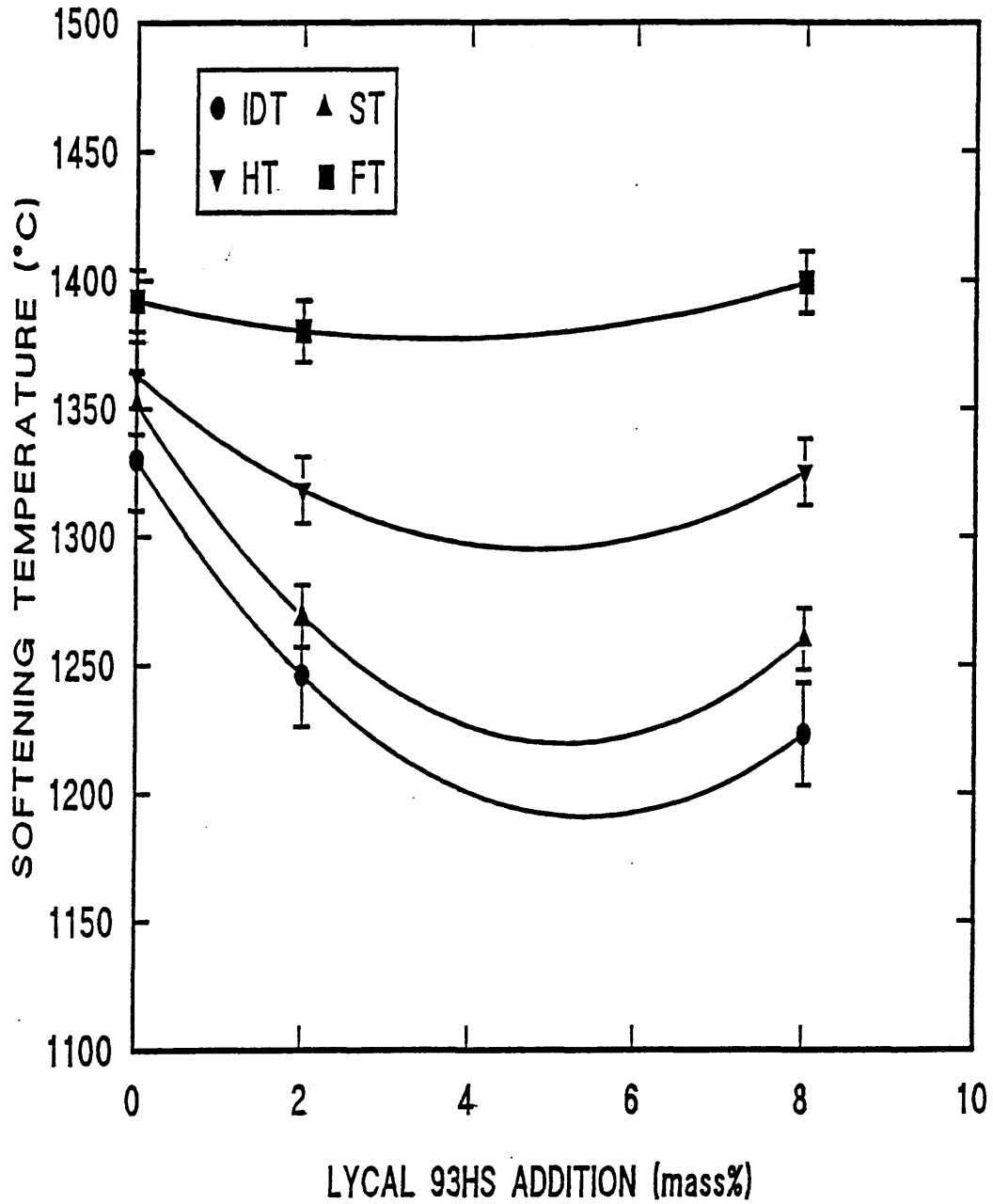


Figure 4-4: Effect of Lycal 93HS on the softening characteristics of the lower furnace "Rear wall" deposit samples from the first batch of deposits before on-line injection of Lycal.

Table 4-16: Results of cone-fusion tests for the "Reconstituted" cone samples of F1 and F2 type of deposits for selected deposits from the "third" sample batch, investigating the effect of 3 mass% additional Lycal 93 HS.

DEPOSIT SPECIFICATION	BOILER SIDE	TEXT. TYPE	SOFTENING TEMPERATURE (°C)			
			IDT	ST	HT	FT
FRONT WALL	A	F1	1314	1382	1444	> 1450
FRONT WALL	B	F1	1322	-	1385	> 1450
FRONT WALL	A	F2	1310	-	1363	1446
FRONT WALL	B	F2	1324	-	1375	1443
REAR WALL	A	F1	1324	-	1403	> 1450
REAR WALL	B	F1	1325	-	1385	1429
REAR WALL	A	F2	1321	1360	1343	1433
REAR WALL	B	F2	1319	-	1345	1420

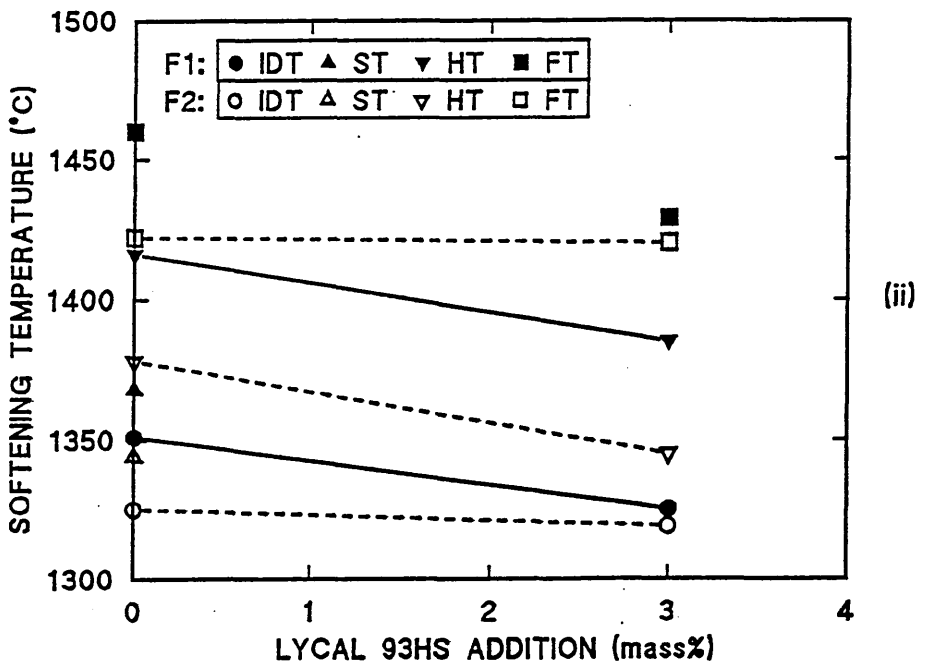
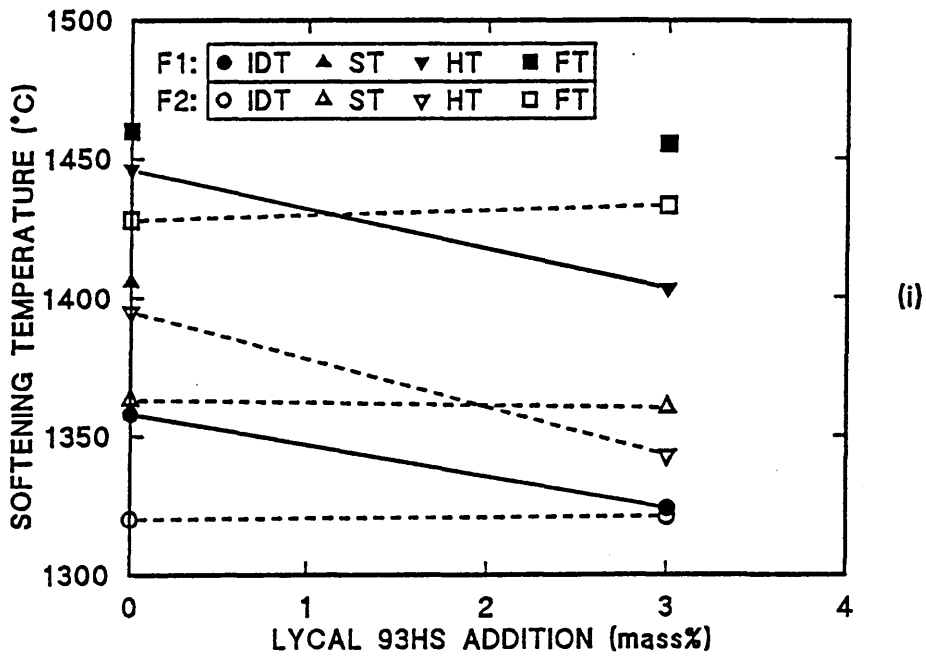


Figure 4-5: Effect of 3 mass% Lycal 93HS addition on the softening characteristics of the "F1" and "F2" type "Rear wall" deposit samples received from the (i) A-side (normal injection) and (ii) B-side (reduced injection) of boiler No.6.

4.3.4 Heat Treatment of Selected Deposits Under Controlled Conditions

The two "friable" types of deposit sample, "F1" and "F2", were investigated in this experiment. The samples were heat treated as described in Section 3.3.5.

A total of eighteen samples, nine of each type, were tested over a range of temperatures and time periods. The results of this study are tabulated in Table 4-17. It is evident that the "F1" type deposit samples were physically unaltered even after 60 minutes of heat treatment at 1275°C. After 60 minutes of heating at 1350°C, the sample was found to be in a molten state. The "F2" samples however experienced a partial physical deformation after just 10 minutes of heat treatment at 1200°C with more extensive melting at longer intervals and higher temperatures.

4.4 DEPOSITION PROBE SAMPLING OF THE COAL FLY ASH

The retention of coal fly ash as well as simultaneous involvement of injected Lycal 93HS within the upper furnace region of boiler No.6 was investigated through a series of short run residential tests, using an air cooled deposition probe.

The probe was inserted at the vicinity of the bottom screen tubes, where fly ash deposition was of particular importance to the boiler operators at the power station.

The probe used in this study, has been previously described in Section 3.3.7 and Figure 3-8 and is shown in action in Plate 3-3.

4.4.1 Chemical Analysis of the Collected Fly Ash

Table 4-18 gives the chemical composition of the thin layer (i.e. 1-2mm) of fly ash collected after twelve hours of exposure with and without injection of Lycal 93HS into the boiler. In addition to various boiler conditions and parameters which were recorded during the tests (see Table 3-5), samples of stack emissions were also collected and the results of their analyses are presented in Table 4-18. It is clearly

DEPOSIT ORIGIN	TYPE OF TEXTURE	FIRING TEMP (°C)	FIRING TIME (min.)	OBSERVATION
FRONT WALL	F1	1200	10	No change
FRONT WALL	F1	1200	30	No change
FRONT WALL	F1	1200	60	No change
FRONT WALL	F1	1275	10	No change
FRONT WALL	F1	1275	30	No change
FRONT WALL	F1	1275	60	No change
FRONT WALL	F1	1350	10	Partial melting of larger spheres. No change in the smaller spheres
FRONT WALL	F1	1350	30	Extensive necking between spheres. Formation of a glassy melt
FRONT WALL	F1	1350	60	Complete melting of larger spheres partial melting of smaller spheres Formation of a glassy melt
FRONT WALL	F2	1200	10	Deformation of larger spheres
FRONT WALL	F2	1200	30	Partial melting and restricted fusion of ash spheres and cenospheres
FRONT WALL	F2	1200	60	Further fusion of ash spheres, dissolution of outer dust layer into the matrix
FRONT WALL	F2	1275	10	Restricted surface melting of some ash spheres and cenospheres
FRONT WALL	F2	1275	30	Extensive melting of matrix with local formation of pits
FRONT WALL	F2	1275	60	Extensive melting/fusion to form a thick layer with local pitting
FRONT WALL	F2	1350	10	Complete melting of surface-glassy melt with pitting & porosity holes
FRONT WALL	F2	1350	30	Complete melting-flow of a glassy, porous melt-wetting of the surface
FRONT WALL	F2	1350	60	Extensive melting-flow of a glassy porous melt-wetting of the surface

Table 4-18: Chemical analysis of deposited fly ash layer collected from the surface of the test probe after twelve hours of exposure with and without injection of Lycal 93HS on boiler No.6.

SIDE OF BOILER/ +/-LYC.	SAMPLING AREA	COMPOUND MASS PERCENTAGE (%)								
		SiO ₂	Al ₂ O ₃	TiO ₂	Fe ₂ O ₃	CaO	MgO	K ₂ O	P ₂ O ₅	SO ₃
A/+	Btm. Sc.T	29.82	19.91	1.01	24.92	3.56	5.76	2.69	6.91	5.41
A/-	Btm. Sc.T	34.59	23.29	1.06	28.94	3.59	1.58	2.24	3.17	1.62
+	STACK	43.04	27.80	1.16	14.90	3.91	3.80	2.30	2.45	0.95
-	STACK	42.42	29.24	1.14	13.50	3.46	1.25	3.14	3.90	1.17

Note: The stack analysis is included as a reference to the comparative effect of Lycal 93HS on the effluent ash burden being discharged with and without injection of Lycal 93HS into the boiler.

evident from this table that the amount of MgO in the bottom screen tube deposit has increased by almost four fold when Lycal 93HS was being injected into the boiler. Also noticeable are the three and two fold increases in the SO₃ and P₂O₅ contents respectively.

4.4.2 Determination of Deposition Rate

The rate of fly ash depositing on the surface of the probe was evaluated in a series of tests carried out over a period of one, two, four and twelve hours with and without on-line injection of Lycal 93HS. Table 4-19 and Figure 4-6 show the results of the deposition rate determinations.

4.5 THE SURFACE-LEACHING OF DEPOSIT SAMPLES

A range of deposit samples from sample batches 2 to 6, with and without Lycal 93HS injection, were selected for this series of experiments as described in Section 3.3.6. The results of these experiments have been presented in Tables 4-20 to 4-42. Comparative analyses of the surface chemistry of the deposits, in terms of three oxides, namely SiO₂, Fe₂O₃ and MgO has further been depicted in Figures 4-7 to 4-13 for deposits with and without Lycal 93HS injection, received or collected from the same areas within boilers No.6 and No.5 respectively.

Figure 4-7 presents the results of surface leaching for the three nominated oxides, SiO₂, Fe₂O₃ and MgO, from front wall deposits taken from Tables 4-20, 4-21 and 4-22 for the samples with Lycal injection and the single set of results taken from Table 4-23 for the corresponding sampling position within boiler No.5 without Lycal injection.

Figure 4-8 presents the results for the rear wall deposits taken from Tables 4-24 and 4-25 for the with and without Lycal injection samples respectively.

Screen Tubes" in boiler No.6, with and without on-line injection of Lycal 93HS.

BOILER No.6			
Exposure Period (hr.)	Run No.	Lycal 93HS Injection	Mass of Fly Ash Collected (g)
1	1	ON	0.165
2	1	ON	0.406
	2	ON	0.389
	3	ON	0.440
	4	OFF	0.494
4	1	ON	0.581
	2	ON	0.329
	3	ON	0.629
12	1	ON	0.671
	2	OFF	0.969

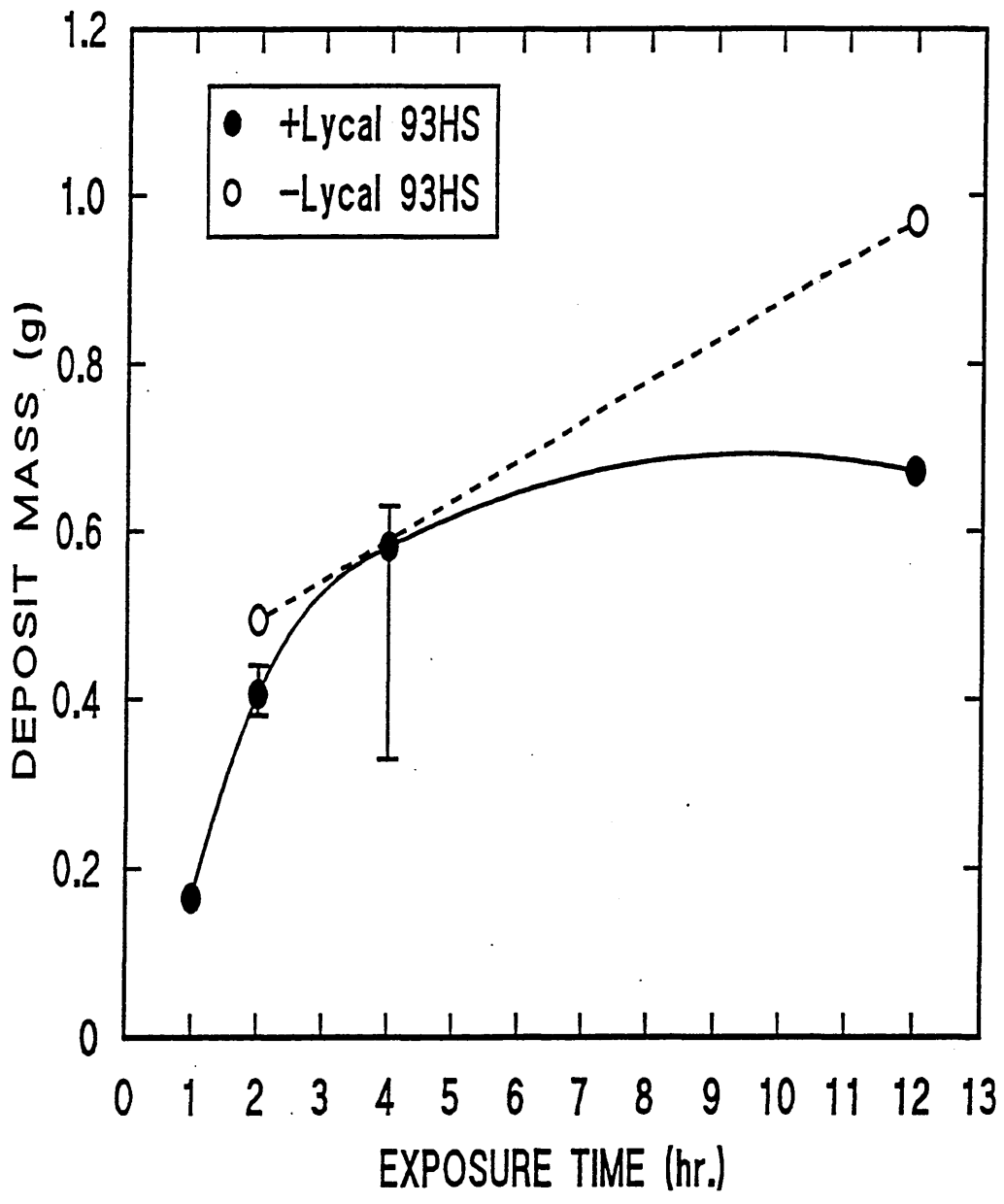
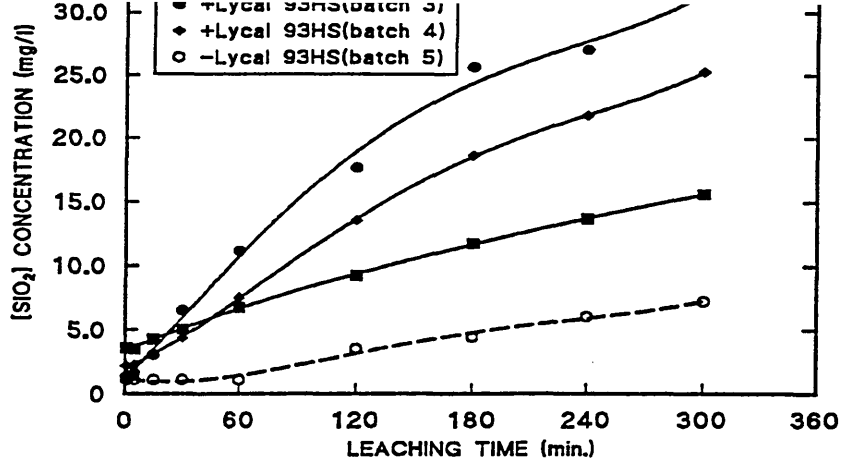
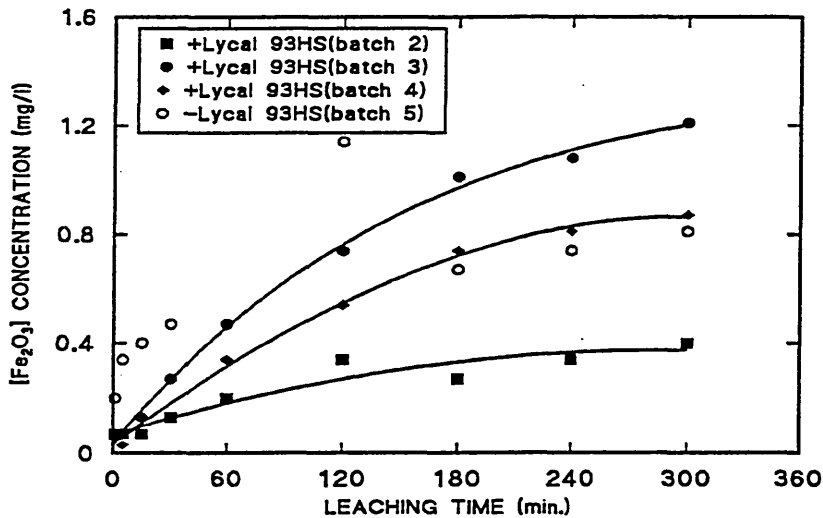


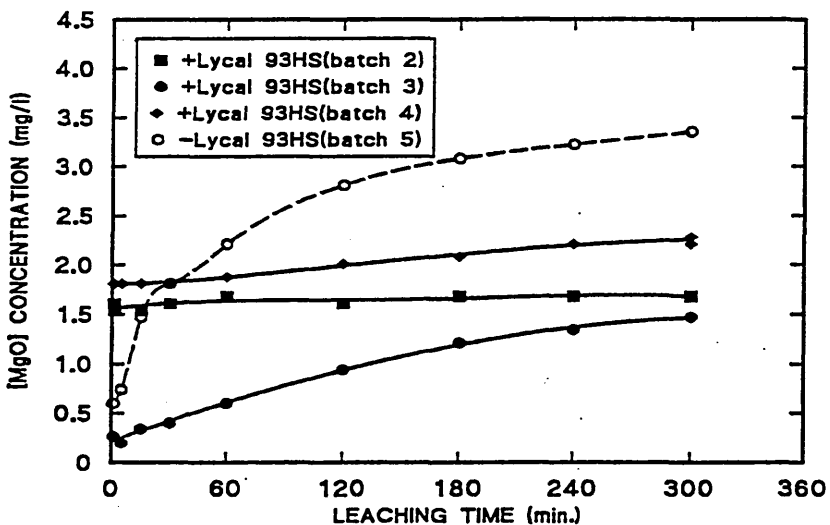
Figure 4-6: Comparison of probe deposition rates before the "Bottom screen tubes" with and without on-line injection of Lycal 93HS in boiler No.6.



(a)



(b)



(c)

Figure 4-7: Determination of HF-solubility rates for (a) $[\text{SiO}_2]$, (b) $[\text{Fe}_2\text{O}_3]$ and (c) $[\text{MgO}]$ concentrations for the "front wall" samples from boilers No.5 and No.6 without and with on-line injection of Lycal 93HS respectively.

received in the "second" batch of samples from boiler No.6 with on-line injection of Lycal 93HS.

FRONT WALL							
Solut. No.	Leach. Time (min.)	Si (mg/L)	SiO ₂ (mg/L)	Fe (mg/L)	Fe ₂ O ₃ (mg/L)	Mg (mg/L)	MgO (mg/L)
1	1.0	7.7	3.59	0.19	0.07	2.7	1.61
2	5.0	7.6	3.52	0.18	0.07	2.6	1.54
3	15.0	9.1	4.26	0.23	0.07	2.5	1.54
4	30.0	10.9	5.05	0.30	0.13	2.7	1.61
5	60.0	14.6	6.78	0.59	0.20	2.8	1.68
6	120.0	19.8	9.24	0.97	0.34	2.7	1.61
7	180.0	25.3	11.77	0.85	0.27	2.8	1.68
8	240.0	29.4	13.70	1.00	0.34	2.8	1.68
9	300.0	33.5	15.63	1.20	0.40	2.8	1.68

in the "third" batch of samples from boiler No.6 with on-line injection of Lycal 93HS.

FRONT WALL							
Solut. No.	Leach. Time (min.)	Si (mg/L)	SiO ₂ (mg/L)	Fe (mg/L)	Fe ₂ O ₃ (mg/L)	Mg (mg/L)	MgO (mg/L)
1	1.0	3.0	1.40	0.1	0.07	0.4	0.27
2	5.0	3.5	1.66	0.2	0.07	0.3	0.20
3	15.0	6.5	3.06	0.4	0.13	0.5	0.34
4	30.0	14.0	6.52	0.7	0.27	0.7	0.40
5	60.0	24.0	11.17	1.3	0.47	1.0	0.60
6	120.0	38.0	17.69	2.0	0.74	1.5	0.94
7	180.0	55.0	25.67	2.8	1.01	2.0	1.21
8	240.0	58.0	27.07	3.1	1.08	2.2	1.34
9	300.0	68.0	31.72	3.4	1.21	2.4	1.47

Note: The deposit analysed was a "Front wall" deposit but it is representative of this type of deposits taken from other locations within the boiler.

received in the "fourth" batch of samples from boiler No.6 with on-line injection of Lycal 93HS.

FRONT WALL							
Solut. No.	Leach. Time (min.)	Si (mg/L)	SiO ₂ (mg/L)	Fe (mg/L)	Fe ₂ O ₃ (mg/L)	Mg (mg/L)	MgO (mg/L)
1	1.0	4.7	2.19	0.18	0.07	3.0	1.81
2	5.0	4.9	2.26	0.07	0.02	3.0	1.81
3	15.0	6.7	3.13	0.39	0.13	3.0	1.81
4	30.0	9.4	4.39	0.41	0.13	3.1	1.88
5	60.0	16.1	7.51	0.85	0.34	3.3	2.01
6	120.0	29.1	13.57	1.5	0.54	3.5	2.08
7	180.0	39.9	18.62	2.0	0.74	3.6	2.21
8	240.0	46.8	21.81	2.3	0.81	3.6	2.21
9	300.0	54.2	25.27	2.5	0.87	3.8	2.28
10	360.0	55.8	26.00	2.5	0.87	3.7	2.28

in the "fifth" batch of samples from boiler No.5 without any injection of Lycal 93HS.

FRONT WALL							
Solut. No.	Leach. Time (min.)	Si (mg/L)	SiO ₂ (mg/L)	Fe (mg/L)	Fe ₂ O ₃ (mg/L)	Mg (mg/L)	MgO (mg/L)
1	1.0	<2.5	<1.20	0.6	0.20	1.0	0.60
2	5.0	<2.5	<1.20	1.0	0.34	1.2	0.74
3	15.0	<2.5	<1.20	1.1	0.40	2.4	1.47
4	30.0	<2.5	<1.20	1.3	0.47	3.0	1.81
5	60.0	<2.5	<1.20	1.4	0.47	3.6	2.21
6	120.0	7.5	3.52	3.3	1.14	4.6	2.81
7	180.0	9.5	4.46	1.9	0.67	5.1	3.08
8	240.0	13.0	6.05	2.0	0.74	5.3	3.22
9	300.0	15.5	7.25	2.3	0.81	5.5	3.35

Note: This was a layered sample which was found to contain large quantities of MgO and Cr₂O₃ > 20%.

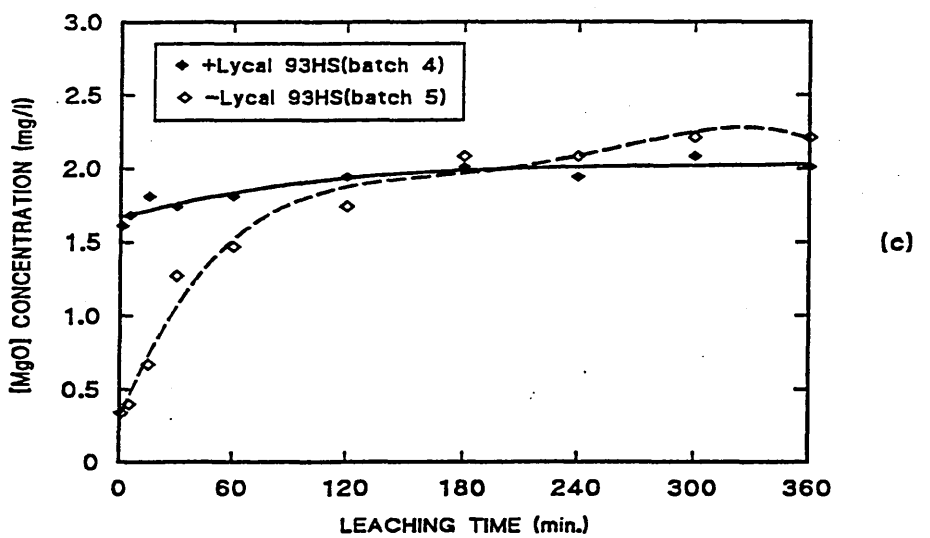
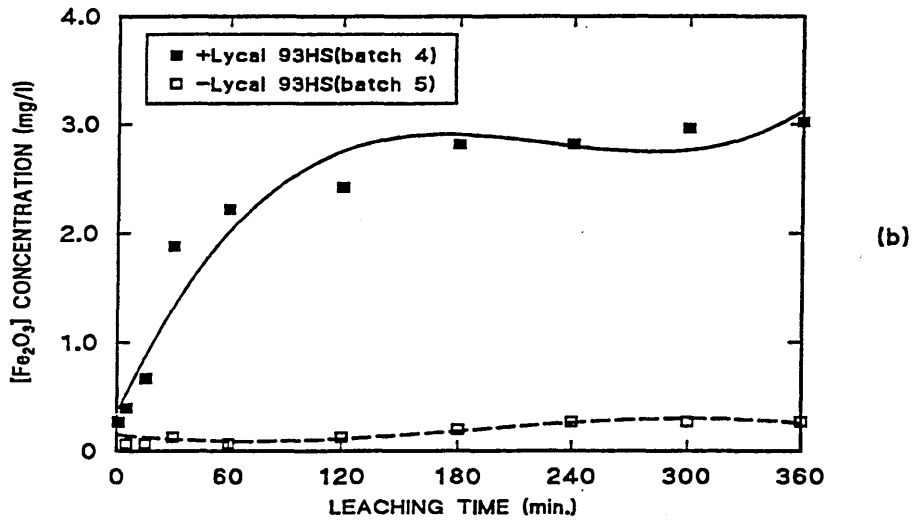
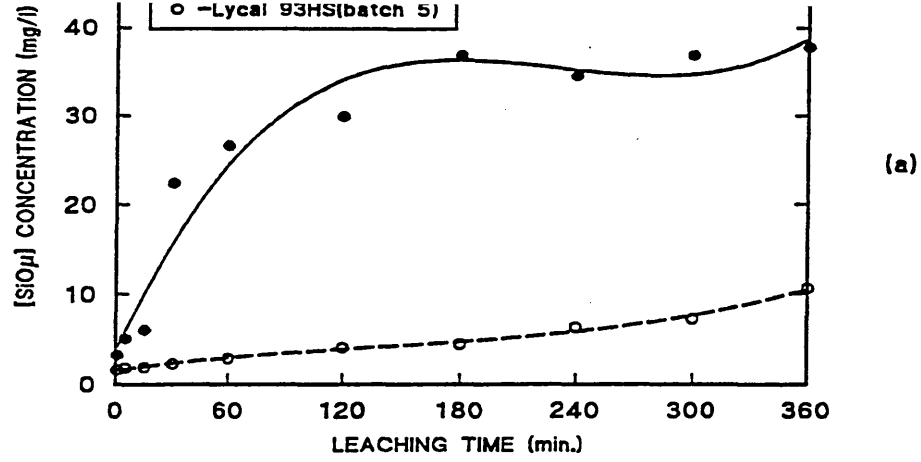


Figure 4-8: Determination of HF-solubility rates for (a) [SiO₂], (b) [Fe₂O₃] and (c) [MgO] concentrations for the "rear wall" deposit samples from boilers No.5 and No.6, without and with injection of Lycal 93HS respectively.

in the "fourth" batch of samples from boiler NO.6 with on-line injection of Lysal 93HS.

REAR WALL							
Solut. No.	Leach. Time (min.)	Si (mg/L)	SiO ₂ (mg/L)	Fe (mg/L)	Fe ₂ O ₃ (mg/L)	Mg (mg/L)	MgO (mg/L)
1	1.0	7.0	3.26	0.7	0.27	0.5	0.34
2	5.0	11.0	5.12	1.1	0.40	0.7	0.40
3	15.0	13.0	6.05	1.9	0.67	1.1	0.67
4	30.0	48.0	22.41	5.3	1.88	2.1	1.27
5	60.0	57.0	26.60	6.3	2.22	2.4	1.47
6	120.0	64.0	29.86	6.8	2.42	2.9	1.74
7	180.0	79.0	36.84	8.0	2.82	3.4	2.08
8	240.0	74.0	34.51	8.0	2.82	3.4	2.08
9	300.0	79.0	36.84	8.3	2.96	3.6	2.21
10	360.0	81.0	37.77	8.5	3.02	3.7	2.21

in the "fifth" batch of samples from boiler No.5 without any injection of Lycal 93HS.

REAR WALL							
Solut. No.	Leach. Time (min.)	Si (mg/L)	SiO ₂ (mg/L)	Fe (mg/L)	Fe ₂ O ₃ (mg/L)	Mg (mg/L)	MgO (mg/L)
1	1.0	3.4	1.60	0.80	0.27	2.6	1.61
2	5.0	3.8	1.80	0.27	0.07	2.8	1.68
3	15.0	4.0	1.86	0.18	0.07	3.0	1.81
4	30.0	4.8	2.26	0.32	0.13	2.9	1.74
5	60.0	6.2	2.86	0.27	0.07	3.0	1.81
6	120.0	8.7	4.06	0.42	0.13	3.2	1.94
7	180.0	11.7	5.45	0.60	0.20	3.3	2.01
8	240.0	13.5	6.32	0.85	0.27	3.2	1.94
9	300.0	15.6	7.25	0.72	0.27	3.4	2.08
10	360.0	16.8	10.64	0.81	0.27	3.3	2.01

Figure 4-9 presents the results for the side wall deposits taken from Tables 4-26 and 4-27 for the with and without Lycal 93HS injection samples respectively.

Figure 4-10 presents the results for the bottom screen tubes deposit taken from Tables 4-28, 4-29, 4-30 and 4-31 for the samples with Lycal 93HS injection and the single set of results taken from Table 4-32 corresponding to values for the sample without Lycal 93HS injection from boiler No.5.

Figure 4-11 presents the results for the economiser ash hopper medium size particulate samples ($-500\mu\text{m} +63\mu\text{m}$) taken from Table 4-33 for the samples with Lycal injection and Table 4-34 is the corresponding values for the samples without Lycal 93HS injection from boiler No.5.

Figure 4-12 presents the result for the grit arrestor medium size particulate samples ($-500\mu\text{m} +63\mu\text{m}$) taken from Table 4-35 for the samples with Lycal 93HS injection and Table 4-36 is the corresponding results for the samples without Lycal injection from boiler No.5.

Figure 4-13 presents the result for the grit arrestor fine size particulate samples ($-45\mu\text{m}$) taken from Table 4-37 and Table 4-38 for the samples with and without Lycal 93HS injection respectively. The relatively higher concentration values obtained for the particulate grit arrestor and economiser ash hopper samples compared to the values obtained for the bulk deposit samples is due to the larger surface area of the samples being available for surface leaching in the HF-solutions.

Tables 4-39 to 4-42 represent the results for those samples which were received or collected from dissimilar areas within boilers No.6 and No.5 and as such are only presented in the tabular form.

Comparative analysis of the corresponding results for the samples from boilers No.6 and No.5 show that:

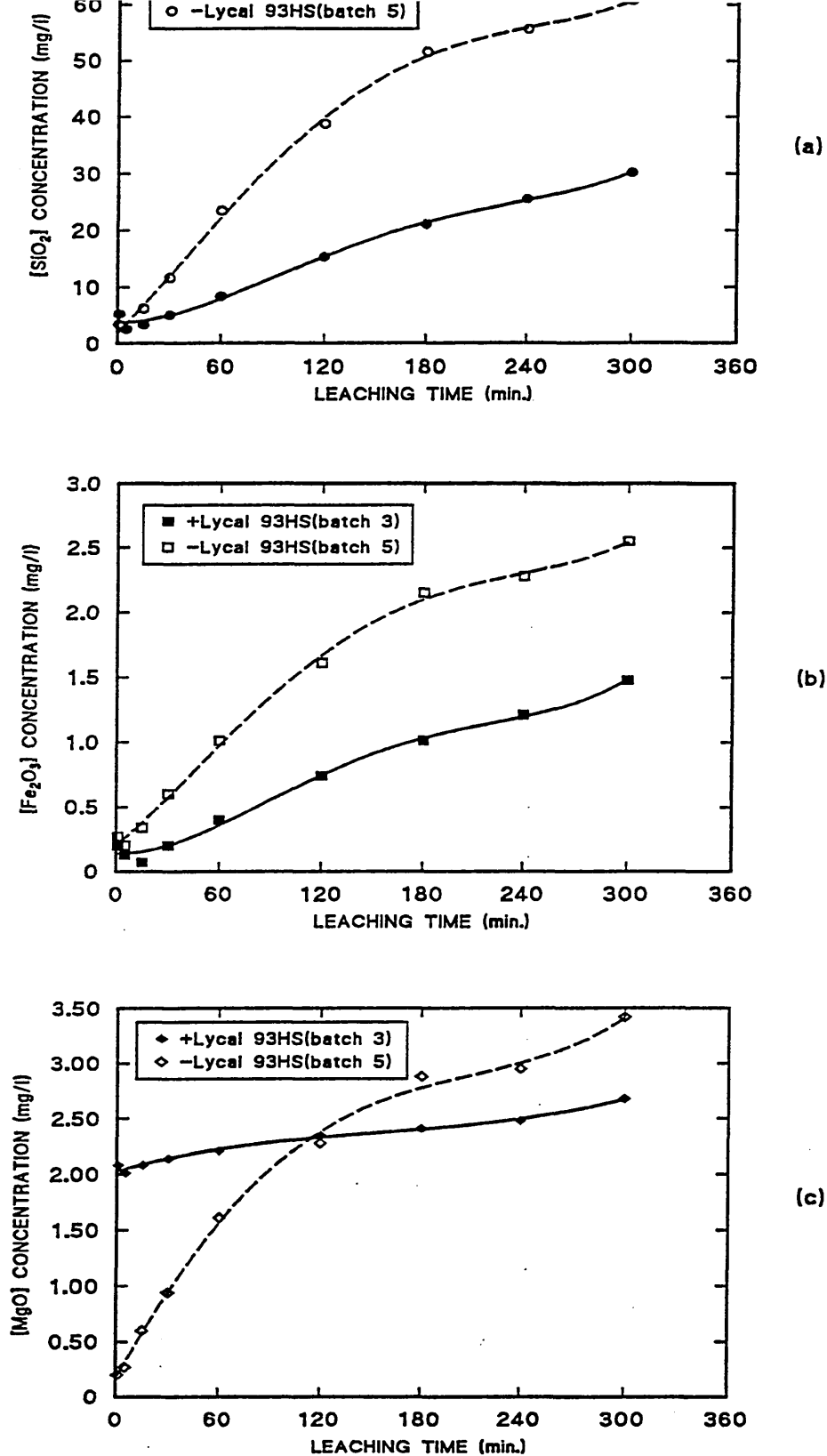


Figure 4-9: Determination of HF-solubility rates for (a) [SiO₂], (b) [Fe₂O₃] and (c) [MgO] concentrations for the "side wall" deposit samples from boilers No.5 and No.6, without and with on-line injection of Lycal 93HS respectively.

in the "third" batch of samples from boiler No.6 with on-line injection of Lycal 93HS.

SIDE WALL							
Solut. No.	Leach. Time (min.)	Si (mg/L)	SiO ₂ (mg/L)	Fe (mg/L)	Fe ₂ O ₃ (mg/L)	Mg (mg/L)	MgO (mg/L)
1	1.0	11.2	5.25	0.56	0.20	3.4	2.08
2	5.0	5.5	2.59	0.37	0.13	3.3	2.01
3	15.0	7.1	3.33	0.27	0.07	3.4	2.08
4	30.0	10.8	5.05	0.53	0.20	3.5	2.14
5	60.0	17.9	8.38	1.1	0.40	3.6	2.21
6	120.0	32.9	15.36	2.0	0.74	3.9	2.35
7	180.0	45.2	21.08	2.9	1.01	4.0	2.41
8	240.0	54.7	25.54	3.4	1.21	4.1	2.48
9	300.0	64.7	30.19	4.1	1.48	4.4	2.68

Note: The deposit analysed was a "side wall" deposit but it is representative of this type of deposits taken from other locations within the boiler.

in the "fifth" batch of samples from boiler No.5 without any injection of Lycal 93HS.

SIDE WALL							
Solut. No.	Leach. Time (min.)	Si (mg/L)	SiO ₂ (mg/L)	Fe (mg/L)	Fe ₂ O ₃ (mg/L)	Mg (mg/L)	MgO (mg/L)
1	1.0	7.2	3.39	0.82	0.27	0.39	0.20
2	5.0	5.4	2.53	0.54	0.20	0.48	0.27
3	15.0	13.3	6.18	0.94	0.34	1.00	0.60
4	30.0	24.9	11.64	1.60	0.60	1.50	0.94
5	60.0	50.4	23.47	2.80	1.01	2.60	1.61
6	120.0	83.2	38.77	4.50	1.61	3.80	2.28
7	180.0	110.6	51.60	5.90	2.15	4.70	2.88
8	240.0	119.3	55.66	6.40	2.28	4.90	2.95
9	300.0	130.5	60.85	7.20	2.55	5.60	3.42
10	360.0	135.9	63.37	7.30	2.62	5.40	3.28

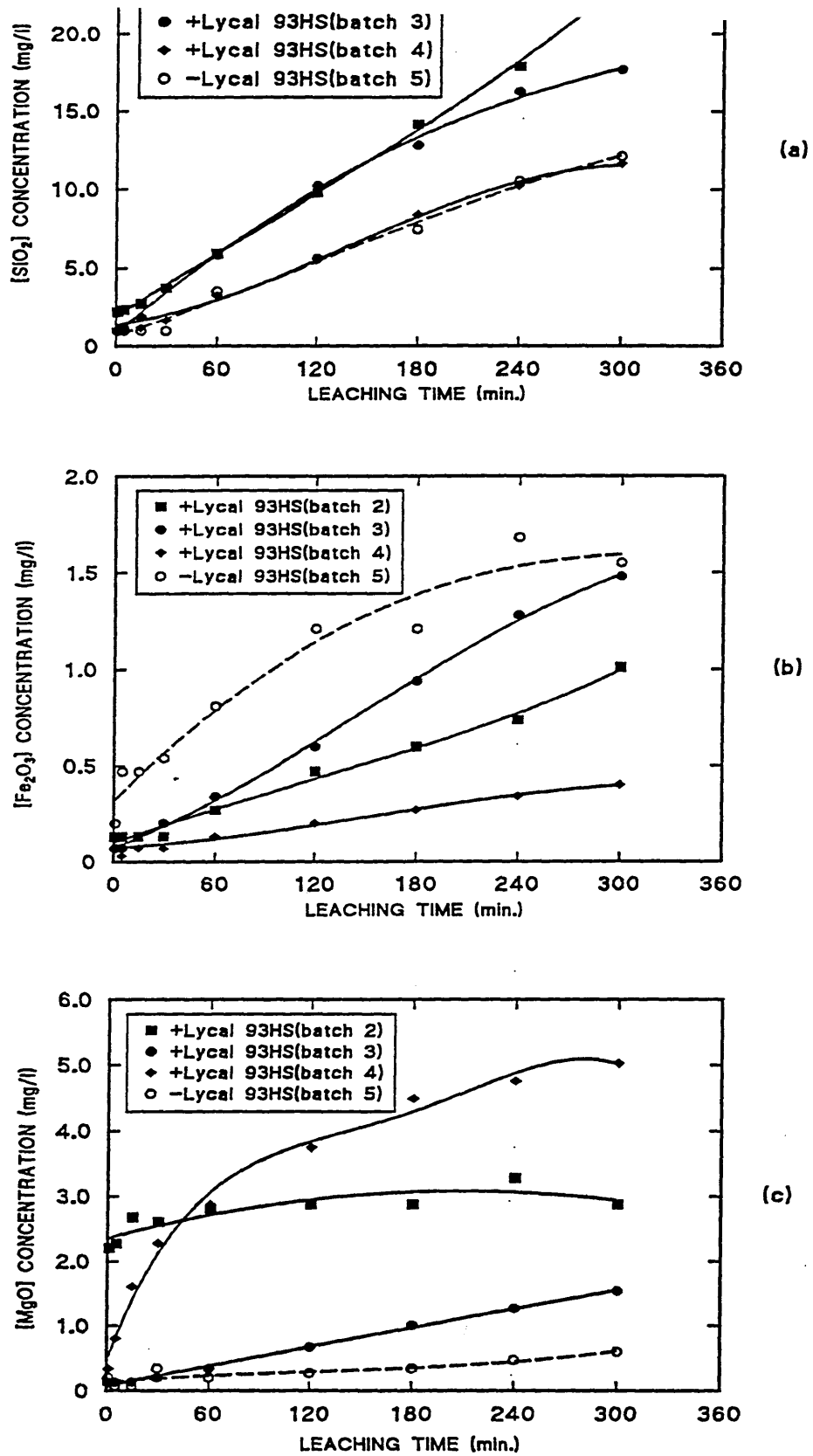


Figure 4-10: Determination of HF-solubility rates for (a) [SiO₂], (b) [Fe₂O₃] and (c) [MgO] concentrations for the "bottom screen tubes" deposit sample from boilers No.5 and No.6, without and with on-line injection of Lycal 93HS respectively.

received in the "second" batch of samples from boiler No.6 with on-line injection of Lycl 93HS.

BOTTOM SCREEN TUBES							
Solut. No.	Leach. Time (min.)	Si (mg/L)	SiO ₂ (mg/L)	Fe (mg/L)	Fe ₂ O ₃ (mg/L)	Mg (mg/L)	MgO (mg/L)
1	1.0	4.7	2.19	0.37	0.13	3.6	2.21
2	5.0	5.0	2.33	0.40	0.13	3.8	2.28
3	15.0	5.9	2.73	0.34	0.13	4.4	2.68
4	30.0	8.0	3.72	0.42	0.13	4.3	2.61
5	60.0	12.7	5.92	0.69	0.27	4.6	2.81
6	120.0	20.9	9.78	1.3	0.47	4.7	2.88
7	180.0	30.4	14.16	1.7	0.60	4.8	2.88
8	240.0	38.4	17.89	2.1	0.74	4.7	2.88
9	300.0	50.7	23.61	2.9	1.01	5.4	3.28
10	360.0	49.8	23.21	2.9	1.01	4.8	2.88

received in the "third" batch of samples from boiler No.6 with on-line injection of Lycal 93HS.

BOTTOM SCREEN TUBES							
Solut. No.	Leach. Time (min.)	Si (mg/L)	SiO ₂ (mg/L)	Fe (mg/L)	Fe ₂ O ₃ (mg/L)	Mg (mg/L)	MgO (mg/L)
1	1.0	6.1	2.86	0.60	0.20	3.3	2.01
2	5.0	7.1	3.33	1.1	0.40	3.2	1.94
3	15.0	10.5	4.92	0.57	0.20	3.3	2.01
4	30.0	18.6	8.65	1.1	0.40	3.6	2.21
5	60.0	33.8	15.76	2.0	0.67	3.9	2.35
6	120.0	57.2	26.67	3.6	1.28	4.0	2.41
7	180.0	75.7	35.31	5.1	1.81	4.3	2.61
8	240.0	118.0	55.00	7.9	2.76	6.1	3.69
9	300.0	104.0	48.48	7.2	2.55	4.9	2.95
10	360.0	125.0	58.25	8.5	3.02	5.7	3.48

Note: The deposit analysed was a "Bottom screen tubes" deposit but it is representative of this type of deposits taken from other locations within the boiler.

in the "third" batch of samples from boiler No.6 with on-line injection of Lycal 93HS.

BOTTOM SCREEN TUBES							
Solut. No.	Leach. Time (min.)	Si (mg/L)	SiO ₂ (mg/L)	Fe (mg/L)	Fe ₂ O ₃ (mg/L)	Mg (mg/L)	MgO (mg/L)
1	1.0	<2.5	<1.20	0.2	0.07	0.2	0.13
2	5.0	2.5	1.20	0.2	0.07	0.2	0.13
3	15.0	4.0	1.86	0.3	0.13	0.2	0.13
4	30.0	8.0	3.72	0.5	0.20	0.3	0.20
5	60.0	12.0	5.85	1.0	0.34	0.6	0.34
6	120.0	22.0	10.24	1.8	0.60	1.1	0.67
7	180.0	27.0	12.83	2.7	0.94	1.6	1.01
8	240.0	35.0	16.29	3.6	1.28	2.1	1.27
9	300.0	38.0	17.69	4.2	1.48	2.5	1.54

Note: The deposit analysed was a "Bottom screen tubes" deposit but it is representative of this type of deposits taken from other locations within the boiler.

sample received in the "fourth" batch of samples from boiler NO.6 with on-line injection of Lycal 93HS.

BOTTOM SCREEN TUBES							
Solut. No.	Leach. Time (min.)	Si (mg/L)	SiO ₂ (mg/L)	Fe (mg/L)	Fe ₂ O ₃ (mg/L)	Mg (mg/L)	MgO (mg/L)
1	1.0	5.0	2.33	0.3	0.13	0.6	0.34
2	5.0	2.0	0.93	0.1	0.03	1.3	0.80
3	15.0	2.5	1.20	0.2	0.07	2.6	1.61
4	30.0	3.5	1.66	0.2	0.07	3.7	2.28
5	60.0	7.0	3.26	0.4	0.13	4.7	2.88
6	120.0	12.0	5.59	0.6	0.20	6.2	3.75
7	180.0	18.0	8.38	0.8	0.27	7.4	4.49
8	240.0	22.0	10.24	1.0	0.34	7.8	4.76
9	300.0	25.0	11.64	1.2	0.40	8.3	5.03
10	360.0	28.0	13.03	1.3	0.47	8.5	5.16

Table 4-32. Results of surface leaching analysis of a Bottom Screen Tubes deposit sample collected in the "fifth" batch of samples from boiler No.5 without any injection of Lycal 93HS.

BOTTOM SCREEN TUBES							
Solut. No.	Leach. Time (min.)	Si (mg/L)	SiO ₂ (mg/L)	Fe (mg/L)	Fe ₂ O ₃ (mg/L)	Mg (mg/L)	MgO (mg/L)
1	1.0	<2.5	<1.20	0.50	0.20	0.30	0.20
2	5.0	<2.5	<1.20	1.30	0.47	0.10	0.07
3	15.0	<2.5	<1.20	1.40	0.47	0.10	0.07
4	30.0	<2.5	<1.20	1.60	0.54	0.50	0.34
5	60.0	7.5	3.52	2.30	0.81	0.30	0.20
6	120.0	12.0	5.59	3.40	1.21	0.45	0.27
7	180.0	16.0	7.45	3.50	1.21	0.60	0.34
8	240.0	22.5	10.51	4.70	1.68	0.80	0.47
9	300.0	26.0	12.10	4.40	1.55	1.00	0.60

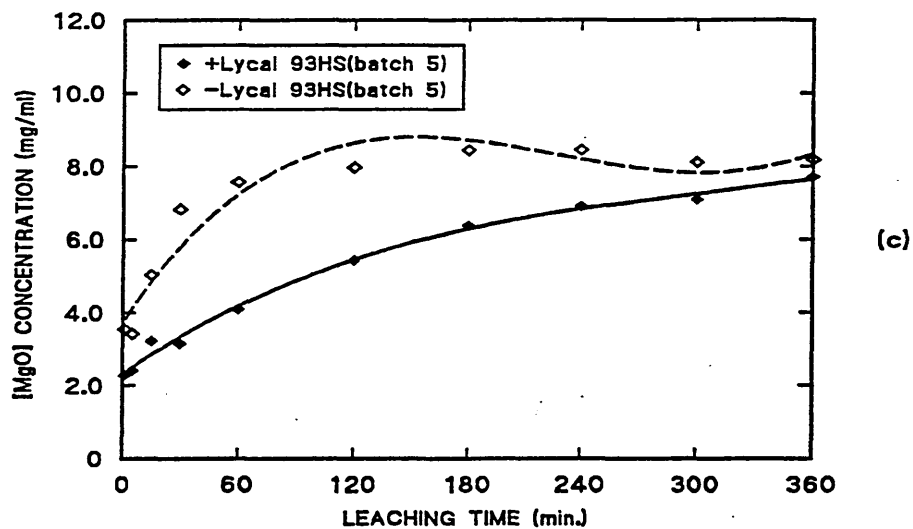
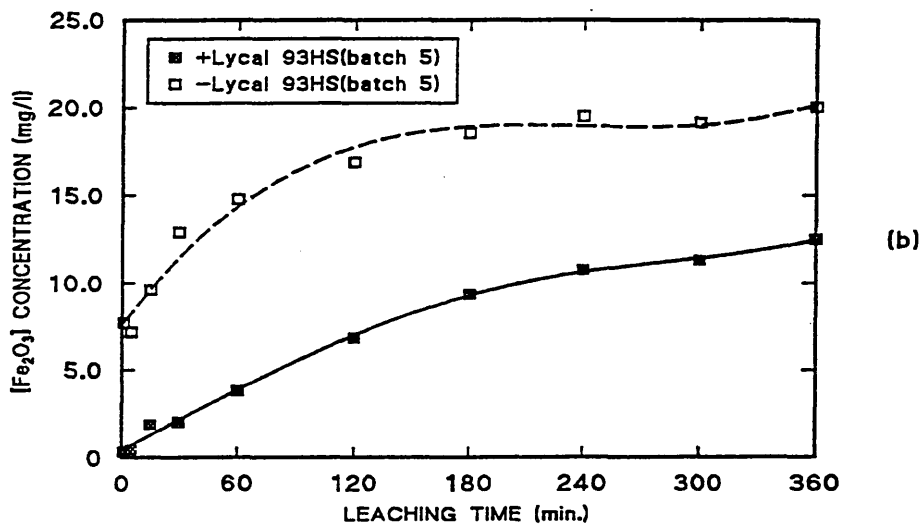
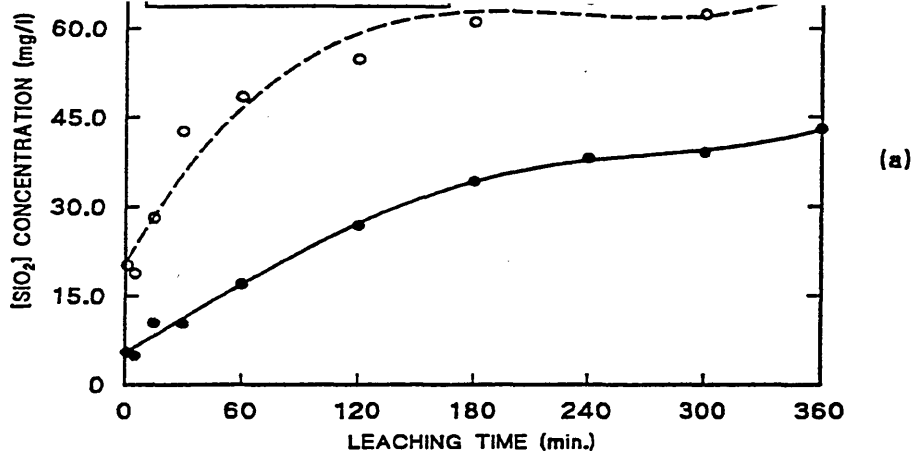


Figure 4-11: Determination of HF-solubility rates for (a) $[\text{SiO}_2]$, (b) $[\text{Fe}_2\text{O}_3]$ and (c) $[\text{MgO}]$ concentrations for "economiser ash hopper" medium size particulate samples ($-500\mu\text{m} +63\mu\text{m}$) from boiler No.6 with and without on-line injection of Lycal 93HS.

"Economiser ash hopper" sample collected in the "fifth" batch of samples from boiler No.6 with on-line injection of Lyclal 93HS.

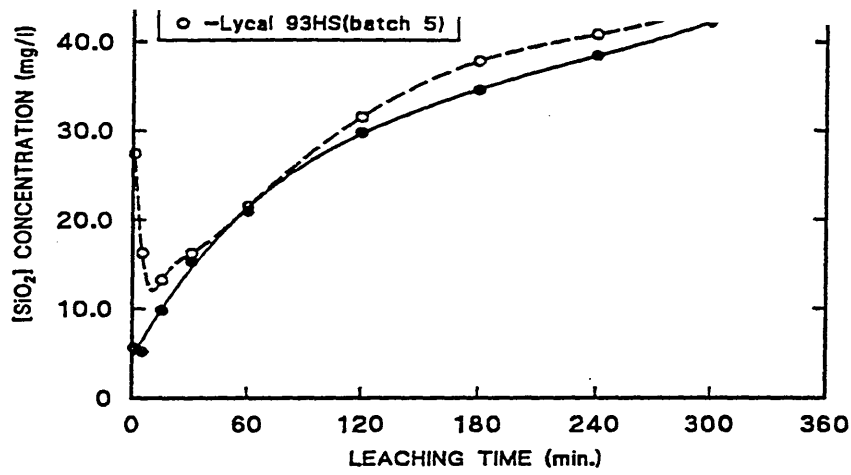
ECONOMISER ASH HOPPERS							
Solut. No.	Leach. Time (min.)	Si (mg/L)	SiO ₂ (mg/L)	Fe (mg/L)	Fe ₂ O ₃ (mg/L)	Mg (mg/L)	MgO (mg/L)
1	1.0	11.8	5.52	0.9	0.34	3.7	2.28
2	5.0	10.6	4.92	1.4	0.47	4.0	2.41
3	15.0	22.4	10.44	5.3	1.88	5.3	3.22
4	30.0	22.3	10.37	5.7	2.02	5.2	3.15
5	60.0	36.3	16.96	10.8	3.83	6.7	4.09
6	120.0	57.6	26.87	19.4	6.85	8.9	5.43
7	180.0	73.4	34.25	26.4	9.34	10.5	6.37
8	240.0	81.9	38.17	30.5	10.75	11.4	6.90
9	300.0	83.9	39.10	32.1	11.29	11.7	7.10
10	360.0	92.3	43.03	35.4	12.50	12.7	7.71

Note: This sample was collected during the deposition probe studies.

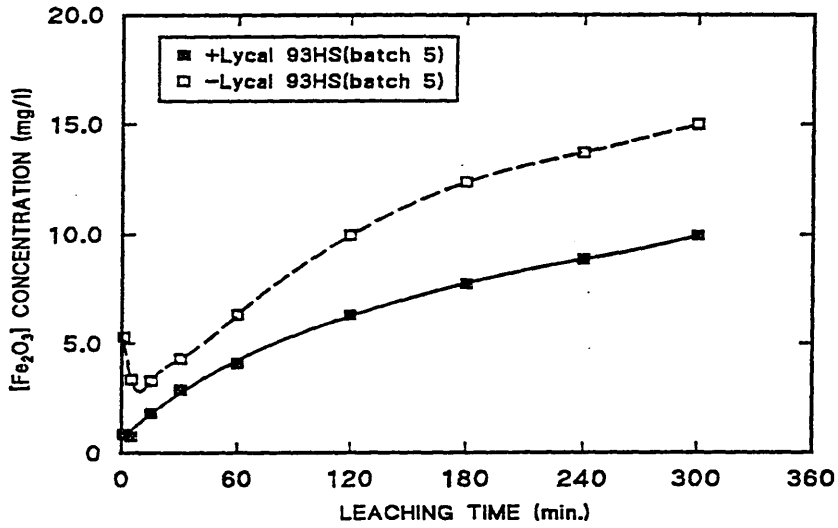
"Economiser ash hopper" sample collected in the "fifth" batch of samples from boiler No.6 without injection of Lyclal 93HS.

ECONOMISER ASH HOPPERS							
Solut. No.	Leach. Time (min.)	Si (mg/L)	SiO ₂ (mg/L)	Fe (mg/L)	Fe ₂ O ₃ (mg/L)	Mg (mg/L)	MgO (mg/L)
1	1.0	43.3	20.22	21.5	7.73	5.8	3.55
2	5.0	40.4	18.82	20.0	7.19	5.6	3.42
3	15.0	60.4	28.20	26.8	9.61	8.3	5.03
4	30.0	91.5	42.69	35.9	12.90	11.3	6.83
5	60.0	104.0	48.48	41.1	14.78	12.5	7.57
6	120.0	117.7	54.86	46.9	16.87	13.2	7.97
7	180.0	131.2	61.18	51.6	18.55	13.9	8.44
8	240.0	139.6	65.10	54.3	19.49	13.9	8.44
9	300.0	133.9	62.44	53.3	19.15	13.4	8.11
10	360.0	142.2	66.30	55.8	20.03	13.5	8.17

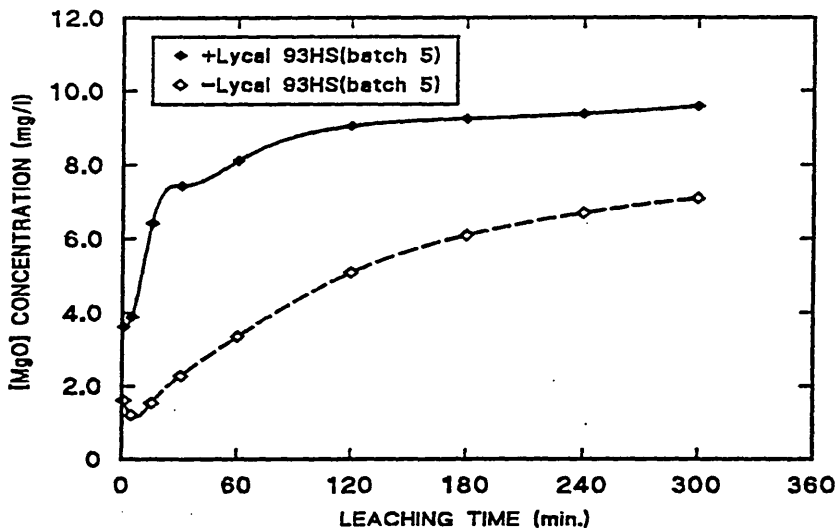
Note: This sample was collected during the deposition probe studies.



(a)



(b)



(c)

Figure 4-12: Determination of HF-solubility rates for (a) $[SiO_2]$, (b) $[Fe_2O_3]$ and (c) $[MgO]$ concentrations for the "grit arrester" medium size particulate samples ($-500\mu m +63\mu m$) from boiler No.6, with and without on-line injection of Lycal 93HS.

"Grit arrestor" sample collected in the "fifth" batch of samples from boiler No.6 with on-line injection of Lycal 93HS.

GRIT ARRESTORS							
Solut. No.	Leach. Time (min.)	Si (mg/L)	SiO ₂ (mg/L)	Fe (mg/L)	Fe ₂ O ₃ (mg/L)	Mg (mg/L)	MgO (mg/L)
1	1.0	12.1	5.65	2.5	0.87	6.0	3.62
2	5.0	11.1	5.19	2.1	0.74	6.4	3.89
3	15.0	21.1	9.84	5.1	1.81	10.6	6.43
4	30.0	32.8	15.30	8.2	2.89	12.3	7.44
5	60.0	44.9	20.95	11.7	4.10	13.4	8.11
6	120.0	63.9	29.79	17.9	6.32	14.9	9.05
7	180.0	74.2	34.58	22.0	7.73	15.3	9.25
8	240.0	82.4	38.44	25.1	8.87	15.5	9.38
9	300.0	90.6	42.23	28.2	9.95	15.8	9.58

Note: This sample was collected during the deposition probe tests.

"Grit arrestor" sample collected in the "fifth" batch of samples from boiler No.6 without injection of Lyclal 93HS.

GRIT ARRESTORS							
Solut. No.	Leach. Time (min.)	Si (mg/L)	SiO ₂ (mg/L)	Fe (mg/L)	Fe ₂ O ₃ (mg/L)	Mg (mg/L)	MgO (mg/L)
1	1.0	58.7	27.40	14.7	5.31	2.6	1.61
2	5.0	34.9	16.29	9.3	3.36	2.0	1.21
3	15.0	28.4	13.23	9.1	3.29	2.5	1.54
4	30.0	34.8	16.23	12.0	4.30	3.7	2.28
5	60.0	46.0	21.48	17.5	6.32	5.5	3.35
6	120.0	67.6	31.52	27.7	9.95	8.4	5.09
7	180.0	81.1	37.84	34.5	12.36	10.1	6.10
8	240.0	87.6	40.83	38.2	13.71	11.0	6.70
9	300.0	93.6	43.62	41.7	14.99	11.7	7.10
10	360.0	97.9	45.62	44.1	15.86	12.0	7.30

Note: This sample was collected during the deposition probe tests.

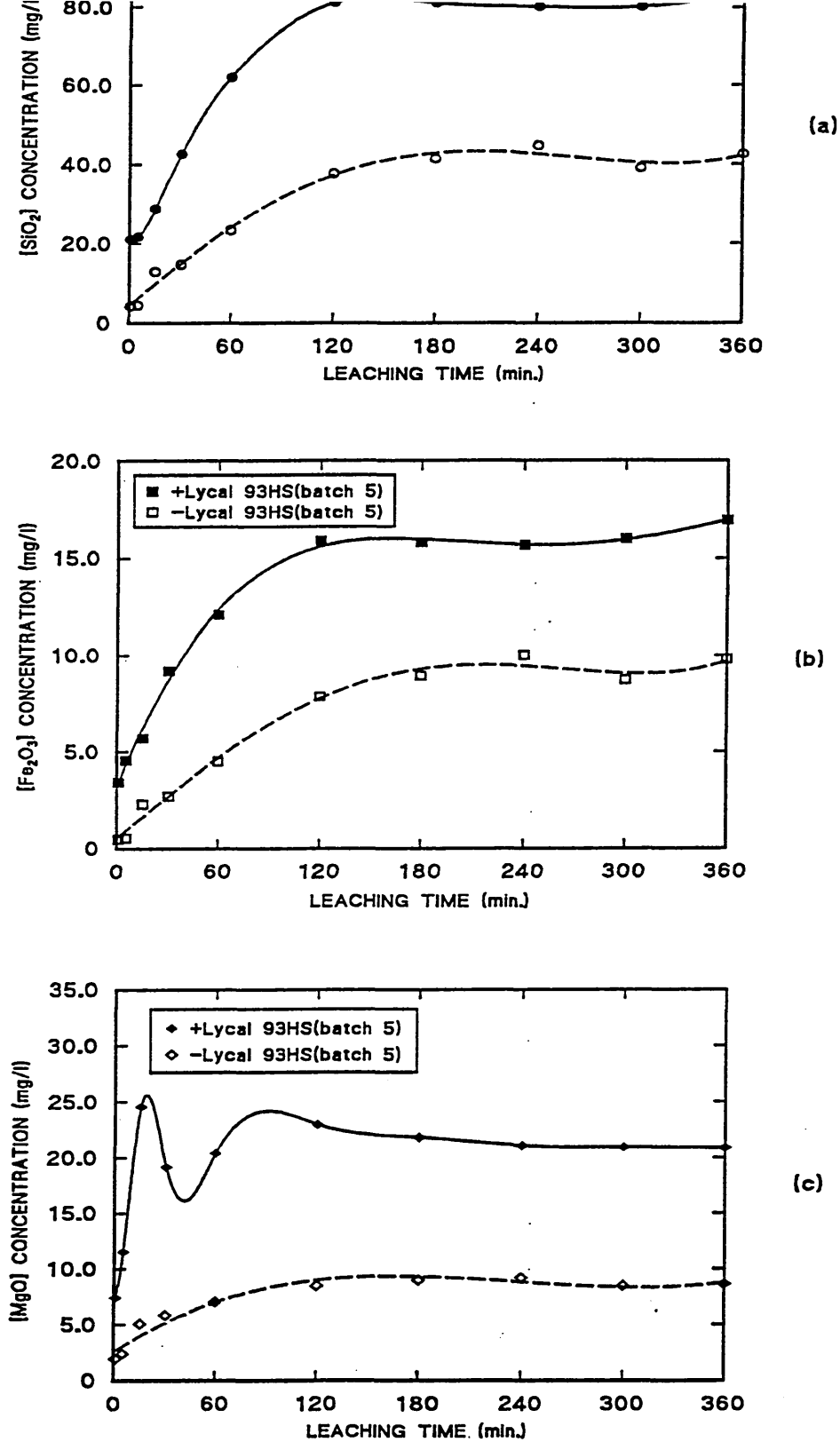


Figure 4-13: Determination of HF-solubility rates for (a) [SiO₂], (b) [Fe₂O₃] and (c) [MgO] concentrations for the "grit arrester" fine size particulate samples (-45 μ m) from boiler No.6 with and without on-line injection of Lycal 93HS.

"Grit arrestor" sample collected in the "fifth" batch of samples from boiler No.6 with on-line injection of Lycal 93HS.

GRIT ARRESTORS							
Solut. No.	Leach. Time (min.)	Si (mg/L)	SiO ₂ (mg/L)	Fe (mg/L)	Fe ₂ O ₃ (mg/L)	Mg (mg/L)	MgO (mg/L)
1	1.0	45.2	21.08	9.7	3.43	12.3	7.44
2	5.0	46.5	21.68	13.0	4.57	19.0	11.52
3	15.0	61.6	28.73	16.1	5.71	40.6	24.59
4	30.0	91.5	42.69	26.1	9.21	31.6	19.16
5	60.0	133.0	62.04	34.3	12.10	33.7	20.44
6	120.0	174.0	81.13	44.9	15.86	37.9	22.98
7	180.0	174.0	81.13	44.7	15.79	36.0	21.84
8	240.0	172.0	80.20	44.4	15.66	34.8	21.11
9	300.0	172.0	80.20	45.3	15.99	34.6	20.97
10	360.0	180.0	83.92	48.1	16.93	34.5	20.90

Note: This was a sieve size fractioned sample collected on the pan (-45um).
The bulk sample was originally collected during the deposition probe tests.

Table 4-38: Results of surface leaching analysis of "fine" size fractionated particulate "Grit arrestor" sample collected in the "fifth" batch of samples from boiler No.6 without injection of Lycal 93HS.

GRIT ARRESTORS							
Solut. No.	Leach. Time (min.)	Si (mg/L)	SiO ₂ (mg/L)	Fe (mg/L)	Fe ₂ O ₃ (mg/L)	Mg (mg/L)	MgO (mg/L)
1	1.0	9.1	4.26	1.4	0.47	3.2	1.94
2	5.0	9.6	4.46	1.6	0.54	4.0	2.41
3	15.0	27.7	12.90	6.4	2.28	8.4	5.09
4	30.0	31.5	14.70	7.7	2.69	9.6	5.83
5	60.0	50.0	23.34	12.8	4.50	11.6	7.04
6	120.0	80.8	37.71	22.3	7.86	14.0	8.51
7	180.0	89.1	41.56	25.4	8.94	14.8	8.98
8	240.0	96.1	44.82	28.4	10.01	15.2	9.18
9	300.0	83.8	39.10	24.8	8.74	14.0	8.51
10	360.0	91.3	42.56	27.9	9.81	14.3	8.64

Note: This was a sieve size fractionated sample collected on the pan (-45) from the original bulk sample.

Table 4-39: Results of surface leaching analysis of a "Passage between Screen Tubes & Superheaters" deposit sample received in the "second" batch of samples from boiler No.6 with on-line injection of Lycal 93HS.

PASSAGE BETWEEN SCREEN TUBES & SUPERHEATERS							
Solut. No.	Leach. Time (min.)	Si (mg/L)	SiO ₂ (mg/L)	Fe (mg/L)	Fe ₂ O ₃ (mg/L)	Mg (mg/L)	MgO (mg/L)
1	1.0	8.2	3.79	0.35	0.13	3.7	2.21
2	5.0	9.8	4.59	0.62	0.20	3.9	2.35
3	15.0	15.9	7.38	1.0	0.34	4.3	2.61
4	30.0	24.9	11.64	1.2	0.40	4.7	2.88
5	60.0	41.5	19.35	2.2	0.81	5.2	3.15
6	120.0	67.9	31.65	4.0	1.41	5.9	3.55
7	180.0	81.0	37.77	5.2	1.81	6.0	3.62
8	240.0	92.6	43.16	6.4	2.28	6.4	3.89
9	300.0	105.0	48.94	7.6	2.69	7.4	4.49
10	360.0	118.0	55.00	9.0	3.16	7.6	4.62

Table 4-40: Results of surface leaching analysis of a "Front Arch" deposit sample collected in the "fifth" batch of samples from boiler No.5 without any injection of Lycal 93HS.

FRONT ARCH							
Solut. No.	Leach. Time (min.)	Si (mg/L)	SiO ₂ (mg/L)	Fe (mg/L)	Fe ₂ O ₃ (mg/L)	Mg (mg/L)	MgO (mg/L)
1	1.0	3.4	1.60	0.91	0.34	0.24	0.13
2	5.0	2.1	1.00	0.26	0.07	0.10	0.06
3	15.0	2.2	1.00	0.20	0.07	0.11	0.07
4	30.0	2.6	1.20	0.22	0.07	0.15	0.07
5	60.0	3.6	1.66	0.25	0.07	0.25	0.13
6	120.0	5.6	2.59	0.32	0.13	0.46	0.27
7	180.0	7.6	3.52	0.39	0.13	0.67	0.40
8	240.0	9.2	4.32	0.44	0.13	0.84	0.54
9	300.0	10.9	5.05	0.48	0.20	1.00	0.60
10	360.0	12.6	5.85	0.58	0.20	1.02	0.60

Table 4-41: Results of surface leaching analysis of a "Rear Arch" deposit sample collected in the "fifth" batch of samples from boiler No.5 without any injection of Lycal 93HS.

REAR ARCH							
Solut. No.	Leach. Time (min.)	Si (mg/L)	SiO ₂ (mg/L)	Fe (mg/L)	Fe ₂ O ₃ (mg/L)	Mg (mg/L)	MgO (mg/L)
1	1.0	<2.5	<1.20	0.30	0.13	0.30	0.20
2	5.0	<2.5	<1.20	0.20	0.07	0.10	0.07
3	15.0	<2.5	<1.20	0.25	0.07	0.10	0.07
4	30.0	4.0	1.86	0.30	0.13	0.50	0.34
5	60.0	9.0	4.19	0.60	0.20	0.30	0.20
6	120.0	19.0	8.84	0.90	0.34	0.45	0.27
7	180.0	28.0	13.03	1.20	0.40	0.60	0.34
8	240.0	33.0	15.36	1.40	0.47	0.80	0.47
9	300.0	39.5	18.42	1.60	0.54	1.00	0.60

Table 4-42: Results of surface leaching of a "Steam Generating Tubes" deposit sample collected in the "fifth" batch of samples from boiler No.5 without any injection of Lyclal 93HS.

STEAM GENERATING TUBES							
Solut. No.	Leach. Time (min.)	Si (mg/L)	SiO ₂ (mg/L)	Fe (mg/L)	Fe ₂ O ₃ (mg/L)	Mg (mg/L)	MgO (mg/L)
1	1.0	3.0	1.40	0.5	0.20	0.5	0.34
2	5.0	3.0	1.40	0.4	0.13	1.2	0.74
3	15.0	4.0	1.86	0.5	0.20	2.1	1.27
4	30.0	7.0	3.26	0.6	0.20	3.0	1.81
5	60.0	13.0	6.05	1.1	0.40	3.5	2.14
6	120.0	23.0	10.71	1.9	0.67	3.9	2.35
7	180.0	33.0	15.36	2.3	0.81	4.0	2.41
8	240.0	33.5	15.63	2.8	1.01	4.2	2.55
9	300.0	37.0	17.22	3.2	1.14	4.1	2.48

- After the period of 5 to 6 hours, the [MgO] concentrations for samples from boiler No.6, with Lycal injection, had reached a saturation level within the leaching solutions.
- The [MgO] concentrations for the corresponding samples from boiler No.5, without Lycal 93HS injection, did not as clearly reach a saturation level by the end of the experimentation.
- The ratio of the [MgO] concentration to [Fe₂O₃] and [SiO₂] concentrations leached from the surface of each deposit sample from boiler No.6, is invariably significantly greater than the ratio of the amount of MgO to Fe₂O₃ and SiO₂ in mass%, for each of these samples.
- The amount of [MgO] leached from the surface of the samples from boiler No.6, particularly at the initial stages of the leaching process is significantly higher than the values for the corresponding samples from boiler No.5.
- The concentration of the [MgO], Fe₂O₃ and SiO₂ for the particulate economiser ash hopper and grit arrester samples in solution, with and without Lycal injection is much greater than the corresponding concentrations from the bulk deposit samples.
- The ratio of [MgO] concentration to [Fe₂O₃] and [SiO₂] concentrations for the particulate samples with Lycal 93HS injection is significantly greater than the same ratios for the particulate samples without Lycal 93HS injection. This is also the case for the corresponding ratios for the bulk deposit samples with and without Lycal 93HS injection.

4.6 COAL CHARACTERISATION

The coal used at West-Belfast power station was of a mixed lump and smalls, bituminous type, mined from open-cast coal fields in the Ayrshire region of

Scotland. The coal was taken from a number of pits and inevitably from different seams within the pits. This coal is especially suitable for stocking and storage for long periods without the possibility of spontaneous combustion.

The investigation of the coal and its residual ash, which will be considered in this section, was based on a sample weighing 4.783 kg obtained from the boiler feeders by one of the operators at the power station.

4.6.1 Proximate Analysis

The proximate analysis of a coal involves the determination of moisture, volatile matter, ash and fixed carbon content by difference,^{175,176} as described in Section 3.4.1. This data was determined by the power station personnel and the author and is presented in Table 3-2.

4.6.2 Ultimate Analysis

The ultimate analysis expresses the composition of a coal in mass percentages of carbon, hydrogen, nitrogen, sulphur, chlorine and oxygen regardless of the origin.¹⁷⁶ This data as well as additional data for the Ayrshire coal has been included in Table 3-2.

4.6.3 Particle Size Analysis

The whole sample, representing the coal as introduced onto the chain-grate for burning, was subjected to a sieve analysis to determine the quantity of various size fractions present. This was carried out before samples were taken from the bulk for the proximate and ultimate analysis.

Table 4-43 presents the results which are plotted as a bar chart in Figure 4-14. This shows that approximately 80% of the total mass of the coal in the sample had a size greater than 8 mesh.

Table 4-43: Result of sieve size analysis of the sample batch of coal collected from the chain-grate before it's introduction to boiler No.6.

Sieve Size (B.S.410)		Mass Oversize Collected (kg)	Mass Percent. Oversize (%)
Mesh No.	Aperture (μm)		
>> 1/4"	>> 6350	1.832	38.30
+1/4"	+6350	0.727	15.20
-1/4" +3/16"	-6350 +4760	0.385	8.05
-3/16"+8	-4760 +2057	0.760	15.90
-8 +14	-2057 +1200	0.325	6.80
-14 +18	-1200 +850	0.159	3.32
-18 +25	-850 +600	0.137	2.90
-25 +44	-600 +355	0.138	2.90
-44 +52	-355 +300	0.032	0.67
-52 +100	-300 +150	0.116	2.40
-100 +200	-150 +75	0.062	1.30
-200 +300	-75 +53	0.016	0.30
-300 +350	-53 +45	0.094	1.96
		----- 4.783	----- 100%

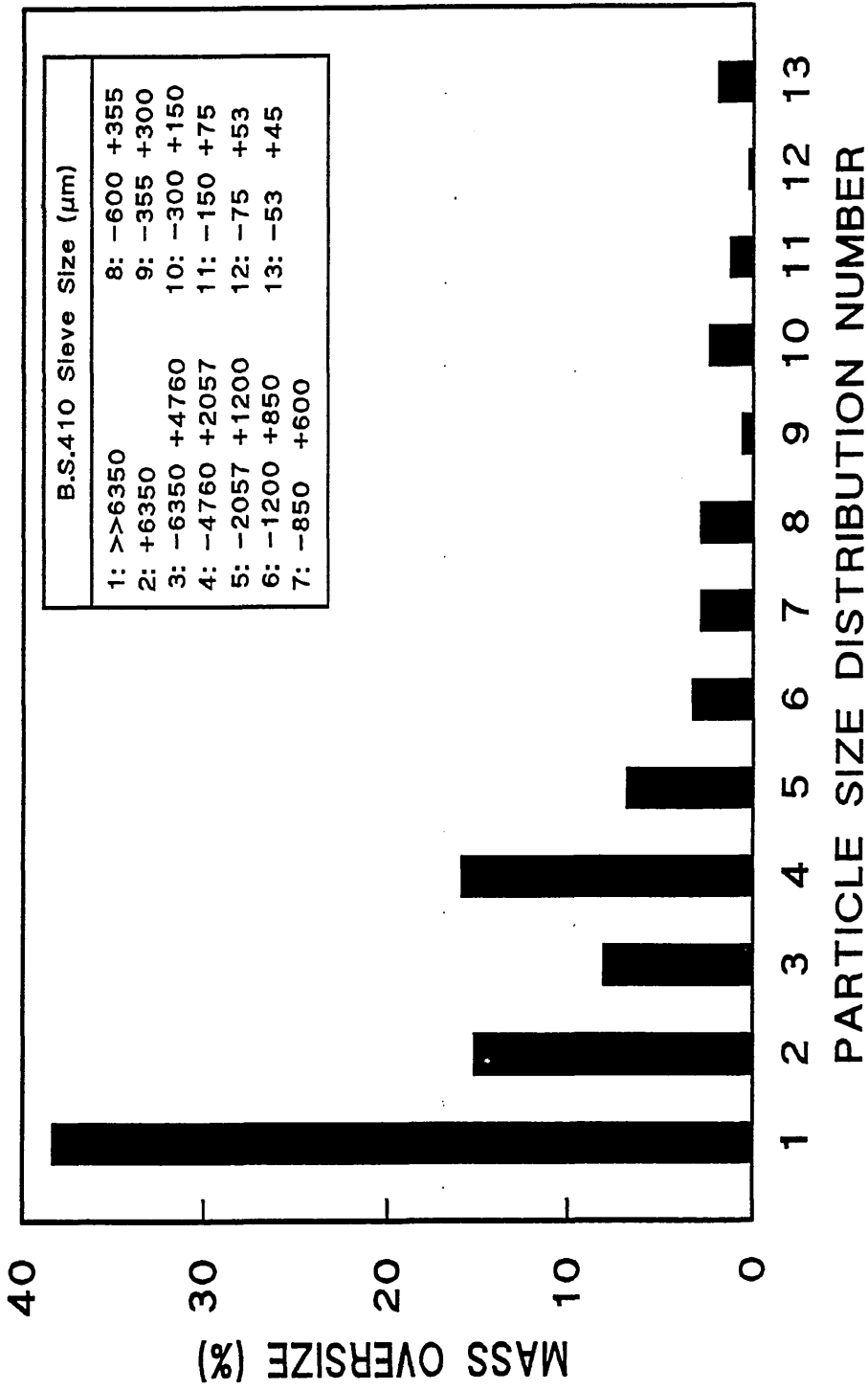


Figure 4-14: Particle size analysis for "Ayrshire" coal.

4.6.4 Variation of Moisture with Coal Particle Size

The inherent moisture content for each particle size range from the sieve analysis was determined using the "vacuum" method described in Section 3.4.1 (b). The results are presented in Table 4-44.

As can be seen for the same results plotted in Figure 4-15, the inherent moisture content generally increased as the particle size decreased. The values plotted are averages of a number of determination for each size band. The bars represent the maximum and minimum values in each set of results.

4.6.5 Variation of Ash Content with Particle Size

The sub-samples of each size fractioned samples of coal were ground to -72 mesh ($-210 \mu\text{m}$) and subsequently ashed as previously described in Section 3.4.1(c). Table 4-45 shows the ash content of each particle size fraction.

Figure 4-16 illustrates the variation in ash content with particle size. This is quite considerable, ranging from 5 mass% for +1/4" mesh size ($> 6350 \mu\text{m}$) coal upto 20% for -200 +300 mesh size ($-75 +53 \mu\text{m}$) coal particles. The average ash content for the coal as received at the power station was 11.3 mass% (see Table 4-43).

4.6.6 Variation of Ash Chemistry with Coal Particle Size

In order to determine whether the variation in the ash content of the different coal particle size fractions would also result in a compositional change, four different groups of "Ash admixtures" designated AM1 to AM4 were prepared. These admixtures were made up from the coal ash derived from four different groups of coal size particles which are defined in Table 4-46. The results of the chemical analysis of the admixtures is given in Table 4-47.

Table 4-44: Result of inherent moisture determination for sieve size particle fractions of Ayrshire coal collected from the chain-grate before it's introduction to boiler No.6.

Particle size (μm)	Min. Moisture (mass%)	Max. Moisture (mass%)	Mean Moisture (mass%)
> > 6350	3.625	3.889	3.761
+6350	4.138	4.227	4.184
-6350 +4760	4.132	4.360	4.240
-4760 +2057	4.996	5.266	5.135
-2057 +1200	4.950	5.728	5.362
-1200 +850	5.150	5.334	5.255
-850 +600	4.458	4.559	4.491
-600 +355	5.096	5.371	5.194
-355 +300	4.743	5.081	4.907
-300 +150	4.926	5.012	4.966
-150 +75	4.992	5.574	5.277
-75 +53	5.266	5.731	5.564

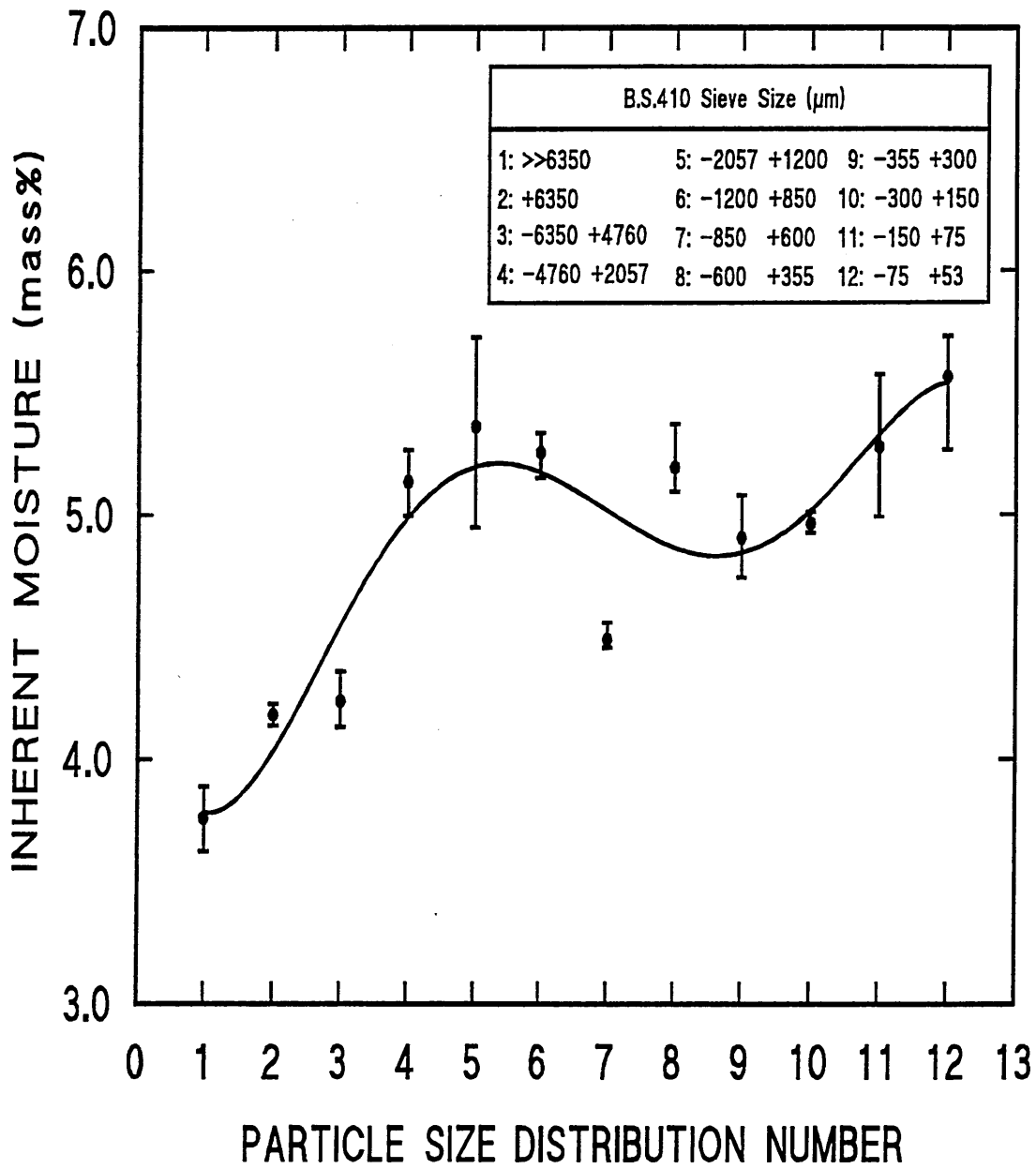


Figure 4-15: Variation in moisture content with particle size for the Ayrshire coal sample.

Table 4-45: Result of ash content determination (a.d.b) for sieve size particle fractions of Ayrshire coal collected from the chain-grate before it's introduction to boiler No.6.

Particle size (μm)	Ash Content Min. (mass%)	Ash Content Max. (mass%)	Ash Content Mean (mass%)
> > 6350	4.675	5.213	4.889
+6350	5.557	5.988	5.724
-6350 +4760	5.195	7.146	5.926
-4760 +2057	5.526	5.890	5.681
-2057 +1200	6.074	6.402	6.265
-1200 +850	6.940	8.199	7.557
-850 +600	8.571	10.169	9.157
-600 +355	9.237	10.101	9.752
-355 +300	14.952	16.621	15.764
-300 +150	15.746	16.577	16.271
-150 +75	17.047	18.850	18.064
-75 +53	18.588	19.930	19.395

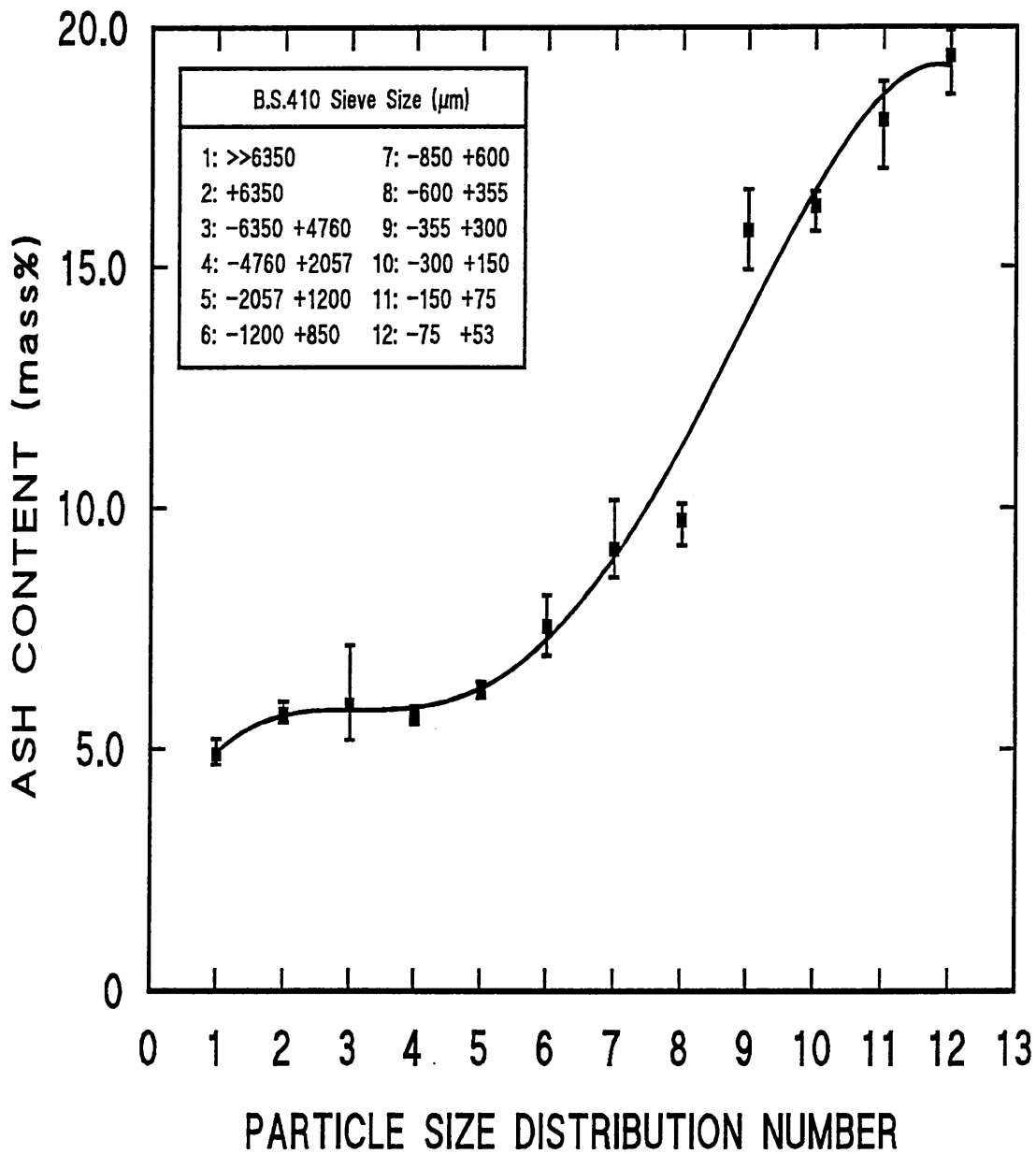


Figure 4-16: Variation in ash content with particle size for the Ayrshire coal sample batch on air-dried basis.

Table 4-46: Description of various "ash admixture" groups derived from the Ayrshire coal size ranges present in the sample batch.

ASH ADMIX. NO.	SCREEN SIZE SPECIFICATIONS (μm)
AM1	+6350, -6350 +4760, -4760 +2057
AM2	-2057 +1200, -1200 +850
AM3	-850 +600, -600 +355, -355 +300
AM4	-300 +150, -150 +75, -75 +53
C.A	+6350 -53

Note: C.A is the average coal ash comprising the entire range of the size fractioned coal particles.

Table 4-47: Chemical analysis of "ash admixture" groups made from various coal size fractions.

ASH ADMIX. NO.	COMPOUND MASS PERCENTAGE (%)								
	SiO ₂	Al ₂ O ₃	TiO ₂	Fe ₂ O ₃	CaO	MgO	K ₂ O	P ₂ O ₅	SO ₃
AM1	48.10	30.60	1.40	12.25	4.74	1.24	1.45	0.21	n.d
AM2	50.40	30.77	1.25	8.96	4.73	1.73	1.95	0.16	n.d
AM3	49.40	30.00	1.17	8.61	6.68	1.79	2.20	0.13	n.d
AM4	49.35	27.66	1.08	9.12	8.84	1.79	1.98	0.16	n.d
C.A	49.30	29.75	1.22	9.73	6.25	1.64	1.90	0.20	n.d

Note: The "ash admixture" groups have been described in Table 4-46. The average coal ash analysis (C.A) has been included for comparative purposes. The Na₂O content has been omitted for the same reason. n.d : not determined.

There appears to be a relative depletion in Fe_2O_3 , TiO_2 and Al_2O_3 and enrichment in CaO , MgO and possibly K_2O contents as the coal particle size decreases. There appears to be no correlatable trend in the SiO_2 content.

4.6.7 Determination of the Softening Characteristics of Selected Ash Admixtures With and Without Additions of Lycal 93HS.

The ash admixtures AM1 and AM4 representing the upper and lower particle size ranges were selected for a series of softening tests with up to 3 mass% additions of Lycal 93HS, using the cone fusion technique described previously in Section 3.3.4.

Table 4-48 shows the effect of additions of Lycal 93HS on the two selected admixtures. It can be seen that whereas the additions of Lycal 93HS had no discernible effect on the temperature of the various softening stages of the AM1 admixture, it proved to decrease them for the AM4 admixture. These results seem to indicate that AM1 admixture is relatively more refractory than the AM4 admixture. From the chemical analysis results in Table 4-47, the higher CaO content and lower Al_2O_3 content of the AM4 admixture compared to the corresponding oxides in AM1 admixture tend to confirm these observations.

Figure 4-17 further highlights the effect of increasing additions of Lycal 93HS on the various softening stages of the AM4 admixture.

4.7 THE CHARACTERISATION OF ASH COMPONENTS IN AYRSHIRE

COAL

The reason for carrying out this work, as explained in Section 3.4.2(a), was four fold:

- To assess the degree of variation in the individual components comprising the coal ash matter.

Table 4-48: Results of cone-fusion tests for the "ash admixture" cone samples of the upper and lower size fractions (AM1 & AM4) with the effect of additions of Lycal 93HS on their softening behaviour.

ASH ADMIX. NO.	LYCAL 93HS (mass%)	SOFTENING TEMPERATURE (°C)			
		IDT	ST	HT	FT
AM1	0.0	>1450	-	-	-
AM1	0.5	>1450	-	-	-
AM1	1.5	>1450	-	-	-
AM1	3.0	1420	>1450	-	-
AM4	0.0	1392	1419	1436	>1450
AM4	0.5	1380	>1450	-	-
AM4	1.5	1365	-	1396	1427
AM4	3.0	1334	1360	1392	1430

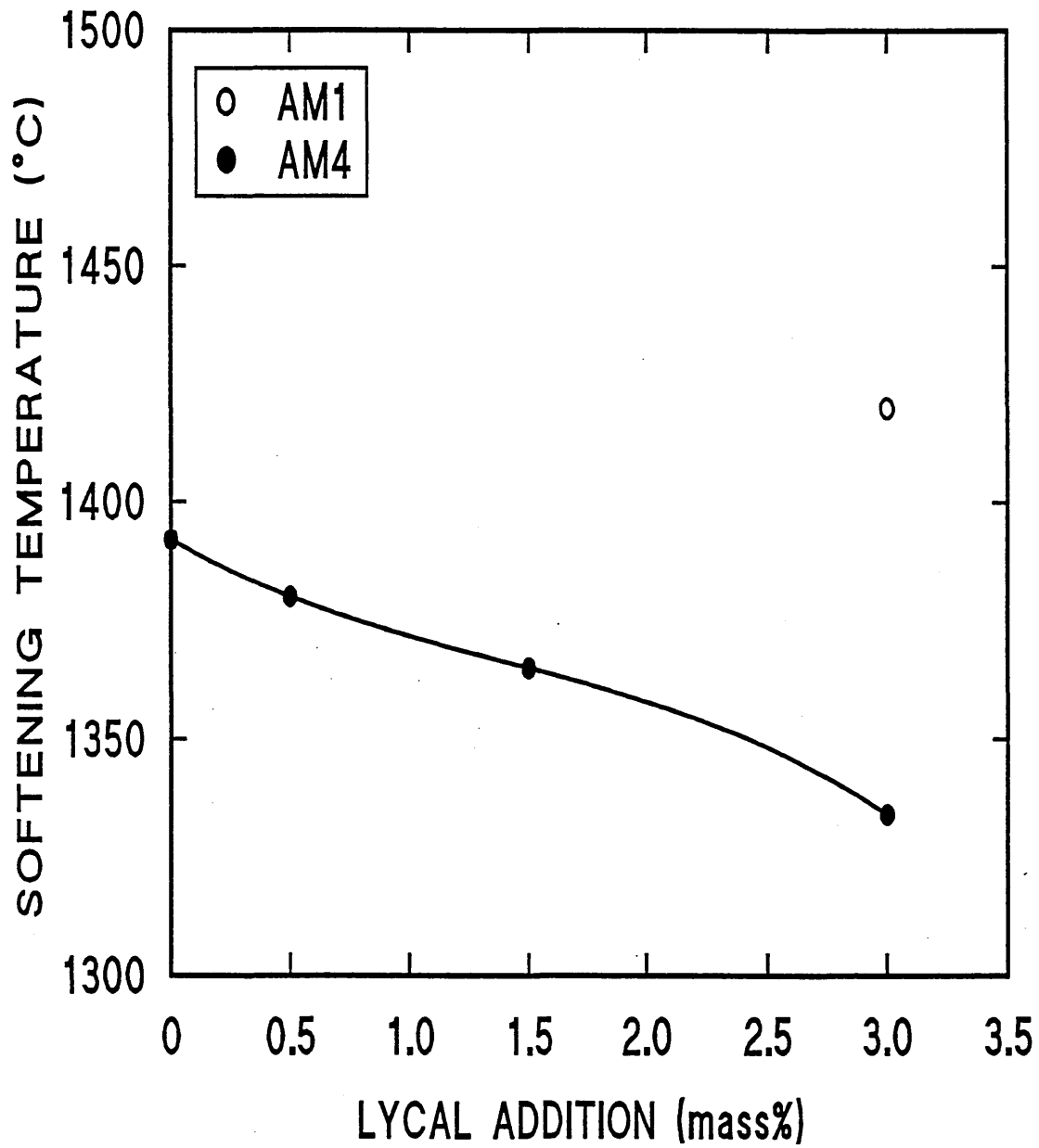


Figure 4-17: Effect of Lycal 93HS on the softening characteristics of the "IDT" ranges for the two "ash admixtures" as defined in Table 4-46.

- To determine the chemical composition of the main constituents within the separated ash components.
- To investigate the softening characteristics of the individual ash components.
- To evaluate the effect of additions of Lycal 93HS in the range of 0% to 10%, on the softening characteristics of a selected number of ash components.

4.7.1 Separation of Coal Ash Components

Plates 4-70 to 4-73 illustrate the entire range of the ash components separated on the basis of their colour and textural differences as described in Section 3.4.2.

Table 4-49 further summarises the characteristics of the separated ash components. Table 4-50 is the evaluation of the amount and the degree of occurrence of each of the separated ash components. The mass percentage distribution of the various ash components which has been calculated from the results shown in Table 4-50, is further illustrated in the form of a bar-chart in Figure 4-18.

4.7.2 Chemical Constituents of the Coal Ash Components

Table 4-51 gives the chemical analyses of the separated ash components which featured more prominently. The selection criteria was either in favour of those components which had occurred more than 60 times and/or those with a collected total mass of more than 0.3 grams. Overall, 29 of the ash components met one or both of these criteria and as such were selected for further analysis.

As can be seen from Table 4-51, compositions of the ash components varied significantly. The SiO₂ content of the analysed ash components varied between 23% and 91%, the Al₂O₃ content between 4% and 40%, the Fe₂O₃ content between 2% and 61%, the CaO content between 0.1% and 7.5% and the K₂O content between 0.08% and 5.71%.

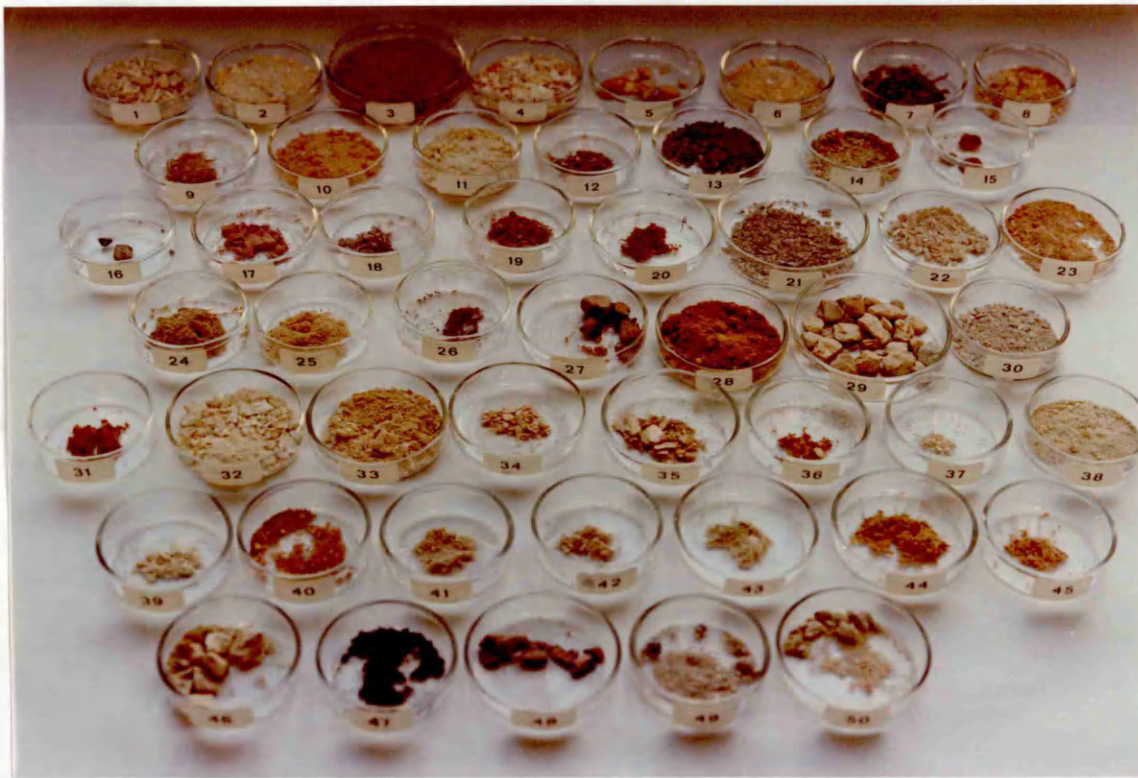


Plate 4-70:

The separated high temperature coal ash components.



Plate 4-71:

Illustration of the soft, powdery ash components of the high temperature coal ash.



Plate 4-72:

Illustration of semi-hard, layered, ash components of the high temperature coal ash.



Plate 4-73:

Illustration of hard, densely compacted or layered ash components of the high temperature coal ash.

Table 4-49: The characterisation of the coal ash components on the basis of texture and colour.

ASH COMP. NO.	TEXTURE & COLOUR DESCRIPTION	ASH COMP. NO.	TEXTURE & COLOUR DESCRIPTION
1	semi-hard, stratified - milky white outer surface, light grey / blue inner matrix.	14	semi-hard dissociating into brittle thin layers-light/tuffly-brown colour matrix.
2	soft, light white powder matrix with limited bands of beige/ creamy intertwings.	15	hard, smoothly surfaced slab type texture-brown/dark purple tone matrix.
3	highly porous, light powder with a reddish-brown colour.	16	very hard, dense, dark brown/ black matrix-intermittant white dust over the surface.
4	semi-soft, pad-like, layered - white/ light beige matrix.	17	hard, densely layered matrix with a pinky/purple colour.
5	very hard, dense, beige matrix smooth yellow outer surface.	18	semi-soft layered breaking into coarse particles-pink/blue matrix, orange surface.
6	soft, dusty, non-porous powder milky white matrix with white patches dispersed randomly.	19	soft, granular texture with a red-brown "saphron" colour matrix.
7	soft, porous, dark maroon powder matrix enveloped in a thin brittle layer.	20	soft, granular, spongy powder - dark brown/red colour matrix.
8	spongy, thinly layered white and beige powder mixture.	21	very soft, coagulated powder light grey/purple matrix - a thin, beige outer surface.
9	spongy, dusty matrix - light grey/ creamy colour.	22	very soft powder like "21". light grey/white matrix.
10	soft powder with a beige matrix and darker exterior.	23	honeycomb, lightly bonded-spread of white thin plate-like particles-brown/white.
11	very soft, granular powder - yellow / beige colour matrix.	24	soft powder in the form of cream / light brown strands.
12	soft powder of mixed matrix-light grey/creamy matrix.	25	very soft granular, spongy - milky white/creamy matrix.
13	finely layered, soft, smooth powdery carbonaceous - like light and dark grey matrix.	26	granular, spongy powder - dark brown/ maroon colour matrix.

Table 4-49: (Continued.)

ASH COMP. NO.	TEXTURE & COLOUR DESCRIPTION	ASH COMP. NO.	TEXTURE & COLOUR DESCRIPTION
27	hard, densely layered - purple internal layer, light brown outer surface.	39	soft, fibrous, white matrix with an inseparable thin creamy layer on the outside.
28	highly porous, light powder - light/dark brown colour - this is very similar to sample "3".	40	soft, padded powder matrix of orange/ light brown colour - a smooth brown outer surface.
29	very hard, dense, smooth, white matrix - similar to sample "5".	41	soft, granular, honey-comb kharky colour matrix.
30	soft, thinly padded, layered light grey powdery matrix enveloped by a light brown, very thin inseparable layer.	42	granular, white/creamy powder matrix with a creamy fragmentable, granular shell.
31	soft dark brown powder similar to sample "20" & "3".	43	soft, fragmentary granular powder - homogenously beige.
32	soft, thinly layered compact - milky white/beige matrix - similar to samples "1" & "4"	44	soft, layered light brown/beige matrix with the layers forming a fine powder.
33	spongy powder - beige/light brown with occasionally very thin white plates.	45	soft, spongy, porous matrix forming a thin waferous structure - light brown/beige.
34	soft, plated, powder formation milky white / creamy matrix.	46	hard, rock-like matrix with shiny-glassy fine nodules.
35	semi-soft, homogenous matrix - fragile texture, fragment into smaller parts - beige colour.	47	coarse, bulky, carbonaceous black powder matrix with sporadic white patches.
36	soft, particulate, fragmentary matrix - orange/light brown.	48	hard, brittle, smooth, rocky matrix - purple/ light grey - similar to sample "27".
37	particulate white powder, with thin creamy outer surface.	49	very soft, porous, particulate powder - uniform light grey.
38	soft powder of light grey / beige matrix - similar to "30".	50	soft, compact powder matrix - milky grey/ creamy surface.

Table 4-50: Quantitative analysis of the separated ash components from high temperature ashing of the coal particle size (+6350, -6350 +4760 μm), stating the amount and frequency of occurrence of the ash components after a total of 100 ashing sessions.

ASH COMP. NO.	AMOUNT COLLECT. (g)	FREQ. OF OCCUR.	ASH COMP. NO.	AMOUNT COLLECT. (g)	FREQ. OF OCCUR.	ASH COMP. NO.	AMOUNT COLLECT. (g)	FREQ. OF OCCUR.
1	3.383	52	18	0.106	4	35	0.224	8
2	1.346	96	19	0.077	36	36	0.074	8
3	1.007	100	20	0.053	12	37	0.063	4
4	2.241	80	21	0.427	28	38	0.379	8
5	2.589	24	22	0.189	20	39	0.123	4
6	0.494	80	23	0.345	56	40	0.044	8
7	0.561	60	24	0.284	44	41	0.036	12
8	0.162	52	25	0.225	40	42	0.039	8
9	0.043	40	26	0.011	8	43	1.915	4
10	0.344	92	27	3.122	12	44	0.130	4
11	0.410	52	28	0.412	96	45	0.030	8
12	0.128	4	29	8.087	36	46	2.664	16
13	0.669	48	30	0.616	24	47	0.136	4
14	0.439	20	31	0.059	32	48	1.680	8
15	0.869	4	32	0.470	40	49	0.090	8
16	0.621	4	33	0.579	52	50	0.017	4
17	0.642	4	34	0.112	8	TOTAL=	38.766	-

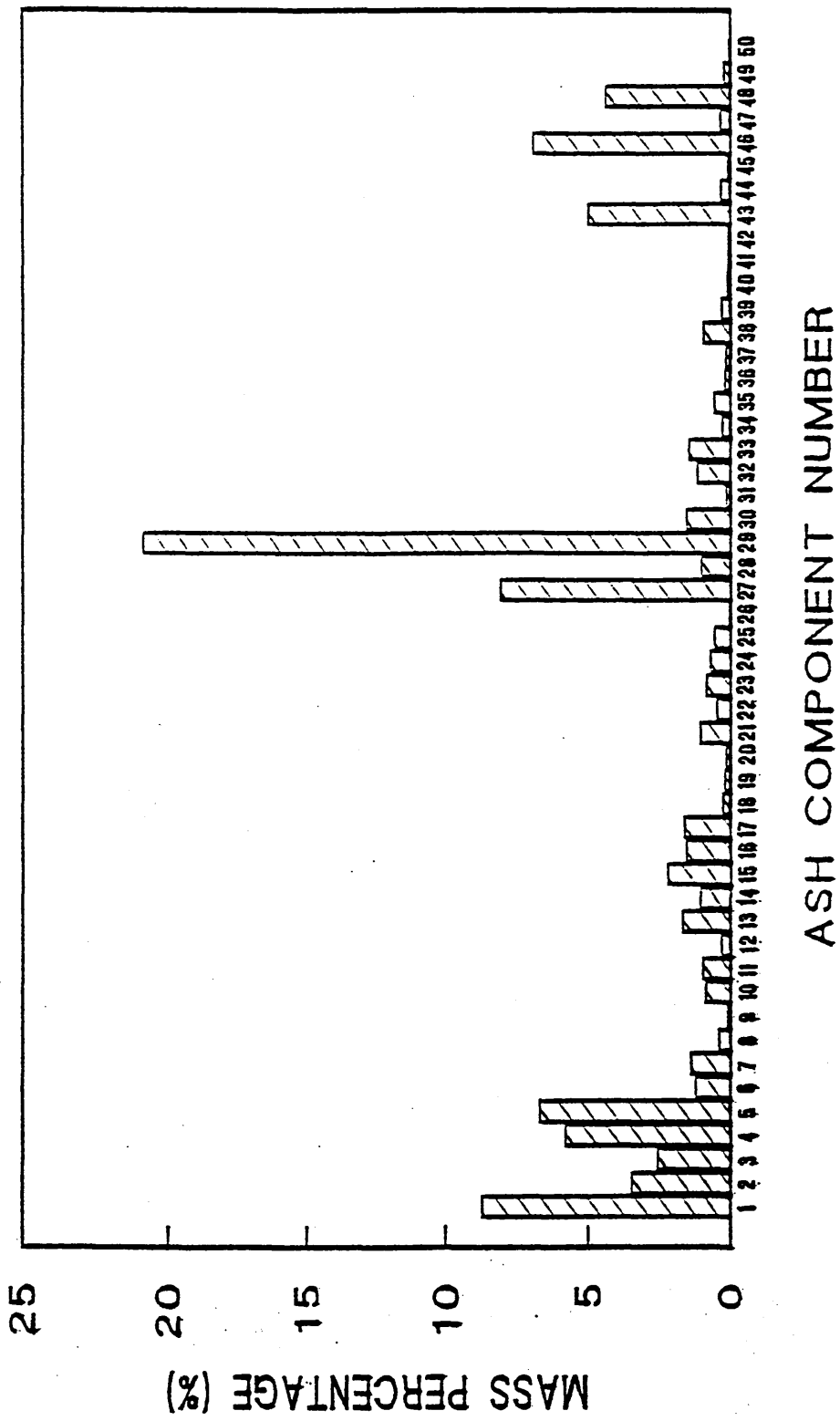


Figure 4-18: Quantitative distribution analysis of various separated coal ash components.

Table 4-51: The chemical analysis of the major separated ash components.

ASH COMP. NO.	COMPOUND MASS PERCENTAGE (%)								
	SiO ₂	Al ₂ O ₃	TiO ₂	Fe ₂ O ₃	CaO	MgO	K ₂ O	P ₂ O ₅	SO ₃
1	59.13	33.61	1.66	2.11	0.37	0.63	2.23	0.15	n.d
2	55.70	38.34	1.22	1.45	2.20	0.35	0.52	0.21	n.d
3	39.60	32.65	1.93	15.25	7.48	1.64	0.75	0.62	n.d
4	58.28	35.44	1.75	1.69	0.44	0.51	1.71	0.18	n.d
5	62.27	25.12	1.18	2.04	0.23	1.09	2.10	0.06	n.d
6	58.16	33.23	2.21	2.66	2.10	0.52	0.67	0.42	n.d
7	23.41	12.95	0.52	60.89	1.19	0.18	0.79	0.06	n.d
10	58.97	27.86	2.90	4.11	3.86	0.86	0.52	0.92	n.d
11	54.63	39.40	1.43	1.31	1.95	0.41	0.50	0.35	n.d
13	36.33	15.66	0.88	38.99	3.11	2.61	1.14	1.28	n.d
14	57.08	25.50	1.18	9.90	1.73	1.24	2.31	1.05	n.d
15	60.38	26.20	0.86	4.42	0.43	1.84	5.71	0.14	n.d
16	52.42	34.19	1.52	3.41	1.93	1.64	3.98	0.88	n.d
17	58.58	30.21	1.05	5.08	0.73	0.98	2.86	0.44	n.d
21	54.50	26.45	1.41	12.02	1.62	1.10	1.81	1.10	n.d

Note: n.d = not determined

Table 4-51: (Continued)

ASH COMP. NO.	COMPOUND MASS PERCENTAGE (%)								
	SiO ₂	Al ₂ O ₃	TiO ₂	Fe ₂ O ₃	CaO	MgO	K ₂ O	P ₂ O ₅	SO ₃
23	53.90	33.40	1.59	6.26	2.71	0.81	0.86	0.46	n.d
24	59.98	31.33	2.03	4.17	2.22	0.51	0.59	0.16	n.d
25	61.73	27.52	2.87	2.98	2.96	0.37	0.43	1.12	n.d
27	47.80	19.80	0.58	22.43	0.97	3.85	4.29	0.27	n.d
28	45.45	30.51	2.74	10.70	7.55	1.73	0.85	0.48	n.d
29	59.05	32.93	1.25	2.92	0.31	1.31	2.12	0.09	n.d
30	63.14	29.52	1.70	2.91	0.52	0.37	1.53	0.29	n.d
32	56.10	37.63	1.97	1.33	0.61	0.34	1.81	0.19	n.d
33	56.02	37.95	1.44	1.88	0.90	0.50	1.07	0.29	n.d
35	62.74	27.52	1.27	3.02	0.23	1.26	3.85	0.11	n.d
38	55.97	40.14	1.09	0.78	1.18	0.10	0.33	0.41	n.d
43	91.60	4.41	3.41	0.21	0.12	0.01	0.08	0.16	n.d
46	69.24	25.85	1.51	1.18	0.11	0.43	1.61	0.04	n.d
48	59.10	28.21	0.79	4.69	0.32	1.35	5.28	0.29	n.d

Note: n.d= not determined

4.7.3 Mineralogy of the LTA and Separated HTA Components

Figure 4-19 characterises the X-ray diffraction spectrum of the mineral constituents in the LTA sample of the Ayrshire coal, using X-ray diffractometry analysis, as described in Section 3.3.3.

The major minerals identified were quartz, illite, kaolinite, chlorite, muscovite, calcite, dolomite, anhydrite, pyrite and iron sulphate. Other minerals which were also present in minor amounts were rutile, jarosite, ankerite and halite.

The mineralogical constitution of 24 of the 29 more prominently featured, separated ash components as shown in Table 4-51 were also determined using X-ray diffractometry analysis as described in Section 3.3.3. Unfortunately the other 5 samples were damaged and could not be considered for this analysis.

Further to the wide variation in physical and chemical characteristics of the ash components, as summarised in Tables 4-49 and 4-51 respectively, the mineralogical constitution of the selected ash components are categorised in Figures 4-20 to 4-22. Figure 4-20 characterises mainly the diffraction spectra for the "acidic" ash components with $\text{SiO}_2 + \text{Al}_2\text{O}_3 > 90$ mass%. Figure 4-21 characterises mainly the diffraction spectra for the "basic" ash components with $\text{CaO} + \text{K}_2\text{O} > 3.50$ mass%. Figure 4-22 characterises the diffraction spectra for the "ferriferous" ash components with $\text{Fe}_2\text{O}_3 > 9.0$ mass%, and the sum of their basic oxides, i.e. $\text{K}_2\text{O} + \text{CaO} + \text{MgO} < 10$ mass%.

The major and minor minerals in the LTA sample, the separated ash components as well as those for the selected deposit samples from batches No.2 and No.3, included for comparative reasons, are listed in Table 4-52.

Peak intensities reflect the relative quantities of the various phases in ash, if only on a semi-quantitative basis. It is also evident from the diffraction spectra,

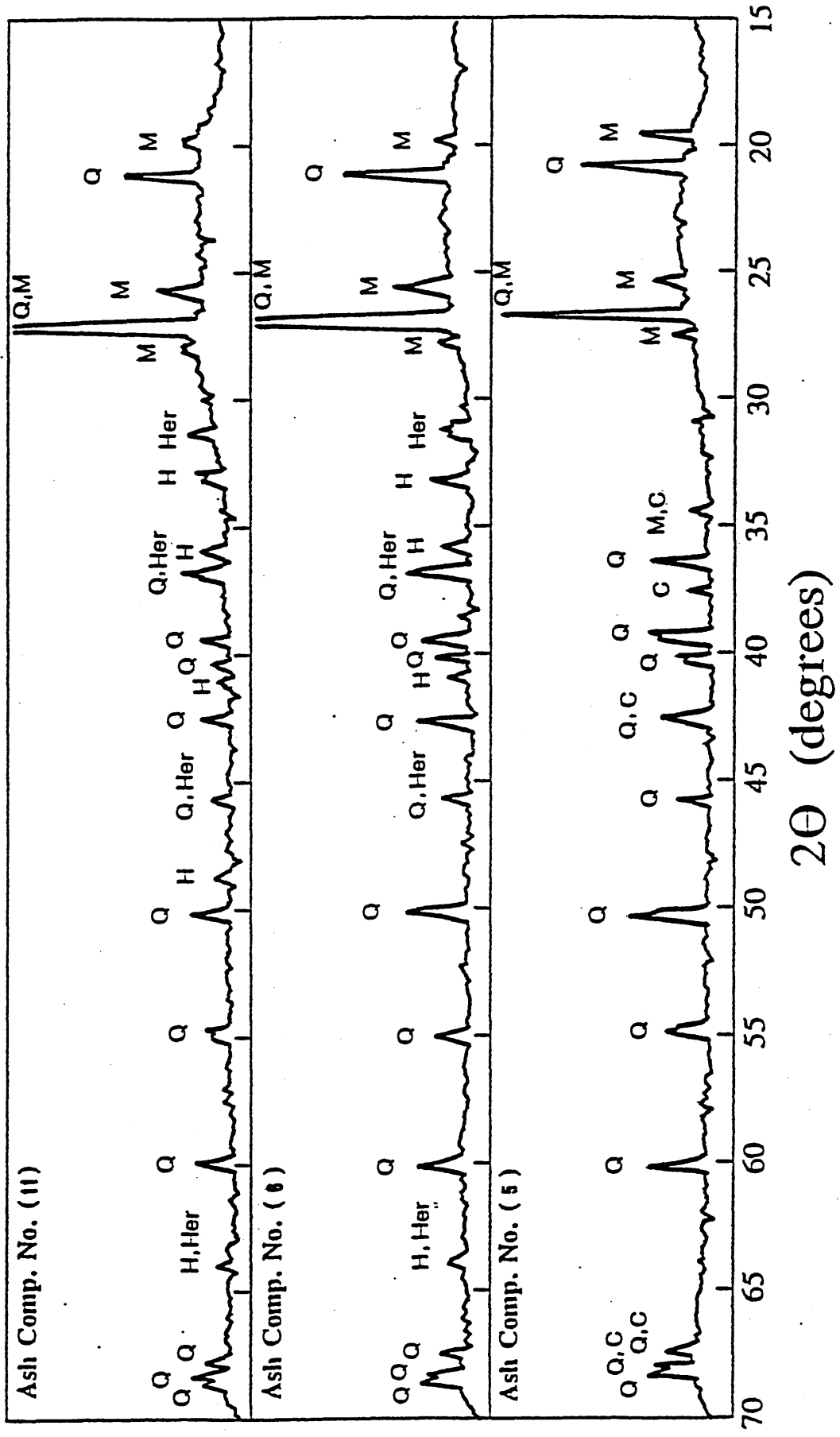


Figure 4-20: (Continued).

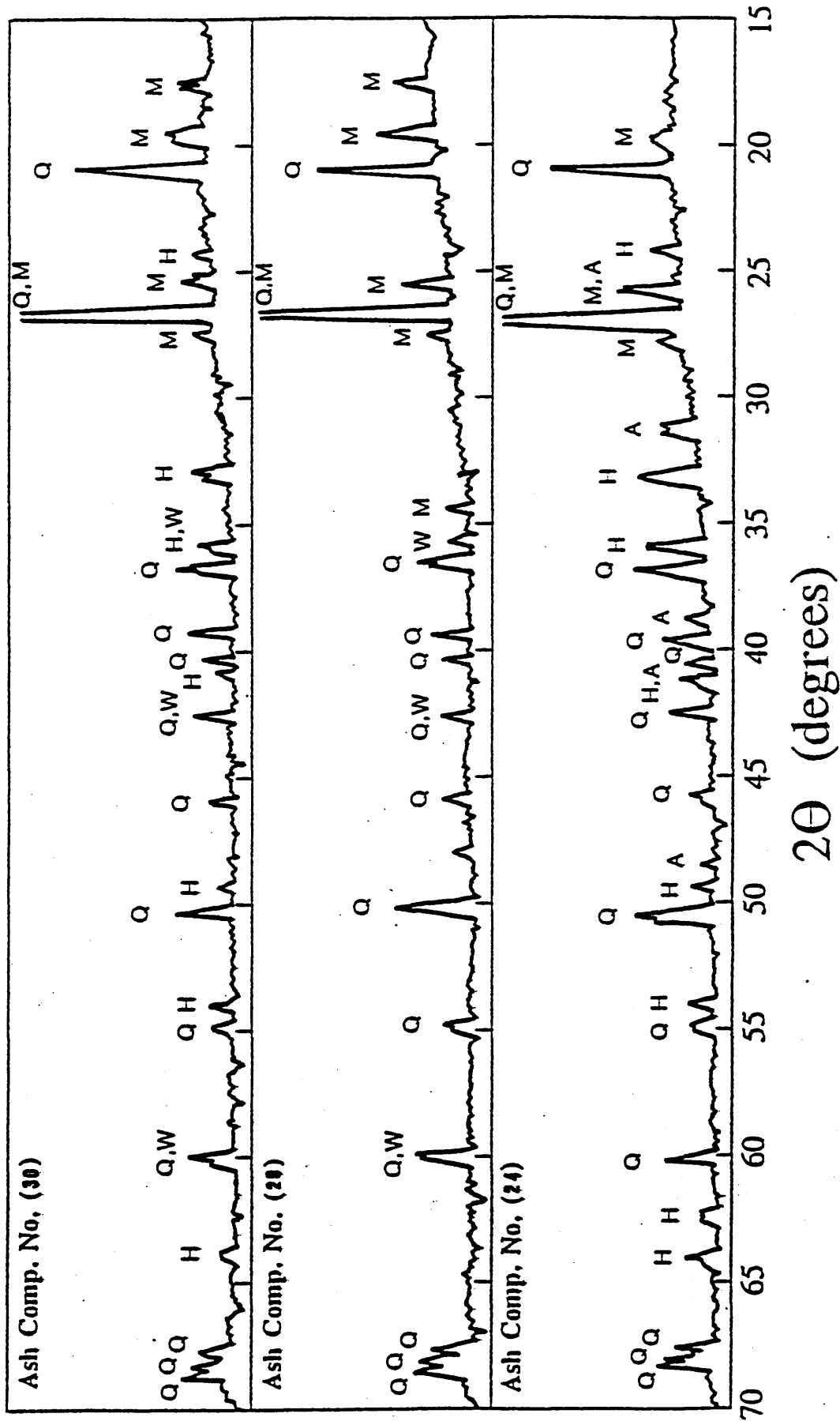


Figure 4-20: (Continued).

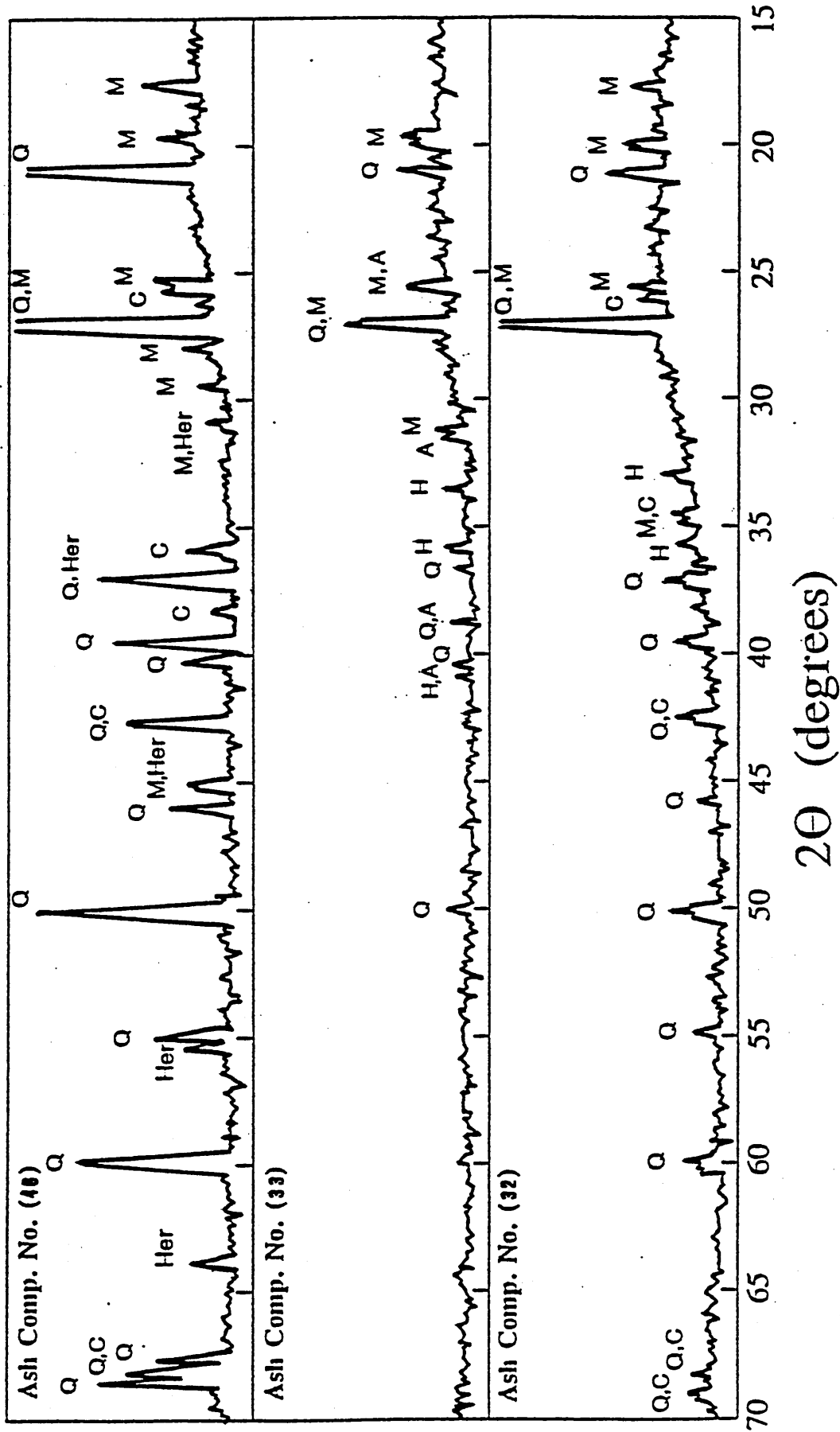


Figure 4-20: (Continued).

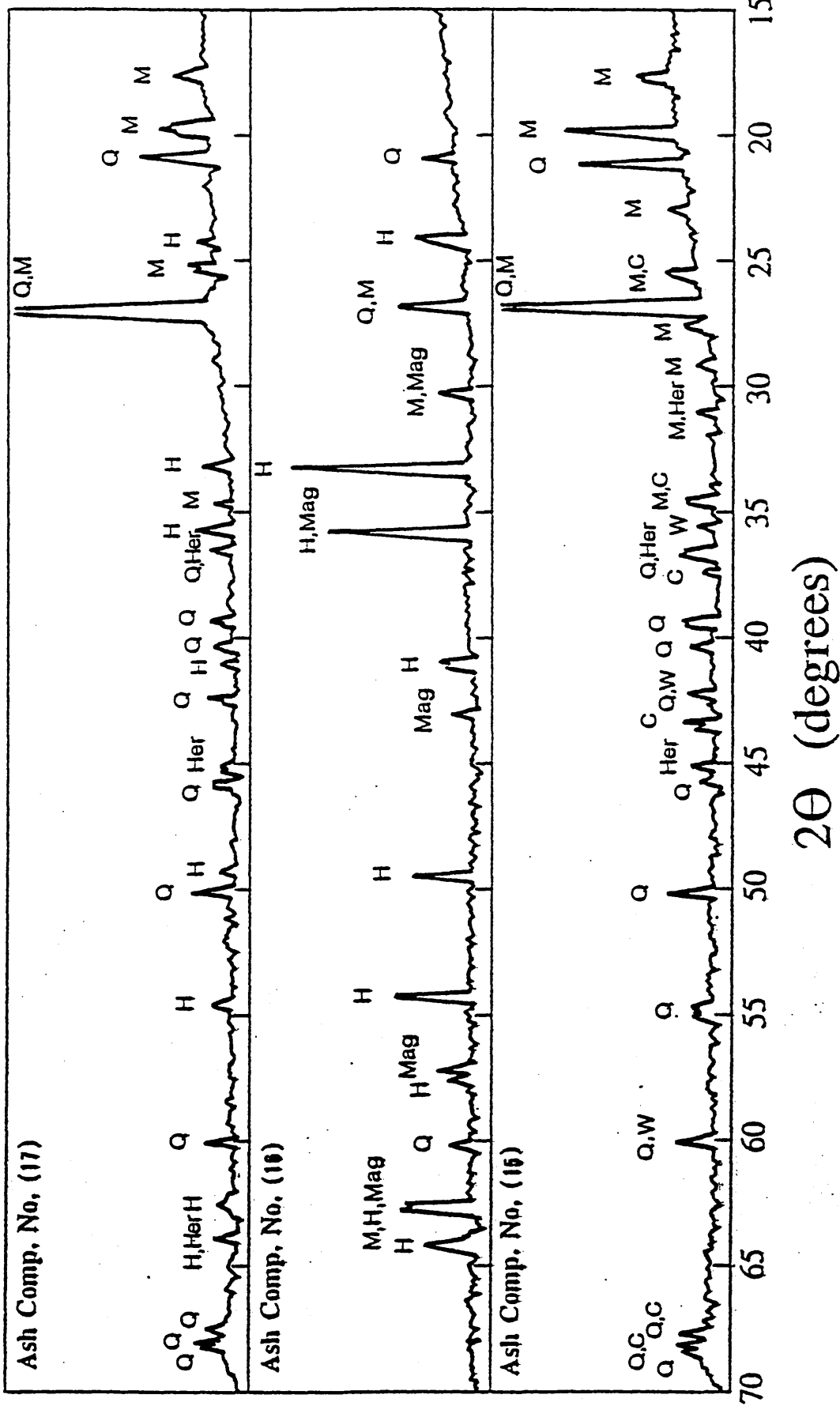


Figure 4-21: X-ray diffraction spectra for the "basic" HTA components.

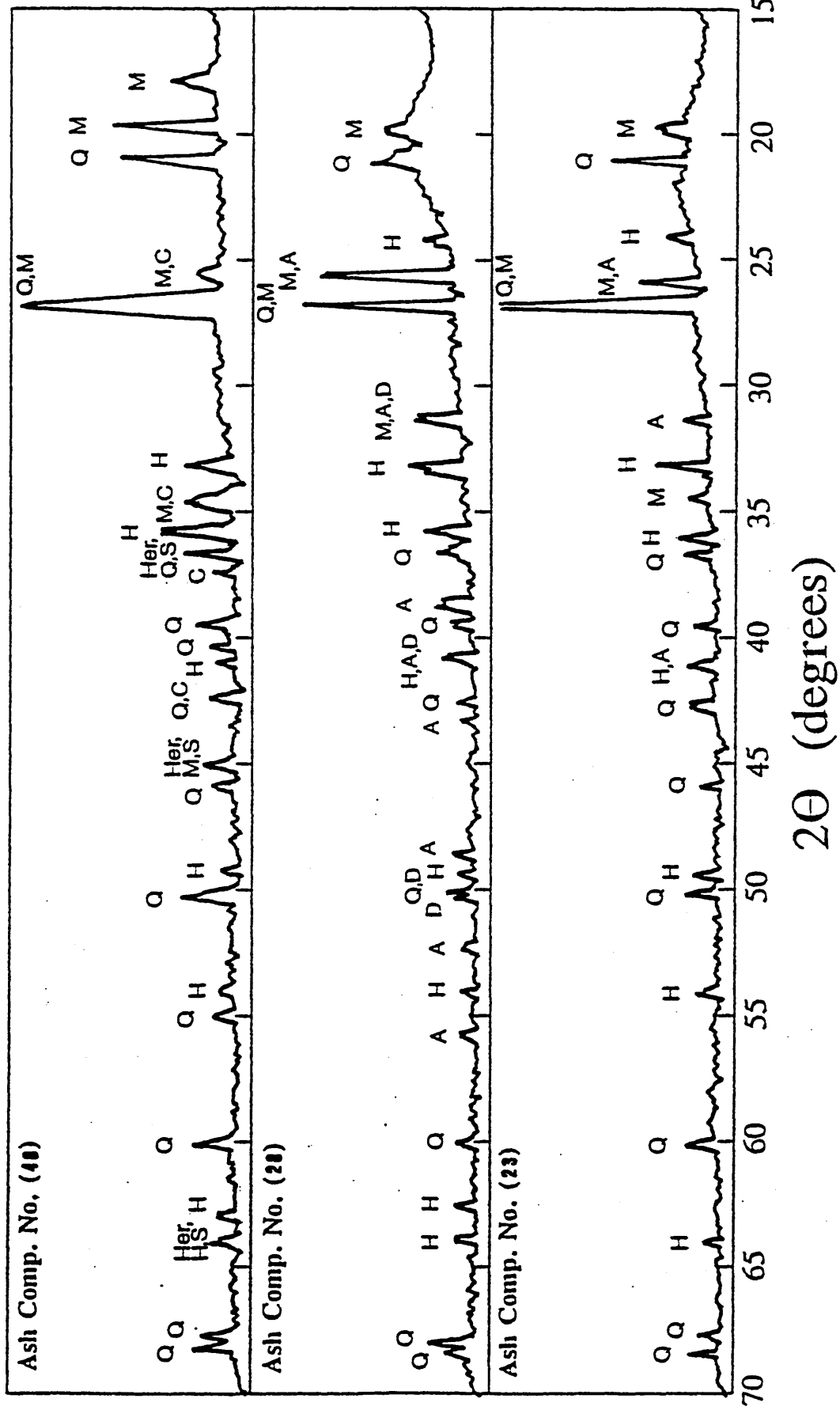


Figure 4-21: (Continued).

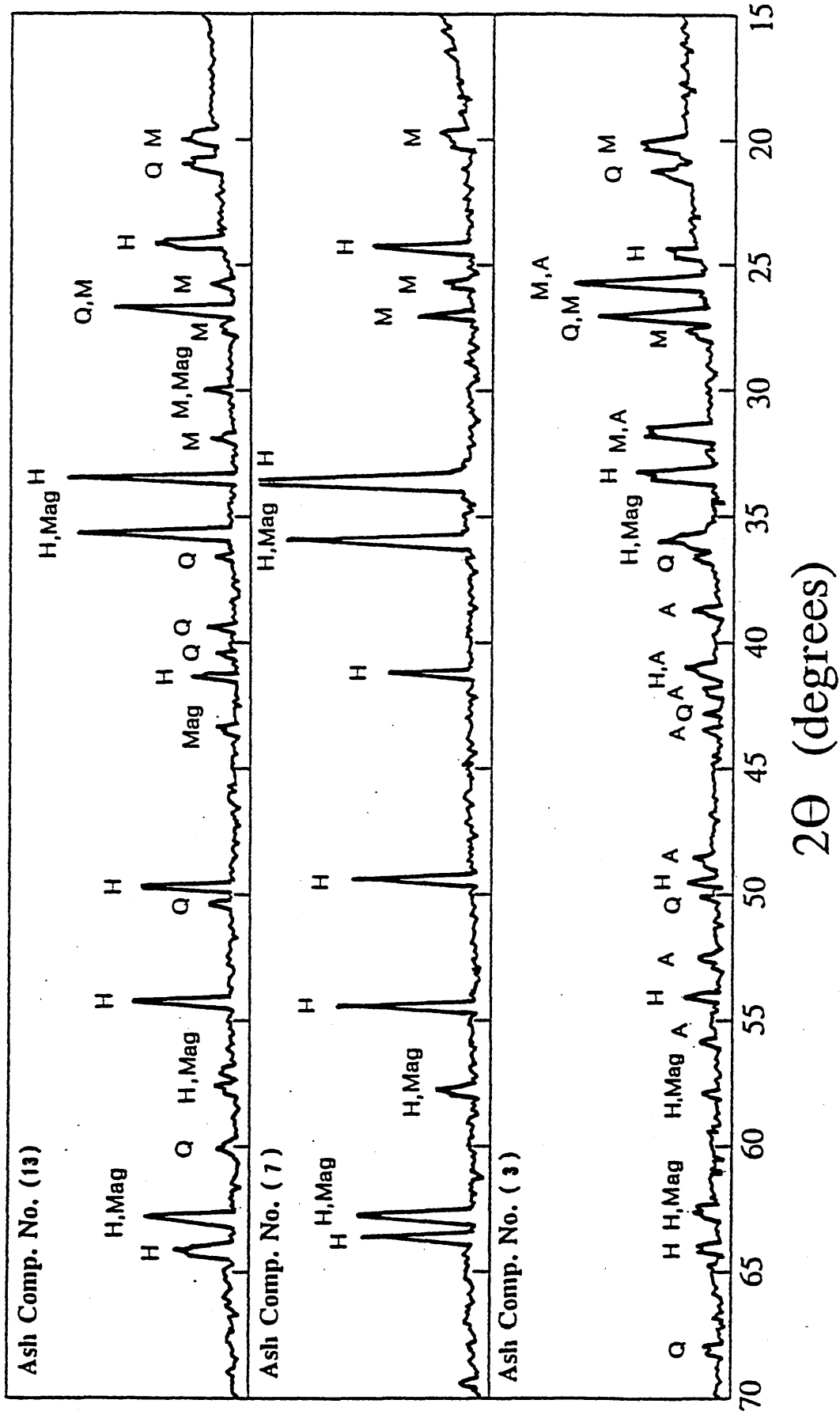


Figure 4-22: X-ray diffraction spectra for the "ferriferous" HTA components.

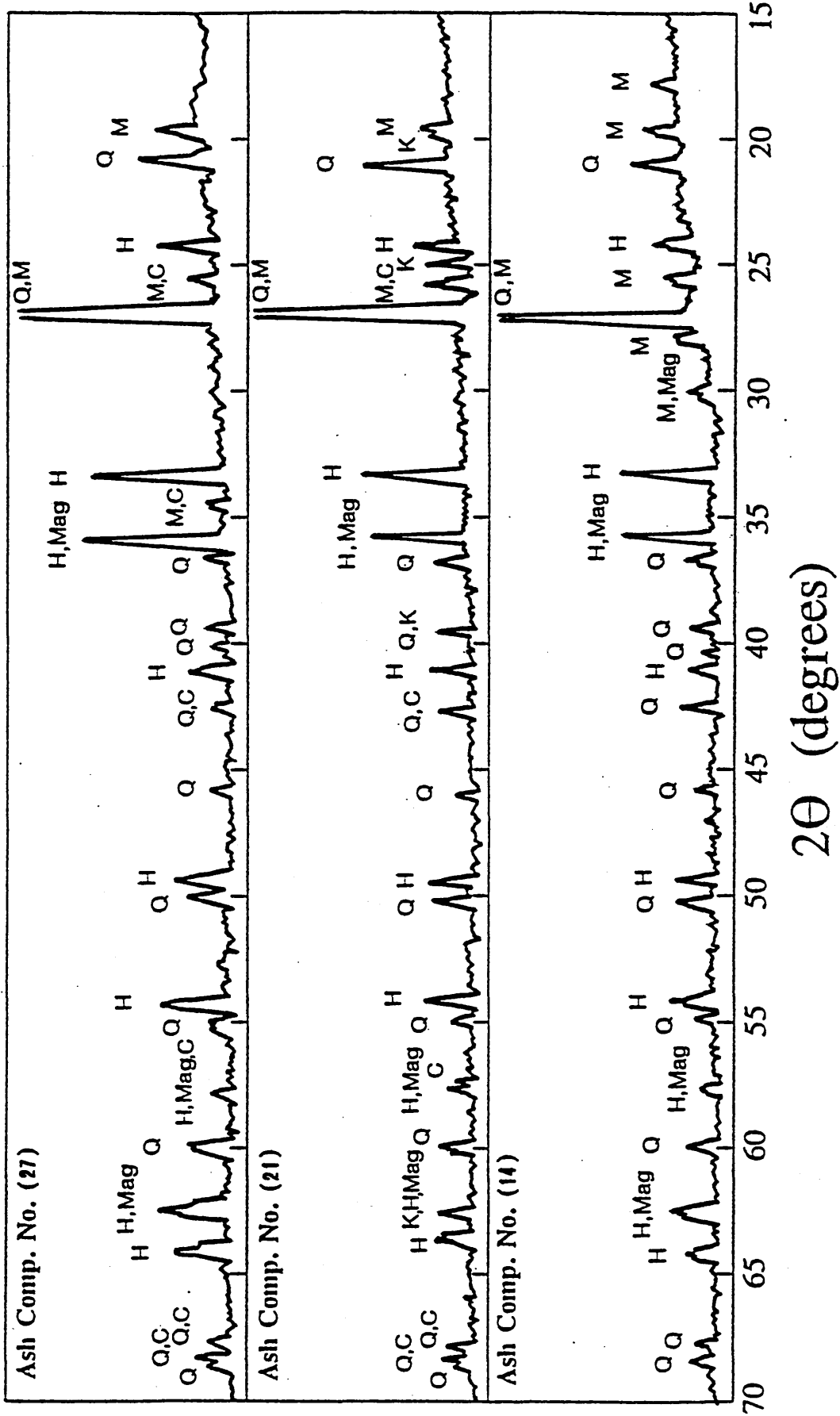


Figure 4-22: (Continued).

Minerals (Symbol)	Formula	LTA	HTA	Deposit
Silicates:				
Quartz (Q)	SiO ₂	●	●	
Cristobalite (αCs.)	SiO ₂			●
Mullite (Mul)	3Al ₂ O ₃ ·2SiO ₂			●
Sillimanite (Sil)	Al ₂ SiO ₅			○
Anorthite (An)	CaAl ₂ Si ₂ O ₈			○
Clays:				
Kaolinite (K)	Al ₂ Si ₂ O ₅ (OH) ₄	●	○	
Illite (I)	(K,H ₃ O)Al ₂ Si ₃ AlO ₁₀ (OH) ₂	●		
Chlorite (Cl)	Mg ₅ Al(AlSi ₃ O ₁₀)(OH) ₈	●		
Muscovite (M)	KAl ₂ (Si ₃ AlO ₁₀)(OH) ₂	●		
Sulphides:				
Pyrite (P)	FeS ₂	●		
Carbonates:				
Calcite (C)	CaCO ₃	●		
Dolomite (D)	(Ca,Mg)CO ₃	●	○	
Ankerite (Ank)	(Ca,Fe,Mg)CO ₃	○		
Sulphates:				
Anhydrite (A)	CaSO ₄	●	●	
Jarosite (J)	KFe ₃ (SO ₄) ₂ (OH) ₆	●		
Iron Sulphate (IS)	Fe ₂ (SO ₄) ₃	○		
Oxides:				
Hematite (H)	α-Fe ₂ O ₃		●	●
Magnetite (Mag)	Fe ₃ O ₄		●	○
Wustite (W)	FeO		○	○
Hercynite (Her)	FeO·Al ₂ O ₃		●	●
Corundum (Cor)	α-Al ₂ O ₃		●	○
Spinel (S)	MgAl ₂ O ₄		○	
Rutile (R)	TiO ₂	○	○	
Calcium Aluminate(Ca.mAl.)	CaAl ₂ O ₄			○
Chlorides:				
Halite (Hal)	NaCl	○		
Others:				
Glass	-			?
Unknown (U)	-			?

Note: ●, Major phases:(LTA > 2 d-spacing values-HTA components > 6 occurrences in the 24 separated ash components - Deposit is the deposit samples from batches No.2 and 3 > 6 occurrences in the 17 samples analysed).

○, Minor phases:(LTA < 2 d-spacing values-HTA components < 6 occurrences in the 24 separated ash components - Deposit < 6 occurrences in the 17 samples analysed).

particularly those designated within the "acidic" category in Figure 4-20, that a large fraction of the minerals transformed into undetectable amorphous phases.

Despite physical, textural and chemical variations for the reviewed ash components, presence of the same group of minerals are in evidence through similar diffraction spectra. For example; ash component numbers 3, 23, 24 and 33 were found to be mainly comprised of quartz (SiO_2), muscovite [$\text{K}_2\text{Al}_4(\text{Si}_6\text{Al}_2\text{O}_{20})(\text{OH})_4$], hematite($\alpha\text{-Fe}_2\text{O}_3$) and anhydrite (CaSO_4). Ash component numbers 13, 14 and 16 were found to be comprised of quartz, muscovite, hematite and magnetite (Fe_3O_4). Ash component numbers 6, 11 and 17 were found to be comprised of quartz, muscovite, hematite and hercynite ($\text{FeO}.\text{Al}_2\text{O}_3$).

4.7.4 Softening Characteristics of Selected Coal Ash Components With and Without Additions of Lycal 93HS

Separated ash components which had met the selection criteria specified in Section 3.4.2 were further investigated for their softening characteristics using both cone fusion and hot-stage microscopy techniques. In addition, samples of high and low temperature ashes (HTA & LTA) from the Ayrshire coal sample were also investigated using hot-stage microscopy.

4.7.4 (a) Cone-Fusion Investigation

Table 4-53 summarises the results of the cone fusion tests carried out on undoped and Lycal 93HS doped ash component samples. It is evident that the majority of the separated ash components did not exhibit any degree of softening. This was consistent with their respective chemical compositions. The ash components with relatively larger Fe_2O_3 and/or CaO contents were more readily softened and melted. The effect of a 0.5 mass% addition of Lycal 93HS on the softening characteristics

Table 4-55: Result of the cone-fusion tests for the selected ash component cone samples with and without Lycal 93HS addition.

ASH COMP. NO.	NO LYCAL 93HS				0.5% LYCAL 93HS			
	SOFTENING TEMPERATURE (°C)				SOFTENING TEMPERATURE (°C)			
	IDT	ST	HT	FT	IDT	ST	HT	FT
1	>1450	-	-	-	>1450	-	-	-
2	>1450	-	-	-	>1450	-	-	-
3	1343	-	1368	1385	1346	1366	1420	>1450
4	>1450	-	-	-	>1450	-	-	-
5	>1450	-	-	-	>1450	-	-	-
6	>1450	-	-	-	>1450	-	-	-
7	1411	>1450	-	-	1380	1438	>1450	-
10	>1450	-	-	-	>1450	-	-	-
11	>1450	-	-	-	>1450	-	-	-
13	1286	-	1319	1334	1301	1313	1328	1338
14	1392	1439	>1450	-	1386	1432	>1450	-
15	>1450	-	-	-	>1450	-	-	-
16	1388	1420	>1450	-	1371	1399	1438	>1450

Table 4-53: (Continued)

ASH COMP. NO.	NO LYCAL 93HS				0.5% LYCAL 93HS			
	SOFTENING TEMPERATURE (°C)				SOFTENING TEMPERATURE (°C)			
	IDT	ST	HT	FT	IDT	ST	HT	FT
17	>1450	-	-	-	>1450	-	-	-
21	1364	1395	1420	>1450	1357	1389	1425	>1450
23	>1450	-	-	-	>1450	-	-	-
24	>1450	-	-	-	>1450	-	-	-
25	>1450	-	-	-	>1450	-	-	-
27	1310	1332	1359	1392	1319	1341	-	1398
28	1405	1428	1433	1449	1408	-	1431	1446
29	>1450	-	-	-	>1450	-	-	-
30	>1450	-	-	-	>1450	-	-	-
32	>1450	-	-	-	>1450	-	-	-
33	>1450	-	-	-	>1450	-	-	-
35	1432	>1450	-	-	1424	>1450	-	-
38	>1450	-	-	-	>1450	-	-	-
43	>1450	-	-	-	>1450	-	-	-
46	>1450	-	-	-	>1450	-	-	-
48	1418	>1450	-	-	1410	>1450	-	-

of the ash components was found to be inconsistent, in some cases promoting softening and melting, in others inhibiting it. This single addition of 0.5 mass% is compatible with the actual amount available for reaction within the boiler atmosphere, as calculated below, based on the information provided by Steetley personnel¹⁷¹, concerning Lycal 93HS injection trials at West Belfast power station:

Rate of Lycal 93HS injection is: 5 Kg / hr \equiv 0.05 mass% of fuel consumed,

$$\begin{aligned} \therefore \text{Hourly rate of fuel consumption is: } & \frac{5 \times 100}{0.05} = 10,000 \text{ Kg / hr} \\ & = 10 \text{ tonnes / hr} \end{aligned}$$

$$\therefore \text{Amount of Lycal 93HS per tonne of coal per hour is: } \frac{5}{10} = 0.5 \text{ Kg / tonne, hr}$$

At 66.7% purity of MgO in Lycal 93HS;

$$\begin{aligned} \therefore 0.5 \text{ Kg of Lycal 93HS is: } & \equiv \frac{66.7}{100} \times 0.5 \\ & = 0.3335 \text{ Kg MgO} \end{aligned}$$

Hence, considering 10 mass% ash content in the coal;

$$\begin{aligned} \text{The ash yield from 1 tonne of coal is: } & = \frac{1000 \times 10}{100} \\ & = 100 \text{ Kg} \end{aligned}$$

$$\begin{aligned} \therefore \text{The mean MgO content present within the boiler for} & \\ \text{reaction due to Lycal 93HS injection should be: } & = \frac{0.3335}{100} \times 100 \\ & = 0.3335 \text{ mass\% MgO} \end{aligned}$$

The effect of Lycal 93HS addition on decreasing the softening and melting temperatures of ash component numbers 7, 14, 21 and 28 was in agreement with the previous observations of the softening and melting behaviour of deposit samples and ash admixtures of similar composition. However the inhibitive influence

of Lycal 93HS on the softening and melting temperatures of certain ash components was unexpected. This latter phenomenon was evidently associated with those ash components which had Fe_2O_3 contents, in the range of 15% to 40%, such as ash components number 3, 13 and 27.

4.7.4 (b) Hot-stage Microscopic Investigation

The effect of additions of Lycal 93HS in the range of 0 - 10 mass% on the various stages of the softening process as well as the crystallisation behaviour on cooling, from the fluid melt, of the selected ash components, the HTA and LTA samples are summarised in Tables 4-54 to 4-74. It is evident from these observations as depicted in the following plates that in the iron enriched ash components No. 3, 7, 13 and 27, additions of only 1 mass% and for No. 21 an addition of 3 mass% Lycal 93HS was sufficient to cause the formation and growth of crystalline needles over the surface of the molten ash components. These observations are presented in Plates 4-76, 4-80, 4-84, 4-87 and 4-85 (b) - (c) respectively. However, in the case of other selected ash components, additions of 5 mass% and 10 mass% were necessary to cause crystallisation of their fluid melts. These observations are presented in Plates 4-75 (a) - (c), 4-77 (a) - (d), 4-79 (a) - (f), 4-81, 4-82 (a) - (d), 4-83 (a) - (d).

Plates 4-74 (a)-(c) are generally representative of the fully softened, fully molten and fluid stages respectively, of an ash component sample being heated within the thermocouple junction of the hot-stage microscope's furnace cell.

Plates 4-75 (a)-(c) show the consecutive stages in the transformation of the fluid ash component No.(1) after 15 minutes, containing 10 mass% Lycal 93HS.

Plate 4-76 shows the formation and growth of fine needles from the viscous fluid melt of ash component No.(3) after 20 minutes, containing 1 mass% Lycal 93HS.

Table 4-54: Hot-stage microscopic observation of softening and crystallisation behaviour of ash component No.(1) without and with additions of Lycal 93HS.

ASH COMPONENT NO. (1)				
Lycal (%)	Run No.	Melt. Temp.(°C)	Crystal. Temp.(°C)	Observations
0	1	1600	-	No trace of softening.
1	1	1600	-	No trace of softening.
3	1	1588	-	Traces of softening near thermocouple tip.
5	1	1440	-	Formation of a molten layer near thermocouple wires-softened tip.
	2	1500	-	Extended fluid melt on thermocouple wires-fully softened bulk.
10	1	1270	-	Initiation of softening.
		1370	-	Partially molten bulk.
		1450	-	Fully molten bulk.
		1550	-	Formation of a viscous fluid.
	2	1600	1400	Formation of very fine crystals. after 15 minutes, filling the melt.
	3	1600	1200	No change.
4	1600	1000	No change.	

Table 4-55: Hot-stage microscopic observation of softening and crystallisation behaviour of ash component No.(2) with and without additions of Lycal 93HS.

ASH COMPONENT NO. (2)				
Lycal (%)	Run No.	Melt. Temp.(°C)	Crystal. Temp.(°C)	Observations
0	1	1580	-	Very small trace of softening.
1	1	1560	-	Very small trace of softening.
3	1	1400	-	Restricted trace of softening.
5	1	1260	-	Initiation of softening.
		1400	-	Partial softening of the bulk.
		1550	-	Extended softening of the bulk.
10	1	1300	-	Trace of softening-sample tilted.
		1400	-	Partial softening & bond formation.
		1500	-	Partially molten bulk.
		1600	-	Fully molten bulk.

Table 4-56: Hot-stage microscopic observation of softening and crystallisation behaviour of ash component No.(3) with and without additions of Lycal 93HS.

ASH COMPONENT No. (3)				
Lycal (%)	Run No.	Melt. Temp.(°C)	Crystal. Temp.(°C)	Observations
0	1	1215	-	Initiation of bulk softening.
		1310	-	Partially molten bulk.
		1340	-	Fully molten bulk.
		1370	-	Onset of fluidity-viscous flow.
	2	1400	-	Fully fluid bulk-free flow.
		3	1450	1300
			1450	1150
1	1	1240	-	Initiation of softening.
		1280	-	Fully molten bulk.
		1320	-	Formation of a viscous fluid.
	2	1450	1350	Formation and growth of fine needle.
		3	1450	1150
3	1	1255	-	Initiation of softening.
		1330	-	Fully molten bulk.
		1380	-	Fully fluid-free flow.
	2	1550	1350	No change after 30 minutes.
		3	1550	1150
5	1	1270	-	Initiation of softening.
		1300	-	Full softening & bond formation.
		1370	-	Fully molten bulk.
		1400	-	Fully fluid-free flow.
	2	1550	1350	No change after 30 minutes.
		3	1550	1150
10	1	1160	-	Initiation of softening.
		1240	-	Fully softened bulk.
		1280	-	Fully molten bulk.
		1310	-	Fully fluid-viscous flow.
		1370	-	Fully fluid-free liquid flow.
	2	1550	1350	No change after 30 minutes.
		3	1550	1150

Table 4-57: Hot-stage microscopic observation of softening and crystallisation behaviour of ash component No.(4) with and without additions of Lycal 93HS.

ASH COMPONENT No. (4)				
Lycal (%)	Run No.	Melt. Temp.(°C)	Crystal. Temp.(°C)	Observation
0	1	1600	-	No trace of softening.
1	1	1310	-	Very limited trace of softening.
		1590	-	Fully softened bulk.
3	1	1350	-	Initiation of softening-bonding of ash to the thermocouple wire.
		1560	-	Formation of viscous melt next to the thermocouple surface.
		1600	-	Fully softrened bulk.
5	1	1360	-	partial softening of the bulk.
		1560	-	Fully softened bulk.
		1600	-	Extensive mlting of the bulk.
10	1	1290	-	Partial softening-restricted bondage between ash & wire surface.
		1385	-	Formation of a molten bulk.
		1480	-	Formation of a free flowing liquid.
	2	1600	1300	No change after 30 minutes.
	3	1600	1100	No change after 30 minutes.

Table 4-58: Hot-stage microscopic observation of softening and crystallisation behaviour of ash component No.(5) with and without additions of Lycal 93HS.

ASH COMPONENT No. (5)				
Lycal (%)	Run No.	Melt. Temp.(°C)	Crystal. Temp.(°C)	Observation
0	1	1500 1600	- -	Initiation of softening. No change.
1	1	1420 1540	- -	Limited softening & bonding between ash & thermocouple wire. Partial softening of the bulk.
3	1	1260 1340 1480 1600	- - - -	Limited softening & bonding between ash & thermocouple wire. Fully softened. Fully molten. Partial fluidity.
5	1	1312 1420 1590	- - -	Initiation of softening. Fully softened bulk-limited bonding between ash and thermocouple wire. Partially molten bulk.
10	1	1270 1360 1458 1510	- - - -	Initiation of softening. Extensive softening of the bulk. Fully molten bulk. Fully fluid-free flow.
	2	1600	1400	Inter-crossing formation of fine lath-like stacks of crystals after 2-5 seconds, growing conically.Full
	3	1600	1350	crystalisation of melt after 1 min. Identical to previous run-slower
	4	1600	1300	formation & growth of crystals. Similar but slower recurrence and growth of crystals as observed in previous runs.

Table 4-59: Hot-stage microscopic observation of softening and crystallisation behaviour of ash component No.(6) with and without additions of Lycal 93HS.

ASH COMPONENT No. (6)				
Lycal (%)	Run No.	Melt. Temp(°C)	Crystal. Temp(°C)	Observation
0	1	1350	-	Initiation of softening.
		1480	-	Fully softened bulk.
		1600	-	No change.
1	1	1350	-	Initiation of softening.
		1470	-	Fully softened bulk.
		1600	-	No change.
3	1	1330	-	Initiation of softening.
		1417	-	Fully softened bulk.
		1480	-	Fully molten bulk.
		1575	-	Fully fluid-free flow.
	2	1600	1350	No change after 30 minutes.
3	1600	1200	No change after 30 minutes.	
5	1	1220	-	Initiation of softening.
		1370	-	Fully softened bulk.
		1410	-	Fully molten bulk.
		1485	-	Formation of fluid-free flow.
	2	1550	1350	Formation of Large laths across the melt & finer laths from the tip of thermocouple towards the centre after a few minutes.
	3	1550	1200	As before with further extension of finer laths from all corners of the melt towards the centre.
4	1550	1100	Limited formation of fine laths.	
10	1	1235	-	Fully softened bulk.
		1360	-	Fully molten bulk.
		1418	-	Formation of fluid-free flow.
	2	1550	1400	Large & smaller laths growing from the top to the bottom of the melt after 2 minutes. Little growth after 75 minutes.
	3	1550	1300	Formation and growth of laths after 10 seconds. Further formation and growth of lath-like stacks crystallising the melt after 8 min.
	4	1550	1200	As above-full crystallinity- 5 min.
5	1550	1100	Limited growth of laths after 10 min.	

Table 4-60: Hot-stage microscopic observation of softening and crystallisation behaviour of ash component No.(7) with and without additions of Lycal 93HS.

ASH COMPONENT No. (7)				
Lycal (%)	Run No.	Melt. Temp(°C)	Crystal. Temp(°C)	Observation
0	1	1245	-	Initiation of softening.
		1340	-	Fully softened.
		1480	-	Fully molten.
		1516	-	Formation of fluid-free flow.
2	1600	1300	Formation and growth of fine, short needles after 30 minutes.	
	1600	1200	No change after 30 minutes.	
4	1600	1100	No change after 30 minutes.	
3	1	1260	-	Initiation of softening.
		1380	-	Fully softened bulk.
		1424	-	Fully molten bulk.
		1504	-	Formation of fluid-free flow.
2	1600	1350	Formation of white stretch marks after 20 minutes.	
	1600	1200	No change.	
5	1	1200	-	Initiation of softening.
		1350	-	Fully softened bulk.
		1450	-	Fully molten bulk.
		1540	-	Formation of fluid-free flow.
2	1600	1300	Formation of a precipitating phase after 10 minutes.	
	1600	1100	Formation of truncated laths within the melt after 20 minutes. Growth of fan type structure needles outwards from the surface of the fluid meniscus.	
10	1	1235	-	Initiation of softening.
		1270	-	Fully softened bulk.
		1450	-	Partially molten bulk.
		1600	-	Formation of a fluid-free flow after 30 minutes.
2	1600	1300	Formation and growth of bifurcating and singular needles up to 60 mins. Further formation of precipitating arrow head-like phase within melt.	
	1600	1100	As above - thickening of the needles.	

Table 4-61: Hot-stage microscopic observation of softening and crystallisation behaviour of ash component No.(11) with and without additions of Lycal 93HS.

ASH COMPONENT No. (11)				
Lycal (%)	Run No.	Melt. Temp(°C)	Crystal. Temp(°C)	Observation
0	1	1325	-	Initiation of softening.
		1470	-	Fully softened bulk.
		1600	-	No further change.
1	1	1350	-	Initiation of softening.
		1550	-	Fully softened bulk.
		1600	-	No further change.
3	1	1250	-	Initiation of softening.
		1440	-	Formation of restricted bonds between the softened ash and thermocouple wire.
		1600	-	No further change.
5	1	1280	-	Initiation of softening.
		1547	-	Fully softened bulk.
		1600	-	Fully molten bulk-partial fluidity.
10	1	1250	-	Initiation of softening.
		1460	-	Fully molten bulk.
		1525	-	Formation of a fluid-viscous flow.
		1580	-	Formation of liquid-free flow.
	2	1600	1350	No change after 30 minutes.
	3	1600	1150	No change after 30 minutes.

Table 4-62: Hot-stage microscopic observation of softening and crystallisation behaviour of ash component No.(13) with and without additions of Lycal 93HS.

ASH COMPONENT No. (13)					
Lycal (%)	Run No.	Melt. Temp(°C)	Crystal. Temp(°C)	Observation	
0	1	1190	-	Initiation of softening.	
		1280	-	Fully softened bulk.	
		1350	-	Fully molten bulk.	
		1405	-	Formation of a fluid-free flow.	
	2	1550	1300	Formation of needles after 15 min.	
				Further formation of arrow head-like phase. Growth of needles-75min.	
	3	1550	1150	Formation of smaller, thicker needles-branching after 30 minutes.	
		1	1197	-	Initiation of softening.
			1310	-	Fully softened bulk.
1360	-		Fully molten bulk.		
1410	-		Formation of a fluid-free flow.		
1550	1500		Formation of needles after 15 min.		
3	1550	1350	Formation of arrow head-like phase Further branching of needles.		
3	1	1160	-	Initiation of softening.	
		1230	-	Fully molten bulk.	
		1285	-	Formation of fluid-free flow.	
	2	1500	1450	No change after 30 minutes.	
		1500	1350	No change after 30 minutes.	
		1500	1150	No change after 30 minutes.	
5	1	1100	-	Initiation of softening.	
		1130	-	Fully softened bulk.	
		1220	-	Fully molten bulk.	
		1290	-	Formation of fluid-viscous flow.	
		1340	-	Formation of fluid-free flow.	
	2	1450	1350	No change after 30 minutes.	
		1450	1150	No change after 30 minutes.	
		10	1	1180	-
1235	-			Fully molten bulk.	
1365	-			Formation of fluid-free flow.	
2	1500		1350	No change after 30 minutes.	
	3		1500	1150	No change after 30 minutes.

Table 4-63: Hot-stage microscopic observation of softening and crystallisation behaviour of ash component No.(14) with and without additions of Lycal 93HS.

ASH COMPONENT No. (14)					
Lycal (%)	Run No.	Melt. Temp (°C)	Crystal. Temp (°C)	Observation	
0	1	1220	-	Initiation of softening.	
		1335	-	Partially molten bulk.	
	2	1400	-	Fully fluid bulk.	
		1500	1350	No change after 30 minutes.	
3	1500	1150	No change after 30 minutes.		
	1	1120	-	Initiation of softening.	
3	1	1260	-	Fully molten bulk.	
		1350	-	Formation of fluid-viscous flow.	
		1400	-	Formation of fluid-free flow.	
		1500	1350	No change after 30 minutes.	
	2	1500	1150	Formation of white colour angular particles suspended within melt.	
		1	1075	-	Initiation of softening.
		1200	-	Fully softened bulk.	
5	1	1360	-	Fully molten bulk.	
		1410	-	Formation of fluid-viscous flow.	
		1550	-	No change.	
		1600	1350	No change after 30 minutes.	
	2	1600	1150	No change after 30 minutes.	
		1	1125	-	Initiation of softening.
10	1	1200	-	Fully softened bulk.	
		1275	-	Fully molten bulk.	
		1300	-	Formation of fluid-free flow.	
		1400	1350	No change after 30 minutes.	
	2	1440	1150	No change after 30 minutes.	

Table 4-64: Hot-stage microscopic observation of softening and crystallisation behaviour of ash component No.(21) with and without additions of Lycal 93HS.

ASH COMPONENT No. (21)				
Lycal (%)	Run No.	Melt. Temp (°C)	Crystal. Temp (°C)	Observation
0	1	1180	-	Initiation of softening.
		1285	-	Fully softened bulk.
		1380	-	Fully molten bulk.
		1420	-	Formation of fluid-free flow.
	2	1500	1300	Formation and growth of fine and large needles after 15 minutes.
		1500	1150	As above-limited branching of fine needles.Presence of a second phase as stretched and truncated laths.
1	1	1170	-	Initiation of softening.
		1300	-	Fully softened bulk.
		1350	-	Fully molten bulk.
		1405	-	Formation of fluid-free flow.
	2	1450	1300	No change after 30 minutes.
		1450	1150	No change after 30 minutes.
3	1	1205	-	Initiation of softening.
		1280	-	Fully softened bulk.
		1350	-	Fully molten bulk.
		1415	-	Formation of fluid-free flow.
	2	1500	1300	Formation and growth of fine needles after 30 minutes.
		1500	1150	As above.
5	1	1215	-	Initiation of softening.
		1260	-	Fully softened bulk.
		1305	-	Fully molten bulk.
		1485	-	Formation of fluid-free flow.
	2	1500	1300	Formation of thick,short needles after 17 minutes.
		1500	1150	As above-branching of some needles.
10	1	1235	-	Initiation of softening.
		1280	-	Fully softened bulk.
		1360	-	Fully molten bulk.
		1450	-	Formation of fluid-free flow.
	2	1500	1300	Formation of fine needles after 15 minutes. Expansion of tips by time.
		1500	1150	As above-No change after 30 min.

Table 4-65: Hot-stage microscopic observation of softening and crystallisation behaviour of ash component No.(27) with and without additions of Lycal 93HS.

ASH COMPONENT No. (27)				
Lycal (%)	Run No.	Melt. Temp.(°C)	Crystal. Temp.(°C)	Observation
0	1	1130	-	Initiation of softening.
		1250	-	Fully softened bulk.
		1330	-	Fully molten bulk.
		1420	-	Formation of fluid-free flow.
	2	1500	1300	No change after 30 minutes.
3	1500	1100	No change after 30 minutes.	
1	1	1110	-	Initiation of softening.
		1240	-	Fully softened bulk.
		1280	-	Fully molten bulk.
		1330	-	Formation of fluid-free flow.
	2	1400	1300	No change after 30 minutes.
3	1400	1100	Formation of very fine, small needles after 20 minutes.	
3	1	1265	-	Fully softened bulk.
		1330	-	Fully molten bulk-partially fluid.
		1380	-	Formation of fluidity-viscous flow.
		1400	-	Partial evaporation of melt.
	2	1380	1300	No change after 30 minutes.
3	1380	1100	No change after 30 minutes.	
5	1	1250	-	Sudden formation of partially molten bulk.
		1355	-	Fully molten bulk.
		1370	-	Formation of fluid-viscous flow.
		1400	-	Evaporation of melt.
	2	1380	1300	No change after 30 minutes.
3	1380	1100	No change after 30 minutes.	
10	1	1170	-	Partial softening of the bulk.
		1305	-	Fully molten bulk.
		1348	-	Formation of fluid-free flow.
		1400	-	Evaporation of fluid melt.
	2	1350	1300	No change after 30 minutes.
3	1350	1100	Formation of very fine needles after 40 minutes.	

Table 4-66: Hot-stage microscopic observation of softening and crystallisation behaviour of ash component No.(28) with and without additions of Lycal 93HS.

ASH COMPONENT No. (28)				
Lycal (%)	Run No.	Melt. Temp.(°C)	Crystal. Temp.(°C)	Observation
0	1	1120	-	Initiation of softening.
		1230	-	Fully softened bulk.
		1330	-	Fully molten bulk.
		1450	-	Formation of fluid-viscous flow.
		1600	-	No change.
	2	1600	1300	No change after 30 minutes.
3	1600	1100	No change after 30 minutes.	
1	1	1220	-	Initiation of softening.
		1310	-	Fully molten bulk.
		1390	-	Formation of fluid-free flow.
	2	1450	1300	No change after 30 minutes.
	3	1450	1100	No change after 30 minutes.
3	1	1240	-	Initiation of softening.
		1370	-	Fully molten bulk.
		1540	-	Partial fluidity-visous flow.
	2	1600	1300	No change after 30 minutes.
	3	1600	1100	No change after 30 minutes.
5	1	1210	-	Partial softening of the bulk.
		1310	-	Fully molten bulk.
		1340	-	Formation of fluid-viscous flow.
		1400	-	Formation of fluid-free flow.
	2	1450	1300	No change after 30 minutes.
	3	1450	1100	No change after 30 minutes.
10	1	1200	-	Initiation of softening.
		1240	-	Fully softened bulk.
		1280	-	Fully molten bulk.
		1340	-	Formation of fluid-free flow.
	2	1400	1300	No change after 30 minutes.
	3	1400	1100	No change after 30 minutes.

Table 4-67: Hot-stage microscopic observation of softening and crystallisation behaviour of ash component No.(29) with and without additions of Lycal 93HS.

ASH COMPONENT No. (29)				
Lycal (%)	Run No.	Melt. Temp.(°C)	Crystal. Temp.(°C)	Observation
0	1	1205	-	Initiation of softening.
		1300	-	Fully softened bulk.
		1550	-	Partially molten bulk.
1	1	1490 1550	- -	Initiation of softening. No further change.
3	1	1380 1550	- -	Initiation of softening. No further change.
5	1	1330 1550	- -	Initiation of softening. Fully softened bulk.
10	1	1200	-	Initiation of softening.
		1410	-	Fully softened bulk.
		1470	-	Fully molten bulk.
		1500	-	Formation of fluid-free flow.
	2	1550	1300	No change after 30 minutes.
3	1550	1100	No change after 30 minutes.	

Table 4-68: Hot-stage microscopic observation of softening and crystallisation behaviour of ash component No. (30) with and without additions of Lycal93HS.

ASH COMPONENT No. (30)				
Lycal (%)	Run No.	Melt. Temp.(°C)	Crystal. Temp.(°C)	Observation
0	1	1310	-	Initiation of softening.
		1470	-	Fully softened bulk.
		1550	-	Partially molten bulk.
1	1	1315	-	Initiation of softening.
		1480	-	Fully softened bulk.
		1550	-	Partially molten bulk.
3	1	1340	-	Initiation of softening.
		1480	-	Fully softened bulk.
		1550	-	Fully molten bulk.
5	1	1360	-	Initiation of softening.
		1430	-	Fully softened bulk.
		1500	-	Fully molten bulk.
		1550	-	Formation of fluid-viscous flow.
	2	1600	1300	No change after 30 minutes.
3	1600	1100	No change after 30 minutes.	
10	1	1260	-	Initiation of softening.
		1300	-	Fully softened bulk.
		1400	-	Fully molten bulk.
		1440	-	Formation of fluid-free flow.
	2	1500	1300	No change after 30 minutes.
	3	1500	1100	No change after 30 minutes.

Table 4-69: Hot-stage microscopic observation of softening and crystallisation behaviour of ash component No. (32) with and without additions of Lycal 93HS.

ASH COMPONENT No. (32)				
Lycal (%)	Run No.	Melt. Temp.(°C)	Crystal. Temp.(°C)	Observation
0	1	1300	-	Initiation of softening.
		1460	-	Fully softened bulk.
		1550	-	No change.
1	1	1300	-	Initiation of softening.
		1445	-	Fully softened bulk.
		1550	-	No change.
3	1	1320	-	Initiation of softening.
		1420	-	Fully softened bulk. "Neck" growth between the softened ash at the top and bottom thermocouple wires.
	2	1550	-	Formation of a glassy, shiny melt.
		1600	20	Formation of a transparent residue, confirming the vitreous nature of the softened residue.
5	1	1320	-	Initiation of softening.
	2	1550	-	Partially softened bulk.
		1600	20	Formation of some transparent parts confirming the partially vitreous nature of the residue.
10	1	1260	-	Initiation of softening.
		1360	-	Fully softened bulk.
		1465	-	Fully molten bulk.
		1540	-	Formation of fluid-viscous flow.
	2	1600	20	No transformation of the melt.

Table 4-70: Hot-stage microscopic observation of softening and crystallisation behaviour of ash component No. (33) with and without additions of Lycal 93HS.

ASH COMPONENT No. (33)				
Lycal (%)	Run No.	Melt. Temp(°C)	Crystal. Temp(°C)	Observation
0	1	1350 1450 1550	- - -	Initiation of softening. Partial softening of the bulk. No change.
	2	1600	20	Transparency of the softened parts.
1	1	1380 1550	- -	Initiation of softening. Partial softening of the bulk.
	2	1600	20	Tranparency of the softened parts.
3	1	1330 1420 1550	- - -	Initiation of softening. Partial softening of the bulk. No change.
	2	1600	20	Transparency of the softened parts.
5	1	1240 1420 1550	- - -	Initiation of softening. Fully softened bulk. Partially molten bulk.
	2	1600	20	Transparency of the softened parts.
10	1	1280 1370 1420 1515	- - - -	Initiation of softening. Fully softened bulk. Fully molten bulk. Formation of fluid-viscous flow.
	2	1600	1300	No change after 30 minutes.
	3	1600	1100	No change after 30 minutes.

Table 4-71: Hot-stage microscopic observation of softening and crystallisation behaviour of ash component No. (46) with and without additions of Lycal 93HS.

ASH COMPONENT No. (46)				
Lycal (%)	Run No.	Melt. Temp.(°C)	Crystal. Temp.(°C)	Observation
0	1	1380 1550	- -	Initiation of softening. No change.
1	1	1350 1540	- -	Initiation of softening. Partial softening of the bulk.
3	1	1340 1470 1550	- - -	Initiation of softening. Formation of bonds between separate parts of softened ash. Fully softened bulk- limited transparency of some parts.
5	1 2	1240 1450 1550 1600	- - - 20	Initiation of softening. Fully softened bulk. No change. No change-No degree of transparency
10	1 2 3	1210 1340 1380 1520 1600 1600 1600	- - - - - 1300 1100	Initiation of softening. Fully softened bulk. Fully molten bulk. Formation of fluid-viscous flow. No change. No change after 30 minutes. No change after 30 minutes.

Table 4-72: Hot-stage microscopic observation of softening and crystallisation behaviour of ash component No. (48) with and without additions of Lycal 93HS.

ASH COMPONENT No. (48)				
Lycal (%)	Run No.	Melt. Temp.(°C)	Crystal. Temp.(°C)	Observation
0	1	1240	-	Initiation of softening.
		1380	-	Fully softened bulk.
		1490	-	Fully molten bulk.
		1550	-	Formation of fluid-viscous flow.
	2	1600	1300	No change after 30 minutes.
3	1600	1100	No change after 30 minutes.	
1	1	1230	-	Initiation of softening.
		1350	-	Fully softened bulk.
		1520	-	Fully molten bulk.
		1550	-	Limited fluidity.
	1600	1300	No change after 30 minutes.	
1600	1100	No change after 30 minutes.		
3	1	1140	-	Initiation of softening.
		1310	-	Fully softened bulk.
		1400	-	Fully molten bulk.
		1480	-	Formation of fluid-free flow.
	2	1500	1300	No change after 30 minutes.
3	1500	1100	No change after 30 minutes.	
5	1	1200	-	Initiation of softening.
		1270	-	Fully softened bulk.
		1340	-	Fully molten bulk.
		1385	-	Formation of fluid-free flow.
	2	1400	1300	Formation and limited growth of fine needles after 20 minutes.
3	1400	1100	Formation and growth of a few fine needles after 15 minutes.	
10	1	1180	-	Initiation of softening.
		1270	-	Fully softened bulk.
		1315	-	Fully molten bulk.
		1360	-	Formation of fluid-free flow.
	2	1400	1300	No change after 30 minutes.
3	1400	1100	No change after 30 minutes.	

Table 4-73: Hot-stage microscopic observation of softening and crystallisation behaviour of a high-temperature ash (HTA) sample with and without additions of Lycal 93HS.

HIGH TEMPERATURE ASH (HTA)				
Lycal (%)	Run No.	Melt. Temp.(°C)	Crystal. Temp.(°C)	Observation
0	1	1250	-	Initiation of softening.
		1450	-	Fully softened bulk.
		1550	-	Partially molten bulk.
		1600	-	No further change.
1	1	1240	-	Initiation of softening.
		1430	-	Fully softened bulk.
		1510	-	Fully molten bulk.
		1600	-	No further change.
3	1	1210	-	Initiation of softening.
		1240	-	Fully softened.
		1360	-	Fully molten bulk.
		1435	-	Formation of fluid-free flow.
	2	1500	1300	No change after 30 minutes.
	3	1500	1100	No change after 30 minutes.
5	1	1200	-	Initiation of softening.
		1290	-	Fully softened bulk.
		1390	-	Fully molten bulk.
		1435	-	Formation of fluid-free flow.
	2	1500	1300	No change after 30 minutes.
	3	1500	1100	Formation and growth of two fine needles after 8 minutes.
10	1	1220	-	Fully softened bulk.
		1280	-	Fully molten bulk.
		1320	-	Formation of fluid-viscous flow.
		1370	-	Formation of fluid-free flow.
	2	1400	1300	No change after 30 minutes.
	3	1400	1100	No change after 30 minutes.

Table 4-74: Hot-stage microscopic observation of softening and crystallisation behaviour of a low-temperature ash (LTA) sample with and without additions of Lycal 93HS.

LOW TEMPERATURE ASH (LTA)				
Lycal (%)	Run No.	Melt. Temp.(°C)	Crystal. Temp.(°C)	Observation
0	1	1235	-	Initiation of softening.
		1280	-	Fully softened bulk.
		1380	-	Fully molten bulk.
		1520	-	Formation of fluid-free flow.
	2	1550	1300	No change after 30 minutes.
3	1550	1100	No change after 30 minutes.	
1	1	1220	-	Initiation of softening.
		1290	-	Fully softened bulk.
		1350	-	Fully molten bulk.
		1470	-	Formation of fluid-free flow.
	2	1500	1300	No change after 30 minutes.
3	1500	1100	No change after 30 minutes.	
3	1	1210	-	Initiation of softening.
		1330	-	Fully molten bulk.
		1420	-	Formation of fluid-free flow.
		1450	1300	No change after 30 minutes.
	3	1450	1100	No change after 30 minutes.
5	1	1200	-	Initiation of softening.
		1320	-	Fully molten bulk.
		1460	-	Formation of fluid-free flow.
		1500	1300	No change after 30 minutes.
	3	1500	1100	No change after 30 minutes.
10	1	1110	-	Initiation of softening.
		1230	-	Fully softened bulk.
		1270	-	Fully molten bulk.
		1330	-	Formation of fluid-free flow.
	2	1400	1300	No change after 30 minutes.
3	1400	1100	No change after 30 minutes.	



(a)



(b)



(c)

Plate 4-74:

Illustration of different stages of deformation for the separated ash components heated between the thermocouple wires of the hot-stage microscope: (a) softening, (b) melting, (c) fluid.

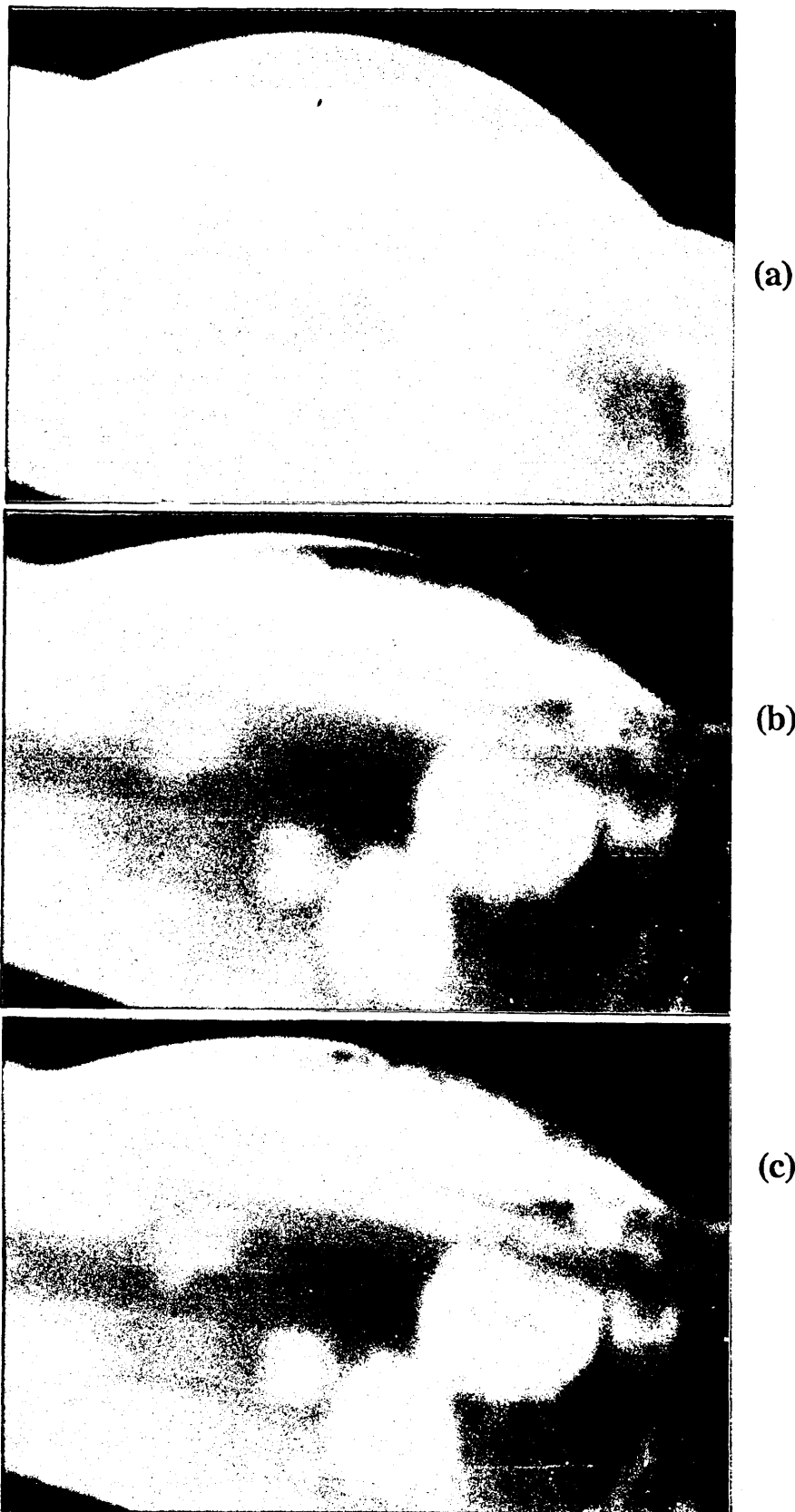


Plate 4-75:

Transformation of a drop of fluid ash component No.(1) with the addition of 10 mass% Lycal 93HS, at 1400°C: (a) fluid (b) crystallisation of fluid melt after 10 minutes, (c) crystallisation of fluid melt after 15 minutes.



Plate 4-76:

Formation and growth of fine needles from the surface of viscous fluid melt of ash component No.(3) with the addition of 1 mass% Lycal 93HS, after 20 minutes at 1350°C.

Plates 4-77 (a)-(d) show the consecutive stages in the transformation of the fluid ash component No.(5), containing 10 mass% Lycal 93HS. The formation of long, conical crystalline needles in the liquid melt was completed between 1-2 minutes depending on the crystallisation temperature. Plate 4-78 is a scanning electron micrograph of this sample, illustrating the extent of crystallisation, the crystalline phase resembling the shape of lozenges with well defined boundaries. The accompanying EDX-analysis denotes the relative enrichment of MgO in the crystalline phase, by approximately 47% compared to that found within the matrix.

Plates 4-79 (a)-(f) show the consecutive stages in the transformation of fluid ash component No.(6), when it contains 5 mass% and 10 mass% Lycal 93HS. The formation and growth of the crystalline phase was completed between 2 to 10 minutes, with the crystallisation temperatures held at 1400°C and 1100°C respectively. Plate 4-80 shows the formation of a precipitating phase within the fluid ash component No.(7) containing 1 mass% Lycal 93HS, after being kept at 1300°C for 10 minutes.

Plate 4-81 shows the formation of truncated, arrow-head like phase within the molten ash component No.(7), with additional fine needles growing outwards from the surface of the melt. Samples containing 5 mass% and 10 mass% Lycal 93HS both behaved in this way when kept at crystallisation temperatures of 1100°C and 1300°C for up to 30 minutes respectively.

Plates 4-82 (a)-(d) show the formation and growth of needles from the surface of molten ash component No.(7) containing 10 mass% Lycal 93HS. The samples were kept at 1100°C and 1300°C between 40 minutes to 2 hours. No further growth or bifurcation (branching) of needles was detected beyond this time.



(a)



(b)



(c)



(d)

Plate 4-77:

Transformation of fluid ash component No.(5) with the addition of 10 mass% Lycal 93HS, at 1400°C: (a) formation of fine conically shaped stacks of crystalline needles after 30 sec. (b) growth of the crystalline needles after 45 sec. (c) growth of the crystalline needles after 1 min. (d) fluid melt after 1 min. 30 sec.

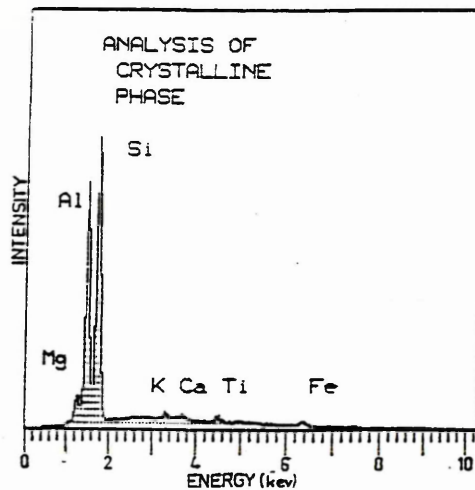
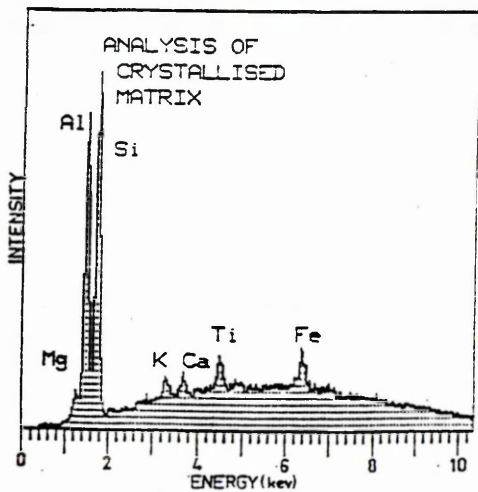
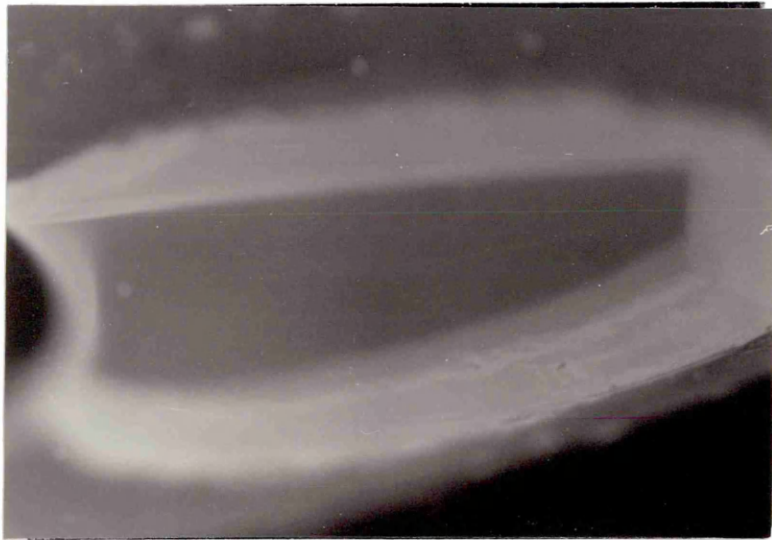


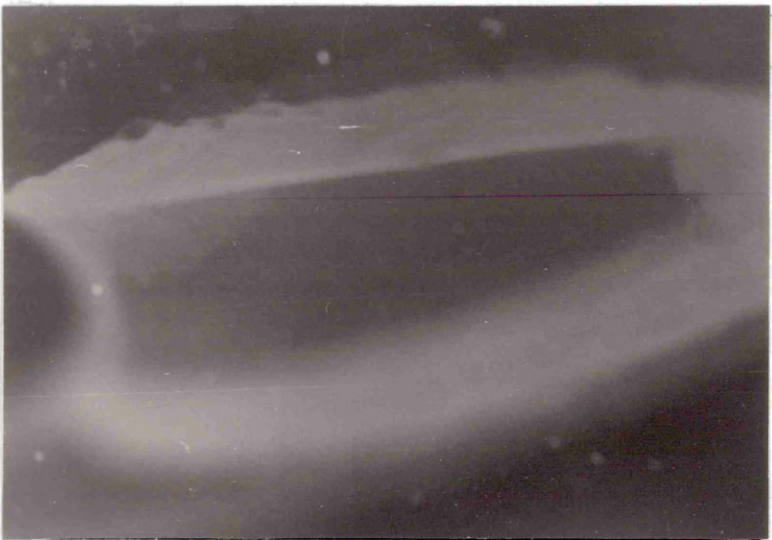
Plate 4-78:

SEM-micrograph of the fluid ash component No.(5) with the addition of 10 mass% Lycal 93HS, showing crystalline lozenges with well defined boundaries. The EDX-analyses show the composition of the matrix and crystalline phase.

[Mag: x880]



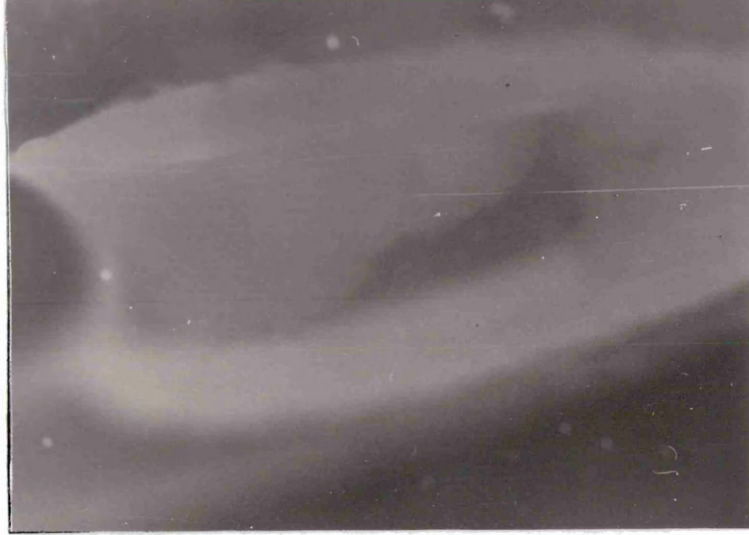
(a)



(b)



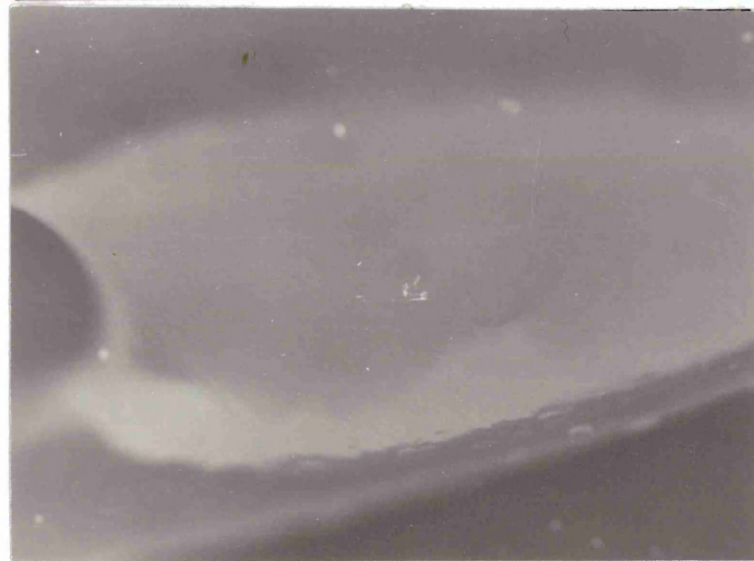
(c)



(d)



(e)



(f)

Plate 4-79:

Transformation of fluid ash component No.(6) with the additions of 5 mass% Lycal 93HS, at 1350°C: (a) fluid pool, (b) formation of crystals from the meniscus and the tip regions, (c) growth of crystals into the centre of the pool, (d) further growth of crystals, (e) conversion of the pool into a crystalline phase, (f) complete crystallisation of the fluid pool.

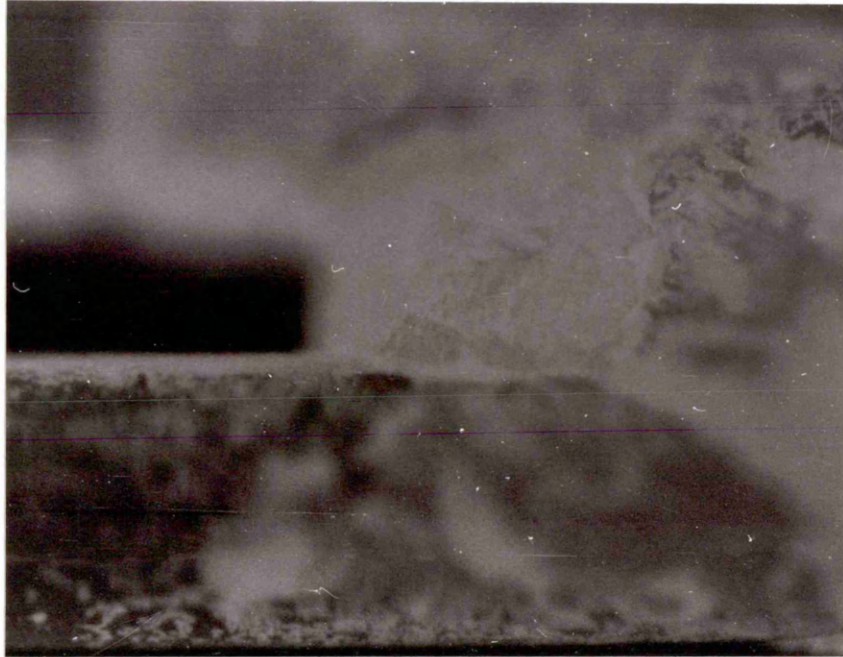


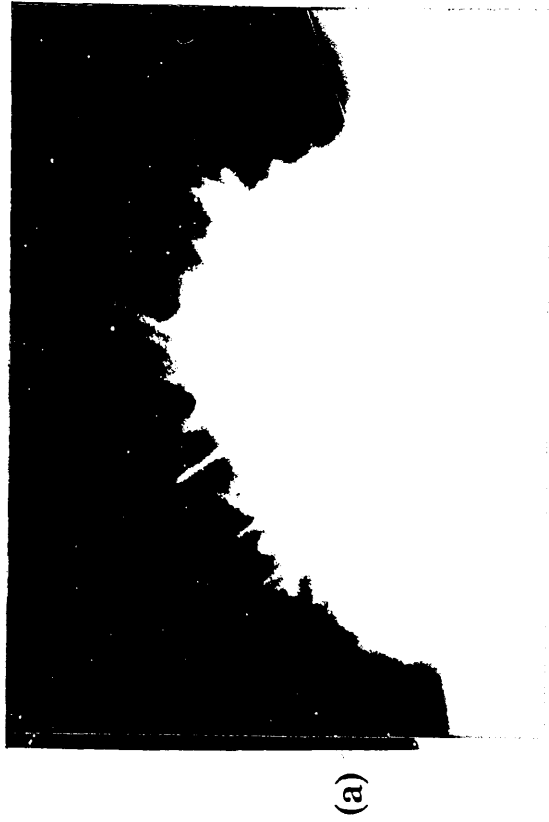
Plate 4-80:

Formation of a precipitating phase within the fluid ash component No.(7) with the addition of 1 mass% Lycal 93HS, after 10 minutes held at 1300°C.

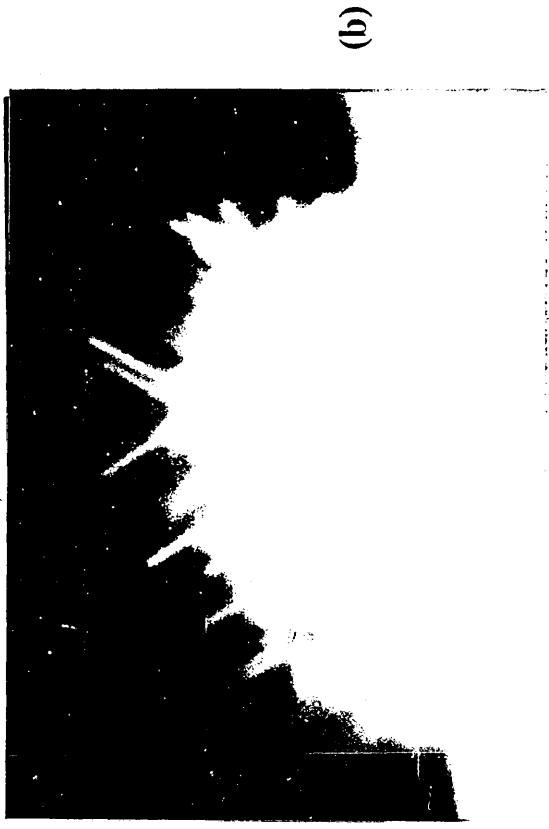


Plate 4-81:

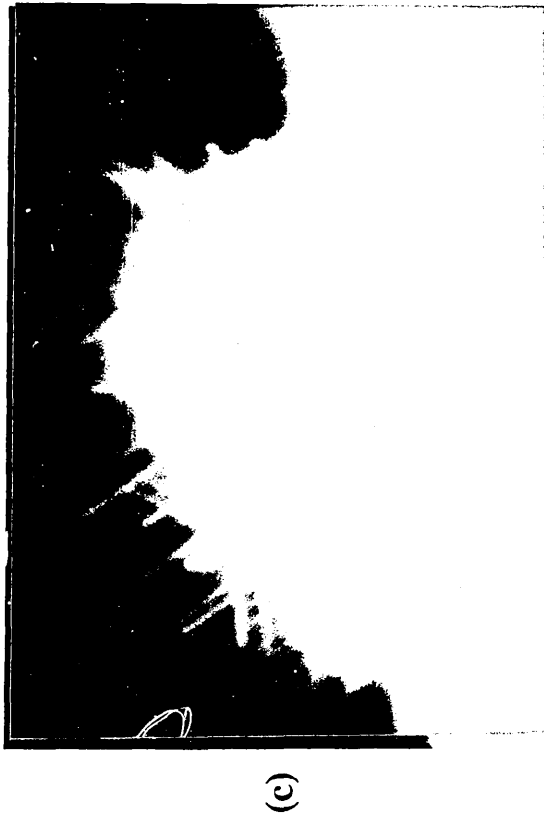
Formation of needles and arrow-head crystals from the surface and within the viscous fluid melt of ash component No.(7) with the addition of 5 mass% Lycal 93HS, after up to 30 minutes held at 1100°C.



(a)



(b)



(c)



(d)

Plate 4-82:

Formation and growth of fine needles from the surface of the viscous fluid melt of ash component No.(7) with the addition of 10 mass% Lycal 93HS, held at 1100°C: (a) initial formation of fine needles after 10 min. (b) growth of needles after 30 min. (c) further growth of needles after 45 min. (d) bending and bifurcation of further grown needles.

Plates 4-83 (a)-(b) are the scanning electron micrographs depicting the fully grown status of needles from the surface of ash component No.(7) containing 10 mass% Lycal 93HS. The EDX-analysis of the needles indicates an eight-fold enrichment of MgO content associated with an Fe₂O₃ rich substrate. Plate 4-83 (b) particularly shows the bifurcation of the needles as they have grown in length.

Plate 4-84 shows the growth of fine needles from the surface of ash component No.(13) with 1 mass% of Lycal. The sample was kept at 1500°C for over 1 hour until no further growth was evident. Some needles had bifurcated when cooled to 1350°C and kept at this temperature for 30 minutes.

Plates 4-85 (a)-(c) represent the formation and growth of a single needle from the fluid melt of ash component No.(21) without any addition of Lycal 93HS. Plates 4-85 (b) and 4-85 (c) depict the growth of the needles after being held at 1300°C for 30 and 45 minutes respectively. Similar observations were made for the sample with 3 mass% addition of Lycal 93HS.

Plates 4-86 (a)-(b) represent the growth and thickening of the needles from the molten surface of ash component No.(21) with 10 mass% addition of Lycal 93HS after 30 and 60 minutes respectively, held at 1300°C.

Plate 4-87 shows the growth of very fine needles from the surface of the molten bulk of the ash component No.(27) with 1 mass% addition of Lycal 93HS held at 1100°C for 20 minutes.

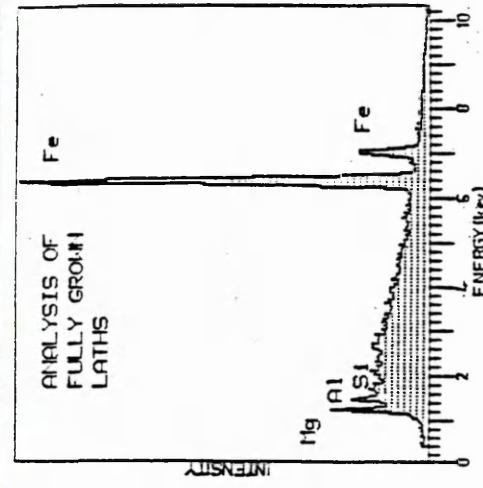
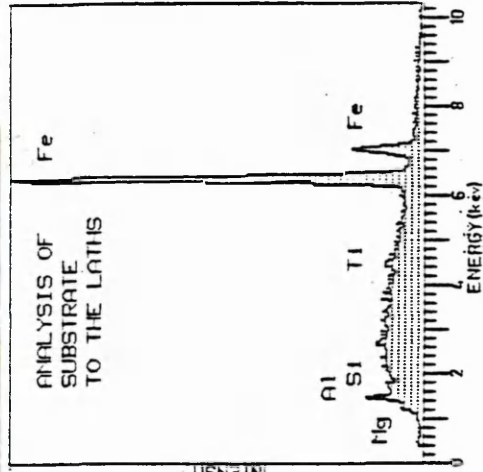
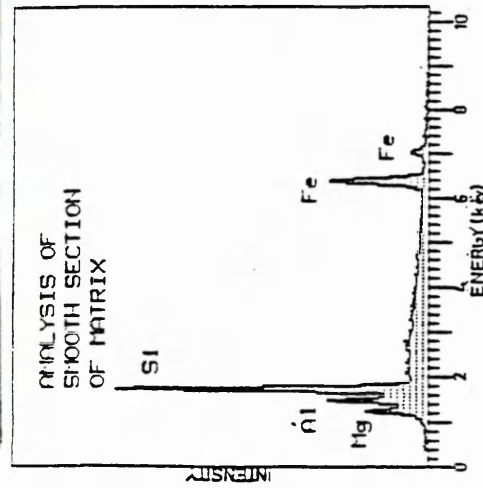
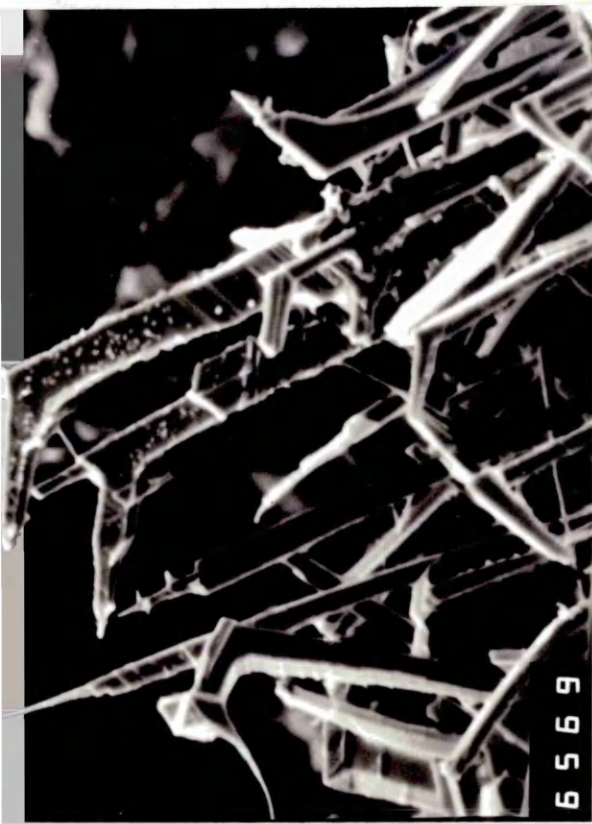
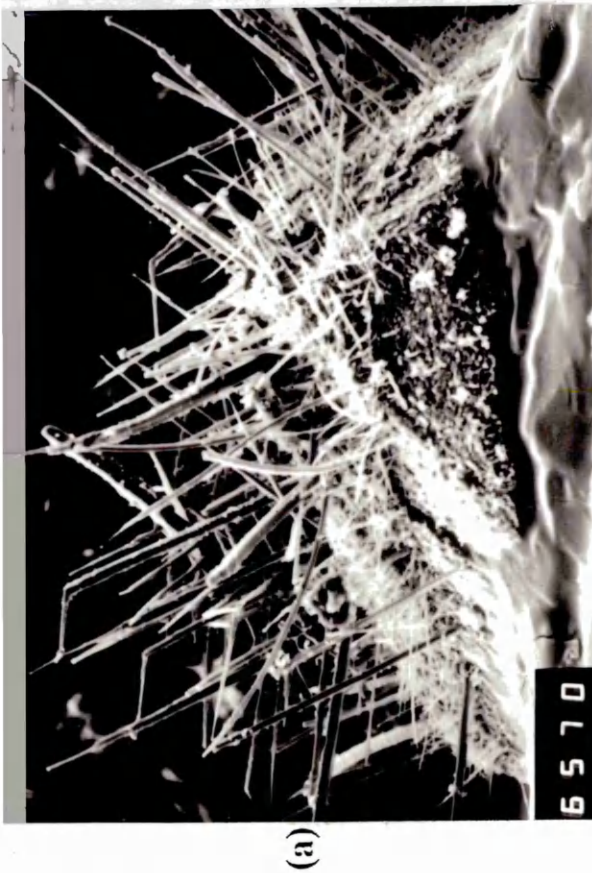


Plate 4-83:

SEM-micrographs of the fully grown needles from the surface of the viscous fluid melt of ash component No.(7) with the addition of 10 mass% Lycal 93HS, quenched to room temperature:

(a) matrix and the substrate to the fully grown laths from the surface.

(b) high magnification of the fully grown laths with bifurcating ends.

The EDX-analyses show the compositions of the smooth and rough part of matrix as well as the laths.

[Mag: x1000]

[Mag: x1000]

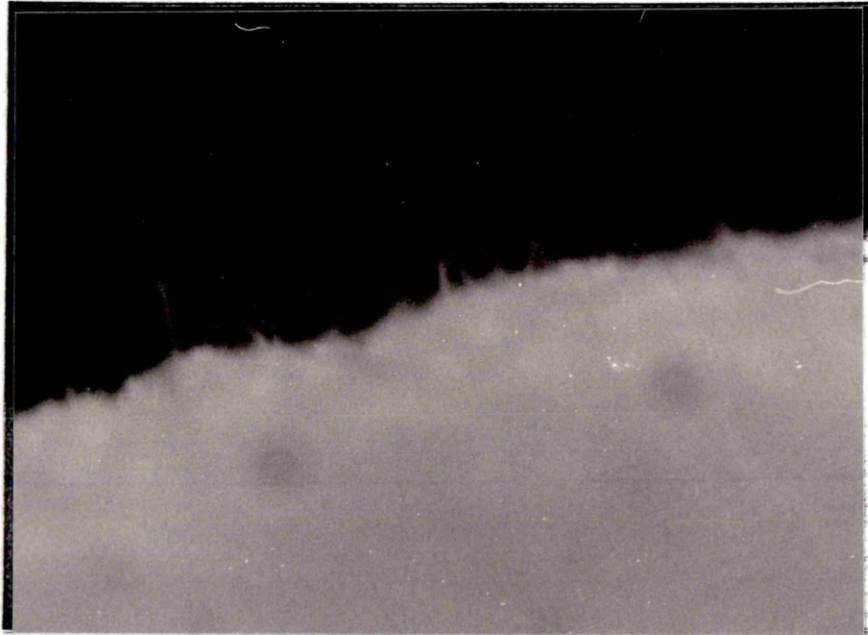


Plate 4-84:

Formation and growth of fine needles from the surface of the viscous fluid melt of ash component No.(13) with the addition of 1 mass% Lycal 93HS, after 1 hour at 1500°C.

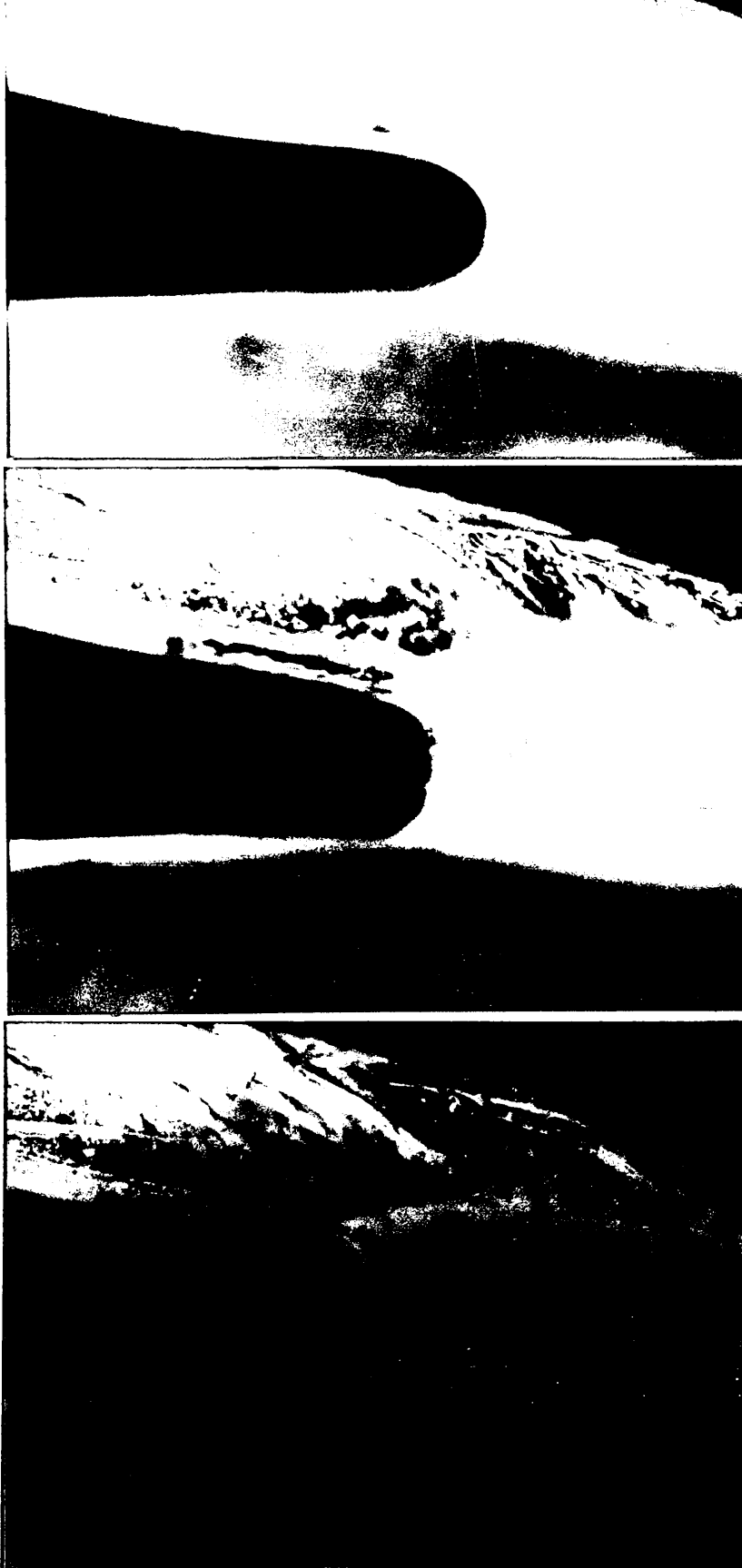
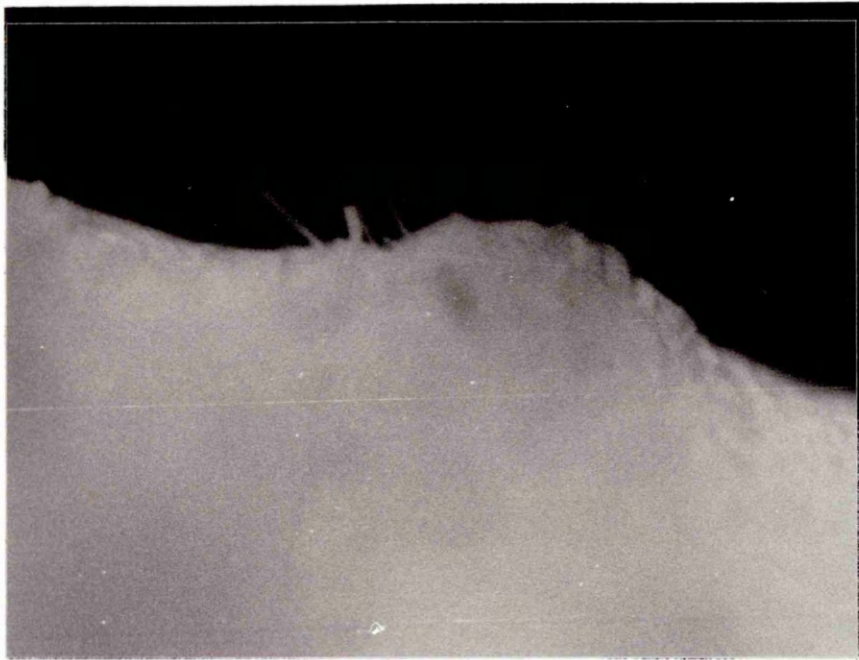
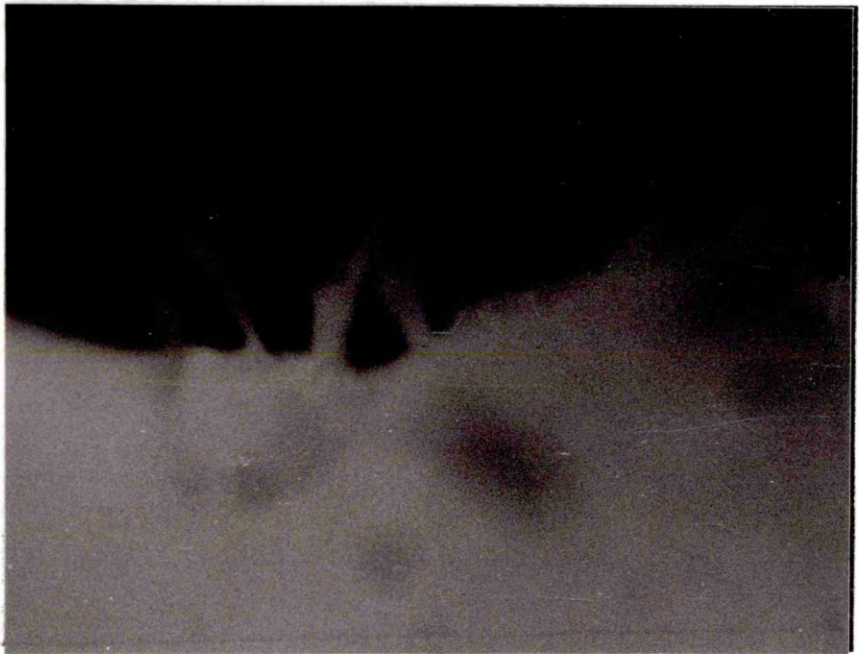


Plate 4-85:

Formation and growth of a single needle from the fluid meniscus of ash component No.(21), without and with addition of 3 mass% Lycal 93HS, at 1300°C: (a) after 10 minutes, (b) after 30 minutes, (c) after 45 minutes.



(a)



(b)

Plate 4-86:

Formation and growth of fine needles from the surface of viscous fluid melt of ash component No.(21), with the addition of 10 mass% Lycal 93HS at 1300°C: (a) after 30 minutes, (b) after 1 hour.

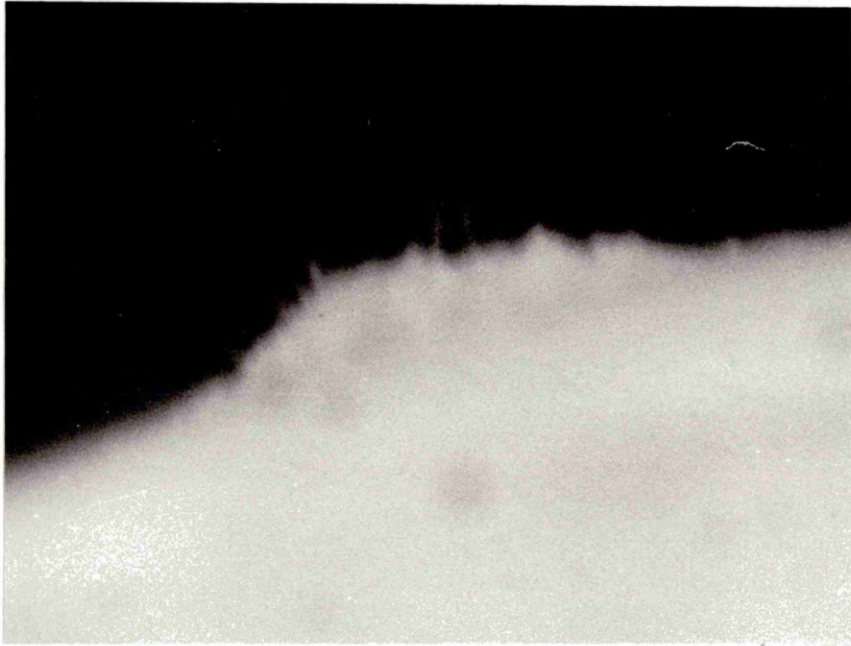


Plate 4-87:

Formation and growth of fine needles from the surface of viscous fluid melt of ash component No.(27), with the addition of 1 mass% Lycal 93HS, after 20 minutes at 1100°C.

5.1 GENERAL INTRODUCTION

It is generally accepted that formation of fire-side deposits within a coal fired boiler system is as a result of many different and complex processes which the coal ash particles undergo during their deposition onto boiler tube surfaces. In order to be able to discuss the role of Lycal 93HS as an additive to alleviate deposit formation, a thorough understanding of the characteristics of the coal ash and fly ash particulates formed within the boiler system is important.

The work presented in this thesis, then, will initially be discussed from the point of view of the characterisation of the physical and chemical constitution of the LTA, HTA and the economiser ash hopper particulates as the fly ash, and the softening behaviour of the LTA and HTA components with and without additions of Lycal 93HS. Secondly the physical, morphological and chemical composition of deposit samples received with and without on-line injection of Lycal 93HS will be discussed through a range of macro/microscopic observations. The role of Lycal 93HS will then be discussed with respect to two possible ways through which it could become associated with the depositing ash matter within the boiler environment. As an "internal" modifier, simulated effect of Lycal 93HS is discussed through softening behaviour of the reconstituted cone samples of the original deposits. As an "external" modifier, the variation in the surface chemistry of the selected deposits formed under the influence of Lycal 93HS injection will be comparatively discussed against those collected from boiler No.5 without on-line injection of Lycal 93HS.

Finally a number of mechanisms for the formation of deposits and the possible interaction of Lycal 93HS within the boiler system will be proposed. These will be based on the extended range of observations for the ash and deposit samples studied.

AYRSHIRE COAL

The characterisation of ash from Ayrshire coal is significant so as to understand better its possible deposit behaviour. This was carried out for both the LTA and HTA.

The LTA being the unadulterated, original ash from the coal, formed the definitive ash to be used to describe its mineralogical constitution. It was also used to show the softening behaviour of this ash under a regime of Lycal 93HS additions.

The HTA was used not only to define the basic composition of the ash, but also to yield the composition of the ash derived from different size fractions of the coal, forming admixtures of ash. The use of these admixtures in the cone fusion tests, with and without additions of Lycal 93HS, was instrumental in showing the softening behaviour of the ash and the effect of its heterogeneity which was in turn dependent on the coal particle size. Also since the HTA was formed at much higher temperatures than the LTA and the ash could be derived from bigger particles of coal than are usually used as standard (i.e. $-210\mu\text{m}$), the ash was investigated in terms of physical variations between some fifty different separated components. These formed the basis to establish the morphological heterogeneity, the compositional variation and the mineralogical diversity of the ash. The extent of interaction between these components would then be expected to be a measure of deposit heterogeneity. The subsequent softening behaviour of these components with and without on-line injection of Lycal 93HS within the boiler environment would then be inferred from the discussion of hot-stage microscopy and cone fusion tests. The possible effect of Lycal 93HS on the degree of crystallinity of the various ash components is also important with respect to their deposit forming propensities, and as such will be discussed.

5.2.1 Physical and Chemical Constitution of Ash Derived from Ayrshire Coal

X-ray diffraction analysis of both the LTA and HTA samples from the Ayrshire coal established the presence of a wide range of mineral species. In the LTA sample, 14 mineral species were detected to be present, although diffraction peak intensities suggested that four of these were present in only minor amounts, suggesting 10 major species (see Figure 4-19 and Table 4-52).

X-ray diffraction analysis (Figures 4-20 to 4-22) of HTA indicated the presence of 12 mineral species with 7 of these being particularly abundant - see Table 4-52 for a comparison of the HTA and LTA. On the basis of visual appearance, texture and chemical composition, the separated ash components derived from ashing +1/4" and +3/16" coal particles (see Plates 4-70 to 4-73 and Table 4-51) appeared to exhibit a much greater diversity - 50 different types being identified. The overall results of these investigations illustrated the complex nature of the coal ash, although based on the limited number of major minerals identified, this complexity simply arises from the way the ash components are mixed together.

Considering that the minerals identified for the LTA are as near to the coal minerals as one can get, the evolution of other minerals identified for the HTA components (see Table 4-52) are clearly as a result of changes taken place on heating, as suggested in Table 2-4. The clays and quartz can both be considered as the source of silica as the coal burns and mineral constituents of its ash are released. The oxidation of pyrites, ankerite and other sulphates (e.g. anhydrite and jarosite) as the original minerals can form different compositions of iron oxides (e.g. hematite, magnetite, wustite). The decomposition of carbonates (e.g. calcite and dolomite) singularly and in combination with minerals from previous groups, form the source of various oxides found in the HTA (e.g. lime, hercynite, corundum, spinel). Hence, the 50 ash

components serve to illustrate the heterogeneities of the ash mineral distribution in the original coal, especially the clay, silica and pyrite distribution. Differences in these have given rise to the different mixes in the ash components, with further subtle differences in the route by which the same mineral species may have formed from different origin in the coal mineral. These explain the differing texture, colour (see Plates 4-70 to 4-73) and composition (see Table 4-51). However, this is less important here than later on where similar differences will manifest themselves in the deposits in the boiler giving rise to differences in colour, texture, composition, hardness and softening behaviour.

The variations in the chemical composition of various ash components can further be illustrated through a rationalised ternary phase diagram for $\text{SiO}_2 - \text{Al}_2\text{O}_3 - \text{Fe}_2\text{O}_3$ system. Figure 5-1¹⁷⁹ shows the dispersion of the ash components at equilibrium with respect to their phase stabilities at 1000°C. Apart from ash components No.(13) and No.(7) which are shown to lie in the $\text{SiO}_2 + \text{Fe}_2\text{O}_3$ region, all of the ash components lie in the main Mullite+ $\text{SiO}_2 + \text{Fe}_2\text{O}_3$ region. The distribution profile of ash components is further depicted in terms of five main regions, each region comprised of ash components with similar mineralogies, as previously identified in Figures 4-20 to 4-22. These regions are outlined in Figure 5-2. The ash component within Region A which is the smallest region, is almost entirely comprised of silica derived from quartz, whereas ash components within region B, which forms the largest region and contains the highest proportion of the ash components, can be seen to have derived mainly from the quartz - kaolinite - muscovite type minerals with limited amount of hematite and/or magnetite minerals derived from the pyrites. The ash components within Regions C and D are identified in terms of their similar mineralogical characteristics (see Figures 4-21 and 4-22). The marginal difference in terms of the distribution profile of the ash

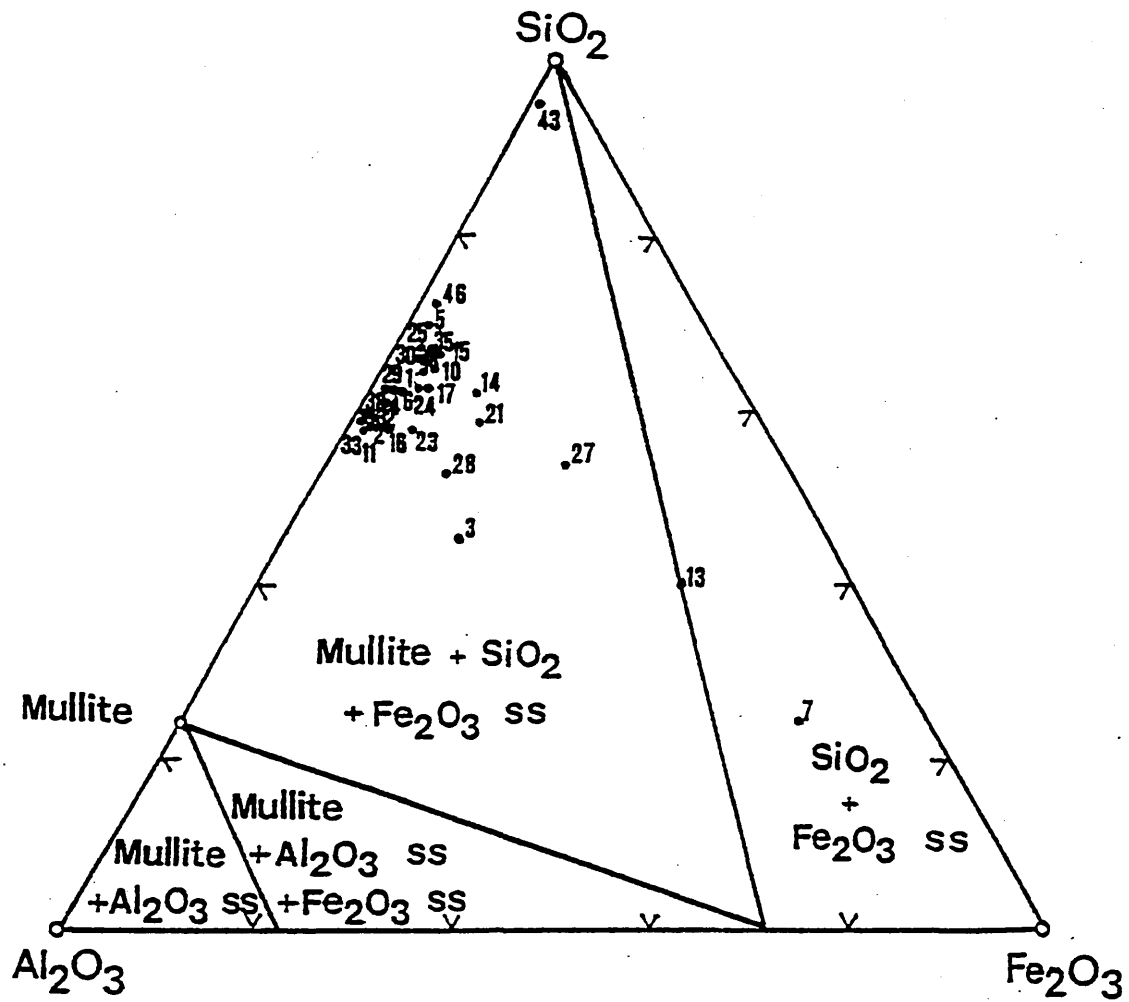


Figure 5-1: Variation in the dispersion of various ash components illustrated through a rationalised ternary SiO_2 - Al_2O_3 - Fe_2O_3 phase diagram at 1000°C .

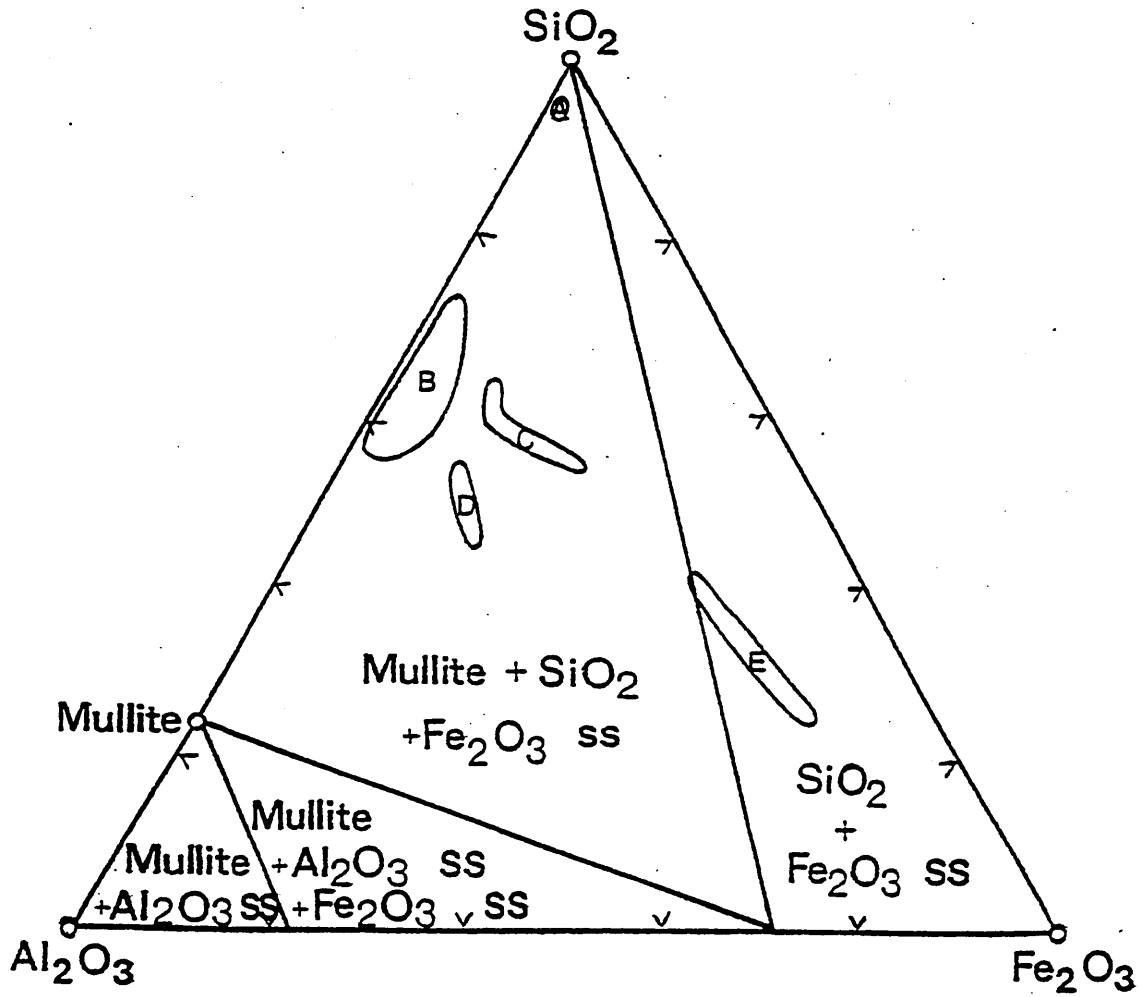


Figure 5-2: Distribution profile of ash components with similar mineralogies illustrated in terms of five main regions on a rationalised ternary $\text{SiO}_2 - \text{Al}_2\text{O}_3 - \text{Fe}_2\text{O}_3$ phase diagram at 1000°C .

components within regions C and D confirms the extent of variation in the proportion of quartz - kaolinite - muscovite type minerals as well as hematite and/or magnetite minerals for the ash components within the two regions as suggested by the relevant peak intensities in Figures 4-21 and 4-22. Region E is comprised of two ash components namely ash components No.(7) and (13). The strong concentration of iron oxide in these components within region E, suggested by their presence within the iron rich corner of the phase diagram, is compatible with the X-ray diffraction spectra for the two components in Figure 4-22 which exhibited strong peak intensities for hematite and/or magnetite peaks. However, whereas in ash component No.(13), the silica could have derived from quartz and/or muscovite minerals, for ash component No.(7), silica must have formed through dissociation of muscovite minerals, since only this mineral was identified in its X-ray diffraction spectra. This further highlights the variation in the source and routes through which similar ash compounds can be formed.

The variation in the size distribution of the coal showed that the coal lumps constituted about 40 mass% of the coal batch whereas the fines constituted only 4 mass% of the total coal burned (see Table 4-43 and Figure 4-14). However as a result of the variation in the ash content with respect to the coal particle size (see Table 4-45 and Figure 4-16), the coal lumps (excluding >> 6350 μm) would only produce $[(\frac{5.724 + 5.926 + 5.681}{124.445}) \times 100\%] = 13.93 \text{ mass\%}$ of the total ash whereas the fines would produce $[(\frac{16.271 + 18.064 + 19.395}{124.445}) \times 100\%] = 43.175 \text{ mass\%}$ of the total ash. It is therefore reasonable to suggest that since the fine coal particles are also more likely to become airborne, the depositing fly ash would be mostly derived from the fines, whereas the lumps are more likely to remain on the grate to form the grate clinker.

From measurements on operational plants it has been inferred¹⁷⁹ that under typical stoker conditions, between 10 and 40 mass% of the coal ash was elutriated from the

bed. The amount of ash becoming air born as fly ash has been found^{181,180} to be dependent on the amount of fine elutriable material in the original coal, the velocity of combustion air through the bed and the general structure of the fuel bed.

The variation in the elemental chemical composition of the ash derived from the coal lumps, coarse, smalls and fines - see Table 4-46, for size description - was shown in Table 4-47 in comparison to the mean ash composition. The resultant ash admixtures, AM1 to AM4 showed some relative enrichment of the main basic oxides (i.e. CaO, MgO and K₂O) as well as depletion of Al₂O₃ in the ash from the fines (i.e. AM4) compared to the ash from the lumps and coarse particles (i.e. AM1 and AM2 respectively). Although the iron content (as Fe₂O₃) of the AM1 is higher than in AM4, CaO alone is generally considered to be a much stronger basic oxide to act as a flux under oxidising conditions.⁵⁸

The mean ash composition, perhaps expectedly, showed a composition representing the averaged position of the ash admixtures AM1 to AM4 (see Table 4-47).

5.2.2 Assessment of Softening Behaviour of High Temperature Ash and its Relationship to Ash Deposition

The softening characteristics of high temperature ash were investigated for:

- (i) Ash admixtures AM1 (derived from the coal lumps) and AM4 (derived from the coal fines) as described in Section 3.4.2 (c).
- (ii) Ash components of sufficient quantity, as described in Sections 3.4.2 and 4.7.

5.2.2 (a) Critical Assessment of the Cone Fusion Technique

It is believed^{58,182} that most coal ashes are almost completely molten at IDT, and the progression to the FT, illustrated in Figure 3-4, is principally the result of lowering slag viscosity rather than production of more molten ash. It has also been shown in these

studies that the degree of partial melting is significant at temperatures as low as 200 to 400°C below IDT. This is indicative of the difference in behaviour when the ash matter is coalesced to form a complex compound as opposed to its original form, comprised of a range of inorganic compounds and minerals. The significance of temperature would thus tend to diminish progressively as some or all of the inorganic mineral matter within the ash are transformed into various crystalline and glassy compounds (see Tables 2-4 and 2-5).

Another factor is that cone fusion temperatures represent the temperatures at which a thorough "mixture" of the whole ash of the coal would melt. This mixing, prior to the application of heat, does not simulate what takes place in practice, as also pointed out by other researchers.^{45,183} The significance of this observation can be seen when the results of the softening temperatures for the HTA of the Ayrshire coal in Table 3-2 is compared to the corresponding temperature regimes for the reconstituted deposit samples in Table 4-14. All the reconstituted deposit samples show lower temperatures for the various stages in their softening than the HTA sample. Also with respect to the possibility of extensive particle to particle bonding without any visible sign of deformation in the shape of the cones, some workers have found misleading results using this technique.¹²⁶

Despite these limitations, the cone fusion test is probably the most widely used method for ash fusion characterisation, allowing comparative analysis to be made between different studies. The various stages in the softening of the ash as described in Section 3.3.4(a) and Figure 3-4 have further been related^{56,126} to the progressive stages in deposit formation of ash inside a boiler. These are as follows:

IDT - Corresponds to the temperature in an operating furnace at which the particles of ash, in transit through the furnace, have been cooled sufficiently to stick

together and gradually form a deposit on heat exchanger surfaces.

ST / HT - Correspond to conditions at which coal ash shows a greatly accelerated tendency to conglomerate together and stick in large quantities to heat exchange surfaces.

FT - Corresponds to the temperature at which the coal ash may be expected to flow in drips or streams from furnace walls.

If the ash fusion range of the deposit is wide, i.e. if the temperature difference between IDT and ST is greater than 150°C, the deposit remains plastic over a wide range of temperatures without becoming actually fluid. This has been shown^{182,184} to cause the deposit layer to become thicker than if the fusion range was narrow. If the temperature difference between the IDT and ST is less than 100°C, the ash has been shown¹⁸⁴ to form "short slags". Such ashes were found to be particularly sensitive to small temperature differences, because they move from the solid into the liquid phase and vice versa, within a closely defined range. They also crystallise quickly out of the molten state.

The use of cone fusion test in this study was based on the relative ease of sample preparation, the immediacy of the results through observation of the cone softening temperatures and the high degree of reproducibility of results.

5.2.2 (b) Variation in the Softening Behaviour of Coal Ash with Respect to its Size and Composition and its Relevance to Deposition

The results of ash admixture softening tests presented in Table 4-48 and Figure 4-17 clearly demonstrated that the ash admixture derived from the coal lumps (AM1) has a much more refractory nature than that derived from the fine coal particles (AM4). These results mostly reflect the collective influence of the strong fluxing oxides such

as CaO, MgO and K₂O at 7.43 mass% for the AM1 and 12.61 mass% for the AM4.

The appreciation of the relationship between the nature of the ash in terms of its refractory and fusible constitution, and the coal particle size is directly relevant to the deposit formation on boiler tubes. The free fusible matter in the ash can quickly melt in the furnace and adhere to walls to form a sticky film. This can also act as a bonding agent for less fusible constituents, as superheater slag deposits from p.f. fired boilers have been shown¹⁸³ to be composed entirely of refractory material bound by a very small proportion of fusible ash. The role of Lycal 93HS on the softening behaviour of the ash will be discussed in later Sections.

5.2.2 (c) Variation in the Softening Behaviour of the Coal Ash Components and its Relevance to Deposition

The results of the ash softening tests presented in Table 4-53 show that 23 of the 29 ash components which comprised the major part of the separated ash, had a refractory nature with IDT values greater than 1400°C. Moreover, 19 of the 23 components had IDT values greater than 1450°C. These constituted approximately 80 mass% of the total separated ash and more than 83 mass% of the major separated ash components (see Figure 4-18).

The analysis of the ash fusion characteristics (see Table 4-53) for the separated ash components with respect to their chemical composition (see Table 4-51) shows that:

a. All the refractory ash components (i.e IDT > 1400°C), with the exception of ash components No.(7) and (28) had a very acidic composition (i.e. SiO₂ + Al₂O₃ + TiO₂ > 87 mass%). This is consistent with the mineral constitution of these two components (see Figures 4-21 and 4-22) where anhydrite, hematite, magnetite and dolomite comprised a basic mineralogy. Similar observations have already been made

for the softening behaviour of the more acidic ash admixture AM1 as compared to that of the more basic ash admixture AM4, discussed previously in Section 5.1.2 (b).

b. Despite an $\text{Fe}_2\text{O}_3 > 60 \text{ mass\%}$, ash component No.(7) displayed a refractory nature (i.e. $\text{IDT} > 1400^\circ\text{C}$). This can be as a result of the way the pyritic iron (as Fe_2O_3) and in the form of hematite and magnetite (see Figure 4-22), is distributed within the extraneous ash. For example if the Fe_2O_3 was present as discrete particles, the ash softening temperatures would be expected to be much lower than if these particles were to be 'contaminated' by alumino-silicates within the extraneous ash as could in this case, suggested by the chemical analysis shown in Table 4-51. Furthermore the degree of sulphur reduction and iron oxidation has been shown⁴⁷ to influence the melting temperature of the pyrite, increasing with increase in oxidation. It is expected that at the ashing temperature of 815°C , all of the pyrite in the ash component would have been converted to iron oxide, as illustrated in Table 2-4.

c. Despite very similar chemical compositions, ash component No.(48) was shown to have an IDT value at least 32°C lower than No.(15) which did not exhibit any deformation at all. Since the mineralogy of these two components is almost identical (see Figure 4-21), the variation in the IDT could perhaps be attributed to the state of oxidation of iron oxide, as FeO in ash component No.(15) and Fe_2O_3 in ash component No.(48). This variation in the IDT temperatures could also reflect the extent of the distribution of other minerals, detected from their peak intensities.

d. Ash component No.(16) with a highly acidic composition (i.e. $\text{SiO}_2 + \text{Al}_2\text{O}_3 + \text{TiO}_2 = 88 \text{ mass\%}$) was the only such component which was softened at the temperature of 1420°C , with its $\text{IDT} = 1388^\circ\text{C}$. This is consistent with the mineral constitution of this component (see Figure 4-21), showing a highly basic mineralogy in the form of hematite and magnetite comprising the major constituents of the ash minerals.

e. Ash component No.(28) with large concentration of basic fluxing oxides (i.e $\text{Fe}_2\text{O}_3 = 11 \text{ mass\%}$ and $\text{CaO} = 7.5 \text{ mass\%}$), unexpectedly exhibited a refractory nature with $\text{IDT} > 1400^\circ\text{C}$. This apparent anomaly could be due to the presence of calcium as CaSO_4 as determined in Figure 4-21 or anorthite ($\text{CaAl}_2\text{Si}_2\text{O}_8$) as shown formed in minor quantities in some ash deposits (see Table 4-52) as well as the extent of clay (muscovite) and silica as quartz minerals exhibited by their corresponding peak intensities.

The softening behaviour of the separated ash components defined by their corresponding compositions in Table 4-51 are in general agreement with that shown in Figure 2-7.^{54,19} For the most acidic components (i.e $\Sigma[\text{Fe}_2\text{O}_3 + \text{CaO} + \text{MgO} + \text{K}_2\text{O} + \text{P}_2\text{O}_5] < 10\%$), the recorded temperatures correlated well with those evaluated from Figure 2-7. This is evident from Table 5-1 which shows that the softening temperatures (i.e. HT values) for all of these components at $> 1450^\circ\text{C}$, is compatible with the softening temperatures for a range of bulk ash samples with basic oxide contents identical to the ash components.

For the basic ash components (i.e $\Sigma[\text{Fe}_2\text{O}_3 + \text{CaO} + \text{MgO} + \text{K}_2\text{O} + \text{P}_2\text{O}_5] = 10\text{-}15\%$) such as ash No. (10),(15),(16),(17),(23),(48), the recorded fusion temperatures were all higher than those evaluated from Figure 2-7. This is evident from Table 5-2 which shows that the HT-values determined in this study are approximately $30\text{-}55^\circ\text{C}$ higher than those evaluated from Figure 2-7 for bulk ash samples with basic oxide contents identical to the ash components.

Similarly, for the ferriferous ash components (i.e $\text{Fe}_2\text{O}_3 > 9.5\%$ and $\Sigma[\text{Fe}_2\text{O}_3 + \text{CaO} + \text{MgO} + \text{K}_2\text{O} + \text{P}_2\text{O}_5] > 15\%$) such as ash No. (3),(7),(13),(14),(21),(27),(28), the recorded fusion temperatures are significantly higher than those evaluated from Figure 2-7. This is evident from Table 5-3 which shows that the HT-values determined

Table 5-1: Results of cone fusion tests for the selected range of acidic ash components showing the softening temperatures as determined in this study, compared to those evaluated in the literature for a range of ash compositions with identical basic oxide contents.

HIGH TEMPERATURE ASH			
ASH COMP. No.	MASS PERCENTAGE BASIC** (%ΣFe₂O₃+CaO+MgO+K₂O+P₂O₅)	EXPERIMENTAL* HT-VALUES (°C)	LITERATURE† HT-VALUES (°C)
1	5.49	> 1450	> 1450
2	4.73	"	"
4	4.53	"	"
5	5.52	"	"
6	6.37	"	"
11	4.52	"	"
24	7.65	"	"
25	7.86	"	"
29	6.32	"	"
30	5.62	"	"
32	4.28	"	"
33	4.64	"	"
35	8.47	"	"
38	2.80	"	"
43	0.58	"	"
46	3.37	"	"

Note: acidic ash components are those components with SiO₂ + Al₂O₃ > 90%.

* these values were evaluated from Table 4-53.

** these values were previously presented in Table 4-51.

† these values were evaluated from Figure 2-7 (oxidising atmosphere) and correspond to bulk ash compositions having identical basic oxide content as ash components in this study.

Table 5-2: Results of cone fusion tests for the selected range of basic ash components showing the softening temperatures as determined in this study, compared to those evaluated in the literature for a range of ash compositions with identical basic oxide contents.

HIGH TEMPERATURE ASH			
ASH COMP. No.	MASS PERCENTAGE BASIC** (%ΣFe₂O₃+CaO+MgO+K₂O+P₂O₅)	EXPERIMENTAL* HT-VALUES (°C)	LITERATURE† HT-VALUES (°C)
10	10.27	> 1450	1418
15	12.54	"	1394
16	11.84	"	1406
17	10.09	"	1414
23	11.10	"	1410
48	11.93	"	1398

Note: basic ash components here are those with the basic oxide content between 10-15 mass percentage.

* these values were evaluated from Table 4-53.

** these values were previously presented in Table 4-51.

† these values were evaluated from Figure 2-7 (oxidising atmosphere) and correspond to bulk ash compositions having identical basic oxide content as ash components in this study.

Table 5-3: Results of cone fusion tests for the selected range of ferriferous ash components showing the softening temperatures as determined in this study, compared to those evaluated in the literature for a range of ash compositions with identical basic oxide contents.

HIGH TEMPERATURE ASH			
ASH COMP. No.	MASS PERCENTAGE BASIC** (% Σ Fe ₂ O ₃ +CaO+MgO+K ₂ O+P ₂ O ₅)	EXPERIMENTAL* HT-VALUES (°C)	LITERATURE† HT-VALUES (°C)
3	25.74	1368	1264
7	63.11	> 1450	1432
13	47.13	1319	1272
14	16.23	> 1450	1353
21	17.65	1420	1337
27	31.81	1359	1248
28	21.31	1433	1308

Note: ferriferous ash components here are those with approximately 10% Fe₂O₃ and total basic oxide content greater than 15 mass percentage.

* these values were evaluated from Table 4-53.

** these values were previously presented in Table 4-51.

† these values were evaluated from Figure 2-7 (oxidising atmosphere) and correspond to bulk ash compositions having identical basic oxide content as ash components in this study.

in this study are approximately 47-125°C higher than those evaluated from Figure 2-7 for bulk ash samples with basic oxide contents identical to the ash components.

These variations in the softening temperatures for the basic and ferriferous ash components and comparable bulk ash samples could be due to factors such as the mineralogical distribution or the extent of free fusible material in the ash as well as variations in the experimental procedures between this and other studies.

Further investigation of the softening characteristics of the major ash components on heating and their possible crystallisation behaviour on cooling was carried out using high temperature microscopy. This technique has frequently been used for such determinations.¹⁸⁵⁻¹⁸⁷ The comparable temperatures for various stages of ash fusion using this technique have in some studies¹⁸⁵ been found to be much lower than those determined by the cone fusion technique. In other studies¹⁸⁸ they have been found to be slightly higher.

Comparison of the two techniques in this work shows that the IDT values determined by the cone fusion test and shown in Table 4-53, are between 166-173°C and >130-227°C higher for the fusible and refractory ash components respectively than temperatures determined by high temperature microscopy, as presented in Tables 4-54 to 4-72.

The HTA and LTA samples of the bulk coal were observed to have IDT values of 1432 and >1450°C respectively, determined by cone fusion tests (see Table 3-2). Comparing these values with those determined through hot-stage microscopy tests for the LTA and HTA samples (see Tables 4-73 and 4-74), shows that the corresponding values for the initiation of softening are respectively 180 and >215°C lower using this method.

These differences are comparable to those of the refractory ash components described previously.

The differences in softening initiation temperatures between the two techniques could be attributed to the ease by which the samples could be observed as they were being heated in the microscope's cell. This allowed close observation and more accurate determination of changes incurred in the study of the samples. This would mean that liquid phases are present at lower temperatures and therefore the fusible part of the ash acting as the bonding agents within the ash would be active over longer period of time. The implication for the formation of deposits within the boiler environment would be that contrary to the refractoriness of the ash determined by cone fusion test (see Table 3-2), deposits are formed at lower temperatures.

These observations seem to generally support the previous ones concerning the refractoriness of the ash derived from the larger coal particulates. Hence as far as the formation of deposits on boiler tubes is concerned, it can be said that the fusible components of the ash are derived from the finer coal, which would then help to glue the more refractory part of the ash to form extended areas of deposition at much lower temperatures than otherwise predicted.

5.3 INTERPRETATION OF THE TRANSFORMATION AND CRYSTALLISATION BEHAVIOUR OF ASH COMPONENTS ON PROGRESSIVE HEATING

5.3.1 Without Additions of Lycal 93HS

Although the study of melting and solidification behaviour of ash components on heating and cooling respectively in the hot-stage microscope was carried out for all the

major ash components, as defined in Section 4.7.2, the discussion here would be limited to only those components which were more readily fusible in the operating temperature range of the microscope. These were mainly those components with high Fe_2O_3 and CaO content, namely No.(3), (7), (13) and (21).

Solidification commenced with the formation of very fine dendrites or a precipitating phase within the semi-fluid melt and generation and growth of fine needle-like structures outwards from the surface of the melt. Such features are illustrated in Plates 4-76, 4-80, 4-81, 4-84 and 4-85. The rather peculiar formation of the fine needles from the surface of the melts have also uniquely been observed in another study.¹⁸⁹ It was noted that the first product of oxidation of a variety of steel alloys was a fine needle-like growth. These needles were identified as $\alpha\text{-Fe}_2\text{O}_3$, with the main oxide composition as $\alpha\text{-Fe}_2\text{O}_3$ and $(\text{Fe}_3\text{O}_4, \text{Fe}_2\text{O}_3)$ was also found in the scale. Although the oxidation of steel is a solid oxidation and does not include a liquid phase, the purpose and the relevance of this analogy here is merely to draw on the formation of the needle-like features, which seemingly were formed as a consequence of iron oxide participation, in the case of this study as well as the one cited above.

For the ash components, the presence of iron oxide in the constitution of the needles is illustrated in the EDX-analysis for the SEM-micrograph in Plate 4-83(a). The formation of iron oxide rich needles from a crusty, ferriferous region of ash component No.(7), also representative of the other three components examined in this way, was clearly evident. The iron oxide in needles could be due to the hematite ($\alpha\text{-Fe}_2\text{O}_3$) and/or magnetite (Fe_3O_4) minerals as the major crystalline phases present within these components.

The implication of these needle formations is that they could act to trap the very fine solid ash particles in the burnt gases and thus act as nucleation sites for the build-up of

ash deposits. This would be particularly significant for the upper furnace regions (i.e. screen tubes, passage between screen tubes and superheaters) where the deposits from boilers No.6 were found to contain on average more than 25 mass% iron oxide (see Tables 4-1 to 4-5).

5.3.2 With Additions of Lycal 93HS

The deposit forming propensity of the selected ash components under increasing additions of Lycal 93HS can be discussed in terms of two main categories:

1. Ferriferous
2. Acid and Basic

1. For all the "ferriferous" ash components as defined in terms of their constitution in Figure 4-22 and Table 4-51, increasing additions of Lycal 93HS effected their softening regimes differently. For ash components with higher Fe_2O_3 and basic oxide concentrations [e.g. ash components No. (7), (13)] small additions of Lycal 93HS increased their initial softening temperatures but higher additions depressed it (see Tables 4-60 and 4-62). With Fe_2O_3 concentrations of 60.89 and 38.99 mass% (see Table 4-51) and mineral compositions almost entirely made up of hematite and/or magnetite (see Figure 4-22), the increasing additions of Lycal 93HS to ash components No.(7) and (13) would act as a strong fluxing oxide, decreasing the softening temperatures.

For ash components No.(21) and (27) with very different chemical composition (see Table 4-51) but almost identical mineralogy (see Figure 4-22), small additions of Lycal 93HS decreased their initial softening temperatures but higher additions increased them (see Tables 4-64 and 4-65). This apparent anomaly in the effect of Lycal 93HS on the softening characteristics of these two components could be due to the formation

of complex compounds between the added Lycal 93HS and other mineral oxides such as calcite (see Figure 4-22) as well as masking the usual fluxing effect of iron oxide.

The effect of Lycal 93HS on the crystallisation behaviour of the ferriferous ash components has been described in Section 4.7.4 (b). It was observed that in some components, e.g. ash No.(7), increases in Lycal 93HS additions promoted the growth of needles. This can be seen in Plates 4-82, 4-86 and 4-83(b) with the accompanying EDX-analysis, showing an eight fold increase in MgO, presumably derived from Lycal 93HS in the fully grown needles compared to the substrate. In other ferriferous components the change in crystalline configuration of the fluid melts, under higher additions of Lycal 93HS was negligible. This variation in behaviour could be attributed to the reactions between MgO (i.e Lycal 93HS) and hematite and magnetite (see Table 4-51 and Figure 4-22), forming the highly refractory magnesium ferrite and thus increasing the ash softening temperatures. This is in accordance with observations in other studies.⁵³

2. For the "acidic" and "basic" ash components as defined in terms of their constitution in Figures 4-20, 4-21 and Table 4-51, increasing additions of Lycal 93HS effected their softening regimes differently. Whereas increasing additions of Lycal 93HS up to 3 mass% caused a reduction in softening, melting and fluid temperatures for some ash components [e.g No. (1), (2), (4), (11), (46)] (see Tables 4-54, 4-55, 4-57, 4-61, 4-71), in others it only did so for the melting and fluid temperatures. However, the higher additions of 5 and 10 mass% Lycal 93HS invariably reduced the temperatures for the three stages in all the components (see Tables 4-54, 4-55, 4-57 to 4-59, 4-61, 4-63, 4-66 to 4-72).

Like the observations for the ferriferous ash components, the influence of ash mineralogy is not apparent. Consider for example ash components No.(6) and (11) with very similar chemical composition (see Table 4-51) and identical mineralogy (see Figure 4-20), additions of Lycal 93HS between 1-10 mass% decreased the softening, melting and fluid temperatures for ash component No. (6) (see Table 4-59). However for ash component No.(11), the effect of Lycal 93HS on the softening temperatures was inconsistent and only higher additions of 5 and 10 mass% showed a fluxing effect on the melting and fluid temperatures (see Table 4-61). On the other hand ash components No.(5) and (48) with different chemical composition and mineralogy (see Table 4-51 and Figures 4-20 and 4-21), exhibited identical regimes for the various stages in their softening with additions of Lycal 93HS between 1-10 mass%. Ash components No.(29) and (30) with very similar composition (see Table 4-51) and mineralogy (Figure 4-20), also exhibited identical regimes for the various stages in their softening with additions of Lycal 93HS between 1-10 mass%.

Ash components No.(5) and (6) were the only samples amongst the "acidic" and "basic" ash components in which additions of 5 and 10 mass% Lycal 93HS promoted crystallisation within the fluid melt(see Tables 4-58 and 4-59). The rate and extent of crystallisation was found to increase with decreasing temperatures between 1400-1300°C for ash No.(5) and 1400-1100°C for ash No.(6).

A quantitative evaluation of the EDX-analyses presented for Plate 4-78 showed a 47% increase in the MgO content of the crystalline phase compared to the matrix of the ash component No.(5) with 10 mass% Lycal 93HS. Similar observations were made for ash component No.(6).

It is evident from these examples that it is difficult to arrive at any unique correlations between ash mineralogy, its composition and its softening behaviour under the influence of Lycal 93HS additions. However, in terms of the softening behaviour of the ash components, it is clear that whereas additions of Lycal 93HS can both increase and decrease the softening of "ferriferous" ash components, for the "acidic" and "basic" components Lycal 93HS always acts as a flux, thereby reducing their softening temperatures. In terms of the transformation and crystallisation of fluid melts, additions of Lycal 93HS promoted growth of needles on the surface of the "ferriferous" ash components. In the "acidic" ash components, Lycal 93HS additions promoted crystallisation of fluid melt and did not have any surface effect. In the "basic" ash components, additions of Lycal 93HS did not seem to have any effect on their transformations.

5.4 CHARACTERISATION OF PARTICULATE FLY ASH SAMPLES FROM ASH HOPPERS AND GRIT ARRESTORS

5.4.1 Introduction

The previous sections looked at the coal and its ash in terms of its chemical and mineralogical constitution as well as its softening behaviour and the effect of Lycal 93HS on it. Now within the boiler system, the combustion releases the mineral matter which changes to form the clinker on the grate and the fly ash airborne within the boiler atmosphere. The nearest thing to the bulk of the original airborne fly ash particles are the samples in the economiser ash hoppers and grit arrestors. As illustrated in Plate 4-29, these are small, discrete, mostly spherical particles in the range of 45 to 700 μ m in diameter. These samples having cooled and solidified rapidly, have had little time for coalescence and since the temperatures in the economiser hoppers and grit

arrestors are much lower than the furnace region, these samples have little time for further heat treatment and unlike in boiler deposits maintain their original form.

5.4.2 Variation in Fly Ash Morphology and Chemistry

Plates 4-30 and 4-31 showed the extent of variation in fly ash morphology, with the EDX - analyses similarly showing corresponding variation in the composition of the smooth and rough surface fly ash spheres as well as non-spherical particulates. Although some limited degree of coalescence can be seen between some fly ash particles, they can still be considered as representative of the bulk fly ash matter within the furnace. The differences in the morphology and chemistry of the fly ash particulates can be related to the conditions of formation and the amount of crystalline and non-crystalline components in them. The EDX analyses show that:

- (a). Rough textured coarse spheres had a surface chemistry rich in phosphorus, magnesium, iron, calcium, silicon and sulphur which could be present as oxides, sulphates, phosphates or other compounds. The enrichment of these substances can be due to their migration from within to the surface of the siliceous ash sphere as it develops to its final size during its flight within the boiler. They can also have arrived on the surface of the ash spheres as broken fine fragments of ash mineral matter suspended in the gases flowing upward within the boiler environment (see Figure 2-13).
- (b). Smooth textured coarse spheres had a surface chemistry rich in silicon, aluminium, iron and calcium present as silicates. The smoothness of the surface of these ash spheres which are the dominant feature amongst the spherical particles, could be explained by either their rapid formation and exit from the furnace environment, thereby not allowing for the migration of minor oxides or by the lack of interaction between ash spheres and suspended ash mineral fragments as explained above.

(c). The coagulated ash matter with a semi-smooth, porous surface was shown to have an alumino-silicate rich surface. The non-spherical shape of these particles suggests some degree of coalescence between different ash particles.

(d). Some medium size (-55 +63 μ m) ash spheroids had a highly porous structure (see Plate 4-31), indicative of the evolution of carbon and other gases from the centre of the particles. The EDX analysis of the surface illustrates a composition mainly enriched by silicon, aluminium, calcium and sulphur oxides.

Table 4-7 further characterised the variation in the chemical composition of the bulk grit arrestor and economiser ash hopper particulate samples. It can be seen that with or without on-line injection of Lyclal 93HS, fine particulates exhibited higher concentrations of iron, magnesium, phosphorus and sulphurous oxides than those associated with the medium and coarse particles. This size related variation in the elemental composition of fly ash particulates could be as a result of the natural distribution of the mineral matter which exists as large bits and finely divided and uniformly dispersed particles within the coal. Depending on the degree of segregation of various mineral species within a coal particle as well as the conditions within the furnace, the ash derived from various mineral concentrates can assume wide ranging sizes and exhibit different elemental compositions.

The significance of these observations is to illustrate the morphological and compositional non-uniformities which are present amongst the particulate fly ash matter representative of the ash particulates depositing on boiler tube surfaces. It is interesting to note that whereas the smaller and smooth surfaced ash spheres seem to have coalesced to form larger, irregularly shaped agglomerates of similar composition, the rough surfaced spheres and spheroids have essentially remained as individual

particulates. This is indicative of the propensity of the smooth fly ash spheres to fuse together and form larger conglomerates which may be propelled upwards and exit the furnace or be projected side ways and impact the boiler tube surfaces. Hence, it can be deduced that upon deposition on boiler tube surfaces, the smooth surfaced ash spheres proceed much more quickly to form a bond with the cooler metal surfaces or the existing oxide films on the metal surfaces. The smooth ash spheres can also adhere more freely to each other and the rough surfaced ash spheres, forming a bonded sintered deposit layer.

5.4.3 Comparative Analysis of the Effect of Lycal 93HS on the Fly Ash and Ash Particles Collected on a Probe Surface

The compositional analysis of the white particles over the surface of the rough surfaced ash spheres from economiser ash hoppers (see EDX for Plate 4-30) in terms of its phosphorus, magnesium and sulphur content was proportionally similar to their ratios in the ash particulates from the bottom screen tubes region collected on the probe, with on-line injection of Lycal 93HS (see Table 4-18). These particles could either have deposited as fine fumes present in the entrained fly ash or as condensing volatile vapour phases.

It can also be seen from Table 4-7 that when Lycal 93HS was on-line, the fine grit arrestor particles which were generally of the same size range as the ash particulates from the probe, also had higher concentrations of magnesium associated with higher amounts of phosphorus and sulphur oxides than the coarse or medium size particles. This demonstrates that it is the fine ash particles impacting and covering the boiler tube surfaces with a fine layer of ash dust, which act as carriers for the injected Lycal. The presence of Lycal 93HS can further be deduced by higher concentrations of MgO

for all the various size fractions of grit arrestor and economiser ash hopper samples with Lycal 93HS injection compared to those without Lycal 93HS injection.

The difficulty in identifying the causes of morphological variations of fly ash particulates as discussed here, have been considered by other researchers^{190,191} who have shown the dependence of these variations on:

- (a) Particle properties such as chemistry, mineralogy, residual carbon content, degree of coalescence or fragmentation of minerals and size, and
- (b) Boiler conditions such as local furnace temperatures, furnace gas flow and generated eddies, concentration gradient of gases and solids and excess oxygen levels.

Further to the chemical variations amongst the particulate grit arrestor and economiser ash hoppers samples, the unburned carbon content associated with different particulate size fractions with and without Lycal 93HS were shown to decrease significantly with particle size (see Table 4-8 and Figure 4-1). The role of carbon is important since higher concentrations of carbon would allow for extended burning of the fly ash particles in suspension, rendering them more softened and therefore more likely to coalesce with other fly ash particles¹⁹². For those softened fly ash particles which impact the heat receiving tube surfaces, the burning of the residual carbon could also further expand their collapse and enhance the growth of bond formation between these and other ash particles residing on tube surfaces.

Although additions of magnesia (MgO) to an oil-fired boiler have been shown¹⁶⁵ to reduce the unburnt carbon portion of the fly ash, the same effect can not conclusively be shown for the grit arrestor and ash hopper samples(see Table 4-8). However, for the fine grit arrestor particles which have previously been shown in Table 4-7 to carry the highest amount of magnesia, the amount of unburnt carbon are lower when Lycal 93HS was on-line than when it was off-line. The effect of Lycal 93HS can similarly be seen

for the fine economiser ash hopper samples.

It is perhaps important to note that with stoker fired boilers, like the one in this study, the bulk of the fly ash is collected as coarse ashes (75-85%) from the boiler furnaces and comparatively little grit (10-20%) from the boiler passes¹⁸¹. Tables 4-9 and 4-10 similarly show that the amount of coarse (+1200 +75 μ m) fly ash particles with and without Lycal 93HS varied between 57-98% and 54-98% respectively. It has already been shown in Table 4-7 that most of the injected Lycal 93HS was associated with the fine (-45 μ m) grit arrestor or medium (-500 +63 μ m) economiser ash hopper particulate samples. It would therefore be expected that as the bulk of particulate fly ash adheres onto the boiler tubes, the coarser particles would form a higher proportion of the fused deposit and finer particles, present in lower proportions would less readily become incorporated into the fused deposit and would act to retard the coalescence of ash particulates.

5.5 COMPARATIVE EXAMINATION AND ASSESSMENT OF THE EFFECT OF LYCAL 93HS ON BOILER DEPOSIT SAMPLES

5.5.1 Macroscopic-Scale Examination

The most clear indication of the beneficial effect on ash deposit adhesion of Lycal 93HS into the atmosphere of boiler No.6 is illustrated by Plate 4-1. The furnace area was generally found to be clear of the usual extensive deposit accumulation. Plates 4-2 and 4-3 show how over three months period of regular, unhindered injection of Lycal 93HS to the left hand side (i.e. A-side), boiler tubes had remained relatively clean. Plates 4-4 and 4-5 showed on the other hand that over the same period because of irregularity in the injection of Lycal 93HS to the right hand side (i.e. B-side), relatively extended areas of deposit had formed on the boiler tubes leading to the upper furnace regions.

The variation in physical and textural differences observed between deposit samples collected from boilers No.6 and No.5 with and without Lycal 93HS injection respectively, are illustrated in Plate 4-6 and described in Section 4.2.3. The two boilers were of the same size, operating under the same conditions with similar furnace temperatures and gas flow regimes and used the same coal for burning. Therefore it must be considered that the variations in the deposit samples from the two boilers is as a consequence of Lycal 93HS injection.

The most notable differences between the range of deposit samples from boilers No.6 and No.5, as previously described in Section 4.2.3(c), were found to be the greater size, thickness and density of samples from boiler No.5 compared to those from boiler No.6. Furthermore, most of deposits, except some within the fourth batch from boiler No.6, were monolithic, whereas for boiler No.5 samples were mostly layered. They either displayed an inner and outer layer or they had an inner, middle and outer layer (see Plate 4-13).

Contrary to a large number of observations in the literature^{82,86,97-99,104,134,135}, deposits on boiler tubes in boilers No.6 or No.5 did not exhibit a thin inner white layer of ash. However, in other studies^{60,96} where increased amounts of alkali oxides (i.e. Na_2O , K_2O), sulphurous oxides (i.e. SO_2) or chlorides¹⁰⁴ (i.e. NaCl) responsible for the white colour, were absent from the inner layer, the colour variations across the deposit layers were generally compatible with those in this study. This suggests that the chemical and/or mineralogical variations have a more determinant effect on the colour and layering orientation of deposits than the temperature ranges and their variations within the boiler furnaces. Other workers have shown⁴⁷ the existence of an initial layer to be related to the potassium level alone or to have been due to calcium sulphate and iron oxide enrichment.¹⁰⁹ In the absence of significant amounts of potassium oxide in the coal ash

(see Table 3-2) and the deposit samples, high concentrations of iron, calcium and sulphur oxides within the layered bottom screen tube deposit samples were significantly shown in Tables 4-5 and 4-6. This is particularly revealing since most of the deposition problems within boiler No.6 was associated with this region. The role of Lyclal 93HS and its combination with a calcium sulphate and iron oxide enriched ash sphere was shown in Plate 4-44 (see EDX analyses for regions B and C). Although the micrograph is representative of a lower furnace (i.e. front or rear walls) deposit sample, it still illustrates the way these components are combined to form the ash sphere. The presence of Lyclal 93HS can be detected from the magnesium peak.

5.5.2 Microscopic Examination and Analysis of Boiler Deposits

5.5.2 (a) Unpolished Deposit Samples

For the unpolished deposit samples in Plates 4-14 to 4-22 and 4-23 to 4-28, with and without Lyclal 93HS injections respectively, the main points of observations were:

- For boiler No.6, the degree of bonding, neck growth and coalescence between spherical ash particles was found to be much more limited in the lower furnace deposits (i.e. Plates 4-14, 4-16) than the upper furnace samples (i.e. Plates 4-17, 4-18, 4-21, 4-22). For boiler No.5, both lower furnace and upper furnace deposit samples (i.e. Plates 4-23 to 4-25 and 4-26 to 4-27 respectively), appeared to have the same degree of bonding and coalescence. This was much more extensive, forming larger agglomerates of fused, sometimes porous morphologies (e.g Plate 4-25).
- A crusty iron-silicate matrix was found acting as the bonding agent between spherical ash particles in deposits from the lower furnace region within boiler No.6 (see Plates 4-14, 4-16). The two elemental oxides of Si and Fe have been found¹⁹³ to have a strongly adhesive affect, even at relatively low temperatures, in binding the ash

particles. A small amount of magnesia was shown associated with the crusty region (see Plate 4-16: EDX for point C). The presence of magnesia could be as the result of Lycal 93HS injection.

- Lower and upper furnace deposit samples from boilers No.6 and No.5 contained particles of pure iron oxide spread over the surface of singular or bonded ash spheres (see Plates 4-15, 4-17 and 4-24). This was particularly extensive for the upper furnace samples, where coalesced ash particles were found to be enveloped in iron oxide enriched phases (see Plates 4-17, 4-18 and 4-26). This produces a surface texture which can readily act as an anchoring site for finer ash cenospheres or solid spheres (see Plates 4-17, 4-18).

The enrichment of the upper furnace deposit samples in iron rich particles has been suggested⁴⁷ to be due to their concentration in the centre of the gas flow streams within the boiler, therefore impinging on the screen tubes laid horizontally on their path upward in the direction of furnace roof. This means that due to accelerated gas flow regimes, iron rich gravity fractions of the fly ash particulates are carried upwards and not sideways towards the front, rear or side walls.

- A selection of cenospheres of a few microns in size as well as angular molten ash particles of similar texture and size within upper furnace deposit samples from boilers No.6 and No.5 are illustrated in Plates 4-19, 4-20 and Plates 4-27, 4-28 respectively. The variation in shape and the extent of softening for these particles could be a measure of their softening and melting characteristics within the boiler environment.

5.5.2 (b) *Polished Deposit Samples*

For the polished deposit samples in Plates 4-42 to 4-57 and 4-58 to 4-69, with and without Lycal 93HS injections respectively, the main points of observations were:

- The low magnification photographs of lower and upper furnace deposit samples from boiler No.6, shown in Plates 4-42 and 4-53 respectively, showed a very open, highly porous, skeletal structure. The corresponding photographs from boiler No.5, shown in Plates 4-58, 4-60 and 4-62 for the lower furnace and Plates 4-64, 4-65 and 4-68 for the upper furnace deposit samples showed highly porous, fully fused, continuous structures. The changes thus observed show that Lycal 93HS has changed the microstructure of the deposits in a fundamental way. In addition Plates 4-1 to 4-5 in Section 4.2.1 have shown categorically that Lycal 93HS has a bulk effect on the extent of deposit formation on boiler tube surfaces by making them friable and more easily removed through the intermittent action of soot blowers.

- The enrichment of deposits in iron oxide, was most evident with the upper furnace samples from both boilers. These are depicted in Plates 4-53 to 4-57 and 4-65 to 4-69 for boilers No.6 and No.5 respectively. The iron oxide was found in a variety of crystalline forms such as: euhedral hematite particles (see Plates 4-46, 4-47, 4-49, 4-66, 4-68), dendritic hematite particles (see Plates 4-43, 4-45, 4-55, 4-57, 4-69), dendritic iron-spinel particles (see Plate 4-47, 4-63, 4-69), angular iron-spinel particles (see Plate 4-48), angular cuboid particles (see Plate 4-43, 4-66, 4-67, 4-69), very fine dendritic particles (see Plate 4-45).

The variation in the morphology of iron oxide and iron oxide containing compounds are further displayed under polarised, crossed illumination in Plates 4-37, 4-39, 4-41. The iron rich regions and phases as fused, coalesced or well rounded spheres appeared as black and grey, red, orange or greyish green depending on their mineralogy (i.e. as hematite, magnetite, wustite or iron-spinel) and morphology (i.e. as dendrites, euhedral spheres, angular cuboids, hexagonal particles). The non-ferrous regions of the matrix and spherical ash particles appeared as mixtures of white, yellow, beige and colourless

thus reflecting the mineralogical variations between the heavier (i.e. iron rich minerals) and lighter (alumino-silicate based minerals) components of the ash.

Iron oxide predominantly appeared as the bonding phase between spherical ash particles, particularly for the upper furnace deposit samples (see Plates 4-53 to 4-56).

- In some samples it was found that at the point where two spherical ash particles were joined together, significantly higher concentrations of calcium and sulphur were present (see Plate 4-44: EDX for point B). These two elements alone^{104,194} as oxides or sulphates or in conjunction with iron¹⁸ or sodium⁹⁸ have been found to be responsible for bond formation between ash spheres. Identification of these oxides is important with respect to characterisation of the possible phases in the boundary regions of spherical ash particles.

- The main crystalline phases in addition to the ferrous ones described previously, were also observed in a variety of forms such as:

Large mullite needles (see Plate 4-63), medium-sized mullite needles (see Plate 4-49), fine mullite needles (see Plate 4-50), fine dendrites of iron - aluminium - magnesium oxides (see Plate 4-46).

These variations in the form and type of ferrous and non-ferrous crystalline phases are further indications of the heterogeneous environment in which the crystal phases nucleate and develop. Formation of crystal phases present within various ash particles are thus influenced by the local environment, the rate of cooling and the general boiler atmosphere.

5.6 APPLICATION OF LABORATORY-BASED TECHNIQUES TO DEPOSIT SOFTENING BEHAVIOUR INSIDE THE BOILER SYSTEM

5.6.1 Correlation of the Softening Regimes for Fashioned Deposits to Boiler Environment

From Table 4-12 it can be seen that the IDT values for all of the deposit samples collected under the influence of Lycal 93HS injection were invariably higher than 1340°C. The ST values were in turn above 1450°C and 1370°C for the lower and upper furnace samples respectively. Studies of ash fusion have shown^{55,183} that ashes with IDT values between 1260-1430°C and ST (i.e. melting temperature) values between 1300-1500°C have respectively been designated as marginally fusible and relatively non-fusible. Therefore, considering that the furnace gas temperatures inside a stoker boiler system, depending on the furnace residence time and location, can vary between 1200 and 700°C¹⁸⁰, no deposit formation would have been expected. The fact that formation of deposits did occur, can only further indicate the complex interaction between the ash matter and its environment within the boiler system. The combination of these complex interactions make any characterisation of factors responsible for deposit formations extremely difficult and therefore the use of an additive such as Lycal 93HS, towards alleviation of deposit formation would have to be based on the analysis of deposit samples.

5.6.2 Relevance of Deposit Reconstitution to its Softening Behaviour Within the Boiler Environment

The formation and morphology of the deposit is the result of coalescence of softened or molten ash particles that arrive on the boiler tubes, largely as a matter of chance. This was simulated through evaluation of the softening of the "reconstituted" deposit

samples. The dependence of the segregation of individual ash constituents on the softening of resulting deposits can be detected from comparison of the results presented in Tables 4-12 and 4-13. The reconstituted samples displayed a decrease in their softening temperatures, ranging from 36 to 124°C and 10 to 70°C for their IDT and ST values respectively compared to their corresponding values in the fashioned state. Furthermore, the reconstituted samples were plastic over broader temperature ranges for the ST to HT and HT to FT than the fashioned samples. This is significant in terms of deposit build up since deposits most difficult to remove have been shown⁸² to have been plastic over a broader temperature range.

5.6.3 Role of Iron Oxide on the Softening Behaviour of Deposits on Boiler Tube Surfaces

Results of the heat treatment of the fashioned F1 and F2 type deposit samples are shown in Table 4-17. It is clear that the F1 type samples with much lower Fe₂O₃ content (9-13 mass%) could be considered as difficultly fusible at 1350°C whereas the F2 type samples with much higher Fe₂O₃ content (24-40 mass%), were readily fusible at 1200°C.

The variation in the extent of melting and fusion of the two type of samples was seen to be very much as a result of both the production of more molten ash and the lowering of deposit viscosity. It seemed that at lower temperatures (i.e. 1200°C), further softening was due to the increase in the molten matter whereas at higher temperatures (i.e. 1275 and 1350°C), the reduction in the viscosity of the bulk sample seemed to be the main cause for further softening. This was particularly evident for the F2 type samples. These observations are in agreement with other studies.^{58,182}

The results of the cone fusion tests on the reconstituted F1 and F2 deposit samples

presented in Table 4-14 showed relatively smaller differences in the softening stage (i.e. ST) compared to the results for fashioned deposit specimens presented in Table 4-17. The IDT values of 1350-1400°C for the reconstituted F1 type samples are close to the equivalent values for the fashioned samples at 1350°C. However, for the iron enriched F2 type samples, the IDT values of 1320-1350°C were significantly higher than the equivalent value of 1200°C for the fashioned samples. The difference in these observations can be related to the role of iron rich particles of ash. In the fashioned state these particles were mostly associated with the outer surface of the deposit (see Plates 4-9, 4-10). The evidence for the presence of iron oxide enriched outer dust layer for the F2 type deposits can be deduced from their significantly high iron oxide contents compared to the F1 type deposits (see Table 4-3). On heating, the surface of the sample first softens and forms a glazed structure. Gradually molten matter flows into the sample as the temperature is raised and the whole of the sample becomes molten. However in the reconstituted samples, the iron rich particles are well mixed with other particles within the sample. The iron rich particles can now only form soft or molten spots within the sample, bonding other solid ash spheres together. Also as suggested in other investigations^{50,185} these particles can be the main source of deposit strength, and hence support for massive slagging deposits by re-enforcing the adhesive bonds between the slag and the collecting tube surfaces. Therefore higher temperature would be required before the whole of the sample becomes molten. This could account for the particular deposition problems associated with the upper furnace regions with much higher iron oxide concentrations in deposits, as stated previously and observed in other investigations.^{45,47,50,111}

5.7 PROPOSALS FOR THE ROLE OF LYCAL 93HS IN BOILER No.6

5.7.1 Introduction

The most evident bulk effect of Lycal 93HS can be observed from Plates 4-1 to 4-5 which demonstrate how its continuous injection has effectively helped to maintain the boiler tube surfaces clean. At some regions (side B) where Lycal 93HS injection had been reduced some deposit formation can be seen (see Plates 4-4, 4-5). Lycal 93HS was injected with the secondary air (138°C)¹⁷¹ into the combustion chamber at both the front and rear of the grate along the width of the furnace in a position about 30 cm above the fuel bed. This ensures good mixing with the air-borne fly ash before it is thrown outwards toward the front, rear and side walls. The fine Lycal 93HS particles can thus react with the fly ash matter before they are deposited on boiler tube surfaces or escape the boiler environment.

The formation of friable deposits under the influence of Lycal 93HS injection into boiler No.6 has already established its beneficial effect (see Plates 4-8 to 4-10). The evidence of microstructural changes previously discussed in Section 5.4.2 (b) has shown how Lycal 93HS injection into boiler No.6 was instrumental in transforming highly porous, fully fused deposit samples with continuous structures into highly porous, very open skeletal structures. In order to determine the possible mechanisms involved, the effect of Lycal 93HS has been investigated in two ways:

1. As an "internal" modifier of the molten fly ash particles with respect to their bulk softening behaviour.
2. As a "external" surface modifier of the molten fly ash particles with respect to their adhesion and coalescence properties.

Additives can also act on the gaseous and vapour phases as well as on the particulate materials in the system. However the results of elemental chemical composition for the

deposit samples (see Tables 4-2 to 4-6) and particulate ash hopper and grit arrestor samples (see Table 4-7) did not show any significant enrichment in the volatile alkali oxides $(\text{Na,K})_2\text{O}$ and sulphur oxide (SO_3). Furthermore, the SEM-EDX analysis of the bulk deposit samples from boilers No.6 and No.5 did not exhibit any notable association of these oxides which are usually indicative of their presence within the inner layer of deposits as K_2SO_4 , Na_2SO_4 and / or more complex sulphates (see Table 2-2). Hence, these aspects were not considered in this study.

The role of Lycal 93HS in terms of the first, second or both of the particulate mechanisms above, can occur before, during or after the deposition of fly ash particles. This would be dependent on the prevailing conditions at various regions within the boiler, subsequently affecting the texture and morphology of the deposit.

5.7.2 The Role of Lycal 93HS as an Internal Modifier of Deposit Particles With Respect to their Softening Behaviour

Table 4-15 shows that for a range of deposit samples collected under the pre-Lycal injection conditions, additions of Lycal 93HS upto 8 mass% acted as a strong fluxing agent under cone fusing test conditions. The temperatures for various softening stages were progressively decreased with increasing additions for all of the upper furnace deposit samples. However for the lower furnace deposit samples, the fluxing effects of Lycal 93HS were more limited, in some cases even increasing the HT and FT values. For all of the deposit samples the extent of plasticity was enhanced by the additions of Lycal 93HS, thus delaying or preventing the fluid formation for the maximum operating furnace temperature of 1450°C.

The fluxing action of Lycal 93HS is further demonstrated by comparison of Tables 4-14 and 4-16 for a selected number of lower furnace deposit samples collected during the

Lycal 93HS injection conditions. Similar to the iron enriched upper furnace deposit samples collected under the pre-Lycal 93HS conditions, the iron enriched F2 type samples showed either little reduction or indeed increased FT values. The extent of plasticity was again extended for both the F1 and F2 type deposits.

These observations can be correlated to the behaviour of depositing fly ash particles by comparing them with the ash admixture results (see Table 4-48 and Figure 4-17). It can clearly be seen that increasing additions of Lycal had only a marginal effect on the softening temperatures of AM1 ash admixture but generally decreased the corresponding temperatures for the AM4 admixture. Comparison of these results with those from the reconstituted deposits (see Figures 4-4 and 4-5) shows that ash from the fine particles (AM4) had behaved similarly to the deposit samples. The IDT values for AM4 and deposit samples were lowered by an average of 19.4 and 9.4°C per 1 mass% of added Lycal 93HS respectively. However, the ash from the coarse particles (AM1) had behaved very differently and had shown only marginal sintering with 3 mass% addition of Lycal 93HS. This behaviour could be attributed to the lower basic oxide (i.e. CaO + MgO + K₂O) content (see Table 4-47) or the presence of more refractory mineral phases within the AM1 compared to AM4.

These reductions in cone fusion temperature values are somewhat higher than data in the literature¹⁹⁵ reporting that up to about 18 mass% magnesia in a magnesia-kaolin system would lower the IDT values by 2.7°C for every 1 mass% of magnesia present. Others^{196,197} have also shown that additions of magnesia produced effects dependent on the composition of the ash. If much iron was present, magnesium ferrite¹⁹⁶ might form, making the ash more refractory.

The relevance of these observations to the effect of Lycal 93HS injection on the ash within boiler atmosphere can be summarised as follows:

For the ash particles in flight, their plasticity over lower and extended temperature ranges would make them stickier over a longer period of time. Therefore their propensity to adhere onto the boiler tubes would be significantly increased. However if Lycal 93HS is absorbed onto the surface of the fly ash particulates, it can significantly reduce their sintering through transformation of glass to crystalline species on the surface layer of silicate ash particles.¹⁶³ For the softened ash particles already impacted onto the boiler tubes to form part of a maturing deposit, the extended plasticity range would cause the enhancement of devitrification range. This could be achieved via increased rate of crystallisation and crystalline growth induced by the presence of Lycal 93HS. The ratio of glassy to crystalline fraction of the ash as previously expressed in equation (2-27) significantly determines the rate of deposit formation, increasing with increase in glassy fraction. Additions of 2 and 8 mass% Lycal 93HS increased the sinter point of the pre-Lycal 93HS injected samples by 50 and 30°C respectively. This would provide an extended vitrification range for the deposited ash over the boiler tubes.

The possible devitrification enhancing mechanism of Lycal 93HS may involve the promotion of nucleating agents or phases derived from iron rich particles within the melt. These agents or iron rich phases can promote the separation of various phases within the fluid ash, assisted by the temperature gradients across the thickness of the forming deposit layer. The enrichment of iron oxide in the deposits from bottom screen tubes region within boiler No.6 could hence particularly influence the effectiveness of injected Lycal 93HS. Formation of nucleating sites promoted by copper oxychloride as the additive have been proposed by other researchers.^{144,145,198,199} A general trend was shown¹⁶³ whereby this additive was more effective with ashes containing 10-20 mass% Fe₂O₃.

5.7.3 The Role of Lycal 93HS as an External Modifier of Deposit Particles With

Respect to their Surface Properties

If the solid particles of Lycal 93HS (as MgO) come into contact with the spherical ash particles during their flight or immediately after their deposition on boiler tube surfaces, the particles and hence resulting deposit would have a different characteristic. This difference however would depend on the degree of impingement of the fine MgO particles which might fully or partially cover the surface of the ash particle. Although, contrary to suggestions in one study¹⁶² which has proposed a change in terms of crystallisation of ash particles through their instantaneous reaction between an additive, it would seem unlikely, due to very short residence times, that an instantaneous reaction between an additive (e.g MgO) and ash particulates would modify their crystallisation and hence by making them harder, render them less sticky. If Lycal 93HS modifies the surface properties, it might be expected to also modify the strength of deposits formed by the fly ash. It should be mentioned that the ability of small amounts of an additive to transform the surface of the ash matter would be dependent on whether the surface constitution of the ash was of a glassy or crystalline nature. This aspect has been discussed by some other researchers.^{84,164} Furthermore it has been shown that the surface properties of the ash particles could change in two ways:^{167,168}

1. Indirectly, through substantial migration of major elements towards the injected additive (i.e. MgO) within deposits, in sufficiently large enough quantities. These elements were found to react with the MgO particles as volatile species. The MgO particles would thus have neutralised them and inhibited their deleterious softening effect on the ash.

2. Directly, by adherence of MgO to the molten surface of the glassy ash spheres, forming an insulating layer. This layer would thus neutralise the effect of volatile species which on condensation on and coating of the ash particles would form a sticky layer. The layer of MgO coating can also act as a physical, refractory barrier to ash particle - ash particle contact.

The results of HF-dissolution experiments for a range of samples from boiler No.6 and No.5 with and without injection of Lycal 93HS respectively are presented in Figures 4-7 to 4-13 and can thus be discussed with respect to the above observations. This series of experiments were carried out to determine if the propositions regarding the surface effects of Lycal 93HS on matured deposit samples and fly ash particulate matter (i.e. economiser ash hoppers and grit arrestors) could be detected from comparison of results with and without Lycal injection. The bulk solubility is clearly a property of both the glassy and crystalline matrix which was discussed previously, and it would be expected that those elements that are either chemically or physically trapped within this matrix to exhibit low solubility. The provision of fresh solvent immediately after extraction of solutions at every point during the tests further allowed for the potentially soluble material to ultimately enter the solutions.

Figures 4-8 and 4-9 show that the MgO concentrations in the leachate were initially much higher for samples with Lycal 93HS injection than the corresponding samples without Lycal 93HS injection for rear and side wall deposits respectively. The initial high concentrations (1.68-2.35 mg/L) are indicative of the readily soluble nature of MgO from the surface of the deposit samples with Lycal 93HS injection compared to much lower values (0.34-2.0 mg/L) for the samples without Lycal 93HS injection. The MgO concentrations for the samples with Lycal 93HS approached a constant value after

one hour, increasing only marginally from the initial leachate concentration. The MgO concentrations for the samples without Lycal 93HS increased rapidly, approaching similar values after two hours. Thereafter the rate of increase in the MgO concentration is relatively slower, final concentration values are found to be higher than the samples with Lycal 93HS injection and particularly for the side wall sample, where the values continue to increase and do not level off. The bulk elemental oxide concentrations of MgO are found to be very similar for both the samples with and without Lycal 93HS injection (see Tables 4-4 to 4-6). This further emphasises the point that significantly higher concentrations of MgO in the leachates for the two samples with on-line injection of Lycal 93HS must be due to the free MgO (from Lycal 93HS).

The concentrations of Fe_2O_3 and SiO_2 in the leachate in Figure 4-8 are much higher for the deposit sample with Lycal 93HS injection than the sample without. Although the initial concentrations after 15 minutes are very similar for all the samples. Furthermore, the leachate concentrations increase only marginally after 3 hours for the sample with Lycal, the SiO_2 concentration for the sample without Lycal shows a continuous increase up to 6 hours. With respect to the bulk elemental composition of these oxides in Table 4-4 to 4-6 which show very similar concentrations, the difference in behaviour can be accounted for by the way these oxides could be associated. If Fe_2O_3 and SiO_2 are absorbed indirectly as volatile species onto the surface of fine microcrystalline MgO particles, they would show much higher solubility than the Fe_2O_3 and SiO_2 compounds which could be present as part of the alumino-silicate matrix. The variation in the leachate concentration of these two oxides, despite their similar concentrations in the bulk samples could depend on their status within the bulk deposit samples. If for example the source of SiO_2 and Fe_2O_3 in one sample happened to be quartz and hematite / magnetite or iron-spinel respectively, then they can much more readily

dissolve in the solution than if they are present as part of a complex alumino-silicate matrix structure. These results are reversed for the side wall samples in Figure 4-9 which showed the enrichment of Fe_2O_3 and SiO_2 for the sample without Lycal 93HS injection despite very similar values for the bulk samples (see Tables 4-4 and 4-6). This time, the variation could reflect the status of the two oxides as discrete minerals within the sample without Lycal 93HS injection.

Figure 4-10 for bottom screen tube deposit samples illustrated significantly higher initial leachate concentration of MgO for the sample with Lycal 93HS injection from the second batch. Other samples with and without Lycal showed almost identical initial concentrations. However, whereas for two of the samples with Lycal injection, the concentration changes, from their initial to their final values, were limited over the test period (i.e. maximum of 0.2 mg/L), for the other sample (i.e. batch 4), the concentration change was 0.7 mg/L. The higher initial MgO concentration for the second batch sample can be reflected from its higher concentration in the bulk sample (see Table 4-2) compared to similar samples from other batches (see Tables 4-3 and 4-4). Furthermore, it is evident that whereas concentration values for the samples from the second and fourth batches approached a constant level, the values for the sample from the third batch (i.e. F1 type) increased continuously. This can be attributed to the highly porous nature of this sample (see Plate 4-8), allowing for a more gradual and continuous leaching of the sample.

The greater Fe_2O_3 leachate concentrations for the deposit sample without Lycal 93HS compared to other samples, is reflected in the bulk composition of this sample (see the composition for the inner layer in Table 4-6 compared to Tables 4-2 to 4-4). Continuous dissolution of Fe_2O_3 for all of the samples, reflected by the slope of their

leachate concentrations is indicative of their availability as discrete minerals. However, the general Fe_2O_3 leachate concentrations for all of the samples were comparatively lower than corresponding values for the lower furnace deposit samples in Figures 4-8 and 4-9. This is unexpected considering the much higher Fe_2O_3 contents of the upper furnace samples. However, it could indicate that the Fe_2O_3 is mostly concentrated within rather than on the surface of the upper furnace deposits. This however was certainly not the case for the F2 type deposits which have already been shown to have a coating of iron rich particles (see Plate 4-9, 4-10).

The SiO_2 contents of the leachate for all of the samples were generally lower than corresponding values from lower furnace deposit samples (see Figures 4-7 to 4-9). Continuous dissolution of SiO_2 for all of the samples, reflected by the slope of their leachate concentrations is indicative of its availability on the surface. Furthermore, the extent of variation in the leachate concentrations is compatible with the concentration differences for the bulk compositions, with higher SiO_2 contents for samples from second and third batches compared to samples from the fourth and fifth batches (see Tables 4-2 to 4-4 and Table 4-6).

Figure 4-7 for front wall deposit samples illustrated significantly high initial leachate concentrations of MgO for samples with Lycal injection from the second and fourth batches. For the other samples with and without Lycal injection, initial leachate concentrations were similar but much lower. However, whereas the leachate concentration profiles increased only marginally after 5 hours for the samples with Lycal, the leachate concentration profile for the sample (inner layer) without Lycal increased rapidly by threefold after 1 hour and thereafter it increased at a slower rate, approaching a constant value at 5 mg/L. This high leachate concentration of MgO could

be due to the residual effect of chrome-magnesite refractory brick lining between boiler tubes which was shown in the bulk chemical composition in Table 4-6. It is further evident that although MgO concentration in the bulk sample without Lycal was more than eight fold higher than that of Lycal injected samples, its initial leachate concentration after 15 minutes was still lower. This could be due to the nature of MgO, as particulates (i.e. from Lycal 93HS), readily available for dissolution compared to the MgO in the MgO-Cr₂O₃ refractory layer contaminating the deposit sample.

The leachate concentration profiles for Fe₂O₃ in samples with Lycal shows similar rates of increase with Lycal, although the sample from the second batch with the highest Fe₂O₃ content amongst the bulk samples (compare Table 4-2 with Tables 4-3 and 4-4) showed the lowest leachate concentration profile. The leachate concentration for the sample without Lycal shows higher initial values up to 1 hour followed by a sudden jump after 2 hours and decreasing thereafter to a final concentration which is lower than samples from the third and fourth batch. This anomalous behaviour can reflect the nature of Fe₂O₃ within the inner layer, mixed with the alumino-silicate matrix of the ash and not as discrete individual minerals, as was the case for the bottom screen tubes.

For the SiO₂, the leachate concentration profiles for the samples with Lycal are comparable to those for the corresponding Fe₂O₃ concentrations. the leachate concentration profile is significantly lower for the sample without Lycal, reaching a maximum value of 1 mg/L after 5 hours. The difference in the SiO₂ concentrations between samples with and without Lycal can however be clearly expected from their bulk compositions (see Tables 4-2 to 4-4 and Table 4-6). The concentration profiles for all of the samples however shows a continuous and constant increase which could indicate that SiO₂ is mostly present as discrete particles such as quartz.

For the particulate ash hopper and grit arrestor samples in Figures 4-11 to 4-13, the

leachate concentration values for all of the three oxides were relatively higher than the leachate concentration values for the bulk deposit samples (Figures 4-7 to 4-10). This can be attributed to the fact that although the amount of particulate samples was identical to the mass of bulk deposit samples (i.e. 1 gram), the particulate samples would have larger surface areas available for leaching in the solution.

Figure 4-11 shows that leachate concentrations of the three oxides were higher for the particulate sample without Lycal 93HS, despite lower bulk values (see Table 4-7). However, although the initial and final values of MgO concentrations are higher for the sample without Lycal, its leachate concentration values remain almost constant after 1 hour. This is unlike the leachate concentration profile for the sample with Lycal, which shows a continuous increase at an almost constant rate. The higher initial MgO values for the particulate sample without Lycal is despite lower MgO content for the bulk sample as determined in Table 4-7. However, since this sample was collected from boiler No.6 during the time when Lycal was off-line, the relatively high MgO leachate concentration could be due to the residual Lycal in the system, which could have been collected by the particles as they traversed through the boiler and down the economisers.

The Fe_2O_3 and SiO_2 leachate concentration profiles are very similar for both samples. However, significantly higher initial values for the sample without Lycal is indicative of the relative availability of these components on the surface of the ash particles possibly as discrete minerals. The results of the bulk composition for the two samples (see Table 4-7), does not show any significant difference in terms of Fe_2O_3 and SiO_2 contents, suggesting therefore the presence of the more easily soluble components for the sample without Lycal. However, the leachate concentration profiles for the two oxides continue at a relatively more constant rate for the sample with Lycal, indicating

a constant rate of dissolution which could be due to the masking effect of Lycal, promoting a slower but more continuous rate of release for these components into the solution.

Figure 4-12 showed significantly higher initial MgO leachate concentration for the grit sample with Lycal injection, increasing by two-fold after 1 hour, after which the leachate concentration remained almost constant. This suggests that a state of chemical equilibrium might have been achieved with respect to the MgO dissolution. The leachate concentration for the sample without Lycal decreased initially up to 5 seconds and then increased gradually thereafter. The possibility that Lycal is the source of MgO in the leachate for the sample with Lycal injection, can further be deduced from Table 4-7. It can be seen that the bulk MgO contents are higher for the sample without Lycal than the samples with Lycal. It is evident therefore that although lower in content, the MgO from sample with Lycal was more readily soluble than sample without Lycal but with originally higher MgO content.

The leachate concentration profiles for Fe_2O_3 and SiO_2 for samples with and without Lycal showed similar patterns. However, despite initial reductions up to 15 seconds which could be due to sampling errors, the leachate concentration values of Fe_2O_3 and SiO_2 were generally higher for the sample without Lycal. Since the amount of these two oxides in the bulk composition of the sample with Lycal were either slightly higher (i.e. SiO_2) or lower (i.e. Fe_2O_3) than their content in the bulk composition of sample without Lycal, the variation in the profiles can be attributed to the masking effect of Lycal which could inhibit the dissolution of these oxides.

Figure 4-13 showed much higher leachate concentration levels for all the three oxides than the other particulate samples in Figures 4-11 and 4-12. This is due to the very fine size of the particles and their extended surface area. MgO leachate concentration

significantly increased initially up to 15 seconds for the particulate sample with Lycal injection and then decreased up to 1 hour before it increased again and approached a constant value thereafter. The unusual shape of the leachate concentration profile can be due to the residual effect of some of the very fine particulates in sampling process. The high initial leachate concentration values and the final levelling of the profile can once again be attributed to the availability of MgO as Lycal 93HS over the surface of the fine particles and the subsequent attainment of equilibria. The MgO leachate concentration values for the sample without Lycal are significantly lower and remained relatively constant after an initial increase up to 1 hour. It is further evident from Table 4-7 that the MgO content in the bulk composition for the sample with Lycal is higher. This could be attributed to the presence of Lycal which would more readily be available as MgO on the surface of the particles.

The leachate concentration values for Fe_2O_3 and SiO_2 for the sample with Lycal are significantly higher than the values for the sample without Lycal. After initial increases up to 2 hours, the concentration profiles for the two oxides approached a constant value. This suggests a continuous dissolution at a constant rate which could be attributed to separate mineral species such as hematite/magnetite and/or iron-spinels (i.e. Fe_2O_3 enriched) and quartz (i.e. SiO_2) on the surface of particles.

Studies of coal fly ash surface chemistry have shown¹⁶ that unlike many trace elements, the major oxides such as those of Si, Al, Mg, Na and P do not segregate to the surface. The percentage of some of these elements is shown in Table 5-4¹⁶. Therefore, considering the very low concentrations of hydrofluoric acid used in this study (i.e. 0.05 molar), the evaluated concentrations for the three oxides including MgO must be attributed to the surface of the samples. Also it can further be seen that whereas for

**Table 5-4: Percentage of elements leached
from a typical coal fly ash¹⁶**

Element	% Leached
Al	0.2
B	5
Ba	4
Ca	35
Cr	30
K	40
Mg	0.2
Mn	0.4
Mo	85
Na	10
P	6
Pb	100
Si	0.1
Sr	6
Zn	6

most of the samples, particularly the non-particulate samples, the MgO leachate concentration profiles for samples with Lycal were almost level after 5 to 6 hours, those for samples without Lycal increased continuously at reduced rates.

5.8 PROPOSALS FOR A MECHANISM FOR THE EFFECT OF LYCAL 93HS ON DEPOSIT FORMATION

5.8.1 Introduction

The formation of fly ash deposits in boilers is a very complex process and it is generally believed that it is mainly the combination of coal ash composition and the high temperatures within boiler environment which determine the type of deposit.

Many other factors contributing to deposit formation, such as high alkali oxides, sulphur and chlorine contents of the ash or very high temperatures within the boiler environment as in p.f. fired boilers, found responsible for deposit formation, were not present in significant amounts in this study. In spite of this, deposits were formed and operational problems were encountered by boiler operators at West Belfast power station as discussed previously. The injection of Lycal 93HS alleviated these problems by making the boiler deposits weaker and more friable and thus more easily removable through the action of sootblowers.

5.8.2 Consideration of Factors Involved in Deposition

The various stages contributing to the formation of deposits in this study could be characterised as follows:

On entry into the boiler, as the coal particles on the grate become subjected to heat, they undergo pyrolysis, releasing their water and volatile matter with subsequent burning of the carbonaceous residue. However, unlike the coal lumps, which release most of their mineral matter which becomes airborne as ash whilst they are burning on

the grate, the coal smalls and fines because of their size and density are readily elutriated and burn in suspension above the grate. The ash derived from the smalls and fines was shown to be much more readily fusible than the ash derived from the larger coal lumps (see Table 4-48). This softened ash which exists mostly as fine solid or hollow spheres (cenospheres) within the boiler environment may arrive on boiler tube surfaces as single particles or agglomerates of two or more spheres of similar or different sizes as was observed for some of the fly ash particles from the ash hoppers presented in Plates 4-30 and 4-31.

The significantly lower unburned carbon content for the medium and fine spherical ash hopper and grit arrestor particles compared to the coarse particles (see Table 4-8 and Figure 4-1) is indicative of a much higher release and burning of carbon within these particles, which could enhance their softened and/or molten status as they are propelled towards boiler tube surfaces. On impaction on the boiler tube surfaces, these particles may either freeze and stick or may rebound and become entrained in the gas flow, depending on their physical status and surface texture as well as regional gas flow regimes and temperatures. The formation of a very thin layer (i.e. 1-2 mm) of fine ash particles on the test probe after 12 hours as explained in Section 4.4.1, further indicates their role in deposit formation.

The larger spherical and cenospherical ash particles derived from the larger ash particles would then start adhering to the finer ash spheres once a layer of some thickness (i.e. a few millimeters) with a sticky molten layer has been formed. However, the very high unburned carbon content (see Table 4-8 and Figure 4-1) and the refractory nature of the ash derived from the coal lumps, as presented in Table 4-48 would suggest that these ash spheres and cenospheres would less readily be in a softened state and therefore would not easily coalesce with other ash particles during

their flight within the boiler environment. Significant bond formation and bridging between spherical ash particles would take place after these larger ash spheres have impinged on the forming deposit layer.

Regions of significant iron enrichment around and in between spherical ash particles were found to be particularly instrumental in bond formation within the upper furnace deposit samples (see Plates 4-53, 4-54 and 4-55). For the lower furnace deposit samples with generally much lower iron oxide contents (see Tables 4-2, 4-4, 4-5 and 4-6), the influence of ferrous regions was less pronounced. For the layered deposits, the bulk analyses of the lower furnace samples showed that iron oxide (i.e. Fe_2O_3) concentrations in the outer layers were almost similar or twice those in the inner layers. For the upper furnace deposits the situation was reversed and the inner layers showed similar or much higher Fe_2O_3 contents, up to three times, compared to the outer layers (see Tables 4-3, 4-5, 4-6).

This enrichment of Fe_2O_3 can take place via different processes. For the upper furnace deposits, the ferro-spheres impact the tubes directly on their flow path. Since the temperature gradients due to lower gas temperatures are not high enough, the cross boundary diffusion of volatilised oxides (i.e. iron oxides or sulphides) from inner to outer layers would be limited. For the lower furnace deposits, the enrichment of iron oxides or sulphides in the outer layer could be assisted by the process of cross boundary diffusion outwards, towards the much higher flame temperatures. This could also be promoted by the higher temperature gradients across the somewhat thicker deposit which could further advance the combustion of residual carbon within the deposited ash particles which in conjunction with iron could either be present as carbonates (see Section 2.3.2(a)) or as iron carbide (Fe_3C) which on further reaction with the silica within the deposit would release the iron and further

form an iron-silicon compound (Fe_3Si) as explained in Section 2.4.2 (a). Iron can thus be released to migrate to the outer surface of the molten deposit layer.

In addition to iron compounds, calcium and sulphur (as calcium sulphate, CaSO_4) were also shown to act as the bonding agent within the boundary layer between some spherical ash particles in lower furnace deposits (see Plate 4-44). This is a compound which could have derived either directly from the sulphatic minerals (e.g. CaSO_4) or indirectly through decomposition of carbonate minerals (e.g. CaCO_3) and their further reactions with sulphurous oxides within the boiler atmosphere.

5.8.3 The Role of Lycal 93HS With Respect to Deposit Formation

As Lycal 93HS which is principally $\text{Mg}(\text{OH})_2$ enters the furnace, it calcines and forms magnesia, MgO by the release of H_2O . This may further cause the fragmentation of already small MgO particles to even smaller particles. It is expected that as a highly refractory oxide (i.e. melting point = 2800°C), the pure MgO would not melt or even soften within the furnace atmosphere and thus keep its solid form. It has been shown¹⁶⁷ that MgO has a very fine microcrystalline structure capable of absorbing the volatile species of silica, phosphorus and sulphur present within the gas flow regime or on the surface of particulate ash matter within sintered coal ash compounds.

The analysis of collected fine fly ash from the surface of the deposition probe after the 12 hour tests (see Table 4-18) showed that with Lycal 93HS injection the amount of sulphate, phosphate and MgO were significantly higher than the trials without Lycal 93HS injection. The association of the volatile species with the deposited ash particles on the probe after only 12 hours seems to have been promoted by the Lycal injection, although the possibility and the extent of this association was not firmly established. However, in essence if there is an interaction between the MgO particles

and the volatile species, this could have taken place via two routes:

(a). Direct impingement of volatile species onto the surface of the solid MgO particles and further diffusion into the body of the particle where they are absorbed by the microcrystalline constituents of MgO particles. This would immobilise these deleterious compounds and would render them ineffective.

(b). Indirectly through coating of the fine ash spheroids and cenospheres which have already absorbed the deleterious volatile species. This would inhibit any further participation of these species over the surface of the ash particulates to form further bonds with other ash matter.

Although direct supportive evidence can not be given for the first of these processes, it could feasibly occur when Lycal 93HS is in flight within the gas flow stream. For the second process, the evidence could be found in the form of association between Mg and P, Fe and S as oxides which were shown to form the bulk of composition for a dispersion of fine, white particles on cenospherical ash matter from economiser ash hopper region (see Plate 4-30: EDX analysis). Further evidence of such association between MgO and some volatile species could also be suggested from the bulk analysis of the thin layer of fine ash matter collected on the surface of the test probe with and without injection of Lycal 93HS (see Table 4-18). The collection of MgO particles on the surface of fly ash particles would most effectively take place when they are in a softened state within the boiler atmosphere or on boiler tube surfaces.

Limited short term probe deposition trials showed that Lycal 93HS injection was influential in lowering the deposition rate (see Figure 4-6). In view of the different routes suggested concerning the role of Lycal 93HS, the neutralisation of volatile species would create less "sticky" fly ash particles and/or the deposit surfaces. Further deposition of colliding ash particles onto the deposit layer already formed may

consequently be hindered by their rebound and re-entrainment into the gas flow stream. In a separate study carried out on boiler No.6, it was shown²⁰⁰ that the fly ash dust emission rates from the discharge side of the I.D fans (i.e. approach duct to stack), with Lycal 93HS injection, were more than twice the emission rates without Lycal injection. This would mean a lowering of the fly ash content available for deposition within the furnace atmosphere although the higher ash burden was also shown²⁰⁰ to lower the collector efficiencies by 10%.

The extent of crystallinity within the deposit samples with and without Lycal 93HS injection was found to be similar. However, laboratory determinations showed that additions of Lycal 93HS between 5-10 mass% influenced the formation of crystalline laths similar in composition to mullite, within the fluid melt of same acidic ash components. Although many of the other acidic ash components had very similar compositions, they did not exhibit any crystallisation on cooling their fluid melt which contained increasing additions of Lycal 93HS. This could be due to mineralogical variations or the extent of miscibility of Lycal 93HS and the fluid melt of the ashes. For the iron enriched ash components, even lower additions of Lycal 93HS at 1-3 mass% transformed the molten ashes and formed highly enriched iron-magnesium oxide or compounds in the form of spikes growing from a siliceous matrix. This has been previously described in Section 5.3.2.

These additions of Lycal 93HS, particularly in the range of 3-10 mass%, are significantly higher than the amount of Lycal 93HS (i.e. at mean value of 0.3 mass%) which was available for reaction with the fly ash matter within the boiler atmosphere. However, the MgO concentration increased significantly by more than threefold to approximately 5.8 mass% within the thin layer of ash sample collected on the surface

of the test probe (see Table 4-18) with on-line injection of Lyclal 93HS. This is indicative of the enrichment of ash by amounts relatively compatible with the Lyclal additions for the ash components in this study.

The work reported in this thesis suggests that the presence of Lyclal 93HS as an additive has an important role to play in reducing the strength of coal ash deposits formed on boiler tube surfaces, by making them friable and easily removed by soot-blowers. Depending on certain factors, most importantly the composition of the coal fly ash and the temperature distribution within the boiler regions, Lyclal can assume more than one role. If much iron (i.e. as iron oxide) was present within the ash, increasing additions of Lyclal 93HS lead to increases in the softening temperatures of the ash. This would prevent the ash from becoming readily softened and thus reduce its tendency to coalesce and form regions of hard, fully fused, slag-type deposits on boiler surfaces. If the ash was of an acidic nature, as defined in this study, increasing additions of Lyclal was influential in both reducing its devitrification temperature as well as increasing the rate of its crystallisation. This would make the fluid ash more viscous and at deposit forming temperatures and therefore less prone to make extended regions of molten ash deposit on boiler tube surfaces.

The presence of fine particulate matter enriched in oxides of Mg, P, S and Fe on the surface of some spherical fly ash particles suggested a certain degree of interaction between Lyclal 93HS and these injurious species. However it could not be ascertained whether such interactions would mostly occur before or after the fly ash particulates have deposited on the boiler surfaces as suggested by the analysis of the collected layer of ash on the test probe.

The results attained here certainly suggest that a full understanding of the principles and the extent of interaction between the additive (i.e. Lycal 93HS) and ash requires a thorough study of the softening and melting behaviour of ash and its components under various temperature and gas flow regimes and compositions.

6. CONCLUSIONS

- (1). External trials at West Belfast Power Station have shown Lycal 93HS injection at the rate of 5 kg/hr to be effective in reducing ash deposit build up by making it more easily removed through the action of soot-blowers.
- (2). The role of Lycal 93HS in formation of friable deposits is very much dependent on the chemical composition of the coal ash within the boiler, particularly its iron oxide content which affects its softening behaviour, determined by laboratory based cone fusion technique.
- (3). The role of Lycal 93HS on the softening behaviour of boiler deposits, using laboratory based cone fusion technique, is dependent on the composition and the arrangement of ash particulates within the softening bulk sample.
- (4). For iron rich components of ash (i.e. 15-39 mass% Fe_2O_3), addition of 0.5 mass% Lycal 93HS, which was compatible with its injection rate into boiler No.6, increased softening temperatures, using the laboratory based cone fusion technique. For other ash components below or above this range (i.e. 12 and 60 mass%) the cone fusion softening temperatures decreased through fluxing action of Lycal 93HS.
- (5). Additions of 5 and 10 mass% Lycal 93HS to the acidic components of the coal ash induced crystallisation of the fluid melt, using laboratory based hot - stage microscopy technique. The crystalline phase was similar to large mullite needles in terms of its composition and structure.

- (6). Additions of 1 to 10 mass% Lycal 93HS to the ferriferous components of the coal ash encourages the formation and growth of fine needles from the surface of some melts but hinders their formation in others, determined by hot-stage microscopy technique. This was shown to be dependent on the iron oxide content of the ash component.
- (7). The proportion of the acidic, basic and ferriferous components of ash either remaining on the grate or becoming air-born as fly ash was shown to be partly dependent on the physical form that these components assume within the coal ash. The basic components were found to be mostly associated with the hard parts of the ash probably remaining on the grate. The acidic and ferriferous components with a powdery texture would readily become air-born as fly ash.
- (8). For the upper furnace deposits, iron oxide was found to invariably act as the bonding phase between spherical ash matter within the deposits. Calcium and sulphur (probably as Ca_2SO_4) was also found in the binding region within spherical ash particles in some lower furnace deposits.
- (9). For the particulate fly ash matter, MgO (i.e. Lycal 93HS) was mostly associated with the fine ($-45\mu\text{m}$) particles. The presence of Lycal 93HS on the surface of these particles was also found to be rich in sulphur and phosphorus oxides or compounds. This suggests a form of interaction between Lycal 93HS and these injurious species.

CHAPTER

(7)

SUGGESTIONS FOR FURTHER WORK

7. SUGGESTIONS FOR FURTHER WORK

The present work was carried out through a wide range of investigations which would directly or indirectly affect the formation of deposits. However, in order to investigate the role of any additive in the way that we have been concerned with in this study, the use of small physical models is conceived to be invaluable. This would allow for the comparative analysis of the pilot scale observations and results with those obtained through the model which provides a more controlled environment.

By using the physical model, the role of Lycal 93HS can also be evaluated for a wide range of gaseous environments and heat cycles as well as its physical interaction with and its effect on the generated ash particles.

The use of hot-stage microscopy technique can be further realised through more elaborate investigation with known minerals and mineral compounds simulating a range of mineralogical compositions. The role of Lycal 93HS through various additions can be more fully investigated and the extent of its influence on each of these minerals and their various combinations can further be shown . These can further be compared against known phase-equilibria diagrams for similar mineralogical compositions.

More sophisticated techniques such as Auger spectroscopy could be used to determine the surface effect of Lycal 93HS in terms of its reaction or combination with a wide range of major, minor or trace elements within the ash. This can also provide information on the extent of reactions of Lycal 93HS with volatile species. This is particularly important with respect to the emission of injurious by-products such as sulphates and phosphates, towards cleaner coal combustion technology.

8. REFERENCES

- 1 Babcock and Wilcox., Steam-It's Generation and Use, 1978, Ch. 9, pp. 1-16.
- 2 Gunn D., Horton R., Industrial Boilers, 1989, Ch. 4, pp. 64-69.
- 3 Williams J.N., Steam Generation, 1969, Ch. 7, pp. 181-191.
- 4 Ambler R.G., Boiler House Design for Solid Fuel, Combustion equipment, NCB-Publication 1976, Six: Combustiin Equipment, pp. 6-19.
- 5 Elonka S.M., Kohan A.L., Standard Heating and Power Boiler Plant Questions and Answers, Ch. 11, pp. 414-415.
- 6 Woodruff E.B., Lammers H.B., Steam Plant Operation, 1967, 3rdEd., Ch. 3, p.88.
- 7 Macek A., Coal Combustion in Boilers: A Mature New Constraints, Combustion, 1983, pp. 65-73.
- 8 Merrell G.A., Knight R.S., Combustion Catalysts in Industry - An Update., Purdue Industrial Fuel Conference 5-6 October 1983, pp. 5-7.
- 9 Macdonald J.R., Shah J., Collins J., Spiker J.S., Combustion Catalysts Effect on Stoker Boiler Efficiency, Purdue Industrial fuel conference, 5 - 6 October 1983, pp. 3-6.
- 10 Coe A., Coe I.M., An Introduction to the Industrial Use of Coal, Technical Information Services-College of Fuel Technology, March 1964, Pt.1, Ch. 1, p.176.
- 11 Woodruff E.B., Lammers H.B., Steam plant Operation, 1967, 3rd Ed., Ch. 4, pp. 136-137.
- 12 Kenton F., Thermal Efficiency and power Production, 1966, Ch. 6, p. 200.
- 13 Gunn D., Horton R., Industrial Boilers, 1989, Ch. 4, pp. 71-73.
- 14 Williams J.N., Steam Generation, 1969, Ch. 10, p. 327.
- 15 Gunn D., Horton R., Industrial Boilers, 1989, Ch. 10, pp. 212-213.
- 16 Fisher G.L., Natusch D.F.S., Size Dependence of Physical and Chemical Properties of Coal Fly Ash, Analytical Methods for Coal and Coal Products, 1979, Vol. III, Ch. 54, pp. 489-541.
- 17 Garner L.J., The Formation of Boiler Deposits from the Combustion of Victorian Brown Coals, J. Inst. Fuel, 1967, 40, pp. 107-115.

- 18 Fessler R.R., Skidmore A.J., Hazard H.R., Dimmer J.P., Composition and Microstructure of a Furnace Ash Deposit from a Coal Fired Utility Boiler, Trans. ASME, J. Eng. Power, 1980, 102, pp. 692-697.
- 19 Bryers R.W., Taylor T.E., An Examination of the Relationship Between Ash Chemistry and Ash Fusion Temperatures in Various Coal Size and Gravity Fractions, Using Polynomial Regression Analysis, Trans. ASME, J. Eng. Power, 1976, 98, pp. 528-539.
- 20 Adams A.M., Raask E., Complex Sulphates in Coal - Fired Boiler Deposits, Mechanism of Corrosion by Fuel Impurities, Proc. of the Int. Conf. - Marchwood, 20-24 May 1963, p. 469-483.
- 21 Jackson P.J., The Physio-chemical Behaviour of Alkali - Metal Compounds in Boiler Deposits, Mechanism of Corrosion by Fuel Impurities, Proc. of Int. Conf. - Marchwood, 20-24 May 1963, p. 484-495.
- 22 Wibberley L.J., Wall T.F., Deposit Formation and Sticky Particles from Alkali-Ash Reactions, Fouling and Slagging from Combustion Gases, pp. 493-513.
- 23 IEA Coal Research, Molecular Structure of Coal, 1980, pp. 5-86.
- 24 Thiessen G., Chemistry of Coal Utilisation (Editor: Lowry H.H.), 1945, Vol.1, Ch. 14, pp. 485-494.
- 25 Elliot M.A.(Edit.), Chemistry of Coal Utilisation, 1981, 2nd Suppl. Vol., NAS-NRC Committee on Chemistry of Coal, Ch. 7, p. 415.
- 26 Francis W., Coal - It's Formation and Composition, 1961, 2nd Ed., pp. 635-667.
- 27 Sarofim A.F., Howard J.B., Padia A.S., Combustion Science Technology, 1977, 16, pp. 187-204.
- 28 Raask E., Mineral Impurities in Coal Combustion, 1985, Ch. 4, p. 29.
- 29 Raask E., Mineral Impurities in Coal Combustion, 1985, Ch. 3, pp. 9-22.
- 30 Reid W.T., Chemistry of Coal Utilisation (Editor: Elliot M.A), 1981, 2nd Suppl. Vol., NAS-NRC Committee on Chemistry of Coal, Ch. 21, pp. 1389-1445.
- 31 Brume J.S.S., King J.G., Fuel-Solid, Liquid and Gaseous, 1961, 5th Ed., Ch.5, p.82
- 32 Mitchell R.S., Gluskoter H.J., Mineralogy of Ash of Some American Coals: Variation With temperature and Source, Fuel, 1976, 55, pp. 90-96
- 33 O'Gorman J.V., Walker Jr. P.L., Thermal Behaviour of Mineral Fractions Separated From Selected American Coals, Fuel 1973, 52, pp. 71-79.
- 34 Richardson H.M., Atlas of Electron Microscopy of Clay Minerals, Ch. 3, pp.132-141.

- 35 Ibid, Ch. 5, pp. 232-237.
- 36 Gluskoter H.J., Electronic Low Temperature Ashing of Bituminous Coal, Fuel, 1965, 44, pp. 285-291.
- 37 Stinespring C.D., Zulkoski M., Chemical Transformation of Minerals in Eastern Bituminous Coals Under Simulated Pulverized Coal Firing Conditions, Proc. of the Int. Conf. on Ash Deposits and Corrosion From Impurities in Combustion Gases, 26 June - 1 July, 1977, ASME, EPRI, DOE
- 38 Padia A.S., Behaviour of Ash in Pulverised Coal Under Simulated Combustion Conditions, PhD thesis, 1976.
- 39 Watt J.D., The Physical and Chemical Behaviour of the Mineral Matter in Coal Under Conditions Met in Combustion Plant-Pt. 1: The Occurrence, Origin, Identity Distribution and estimation of the Mineral Species in British Coals. BCURA Literature Survey, 1968.
- 40 Watt J.D., The Physical and Chemical Behaviour of the Mineral Matter in Coal Under Conditions Met in Combustion Plant - Pt.2: Thermal Decomposition of the Mineral Species: Volatilisation of Fouling Components; Sintering and Melting of Coal Ashes; Ash fusibility, BCURA Literature Survey, 1968.
- 41 Raask E., Creation, Capture and Coalescence of Mineral Species in Coal Flames, J. Inst. Energy, 1984, 57, pp. 231-239.
- 42 Crossley H.E., External Boiler Deposit, J. Inst. Fuel, 1952, 25, pp. 221-225.
- 43 Bryers R.W., The Physical and Chemical Characteristics of Pyrite and Their Influence on Fireside Problems in Steam Generators, Trans. ASME, J. Eng. Power, 1976, 98, pp. 517-527.
- 44 Raask E., Mineral Impurities in Coal Combustion, 1985, Ch. 6, pp. 62-75.
- 45 Bryers R.W., Influence of the Distribution of Mineral Matter in Coal on Fireside Ash Deposition, Trans. ASME, J. Eng. Power, 1979, 101, pp. 506-515.
- 46 Borio R.W., Narciso R.R., The Use of Gravity Fraction Techniques for Assessing Slagging and Fouling Potential of Coal Ash, Trans. ASME, J. Eng. Power, 1979, 101, pp. 500-503.
- 47 Bryers R.W., Walchuk O.R., Influence of Pyrite on Furnace Slagging, Proc. Int. Conf. on Slagging, Fouling and Corrosion in Thermal Power Plants, 29 February - 2 March 1984, pp. 276-311.
- 48 Raask E., Mineral Impurities In Coal Combustion, 1985, Ch. 7, pp. 85-88.
- 49 Schwab G.M., Phillips J., Reaction of Iron Pyrites: Thermal Decomposition Reduction by hydrogen and Aerial Oxidation, J. Am. Chem. Soc., 1947, 69, pp. 2588-2596.

- 50 Groves S.J., Williamson J., Sanyal A., Decomposition of Pyrites During Pulverized Coal Combustion, *Fuel*, 1987, 66, pp. 461-466.
- 51 Ghosh S.K., Understanding thermal Coal Ash Behaviour, *Mining Engineering*, February 1985, pp. 158-162.
- 52 Ely F.G., Barnhart D.H., Coal Ash - It's Effect on Boiler availability, *Chemistry of Coal Utilisation*, (Editor: Lowry H.H.), 1963, Suppl.vol., Ch. 19, pp. 822-891.
- 53 Barrett E.P., *Chemistry of Coal Utilisation*, (Editor: Lowry H.H.), 1945, Vol. 1, Ch. 15, pp. 497-571.
- 54 Winegartner E.C., Rhodes B.T., An Empirical Study of the Relation of Chemical Properties to Ash Fusion Temperatures, *Trans. ASME., J. Eng. Power*, 1975, 97, pp. 395-406.
- 55 Bunte K., Baum K., Investigation into the Fusion Processes in Fuel Ashes, *Das Gas Und Wasserfach*, 1928, 71, pp. 97-101.
- 56 Tsukii J., Kasen B., Kober A.E., Chemical Technology to Reduce Radiant Wall Slagging in Coal-Fired Boilers, *Coal Technology*, 1981, 3, pp. 65-80.
- 57 Hodges N.J., Marsh M.K., Martin T.G., McCaffery D.J., Williamson J., 1st European Conf. on the Influence of Inorganic Constituents on Coal Combustion (in Small to Medium Sized Boilers), *Inst. of Energy*, September 1987, pp. 1-13.
- 58 Huffman G.P., Huggins F.E., Investigation of the High Temperature Behaviour of Coal Ash in Reducing and Oxidising Atmosphere, *Fuel*, 1981, 60, pp. 585-597.
- 59 Reid W.T., Fouling of Heat Transfer Surfaces in Large Steam Generators - Fouling of Heat Exchanger Surfaces, *Proc. of Eng. Foundation Conf.*, November 1982, pp. 389-417.
- 60 Hupa M., Predicting Slagging and Fouling Tendency, *VTT Symposium on Low Grade Fuels*, Pt. 2, 1989, 2 (108), pp. 57-72.
- 61 Badin E.J., *Coal Combustion Chemistry - Correlation Aspects*, *Coal Science and Technology* 6, 1984, Pt. I, Ch. 2, pp. 9-26.
- 62 Vorres K.S., Melting Behaviour of Coal Ash Materials From Coal Ash Composition *ASC-CIC Fuel Chem. Symposium on Properties*, May 1977.
- 63 Vorres K.S., Effect of Composition on Melting Behaviour of Coal Ash, *Trans. ASME, J. Eng. Power*, 1979, 101, pp. 497-499.
- 64 Dutta B.K., Rai B., Chakravorty K.R., A Study of the Fusion Characteristics of Coal Ashes: Softening Temperature of Coal Ashes in Oxidising Atmosphere, *J. of Science and Industrial research*, 1966, 19B, pp. 206-212.

- 65 Szulakowski W., The Influence of Finely Ground Silica on the Ash Fluidity, J. Inst. Fuel, 1968, 47, pp. 25-27.
- 66 Badin E.J., Coal Combustion Chemistry - Correlation Aspects, Coal Science and Technology 6, 1984, Pt. I, Ch. 1, pp. 1-8.
- 67 Kosaka Y., Toda H., Kitagowa C., J. Soc. Chem. Ind. Japan, 1936, 39, Suppl. binding, pp. 36-40.
- 68 Saphtharishi L.R., Elanchezhan P.K., Damodara M., Ekambaran A., An Investigation Report on Slagging in a 60MW Indirect-Fired Boiler - Slagging, Fouling and Corrosion in Thermal Power Plants, February 1984, pp. 390-401.
- 69 Raask E., Mineral Impurities in Coal Combustion, 1985, Ch. 15, p. 275.
- 70 Sanyal A., Williamson J., Slagging in Boiler Furnaces: An Assessment Technique Based on Behaviour of Coal Minerals, J. Inst. Energy, 1981, 54, pp. 158-162.
- 71 Raask E., Mineral Impurities in Coal Combustion, 1985, Ch. 8, pp. 103-119.
- 72 Williamson J., I'll Take Any Coal As Long As It Burns, 1st European Conf. on the Influence of Inorganic Constituents on Coal Combustion (in Small to Medium Size Boilers), 24-25 September 1987, Vol 1, pp. II/1-13
- 73 Dutta B.K., Rai B., Chakravorty K.R., A Study of the Fusion Characteristics of Coal Ashes: Softening Temperature of Coal Ashes in Mild Reducing Atmosphere, J. of Science and Industrial Research, 1962, 210, pp. 44-48.
- 74 Huggins F.E., Kosmack D.A., Huffman G.P., Correlation Between Ash Fusion Temperatures and Ternary Equilibrium Phase Diagrams, Fuel, 1981, 60, pp. 577-584
- 75 Reid W.T., Cohen P., The Flow Characteristics of Coal Ash Slags in the Solidification Range, Trans. ASME, (Special Edition), February 1944, 66, pp. 83-97.
- 76 Reid W.T., External Corrosion and Deposits (Boilers and Gas Turbines), 1971, Ch. 2, pp. 50-73.
- 77 Watt J.D., The Flow Properties of Slag Formed From the Ashes of British Coals: Pt.1 - Viscosity of Homogenous Liquid Slags in Relation to Slag Composition, J. Inst. Fuel, 1969, 42, pp. 99-103.
- 78 Watt J.D., The Flow Properties of slag Formed From the Ashes of British Coals: Pt.2 - The crystallising Behaviour of the Slags, J. Inst. Fuel, 1969, 42, pp. 131-134.
- 79 Gibb W.H., The Slagging and Characteristics of Coals, I. Ash Viscosity measurements for the Determination of Slagging Propensity, Power Industry Research, 1981, 1, pp. 29-42.
- 80 Raask E., Mineral Impurities in Coal Combustion, 1985, Ch. 9, pp. 121-135.

- 81 Winegartner E.C., Coal Fouling and Slagging Parameters, ASME Committee on Corrosion and Deposits From Combustion Gases, 1974, pp. 1-34.
- 82 Babcock and Wilcox, Steam - Its Generation and Use, Ch. 15, pp. 15.1-15.21
- 83 Badin E.J., Coal Science and Technology 6, Coal Combustion Chemistry - Correlation Aspects, Elsevier Science Publishing, 1984, Ch.9, pp. 105-116.
- 84 Raask E., Mineral Impurities in Coal Combustion, 1985, Ch. 12, pp. 189-214.
- 85 Zinzen A., Investigation of the Fusion Behaviour of Fuel Ash, Arch. Warmew, Verein Duetsch Ingenieure, 1943, 24, pp. 199-201.
- 86 Grant K., Weymouth J.H., The Nature of Inorganic Deposits Formed During the Use of Victorian Brown coals in Large Industrial Boilers, J. Inst. Fuel, 1962, 35, pp. 154-159.
- 87 Hein H.K., Formation of Fireside Deposits During Brown Coal Combustion, Proc. of the Eng. Foundation Conf., 12-13 July 1981, pp. 69-83.
- 88 Raask E., Cenospheres in Pulverised Fuel Ash, J.Inst. Fuel, 1968, 41, pp. 339-344
- 89 Lauf R.J., Cenospheres in Fly Ash and Conditions Favouring Their Formation, Fuel, 1981, 60, pp. 1177-1179
- 90 Hazard H.R., Influence of Coal Mineral Matter on Slagging of Utility Boilers, Battle Columbus Lab., CS 1418, June 1980, p. 8-18, 9-24 to 9-26.
- 91 Hazard H.R., Barrett R.E., Dimmer J.P., Coal Mineral Matter and Furnace Slagging, Battle Columbus Labs. and Electric Power Research Institute, Proc. of the Am. Power conf., 1979, 41, pp. 610-617.
- 92 Raask E., Mineral Impurities in Coal Combustion, 1985, Ch. 11, pp. 169-187.
- 93 Grant K., Weymouth J.H., The Influence of the Inorganic Constituents in Victorian Brown Coals on the Fouling Properties of the Coal When Used in Gas Generators and Industrial Boilers, Symp. Inorganic Constituents of Fuel, 1964, pp. 127-137.
- 94 Borio R.W., Hensel R.P., Coal Ash Composition as Related to High Temperature Fire Side Corrosion and Sulphur Oxide Emissions Control, Trans. ASME, J. Eng. Power, 1972, 94, pp. 142-148.
- 95 Hupa M., Backmann R., Sundberg L., Slagging and Fouling Studies in Coal Fired Boilers Using Air-Cooled Deposit Probes, Slagging, Fouling and Corrosion in Thermal Power Plants, February 1984, pp. 257-274.
- 96 Shigeta J.I., Hamao Y., Aoki H., Kajigaya I., Development of a Coal Ash Corrosivity Index for High Temperature Corrosion, Trans. ASME, J. Eng. Materials and Technology, 1987, 109, pp. 299-305.

- 97 Brown H.R., Durie R.A., Taylor G.H., Factors Influencing the Formation of Fireside Deposits During the Combustion of Morwell Brown Coals - Mechanism of Corrosion by Fuel Impurities, Proc. of the Int. Conf.- Marchwood, 20-24 May 1963, pp. 469-483.
- 98 Rindt D.K., Jones M.L., Schobert H.H., Investigation of the Mechanism of Ash Fouling in Low-Rank Coal Combustion, Fouling and Slagging From Combustion Gases, Proc. of the Eng. Foundation Conf., 12-17 July 1981, pp. 17-35.
- 99 Sondreal E.A., Gronhovd G.H., Ash Fouling Studies of Low Rank Western U.S. Coals, Proc. of Int. Conf. on Ash Deposits and Corrosion from Impurities in Combustion Gases, 1 June - 26 July 1977, pp. 85-111.
- 100 Wibberley L.J., Wall T.F., Alkali - Ash Reactions and Deposit Formation in pulverized Coal Fired Boilers: Experimental Aspects of Sodium-Silicate Formation and the Formation of Deposit, Fuel, 1982, 6, pp. 93-99.
- 101 Raask E., Goetz L., Characterisation of Captured Ash, Chimney Solids and Trace Elements, J. Inst. Energy, 1981, 54, pp. 163-173.
- 102 Reid W.T., External Corrosion and Deposits (Boilers and Gas Turbines), 1971, Ch. 6, pp. 144-159.
- 103 Gronhovd G.H., Beckering W., Study of Factors Affecting Ash Deposition From Lignite and other Coals, Proc. of Annual Meeting of ASME, July 1969, Paper No. 69-WA / CD-1, pp. 1-9.
- 104 Procter N.A., Taylor G.H., Microscopical Study of Boiler Deposits Formed from Australian Brown Coals, J. Inst. Energy, 1966, 39, pp. 284-293.
- 105 Rahmel A., Influence of Calcium and Magnesium Sulphate in the High Temperature Oxidation of Austenitic - Chrome Nickel Steels in the Presence of Alkali Sulphate and Sulphur Trioxide, Proc. of the Int. Conf - Marchwood, 1963.
- 106 Lebedev I.K., Mikhaielenko S.A., The Effect of the Gaseous Medium on the Tendency of Ash to Foul the Heating Surfaces of Boilers, Thermal Engineering, 1982, 29 (1), pp. 43-46.
- 107 Clark F., Morris C.W., Combustion Aspects of Furnace Wall Corrosion- Corrosion Resistance Material for Coal Conversion System, Proc. Int. Conf., 1982 (Published 1983), pp. 47-61.
- 108 Kirsch H., Corrosion in Combustion Chambers Caused by Slag Attack and Flue Gases of Varying Composition, Mechanism of Corrosion by Fuel Impurities, Proc. of the Int. Conf. - Marchwood 20-24 May 1963, pp. 508-528.
- 109 Hupa M., Eriksson B.E., Slagging of the Furnace Walls in Pulverized Coal-Fired Steam Boilers, Kemia-Kemi, 1979, 11, pp. 607-611.

- 110 Pollock W.H., Goetz G.J., Park E.D., Advancing the Art of Boiler Design by Combining Operating Experience and Advanced Coal Evaluation Techniques, Proc. of the Am. Power Conf., 1983, 45, pp. 102-117.
- 111 Bonafede G., Kiss L.T., Study of Ash Deposits From Brown Coal Fired boilers With the Aid of Scanning and Transmission Electron Microscopy, ASME Paper No. 73 - WA / CO-7, p. 12.
- 112 Reid W.T., Chemistry of Coal Utilisation (Editor: Elliot M.A.), 1981, 2nd Suppl. Vol., NAS-NRC Committee on Chemistry of Coal, Ch. 21, pp. 1391-1403.
- 113 Pacer D.W., Duzzy A.F., How Coal Affects Boiler Design, Coal Mining and Processing, 1982, 19, pp. 72-78.
- 114 Richards C.L., The Effect of Coal Properties on Boiler Design, Coal Technology 78 - The Int. Coal Utilisation Conf. and Exhibition, October 1978, pp. 283-311.
- 115 Keyes H.E., Alleviation of a Superheater Fouling Problems in a Cyclone-Fired Boiler Unit, Coal Technology 1983, 6 (3), p. 76.
- 116 Beer J.M., The 1986 British Coal Utilisation Research Association Robens Coal Science Lecture: Combustion of Coal; A New Look on a Old Problem, J. Inst. Energy, 1987, 60, pp. 143-151.
- 117 Szpindler G.D., Studies of the Combustion Rate and Structure of Pulverized Fuels Burned in the C-15 Trials (1969) of the International Flame research foundation, Pt.2: Microscopic Examination of the Structural Changes in the Solid Particles in a Pulverized Bituminous Coal Flame, Report No. 87, April 1971, pp. 1-42.
- 118 Kromka D.P., Hayes T.L., Lai C.E., Fisher G.L., Prentice B.A., Comparative Analysis of Coal Fly Ash by Light and Electron Microscopy, AIChE. Symp. Series, 1980, 76 (201), pp. 149-153.
- 119 Lauf R.J., Ceramic Bulletin, 1982, 61 (4), pp. 487-490.
- 120 Raask E., Flame Imprinted Characteristics of Ash Relevant to Boiler Slagging, Corrosion and Erosion, Trans. ASME, J. Eng. Power, 1982, 104, pp. 858-865.
- 121 Gupta A.K., Jackson T.W., Fouling and particulate Deposition in Practical Systems J. Inst. Energy, 1985, 58, pp. 103-111.
- 122 Brown T.D., The Deposition of Sodium Sulphate From Combustion Gases, J. Inst. Fuel, 1966, 39, pp. 378-384.
- 123 Beer J.M., 51st Melchelt Lecture - Clean combustion of Coal, Research and applications - An Overview of Recent Development in the U.S.A., J. Inst. Energy, 1986, 59, pp. 3-19.
- 124 Raask E., Boiler Fouling - The Mechanism of Slagging and Preventive Measures, CEBG Report RD/L/N97/72, January 1976, pp. 1-11.

- 125 Walker R.F., Mechanism of Material transport During Sintering, J. Am. Cer. Soc., 1955, 38 (6), pp. 187-197.
- 126 Raask E., Mineral Impurities in Coal Combustion, 1985, Ch. 10, pp. 137-167.
- 127 Navies L., Sintering Experiments on Sapphire Spheres, J. Am. Cer. Soc., 1956, 39 (4), pp. 141-145.
- 128 Burke J.E., Role of Grain Boundaries in Sintering, J. Am. Cer. Soc., 1957, 40 (3), pp. 80-85.
- 129 Coble R.L., Initial Sintering of Alumina and Hematite, J. Am. Cer. Soc., 1958, 41 (2), pp. 55-62.
- 130 Nowok J.W., Benson S.A., Jones M.L., Kalmanovitch D.P., Sintering Behaviour and Strength Development in various Coal Ashes, Fuel, 1990, 69, pp. 1020-1027.
- 131 Frenkel J.J., Viscous Flow of Crystalline Bodies Under the Action of Surface Tension, J. Physics, 1945, 9, p. 385.
- 132 Barnhart D.H., Williams P.C., The Sintering Test, An Index to Ash Fouling Tendency, Trans. ASME, August 1956, pp. 1229-1236.
- 133 Smith E.J.D., The Sintering of Fly Ash, J. Inst. Energy, 1956, 29, pp. 253-260.
- 134 Anderson C.H., Diehl E.K., Bonded Fireside Deposits in Coal-Fired Boilers - A progress report on the Manner of Formation, ASME Paper 55-A-200, 1955, pp. 1-20
- 135 Tuft P.H., Beckering W., A Proposed mechanism For Ash Fouling, Burning Northern Great Plain Lignite, Trans ASME, J. Eng. Power, 1975, 97, pp.407-412.
- 136 Radway J.E., Hoffman M.S., Operation Guide For the Use of Combustion Additives in Utility Boilers, 1988, Section 9, pp. 9.1-9.25.
- 137 Radway J.E., Hoffman M.S., Operation Guide For the Use of Combustion Additives in Utility Boilers, 1988, Section 3, pp. 3.1-3.6.
- 138 Reid W.T., External Corrosion and Deposits (Boilers and Gas Turbines), 1971, Ch. 7, pp. 160-177.
- 139 Michel J.R., Wilcoxson L.S., Ash Deposits on Boiler furnaces from Burning Central Illinois Coal, ASME Paper 55-A-95, 1955.
- 140 Bennett R.P., Kakin I., Process For Reducing the Fouling Point of Coal Ash, U.S. Patent No. 4,057,398, 8 November, 1977.
- 141 Szladow A.J., Smith D.W., Combating Lignite Ash Fouling at SPC: From Solving Problems of the "60's" to Meeting Demands of the "80's", Fouling of Heat Exchanger Surfaces, Engineering Foundation, 1983, pp. 751-760.

- 142 Radway J.E., Boyce T.R., Reduction of Coal Ash Deposits With Magnesia Treatment - Ash Deposits and Corrosion Due to Impurities in Combustion gases - proc. Int. Conf. on Ash Deposits and Corrosion from Impurities, 26 June - 1 July, 1977.
- 143 Gibb W.H., The Role of Calcium in the Slagging and Fouling Characteristics of Bituminous Coals, J. Inst. Energy, 1986, 59, pp. 206-213.
- 144 James W.G., Fisher A.H., A New Fuel Additive For Coal-Fired Boilers, J. Inst. Fuel, 1967, 40, pp. 170-172.
- 145 Kiss L.T., LLOYD B., Raask E., The Use of Copper Oxychloride to Alleviate Boiler slagging, J. Inst. Fuel, 1972, 45, pp. 212-223.
- 146 Libutti B.L., Pall R.L., Criteria For Selection of Coal Additives, Am. Chem. Soc.- Division of Fuel Chem., Prep. Paper, 1978, 23 (1), pp. 206-213.
- 147 Nelson W., Spencer E., Additive Mixtures to Combat High Temperature Corrosion and Ash Boning During the Operation of Furnaces, Patent No. 3,249,075, May 1966.
- 148 Radway J.E., Hoffman M.S., Operation Guide For the Use of Combustion Additives in Utility Boilers, 1988, Section 10, pp. 10.1-10.17.
- 149 O'Connor E.F., Use of Copper Salts For Inhibition of External Fouling of Peat-Fired Boilers, J. Inst. Fuel, 1970, 43, pp. 449-450.
- 150 Radway J.E., Effectiveness of Fireside Additives in Coal Fired Boilers, 1979.
- 151 Anson D., Status of Fireside Additives in the USA - The Effectiveness of Fuel Additives, Proc. of Conf., Inst. of Energy, 2nd Vol., 1983.
- 152 Merrell G.A., Knight R.S., Combustion Catalysts in Industry-An Update presented at the Purdue industrial Fuel Conf., 5-6 October 1983, pp. 13-21.
- 153 Oschell F.J., Boccuzzi E.J., Improved Coal Combustion through Chemical Treatment Combustion, 1980.
- 154 Harker J.H., Pimparker P.M., The effect of Additives on the Electrostatic Precipitation of Fly Ash, J. Inst. Energy, 1988, 61, pp. 134-142.
- 155 South of Scotland Electricity Board - Plant test and Efficiency Section, Flue Gas Conditioning by "Liquimag", Report No. T.E.77.15, August 1977.
- 156 Lees B., Mustoe D.H., Effect of Magnesium-Based Additives in High Temperature Corrosion in Oil-Fired Boilers, J. Inst. Energy, 1972, 45, pp. 397-405.
- 157 Davies J., Laxton J.W., Owers M.J., The Use of Magnesium-Based Flue Gas Additives in Minimising Acid Smut Emission From Oil-Fired Boilers, J. Inst. Fuel, 1981, 54, pp. 21-29.

- 158 Reid W.T., The Relation of Mineral matter Composition to Slagging, Fouling and Erosion During and After Combustion, Prog. Energy Combustion Science, Vol. 10, 1984, pp. 159-175.
- 159 Libutti B.L., Control of Coal Ash Corrosion by Additives, AIChE, 67th Annual Meeting, Paper No. 78-E, 1-5 December, pp. 1-21.
- 160 Honea F.I., Rindt D.K., Middleton R., Royhe D., The Use of Additives to Reduce Ash Fouling Problems in Lignite-Fired Boilers, ASME Paper No. 80-JPGC/FU-3, 1980, pp. 1-13.
- 161 Radway J.E., Some Consideration in the Application of Fireside Additives, The Effectiveness of Fuel Additives-Proc. of Conf., Inst. of Energy, Vol. 1, 4-5 October 1983.
- 162 Anderson C.H., Diehl E.K., Combustion Science Technology, 1980, **23**, pp. 103-112.
- 163 Raask E., Mineral Impurities in Coal Combustion, 1985, Ch. 16, pp. 283-310.
- 164 Anderson C.H., Goddard C.W., Equilibrium SO₃ Pressures of Inner Layers of Fireside Deposits From Coal-Fired Boilers, J. Inst. Fuel, 1968, 41, pp. 357-364.
- 165 Blaustein E., Technical Evaluation of Magnesia's Influence on Fireside Deposits, Combustion and Emission on Oil-Fired Boilers, Proc. of the Int. Conf. on Ash Deposits and Impurities in Combustion Gases, ASME - EPRI/DOE, 26 June-1 July 1977.
- 166 Hazard H.R., Krause H.H., Sekercioglu I., Use of Additives to Facilitate On-Load Cleaning of Utility Boilers, EPRI Report CS-3270- Res. Project 1839-2, November 1983.
- 167 Anson D., Hazard H., Sekercioglu I., Krause H., Dimmer J., Action of Additives on Fuel Ash Deposit Fouling of Heat Exchanger surfaces, Proc. of the Eng. Foundation Conf., October - November 1982, pp. 761-777.
- 168 Hedges P.E., Turner J.E., Gagg M., Reduction of Slag Deposits by Magnesium Hydroxide Injection - The Effectiveness of Fuel Additives, Proc. of Conf., Inst. of Energy Publications, 4-5 October 1983.
- 169 Jaworowski R.J., Chemical Additives in Coal and oil Fired Boilers Fouling of Heat Exchanger Surfaces - Proc. of the Eng. Foundation Conf., October - November 1982, pp. 785-790.
- 170 Harkin K.J., The effect of a Magnesium Additive on Deposit Formation in a Coal Fired Boiler, Queen's University of Belfast, April 1987.
- 171 Turner J., Application of Lycal 93HS to a Large Coal Fired Boiler, Interim Report I, private Communication, 1986.

- 172 Hedges P., Johnson T.D., Laxton J.W., The Development of Injection Equipment For Magnesium Hydroxide Powder, J. Inst. Energy, 1981, 54, pp. 135-141
- 173 Cullity B.D., Elements of X-Ray Diffraction, Ch. 3, 1967.
- 174 Ibid., Ch. 14.
- 175 B.S. 1016, Pt. 15, 1970.
- 176 B.S. 410, Pt. , 1962.
- 177 B.S. 1016, Pt. 3, 1965.
- 178 Miller R.N., Yarzab R.F., Given P.H., Determination of the Mineral Matter Content of Coal by Low Temperature Ashing, Fuel, 1979, 58, PP. 4-10.
- 179 Roth R.S., Negas T., Cork L.P., Phase Diagrams for Ceramists, Amer. Ceram. Soc., 1969.
- 180 Ford N., Cooke M.J., Pettit M.D., The Use of a Laboratory Fixed-Grate Furnace to Simulate Industrial Stoker-Fired Plant, J. Inst. Energy, 1992, 65, pp. 137-143.
- 181 Marskell W.G., Pratt C.W., A Special Study of Ash and Clinker in Industry, Paper 3. Ash and Clinker in Practice - Handling and Disposal, J. Inst. Fuel, 1952, 25, pp. 212-221.
- 182 Huffman G.P., Huggins F.E., Investigation of Partial Ash Melting by Phase Analysis of Quenched Samples, Fouling and Testing from Impurities in Combustion Gases - Proc. of the 1981 Eng. Foundation Conf. (Edit. Bryers R.W.) pp. 259-279.
- 183 Gould G.B., Bunjes H.L., Proportions of Free Fusible Material in Coal Ash, As an Index of Clinker and Slag Formation, Ash Deposits and Corrosion Due to Impurities in Combustion gases - proc. Int. Conf. on Ash Deposits and Corrosion from Impurities, 26 June - 1 July, 1977.
- 184 Pollman S., Albrecht W., Investigations of the Slagging Behaviour of Bituminous Coals in Dry-Bottom Steam Generators, Proc. of the 1981 Eng. Foundation Conf., pp. 85-99.
- 185 Barratt D.J., Unsworth J.F., Ash Formation During Pulverized Fuel Combustion, 3. The Structure and Strength of Boiler Deposits, Fuel, 1988, 67, pp. 1503-1509.
- 186 Nolan J., Rogers P.S., Williamson J., A Laboratory Study of the Thermal Behaviour of Coal Minerals, Microstructural Sciences, 1981, 9, pp. 99-108.
- 187 Lindsay C.G., Kinetic Studies of the Behaviour of Mineral Associations Commonly Found in the U.S. Coals and Coal Blends By Heating-Stage Microscopy, Int. Coal Testing Conf., Proc. of the 3rd Conf., Vol III, October 24-26, 1983, pp. 158-166.

- 188 Gray V.R., Prediction of Ash Fusion Temperature from Ash Composition for Some New Zealand Coals, Fuel, 1987, 66, pp. 1230-1239.
- 189 Steel J.S., Brandes E.A., Growth and Adhesion of Oxides in Furnace Deposits and Their influence on Subsequent Deposition of Ash Particles as Combustion Products, Fouling and Slagging From Combustion Gases, Proc. of the Eng. Foundation Conf., 12-17 July 1981.
- 190 Erickson T.A., Ludlow D.K., Benson B., Fly Ash Development from Sodium, Sulphur and Silicon During Coal Combustion, Fuel, 1992, 71, pp. 15-18.
- 191 Vassilev S.V., Phase Mineralogy Studies of Solid Waste Products from Coal Burning at Some Bulgarian Thermoelectric Power Plants, Fuel, 1992, 71, pp. 625-633.
- 192 Spiro C.L., Kimura S.G., Chen C.C., Ash Behaviour During Combustion and Deposition in Coal-Fueled Gas Turbines, J. Eng. for Gas Turbines and Power, 1987, 109, pp. 325-330.
- 193 Rost F., Ney P., Information on Boiler Slag, Brenstoff-Chemie, Vol.37, No.13/14, 1956, pp. 201-210, (English Translation 1070, pp. 1-25).
- 194 Moreau A., Barbier J.M., Lecointre D., Gallo P., Analysis of the Fouling Phenomenon in Incinerator, Proc. of the 6th European ABWASSER - ABFALL Symp., 1984, pp. 731-743.
- 195 Rieke R., Sprechsaal, 1910, 16, pp. 229-232 Cited in Hall F.P., Insley H., "A Compilation of Phase-Rule Diagrams of Interest to the Ceramist and Silicate Technologist", J. Am. Cer. Soc., 1933, 16, pp. 463-567.
- 196 Estep T.G., Seltz H., Osborn W.S., Determination of the Effects of Oxides of Sodium, Calcium and Magnesium on Ash Fusion Temperature by the Use of Synthetic Coal Ash, Mining and Metallurgical Investigations Co-op. Bull., 1937, 74, pp. 1-15.
- 197 Kalmanovitch D.P., Reactions in Coal Ash Melts, PhD Thesis, London Univ., 1982, p. 212.
- 198 Livingston W.R., Sanyal A., Williamson J., The Role of Copper Oxychloride in Reducing Slagging in P.F. Fired Boilers, The Effectiveness of Fuel Additives, Proc. of Conf. - Inst. of Energy, 4-5 October 1983, 1st Vol., pp.1-21.
- 199 Raask E., Formation of Coal Fired Boiler Deposits and Remedial Measures, Int. Conf. on Slagging, Fouling and Corrosion in Thermal Power Plants, 29 February - 2 March 1984, pp. 457-492.
- 200 Private Report No. D96, West Belfast Power Station, 1 - 3 September 1987.